الجمهورية الجزائرية الديموقراطية الشعبية
PEOPLE'S DEMOCRATIC REPUBLIC OF ALGERIA

وزارة التعليم العالي و البحث العلمي
MINISTRY OF HIGHER EDUCATION AND SCIENTIFIC RESEARCH

جامعة باجي مختار-عنابة

BADJI-MOKHTAR-ANNABA- UNIVERSITY

FACULTY OF SCIENCE
CHEMISTRY DEPARTMENT
ECO-COMPATIBLE ASYMMETRIC CATALYSIS LABORATORY

THESIS

Submitted in view of obtaining the **Doctorate** degree
Field: Chemistry

Speciality: Organic chemistry

THEME

Chemoenzymatic synthesis of chiral phosphonate derivatives of biological interest

Presented by: M^elle Meriem FERRAH

In front of the jury

Pr. FERKOUS Fouad	President	U. B.M. Annaba
Pr. GUEZANE LAAKOUD Samia	Thesis director	U. B.M. Annaba
Pr. MERABET-KHELASSI Mounia	Thesis co-director	U. B.M. Annaba
Pr. BOUGHELOUM Chafika	Examiner	U. B.M. Annaba
Dr. SAIHI Youcef (MCA)	Examiner	ENSET Skikda
Dr. KRAIM Khairedine (MCB)	Invited	ENSET Skikda

University Year: 2023/2024

Dedication

To my mother and father, who have always been my source of love, support, and encouragement.

To my family.

To everyone who helped me in this work.

Who have contributed their time, expertise, and guidance...

Thank you

Acknowledgments

Above all, I express my gratitude to the Almighty God, who bestowed upon me the will, courage, and patience, guiding my steps on the right path throughout my years of study.

This thesis was conducted at the Eco-Compatible Asymmetric Catalysis Laboratory "L.C.A.E" at the University of Badji Mokhtar in Annaba, Algeria, under the guidance of Professor Madame ***Guezane Laakoud Samia*** *and Professor* ***Mounia MERABET-KHELASSI****.*

I extend my deep thanks to Professor ***Guezane Laakoud Samia****, my thesis director, for her unwavering supervision, scientific counsel, pedagogical excellence, availability, efforts, and support provided during these four years until the completion of the manuscript. I extend my heartfelt thanks for the countless hours you devoted to guiding me through each stage of the thesis. Your mentorship has been invaluable, and I am sincerely grateful for the opportunities you provided for intellectual exploration and academic development.*

Sincere appreciation goes to Professor ***Mounia MERABET-KHELASSI****, the co-director of my doctoral thesis, for her support, kindness, and tremendous patience. I also acknowledge her for the valuable discussions and substantial assistance throughout this research.*

Gratitude is also extended to the esteemed members of the jury who honored me by evaluating this work. I appreciate the significant contribution of ***Mr. FERKOUS Fouad****, a professor at the University of Annaba, for graciously chairing the jury.*

Special thanks to ***Ms. BOUGHELOUM Chafika****, a professor at the University of Annaba, for agreeing to be a jury member, dedicating her time to examine and evaluate this work.*

I express my warm thanks to ***Dr. SAIHI Youcef*** *M.C.A at ENSET in Skikda, for serving as rapporteur for this work and being part of the thesis jury. Sincere appreciation is also extended to* ***Mr. KRAIM Khairedine****, Doctor at ENSET University of Skikda, for his valuable comments and criticisms.*

I cannot overlook acknowledging my family for their unwavering support in all situations.

I extend my gratitude to my friends and colleagues in the laboratory for fostering a friendly atmosphere. Thanks to all the individuals who contributed directly or indirectly to the completion of this work.

In conclusion, my heartfelt thanks to everyone who played a role in the successful accomplishment of this thesis.

الملخص

تتكون الأطروحة المقدمة من ثلاثة أجزاء :

في الجزء الأول، قمنا بتخليق سلسلة جديدة من مشتقات ألفا أمينو فوسفونات من خلال مسار التحفيز العضوي، وذلك باستخدام حمض ثنائي فينيل فوسفينيك وتنفيذ طريقة تصميم التجربة. تم استخدام تفاعل كاباتشنيك-فيلدز في ظل ظروف صديقة للبيئة، مع الالتزام بمبادئ الكيمياء الخضراء. ويؤكد التوليف الناجح لجميع المشتقات على كفاءة هذه المنهجية.

ويركز الجزء الثاني على تصميم وتركيب مشتقات ألفا أمينو فوسفونيت، مع التعرف على أهميتها الدوائية والكيميائية. لعب وجود 2-هيدروكسي ميثيل-18-كراون-6 دورًا محوريًا في عملية التخليق. علاوة على ذلك، تم إجراء دراسة نظرية شاملة تستخدم DFT والإرساء الجزيئي، لتوضيح التفاعل الكيميائي والأهمية البيولوجية للجزيئات المركبة . تم الحصول على النواتج المذكورة بمردود عالي في ظل الظروف المثالية.

في الجزء الختامي، كان تركيزنا على الإزالة الإنتيوإنتقائية لخلات البنزيليك الثانوية المحفزة بواسطة-CAL. Bتم هذا التفاعل في وسط غير مائي، مدعومًا بوجود DABCO كمادة مضافة مهمة. تم الحصول على الكحوليات الناتجة مع فائض إنانتيوميري استثنائي يتجاوز 99% وانتقائية.(E> 200)

كان تطبيق الطرق الطيفية المختلفة، بما في ذلك ^{1}H و^{13}C و^{31}P NMR ، إلى جانب قياس الطيف الكتلي، محوريًا في تحديد الخصائص الهيكلية للمركبات المركبة.

الكلمات المفتاحية: الفوسفات العضوي، ألفا أمينوفسفونات، تفاعل كاباتشنيك-فيلدز، التحفيز العضوي، الاستبانة الحركية الأنزيمية، الليباز.

Abstract

The presented PhD thesis composed of 03 comprises three distinct partis:

In the initial part, we detail the synthesis of a novel series of α-amino-phosphonate derivatives through an organocatalytic pathway, utilizing diphenylphosphinic acid and applying the Design of Experiment method. The *Kabachnik-Fields* reaction was employed under eco-friendly conditions, adhering to the principles of green chemistry. The successful synthesis of all derivatives underscores the efficiency of this methodology.

The second part focuses on the design and synthesis of *α*-aminophosphonate derivatives, recognizing their pharmacological and chemical importance. The presence of 2-Hydroxymethyl-18-Crown-6 played a pivotal role in the synthesis. Furthermore, a comprehensive theoretical study, employing DFT and molecular docking, was conducted to elucidate the chemical reactivity and biological relevance of the synthesized molecules. The mentioned products were obtained with high yields under optimal conditions.

In the last part we focus on the enantioselective deacylation of secondary benzylic acetates catalyzed by *CAL-B* as key pathway to easily access to enantiopure organophosphorus compounds. This reaction unfolded in a non-aqueous medium in the presence of DABCO as a crucial additive. The resulting alcohols were successfully obtained enantiopure 99% ee and selectivity ratio of E > 200.

The application of various spectroscopic methods, including ^{1}H, ^{13}C, and ^{31}P NMR, along with mass spectrometry, was pivotal in establishing the structural characteristics of the synthesized compounds.

Key words: Organophosphates, *α*-aminophosphonates, *Kabachnik-Fields* reaction, organocatalysis, enzymatic kinetic resolution, lipases.

Résumé

Notre travail présenté dans cette thèse est constitué de trois parties :

Dans la première partie, nous avons détaillé la synthèse d'une nouvelle série de dérivés *α*-aminophosphonates par une voie organocatalytique, en utilisant l'acide diphénylphosphinique et en exploitant la méthode du plan d'expérience. La réaction de *Kabachnik-Fields* a été utilisée dans des conditions respectueuses de l'environnement, en adhérant aux principes de la chimie verte. Les différents dérivés sont obtenus avec de bons rendements chimiques isolés.

Dans la deuxième partie, nous avons utilisé un autre type d'organocatalyseurs le 2-Hydroxyméthyl-18-Crown-6 pour la synthèse de dérivés α-aminophosphonate d'intérêt pharmacologique. En outre, une étude théorique complète, utilisant la DFT et le docking moléculaire, a été menée pour élucider la réactivité chimique et la pertinence biologique des molécules synthétisées.

Les produits mentionnés ont été obtenus avec des rendements élevés dans des conditions optimales.

Dans la dernière partie, nous avons étudié la déacylation énantiosélectives d'acétates benzyliques secondaires catalysées par la CAL-B. Cette réaction s'est déroulée dans un milieu non aqueux en présence du DABCO comme en tant que additif cruciale. Les alcools ont étaient obtenus avec un excès énantiomériques ee>99% et un facteur de sélectivité (E > 200).

Les différentes méthodes spectroscopiques, RMN ^{1}H, ^{13}C et ^{31}P, spectrométrie de masse, ont été mises à profit pour établir les caractéristiques structurales des composés synthétisés.

Mots clés : Organophosphates, *α*-aminophosphonates, réaction de *Kabachnik-Fields*, organocatalyse, résolution cinétique enzymatique, lipases.

Table of contents

Chapter II : Multicomponents reactions and catalysis

Chapter III : Design of experiments, density functional theory and molecular docking

Part Two: Results and discussion

Chapter IV: Synthesis of α-aminophosphonates using diphenylphosphinic acid.

Chapter V: Synthesis of α-aminophosphonates using 2-Hydroxymethyl-18-Crown-6

Chapter VI: Enantioselective Biodeacylation of arylalkylacetates as key precursors of enantiopure organophosphorus compounds

Experimental protocols

Annex

List of schemas

General Introduction

Part 01: Chapter I

Chapter II

Chapter III

Part 02: Chapter IV

Chapter V

Chapter VI

List of Figures

General Introduction

Part 1: chapter I

Chapter II

Chapter III

Part 02: Chapter IV

Chapter V

Chapter VI

List of tables

Part 01: Chapter III

Part 02: Chapter IV

Chapter V

Chapter VI

Abreviations list

Reagents and products

DEP: Diethylphosphite

RNA : Ribonucleic acid

DCC: N,N'-dicyclohexylcarbodiimide

DMAP: 4-dimethylaminopyridine

Et_3N: Triethylamine

DABCO: 1,4-Diazabicyclo [2.2.2]octane

SPINOL: 1,1′-spirobiindane-7,7′-diol

Chemical groups

Ph: Phenyl

R: Radical

Alk: alkyl

Ar:aryl

Enzymes

AChE: acetylcholinesterase

PCL: Lipase from Pseudomonas cepacia

CAL-B: Candida antarctica lipase B

PPL: Porcine pancreatic lipase

CCL: Lipase from Candida cylindracea

RGL: Rabbit gastric lipase

Solvents

DCM: dichloromethane

DIPE: Diisopropyl ether

TBME: tertbuthylmethylether

THF: Tetrahydrofuran

EtOH: Ethanol

Spectroscopy and chromatography

CCM: Thin-layer chromotography

CPG: Gas chromatography

HPLC: High performance liquid chromatography

m: multiplet

D: doublet

q: quadruplet

Dd: doublet de doublet

Rf: Rapport frontal

RMN: Nuclear magnetic resonance

s: singulet

t: Triplet

J: Coupling constant

δ: Chemical shift

Physical units and constants

°C: Degree Celsius

min: Minute

eq.g: Number of gram equivalents

mmol: millimole

g: Gramme

mol: Mole

h: Hour

ppm: Part-per-million

Hz: Hertz

s: Second

M: Masse molecular

t: Time

m.p. (°C): Fusion point

T°: Temperature

C: Conversion

E: Selectivity factor

ees/eep: Substrate/product enantiomeric excess

Introduction

Since the progressive developments of organophosphorus compounds, especially the introduction of the phosphonates moieties, there are numerous examples of coordinated main group compounds. Phosphorus can form chemical bonds with many other elements, it has empty *d*-orbital and can have different valencies 3 or 5.

Phosphonates are fascinating groups and they have many technical applications and are a class of drugs. They can play a crucial role in life chemistry and biochemistry, enabling the creation multifunctional compounds and various industrial applications[1]: in fertilizers[2], detergents[3], flame retardants[4], …etc.

α-Aminophosphonates emerge as a notable subset within the expansive realm of phosphonates, distinguished by the incorporation of an amino group at the *α*-carbon atom[5]. Attracting considerable attention, especially in the biological sciences, these compounds captivate researchers with their unique chemical structures and versatile functional properties[6]. In the domain of medicinal chemistry, *α*-aminophosphonates hold great promise, frequently exhibiting bioactivity and pharmacological effects[7]. Their ability to mimic the structural features of natural amino acids contributes to their relevance in drug design and development[8]. This versatility positions them as potent candidates across a diverse range of therapeutic applications, encompassing antitumor[9], antibacterial[10], *α*-glucosidase inhibitors[11], virucidal[12], and anticancer properties[13], as illustrated in ***Figure 1.***

[1] Wan, F., Tang, W. *Chin. J. Chem*, **2021**, *39*(4), 954-968.
[2] Weeks Jr, J. J., & Hettiarachchi, G. M. *J. Environ. Qual*, **2019**, *48*(5), 1300-1313.
[3] Agbazue, V. E., Ekere, N. R., & Shaibu, Y. *Int. J. Chem. Sci*, **2015**, *13*(2), 771-785.
[4] Yu, M., Chu, Y., Xie, W., Fang, L., Zhang, O., Ren, M., & Sun, J. *J. Chem. Eng*, **2024**, *480*, 148167.
[5] Bera, K., & Namboothiri, I. N. *Asian J. Org. Chem*, **2014**, *3*(12), 1234-1260.
[6] Shaikh, S., Dhavan, P., Singh, P., Uparkar, J., Vaidya, S. P., Jadhav, B. L., & Ramana, M. M. V. *J. Biomol. Struct. Dyn*, **2023**, *41*(2), 386-401.
[7] Tsacheva, I., Todorova, Z., Momekova, D., Momekov, G., Koseva, N. *Pharm*, **2023**, *16*(7), 938.
[8] Lokwani, D. K., Chavan, S. R., Ugale, V. G., Kendre, P. N., & Jain, S. P. In *Alzheimer's Disease and Advanced Drug Delivery Strategies,* **2024**, 33-46. Academic Press.
[9] Huang, X. C., Wang, M., Pan, Y. M., Tian, X. Y., Wang, H. S., & Zhang, Y. *Bioorganic Med. Chem. Lett*, **2013**, *23*(19), 5283-5289.
[10] Rasal, S. A., Dhavan, P. P., Jadhav, B. L., & Shimpi, N. G. *Appl. Organomet. Chem*, **2020**, *34*(2), e5317.
[11] Shaik, M. S., Nadiveedhi, M. R., Gundluru, M., Poola, S., Allagadda, R., Chippada, A. R., & Cirandur, S. R. *Synth. Commun*, **2020**, *50*(4), 587-601.
[12] Hkiri, S., Mekni-Toujani, M., Üstün, E., Hosni, K., Ghram, A., Touil, S., Sémeril, D. *Pharm*, **2022**, *15*(1), 114.
[13] Baren, M. H., Ibrahim, S. A., Al-Rooqi, M. M., Ahmed, S. A., El-Gamil, M. M., & Hekal, H. A. *Sci. Rep*, **2023**, *13*(1), 14680.

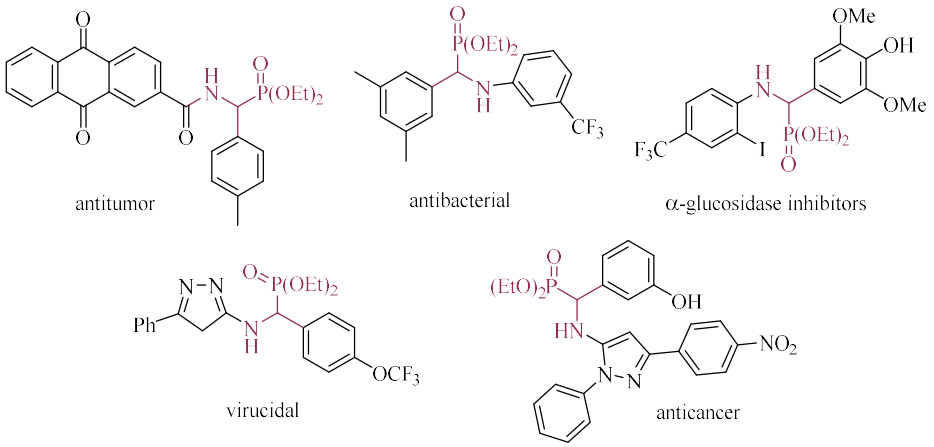

Figure 1: Structures of *α*-aminophosphates exhibiting biological properties.

In the ever-evolving landscape of organic synthesis, multicomponent reactions (MCRs) have risen to prominence as indispensable and efficient tools, bringing about a revolution in the assembly of diverse chemical structures. These reactions hinge on the simultaneous coupling of at least three components in a single step, facilitating the creation of variably functionalized compounds. The integration of multicomponent reactions into phosphonate synthesis stands out as a transformative strategy, providing distinct advantages such as step economy, atom efficiency, and swift access to intricately structured phosphonate derivatives[14].

In recent years, organic chemistry research has been prominently dedicated to exploring innovative, flexible, and modular synthesis methodologies aimed at facilitating the development of novel biologically active molecules. The extensive repertoire of synthesis methods has advanced to a stage where the feasibility of achieving a molecular target is nearly assured, prompting a shift in focus toward refining the precision and efficiency of these syntheses. The significance of experimental design, especially in multicomponent reactions such as the *Kabachnik-Fields* reaction, has emerged as a pivotal factor in optimizing these processes. The meticulous planning of an ideal synthesis route for intricate molecules presents one of the most exhilarating challenges in organic chemistry. Consequently, organic chemists have taken the lead in introducing cutting-edge technologies and refining experimental designs to elevate the overall efficiency and precision of these synthetic endeavors.

[14] Younus, H. A., Al-Rashida, M., Hameed, A., Uroos, M., Salar, U., Rana, S., & Khan, K. M. *Expert Opin Ther Pat*, **2021**, *31*(3), 267-289.

Many chemical reactions necessitate the intervention of catalysis, showcasing its multifaceted influence. The utilization of catalysts plays a pivotal role in elevating reaction rates, curbing energy requirements, and shaping reaction selectivity, thereby enhancing the overall efficiency and sustainability of chemical processes[15].

The significance of organocatalysis, as the third pillar of catalysis, alongside metallocatalysis and biocatalysis, lies in its ability to unlock novel synthetic routes, optimize reaction pathways, and enable the synthesis of complex molecules with high efficiency. As researchers delve deeper into the intricacies of catalytic processes, the development of innovative organocatalytic strategies has become a focal point in the quest for sustainable and greener chemical synthesis.

Among all the organocatalyst, phosphinic acids emerge as notable catalysts, standing out for their substantial potential and diverse applications in organic synthesis[16]. These catalysts, alongside crown ethers, are pivotal elements at the core of our team's focus on advancing the development of new α-aminophosphonates. Our attention is specifically directed towards leveraging the capabilities of these organocatalysts in a multicomponent *Kabachnik-Fields* reaction. ***(Scheme 1)***

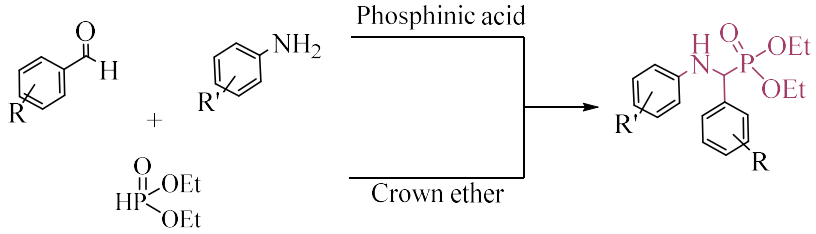

Scheme 1: Synthesis of α-aminophosphonates via *Kabachnik-Fields* reaction using different organocatalysts.

In the pursuit of sustainable and environmentally conscious practices, the concept of green chemistry has emerged as a beacon of innovation, striving to revolutionize traditional chemical processes. Central to this paradigm shift is the prominence of biocatalysis, an integral pillar that embodies the fusion of biology and chemistry. As the demands for cleaner and more resource-efficient technologies intensify, fundamental research is progressively gravitating towards bioconversion processes, recognizing them as indispensable tools to address both environmental and economic imperatives.

[15] Neto, B. A., Rocha, R. O., & Rodrigues, M. O. *Molecules*, **2021**, *27*(1), 132.
[16] Pan, S. C., & List, BAngew. Chem. Int. Ed, **2008**, *47*(19), 3622-3625.

Biocatalysis, at its core, involves the utilization of enzymes, to facilitate chemical transformations. This approach aligns seamlessly with the principles of green chemistry, which seeks to minimize the environmental impact of chemical processes while optimizing resource utilization.

In the dynamic landscape of modern chemistry, the demand for pure chiral molecules has witnessed a remarkable surge, driven by the ever-expanding fields of pharmaceuticals[17], agrochemicals[18], and materials science[19]. The synthesis of enantiopure compounds represents a pivotal challenge due to the inherent complexity of achieving selective transformations. As the quest for more efficient and selective synthesis methods intensifies, kinetic resolution has emerged as a prominent access mode for obtaining enantiomerically pure compounds.

With the objective of obtaining key precursors necessary for synthesizing enantiomerically pure organophosphates from enantiopure alcohols, we have developed a streamlined kinetic resolution via deacylation of chiral aryl alkyl acetates as a promising strategy. ***(Scheme 2)***

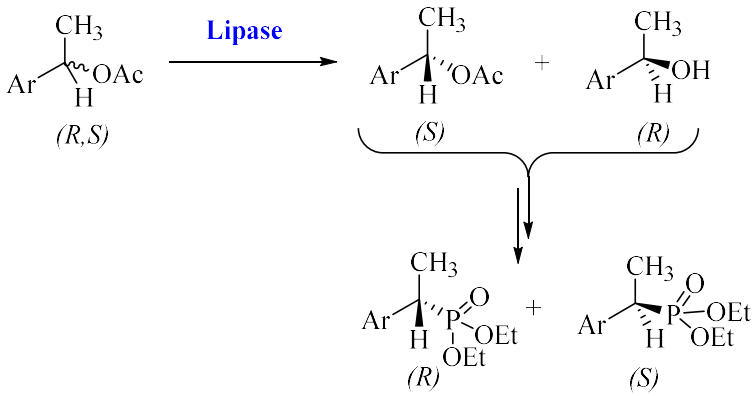

Scheme 2: Enzymatic deacylation of chiral benzyl esters.

This thesis focuses on the exploitation of the oraganocatalysis and biocatalysis methodology for the synthesis of a set of new phosphonate derivatives under ecofriendly conditions.

This manuscript is divided into three parts including a total of 7 chapters.

[17] Teng, Y., Gu, C., Chen, Z., Jiang, H., Xiong, Y., Liu, D., & Xiao, D. *Chirality*, **2022**, *34*(8), 1094-1119.
[18] Wang, F., Li, X., Jiang, S., Han, J., Wu, J., Yan, M., & Yao, Z. *J. Agric. Food Chem*, **2023**, *71*(33), 12372-12389.
[19] Duan, Y., & Che, S. *Adv. Mater*, **2023**, *35*(51), 2205088.

The first part comprises a bibliographical update that delves into the thematic foundation of this research. This section unfolds across three chapters, each intricately exploring facets relevant to the subject matter.

The inaugural chapter encompasses an in-depth bibliographic exploration of the chemistry associated with organophosphates and select phosphonate compound families. This chapter elucidates their diverse applications across various fields and delves into the methods of their synthesis. Subsequently, our attention turns to a detailed analysis of the biological and pharmacological significance of α-aminophosphonates, accompanied by a comprehensive overview of the various synthesis methods documented in the existing literature. Our research will be anchored in these molecules, considering them as fundamental target structures.

The second chapter is dedicated to a comprehensive bibliographic review of green chemistry and its foundational principles, with a specific focus on multicomponent reactions and catalysis. Within this context, we will delve into fundamental concepts of organocatalysis and biocatalysis, elucidating their roles as environmentally friendly methods for activating various organic reactions.

In ***the third chapter***, we provide a concise overview of the theoretical concepts underpinning the calculation methods employed in our study. This includes discussions on modeling through experimental designs with associated statistical notions, as well as an exploration of the principles behind Density Functional Theory (DFT) and molecular docking.

The second part comprises an exposition of the thesis objectives, the attained results, and the drawn conclusions. Comprising two chapters, this part delineates the outcomes of the research efforts undertaken within the thesis.

Chapter four is dedicated to an in depth examination of the impact of various parameters namely, the catalyst, reaction temperature, and reaction time on the advancement of the Kabachnich-Fields reaction. Employing the design of experiments methodology, this chapter explores the optimization of conditions for accessing α-aminophosphonates using diphenylphosphinic acid.

Within the confines of ***the five chapter***, we engage in a detailed discussion on the results derived from our innovative approach to synthesizing α-aminophosphonates through a "one-pot" reaction using crown ether as an organocatalyst. Furthermore, this chapter

meticulously interprets the computational findings, providing a comprehensive analysis of the research findings we have obtained.

Within the confines of ***Chapter six***, we elucidate the findings of kinetic resolution achieved through deacylation catalyzed by *Candida Antarctica* lipase (*CAL-B*), by modulating the different parameters influencing reactivity and lipase selectivity.

The last chapter is devoted to the enantioselective deacylation of alcohol as enantiopure precursors for the synthesis of enantiopure phosphonates.

We conclude this work with a comprehensive conclusion and future perspectives. The detailed operational protocols and spectroscopic identification of the various synthesized structures are consolidated in the ***experimental section***. The published works corresponding to this manuscript are included in the appendix.

First part:

Bibliographic study

Chapter I

Organophosphorus chemistry

I-1 General introduction on organophosphorus

Phosphorus is isoelectronic to nitrogen from the point of view of its valence layer, it has the capacity to form hypervalent compounds and to make bonds with other atoms by virtue from empty *d*-orbitals. Also it has the possibility to form σ and π bonds with metallic and non-metallic elements, consequently the formation of multifunctional organophosphorus compounds[1]. Phosphoryl bonds are generally deemed stable and relatively unreactive, distinguishing them from the reactivity of C=N or C=O bonds. Unlike P=O bonds, which resist nucleophilic addition, oxygen in phosphoryl bonds can react with strong acids or potent electrophiles. This stability is attributed to a high bond dissociation energy, ranging from 129 to 139 kcal mol−1, elucidating the oxophilicity of trivalent phosphorus and its inclination to form P (V) adducts[2].

In recent years, there has been a growing fascination in the preparation of organophosphorus compounds. Various synthetic methods have been documented to explore the applications of phosphorus compounds, aiming to comprehend their roles in biological systems through the study of different derivatives.

The extensive array of organophosphorus species, also known as carbophosphorus (C-P), can be categorized into two groups based on their structure: trivalent and pentavalent species.

Trivalent phosphorus species, denoted as P (III), exhibit a trigonal pyramid geometry with three single bonds and a lone pair of 2p electrons. This lone pair imparts nucleophilic behavior and imparts *Lewis* base characteristics. On the other hand, pentavalent organophosphorus species, P (IV), are generally less reactive. They consist of three single bonds and a phosphoryl bond P=O, arranged in a tetrahedral geometry, as illustrated in ***Figure 1.***[3]

[1] Dillon, K. B.; Mathey, F.; Nixon, J. F. *Phosphorus: The Carbon copy, John Wiley and sons, New York,* **1998.**
[2] Emsley, J.; Hall, D. *The chemistry of Phosphorus, Harper and Row, London*, **1976**.
[3] Sosth ene P.-M. Ung and Chao-Jun Li, *RSC Sustainability*, **2023**, 1, 11–37.

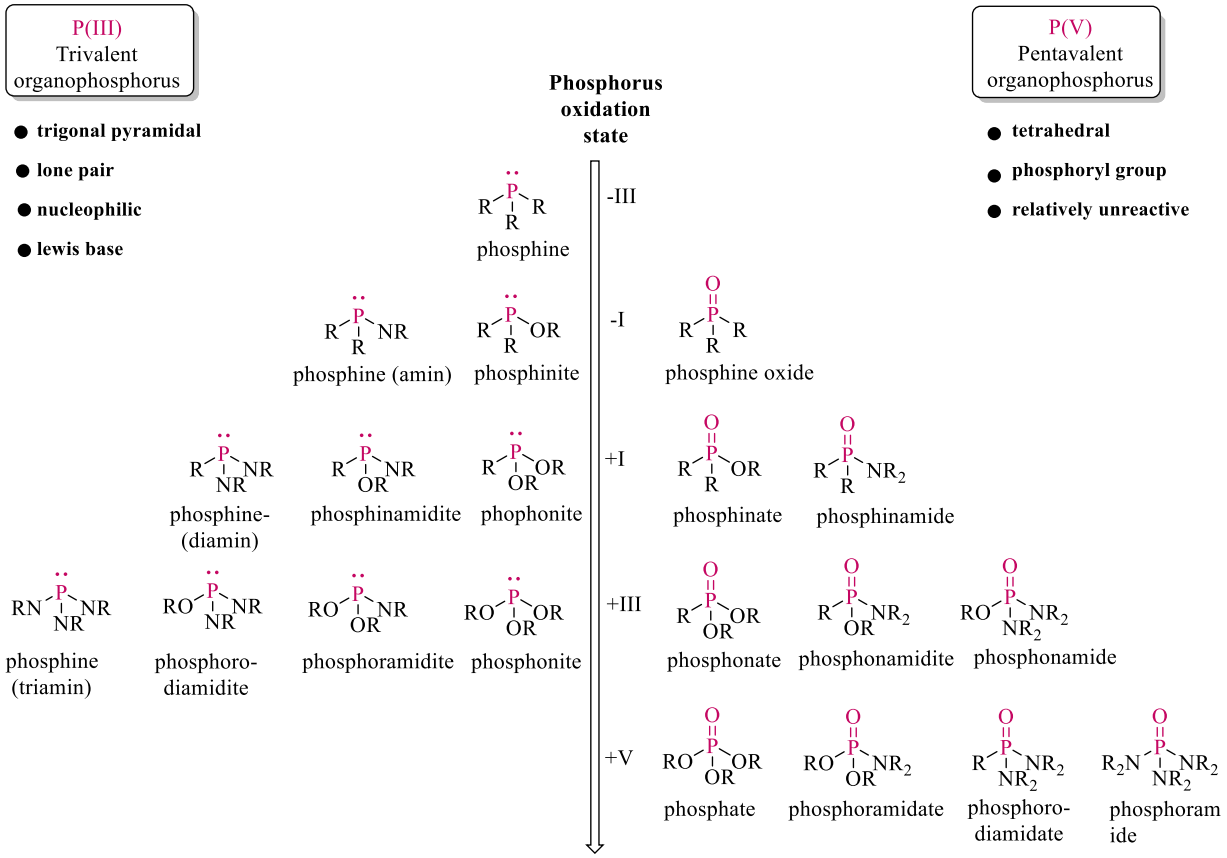

Figure 1: Nomenclature of Organophosphorus Compounds Based on Oxidation Number: Trivalent and Pentavalent Species

Furthermore, crucial tetrahedral ions include ylides **I.1**, which are zwitterionic species carrying a positive charge on the phosphorus and a negative charge on the carbon. They are recognized as effective nucleophiles. Additionally, phosphoniums **I.2** feature a positive charge on the P-center and frequently function as reactive intermediates. (***Figure 2***).

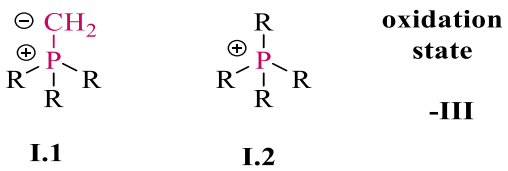

Figure 2: Important tetrahedral organophosphorus ions.

Various factors contribute to the appeal of pentavalent phosphorus for medicinal chemists. Of particular interest are structures such as phosphonic acids and aminophosphonates, which can be regarded as bioisosteres of carboxylic acids. An illustrative

example is the phosphonodipeptide alafosfalin **I.3**, which releases L-aminoethanephosphonic acid after metabolism ***(Figure 3)***. The phosphonate mimics the natural substrate for L-alanine racemase but exhibits a higher binding affinity to the cofactor, resulting in enzyme inhibition and subsequent suppression of cell wall biosynthesis.[4]

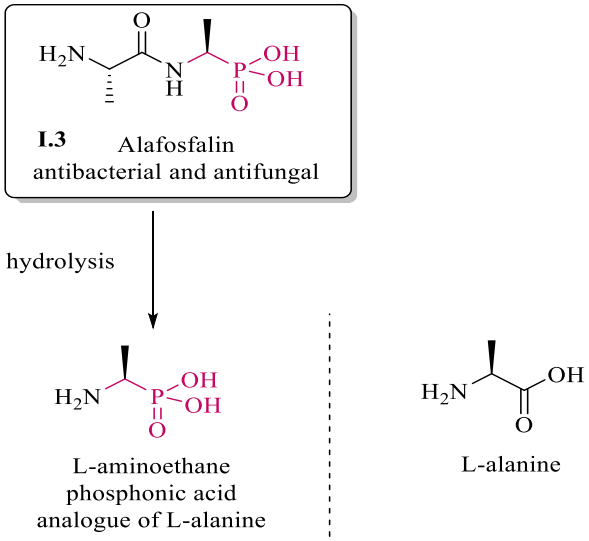

Figure 3: Peptidophosphonates as therapeutic analogs.

On the other hand, employing P (V) compounds, such as phosphonates **I.4**, as substitutes for biologically prevalent phosphates **I.5**, presents another perspective. The CH2 group attached to the phosphonate exhibits isosteric properties with the oxygen connected to phosphates, owing to their comparable size and bond angle. Consequently, these two structures can be essentially superimposed. Nevertheless, the C–P bond in phosphonates displays significantly greater stability against hydrolysis. (***Figure 4*).**

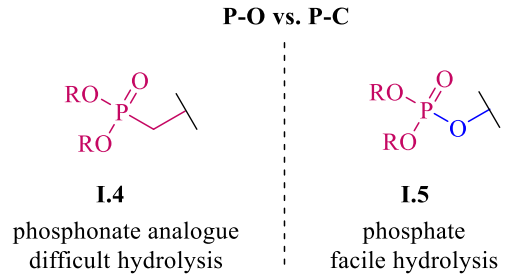

Figure 4: Structures of phosphate/phoshonate.

Organophosphorus play an important role in the chemistry of life, they are often found in nature associated with biomolecules such as carbohydrates, lipids, nucleicacids,

[4] Badet, B., Inagaki, K., Soda, K., & Walsh, C. T. *Biochem*, **1986**, *25*(11), 3275-3282.

and proteins[5]. For example, compound **I.6** has been used for the conservation and transmission of genetic information by being involved in the formation of nucleotides and the assembly of DNA and RNA.[6] ***(Figure 5).***

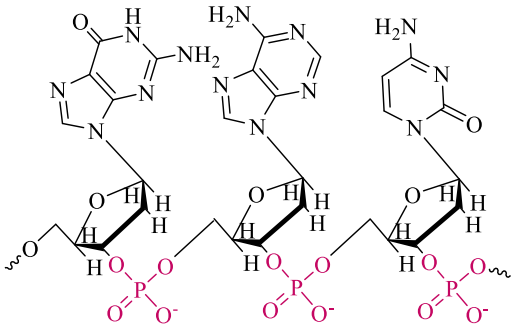

I.6

Figure 5: Structure of ribonucleic acid (RNA).

Organophosphorus compounds are also involved in the synthesis of phosphonolipids, which are lipids containing aminophosphonates and are referred to as phosphonolipids. These phosphonolipids fall into two categories: glycerophosphonolipids **I.7** and sphingophosphonolipids **I.8**. (representative structures are shown in ***Figure 6*****).** They are the structural basis of all cell membranes providing stability, fluidity, and permeability and that due to the amphipathic nature (containing both hydrophobic and hydrophilic groups) that allows them to form a double layer of phosphonolipids[7]. These lipids have been extracted from a wide range of organisms, encompassing humans, various mammals (such as sheep, goats, and rats), egg yolk, fish, insects, sea anemones, sponges, various freshwater and marine mollusk species, plant seeds, protozoa, and bacteria[8].

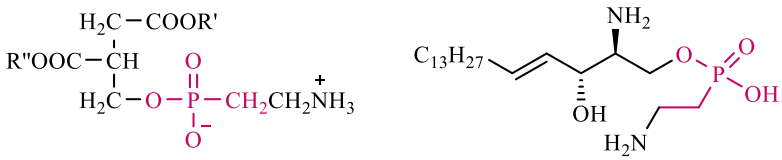

I.7 **I.8**

Figure 6: Structures of glycerophosphonolipids and sphingophosphonolipids.

[5] Petkowski, J. J, Bains, W. Seager, S. *Molecules*, **2019**. *24*(5), 866.
[6] a) Doherty, E. A.; Doudna, J. A. Annu. Rev. *Bioph. Biom*, **2001**, 30(1), 457-475; b) Dickerson, R. E.; Sci. Am, **1983**, 249(6), 94-111; c) Watson, J. D.; Crick, F. H. *Cold Spring Harbor Laboratory Press*, **1953**,(18),123-131.
[7] Kafarski, P. *Contemporary Topics about Phosphorus in Biology and Materials*, **2019**. 1-19.
[8] a) Ju K-S, Doroghazi JR, Metcalf WW. *J. Ind. Microbiol. Biotechnol*. **2014.** 421:345-356. b) Mukhamedova KS, Glushenkova AI. *Chem. Nat. Compd*. **2000**. 36,329-341.3.

I-2 Medicinal chemistry

Amongst the entire organophosphorus, the pentavalent organophosphorus P(V) or phosphonates, possess an important class in therapeutic domain because of their low toxicity. They are generally subdivided into several classes, and depending on their molecular structure, excellent biological and pharmacological activities have been discovered, such as enzyme inhibitors[9], herbicides[10], bactericides[11], fungicides[12], antibiotics[13], antitumor reagents[14], antiviral agents[15], anti-thrombotic agents[16].

α-Hydroxyphosphonates

The *α*-hydroxyphosphonates function as structural counterparts to *α*-hydroxyphosphonic acids[17]and can serve as enzymatic inhibitors for farnesyl protein transferase (FPT)[18], human rennet[19], and human protein tyrosine phosphatase[20]. For example the, representative structures of *α*-hydroxyphosphonates **I.9, I.10** and **I.11** shown in ***Figure 7***, are described as anticancer[21], antioxidant[22], and antimicrobial agent[23]respectively.

Synthetically, these compounds are useful precursors for other valuable derivatives such as *α*-amino[24], *α*-diketo[25], *α*-keto[26], *α*-halo[27], and *α*-acetoxyphosphonates[28].

[9] Park, J., Pandya, V. R., Ezekiel, S. J., & Berghuis, A. M. *Front. Chem*, **2021**. *8*, 612728.
[10] Zhang, S., Guo, X., Zhou, Y., Yang, Y., Peng, H., & He, H. *Phosphorus, Sulfur Relat. Elem*, **2019**. *194*(12), 1158-1163.
[11] Telu, J. R., Kuntala, N., Banothu, V., Mallavarapu, B. D., Pal, S., & Anireddy, J. S. ***Int. j. chem. environ. sci***, **2022.** 3(2), 67-84.
[12] Mihoubi, W., Elleuch, H., Boudabbous, M., Ketata, E., Borgi, I., Rezgui, F., & Gargouri, A. *Mycol. Prog*. **2023**. *22*(8), 58.
[13] Łysakowska, M., Głowacka, I. E., Andrei, G., Schols, D., Snoeck, R., Lisiecki, P. & Piotrowska, D. G. Molecules, **2022**. 27(19), 6526.
[14] Baren, M. H., Ibrahim, S. A., Al-Rooqi, M. M., Ahmed, S. A., El-Gamil, M. M., & Hekal, H. A. *Sci. Rep*, **2023**. *13*(1), 14680.
[15] Xu, Y., Groaz, E., Rihon, J., Herdewijn, P., & Lescrinier, E. *Eur. J. Med. Chem*, **2023**. *255*, 115379.
[16] Chackalamannil, S., Xia, Y., Greenlee, W. J. Clasby, M. Doller, D. Tsai, H., & Chintala, M. *J. Med. Chem*, **2005**. *48*(19), 5884-5887.
[17] a) Samanta, S. Zhao, C. G. Am. J. *Chem. Soc*., **2006**, 128, 7442–7443. b) Kim. D. Y. and Weimer, D. F. *Tetrahedron Lett*., **2003**, 44, 2803–2805
[18] Pompliano. D. L. Rands, E. Schaber, M. D. Mosser, S. D. Anthony, N. J. Gibbs, J. B. *Biochem*, **1992**, 31, 3800–3807.
[19] Dellaria, J. F. Maki, R. G. Stein, H. H. Cohen, J. Whittern, D. Marsh, K. Hoffman, D. J. Plattner, J. J. Perun, . T. *Med. Chem.*, **1990**, 33, 534–542.
[20] Murano, T. Yuasa, Y. Kobayakawa, H. Yokomatsu, T. Shibuya, S. *Tetrahedron*, **2003**, 59, 10223–10230
[21]Kalla, Reddi Mohan Naidu, LEE, Hye Ri, CAO, Jiafu, *et al. New J Chem*, **2015**, 39, 5, 3916-3922.
[22]Gundluru, Mohan, Mallu, Kiran K. R, SARVA, S *et al. J. Mol. Struct*, **2022**, 1256, 132554.
[23]Phillips, Ana Maria F, Barros, M. T. Pacheco, Marta, *et al. Bioorganic Med. Chem. Lett*, **2014**, 24, 1, 49-53.
[24] Kaboudin, B. *Tetrahedron Lett*., **2003**, 44, 1051–1053.
[25] Olah. G. A. and A. Wu, *J. Org. Chem*., **1991**, 56, 902–904.
[26] Firouzabadi, H. Iranpoor. N. and Sobhani. S. *Tetrahedron. Lett*., **2002**, 43, 477–480.
[27] Eymery, F. Lorga, B. and Savignac, P. *Tetrahedron*, **1999**, 55, 2671–2686.
[28] Firouzabadi, H. Iranpoor, N. Sobhani, S. and Z. Amoozgar, *Synthesis*, **2004**, 1771–1774.

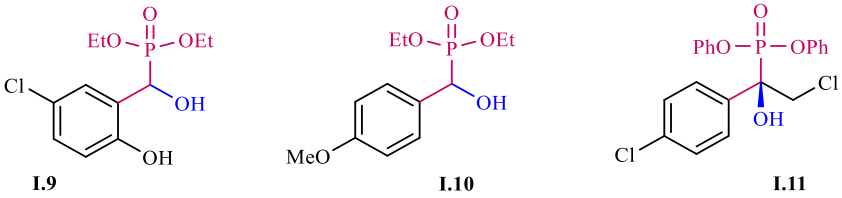

***Figure 7*: Selected structures of α-hydroxyphosphonates having biological activities.**

α-Acyloxyphosphonates

The α-acyloxyphosphonates, generally results from acylation of α-hydroxyphosphonates. They were described in the literature as herbicides, insecticides[29]and anticancer agent[30]for compounds **I.12**, **I.13** and **I.14** respectively as shown in ***Figure 8.***

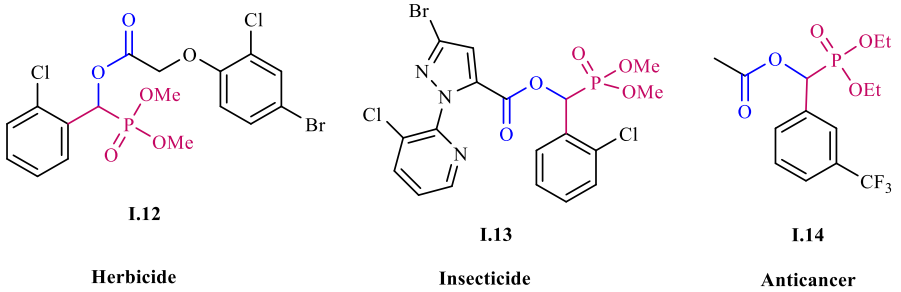

Figure 8: Structures of α-acyloxyphosphonates having biological active.

α-Amidophosphonates

The α-amidophosphonates have the molecular structures similar to those of the aminophosphonic acids. They are used for the extraction of uranium in industry **I.15**,[31] as antitumor agent[32] **I.16** and antimicrobial activity **I.17**.[33] ***(Figure 9)***.

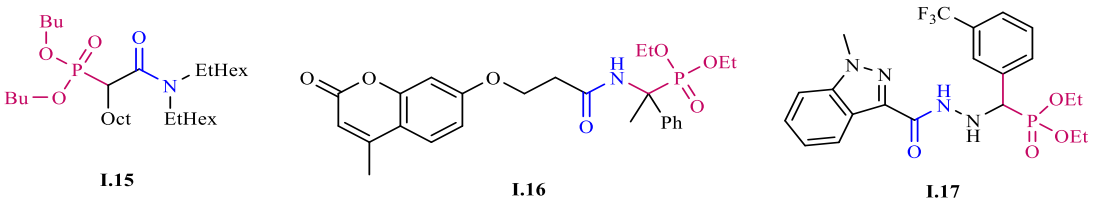

Figure 9: Structures of α-amidophosphonates having biological activities.

α-Aminophosphonates

α-aminophosphonates stand out as highly significant organophosphorus compounds, showcasing a diverse array of biological activities. For example: compound

[29]Jin, C.; He, H. *Phosphorus Sulfur Silicon Relat.Elem* **2011**, 186, 1397–1403.
[30]Varga, P. R., Bilovics, A. Bagi, P *et al. Molecules*, **2022**, 27, 7, 2067.
[31]Arteste, A., Dourdain, S. Felines, N, *et al. Solvent Extr. Ion Exch*, **2020**, 38, 703-718.
[32]Li, Y. Wang, C,Y. YE, M, Y, *et al. Molecules*, **2015**, 20, 8, 14791-14809.
[33]Koszelewoski, D. Kowalczyk, P. Śmigielski. p, *et al. Materials*, **2022**, 15, 11, 3846.

I.18 has antifungal activity[34] while compound **I.19** is described as an anti-inflammatory.[35] (***Figure 10).***

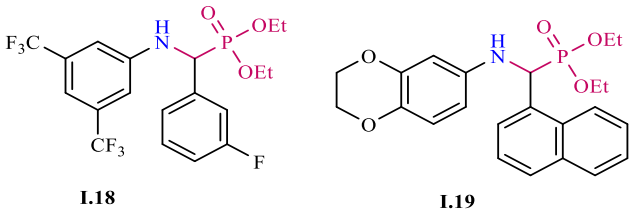

I.18 **I.19**

Figure 10: Structures of biologically active α-aminophosphonates.

Bisphosphonates

Numerous bis α-aminophosphonates demonstrate noteworthy biological activities. Compound **I.20**, for instance, displays antifungal properties[36], while compound **I.21** is recognized as an antioxidant agent.[37] Additionally, compound **I.22** exhibits optimal anti-proliferative activity against human tumor cells in colon carcinoma.[38] ***(Figure 11)***.

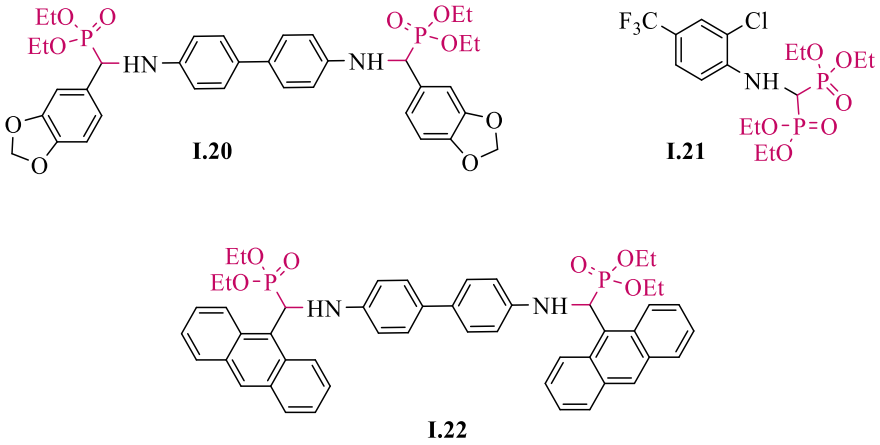

I.20 **I.21**

I.22

Figure 11: Structures of bisphosphonates having biological activities.

I-3 Preparation of the phosphonates

Several approaches have been described in the literature based on the most famous reactions to introduce the phosphonates moieties, among these the best known are:

[34] Sudileti, M., Gundluru, M., Sarva, S., Tellamekala, S., Hari, B., Meriga, B., & Cirandur, S. R. *Monatsh. Chem*, **2019**, l. 150, 1101-1109.
[35] Shaik, Y. H., Chintha, V., Gundluru, M., Sarva, S., & Cirandur, S. R. *Synth. Commun*, **2022**, 52, 1, 129-144.
[36] Aissa, R Guezane-Lakoud, S. Toffano, M. Gali, L. Aribi-Zouioueche, L. *Bioorganic Med. Chem. Lett***. 2021**. 41, 128000
[37]Shaik, M. Nadiveedhi, M. Gundluru, M *et al. Synthetic Communications*, **2021**, 51, 5, 747-764.
[38]Kraicheva, I, Vodenicharova, E, Shivachev, B, et al. *Phosphorus Sulfur Silicon RelatElem*. **2013,** 188, 11, 1535–1547.

I-3-1 *Michaelis-Arbuzov* reaction

The *Michaelis-Arbuzov* reaction, initially identified by *August Michaelis* in ***1989***[39] and subsequently advanced by *Aleksandr Arbuzov*,[40] stands out as one of the foremost approaches to form carbon-phosphorus (C-P) bonds. This reaction consists to react a trialkylphosphite as a good nucleophile with an alkyl halide. ***(Scheme 1).***

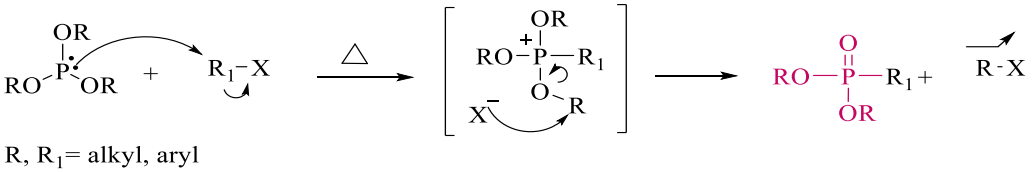

Scheme 1: Synthesis of phosphonates via *Michaelis-Arbuzov* reaction.

I-3-2 *Michaelis-Becker* reaction

In this reaction a base must be used in an anhydrous solvent to deprotonate the diethylphosphite as a nucleophile, which subsequently attacks the alkyl halide **I.23** introducing phosphonates group **I.24**.[41] ***(Scheme 2).***

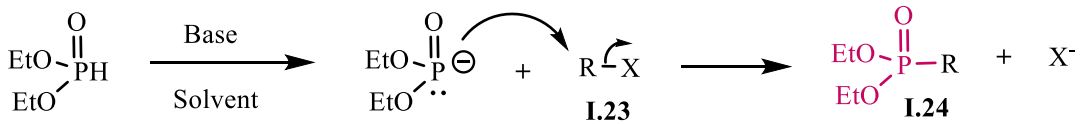

Scheme 2: Introduced of phosphonates group by *Michaelis-Becker*reaction.

I-3-3 *Pudovik/Abramov* reaction

Among the most famous methods for the introduction of phosphonates group **I.25** are the two reactions of *Abramov*[42] and *Pudovik*[43]. The *Abramov* reaction consists of the addition of a trialkylphosphite to a carbonyl compound **I.26**, while the *Pudovik* reaction results in the condensation of a dialkylphosphite to a carbonyl in the presence of base. Both reactions share a comparable mechanism, characterized by the nucleophilic phosphorus atom attacking the carbonyl group. ***(Scheme 3)***.

[39] Michaelis, A. Kaehne, R. Ber. *Dtsch. Chem. Ges*. **1898**, 31, 1048.
[40] Arbuzov. A. E. J. Russ. *Phys. Chem. Soc*. **1906**, 38, 687.
[41] Michaelis, A. T. Becker, *ChemBer*. **1897,** 30, 1003.
[42](a) Abramov, V. S. Dokl. Akad. Nauk SSSR **1950**, 73, 487. *Chem. Abstr*. **1951**, 45, 2855; (b) Abramov, V. S. Zh. Obshch. Khim. **1952**, 22, 647. *Chem. Abstr*.**1953**, 47: 5351e.
[43]a) Pudovic, A. N. *Dokl. Akad. Nauk SSSR*. **1952**, 83, 865; b) Pudovik, A. N. Konovalova, I. V. *Synthesis* **1979**, *1979*, 81.

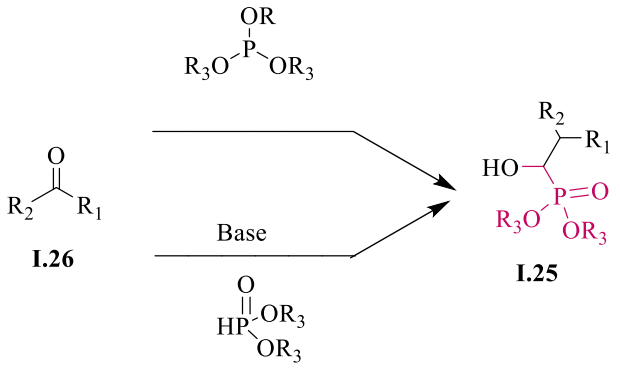

***Scheme 3*:** Synthesis of hydroxyphosphonates via *Pudovik/Abramov* reactions.

I-3-4 Kabachnik-Fields reaction

The *Kabachnik-Fields* reaction, alternatively referred to as the *phospha-Mannich* reaction, enables the one-step synthesis of *α*-aminophosphonates **I.27** through the condensation of three components: aldehyde **I.28**, aniline **I.29**, and H-Phosphonates.[44]. (***Scheme 4).***

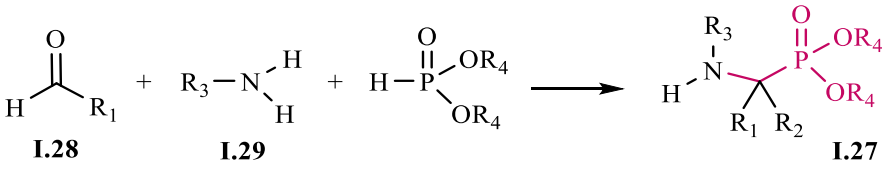

***Scheme 4*:** Synthesis of *α*-aminophosphonates by *Kabachnik-Fields* reaction.

H-Phosphonates display two tautomeric forms: the three-coordinate phosphate and the typically more stable penta-coordinate phosphonate. In aqueous solutions, the proportion of phosphite in diethyl H-phosphonate is estimated to be minimal up to pH 10-9. However, beyond pH 13, it becomes the predominant form of diethyl H-phosphonate, exhibiting a pKa value of 12.7[45]. **(*Scheme 5).***

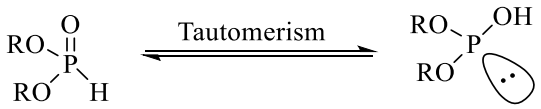

Scheme 5: Phosphonate/phosphinite equilibrium.

[44] a) Kabachnik, M. I., *IzvestiiaAkademiinauk SSSR*, **1953,** 6, 1126-1128; b) Kabachnik, M. I.; Medved, T. Y. *In Dokl. Akad. Nauk. SSSR*, **1952,** 83, 689-692; c) Fields, E. K., *J. Am. Chem. Soc*, **1952,** 74(6), 1528-1531.
[45] Nicholas Powles, John Atherton and Michael I. Page, *Org. Biomol. Chem.*, **2012**, 10, 5940.

In the continuation of our research, we have interested by the preparation of different derivatives of *α*-aminophosphonates by the *Kabachnik-Fields* multi-component reaction, we address their stability and reactivity.

I-4 *α*-Aminophosphonates

α-Aminophosphonates featuring an N–C–P moiety remain a significant area of interest owing to their potential biological activity. Serving as phosphorus structural analogs of amino acids, their bioactivity holds promise for applications in agrochemicals and medicines.[46] These *α*-aminophosphonates have garnered considerable attention for their roles as enzyme inhibitors[47], haptens of catalytic antibodies[48], herbicidals[49], inhibitors of serine hydrolases[50], inhibitors of UDP-galactopyranosemutase[51] and also as anticancer agents.[52]

I-4-1 *α*-Aminophosphonates utility

Over the years, many ***α***-aminophosphonates derivatives have been employed in different domains, such as, medicine, agriculture, industry. For this purpose, we present in the following some fields of application of *α*-aminophosphonates.

I-4-1-1 In medicine

Due to their resemblance to amino acids, *α*-aminophosphonates have received substantial attention as potential candidates for enzyme inhibition and therapeutic applications. In the extensive literature, *Shaikh* et *al.*[53] have developed *α*-aminophosphonate derivatives, including carbazole-based compounds **I.30** and **I.31**, chromone-derived aminophosphonate **I.32**[54] and *α*-aminophosphonate derivatives with 2,3,4,5-tetrahydrobenzothiazepine appendages, specifically **I.33**[55], which tested for Alzheimer's disease. The results show that these derivatives exhibited better AChE inhibition, the examined compounds are represented in ***Figure 12*.**

[46] Kaboudin, B., Daliri, P., Faghih, S., & Esfandiari, H. *Front. Chem*, **2022**. *10*, 890696.
[47] Sobati, M., Abdoli, M., Bonardi, A., Gratteri, P., Supuran, C. T., & Žalubovskis, R. . *ACS Med. Chem. Lett*, **2023**. *14*(8), 1067-1072.
[48] Rassukana, Y. V., Yelenich, I. P., & Onys′ko, P. P. *Ukr. Bioorg. Acta*, **2022**. *17*(1), 101-104.
[49] Che, J. Y., Xu, X. Y., Tang, Z. L., Gu, Y. C., & Shi, D. Q. *Bioorganic Med. Chem. Lett*, **2016**. *26*(4), 1310-1313.
[50] Makhaeva, G. F., Aksinenko, A. Y., Sokolov, V. B., Baskin, I. I., Palyulin, V. A., Zefirov, N. S., & Richardson, R. J. *Chem. Biol. Interact*, **2010**, *187*(1-3), 177-184.
[51] Pan, W., Ansiaux, C., & Vincent, S. P. *Tetrahedron lett*, **2007**, *48*(25), 4353-4356.
[52] Mandour, H. S., Hamed, M. A., Saad-Allah, K. M., Abd Elnabi, M. K., Abosharaf, H. A., & El-Gharably, A. A. *Chem. Selc*, **2023**, *8*(16), e202300254.
[53] Shaikh,S. Dhavan, P. Singh, J. Uparkar, S.P. Vaidya, B.L. Jadhav, M.V. Ramana, *Biomol. Struct. Dyn.* **2020**. 1–23.1861981.
[54] Shaikh, S. Dhavan, P. M. M. V. Ramana, B.L. Jadhav, *Mol. Divers.* ***2021***. 25 (2), 811–825.
[55] Shaikh, S. Dhavan, P. Uparkar, J. Singh, P. Vaidya, S.P. Jadhav, B.L. Ramana, M.M.V . *Bioorg Chem*, **2021**, 116, 105397.

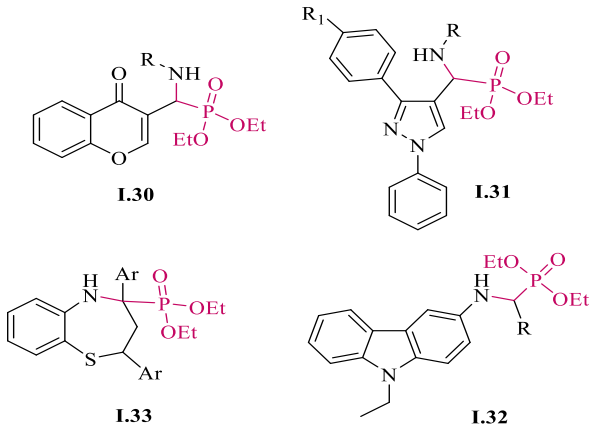

Figure 12: *α*-Aminophosphonates derivatives structures present potential acetylcholinesterase inhibitors.

In a recent study, *Zareei* et *al.*[56] synthesized a novel compound, 4,5-diphenyl-imidazol-*α*-aminophosphonate **I.34**. This compound was subsequently evaluated in vitro as a potential anti-diabetic agent against two important target enzymes in diabetes treatment, namely *α*-glucosidase and *α*-amylase. The assessments revealed that this compound exhibited greater potency compared to the standard inhibitor acarbose against the studied enzymes. ***(Figure 13)***.

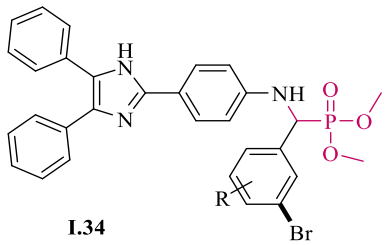

Figure 13: Structure of imidazol-*α*-aminophosphonate having anti-diabetic activity.

Coumarin-amino phosphonate **I.35** as new antibacterial agent was designed and evaluated for antibacterial activity[57]. The findings indicate that, both in vitro and in vivo, this compound demonstrated remarkable inhibitory effectiveness against *Staphylococcus aureus*, particularly at low concentrations, showcasing its substantial antibacterial potential. ***(Figure 14)***

[56] Zareei, S. Ranjbar, S. Mohammadi, M. Ghasemi, Y. Golestanian, S. Avizheh, L. Moazzam, A. Larijani, B. Mohammadi-Khanaposhtani, M. Tarahomi, M. Mahdavi, . M.M Sadeghian, N. Taslimi, P. *BioorgChem* 141 **2023**, 106846.
[57] Yang, X. MeiZeng. C. Avula S, Geng, X, Zhou, C. *Eur. J. Med. Chem*, **2023,** 245, 114891.

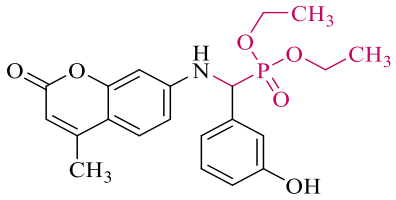

I.35

Figure 14: Structure of coumarin aminophosphonate derivative having antibacterial activity.

I-4-1-2 In agricultural

α-Aminophosphonates are used daily in agriculture due to their various activities. A new category of phosphate-phosphonate compounds **I.36** has been prepared by our laboratory researchers[58]. The evaluation of the antifungal activity against *Fusariumoxysporum* and *Botrytis cinerea*, all tested products exhibited a potent growth inhibitory effect. ***(Figure 15)***.

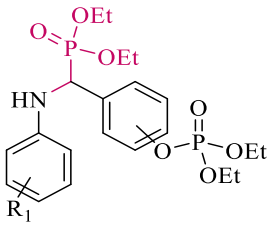

I.36 R_1: 4-CF_3, 4-NO_2, 4-Br.

Figure 15: Structure of phosphate-*α*-aminophosphonate derivatives having antifungal activity.

Organophosphonate pesticides are the most used due to their large broad spectrum of application, high toxicity for insects, and low cost. For example: Dufulin **I.37**[59] is a new commercially produced pesticide derivatives of *α*-aminophosphonate family due to its exceptional efficacy in preventing infections caused by rice viruses and tobacco mosaic virus, this innovation secured a national invention patent in the *People's Republic of China*. Following registration by the *Chinese Ministry of Agriculture*, it was then industrialized for widespread field application. Recently, *α*-aminophosphonate-hydrazone **I.38** was synthesized by *JiaTianet al* and evaluated as antiviral activity, the results show that their efficiency is significantly superior to the commercial antiviral agent **I.37**[60]. **(*Figure 16)***

[58] Aissa,R Guezane-Lakoud, S. Gali, L. Toffano, M. gnaczak, A. Adamiak, M. Merabet-Khelassi, M. Guillot, R Aribi-Zouioueche, L. *J. Mol. Struct*, **2022,** 1247, 131-336.
[59] Song , B. A. Zhang, , G. P. Hu, D. Y. Pang, L., Yang, S., Liu, G., et al. CN 1291993C. **2006**.
[60] Tian, J., Ji, R., Wang, H., Li, S., & Zhang, G. *Front. Chem* ,**2022**, *10*, 911453.

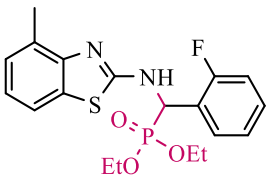

I.37

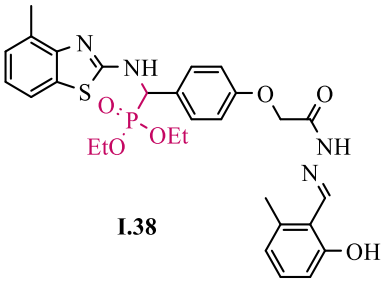

I.38

***Figure 16*:** Structure of α-aminophosphonate-hydrazone derivative having anti-pesticide activity.

Due to the excellent performance of fipronil in managing various agronomic invertebrate pests such as aphids, thrips, domestic musca, and other insects, a synthetic inhibitor of this nature, exemplified by diethyl (3-Cyano-1-(2,6-difluorophenyl)-1H-pyrazol-5-yl) amino)-4-fluorophenyl)methyl phosphonate **I.39**, is employed as an insecticide targeting *Culex pipiens* and *Musca domestica*[61]. In addition, compound **I.40** have interesting herbicidal properties,[62] while the compound **I.41** possess a good fungicidal activity against *Macrophominaphaseolina*[63]. ***(Figure 17).***

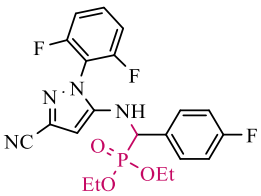

I.39

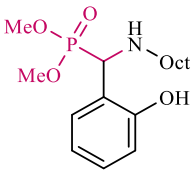

I.40

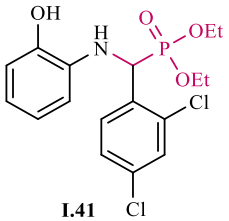

I.41

Figure 17: Structures of α-aminophosphonates derivatives having insecticide, herbicide and fungicidal activities.

I-4-1-3 In industry

Different types of α-aminophosphonates prove to be efficient in serving as corrosion inhibitors for safeguarding oil and gas pipelines. For example, compound **I.42** prevents penetration of corrosive agents on the surface metal, through its ability to the absorb and form a protective layer.[64]

Furthermore, organophosphonates compounds can be used as agents for extracting and precipitating rare earth metals. The compound **I.43** act as good extractant for recovery of

[61] Guo, C. W., Wu, S. H., Chen, F. L., Han, Z. Y., Fu, X. H., & Wan, R. *Phosphorus, Sulfur Relat. Elem*, **2016**, *191*(9), 1250-1255.

[62] Oniţa, N., Şişu, I., Penescu, M., Purcarea, V. L., & Kurunczi, L. *SYNTHESIS*, **2010**, *58*, 5.

[63] Abbod, M., Safaie, N., Gholivand, K., Mehrabadi, M., Bonsaii, M., & Valmoozi, A. A. E. *Chem. Biol. Technol. Agric*, **2021**, *8*, 1-11.

[64] Nikitin, E. N., Shumatbaev, G. G., Terenzhev, D. A., Sinyashin, K. O., & Kazimova, K. S. *Civ. Eng. J*, **2019**, *5*(4), 963-970.

lanthanum and lutetium ions from aqueous solutions.[65] Phosphonates also serve as complexing agents in detergents, and as flame retardants **I.44** for fabrics and plastic plasticizing.[66] They also have been used in textile industry and water treatment.[67] ***(Figure 18)***

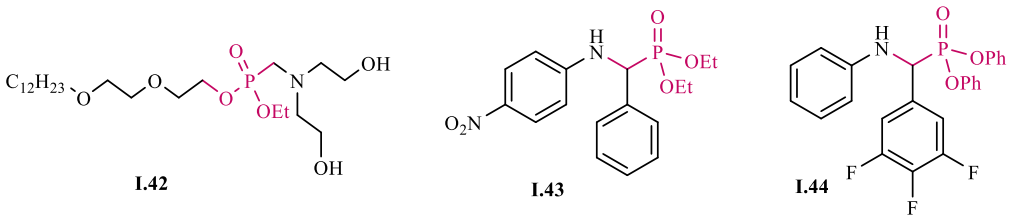

Figure 18: Structures of α-aminophosphonates employed in industry.

I-4-2 Access method to α-aminophosphonates

Due to the importance of α-aminophosphonates in different fields, in the last years numerous procedures for their preparation by multicomponent *Kabachnik-Fields* was described in the literature using different conditions. We can cite the following examples:

I-4-2-1 Using organocatalyst

Reddy et al[68] have applied enantiopure camphor-derived thiourea organocatalyst **I.45**, previousely synthesized, to the one-pot three-component reaction for the asymmetric α-aminophosphonates from 2-cyclopropylpyrimidin-4-carbaldehyde **I.46**, aniline **I.47**, and diphenylphosphite. These compounds exhibited good catalytic activity (up to 80%) chemical yields, but moderate enantioselectivity, as shown in ***Scheme 6***.

[65] Fedorenko, S. V., Mustafina, A. R., Kazakova, E. K., Pod" yachev, S. N., Kharitonova, N. I., Pudovik, M. A., & Myasoedov, B. F. *Russ. Chem. Bull*, **2003**, *52*, 562-566.
[66] Stanfield, M. K., Carrascal, J., Henderson, L. C., & Eyckens, D. J. *Materials*, **2021**, *14*(12), 3230.
[67] Rott, E., Happel, O., Armbruster, D., & Minke, R. *Water*, **2019**, *12*(1), 53.
[68] Reddy, P. S., Reddy, M. V. K., & Reddy, P. V. G. *Chin Chem Lett*, **2016**, *27*(6), 943-947.

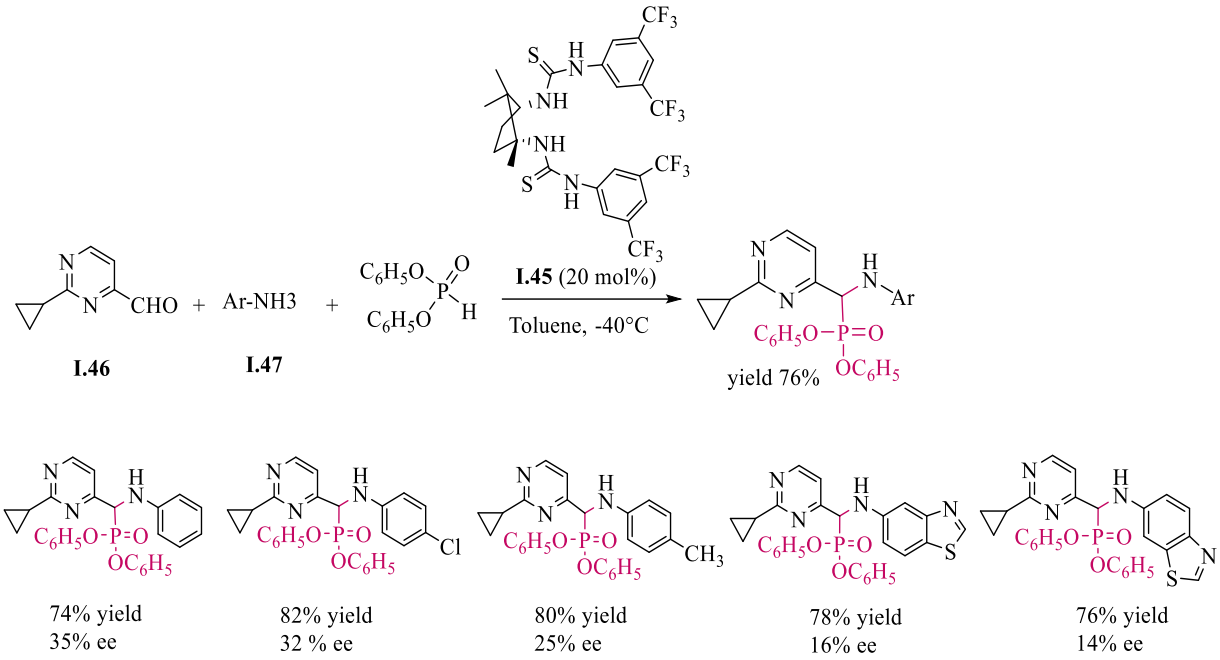

Scheme 6: Synthesis of enantioselective *α*-aminophosphonates derivatives using camphor-derived thiourea.

Biologically promising bis *α*-aminophosphonates, designated as **I.48**, were synthesized by combining 2 equivalents of aromatic aldehyde **I.49**, 1 equivalent of benzidine **I.50**, and 2 equivalents of diethylphosphite. This synthesis employed (S, S)-1-hydroxy-1-oxo-2-c,5-t-diphenylphospholane, commonly known as *Fiaud's* acid, as an innovative and efficient chiral organocatalyst[69]. The targeted compounds were successfully produced with high yields ranging from 63% to 93%, coupled with excellent to good diastereoselectivities, all achieved within a short period of 35 minutes in AcOEt as the solvent at 70°C. ***(Sheme 7).***

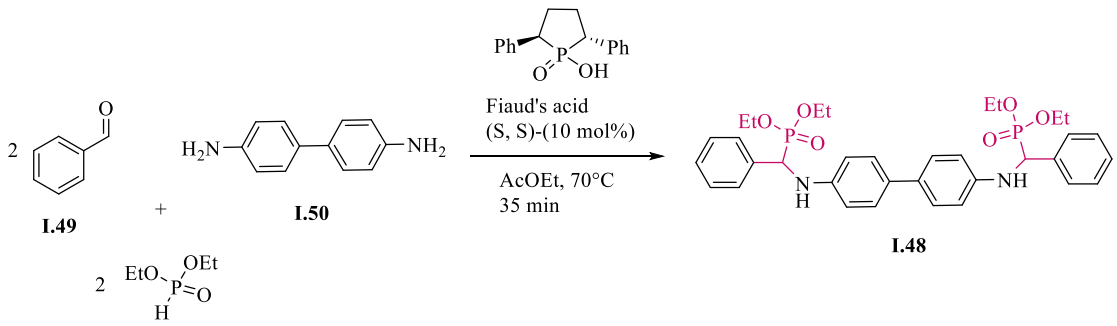

Scheme 7: Synthesis of bis *α*-aminophosphonates using *Fiaud's acid* as organocatalyst.

[69] Aissa, R., Guezane-Lakoud, S., Toffano, M., Gali, L., & Aribi-Zouioueche, L. *Bioorg. Med. Chem. Lett*, **2021**, *41*, 128000.

I-4-2-2 Using nanocatalysts

A series of substituted dimethyl-phenylamino-benzylphosphonates **I.51** was prepared by *Sreelakshmi et al*[70], using CuO/ Au oxide nanocatalyst from 2-hydroxyl aniline **I.52**, substituted benzaldehydes **I.53**, and dimethylphosphite under conventional heating or microwave irradiation. Neat and several solvents are tested such as, EtOH, MeCN and PhMe and THF. The product of this catalyst gave the corresponding product in excellent yields in THF. ***(Scheme 8).***

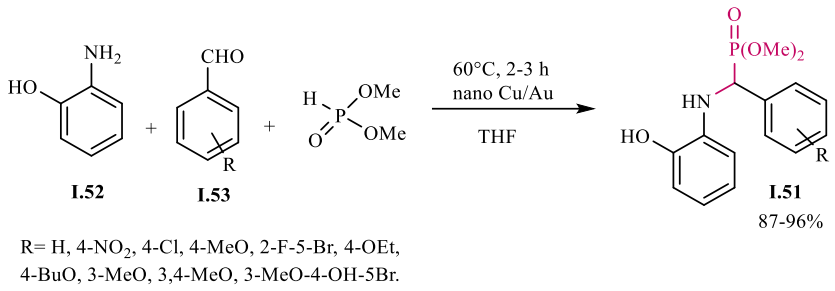

Scheme 8: Nanocatalyst Cuo/Au for α-aminophosphonate synthesis.

Nano Sb_2O_3 has also demonstrated remarkable efficiency as a catalyst in the three-component condensation reaction. This was evident when 3-(4-amino-3-fluorobenzyl)-N-methylbenzamide **1.54** reacted with various substituted aromatic aldehydes **I.55** and dialkyl phosphite, resulting in the synthesis of a series of novel dialkyl (aryl substituted){2-Fluoro-4-[(2-methylcarbamoyl)pyridine-4-yl)oxy)phenyl)amino)methyl)phosphonates derivatives **I.56**. The reaction proceeded under mild conditions, yielding predominantly good results[71]. The authors systematically explored alternative catalysts, varying reaction times, and different concentrations of the nanocatalyst in their study. ***(Scheme 9)***

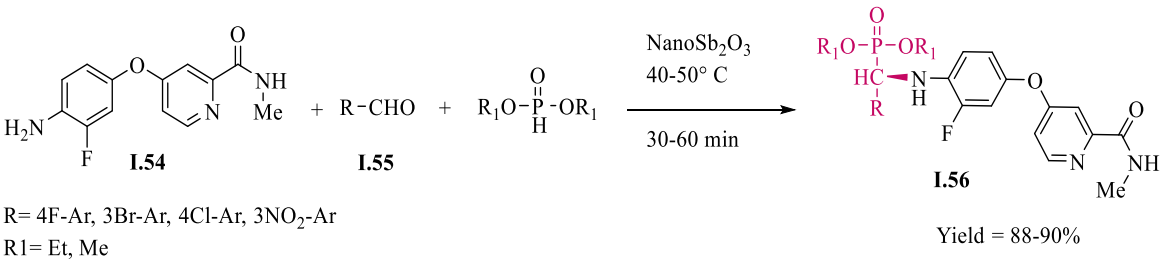

Scheme 9: Synthesis of α-aminophosphonates using $NanoSb_2O_3$.

[70] Sreelakshmi, P., Santhisudha, S., Reddy, G. R., Subbarao, Y., Peddanna, K., Apparao, C., & Reddy, C. S. *Synth. Commun*, **2018**, *48*(10), 1148-1163.
[71] Poola, S., Nadiveedhi, M. R., Sarva, S., Gundluru, M., Nagaripati, S., Shaik, M. S., & Cirandur, S. R. *Med. Chem Res*, **2019**, *28*, 528-544.

I-4-2-3 Using Lipase as catalyst

In **2017**, the first reaction using lipase as catalyst in multicomponent *Kabachnik-Fields* reaction has been designed by *Guezane Lakoud et al*[72], under lipase catalytic promiscuity method. Various commercially available lipases, including PCL, CCL, CAL-B, and PPL, were evaluated in THF as a solvent. However, using PCL, CCL, and PPL, the yields did not surpass 10%. In contrast, the multicomponent condensation reaction involving aromatic aldehydes **I.57**, anilines **I.58**, and diethylphosphite exhibited excellent yields when conducted under solvent-free conditions and at room temperature, the reaction was carried out with 50 mg of CAL-B. (***Scheme 10***, reaction **A**).

In **2019**, *Aissa et al*[73] employed an innovative approach utilizing the lipase catalytic promiscuity to create a novel series of bis (*α*-aminophosphonates) **I.59**. This method exhibited high diastereoselectivity, yielded very satisfactory results, and was characterized by a short reaction time under mild and environmentally friendly conditions. The lipase-catalyzed *Kabachnik–Fields* reaction represents a noteworthy instance of catalytic promiscuity, presenting itself as a valuable synthetic method for bioorganic synthesis. (***Scheme 10***, reaction **B**).

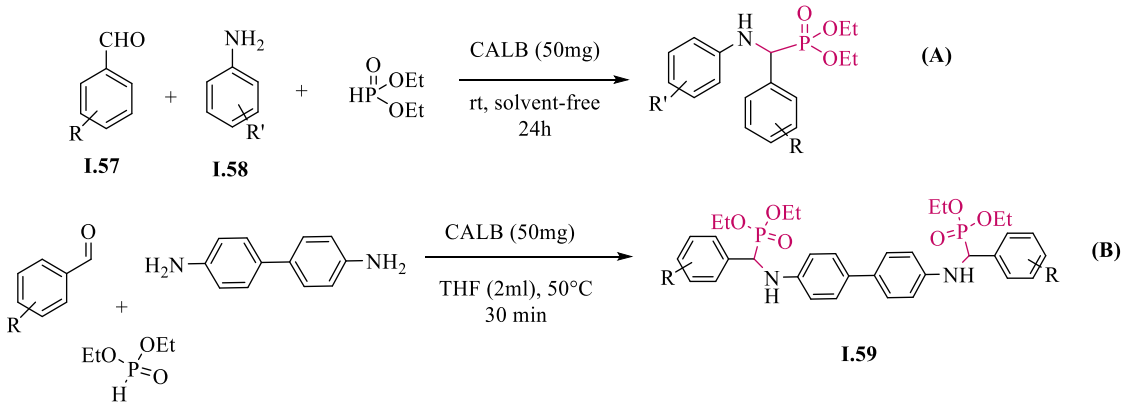

Scheme 10: Synthesis of *α*-aminophosphonates and bis (*α*-aminophosphonates) Catalyzed by *CAL-B.*

After this date and in **2020**, *Sarfaraz Shaikh et al*[74] have prepared the pyrazole *α*-aminophosphonates derivatives **I.60** using the catalytic promiscuity of lipase, specifically *Porcine Pancreatic Lipase* (PPL). The reaction was carried out by multicomponent condensation of 1H-pyrazole-4-carbaldehydes **I.61**, substituted amines **I.62** and diethylphosphite at 45°C. For the optimization of reaction conditions, the authors examined

[72] Guezane-Lakoud, S., Toffano, M., & Aribi-Zouioueche, L. *Heteroat. Chem*, **2017**,*28*(6), e21408.
[73] Aissa, R., Guezane-Lakoud, S., Kolodziej, E., Toffano, M., & Aribi-Zouioueche, L. *New J Chem*, **2019**, *43*(21), 8153-8159.
[74] Shaikh, S., Dhavan, P., Pavale, G., Ramana, M. M. V., & Jadhav, B. L.. *Bioorg Chem*, **2020**, *96*, 103589.

several parameters, including the lipase nature, quantity of lipase, the influence of solvent, temperature variations, and reaction duration. After reaction optimization, the reaction proceeds at 45°C within 3h, obtaining the product in 91% chemical yield. ***(Scheme 11).***

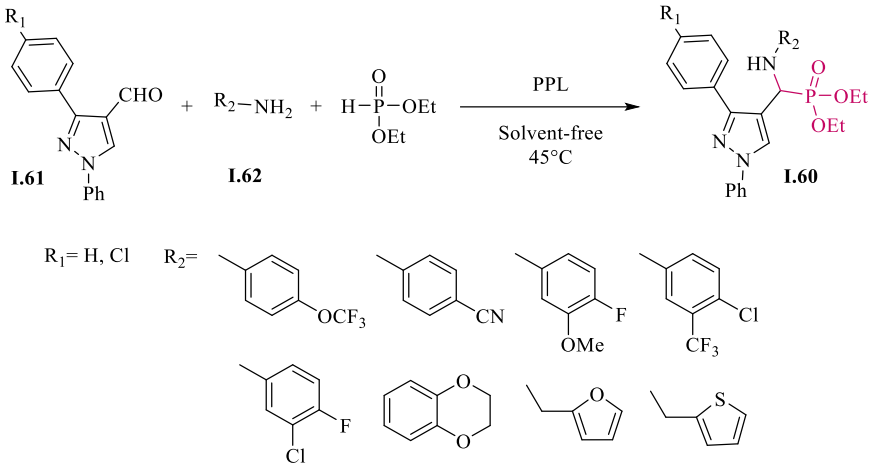

Scheme 11: Synthesis of pyrazole *α*-aminophosphonates using *PPL*.

I-4-2-4 Using microwave irradiation

A catalyst free approach has been developed for the synthesis of new series of N-alkyl-isoindolin-1-one-3-phosphonates ***I.63*** have been realized from 2-formylbenzoic acid ***I.64,*** aliphatic primary amines ***I.65*** and various dialkylphosphites using microwave irradiation at 60°C within short reaction times.[75] ***(Scheme 12)***.

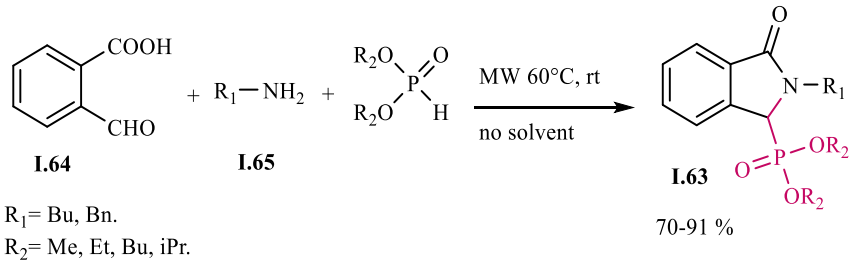

Scheme 12: Microwave-assisted synthesis of isoindolin-1-one-3-phosphonate derivatives.

I-4-2-5 Ultrasound-assisted synthesis

In order to improve the chemical yields of the synthesis of *α*-aminophosphonates within short reaction time, ultrasonic irradiation can be employed. This technique makes it possible to generate or fast and easier work-up compared to the conventional mode. Recently, *Shaikh et al*[76] were carried out the synthesis of novel antipyrine based *α*-aminophosphonates in the presence of TiO_2/CNT nanocomposite as heterogeneous catalyst, using ultrasonication as a

[75] Tajti, Á., Tóth, N., Rávai, B., Csontos, I., Szabó, P. T., & Bálint, E. *Molecules*, **2020**, *25*(14), 3307.
[76] Shaikh, S., Yellapurkar, I., & Ramana, M. M. V. *React. Kinet. Mech. Catal*, **2021**, *134*, 917-936.

green energy source. The reaction was performed by the condensation of 4-aminoantipyrine **I.66**, anilines **I.67** and diethylphosphite and gave the best results (up to 90%) in (5s/ 2s on/off time) ***(Scheme 13).***

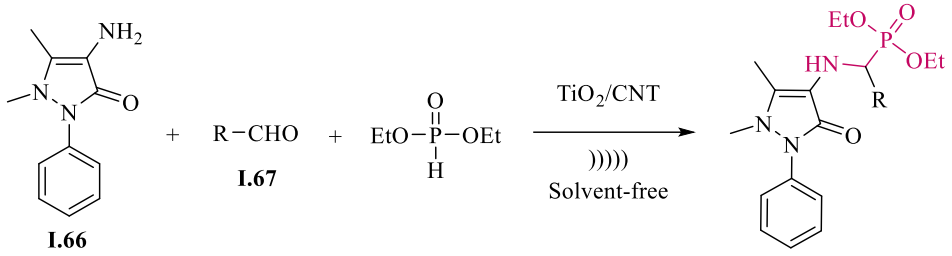

R= Benzaldehyde, 4-CH_3Ar, 4-FAr, 4-ClAr, 3-NO_2Ar, Furan-2-Ar, Thiophene-2-Ar

Scheme 13: Synthesis of antipyrine *α*-aminophosphonates derivatives.

I-4-2-6 Using Lewis acid

A number of reactions were described in the literature detail the synthesis of α-aminophosphonates using Lewis acid. In **2017**, *Guezane Lakoud* et *al.*[77] have developed a $NiSO_4.6H_2O$ as an efficient catalyst for *Kabachnik-Fields* multicomponent reactions conducted under eco-friendly conditions. The reaction proceeds by the condensation of aromatic aldehydes **I.68**, anilines **I.69** and diethylphosphite. $NiSO_4.6H_2O$, employed in catalytic amounts (5 mol%) at room temperature without the use of solvents, facilitates the formation of the desired *α*-aminophosphonates. Following a simple work-up procedure, impressive yields (up to 92%) are achieved within a brief reaction time of 10–20 minutes. The nature of solvent, concentration of catalyst, temperature and the reaction time were examined in order to find the optimal conditions. ***(Scheme 14).***

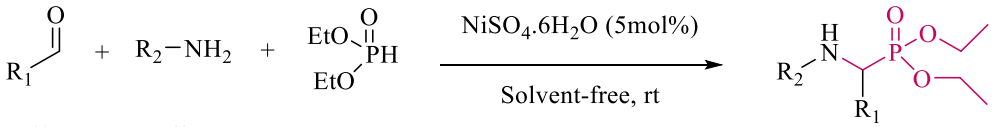

I.68 **I.69**

R_1= aryl, heteroaryl

R_2= H, CF_3, CH_3

Scheme 14: Synthesis of *α*-aminophosphonates using $NiSO_4 \cdot 6H_2O$ as *Lewis* acid.

In **2018**, *Awad* et *al*[78]. utilized zinc chloride as a *Lewis* acid catalyst for the preparation of diphenyl (aryl) (4-oxo-2-phenyl-4H-quinazolin-3-yl)-acetic acid hydrazino methyl phosphonate I.70. The reaction involved the condensation of 3,4-dihydro-(4-oxo-2-phenyl-4H-quinazolin-3-yl)-acetic acid hydrazide **I.71** with various aromatic aldehydes **I.72** and

[77] Guezane Lakoud, S., Merabet-Khelassi, M., & Aribi-Zouioueche, L. *Res. Chem. Intermed*, **2016**, *42*, 4403-4415.
[78] Awad, M. K., Abdel-Aal, M. F., Atlam, F. M., & Hekal, H. A. *J. Mol. Struct*, **2018**, *1173*, 128-141.

triphenylphosphite. The *α*-aminophosphonates were obtained with excellent yields, as illustrated in ***Scheme 15***.

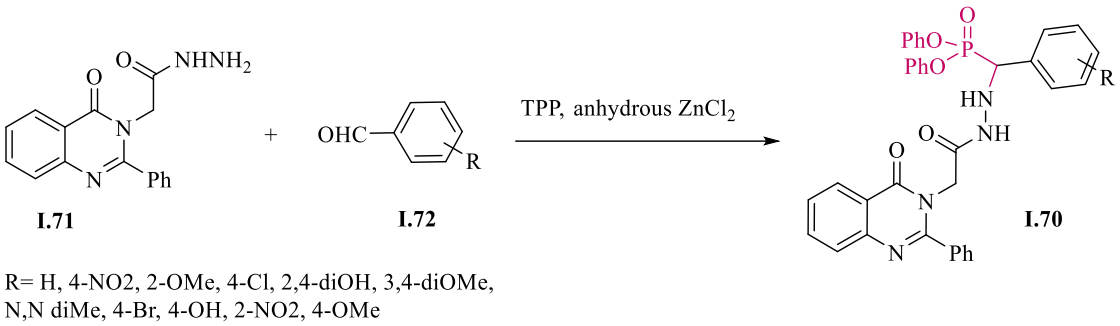

Scheme 15: Synthesis of *α*-aminophosphonates using $ZnCl_2$ as *Lewis* acid.

I-4-2-7 By author procedures

The α-aminophosphonates could be prepared by author procedures, we found for example:

a) From aza-Pudovic reaction:

The *aza-Pudovik* reaction presents an alternative route for synthesizing *α*-aminophosphonates, involving the addition of a dialkyl phosphite to an imine. In this procedure, a carbazole-related imine **I.73** underwent reaction with dialkyl phosphites and diphenylphosphine oxide, using tetramethylguanidine as the catalyst in toluene. The resulting adducts **I.74** were obtained in satisfactory yields.[79] ***(Scheme 16).***

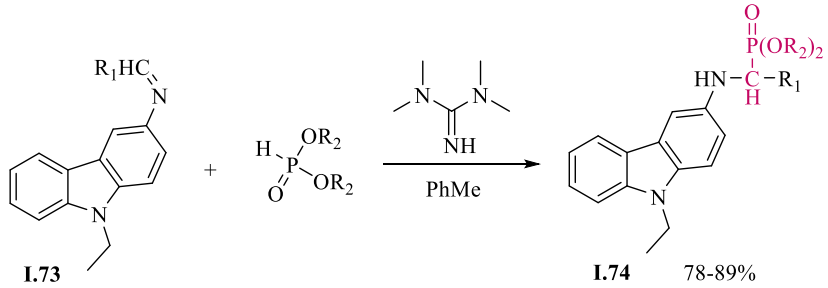

R_2	R_1
Me	3-Me-thiophene, 5-Me-thiophene, 2-HO-5-ClC_6H_3
Et	3-Me-thiophene, 5-Me-thiophene, 2-HO-5-ClC_6H_3
Ph	3-Me-thiophene, 5-Me-thiophene, 2-HO-5-ClC_6H_3

***Scheme 16*:** Synthesis of carbazole-*α*-aminophosphonates by *Pudovic* reaction.

[79] Reddy, S. S., Rao, V. K., Krishna, B. S., Reddy, C. S., Rao, P. V., & Raju, C. N. *Phosphorus, Sulfur Relat. Elem*, **2011**, *186*(7), 1411-1421.

A cinchona-derived thiourea **A-D** was employed for the addition of diphenyl phosphite to ketimines **I.75**. The resulting yields for products **I.76** and **I.77** exhibited variation within the range of 48–88%[80]. (***Scheme 17***)

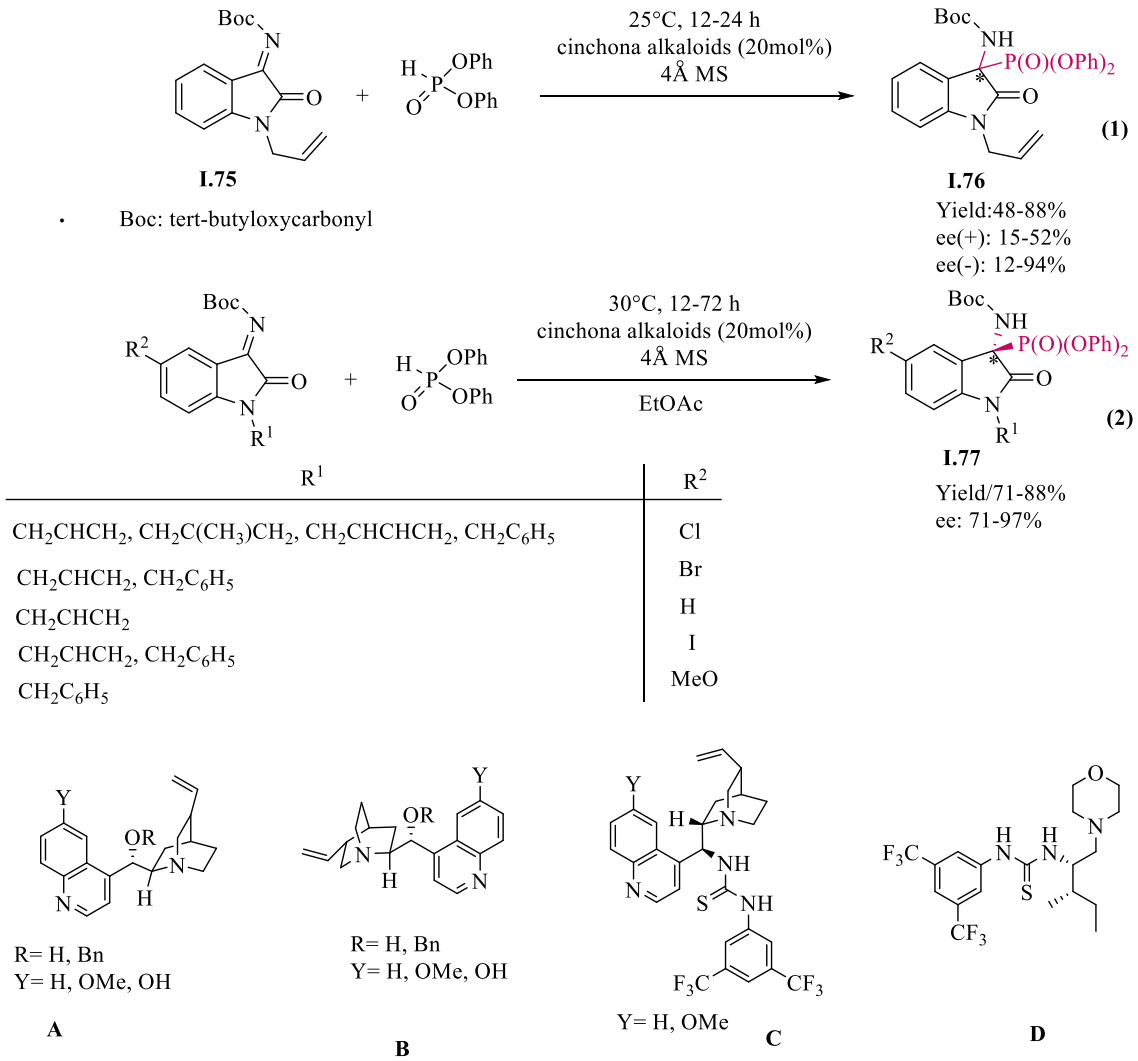

Scheme 17: The use of cinchona-derived thiourea catalysts in the *aza-Pudovik* reaction.

b) From hydroxyphosphonates

A simple procedure has been developed by *Nóra Zsuzsa Kiss et al*[81] for the substitution of *α*-hydroxyphosphonates **I.78**, previousely prepared by *Pudovic* recation, to afford the *α*-aminophosphonates **I.79** under MW irradiation in solvent-free condition. The reaction was performed with primary amine **I.80** as nucleophile targeting the carbon atom with the hydroxy group. The beneficial neighboring effect of the phosphorus atom facilitated the migration of the OH group. This advantageous proximity of the phosphorus atom, aiding in the departure

[80] Kumar, A., Sharma, V., Kaur, J., Kumar, V., Mahajan, S., Kumar, N., & Chimni, S. S. *Tetrahedron*, **2014**, *70*(39), 7044-7049.
[81] Nóra Zsuzsa Kiss, Zita Rádai, Zoltán Mucsi, György Keglevich, *Heteroat Chem*, **2016**; 27; 260-268.

of the OH group, led to a substantial reduction in the enthalpy gap of the reaction. ***(Scheme 18).***

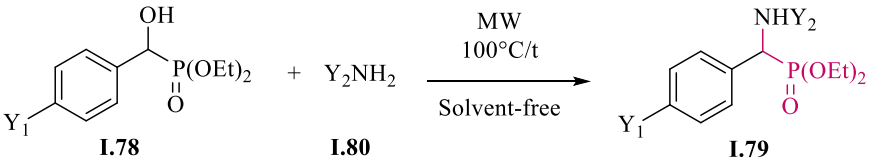

Y_1= H, OMe, Me, Cl

Y_2= ^{n}Pr, ^{n}Bu, Hex

Scheme 18: Synthesis of *α*-aminophosphonates *via α*-hydroxyphosphonates.

I-4-3 Chemical reactivity of the *α*-aminophosphonates

The different functions exist in the structure of aminophosphonate allows it to have an important place in organic synthesis and to use them as precursors in the famous reactions.

I-4-3-1 As precursor in Horner–Wadsworth–Emmons reaction

The *Horner–Wadsworth–Emmons* (HWE) reaction[82], widely utilized in organic chemistry, involving stabilized phosphonate carbanions reacting with aldehydes (or ketones), resulting primarily in the formation of E-alkenes. *Han et al*[83], were described the preparation of piperlongumine-like compounds **I.81** from a novel phosphonoacetamide reagent **I.82** by HWE olefination in good overall yield ***(Scheme 19).***

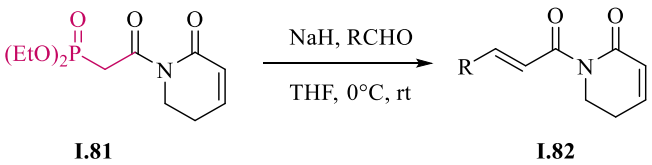

Scheme 19: The use of *α*-aminophosphonates in *HWE* reaction.

I-4-3-2 Using as an organocatalyst

In academic research *α*-aminophosphonates hold significant importance in organic synthesis not only as intermediate but also as organocatalyst in many reactions. *Tao et al.*[84] confirmed the high reactivity of *α*-aminophosphonate to catalysis the *Michael* reactions between the addition of carbonyl compounds **I.83** to nitro-olefins **I.84**, (reaction A***, Scheme***

[82] a) Wadsworth, W. S., Jr.; Emmons, W. D. *J. Am. Chem. Soc.* 1961, *83*, 1733. b) Wadsworth, W. S., Jr.; Emmons, W. D. *Organic Syntheses*, **1973**, 5, 547 45, 44, 1965.

[83] Han, L. C., Stanley, P. A., Wood, P. J., Sharma, P., Kuruppu, A. I., Bradshaw, T. D., & Moses, J. E. *Organic & Biomolecular Chemistry*, **2016**, *14*(31), 7585-7593.

[84] Tao, Q., Tang, G., Lin, K., & Zhao, Y. F. *Chirality: The Pharmacological, Biological, and Chemical Consequences of Molecular Asymmetry*, **2008**, *20*(7), 833-838.

7*). Whereas, *Peter Din´er* and *Mohamed Amedjkouh*[85] evaluated the performance of chiral *α*-aminophosphonates as organocatalysts in the asymmetric aldol reaction. *(*reaction B*, Scheme 20).

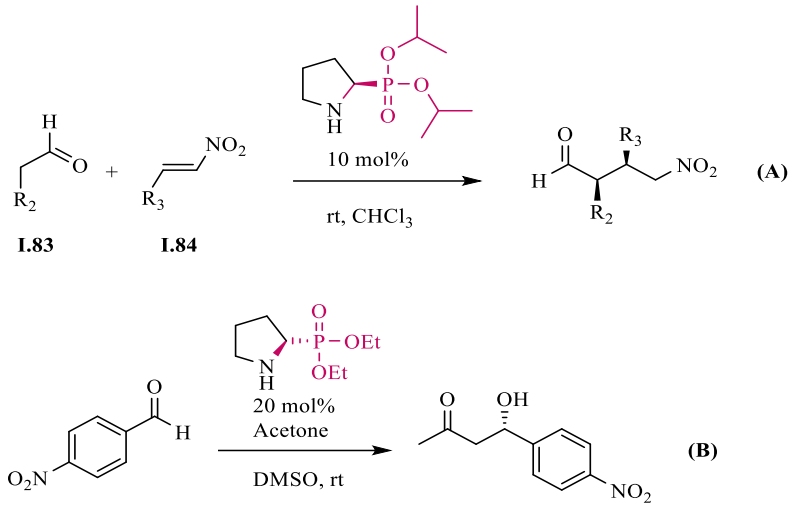

Scheme 20: The use of *α*-aminophosphonates as an organocatalyst *in Michael* reactions.

[85] Dinér, P., & Amedjkouh, M. *Org. Biomol. Chem*, **2006**, *4*(11), 2091-2096.

Conclusion

In this chapter we have provided a comprehensive overview of organophosphonates, their different classes according to their oxidation number, and the versatile range exhibition of properties, making them valuable in numerous applications.

Furthermore, the discussion delved into the extensive use of organophosphonates in pharmaceutical research, where these compounds have been recognized for their ability to act as enzyme inhibitors and drug candidates. Their diverse biological activities and potential therapeutic applications offer new avenues for addressing health challenges and drug development.

We also presented various recent methods employed for the synthesis of organophosphonates compounds via multicomponent *Kabachnik-Fields* reactions using different kinds of catalysts. Also we have highlighted the important reactivity of these compounds.

This chapter serves as a testament to the remarkable contributions and boundless opportunities presented by organophosphonates in the realm of science and technology, which have allowed us to contemplate the synthesis of new molecules derived from α-aminophosphonates using environmentally friendly methods with the aim of evaluating their pharmacological properties and anticancer activity.

Chapter II

Multicomponents reactions and catalysis

II-1 Introduction

The concept of "Green" and "Sustainable Chemistry" goes back to **1990s**, arose by the American chemists *Anastas* and *Warner*. It revolves around the advancement of methodologies and technologies aimed at fostering chemical reactions with enhanced efficiency, thereby producing minimal waste and reduced environmental emissions compared to conventional methods. Grounded in twelve fundamental principles, these innovative approaches underscore a commitment to sustainable and eco-friendly practices within the realm of chemical processes.[1] ***(Figure 1)***.

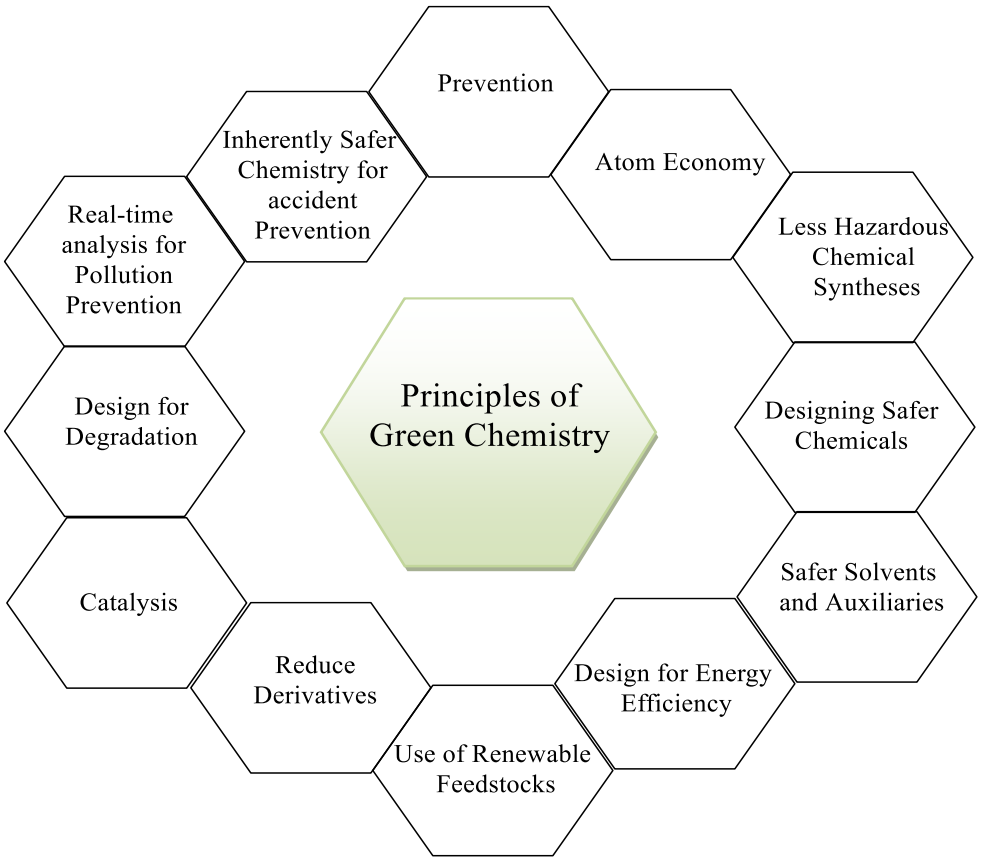

Figure 1: The twelve principles underpinning green chemistry.

This concept provides an attractive technique for chemists and researchers to synthesize chemicals by environmentally friendly processes that reduce waste as well as to search for alternative solutions or to improve existing methods.[2]

[1] Li, C. J., & Anastas, P. T. *Chem. Soc. Rev*, **2012**, *41*(4), 1413-1414.
[2] P.T.Anastas, T.C. Williamson, Green chemistry: frontiers in benign chemical syntheses and processes,Oxford University Press **1999**.

Researchers in organic chemistry are increasingly drawn to the exploration of designing environmentally friendly processes that are both clean and efficient for product preparation.

Within this framework and thanks to their ability to build one product in a single operation from three or more reactant molecules with excellent yields, high atom- and step economy , low waste and environmentally safe multicomponent reactions (MCRs), feet well with the green chemistry criteria's.

Diligent research efforts have yielded numerous advancements in the realm of Multicomponent Reactions (MCRs) coupled with environmentally friendly activation methods. Various synthetic approaches have been explored, encompassing C–H and C-heteroatom activation through processes such as coupling, cycloaddition, and others, all under diverse conditions.

Furthermore, the marriage of both catalysis and MCRs contributes well to more sustainable processes with high selective processes, and that since catalysis is considered as the pillar of the green chemistry concept.[3] Further that, the use of catalysts resolves various problems may be produced in classical MCRs, such as; equilibrium between intermediates, racemisation and certainly lack of selectivity, especially, the enantioselectivity if we used a chiral catalyst.

In the present chapter, we would present an overview on the recent development and the application of MCRs and discuss some of their recent applications. Also, we highlight some literature examples dedicated to the exploitation of catalysis as effective processes to achieve those potential reactions, especially for those concerning the preparation of organophosphorus compounds.

II-2 Multicomponent reactions

Multicomponent reactions (MCRs) have emerged as an advanced approach, revolutionizing conventional sequential multi-step synthesis by offering efficiency, cost-effectiveness, and eco-friendliness.[4]

MCRs streamline the synthesis process by creating a single compound in a "*one-pot*" operation, amalgamating all the atoms from the initial reactants. This is achieved by creating

[3] Török, B. In *Green Chem* (pp. 49-89). Elsevier. **2018**.

[4](a) Zarganes-Tzitzikas, T., Chandgude, A. L., & Dömling, A. *Chem. Rec*, **2015**, *15*(5), 981-996. (b) J. Zhu ; H. Bienaymé, Multicomponent Reaction, **2005**.

new bonds from at least three substrates without changing the conditions during the reaction[5]. (***Scheme 1***)

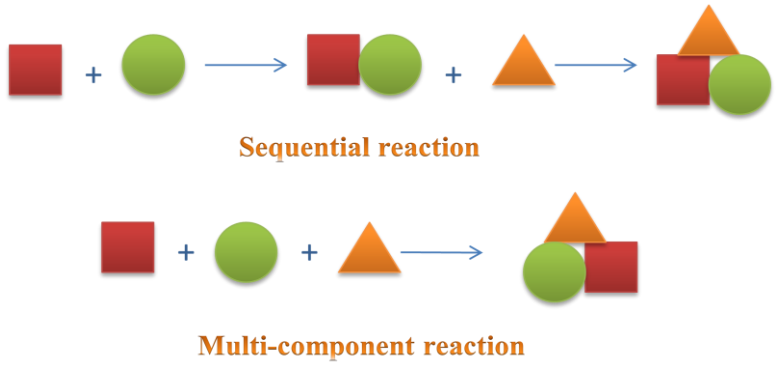

***Scheme 1*:** MCRs *versus* sequential reactions.

Since the early **1990s**, several MCRs have been developed and extensively applied in the synthesis of many drugs[6] and natural products[7] for therapeutic purposes. These reactions allow rapid access to bioactive molecules by improving existing synthetic pathways by reducing the number of steps[8].

MCRs embody key aspects of efficient synthesis, providing benefits such as higher yields, uncomplicated reaction profiles, shorter reaction times, and improved reproducibility.

II-2-1 Classes of MCRs

MCRs are classified based on the the number of starting materials, and more recently, the nature of the resulting products has played a role in their classification. This includes distinctions such as acyclic, heterocyclic, fused heterocyclic, and miscellaneous compounds[9]. As reported in the literature data library, there are MCRs from three to five or more of components giving different kind of compounds (***Scheme 2***).[10]

[5] Keating, T. A.; Armstrong, R. W. *J. Am. Chem. Soc.* **1996**, *118*, 2574–2583.
[6] (a) Kalinski, C., Lemoine, H., Schmidt, J., Burdack, C., Kolb, J., Umkehrer, M., & Ross, G. *Synthesis*, **2008**, 4007-4011. (b) Cores, Á., Clerigué, J., Orocio-Rodríguez, E., & Menéndez, J. C. *J. Pharm*, **2022**, *15*(8), 1009. (c) Zarganes-Tzitzikas, T., Neochoritis, C. G., & Dömling, A. *ACS Med. Chem. Lett*, **2019**, *10*(3), 389-392.
[7] (a) Pettit, G. R., Orr, B., & Ducki, S. *Anti-cancer drug design*, **2000**, *15*(6), 389-395.(b) Tietze, L. F., & Rackelmann, N. *Pure Appl. Chem*, **2004**, *76*(11), 1967-1983..
[8] (a) Xu, S., Zhang, X., Tao, Y., Liu, X., & Zhan, P. *Mini-Rev. Org*, **2022**, *19*(8), 894-897. (b) Graziano, G., Stefanachi, A., Contino, M., Prieto-Díaz, R., Ligresti, A., Kumar, P., & Leonetti, F. *Int. J. Mol. Sci.*, **2023**, *24*(7), 6581.
[9] Fairoosa, J., Saranya, S., Radhika, S., & Anilkumar, G. *ChemistrySelect*, **2020**, *5*(17), 5180-5197.
[10] Zhu, Y. Y., Zhang, T., Zhou, L., & Yang, S. D. *Green Chem*, **2021**, *23*(23), 9417-9421.

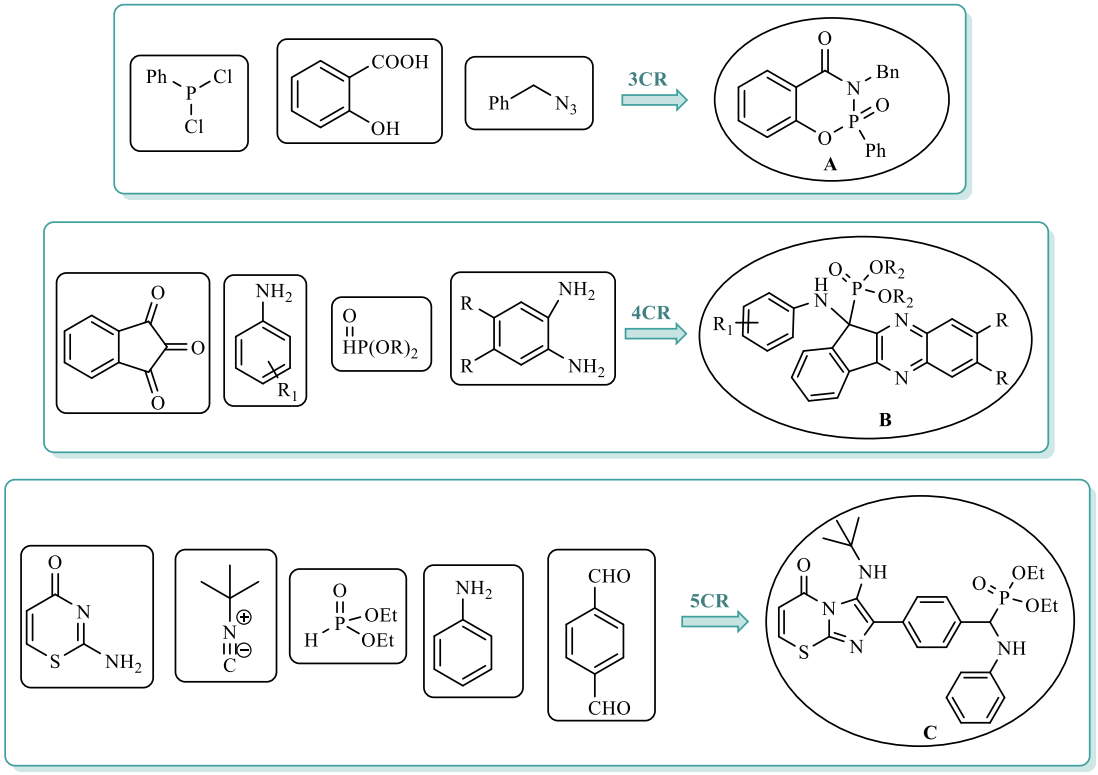

Scheme 2: Classification of multicomponent reactions.

The inaugural MCR dates back to **1838** when *Laurent* and *Gerhardt*[11] reported the synthesis of "Benzoylazotide" through a three-component reaction involving bitter almond oil and ammonia. Subsequently, numerous three-component MCRs surfaced, leading to their classification into two overarching categories: isocyanide-based multicomponent reactions (IMCRs) and nonisocyanide-based multicomponent reactions (NMCRs). The most important examples are the *Hantzsch*[12] synthesis to create analogues of the cardiovascular drug Nifedipin (Procardia®) **II.1** in **1881**, followed by the *Biginelli*[13] reaction to produced 3,4-dihydropyrimidin-2(1H)-ones **II.2** in **1891**. The *Passerini*[14] reaction, introduced in **1921**, played a pivotal role in generating *α*-acyloxy-carboxamides **II.3** and is acknowledged as the first example of isocyanide-based Multicomponent Reactions (MCRs).

Since then, many multicomponent reactions have been developed, among them we mentioned the *Pavarov*[15] reaction to produced tetrahydroquinoline **II.4** by combining of an aniline, aldehyde, and an activated olefin in **1963**, while in **1977** *Van Leusen*[16] reported the three component reaction which involve the one pot condensation reaction of carbonyl

[11] Laurent, A., & Gerhardt, C. F. *Ann Chim Phys*, **1838**, *66*, 181-181.
[12] Hantzsch, A. *Ber. Dtsch. Chem. Ges*, **1881**, *14*(2), 1637-1638.
[13] Biginelli, P. *Ber. Dtsch. Chem. Ges*, **1891**, *24*(1), 1317-1319.
[14] Passerini, M., & Simone, L. J. G. C. I. *Gazz. Chim. Ital*, **1921**, *51*(2), 126-129.
[15] Povarov, L. S.; Grigos, V. I.; Mikhailov, B. M. Izv. Akad. Nauk SSR, Ser. Khim. **1963**, 2039–2041.
[16] Oldenziel, O. H., Van Leusen, D., & Van Leusen, A. M. *J. Org. Chem*, **1977**, *42*(19), 3114-3118.

compounds, aromatic amines and aryl substituted tosylmethylisocyanide (TosMIC) to afford polysubstituted imidazoles **II.5**. The next important example is the *Orru*[17] which provides highly substituted 2-imidazolines **II.6** by utilizing an amine, an aldehyde, and an α-acidic isocyanide in **2003.** (***Scheme 3***).

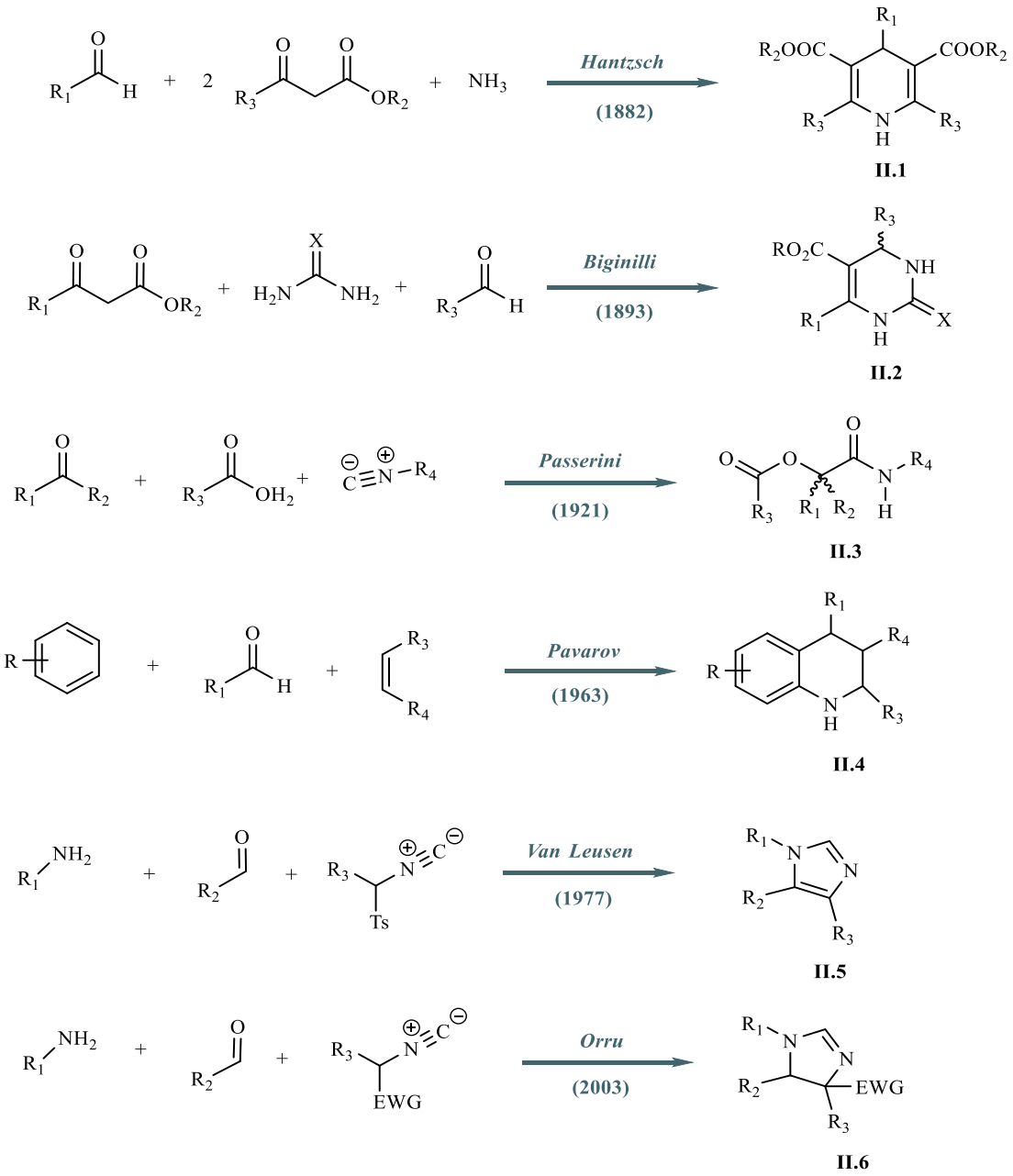

Scheme 3: Most important examples of three component reactions.

For the four component reaction, as exemple, we cite the investigation of *Rashid* and co-woorkers[18] concerning the condensation of ninhydrin **II.7**, anilines **II.8**, 1,2-

[17] Bon, R. S., Hong, C., Bouma, M. J., Schmitz, R. F., de Kanter, F. J., Lutz, M.,. & Orru, R. V. *Org. Lett*, **2003**, *5*(20), 3759-3762.
[18] Rashid, Z., Naeimi, H., & Ghahremanzadeh, R. *RSC adv*, **2015**, *5*(120), 99148-99152.

phenylenediammines **II.9** and dialkyl or diaryl phosphites (***Scheme 4***). This reaction provides series of aminophosphonates derivatives **II.10** that exhibit several biological properties.

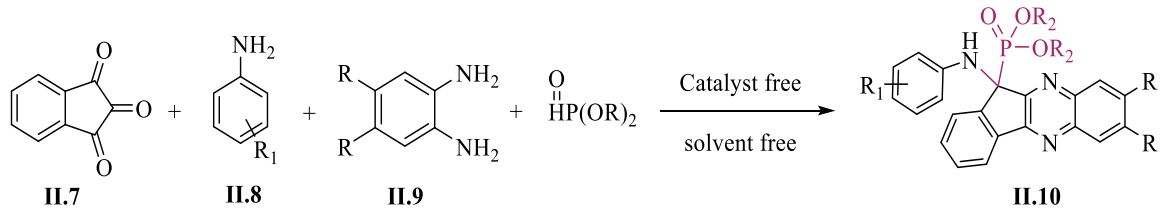

Scheme 4: Streamlined synthesis of diphenyl 11-(p-tolylamino)-11H-indeno[1,2-b]quinoxalin-11-ylphosphonate *via* a four component condensation reaction.

Finally, for the reactions involving five starting materials are known as **five-component reaction**, which incorporate multiple functionalities and demonstrate a elevated bond forming index (BFI). Generally, this reaction is used in the preparation of heterocycles by cycloaddition of nucleophilic and electrophilic intermediates[19]. One prototypical example of a five-component reaction involves the microwave-assisted synthesis of imidazo[2,1-b][1,3]thiazinyl-α-aminophosphonate **II.15**, as conducted by *Kaur* et *al*[20]. This reaction allows the formation of six new bonds in a one procedure between aniline **II.11**, dialdehyde **II.12**, 2-amino-4H-1,3-thiazine-3-one **II.13**, diethylphosphite and isocyanide **II.14**. (***Scheme 5)***

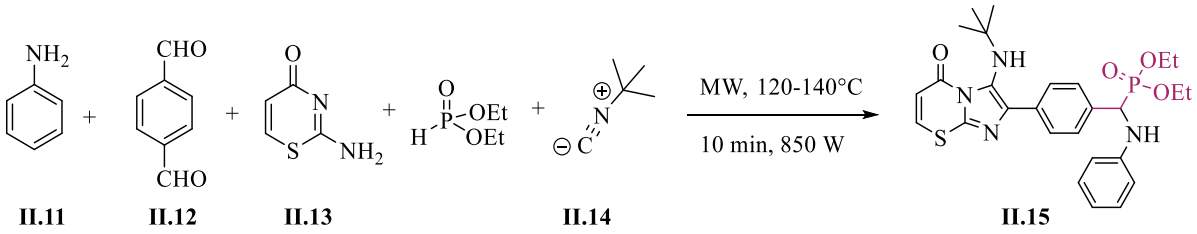

Scheme 5: Synthesis of imidazo[2,1-b][1,3]thiazinyl-*α*-aminophosphonate via five component condensation reaction.

II-3 Catalysis

Catalysis is the action of a substance called a catalyst on a chemical transformation with the aim of modifying its reaction rate by lowering the energy barrier to be crossed (***Figure 2***). Indeed, the catalyst makes it possible to direct the chemical reactions to make them selective, and this reflects its essential role in fields as diverse as oil refining, petrochemicals, fine chemicals, polymerization, depollution,…etc. On the other hand, a

[19] (a) Ambethkar, S., Padmini, V., & Bhuvanesh, N. *New J Chem*, **2016**, *40*(5), 4705-4709. (b) Lu, Z., Xiao, J., Wang, D., & Li, Y. *Asian J. Org. Chem*, **2015**, *4*(5), 487-492.

[20] Kaur, T., Saha, D., Singh, N., Singh, U. P., & Sharma, A. *ChemistrySelect*, **2016**, *1*(3), 434-439.

catalyst provides an alternative, energetically favorable pathway compared to non-catalytic reactions. This allows processes to be conducted under conditions of pressure and temperature that are more practical and achievable.

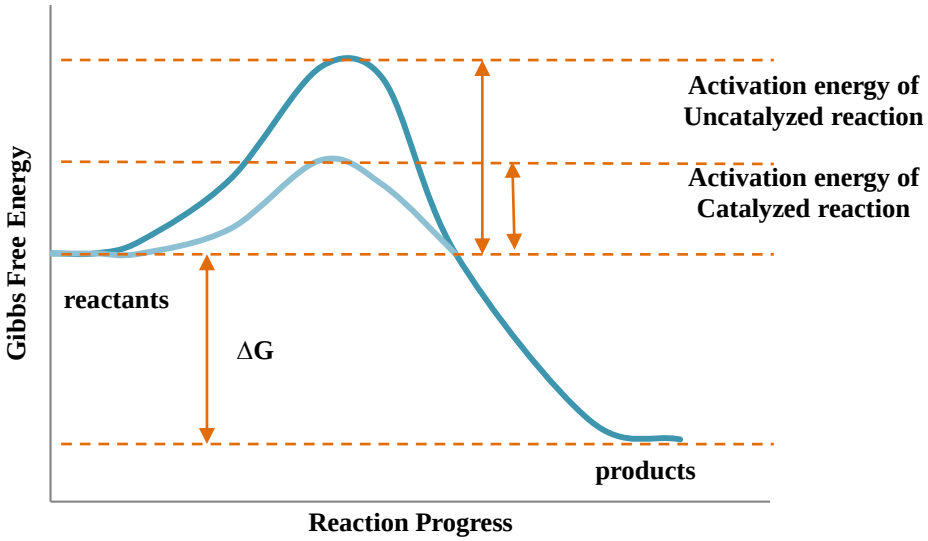

Figure 2: Energetic diagram of uncatalyzed *versus* catalyzed reaction.

Catalysis is subdivided into three main classes referring to the mode of action of the catalyst: a) Heterogeneous, b) Homogeneous, c) Biocatalysis (***Figure 3***)[21].

[21] Chouhan, A. S., & Sarma, A. K. *Renew. Sust. Energ. Rev*, **2011**, *15*(9), 4378-4399.

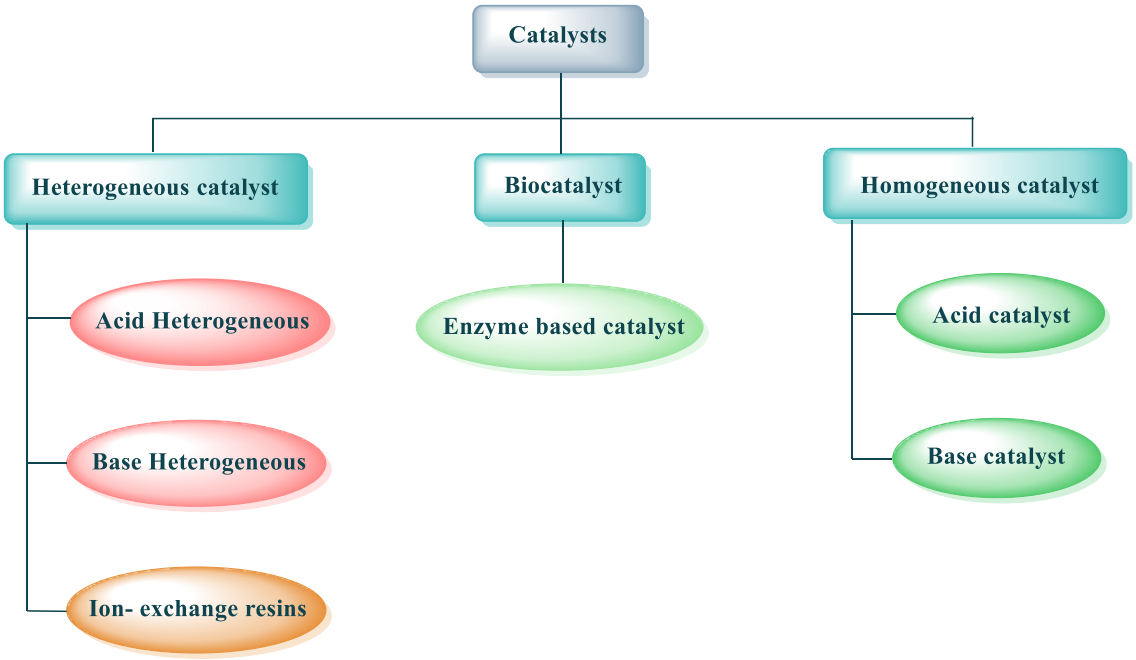

Figure 3: Catalysts classification.

In the main purpose of this thesis, we focused in what follows on the two last classes of catalysts. For the homogeneous catalysis we spotlight the organocatalysis.

II-3-1 Organocatalysis

II-3-1-1 Definition and concept

Organocatalysis consists to use small metal-free organic molecules, mainly named "organocatalyst" to catalyze organic transformations. Organocatalysts can adopt either achiral or chiral configurations, typically composed of C, H, N, S, and P. These catalysts demonstrate inherent stability and offer a straightforward design and synthesis process, enabling the creation of diverse molecules with ease.

Organocatalysts are frequently derived from non-toxic organic compounds sourced from biological materials. These can function as *Lewis* bases, *Lewis* acids, *Brønsted* bases, or *Brønsted* acids, often encompassing sugars, peptides, amino acids (such as proline), and alkaloids like cinchona (***Figure 4***). In the initial stages of organocatalysis, achiral compounds were predominantly employed to drive targeted reactions, resulting in the formation of achiral or racemic products. For the asymmetric version of organocatalysis, the catalyst is a chiral and under single enantiomer form.[22] This concept is recognized due to the independent research works of groups of *Benjamin List* and *David MacMillan*[23].

[22] a) Shaikh, I. R. *J. Catal*, **2014**. b) Oliveira, V. D. G., Cardoso, M. F. D. C., & Forezi, L. D. S. M. *Catalysts*, **2018**, *8*(12), 605. C) Aukland, M. H., & List, B. *Pure Appl. Chem.* **2021**, *93*(12), 1371-1381.
[23] List, B., & MacMillan, D. *Curr. Sci*, **2021**, *121*(9), 1148.

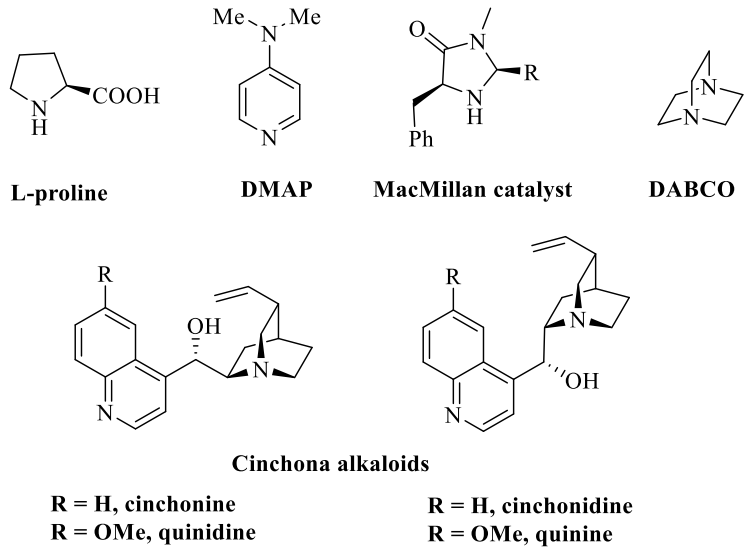

Figure 4: Some potential organocatalysts.

In recognition of their groundbreaking contributions, the *Nobel* Prize in Chemistry was conferred upon them in **2021**[24] for their pioneering efforts in the development of asymmetric organocatalysis. Additionally, *MacMillan* played a key role in establishing the widely accepted term "organocatalysis" to characterize an entire field of chemistry research[25].

II-3-1-2 Early application of organocatalysis

Over the last century, the first organic catalysts employed for the formation of C-C and C-heteroatoms bonds were predominantly sourced from nature such as; amino acid, alkaloid, brucine and cinchona.[26]

In **1974**, *Hajos* and *Parrish*[27] made a groundbreaking contribution by reporting the initial instance of an organocatalyzed enantioselective reaction. They carried out the intramolecular aldolisation catalyzed by *L*-proline to convert quantitatively achiral trione **II.16** into a *β*-keto-hydroxy **II.17** with an impressive enantiomeric excess of 93%. ***(Scheme 6)***

[24] The Nobel Prize in Chemistry 2021—NobelPrize.Org. Available online: https://www.nobelprize.org/prizes/chemistry/2021/summary/ (accessed on 20 July 2022).
[25] García Mancheño, O., & Waser, M. ***Eur. J. Org. Chem.*** **2023**, *26*(1), e202200950.
[26](a) Vavon, M. M., & Peignier, P. *Bull. Soc. chim. Fr*, **1929**, *45*, 293. (b) Wegler, R. *Liebigs Ann*,**1932**, *498*(1), 62-76.
[27] Z. G. Hajos, D. R. Parrish, *J. Org. Chem.* **1974**, *39*, 1615-1621.

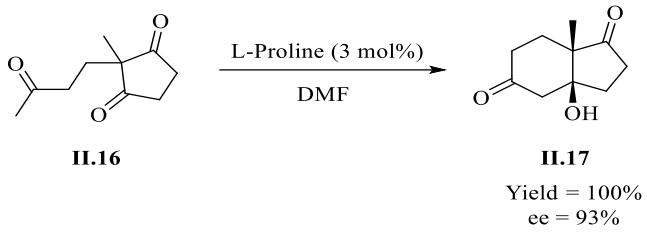

Scheme 6: Intramolecular aldolisation catalyzed by *L*-proline.

In subsequent years, the same chiral catalyst was used by *List* et *al*[28]. in the intermolecular aldolization between acetone **II.18** and various aldehydes **II.19** to obtain the desired product **II.20** with an enantiomeric excess up to 70%. (***Scheme 7***)

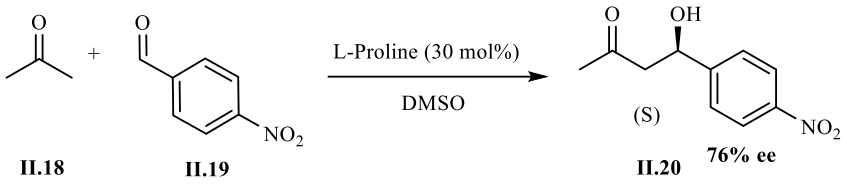

***Scheme 7*:** Intermolecular aldolisation catalyzed by *L*-proline.

Ahrendt et *al.*[29] described the use of chiral imidazolidinone (5 mol %) as catalyst in the asymmetric *Diels-Alder* reaction of various dienes **II.21** and *α, β*-unsaturated **II.22** as electrophile. Accordingly, *Diels-Alder* cycloaddition provided selectively the enantioenriched product **II.23** 82% yield at ee = 94%. (***Scheme 8***)

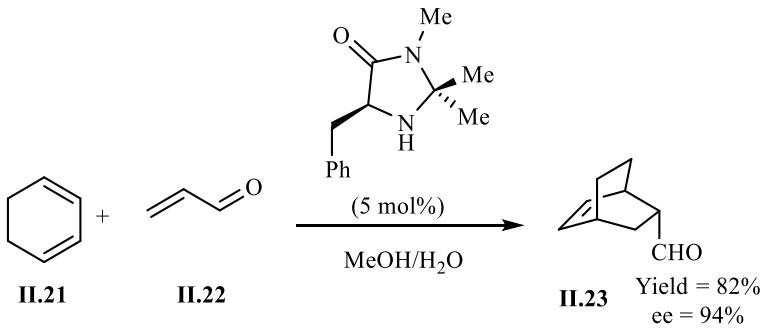

***Scheme 8*:** *Diels-Alder* reaction catalyzed by chiral imidazolidinone.

II-3-1-3 Organocatalytic activation modes

There are two different classifications based on mechanistic perspective. The first pertains to organocatalytic processes forming covalent intermediates between the catalyst and substrate, while the second involves those relying on non-covalent interactions. Additional distinctions within each category can be drawn based on the mode of substrate activation:

[28] List, B., Lerner, R. A., & Barbas, C. F. *J. Am. Chem. Soc*, **2000**, *122*(10), 2395-2396.
[29] Ahrendt, K. A., Borths, C. J., & MacMillan, D. W. *J. Am. Chem. Soc*, **2000**, *122*(17), 4243-4244.

either through highest occupied molecular orbital (HOMO) activation, as observed in enamine and N-heterocyclic carbene catalysis, or lowest unoccupied molecular orbital (LUMO) activation, exemplified by iminium and acylammonium catalysis.[30] (***Figure5***).

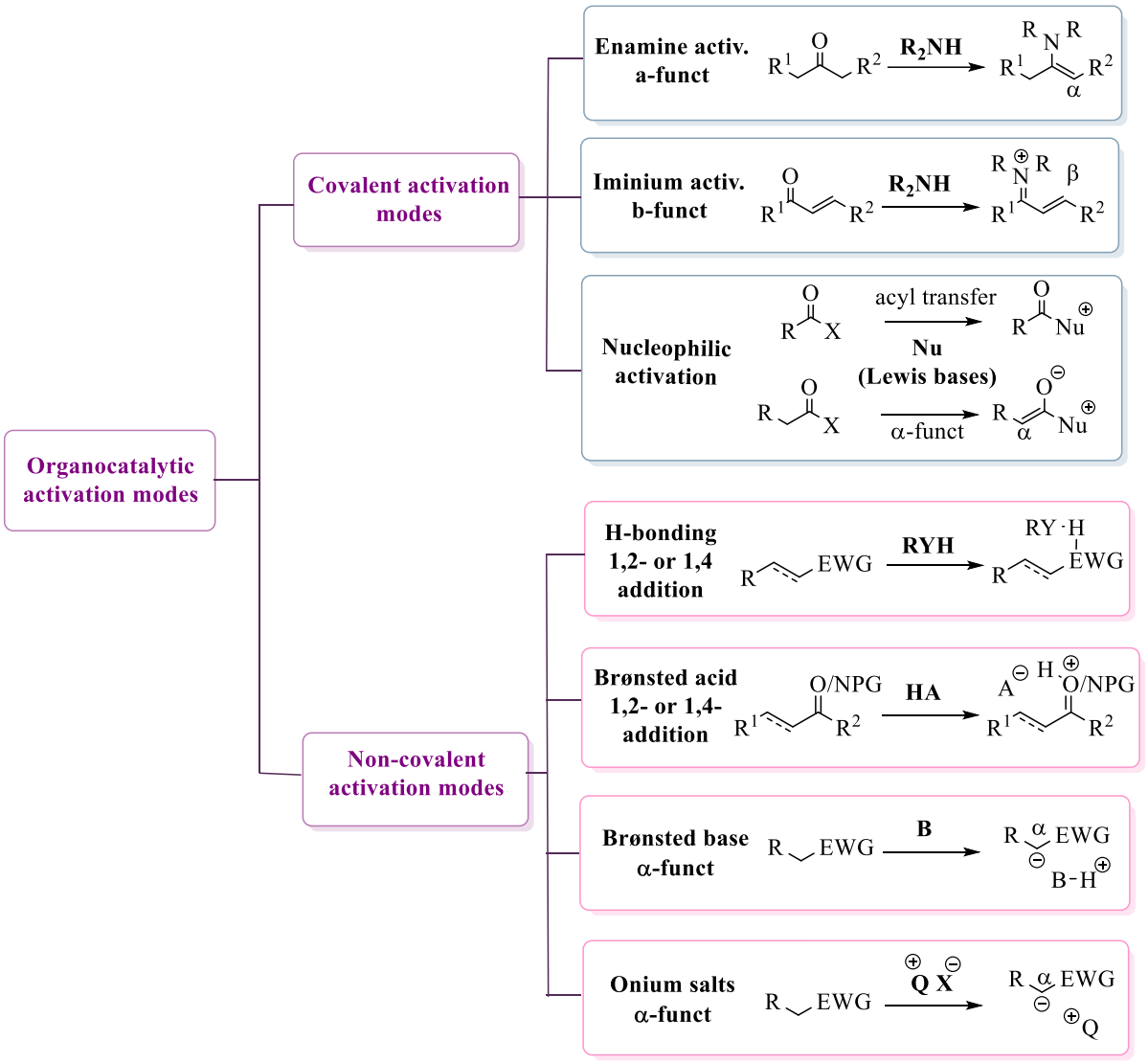

Figure 5: Organocatalytic activation modes.[31]

a) Covalent activation modes

The use of secondary amines catalysts with a carbonyl compound allows the formation of a reversible enamine intermediate, which considered as a good nucleophile and could be used in various synthetic reactions. The addition of the enamine to the elctrophile forms the iminium ion as intermediate. This nucleophilic entity is very reactive (because it has a high molecular orbital energy (HOMO), and reacts with an electrophile to carry out a variety of reactions in a very selective way. The hydrolysis of the resultant iminium ion liberates the

[30] Abbasov, M. E., & Romo, D. *Nat. Prod. Rep*, **2014**, *31*(10), 1318-1327. Abbasov M.E.
[31] García Mancheño, O., & Waser, M. *Eur. J. Org. Chem*, **2023**, *26*(1), e202200950.

carbonyl, facilitating catalyst recovery. This mode of activation finds extensive application in diverse chemical transformations, including *Michael* reactions, *Mannich* reactions, aldolization, and the *α*-alkylation of carbonyl compounds, as illustrated in ***Scheme 9* (A)** [32].

Non-enolizable carbonyl compounds of the *α-β* unsaturated called *"Michael acceptor"* are activated by enamine via the formation of an iminium ion, subsequently engages with a nucleophile resulting in activation at the β position, with the enamine being regenerated in the process.[33] ***(Scheme 9 (B)).***

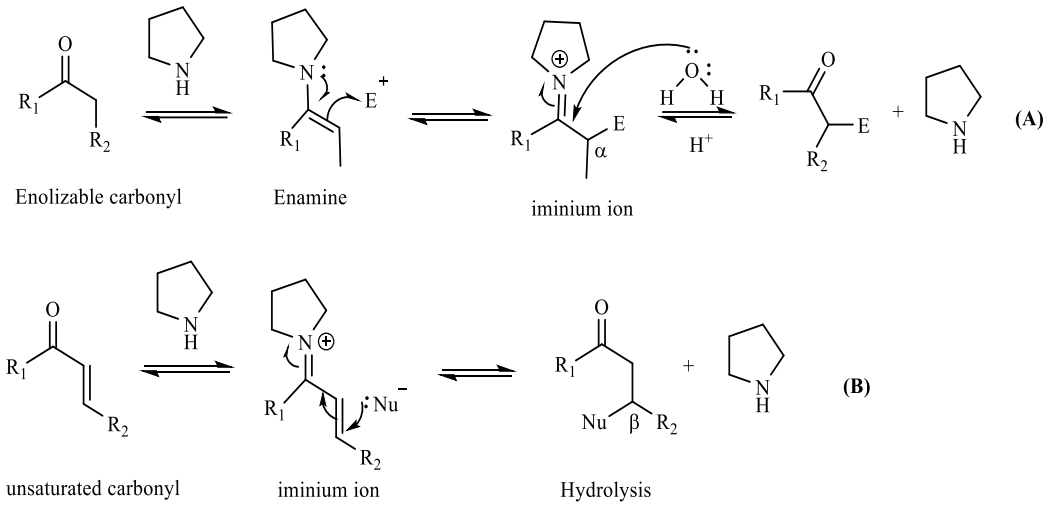

***Scheme 9*:** Modes of activation *via* enamine.

b) Non-covalent activation modes

In this mode of non-covalent activation, the catalyst and the substrate act by weak non-covalent interactions. For example, catalysts of the diol, thiourea or *Lewis* acid can also activate a carbonyl function and thus increase its electrophilicity[34]. ***(Scheme 10)***

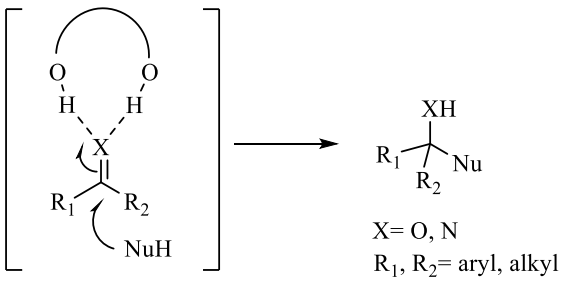

***Scheme 10*:** Mode of activation via hydrogen bonds.

[32] Mukherjee S., Yang J.W., Hoffmann S., List B., *Chem. Rev.*, **2007**, *107*, 5471.
[33] Erkkilۉ A., Majander I., Pihko P.M., *Chem. Rev.*, **2007**, *107*, 5416.
[34] Akiyama T., Mori K., *Chem. Rev.*, **2015**, *115*, 9277 ; Parmar D., Sugiono E., Raja S.

II-3-1-4 Advantages of organocatalysis

Organocatalysis presents a number of advantages like as:

- Organocatalysts are generally stable and less sensitive to water and oxygen[35], which makes them useful under simple and eco-friendly conditions to carry out highly selective reactions.
- Organocatalysis reduces the protection/deprotection of functional group and consequently the overall reaction steps due to its high compatibility that might be delicate to other processes[36].
- The absence of transition metals not only averts the production of metallic waste but also eliminates the presence of metal residues in the products. This attribute is vital for its suitability in pharmaceutical and food industries, guaranteeing a process that is environmentally friendly and free of unwanted metal contaminants.[37]
- Some of the used organocatalysts are biodegradable and easily available in nature like sugars[38], tartaric acid[39] and L-proline[40].
- Immobilization of the catalyst on a support allows resisting at high temperature and prevents their denaturation, to recycle, and reused it by its heterogeneization[41].

II-3-1-5 Highlighted examples of organocatalyzed MCRs (OMCRs)

The use of organocatalysis in multicomponent reactions has become as a potent strategy in contemporary organic synthesis. This approach can significantly streamline the synthesis process, providing a time-efficient route to construction of complex molecular scaffolds in a single step.

a) The *Ugi* reaction

Zhang et *al*[42]. successfully introduced an enantioselective three-component condensation *Ugi* reaction catalyzed by a chiral SPINOL-derived phosphoric acid (CPA). The reaction involved cyclohexyl isocyanide **II.24,** 2-benzyloxy acetaldehyde and 4-nitroaniline in CH_2Cl_2 at -30 °C. The *Ugi* 3RC facilitates the generation of α-amino amide **II.25** with a notable yield of 99% and exceptional enantioselectivity at 97% ee. (***Scheme 12***).

[35] Raj, M., & Singh, V. K. *J. Chem. Soc*, **2009**, (44), 6687-6703.
[36] Sharma, A., & Pandey, S. K. *J. Org. Chem*, **2022**, *87*(15), 10430-10434.
[37] Oliveira, V. D. G., Cardoso, M. F. D. C., & Forezi, L. D. S. M. *J Catal*, **2018**, *8*(12), 605.
[38] Pinheiro, D. L., Batista, G. M., Gonçalves, J. R., Duarte, T. N., & Amarante, G. W. **2016**.
[39] Gangwar, N., & Kasana, V. K. *Synth. Commun*, **2011**, *41*(18), 2800-2804.
[40] Tiecco, M., Alonso, D. A., Ñíguez, D. R., Ciancaleoni, G., Guillena, G., Ramón, D. J., & Germani, R. *J. Mol. Liq.*, **2020**, *313*, 113573.
[41] Steinbauer, J., Longwitz, L., Frank, M., Epping, J., Kragl, U., & Werner, T. *Green Chem*, **2017**, *19*(18), 4435-4445.
[42] Zhang, J., Wang, Y. Y., Sun, H., Li, S. Y., Xiang, S. H., & Tan, B. *Sci. China Chem*, **2020**, *63*, 47-54.

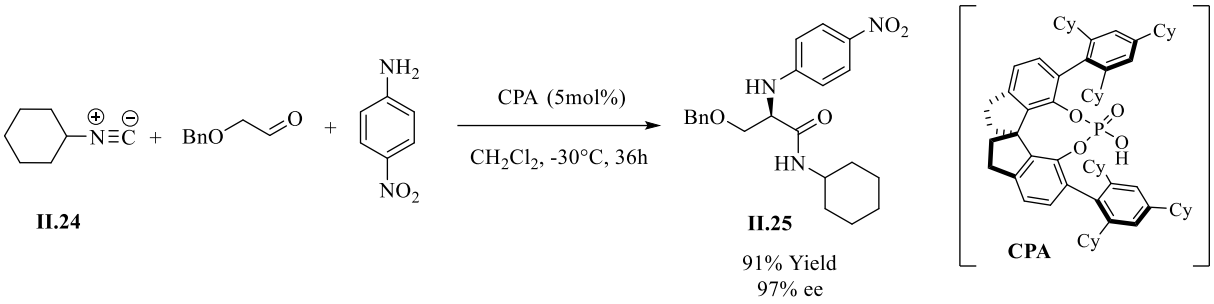

Scheme 12: Enantioselective 3CR-*Ugi* reaction using chiral SPINOL-derived phosphoric acid as catalyst.

b) The *Biginelli* reaction

Hu and co-workers[43]. have reported the one-pot preparation of dihydropyrimidinethiones (DHPMs) **II.27** from aldehydes, benzylthiourea **II.26**, and cyclohexanone via *Biginelli* reaction catalyzed by 10 mol% of chiral TADDOL-derived phosphoric acid, typically derived from enantiopure tartaric acids. After conditions optimization, the results show that a high enantioselectivity observed in chloroform at room temperature. ***(Scheme 13)***

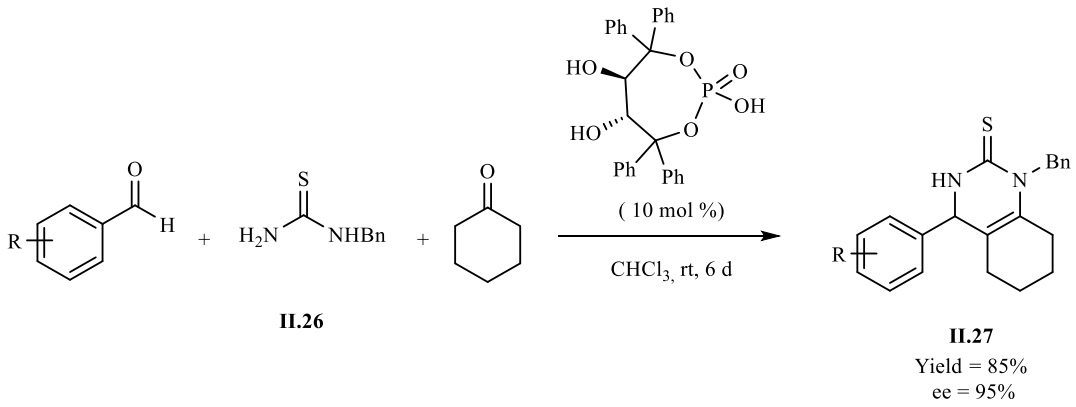

Scheme 13: *Biginelli* reaction catalyzed by a chiral TADDOL-derived of phosphoric acid.

c) Synthesis of azetidines by multicomponent reaction

Recently, *Qian* et *al*.[44] have provided a paradigm for designing of tetrahydroquinoline azetidines **II.30** with high chemo, diastereo, and enantioselectivity through three-component reaction involving anilines, aldehydes, and azetidinones **II.28** in one step. Where they reported the effective contribution of a chiral phosphoric acid (CPA) derived from H8-BINOL **II.29** in catalyzing this reaction to access the desired product with three contiguous stereocenters. **(*Scheme 14)***

[43] Hu, X., Guo, J., Wang, C., Zhang, R., & Borovkov, V. *Beilstein J. Org. Chem*, **2020**, *16*(1), 1875-1880.
[44] Qian, L. L., Hu, Y. C., Min, X. T., Yang, S. N., Shen, B. X., Wan, B., & Chen, Q. A. *Chem Catal*, **2022**, *2*(8), 2024-2033.

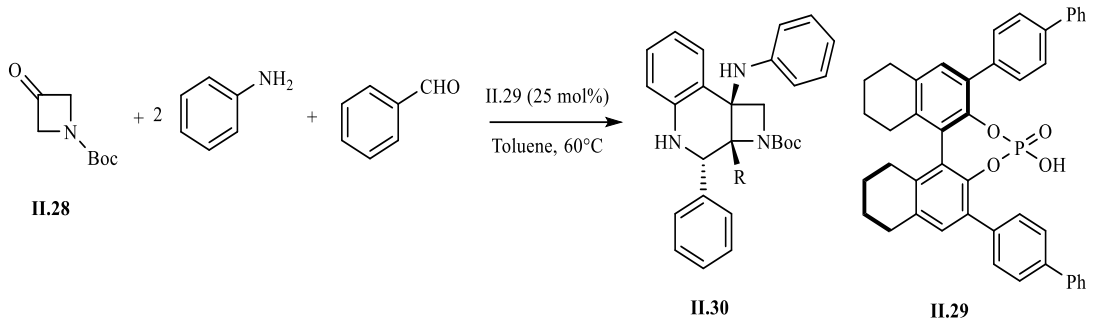

***Scheme 14*:** Synthesis of tetrahydroquinoline azetidines catalyzed by CPA.

d) Multicomponent allylation

Goswami. P et *al.*[45] presented an innovative approach for the synthesis of *α*-tertiary amine (ATA) derivatives **II.33** via multicomponent allylboration in the presence of 4-dodecylbenzenesulfonic acid (DDBSA) as organocatalyst with a squaramide activator (SQA-III). This reaction was carried out with a variety of functionalized ketones, benzhydrazide **II.31**, and allylboronic acid pinacol ester **II.32** under water-rich biphasic condition. The p-p interaction, H-bonding, and hydrophobic interaction resulting from the combination of hydrophobic acid catalyst DDBSA and SQA-III activator made a high chemo-selectivities for this transformation with an excellent yield (>95%). ***(Scheme 15)***

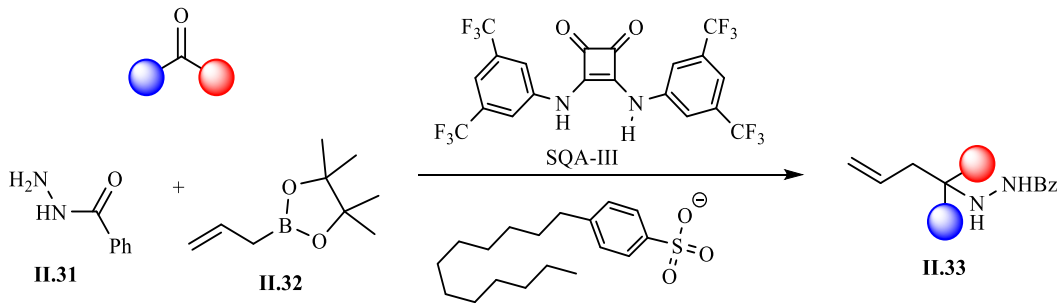

***Scheme 15*:** Multicomponent organocatalytic allylation.

e) DABCO catalyzed synthesis of functionalized curcumin derivatives:

Bhuvaneswari et *al.*[46] have described the effectiveness of utilizing 1,4-diazabicyclo [2.2.2] octane (DABCO) to catalyze for a room temperature three-component reaction of curcumin **II.34**, substituted aromatic aldehydes and malononitrile/ethyl 2-cyanoacetate **II.35** in ethanol. This method yields functionalized curcumin derivatives **II.36** with impressive yields ranging from 80% to 92%. The formation of the cyclohexene ring is orchestrated

[45] Goswami, P., Cho, S. Y., Park, J. H., Kim, W. H., Kim, H. J., Shin, M. H., & Bae, H. Y. *Nat. Commun*, **2022**, *13*(1), 2702..
[46] Bhuvaneswari, K., Sivaguru, P., & Lalitha, A. *ChemistrySelect*, **2017**, *2*(35), 11552-11560.

through a *Knoevenagel*/*Michael*/cyclization sequence catalyzed by DABCO (10 mol%). (***Scheme 16***)

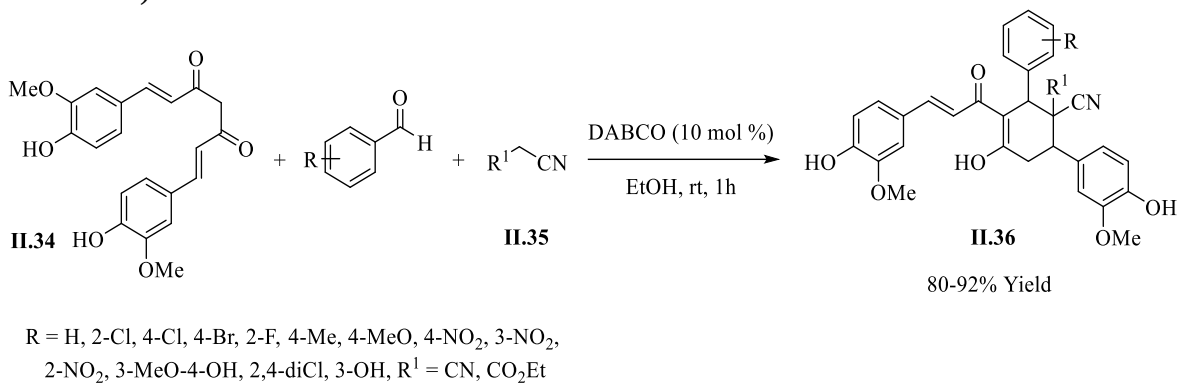

R = H, 2-Cl, 4-Cl, 4-Br, 2-F, 4-Me, 4-MeO, 4-NO_2, 3-NO_2, 2-NO_2, 3-MeO-4-OH, 2,4-diCl, 3-OH, R^1 = CN, CO_2Et

Scheme 16: DABCO catalyzed synthesis of functionalized curcumin derivatives.

f) DMAP catalyzed synthesis of 2-amino-4H-chromenes derivatives

Recently, *Thangallipalli* et *al*.[47] introduced an environmentally friendly pathway for synthesizing 4-chromenes derivatives **II.39** in the presence of DMAP as an organocatalytic in one pot reaction between active methylene compound **II.37**, aromatic aldehydes and resorcinol **II.38** with high yields (up to 98 %) in water. DMAP exhibited efficient recovery and sustained reusability for six cycles without a notable decline in yields. (***Scheme 17***)

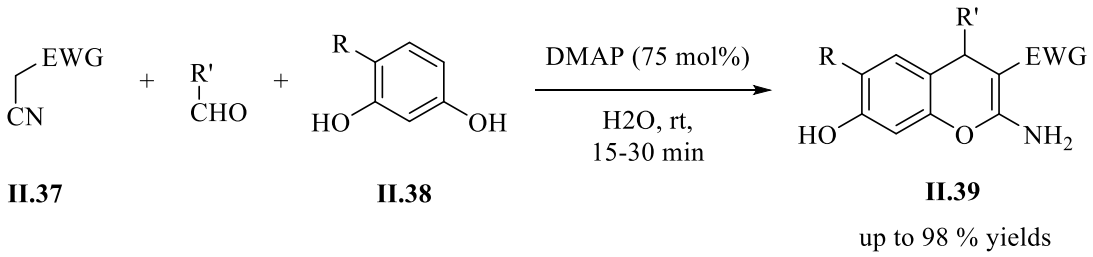

II.37 **II.38** **II.39**

up to 98 % yields

Scheme 17: DMAP- Mediated synthesis of 2-amino-4H-chromenes derivatives.

II-4 Biocatalysis

The biocatalytic process is commonly utilized to describe the conversion of a substrate into a specific target product through one or more enzymatic steps. The term "biocatalysis" encompasses various processes, such as fermentations, biotransformations, and enzyme-mediated reactions. In the purpose of this thesis, we focused on the last one.

II-4-1 Generality on the enzymes

Enzymes are selective macromolecules of protein nature, which possess catalytic activity[48]. These biocatalysts act to specifically accelerate many chemical reactions to rates

[47] Thangalipalli, S., Bandalla, S. G., Gavinolla, V., Panduga, R., & Neella, C. K. *ChemistrySelect*, **2023**, *8*(29), e202302065.
[48] Donald Voet, Judith G. Voet Biochimie, De Boeck Université, Bruxelle. **1998**.

more than 10^{16} times than of uncatalyzed levels without themselves being altered by the reaction. Enzymes are polypeptides present in the cells of all living organisms, characterized by a high molecular mass ranging from 10,000 Da to 1,000,000 Da approximately. They consist of several α-amino acids of the L series linked together by an amide bond, which result from the condensation of the carboxyl group of one amino acid with the amine group of another.

The sequence of amino acids of a protein, i.e. the order in which these are arranged forms the primary structure. As soon as the primary structure folds in on itself, it constitutes the secondary structure. This structure is stabilized through the generation of hydrogen bonds and constitute of primary types: the alpha helix and the beta sheet. The three-dimensional arrangement of these secondary structural elements relative to each other forms a tertiary structure, which stabilizes by disulfide bridges and confers the biological function to a protein. The association of different tertiary units forms the quaternary structure which can be described for very large enzymes[49]. For example, hemoglobin is a tetrameric protein resulting from the assembly of 4 monomers[50]. ***(Figure 6)***

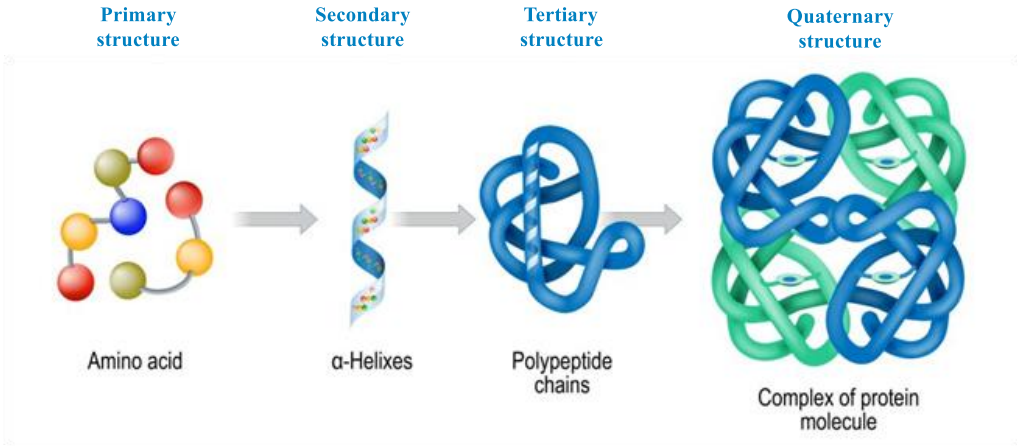

***Figure 6*:** Structure of enzymes.

The important part of the enzyme is the active site. This particular region is made up of a small number of amino acids where the substrate binds through several weak chemical bonds, which can then be subjected to the action of the enzyme in order to transform it into a product.

[49] https://www.nfpt.com/blog/mixology-101-combining-protein-powder-with-hot-liquids.
[50] C. Vollhardt, « Traité de Chimie organique », DeBoeck université, Traduit par P. Depovere, 2ème édition, Bruxelles, **1994**.

The active site is subdivided into two parts[51]:

- **The recognition site:** it recognizes shape complementarity with an enzyme-specific substrate.
- **The catalytic site:** it allows the reaction transforming the substrate into a product.

The three-dimensional structure or the ionization state of this site, is influenced by factors such as pH or temperature, strongly affecting the enzymatic activity.

Catalytic active sites, specific regions on the enzyme surface, create a distinctive reaction environment. Typically, the active site is nestled at the terminus of a channel lined with robust and aromatic amino acids, regulating the entry of substrates and solvents. As a result, the amino acid composition within the channel varies depending on the enzyme type.

The mechanism of enzymatic catalysis has been determined; two models have been proposed to explain the specificity of enzymes with respect to the substrate:

- **Key-lock model (1890):** *Fischer* suggested that the substrate's conformation perfectly complements the shape of the enzyme's active site.
- **Induced fit model (1958):** *Koshland* proposed that enzyme and substrate mutually fit their respective shapes.[52] ***(Figure 7)***

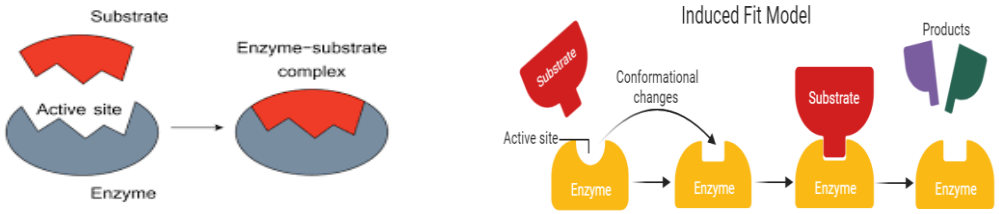

***Figure 7*:** Lock and key model and Induced fit model.[53]

II-4-2 Mode of action of enzymes

Enzymes catalyze the reactions of transformation of substrates (s) into products (p) in a very short time (fractions of seconds). They accelerates the speed of the reaction without modifying the equilibrium state by lowering the activation energy required for substrate. The first step implies the creation of an enzyme-substrate complex and the specificity of a

[51] Pelmont, J. Presse Universitaire de Grenoble, **1995**, 7, 652–654.
[52] R. A. Copeland; « Enzymes: A Practical introduction to structure, Mechanism, and Data Analysis ». 2nd edition., Weiley-VCH, Inc. **2000**, 62, 149, 175.
[53]https://microbenotes.com/enzymes-properties-classification-and-significance/#mechanism-of-action-of-enzymes.

substrate by reciprocal interactions/adaptation via bonds of low types of types: *Van Der Waals*; Electrostatics; Hydrogen bridges.

Enzymes also stabilize the transition state and ensure the transformation of the substrate into product, which is then released with the enzyme.

About a third of known enzymes use metal ions as cofactors such as: Cu^{2+}, Zn^{2+}, Mn^{2+} or Co^{3+}. Cofactors are chemical bodies that necessarily intervene in an enzymatic reaction to transport or complete a substrate and accept a product. Some cofactors are more complex molecules synthesized by cells: called coenzymes.[54]

II-4-3 Classification of enzymes

Since **1961**, the International Union of Biochemistry and Molecular Biology (IUBMB) has organized enzymes into six distinct groups, classifying them according to the specific types of reactions they catalyze. ***(Figure 8)***.

a) Transferases: These enzymes transfer radicals or groups of atoms from a molecule (donor substrate) to a molecule (acceptor substrate) such as methyl, ethyl, carbon group comprising aldehyde or ketone functions (- CHO) or (- CO – R) amine group (NH2). Example: Phosphofructokinase, and L-aspartate-aminotransferase.

b) Oxido-reductases: Enzymes that catalyze redox reactions, and they require the presence of a coenzyme (NAD, NADP, FAD or FMN). Most of these enzymes are dehydrogenases, others are oxidases, peroxidases, reductases...

c) Hydrolases: This class of enzymes is the most used because it does not require a coenzyme, like proteases and peptidases. They allow the hydrolysis of esters, anhydrides, glycosides, amides by cleaving C-C, C-O, and C-N bonds and fix the H and OH radicals of the water on the valences released.

d) Isomerases: They catalyze structural changes in the same molecule without changing its overall formula (isomerization, cis – trans, epimerization, displacement of radicals, etc.).

e) Lyases: Isocitrate glyoxylate lyase represents an example of this type of catalysts, these enzymes promote HX additions on double bonds such as C=C, C=N, C=O and their reverse process.

f) Ligases: They allow the formation of C-C, C-N, C-S, and CO-O-P bonds through the use of ATP. For example pyruvate carboxylase.

[54] B. Augère, "Les enzymes biocatalyseurs protéiques". Ell. Edi. Mark, **2001**.

Hydrolases, constituting 60% of the enzymes utilized in industry, play a pivotal role in processes involving the resolution of racemic mixtures. Within this category, lipases emerge as the most prevalent enzymes employed for resolving racemic mixtures of alcohols, acids, amines, and other compounds.[55]

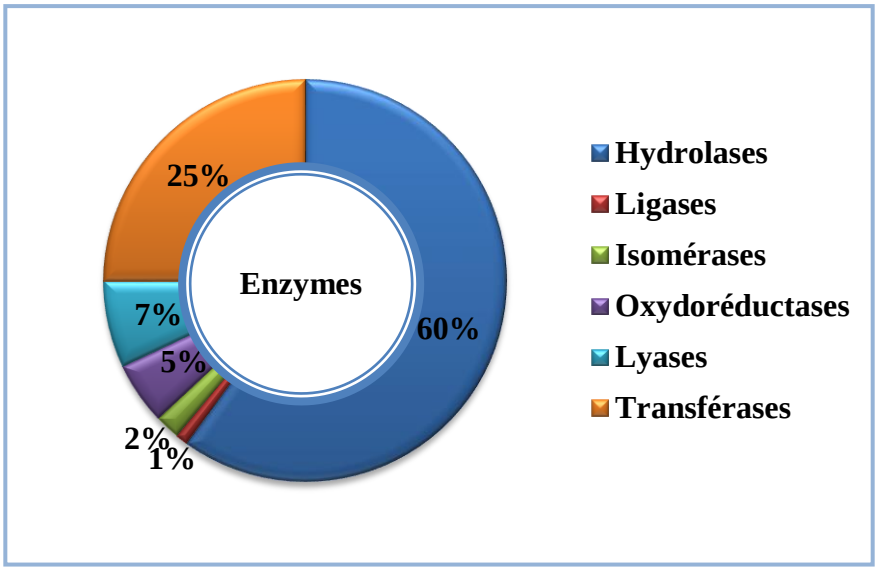

***Figure 8*:** Classification of enzymes.

II-4-4 Lipases in organic chemistry

The hydrolases, especially lipases are the most practical in organic transformation for organic transformations due to their numerous advantages. They are user-friendly, biodegradable, and efficient with minimal waste. Their independence from co-factors, stability in both aqueous and organic solvents, and remarkable *chemo-*, *regio-*, and *enantio-*selectivity contribute to their appeal. Furthermore, their versatility with various substrates and conditions makes them valuable tools in organic synthesis, enabling the creation of greener and more sustainable processes.[56]

II-4-4-1 Unconventional uses of lipases (lipase promiscuity)

Enzyme promiscuity refers to the capacity of enzymes to catalyze alternative reactions that deviate from their natural physiological functions. *Hult* and *Berglund*[57] categorized enzyme promiscuity into three primary categories:

[55] **(a)** J. E. Puskas, K. S. Seo, M. Y. Sen, *Eur. Polym. J*, **2011**,47,524-534 ; **(b)** S. Sen, & J. E. Puskas,*Molecules*, 2015,20(5), 9358-9379. (c) S. H. Krishna, *Biotechnol. Adv.*, **2002**, 20, 239-267.
[56] Sheldon, R. A., Brady, D., & Bode, M. L. *Chem. Sci. J*, **2020**, *11*(10), 2587-2605.
[57] (a) Hult, K., & Berglund, P. *Trends Biotechnol*, **2007**, *25*(5), 231-238. (b) Kapoor, M., & Gupta, M. N. *Process Biochem*, **2012**, *47*(4), 555-569.

- Enzyme condition promiscuity: This involves the enzyme's capability to catalyze reactions under unconventional conditions, such as anhydrous media, extreme temperatures, or pH levels.
- Enzyme substrate promiscuity: Enzymes with substrate promiscuity can efficiently use a diverse range of substrates to perform a similar chemical reaction, showcasing broad substrate specificity.
- Enzyme catalytic promiscuity: This type of promiscuity involves the active site's ability to catalyze chemically distinct transformations. These transformations may differ in the type of bond making/bond breaking and/or the catalytic mechanism employed for these processes.

The enzyme catalytic promiscuity is extensively applied for several organic synthesis to catalyze: C-C, C-N, C-P bonds formation.

The versatile (promiscuous) utilization of lipases is instrumental in various crucial organic reactions, encompassing Aldol condensation, *Hantzsch* reaction, *Canizzaro* reaction, *Mannich* reaction, *Baylis-Hillman* reaction, *Knoevenagel* condensation, *Michael* addition, *Ugi*, *Biginelli* and other processes, including the *Kabachnik-Fields* reaction.[58] Herein, we can sited some examples:

a) Synthesis of 4H-chromenes derivatives via a MCR catalyzed by lipase:

Zhang et *al*[59]. have reported the synthesis of series of indanolyl 4H-chromenes **II.40** via 3MCR catalyzed by *Mucor miehei* lipase (MML) in [EMIM][BF4] as an ionic liquid at 30°C (***Scheme 19***). The obtained products are recovered with high yields (77–98%).

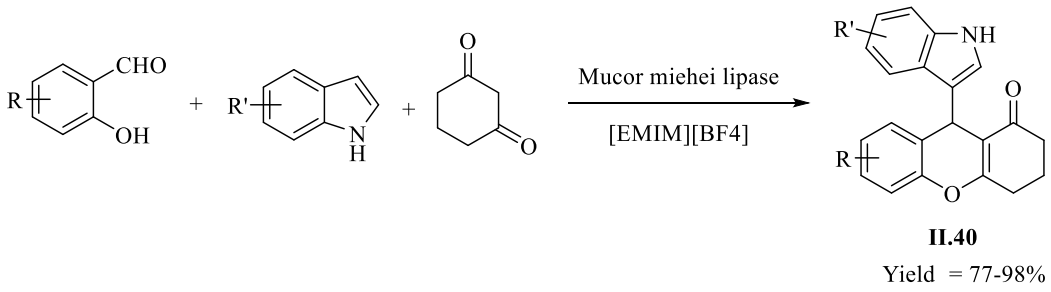

II.40

Yield = 77-98%

Scheme 19: Synthesis of indanolyl 4H-chromenes via MCR catalyzed by lipase.

[58] (a) Dwivedee, B. P., Soni, S., Sharma, M., Bhaumik, J., Laha, J. K., & Banerjee, U. C. *ChemistrySelect*, **2018**, *3*(9), 2441-2466. (b) L Eremeev, N., & Y Zaitsev, S. *Mini-Rev. Org*, **2016**, *13*(1), 78-85.

[59] Zhang, W., Zhao, Z., Wang, Z., Guo, C., Wang, C., Zhao, R., & Wang, L. *J Catal* , **2017**, *7*(6), 185.

b) One-Pot *Knoevenagel–Phospha–Michael* reaction catalyzed by lipase:

Recently, an eco-freindly synthesis method for *β*-phosphonomalononitriles **II.41** in the presence of benzaldehyde, cyanide derivatives and diethylphosphite in a one-pot lipase-catalyzed *Knoevenagel*–phospha–*Michael* reaction[60]. Among various lipases screened, Candida cylindracea (CCL) lipase emerged as an efficient, recyclable catalyst, enabling the production of a series of target compounds with yields varying from 43% to 93% (***Scheme 20***).

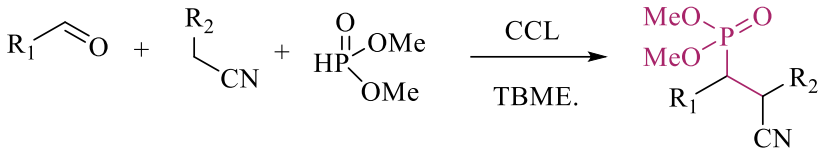

R_1 = alkyl, aryl, 2-furyl, 2-thiophenyl
R_2 = CN, CO_2Et

II.41
Yield = 43-93%

***Scheme 20*:** CCL catalyzed the synthesis of *β*-phosphonomalononitriles.

c) Lipase-catalyzed *Kabachnik-Fields* reaction:

Koszelewski et *al*[61]. introduced a novel approach for synthesizing important α-aminophosphonate derivatives **II.42** using a lipase-catalyzed *Kabachnik-Fields* reaction, achieving impressive yields of up to 93%. Among the examined lipases, the *Porcine pancreas* lipase (PPL) exhibited the best affinity to achieve this MCR at 25°C. (***Scheme 21***)

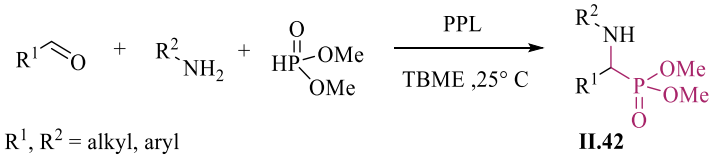

R^1, R^2 = alkyl, aryl

II.42

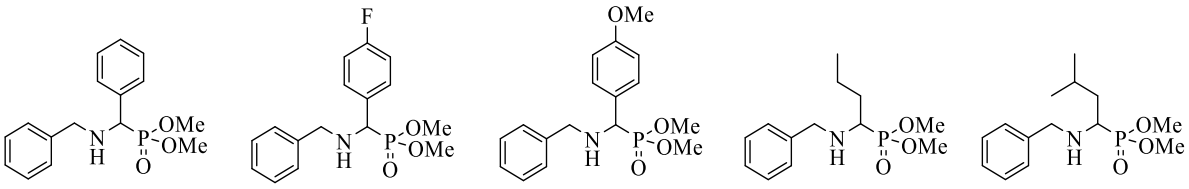

91% 84% 87% 71% 63%

Scheme 21: Synthesis of *α*-aminophosphonates catalyzed by PPL.

[60] Samsonowicz-Górski, J., Koszelewski, D., Kowalczyk, P., Śmigielski, P., Hrunyk, A., Kramkowski, K., & Ostaszewski, R. *Int. J. Mol. Sci*, **2022**, *23*(15), 8819.
[61] Koszelewski, D., Kowalczyk, P., Śmigielski, P., Samsonowicz-Górski, J., Kramkowski, K., Wypych, A., & Ostaszewski, R. *J. Mater*, **2022**, *15*(11), 3846.

II-4-4-2 Conventional use of lipases:

Lipases are commonely used for the preparation of enantiopure compounds through kinetic resolution of racemates (hydrolysis, esterification, transesterification and interesterification) or the enantioselective desymmetrization of meso compounds due to their good stereoselectivity, especially, in organic solvents (***Figure 9***).

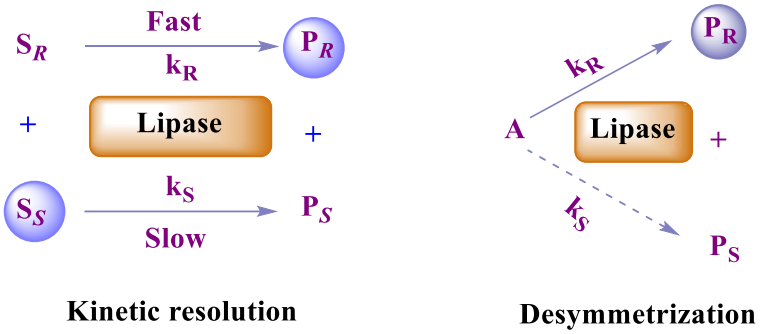

Figure 9: Lipase mediated kinetic resolution versus desymmetrization.

The kinetic resolution of racemates is the most applicable in the industrial scale for their simplicity.

II-4-6 Scopes on the lipase catalyzed kinetic resolution of phosphorous compounds

a) Lipase catalyzed KR of hydroxymethylphosphonates:

Huijuan et *al*[62]. reported the transesterification of racemic *α*-hydroxymethylphosphonates **II.43** by means of lipase from *Pocine Panceas* (PPL) and that using vinyl acetate as acyl donor at 37°C. All furnished (*S*)-acetates are recovered in up to 49% yield and 83% *ee*. The EKR was achieved with selectivity factor E< 40. (**Scheme 22**)

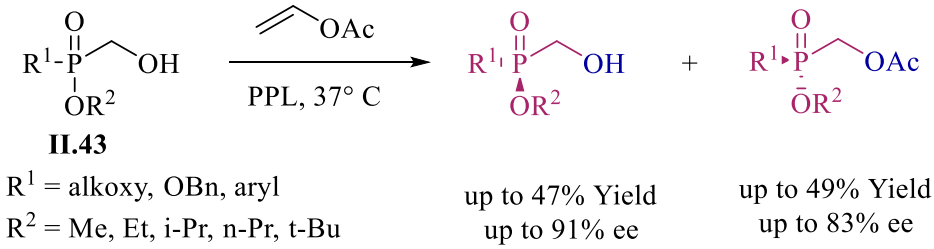

Scheme 22: PPL-catalyzed acylation of racemic *α*-hydroxymethylphosphonates.

[62] Huijuan, H., Qiaoli, Y., Xiaogang, L., Qifan, Y., Chengxin, P., Hongmei, W., & Runli, G. *Chinese J. Org. Chem*, **2023**, *43*(8), 2815.

b) Lipase catalyzed KR of α-hydroxyphosphonates:

In another investigation, *Hu* and co-workers[63] conducted an investigation on the acylation of a set of racemic *α*-hydroxyphosphonates **II.44** by employing lipase CAL-B as the biocatalyst and vinyl acetate as the acyl donor. The researchers noted that the catalytic efficiency and enantioselectivity of CALB varied based on the *α*-carbon substituents. The recovered S-acetates exhibited yields of approximately 50% and an enantiomeric excess (ee) exceeding 99%. (***Scheme 23***).

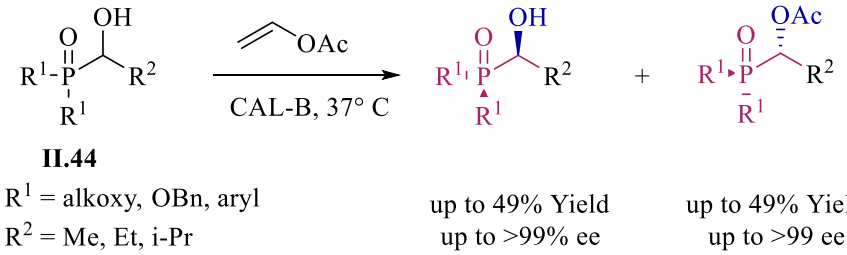

II.44

R^1 = alkoxy, OBn, aryl

R^2 = Me, Et, i-Pr

up to 49% Yield
up to >99% ee

up to 49% Yield
up to >99 ee

Scheme 23: Lipase catalyzed KR of *a*-hydroxyphosphonates.

c) Lipase catalyzed KR Dimethyl and Dibutyl 1-Butyryloxy-1-carboxymethylphosphonates

Majewska et *al.*[64] has reported the enantioselective hydrolysis racemic dimethyl and dibutyl 1-butyryloxy-1-carboxymethylphosphonates **II.45** using the lipases from *Candida rugosa*, *Candida antarctica*, and *Aspergillus niger*. The kinetic resolution leading to optically active dimethyl 1-carboxy-1-hydroxymethylphosphonate **II.46** (58%–98% enantiomeric excess) with high enantiomeric ratio (reaching up to 126). However, during the hydrolysis of dibutyl 1-butyryloxy-1-carboxymethylphosphonate, the best results were obtained by lipases from *Burkholderia cepacia* and *Termomyces lanuginosus*, and leading to optically active dibutyl 1-carboxy-1-hydroxymethylphosphonate (66%–68% enantiomeric excess) with moderate enantiomeric ratio (reaching up to 8.6). (***Scheme 24***)

[63] Hu, H. J., Gao, R. L., Yang, Q. F., Huang, Y. P., Wang, H. M., & Pei, C. X. *New J Chem*, **2022**, *46*(17), 7987-7991.
[64] Majewska, P. *J Catal*, **2021**, *11*(8), 956.

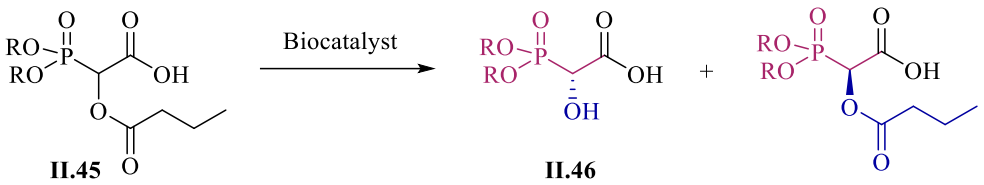

Scheme 24: Lipase catalyzed hydrolysis dimethyl and dibutyl 1-butyryloxy-1-carboxymethylphosphonates.

Conclusion

In the present chapter we have highlighted the importance of the MCRs as greener processes able to create a huge library of bioactive molecules starting by simple reagents to obtain multifunctional compounds containg various bond type. We have also reviewed the catalytic aspect of these reactions that allow to implanted rapid access to bioactive molecules by improving existing synthetic pathways by reducing the number of steps. In addition, some pointed examples of organocatalytic used in MCRs, and the biocatalytic was also underlined using different conditions conventional and unconventional medium. It is important the indicate that the both organocatalytic and biocatalytic classes exhibit high added values to standard MCRs, in term of high selectivity in shortened times.

.

Chapter III

Design of experiments, density functional theory and molecular docking

Introduction

Cheminformatics is a relatively new field of information technology that focuses on the collection, computational, analysis, and manipulation of chemical data. The chemical data of interest typically includes information on small molecule formulas, structures, properties, spectra, and activities (biological or industrial).[1] The global cheminformatics Market Size was estimated at USD 5.5 billion in 2022 and it is projected to grow from USD 6.35 Billion in 2023 to USD 20.11 billion by 2032, with an annual growth rate (CAGR) of 15.5% during the forecast period (2023 - 2032).[2] Cheminformatics originally emerged as a way to predict the outcome of chemical phenomena with the advent of high throughput drug screening and the need for million-compound chemical libraries, it is a powerful discipline that unveils the secrets of molecules and plays a pivotal role in various industries, especially in drug discovery and pharmaceutical development.[3] On the other hand, the technique of experimental design as statistical method still useful way aided to explore several parameters simultaneously in a relatively small number of experiments.[4]

The intent of this chapter is to show some introduction into the field of cheminformatics and how cheminformatics can enhance much of what is currently done in bioinformatics using the synthesized compounds as small molecules.

We have exploring the pivotal components of cheminformatics using the design of experiments, density functional theory (DFT) and molecular docking, which are the three pillars investigated in this thesis.

The following lines are dedicated to outline a comprehensive exploration of these fascinating domains, paving the way for a deeper understanding of the intricate world of molecules and the vital role they play in various scientific disciplines.

III-1 Design of experiments

III-1-1 Generality on design of experiments (DOE)

Design of experiments (DOE) was developed in the early **1920**s by the mathematician *Sir Ronald Fisher* following his employment, in **1919** at the *Roth Amsted* agricultural field

[1] (a) David S. Wishart Current Protocols in Bioinformatics. **2007** 14.1.1-14.1.9. (b) Raslan, M. A., Raslan, S. A., Shehata, E. M., Mahmoud, A. S., & Sabri, N. A. *Pharm*, **2023,** *16*(7), 1050.
[2] https://www.marketresearchfuture.com/reports/cheminformatics-market-11552
[3] Schlotterbeck, G., Ross, A., Dieterle, F., and Senn, H. Pharmacogenomics**, 2006**, 7:1055- 1075
[4] Murray, P. M., Bellany, F., Benhamou, L., Bučar, D. K., Tabor, A. B., & Sheppard, T. D. *Org & biom chem*, **2016**, *14*(8), 2373-2384.

research station in London[5]. His primary focus was to investigate the impact of different fertilizers and the effect of other factors (such as underlying soil condition, moisture content of the soil, etc.) on agricultural outcomes for various plots of land[6]. Since then, a number of successful applications of DOE have been reported by many US and European manufacturers. After **1940**, the concept of experimentation expanded as new other concepts emerged such as the *Plackett* and *Burman* plans[7], the response surface [8-9], the optimal plans[10]...etc.

A design of experiment is a statistical approach derived from simple mathematical notions used to optimize the choice of tests and that of their sequence during the experiment[11]. It is a systematic and comprehensive method to understanding the relationship between input variables (X) called factors and the output or answer (Y) of a system ***Figure 1***, wich it is expressed by $Y = f(x_i)$[12]. Its principle consists in simultaneously varying the levels of one or more factors at each test in order to identify the optimal combination of factor levels that produces the desired answer[13].

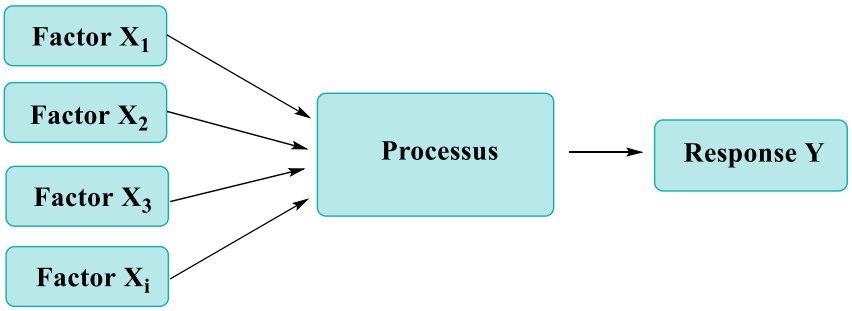

Figure 1: Plans of experiments.

III-1-2 Basic vocabulary of experimental designs

III-1-2-1 Factors

In the design of experiments, a factor refers to a variable which are potentially influence the outcome of an experiment or study. Factors can be qualitative (categorical) or quantitative (continuous), and that can be manipulated or controlled by the experimenter. The factors are limited by two bounds, lower (low) and upper (high). The low level is designated by the sign (-1) and the high level by the sign (+1). The set of all the values that the factor can

[5] Tinsson, W. **2010**, (Vol. 67).
[6] Antony, J. Elsevier. **2023**.
[7] Plackett, R. L., & Burman, J. P. *Biometrika*, **1946**, *33*(4), 305-325.
[8] Box, G. E. *Biometrika*, **1952**, *39*(1-2), 49-57.
[9] Box, G. E. P., & Wilson, K. B. *J R Stat Soc*, **1951**, *13*(1), 1-45.
[10] Kiefer, J. *J R Stat Soc*,***1959***, *21*(2), 272-304.
[11] Gilman, J., Walls, L., Bandiera, L., & Menolascina, F. *Synth. Biol*, **2021**, *10*(1), 1-18.
[12] Dagnelie, P. *Revue Modulad*, **2008**, *38*, 13-36.
[13] Pierre, C. *Revue: Contrôles-Essais-Mesures*, **2005**, 69-72.

take between the low level and the high level is called the domain of variation of the factor or the domain of the factor[14]. (***Figure 2***).

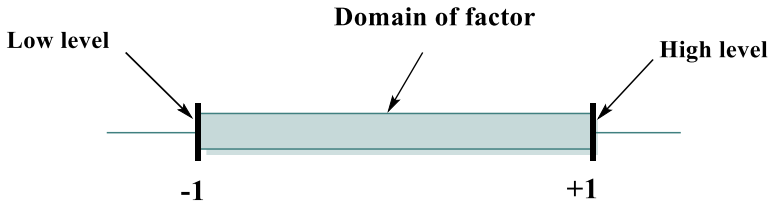

Figure 2: Domain of variation of the factor.

III-1-2-2 Response

The term "answer" refers to the outcome or dependent variable being measured or observed in an experiment. It represents the quantity or characteristic that researchers are interested in studying or optimizing[15].

III-1-2-3 Experimental field and field of study

The experimental domain is the space represented by the axes of the factors which are orthogonal to each other. Moreover, the field of study is the particular zone of the experimental space chosen by the experimenter to carry out his tests. This domain is defined by the high and low levels of each factor.[16] (***Figure 3***)

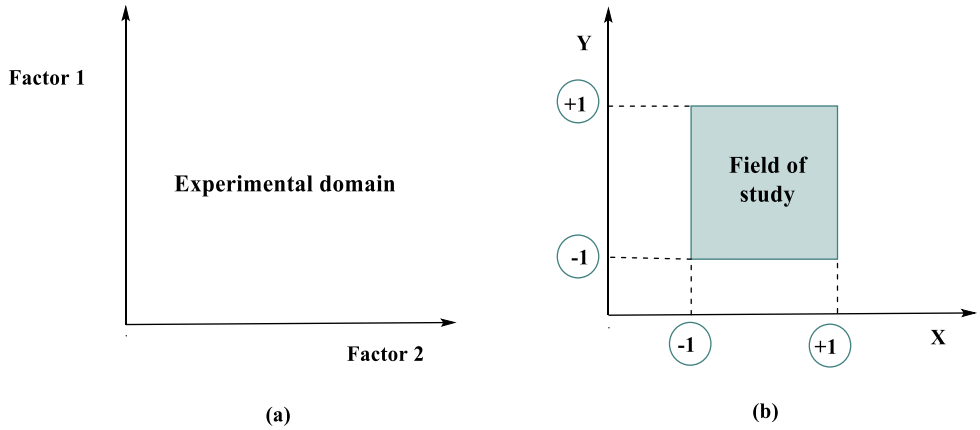

Figure 3: The experimental domain (a) and definition of the field of study (b).

[14] J.J. Rousselle, Thèse de doctorat. Les contours actifs, une méthode de segmentation application à l'imagerie médicale. Université François Robelais, **2003**.
[15] Droesbeke, J. J., Fine, J., & Saporta, G. Editions technip.**1997**.
[16] Goupy, J. P*lans d'expériences*. Ed. Techniques Ingénieur. **2006**.

III-1-3 Application of DOE

III-1-3-1 In pharmaceuticals

In pharmaceutical research, DOE are used to optimize the formulation development of Silver sulfadiazine drug[17], in clinical trial design[18], and to excipients variability on drug product quality attributes of Theophyline drug[19]. In addition, DOE help to identify the critical factors influencing drug efficacy, stability, and safety. It is also applied in Ibuprofen drug to determine the optimal combination of drug ingredients and their levels to achieve desired therapeutic outcomes while minimizing side effects[20-21].

III-1-3-2 In biological and biotechnological

DOE finds a various applications in biological and biotechnological processes, for example the optimization of high performance liquid chromatography separation of neuroprotective peptides wich used by *Novotna* et *al*[22], to optimize a plasmid DNA purification process, and in enzyme production[23]. Overall, DOE provides a systematic and statistical approach to studying the influence of multiple factors on biological systems, for example; the selection of main variables for improving *Tetrahymena thermophila* growth[24], in optimization of the production of poly (γ -glutamic acid) by *Bacillus licheniformis* CCRC 12826[25], in fermentation processes[26], and for production of antifungal and antibiotic compounds by *Thermomonospora sp* MTCC 3340 reported by *M. Gupte* et *al*.[27]

III-1-3-3 In industrial

The versatility and power of DOE in industrial allow improving product quality and enhancing efficiency. We find its application for treatment of plasticized PVC to reduce plasticizer/solvent migration[28], analysis of absorption-dehumidification processes[29], and optimization of mechanical properties of polymer concrete and mix design[30].

---

[17] Kumar, P. M., & Ghosh, AEur. *J. Pharm. Sci*. **2017**, *96*, 243-254.
[18] Khanam, N., Alam, M. I., Ali, Y., & Siddiqui, A. U. R. *Int J App Pharm*, **2018**, *10*(2), 7-12.
[19] Wong, S. N., Weng, J., Ip, I., Chen, R., Lakerveld, R., Telford, R.,& Chow, S. F. *Pharm*, **2022**, *14*(2), 300.
[20] Sütő, B., Weber, S., Zimmer, A., Farkas, G., Kelemen, A., Budai-Szűcs, M., & Csányi, E. *Chem. Eng. Res. Des*, **2015**, *104*, 488-496.
[21] Salunkhe, S. S., Bhatia, N. M., Thorat, J. D., Choudhari, P. B., & Bhatia, M. S. *Pharm. Investig* **2014**, *44*, 273-290.
[22] Novotná, K., Havliš, J., & Havel, J. *Chromatogr A*, **2005**, *1096*(1-2), 50-57.
[23] Eon-Duval, A., Gumbs, K., & Ellett, C. *Biotechnol. Bioeng*, **2003**, *83*(5), 544-553.
[24] De Coninck, J., Leclercq, B., Exbrayat, J. M., & Duyme, F. *J. Ind. Microbiol. Biotechnol*, **2004**, *31*(5), 204-208.
[25] Lungmann, P., Choorit, W., & Prasertsan, P. *Electron. J. Biotechnol*, **2007**, *10*(1), 1-11.
[26] Agbogbo, F. K., Ramsey, P., George, R., Joy, J., Srivastava, S., Huang, M., & McCool, J. *J. Ind. Microbiol. Biotechnol.* **2020**,*47*(9-10), 789-799.
[27] Gupte, M., & Kulkarni, P. *Environ & Clean Technol*, **2003**, *78*(6), 605-610.
[28] Fugit, J. L., Taverdet, J. L., Gauvrit, J. Y., & Lanteri, P. *Polym. Int*, **2003**, *52*(5), 670-675.
[29] Lai, M. H., Chang, Y. N., Wang, C. M., Wu, H., & Chung, T. W. *Sep Sci Technol* **2003**, *38*(11), 2447-2464.
[30] Muthukumar, M., & Mohan, D. *J. Appl. Polym. Sci*,**2004**, *94*(3), 1107-1116.

III-1-4 Types of experimental designs

There are three main families of experimental designs: mixing designs, screening plans and modeling plans or response surfaces (***Figure 4***).

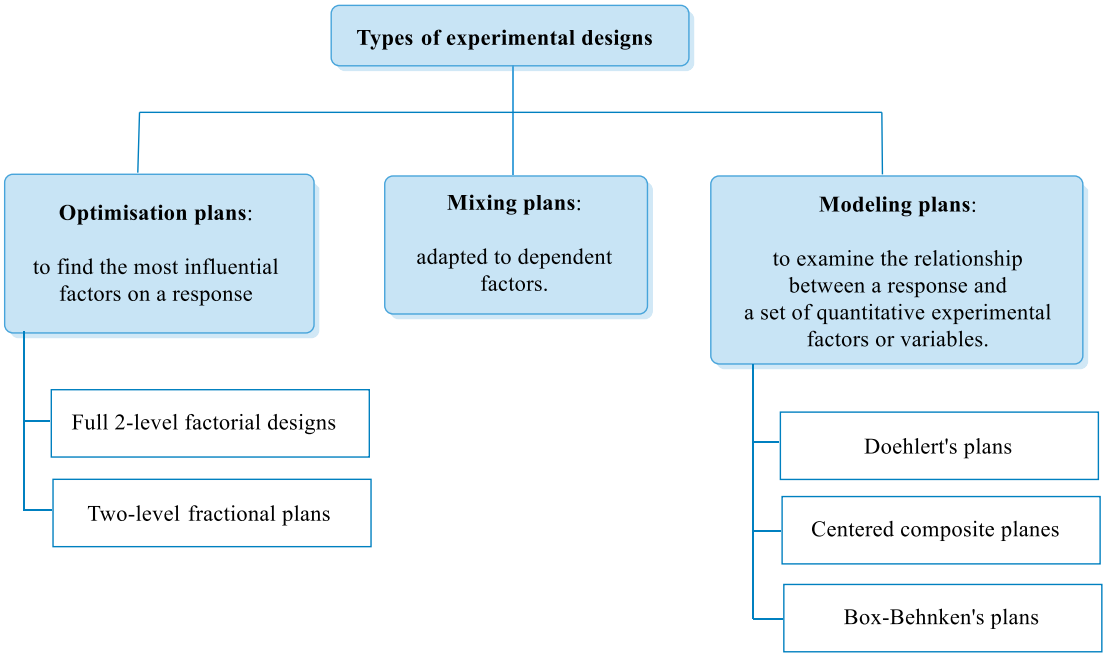

Figure 4: Different types of experimental designs.

In this context, our primary objective was to assess the emphasis on full factorial designs as an essential step in advancing our research.

III-1-5 Full factorial plan

The full factorial plans are the most used because they are the fastest and the easiest to implement. This factorial plan kind, each factor is studied at two distinct levels which delimit the field of factor study. We will therefore have 2^k (k is the number of factors) trials in total. These plans make it possible to study both the main effects of each factor and the interactions between the factors, in which the ***Figure 5*** graphically shows a complete three-factor factorial design. The experimental points will be at the cube vertices[31].

[31] Addelman, S. *Technometrics*, **1969**, *11*(3), 477-509.

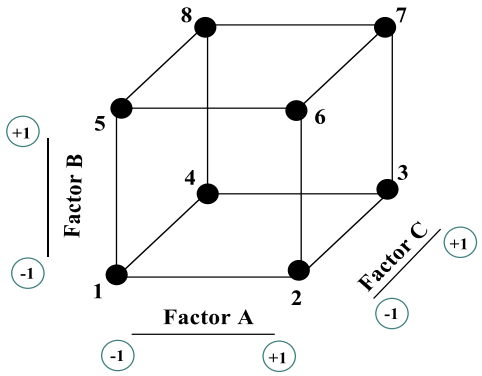

Figure 5: Full factorial plan 2^3

III-1-5-1 Experiment matrix

An experiment matrix refers to a structured table represents in coded or uncoded form, that outlines all possible combinations of factor levels to be tested in an experiment. It is made up of (n) rows corresponding to the (n) experiments to be carried out and (k) columns, corresponding to the (k) variables studied. For example, consider an experiment with three factors: A, B and C, each with two levels (low (-1) and high (+1)). The first column of the experience table is filled according to the formula 2^{K-1} with k = 1, i.e. $2^0 = 1$, or for factor A (high level = 5 and low level = 1) a sequence of -1, + 1, -1, +1, etc. The second column is filled according to the same rule, either 2^{k-1} with k = 2, hence $2^1 = 2$, or for factor B ((-1) = 10 and (+1) = 20) a series of 2 signs (-) followed by 2 signs (+): -1, -1, +1, +1, -1, -1, etc. The third column is filled in analogously[32]. The ***Table 1*** shows the experiment matrices for this example in coded and uncoded form.

Table 1: Experience matrix for a full factorial design 2^3.

Coded					Uncoded				
	Factor A	**Factor B**	**Factor C**	**Response**		**Factor A**	**Factor B**	**Factor C**	**Response**
Exp	X_1	X_2	X_3	Y	**Exp**	X_1	X_2	X_3	Y
1	-1	-1	-1	Y_1	**1**	1	10	4	Y_1
2	+1	-1	-1	Y_2	**2**	5	10	4	Y_2
3	-1	+1	-1	Y_3	**3**	1	20	4	Y_3

[32] Jung, Y., Lee, I. *Reliab. Eng. Syst. Saf.* **2021**, *216*, 107968.

4	+1	+1	-1	Y_4	**4**	5	20	4	Y_4
5	-1	-1	+1	Y_5	**5**	1	10	16	Y_5
6	+1	-1	+1	Y_6	**6**	5	10	16	Y_6
7	-1	+1	+1	Y_7	**7**	1	20	16	Y_7
8	+1	+1	+1	Y_8	**8**	5	20	16	Y_8

Factor	Low	High
A	1	5
B	10	20
C	4	16

III-1-5-2 The mathematical model

This model is also called postulated or a priori model, it is a mathematical relationship that shows the change in a response produced by the change of one or more factors[33]. The purpose of modeling the response by a mathematical model is to be able to calculate then all the answers of the field of study without being obliged to do the experiments[34]. The model can be represented as:

$$y = a_0 + \sum_{i=1}^{k} a_i x_i + \sum\sum_{i<j}^{k} a_{ij} x_i x_j + \varepsilon \qquad (1)$$

Where:

y : represents the response variable.

a_0 : represents the theoretical response.

x_i, x_j : represent the factors (input variables).

a_i, a_j: are the coefficients that quantify the effect of each factor.

ε : represents the error term.

Theoretical response: is the average of the responses observed at levels -1 and +1.

Where:

$$a_0 = \frac{y_1 + y_2 + y_3 + y_i}{n_i} \qquad (2)$$

n_i: number of experiments studied.

[33] Allen, T. T. *Springer Sci. Rev.* **2006**.
[34] Gendre, L., Soulier, B., & Savary, A. **2009**.

III-1-5-3 Factor effect

Corresponds to the variation of the response **y** when **x** changes from a value at level -1 to another value at level +1[35]. For example, in **a** two-factor factorial design, the estimated effect of factors a_1 and a_2 is as follows:

$$a_1 = \frac{-y_1 + y_2 - y_3 + y_4}{4} \qquad (3)$$

$$a_2 = \frac{-y_1 - y_2 + y_3 + y_4}{4} \qquad (4)$$

III-1-5-4 Interaction Effect

In the context of experimental design, the effects of interactions in a full factorial design refer to the combined impact of two or more independent variables on the dependent variable of interest[36]. This interaction is reflected on a diagram by the fact that the two straight lines are not parallel. The further the lines deviate from the parallel, the greater the degree of interaction, as shown in ***Figure 6***.

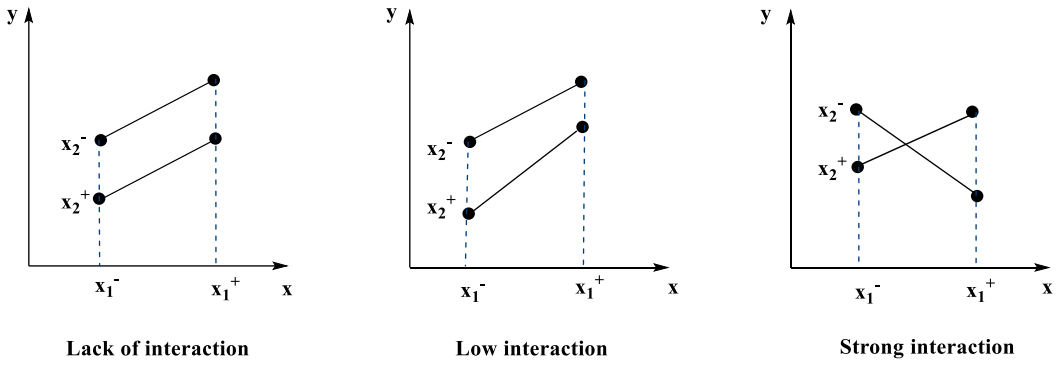

Figure 6: Illustration of an interaction.

We take the previous example to calculate the effect of an interaction for a complete factorial design for two factors. The matrix of main effects and interaction effects is shown in ***Table 2***.

Table 2: Matrix of experiments with effects for a full factorial design 2^2.

Exp	Average	X_1	X_2	X_1X_2	Response (y_i)
1	+1	-1	-1	+1	Y_1
2	+1	+1	-1	-1	Y_2

[35] Kazemi, K., Zhang, B., Lye, L. M., Cai, Q., & Cao, T. *J. Waste Manag*, **2016**, *58*, 107-117.
[36] Agudelo, C., Vedula, R. T., Capecelatro, J., & Wang, Q. *SAE Tech. Pap*. **2019**, 01, 2139.

3	+1	-1	+1	-1	Y_3
4	+1	+1	+1	+1	Y_4
Effects a_i	a_0	a_1	a_2	a_{12}	Y_i

Where:

$$a_{12} = \frac{y_1 - y_2 - y_3 + y_4}{4} \qquad (5)$$

III-1-5-5 Analysis of Variance (ANOVA)

Is a statistical technique used to analyze and compare the means of two or more groups or treatment. It assesses the variation between groups and within groups to determine if there are statistically significant differences in means[37]. The result of ANOVA test can be modeled by a table which provides a structured and organized summary of the statistical obtained results[38]. Below we will show the most important headings that make up the ANOVA table.

a) ***Source of Variation:*** This column lists the different sources of variation that are being investigated or analyzed. It identifies the factors or variables that contribute to the differences between groups.

b) ***Degrees of Freedom (DF):*** Degrees of freedom represent the number of independent pieces of information available for estimation within a statistical analysis which associated with each source of variation[39].

The between treatment degrees of freedom is DF_1 = p-1. The error degrees of freedom is DF_2 = n - p. The total degrees of freedom is n-1, where: p is the number of estimated coefficients of the model and n is the number of experiments performed

c) ***Sum of Squares (SS):*** represents the sum of the squared differences between each observation and the overall mean. It quantifies the variability within and between groups[40].

Sum of Squares for Treatment or the Between Group Sum of Squares

$$SST = \sum_{i=0}^{n} (\hat{y}_i - \bar{y})^2 \qquad (6)$$

[37] St, L., & Wold, S. *Chemometr Intell Lab Syst*, **1989**, *6*(4), 259-272.
[38] ANOVA, O. W. **2007**.
[39] Armstrong, R. A., Slade, S. V., & Eperjesi, F. *Ophthalmic Physiol Opt*, **2000**, *20*(3), 235-241.
[40] Khuri, A. I. *J. Stat. Plan. Inference*, **1998**, *74*(1), 135-147.

Sum of Squares for Error or the Within Group Sum of Squares

$$SSE = \sum_{i=0}^{n} \hat{e}_i^2 = \sum_{i=0}^{n} (y_i - \hat{y}_i)^2 \qquad (7)$$

Total Sum of Squares

$$TSS = \sum_{i=1}^{n} (y_i - \bar{y})^2 \qquad (8)$$

Note that: y_i are the responses observed during the experiments, $\bar{y}$ is the mean of the responses and $\hat{y}_i$ are the responses estimated using the model.

d) ***The p-value:*** The p-value, or probability value, is a statistical measure used to measures the degree of certainty. It is the most important statistic in the analysis of variance table. A small p-value (typically less than 0.05) suggests that the effect is significant.

e) Coefficients of determination (R^2, adjusted R^2):

These measurements make it possible to test the quality of the model. The coefficient of determination R^2 is defined as being the fraction of the variations of the response explained by the model alone[41].

Adjusted R^2adjusts the R^2 value for the number of predictors in the model, providing a more accurate measure of the goodness of fit when multiple predictors are used. It is calculated as:

Adjusted $R^2 = 1 - ((1-R^2)(n-1)/n-p-1)$

where n is the number of observations and p is the number of predictors.

If the R^2 is close to 1, the model makes it possible to find the values of the measured responses. If it is equal to 0, the model does not explain anything. On the other hand, the adjusted coefficient of determination $R^{2\ adju}$ is used to compare the models with a number of different predictors. The $R^{2\ adju}$ is always less than the R^2.

III-1-5-6 Advantages of full factorial design

Due to the complexity and interplay of numerous factors that might affect chemical reactions and processes, full factorial design is particularly helpful in organic chemistry research. The following are some particular benefits of full factorial design in organic chemistry:

a) Analyses of all relevant factors: full factorial design providing to researchers a comprehensive assessment of the factors that influence the chemistry reactions such as

[41] Palacios-González, F., & García-Fernández, R. M. *J. Appl. Stat*, **2012**, *39*(7), 1543-1555.

temperature, reaction time, solvent type and quantity, catalyst quantity and reactant ratio[42]. It also allows to systematically investigate the effects of each factor individually and in combination[43].

b) Finding the ideal conditions: in the using of full factorial design, researchers can find the ideal set of variables that yield of the desired reaction outcome. This aids in establishing exact reaction conditions that might otherwise be difficult to achieve by trial and error, increasing the yield of the target product, minimizing the by-products, or both[44].

c) Efficient use of resources: Organic chemistry experiments can be time-consuming and resource-intensive. FFD allows researchers to gain substantial information from a relatively small number of experiments compared to exploring each factor individually or using less efficient design approaches[45].

d) Versatility and adaptability: Full factorial design can be used for optimization, screening, process development and is also adaptable to various research aims. It can be applied to various types of organic chemistry experiments, ranging from simple reactions to more complex multi-step syntheses[46].

e) Insight into reaction mechanism: Exploring all potential combinations of variables can help researchers to gain valuable insights into the underlying reaction mechanism[47]. This knowledge can lead to a deeper understanding of the reaction pathway, intermediate species, and potential rate-limiting steps[48].

III-1-5-7 Utilization of the full factorial design in different organic reactions:

a) In Michaelis–Becker* reaction*:

Rambali et *al.* [49] used experimental design methodology to optimize the conditions of a *Michaelis–Becker* dibromoalkane monophosphorylation reaction for the synthesis of 4-bromo-1-(diethylphosphono) butane **III.2**. A 2^4 full factorial design (4 factors and 2 levels by factors) was employed to assess the impact of the temperature of reaction, the dibromobutane concentration, the solvent quantity and the reaction time. ANOVA results confirmed the significance of the reaction time on chemical yield of the desired product. Optimization

[42] Hasnain, M., Abideen, Z., Naz, S., Roessner, U., & Munir, N. *Biomass Convers. Biorefin*, **2023**, *13*(7), 6213-6228.
[43] Woloszyk, K., & Garbatov, Y. *Pol. Marit. Res*, **2020**, (3), 109-120.
[44] Taylor, C. J., Pomberger, A., Felton, K. C., Grainger, R., Barecka, M., Chamberlain, T. W., & Lapkin, A. A. *Chem. Rev*, **2023**, *123*(6), 3089-3126.
[45] Kirk, R. E. *Sage handbook of quantitative methods in psychology*, **2009**, 23-45.
[46] Collins, L. M., Dziak, J. J., & Li, R. *Psychol. Methods*, **2009**, *14*(3), 202.
[47] Seh, Z. W., Kibsgaard, J., Dickens, C. F., Chorkendorff, I. B., Nørskov, J. K., & Jaramillo, T. F. *Science*, **2017**, *355*(6321).
[48] Ahn, S., Hong, M., Sundararajan, M., Ess, D. H., & Baik, M. H. *Chem rev*, **2019**, *119*(11), 6509-6560.
[49] Guervenou, J., Giamarchi, P., Coulouarn, C., Guerda, M., Le Lez, C., & Oboyet, T. *Chemometr Intell Lab Syst*, **2002**, *63*(1), 81-89.

studies concluded the following optimum conditions: temperature = 68 °C, dibromobutane concentration = 6 equivalents per liter, solvent percentage = 10%, reaction time = 2h. (***Scheme 1).***

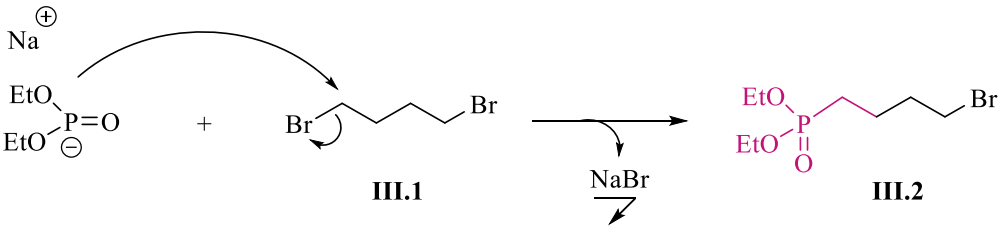

Scheme 1: Used of the full factorial design in *Michaelis–Becker* monophosphorylation reaction.

b) In Biginelli reaction*:*

It proven the use of full factorial design in *Biginelli* multicomponent reactions (MCRs) for the preparation of 3,4-dihydropyrimidin- 2(1H)-ones **III.3** (DHPMs) by *Maryam Khashaei et al*[50]. In this study, 2^3 full factorial designs were realized to find the optimal conditions. It confirmed that the catalyst have a significant effect ($p < 0.05$) than the other factors (temperature and reaction time). From the response surface, the optimum conditions were found to be at T = 90 °C, t = 90 minutes and 60 mg of catalyst. (***Scheme 2)***

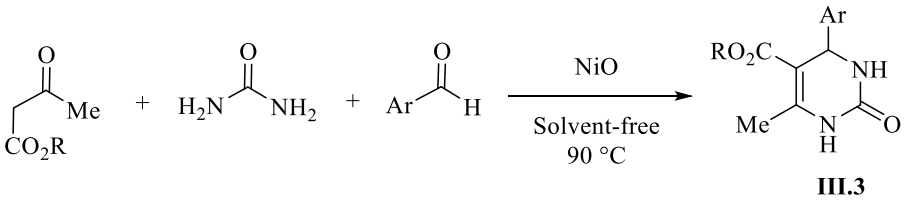

Ar = C_6H_5, 4-Br-C_6H_4, 4-Me-C_6H_4, 4-Cl-C_6H_4, 4-MeO-C_6H_4, 4-NO_2-C_6H_4,

4-HO-C_6H_4, 2-Cl-C_6H_4, 2-HO-C_6H_4, 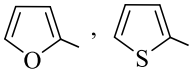

R = Me, Et

Scheme 2: The use of full factorial design in *Biginelli* multicomponent reactions

c) In multicomponent reaction (MCR) of oxazolidines *:*

A full factorial design was also used for multicomponent reaction (MCR) optimizing of oxazolidines **III.7** to explore the effect of temperature, concentration of reagent, quantity of

[50] Khashaei, M., Kafi-Ahmadi, L., Khademinia, S., Poursattar Marjani, A., & Nozad, E. *Sci. Rep*, **2022**, *12*(1), 8585.

catalyst and solvent on the reaction outcome. The reaction proceeds from the condensation of an aminoalcohol **III.4**, carbonyl compound **III.5** and an isocyanide **III.6**, and the results show that the solvent exhibits the most significant parameter promoting the formation of the lactone (***scheme* 3**).[51]

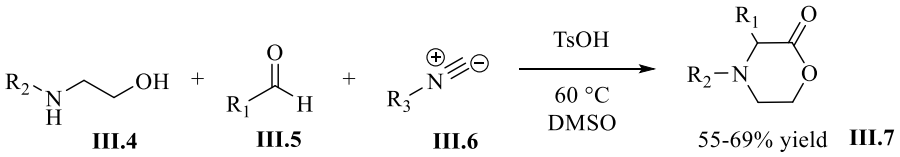

III.4 **III.5** **III.6** **III.7**

Scheme 3: The use of the full factorial design in the synthesis of oxazolidines via MCR.

III-2 Density Functional Theory (DFT)

III-2-1 Principle

The central principle of Density Functional Theory (DFT) is based on the fact that the electronic structure of a quantum system, such as atoms, molecules, or solids, can be accurately described by the electron density rather than the wave function of the system. The *Hohenberg-Kohn* theorem establishes that the ground-state electron density uniquely determines the system's ground-state wave function and, consequently, all observable properties[52].

III-2-2 *Schrödinger* equation

The *Schrödinger* equation constitutes a fundamental concept of quantum chemistry that describes how the wave functions of a certain physical system. It was formulated by the *Austrian* physicist *Erwin Schrödinger* in **1925**[53]. It is universally acknowledged that the *Schrödinger* equation exerts significant effects on electronic structure description:

$$\hat{H}\,\Psi = E\,\Psi \qquad (9)$$

Where:

E: is the total energy of system.

Ψ: its wave function (eigen function).

H: represents the Hamiltonian of a system with several nuclei and electrons, it is expressed in the form of a sum of operators associated with the various kinetic and potential (electrostatic) energy terms:

[51] (a) Diorazio, L. J., Motherwell, W. B., Sheppard, T. D., Waller, R. W. *Synlett*, **2006**, (14), 2281-2283. (b) Waller, R. W., Diorazio, L. J., Taylor, B. A., Motherwell, W. B., & Sheppard, T. D. . *Tetrahedron*, **2010**, *66*(33), 6496-6507.

[52] Geerlings, P., Chamorro, E., Chattaraj, P. K., De Proft, F., Gázquez, J. L., Liu, S., ... & Ayers, P. *Theor. Chem. Accs*, **2020**, *139*(2), 36.

[53] Schrödinger, E. *Annalen der Physik*, **1926**, *79*, 734.

$H = Tel + Tnoy + Vnoy\text{-}noy + Vnoy\text{-}el + Vel\text{-}el$ ***(10)***

Where:

Tel and $Tnoy$: the kinetic energy of repulsion of electrons and nuclei, respectively.

$Vnoy\text{-}noy$ and $Vnoy\text{-}el$: the potential energy of repulsion between nuclei, electrons.

$Vel\text{-}el$: the potential energy of attraction between nuclei and electrons.

Considering the complexities of all related terms, *Schrödinger* equation can only be solved for very simple systems like hydrogen atom and 2 H^+ molecular ion. To address more complex system, numerical approaches are introduced to combine with the *Schrödinger* equation[54].

III-2-3 *Hartree–Fock* approximation

In **1928**, *Hartree* introduced the *Hartree* method, which he termed the self-consistent field method. This technique aimed to streamline the description of wave functions and the calculation of energy for atoms and ions[55]. According to the *Hartree* method, the electron motions can be approximated as largely independent within stable molecules or atoms. Each electron follows its path within the electronic field created by the nucleus and other electrons. Individual electron states can be characterized by their respective single-electron wave functions, and the overall electron states are determined by multiplying all these single-electron wave functions together. The total wave function Ψ is written in the form of a Slater determinant[56], whose abbreviated form for a closed layer system is:

$$\Psi(1,2,\dots n) = \frac{1}{n!^{1/2}}\left|\phi_1\,(1)\overline{\phi_1}\,(2)\dots\,\phi_m\,(2m-1)\overline{\phi_m}\,\,(2m)\right| \qquad \textbf{(11)}$$

With Expression of molecular orbital

$$\phi_1\,(1) = \phi_1(1)\alpha(1) \qquad \textbf{(12)}$$

$$\overline{\phi_1}\,(2) = \,\phi_1(2)\beta(2)$$

Φ: is a single-electron molecular orbital. P and Q are the spin functions.

III-2-4 Notion on Density Functional Theory (DFT)

Most of the properties of a solid depend on the behavior of its electrons. Quantum chemistry employs methods such as Density Functional Theory (DFT) to understand, model

[54] Wang, S. C. *Physical Review*, **1928**, *31*(4), 579.
[55] Hartree, D. R. In *Mathematical Proceedings of the Cambridge Philosophical Society*, **1928**, (Vol. 24, No. 1, pp. 89-110).
[56] Slat Slater, J. C. (1929). The theory of complex spectra. Physical Review, 34(10), 1293.er,J. C. Phys.Rev.1929,34, 1293 ;1931,38,38

or predict these properties[57]. Density Functional Theory (DFT) stands as a potent computational method used for characterizing electronic density rather than the multi-electron wave function. This approach allows to transition from 3N variables (where N is the total number of particles in the system) to only three spatial coordinates (x, y, z), thus significantly reduces computation durations and enabling the examination of large systems with ease[58].
The objective of DFT methods is to derive a functional (a function that depends on another function) for the calculation of a system's ground state energy, where the primary variable is the electron density[59].

Historically, the roots of Density Functional Theory (DFT) can be traced back to the groundbreaking work of *Llewellyn Thomas* and *Enrico Fermi* in **1927**[60-61]. They devised the *Thomas-Fermi* model, which sought to calculate an atom's energy by representing its kinetic energy as a function of the electron density. In **1964**, *Walter Kohn* and *Pierre Hohenberg* formulated two landmark theorems in the context of DFT[62]. The first *Hohenberg-Kohn* theorem proved that the electron density uniquely determines the ground-state energy of a system[63]. The second theorem showed that the ground-state electron density minimizes the energy functional under the constraints of a fixed electron density[64]. A year later, Density Functional Theory (DFT) was developed by Kohn with his collaborator *Lu Sham* by introducing the *Kohn-Sham* equations in **1965**[65]. These equations ingeniously reformulated the complex problem of many interacting electrons into a set of single-electron equations, simplifying the computational treatment.

DFT rapidly gained popularity due to its computational efficiency and accuracy. It has since evolved into the most widely adopted method for elucidating electronic structure and properties. Notably, DFT's profound impact was recognized in **1998** when *Walter Kohn* was awarded the *Nobel* Prize "for his development of density-functional theory"[66].

III-2-5 Different exchange-correlation functional

[57] Geerlings, P., De Proft, F., & Langenaeker, W. *Adv. Quantum Chem.*, **1998**, Vol. 33, pp. 303-328.
[58] Orio, M., Pantazis, D. A., & Neese, F. *Photosynth. Res*, **2009**, *102*, 443-453.
[59] Ziegler, T. *Chem. Rev*, **1991**, *91*(5), 651-667.
[60] Thomas, L. H. *Math. Proc. Cambridge Philos. Soc*, **1927**, (Vol. 23, No. 5, pp. 542-548).
[61] (a) Enrico, F. *Rend. Accad. Naz. Lincei*, **1927**, *6*, 602-607. (b) Fermi, E. Z. Phys. **1928**, 48, 73.
[62] Hohenberg, P., & Kohn, W. *Phyl rev*, **1964**, *136*(3B), B864.
[63] Englisch, H., & Englisch, R. *Physica A: Phys. A: Stat. Mech*, **1983**, *121*(1-2), 253-268.
[64] Görling, A. *Phys Rev A*, **1999**, *59*(5), 3359.
[65] Kohn, W., & Sham, L. J. *Phys rev*, **1965**, *140*(4A), A1133.
[66] Kohn, W. *Rev. Mod. Phy*, **1999**, *71*(5), 1253.

The exchange-correlation functional is a crucial component of the theory's formulation. It is crucial because it corrects the approximate treatment of electron-electron interactions in the *Kohn-Sham* equations. The exchange-correlation functional is typically denoted as E_{xc} [n], where "n" is the electron density of the system[67]. In this context, several functionals calibrated on a type of molecule and with different levels of approximations have been developed in recent years. Some common types of exchange-correlation functionals include:

III-2-5-1 Local density approximation *LDA*

Local Density Approximation is the approximation on which practically all approaches currently employed are based. It was first proposed by *Kohn* and *Sham*, but the philosophy of this approximation was already present in the work of *Thomas* and *Fermi*. The local density approach is based on the homogeneous electron gas model[68]. The functional of the exchange-correlation energy is therefore the simple integral of a density function at any point in space:

$$E_{XC}^{LDA}[\rho] = \int \rho(r)\varepsilon_{xc}(\rho)dr \qquad \textbf{(13)}$$

$$\varepsilon_{xc} = \varepsilon_c(\rho) + \varepsilon_x(\rho) \qquad \textbf{(14)}$$

With ε_{xc} : The exchange-correlation energy for a particle of an electron gas uniform density. It represents a sum of a contribution of exchange and correlation.

LDA functionals have demonstrated computational efficiency when employed to calculate certain molecular properties like equilibrium geometry, vibrational frequencies, and multipolar moments. Nonetheless, they have shown limitations in accurately predicting energy-related data, such as bond energies and ionization energies[69].

III-2-5-2 Generalized Gradient Approximation (GGA)

These methods are commonly referred to as nonlocal approaches. They represent an enhancement over LDA in the treatment of exchange and correlation effects by considering not only the electron density but also its gradient, which accounts for spatial variations. In the Generalized Gradient Approximation (GGA)[70], the exchange-correlation energy is expressed as:

[67] Scuseria, G. E., & Staroverov, V. N. *J Theor Comput Chem*, **2005**, (pp. 669-724). Elsevier.
[68] Perdew, J. P., & Wang, Y. *Phys rev*,**1992**, *B*, *45*(23), 13244.
[69] Ghosh, S., Verma, P., Cramer, C. J., Gagliardi, L., & Truhlar, D. G. *Chem rev*, **2018**, *118*(15), 7249-7292.
[70] Perdew, J. P., Burke, K., & Ernzerhof, M. *Phy rev lett*, **1996**, *77*(18), 3865.

GGA functionals offer improved accuracy when it comes to modeling molecular geometries and bonding properties. Numerous calculations have been conducted using this approximation, including the widely recognized approximations developed by *Perdew*, *Burke*, and *Ernzerhof* in 1996[71].

III-2-5-3 Meta-Generalized Gradient Approximations (meta-GGAs)

Meta-Generalized Gradient Approximations (meta-GGAs) represent an advanced evolution beyond Generalized Gradient Approximations (GGAs) by incorporating additional information about the second-order gradient of the electron density and Laplacians. An example of a highly influential functional within this family is the Staroverov, Tao, and Scuseria (TPSS) functional[72].

III-2-6 Hybrid Methods in Density-Functional Theory:

In the context of computational chemistry hybrid methods are a category of computational approaches that leverage a combination of local exchange-correlation functionals, typically derived from Density Functional Theory (DFT), and a fraction of the exact exchange from *Hartree-Fock* theory[73]. These methods are specifically designed to enhance the accuracy of predictions for a wide range of molecular properties and electronic structures. In this section, we will cite the most used hybrid functionals.

III-2-6-1 The B3LYP

Becke's **1988** exchange functional[74] combined with *Lee-Yang-Parr* correlation functional[75], is a prominent density functional theory (DFT) method. It offers a unique blend of general gradient approximation (GGA) exchange-correlation functionals and *Hartree-Fock* exchange, with 20% of the exchange energy derived from the latter[76]. While widely employed in molecular modeling, B3LYP does come with certain limitations:

a) Alkylation Sensitivity: B3LYP exhibits increased errors in estimating C-X (carbon-halogen) bond energies as alkylation levels rise. This means it may struggle to accurately predict the strengths of these bonds in more complex molecules[77].

Isomer Energy Ordering: B3LYP may not reliably establish the energy order of isomers, potentially leading to incorrect predictions of the stability of different molecular arrangements[78].

[71] Perdew, J. P., Ernzerhof, M., & Burke, K. *J. chem. phy*, **1996**, *105*(22), 9982-9985.
[72] Tao, J., Perdew, J. P., Staroverov, V. N., & Scuseria, G. E. *Phy. rev lett*, **2003**, *91*(14), 146401.
[73] Jones, R. O. In *Strongly correlated systems: Theoretical methods*, **2011**, (pp. 1-28).
[74] Becke, A. D. *J. Chem. Phys.***1988**, *84*(8), 4524-4529.
[75] Lee, C., Yang, W., & Parr, R. G. Phys. Rev, **1988**.
[76] Stephens, P. J., Devlin, F. J., Chabalowski, C. F., & Frisch, M. J. *J. Phys. Chem.* **1994**, *98*(45), 11623-11627.
[77] Sproviero, E. M., Gascon, J. A., McEvoy, J. P., Brudvig, G. W., & Batista, V. S. *J. Inorg. Biochem*, **2006**, *100*(4), 786-800.

b) Size-Dependent Errors: As the size of the molecular system grows, BLYP can accumulate errors in calculating heats of formation. This limitation can hinder its applicability to larger and more intricate chemical structures[79].

c) Neglect of Non-Covalent Bonds: BLYP tends to underestimate the strength of dispersion forces, which are crucial for modeling long-range attractive interactions, such as van der Waals forces. This can result in inaccuracies when characterizing weakly bonded systems.

Despite these drawbacks, B3LYP remains a popular choice for modeling a wide range of chemical compounds in molecular simulations[80]. Researchers often rely on it due to its balance between computational efficiency and accuracy, making it suitable for many applications.

III-2-6-2 The CAM-B3LYP functional

Introduced in **2004** by *Yanai*[81], was specifically engineered to yield more precise results when dealing with heavy atoms and intricate electronic structures in molecular systems. This functional blends the characteristics of both of hybrid qualities B3LYP and Tawada's long-range correction, resulting in an enhanced ability to assess long-range interactions.

CAM-B3LYP incorporates a range of *Hartree-Fock* exchange components, with a clear distinction between short-range and long-range interactions. Specifically, it assigns a substantial 65% proportion of *Hartree-Fock* exchange for long-distance interactions, while only allocating 19% for short-distance ones[82].

One notable strength of CAM-B3LYP lies in its long-range correction capabilities, which enable a more accurate depiction of charge transfer processes within molecules. This stands in contrast to the limitations of the B3LYP method, which is ill-suited for calculating charge transfer energies.

III-2-7 Basis sets in Density-Functional Theory

The choice of a basis set significantly influences the accuracy of electronic structure calculations, serving as the mathematical underpinning for representing atomic orbitals. These basis sets can be categorized into two main classes: *Slater* and *Gaussian* function bases.

---

[78] Tirado-Rives, J., & Jorgensen, W. L. *J. Chem. Theory Comput.*, **2008**, *4*(2), 297-306.
[79] Wenthold, P. G., Squires, R. R., & Lineberger, W. C. *J. Am. Chem. Soc*, **1998**, *120*(21), 5279-5290.
[80] Marom, N., Tkatchenko, A., Scheffler, M., & Kronik, L. *J. Chem. Theory Comput.*, **2010**, *6*(1), 81-90.
[81] Yanai, T., Tew, D. P., & Handy, N. C. *Chem phys lett*, 2004, *393*(1-3), 51-57.
[82] Bircher, M. P., & Rothlisberger, U. *J. Chem. Theory Comput*, **2018**, *14*(6), 3184-3195.

III-2-7-1 *Slater* type orbitals

Slater type orbitals[83], which are hydrogenoid orbitals derived from exact solutions of the Schrödinger equation for hydrogen-like atoms, are characterized by the following general expression:

$$\chi_{\zeta,n,l,m}(r,\theta,\varphi) = N\, r^{n-1}\, Y_{l,m}(\theta,\varphi) e^{-\zeta r} \qquad \textbf{(15)}$$

r, θ, and φ*:* are spherical coordinates.

r: is the distance between the electron and the nucleus at which the STO is centered, *N* is a normalization constant.

$Y_{l,m}$: is a spherical harmonic function (the angular part of the STO).

ζ*:* is called the orbital exponent, and *n* is the principal quantum number.

These orbitals are generally used for atomic and diatomic systems demanding a high degree of calculation precision. Nevertheless, when dealing with bielectronic integrals that encompass orbitals located on distinct atoms, these functions pose considerable numerical challenges.[84]

III-2-7-2 *Gaussian* type orbitals (GTO)

Boys proposed a groundbreaking advancement in quantum chemistry by introducing Gaussian functions (GTOs) as a replacement for Slater orbitals.[85] These GTOs are constructed as powers of X, Y, and Z, all of which are multiplied by the exponential term $e^{-\zeta r2}$:

$$\chi_{\zeta,i,j,k}(x,y,z) = N\, x^i y^j z^k\, e^{-\zeta r^2} \qquad \textbf{(16)}$$

In this equation:

x, *y*, *z* : the Cartesian components of the distance between the electron and the center of the GTO, normally a nuclear position.

N: the normalization factor.

ζ: defines the radial extent of the function.

i, j, and k: integers that emulate the quantum numbers n, l, and m.

i+j+k : type of the atomic orbital.

Or :

- i+j+k = 0 (OA of type s)
- i+j+k = 1 (OA of type p)

[83] Slater, J. C. Atomic shielding constants. *Phys rev*, **1930**, *36*(1), 57.
[84] Avery, J. E., & Avery, J. S. *Adv. Quantum Chem*, ***2015***, Vol. 70, pp. 265-324.
[85] Stewart, R. F. *J. Chem. Phys*, **1970**, *52*(1), 431-438.

- i+j+k = 2 (OA type d)

Notably, multiplying two Gaussian type orbitals (GTOs) results in a Gaussian, simplifying the calculation of multicentric integrals into easily manageable monocentric integrals.[86]

Nevertheless, these functions do have limitations. They fail to precisely describe the orbital behavior in the immediate vicinity of the nucleus (as r approaches 0), and they also decay too rapidly as r approaches infinity. Therefore, the accuracy of the results is significantly influenced by the quantity of Gaussians employed in the construction of atomic orbitals.

III-2-8 Base classification

III-2-8-1 Minimum base/STO-nG

Minimal basis sets include the smallest collection of basis functions necessary to accurately describe the electronic structure of neutral atoms. Among these, the STO-nG minimal basis sets, pioneered by *John Pople's* research group, stand out as the most commonly employed. [87]In this nomenclature, the 'n' value signifies the quantity of primitive *Gaussian* functions employed to approximate a *Slater*-type orbital (STO). For instance, within the minimal STO-3G basis set, the label "3G" denotes that three *Gaussian* functions are employed to optimally replicate the underlying *Slater* orbital[88].

III-2-8-2 Split valence

In the context of split valence basis sets, atomic orbitals are represented by a combination of two *Gaussian* functions. These two distinct functions are employed to characterize the behavior of inner and outer electrons within an atom, acknowledging the disparate nature of these electron populations.[89]

The notation used to describe this type of basis set is typically expressed as "N-MLG," [90]where:

- N: represents the total number of Gaussian functions employed to describe the inner-shell orbitals.
- M: corresponds to the number of Gaussian functions dedicated to modeling the smaller orbital.
- P: corresponds to the number of *Gaussian* functions used to depict the larger orbital.

[86] Huzinaga, S. Gaussian-Type functions for polyatomic systems. I. *J. Chem. Phys*, **1965**, *42*(4), 1293-1302.
[87] Ditchfield, R. H. W. J., Hehre, W. J., & Pople, J. A. *J. Chem. Phys*, **1971**, *54*(2), 724-728.
[88] Pietro, W. J., Levi, B. A., Hehre, W. J., & Stewart, R. F. *Inorg. Chem*, **1980**, *19*(8), 2225-2229.
[89] Binkley, J. S., Pople, J.A, Hehre, W. J., *J. Am. Chem. Soc*., **1980,** 102, 939.
[90] Collins, J. B., Schleyer, Binkley, J. S., J. *Chem. Phys*., **1976**, 64, 5142.

For instance, the 3-21G basis set is a prime example of a split valence basis set. In this case, it comprises two different sizes of basis functions for each valence orbital. This particular type of basis set is commonly referred to as "Split Valence Double Zeta" (DZ)[91]. Beyond DZ, higher levels of approximation are available, including Triple Zeta (TZ)[92], Quadruple Zeta (QZ), and Quintuple Zeta (5Z) bases, each offering progressively greater precision in electronic structure calculations.[93]

III-2-8-3 Polarization functions

These functions enhance the flexibility of the base by accounting for changes in valence orbitals as the molecule undergoes deformation. These orbitals correspond to higher secondary quantum numbers denoted as p and d for hydrogen, and d, f, and g for elements in the 2nd and 3rd rows of the periodic table,..etc. Moreover, they play a crucial role in understanding molecular transitions and locating transition states[94]. For example, popular polarized basis set 6-31G (d,p) used in our calculations, signifies the incorporation of p functions for hydrogen atoms and d functions for all other non-hydrogen atoms, further refining our modeling precision[95].

III-2-8-4 Diffuse functions

Diffuse functions are crucial for the realistic modeling of molecules or systems with long-range dispersion forces, like *van der Waals* interactions, hydrogen bonds. Moreover, they enable the accurate portrayal of electron behavior over extended spatial regions, a necessity for capturing phenomena involving valence electrons in aromatic molecules and species having free doublets[96].

In notation, the inclusion of diffuse functions is denoted by the symbol "+". For instance, the basis set 6-31+G signifies the addition of diffuse orbitals to all atoms except hydrogen[97], while the 6-31++G basis set includes diffuse functions for all atoms within the system[98].

91 Binkley, J. S., Pople, J. A., & Hehre, W. J. *J. Am. Chem. Soc*, **1980**, *102*(3), 939-947.
92 Ditchfield, R. H. W. J., Hehre, W. J., & Pople, J. A. *J. Chem. Phys*, **1971**, *54*(2), 724-728.
93 Dyall, K. G. *Theor. Chem. **Acc***, 2004, *112*, 403-409.
94 Jensen, F. *J. Chem. Phys*, **2001**, *115*(20), 9113-9125.
95 Mitin, A. V. *J. Comput. Chem*, **2013**, *34*(23), 2014-2019.
96 Jensen, F. *J. Chem. Phys*, **2002**, *117*(20), 9234-9240.
97 Mitin, A. V., Baker, J., & Pulay, P. *J. Chem. Phys*, **2003**, *118*(17), 7775-7782.
98 Fábri, C., Szidarovszky, T., Magyarfalvi, G., & Tarczay, G. *J. Chem. Phys A*, **2011**, *115*(18), 4640-4649.

III-2-9 The theory of frontier orbitals

In the **1950**s, *K. Fukui* formulated the theory of frontier orbitals[99], a pioneering contribution that earned him the *Nobel* Prize in Chemistry in **1981**[100]. This theory is centered on unraveling the reactivity of organic molecules and highlighting the prevalent role of interactions between the Highest Occupied Molecular Orbital (HOMO) of one reactant and the Lowest Unoccupied Molecular Orbital (LUMO) of another in chemical reactions between nucleophiles and electrophiles.

The HOMO, short for Highest Occupied Molecular Orbital, is a characteristic feature of nucleophilic components, representing the molecular orbital with the highest energy containing electrons within a given molecular system. The energy level of the HOMO exhibits an inverse correlation with the stability of the molecule, wherein a lower HOMO energy signifies a more stable compound.

Conversely, the LUMO, or Lowest Unoccupied Molecular Orbital, is the molecular orbital with the lowest energy that is unoccupied by electrons. A molecule's LUMO energy is associated with its ability to accept electrons, and a lower LUMO energy indicates a greater propensity for accepting electrons, making the molecule more electrophilic.

The energy difference between the HOMO and LUMO, known as the HOMO-LUMO gap, is a measure of the stability of a molecule. A molecule with a small HOMO-LUMO gap is more likely to react than a molecule with a large HOMO-LUMO gap.

$$\Delta G = E_{LUMO} - E_{HOMO} \qquad \textbf{(17)}$$

III-2-10 Global reactivity descriptors

Global reactivity descriptors are a set of theoretical parameters used in the field of theoretical and computational chemistry to describe the reactivity and chemical behavior of molecules. Global reactivity descriptors are derived from quantum mechanical calculations, which can be mathematically defined by the conceptual density functional theory C-DFT by *R.G. Parr* and *R.G. Pearson*.

In our study, the global descriptors that were processed are:

[99] Fukui, K., Yonezawa, T., & Shingu, H. *J. Chem. Phys*, **1952**, *20*(4), 722-725.
[100] Schwarzschild, B. M. *Physics Today*, **1981**, *34*(12), 20-22.

a) Hardness (η):

Hardness is a measure of the resistance of a molecule to changes in its electron density. It is calculated as the energy required to add or remove an electron from a molecule. It is often used in the context of the HSAB (Hard and Soft Acids and Bases) principle[101].

$$\eta = \frac{E_{LUMO} - E_{HOMO}}{2} \qquad \textbf{(18)}$$

b) Softness (σ):

Softness is the reciprocal of hardness and reflects the ease with which a molecule can accept or donate electrons. Molecules with higher softness are more reactive. (Equation.III.19)[102].

$$\sigma = \frac{1}{\eta} \qquad \textbf{(19)}$$

c) Electronegativity (χ):

Electronegativity measures the ability of an atom within a molecule to attract electrons. It is often used to predict the polarity of chemical bonds and the distribution of charge within a molecule[103].

$$\chi = -\frac{E_{HOMO} + E_{LUMO}}{2} \qquad \textbf{(20)}$$

d) The Global Electrophilicity Index (ω):

Molecules with higher X values are more electrophilic, meaning they are more prone to accept electrons and participate in electrophilic reactions[104].

$$\omega = \left(\frac{\chi^2}{2\eta}\right) \qquad \textbf{(21)}$$

Density Functional Theory has been widely applied in the field of organic chemistry to investigate various aspects of organic reactions, especially for organophosphorus compounds.

A set of elegant examples for the DFT study of aminophosphonates followed by an *in silico* bioactivity evaluation are given by several authors [105].

As an example, the molecular geometries and physical-chemical properties of three *α*-aminophosphonates (**III.8-III.10**) were meticulously examined by *Alkhimova* et *al*[106] using DFT calculations. This investigation unveiled a noteworthy trend in the HOMO–LUMO energy gap values: **III.8** < **III.9** < **III.10**. This sequence suggests that compound **III.8**

[101] Pearson, R. G. *J. Chem. Educ*, **1987**, *64*(7), 561.
[102] Patterson, J. D. **1989**, 333.
[103] Mulliken, R. S. *J. Chem. Phys*, **1934**, *2*(11), 782-793.
[104] Lewis, G. N. *J. Am. Chem. Soc*, **1916**, *38*(4), 762-785.
[105] (a) Awad, M. K., Abdel-Aal, M. F., Atlam, F. M., & Hekal, H. A. *J. Mol. Struct*, **2018**, *1173*, 128-141. (b) Moumeni, O., Chafaa, S., Kerkour, R., Benbouguerra, K., & Chafai, N. *J. Mol. Struct*, **2020**, *1206*, 127693. (c) Shaik, Y. H., Chintha, V., Gundluru, M., Sarva, S., & Cirandur, S. R. *Synth. Commun*, **2022**, *52*(1), 129-144.
[106] Alkhimova, L. E., Babashkina, M. G., Safin, D. A. *Tetrahedron*, **2021**, *97*, 132376.

displays higher polarizability and reactivity, establishing it as a more flexible and reactive soft molecule in comparison to the other two compounds. (***Figure 7***).

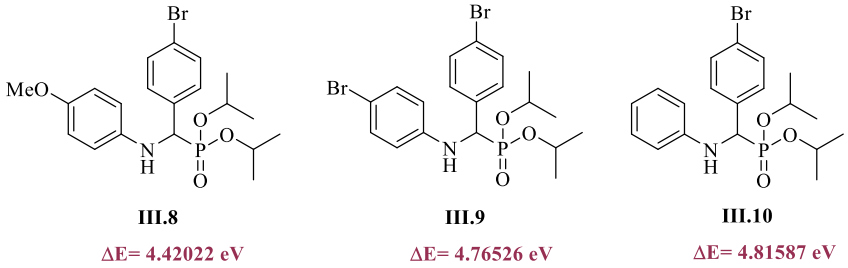

Figure 7: The gap energy (ΔE) of potent *α*-aminophosphonates derivatives.

Additionally, a molecular electrostatic potential analysis of these molecules was performed using the B3LYP/6-311++G(d,p) method to pinpoint the active centers governing electrophilic and nucleophilic reactions. The accompanying figure vividly portrays a distinctive negative region (depicted in red) surrounding the N(H)–C(H) fragment, the bromine, and methoxy oxygen atoms (***Figure 8***). This highlights their inclination towards electrophilic reactivity. Meanwhile, the most prominent nucleophilic center is identified on the P=O oxygen atom.

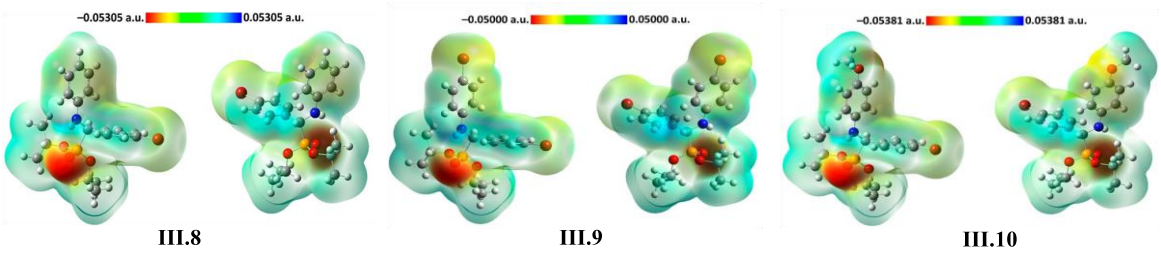

Figure 8: Front (left) and rear (right) views of the molecular electrostatic potential surface of compounds **III.8-III.10**.

III-3 Molecular docking

III-3-1 Generality and definition

Molecular docking is a bioinformatics method used in the pharmacochemistry for drug design and in the field of molecular biology[107]. This method is part of the modeling methods that widely employed ever since the early **1980**s[108]. Molecular Docking is the *in silico* study of the different mechanisms and interactions involved between two molecules[109]:

[107] Singh, S., Florez, H. *F1000Research*, **2020**, *9*.
[108] Kuntz, I. D., Blaney, J. M., Oatley, S. J., Langridge, R., & Ferrin, T. E. *J. Mol. Biol*, **1982**, *161*(2), 269-288.
[109] Mendie, L. E., & Hemalatha, S. *Appl. Biochem. Biotechnol*, **2022**, 1-17.

The first one, is the target considered as, a macromolecular, most often is a protein which known by their three-dimensional structure having one or more active sites capable of binding specifically and reversibly to another molecule called a ligand[110].

The second is the ligand, as a small flexible molecule, which reacts with the protein in a non-covalent manner and plays a role in its functions[111].

Molecular docking is a cost and time-effective alternative to experimental screening methods[112]. It is a powerful tool that plays a crucial role in various scientific disciplines, For instance, in biochemistry to confirm data related to enzyme inhibitory activity[113], such as experimental dissociation constant (K_d) or half-maximal inhibitory concentration (IC_{50})[114], in agrochemicals and pesticide design by assessing their binding to target proteins in pests[115] or plants and in genotoxicity studies by predict the binding modes and affinity of small molecules on DNA[116].

Furthermore, docking has proved to be extremely successful for investigating the correlation between structure and function and finding potential leads by virtual screening. Recently, it was adopted even in the COVID-19 pandemic in drug discovery campaigns against the SARS-CoV-2 virus[117]. So, the main goal of molecular docking is to predict molecular recognition between the ligand and target, both structurally (i.e. finding favorable binding orientation) and energetically (i.e. predicting binding affinity)[118].

The aim of docking step is to understand how ligand is positioned at the active site of the protein to form stable complexes by modifying its structural parameters using search algorithms[119]. The "scoring" is the classification stage which consists of evaluating energetic interactions between the ligand and protein. Lower energy values indicate more favorable binding[120].

[110] Li, X., Moal, I. H., & Bates, P. A. *Proteins: Structure, Function, and Bioinformatics*, **2010**, *78*(15), 3189-3196.
[111] Mobley, D. L., & Dill, K. A. *Structure*, **2009**, *17*(4), 489-498.
[112] Sha, C. M., Wang, J., & Dokholyan, N. V. *Front. Mol. Biosci*, **2022**, *9*, 867241.
[113] Yakan, H., Koçyiğit, Ü. M., Muğlu, H., Ergul, M., Erkan, S., Güzel, E., & Gülçin, İ. *J. Biochem. Mol. Toxicol*, **2022**, *36*(5), e23018.
[114] Chen, H. H., Li, W., Wang, Y., Xu, B., Hu, X., Li, X. B., & Xing, X. H. *J. Agric. Food Chem*, **2023**.
[115] Kumar, R., Das, J., Rode, S., Kaur, H., Shah, V., Verma, P., & Sharma, A. K. *Biotech*, **2023**, *13*(6), 175.
[116] Shmilovich, K., Chen, B., Karaletsos, T., & Sultan, M. M. *J. Chem. Inf. Model*, **2023**, *63*(9), 2719-2727.
[117] Rehman, H. M., Sajjad, M., Ali, M. A., Gul, R., Naveed, M., Aslam, M. S., & Amin, AInt. *J. Biol. Macromol*, **2023**, *237*, 124169.
[118] Singh, S., Baker, Q. B., & Singh, D. B. In *Bioinform*, **2022**, pp. 291-304.
[119] Chaudhary, K. K., & Mishra, N. *Databases*, **2016**, *3*(4), 1029.
[120] Muegge, I., & Rarey, M. *Rev. Comput. Chem* **2001**, *17*, 1-60.

III-3-2 Types of docking

III-3-2-1 Flexible docking

Also known as "induced-fit docking"[121]. It represents the most accurate technique, which is based on the induced-fit hypothesis offered by *Daniel Koshland* in **1958**[122]. In this approach, the side chains of the protein and ligand allow some flexibility to accommodate conformational changes upon binding. This type's disadvantage is that it is both time and cost-consuming.

III-3-2-2 Semi-flexible docking

Semi-flexible docking introduces adaptability to either the ligand, receptor, or both, recognizing the dynamic nature inherent in biological molecules. This methodology aptly addresses the natural flexibility exhibited by ligands due to rotatable bonds and other internal degrees of freedom. Throughout the simulation, the algorithm systematically explores a myriad of ligand conformations, permitting rotations around specific bonds known as torsional angles. While emphasizing the ligand's flexibility, certain semi-flexible docking approaches also take into account constrained modifications in the receptor's structure, such as side-chain flexibility[123]. Through the incorporation of conformational sampling and scoring functions that comprehensively consider various energetic contributions, semi-flexible docking offers a more nuanced and realistic portrayal of ligand-receptor binding. Its particular efficacy shines in drug discovery and structural biology applications, where understanding molecular flexibility is paramount[124].

III-3-2-3 Rigid docking

Involves keeping the fixed geometry of both the target (protein) and the ligand during the docking analysis[125], following *Emil Fischer's* 'Lock and Key' hypothesis[126]. However, this method can lead to challenges in observing interactions, especially when the ligand is rigid and doesn't fit well into the protein's binding pocket. Rigid docking may not capture essential structural modifications for binding, making it primarily suitable for observing interactions

[121] Nabuurs, S. B., Wagener, M., & De Vlieg, J. *J. Med. Chem*, **2007**, *50*(26), 6507-6518.
[122] Stoddard, B. L., & Koshland Jr, D. E. *Nature*, **1992**, *358*(6389), 774-776.
[123] Rondón, P., Arguello, H., & Torres, R. **2011**, pp. 1-4.
[124] Xue, Q., Liu, X., Russell, P., Li, J., Pan, W., Fu, J., & Zhang, A. *Ecotoxicol. Environ. Saf*, **2022**, *233*, 113323.
[125] Duhovny, D., Nussinov, R., & Wolfson, H. J. *Proc*, **2002**, pp. 185-200.
[126] Tripathi, A., & Bankaitis, V. A. *J. Mol. Med*, **2017**, *2*(1).

rather than predicting accurate binding conformations[127]. Despite its simplicity and quick runtime, rigid docking may not provide satisfactory results in some cases[128].

III-3-3 Molecular docking Approaches

III-3-3-1 Stochastic approach

Stochastic algorithms in molecular docking involve sampling ligand binding orientations and conformations. This is achieved by introducing changes to the ligand, guided by one or more randomly generated values at each step[129]. These alterations are either accepted or rejected based on criteria specific to the algorithm being used. The strength of stochastic algorithms lies in their ability to create extensive sets of molecular conformations, enabling them to explore a wide energy landscape effectively[130]. This increased exploration enhances the likelihood of identifying the global energy minimum. Noteworthy examples within this category include GOLD and AutoDock[131].

III-3-3-2 Simulation approach

Simulation methods for studying protein-ligand interactions primarily rely on solving Newton's equations of motion, utilizing techniques such as molecular dynamics and minimization algorithms. Molecular dynamics, though powerful, is rarely employed for ligand flexibility due to its computationally intensive nature, which is impractical for large molecular databases. Instead, minimization algorithms, coupled with other search algorithms, are sometimes utilized in docking programs to achieve low-energy ligand conformations. Notably, Flex and Arguslab are among the most widely used software programs for simulating protein-ligand interactions, with Flex employing an incremental approach and Arguslab employing mixed methods.

III-3-3-3 Systematic approach

The core concept involves dividing the ligand into rigid and flexible segments. Initially, the rigid fragments are positioned within the active site, engaging with the target. Subsequently, the ligand is reassembled by sequentially placing the flexible fragments,

[127] Bolia, A., Gerek, Z. N., & Ozkan, S. B. *J. Chem. Inf. Model*, **2014**, *54*(3), 913-925.
[128] Bursulaya, B. D., Totrov, M., Abagyan, R., & Brooks, C. L. *J. Comput. Aided Mol. Des.***2003**, *17*, 755-763.
[129] Ghosh, P., Ghosh, S., Basu, K., Das, S. K., & Daefler, S. **2006**, pp. 1-8.
[130] Vainio, M. J., & Johnson, M. S. *J. Chem. Inf. Model.* **2007**, *47*(6), 2462-2474.
[131] Novič, M., Tibaut, T., Anderluh, M., Borišek, J., & Tomašič, T. **2016**, pp. 99-127.

making use of torsion angles for adjustment[132]. Software applications like FlexX, and Dock[133] employ this strategy, enabling swift screening of extensive chemical libraries.

III-3-4 Interactions protein-ligand:

Many types of non-covalent interactions have been demonstrated in protein-ligand complexes. Some of these include:

III-3-4-1 Van Der Waals interactions:

Van Der Waals interactions are non-permanent dipoles with limited reach[134]. Yet they are abundant and crucial for establishing a steric fit between the ligand and the receptor protein during molecular interactions.

III-3-4-2 Hydrogen bonds:

Hydrogen bonds originate from a combination of electrostatic and van der Waals interactions[135]. These bonds typically form between an electronegative atom, often oxygen or nitrogen, which possesses a free electron pair, and a hydrogen atom attached to another electronegative atom[136]. Notably, hydrogen bonds are stronger than van der Waals bonds, with energies ranging from 3 to 9 kcal/mol.

III-3-4-3 Electrostatic interactions

Electrostatic interactions, which are essentially weak ionic bonds, occur when two atoms with opposite charges interact, resulting in the formation of an attractive force[137]. Specific amino acids can carry positive or negative charges, leading to electrostatic phenomena that facilitate the formation of distinct protein complexes.

III-3-4-4 Hydrophobic interactions:

Molecules that lack polarity and have low polarizability often exhibit a tendency to aggregate, giving rise to hydrophobic bonding forces[138]. These interactions occur among molecules or groups that show minimal attraction to water. They arrange themselves to minimize contact with the aqueous environment, favoring the least possible surface exposure.[139]

---

[132] Van de Weerd, H. A., Docking, C. M., Day, J. E., Avery, P. J., & Edwards, S. A. ***Appl. Anim. Behav. Sci***. **2003**, *84*(2), 101-118.
[133] Kellenberger, E., Rodrigo, J., Muller, P., & Rognan, D. *Proteins: Structure, Function, and Bioinformatics*, **2004**, *57*(2), 225-242.
[134] Li, A. J., & Nussinov, R. *Proteins: Structure, Function, and Bioinformatics*, **1998**, *32*(1), 111-127.
[135] Van Oss, C. J., Good, R. J., & Chaudhury, M. K. *J. Colloid Interface Sci*, **1986**, *111*(2), 378-390.
[136] Crabtree, R. H. *Science*, **1998**, *282*(5396), 2000-2001.
[137] Sharp, K. A., & Honig, B. *Annu. Rev. Biophys*, **1990**, *19*(1), 301-332.
[138] Scheraga, H. A. *J. Biomol. Struct. Dyn*, **1998**, *16*(2), 447-460.
[139] VESELOVSKY, A. V., IVANOV, Yu D., IVANOV, A. S., *et al. J. Mol. Recognit*, **2002**, vol. 15, no 6, p.405-422.

III-3-4-4 Docking software

In the past two decades, numerous docking programs have been developed, as shown in ***Figure 9*** with their distribution percentages. Autodock Vina, including QuickVina, Smina, and YASARA, stands out as the most frequently cited, featuring in 44.6% of articles (Figure 2B). Other notable choices include the Schrödinger package's Glide (23.2%), Autodock4 (15.5%), and the Molecular Operating Environment platform (MOE; 7.1%) in various research campaigns[140]

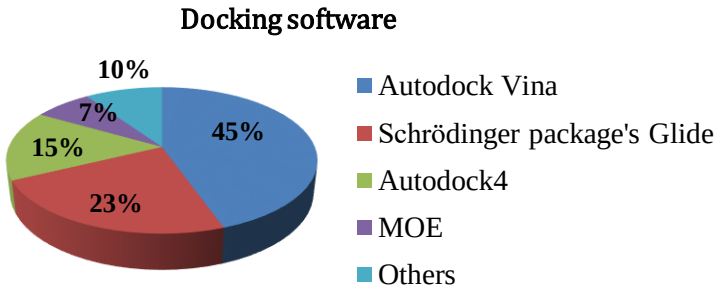

Figure 9: *Different docking programs used.*

It's important to note that these percentages are rough estimates based on the trends observed in the field as of **2021**. The use of docking programs can vary significantly depending on factors such as the specific research domain, the preferences of individual researchers, and the availability of software licenses and resources. In our specific research project, we have selected AutoDock Vina, AutoDock Tools, and Discovery Studio as the software tools for our modeling endeavors.

III-3-5-1 Software used

III-3-5-1-1 AutoDock Tools

AutoDockTools (ADT) serves as the user-friendly graphical interface for configuring and executing AutoDock, streamlining various crucial aspects of molecular docking setup. With a comprehensive toolkit at its disposal, ADT simplifies the preparation of input molecule files by guiding users through essential tasks such as protonation, charge calculations, and definition of rotatable bonds within both the ligand and protein molecules. This tool not only ensures accuracy in predicting the binding pose of small chemical

[140] Dickerhoff, J., Warnecke, K. R., Wang, K., Deng, N., Yang, D. *Int. J. Mol. Sci*, **2021**, *22*(19), 10801.

compounds within their respective receptor pockets but also offers a cost-effective and open-source solution, catering to the needs of computational docking researchers worldwide.[141]

III-3-5-1-2 AutoDock Vina

AutoDock Vina, an off spring of AutoDock Tools, was developed by *Oleg Trott* at the Molecular Graphics Lab within the Scripps Research Institute in **2010**. This software represents a relatively recent addition to the molecular docking landscape and is freely accessible, catering to the needs of researchers in molecular docking, drug discovery, and virtual screening. Its merits include high performance, multi-core optimization, heightened accuracy, and an intuitive user interface. Moreover, Vina takes charge of predicting grid maps and clustering, significantly elevating the precision of interaction mode predictions when compared to its predecessor, AutoDock.

The key distinction between this program and its predecessor lies in the scoring function. AutoDock Tools predominantly relies on a physics-based scoring function, incorporating various terms derived from the Amber family of force-fields. In contrast, AutoDock Vina employs a hybrid scoring function, which combines both empirical and knowledge-based components.[142-143]

***III-3-5-1-3* The Discovery Studio Visualizer**

Biovia Discovery Studio (BDS), a comprehensive software, includes a visualization tools for effectively interpreting and communicating the results of molecular simulations and analysis.[144] The Discovery Studio Visualizer is a free viewer that can be used to open data generated by other software in the Discovery Studio product line.[145]

The Discovery Studio Visualizer is engineered to provide an engaging and interactive environment, enabling users to delve into molecular structures in three dimensions. Its capabilities extend to visualizing intricate interactions between ligands and proteins, as well as depicting the electrostatic potential distribution on the surface of proteins. Moreover, it boasts a diverse array of viewers that empower users to display various plots and graphical representations of their data, further enhancing the utility of this indispensable tool.[146]

[141] Morris, G. M., Huey, R., Lindstrom, W., Sanner, M. F., Belew, R. K., Goodsell, D. S., & Olson, A. J. *J. Comput. Chem.*, **2009**, *30*(16), 2785-2791.
[142] Fuhrmann, J., Rurainski, A., Lenhof, H. P., & Neumann, D. *J. Comput. Chem*, **2010**, *31*(9), 1911-1918.
[143] Trott, O., & Olson, A. J. *J. Comput. Chem*, **2010**, *31*(2), 455-461.
[144] Systèmes, D. *Dassault Systèmes Biovia: San Diego. **2016*** .
[145] Govender, N., Zulkifli, N. S., Hisham, N. F. B., Ab Ghani, N. S., & Mohamed-Hussein, Z. A. *PeerJ*, **2022**, *10*, e14168.
[146] Baskaran, S. G., Sharp, T. P., & Sharp, K. A. *J. Chem. Inf. Model*, **2021**, *61*(3), 1427-1443.

III-3-6 Scoring functions

Scoring functions represent efficient mathematical tools employed to quantitatively assess the affinity with which a ligand binds to a receptor. They provide an estimation of the free energy change associated with the transition from the unbound state of the protein and ligand to their complexed form.[147] This scoring system plays a pivotal role, not only in the selection of the most favorable binding pose from a myriad of possibilities but also in the comparative ranking of diverse ligands to identify the most promising candidate among them. The thermodynamic principle is as follows:

$$\Delta G = \Delta G_{complex} - \Delta G_{ligand} - \Delta G_{protien}$$

Scoring functions divided into two types of classes: classical scoring functions and machine-learning scoring functions[148].

Classical scoring functions include three categories: force-field based, knowledge-based, and empirical-based[149]. These models often employ the straight forward linear additive feature algorithm. In contrast, machine learning-based scoring functions utilize algorithms like neural networks, random forests, or support vector machines[150].

III-3-6-1 Classical scoring functions

a) Empirical scoring functions

Empirical scoring functions gauge the binding affinity of a protein-ligand complex by considering a combination of various energetic factors inherent to the binding process. [151]These factors encompass aspects like hydrogen bonds, hydrophobic interactions, clashes between the protein and ligand, among others. [152]The appeal of these scoring functions lies in their efficiency, making them a favored choice in many docking software applications due to their ability to deliver results quickly and accurately. Nevertheless, their primary limitation arises from their reliance on calibration parameters, which can impact their reliability.[153]

b) Knowledge-based scoring functions

These functions originate from a meticulous examination of three-dimensional structures in ligand-protein complexes, which have been empirically determined through experiments.

[147] Kollman, P. A., Massova, I., Reyes, C., Kuhn, B., Huo, S., Chong, L., Cheatham, T. E. *Acc. Chem. Res*, **2000**, *33*(12), 889-897.
[148] Ain, Q. U., Aleksandrova, A., Roessler, F. D., & Ballester, P. J. *Comput. Mol. Sci*, 2015, *5*(6), 405-424.
[149] Li, J., Fu, A., & Zhang, L. *Interdiscip. sci. comput. life sci*, **2019**, *11*, 320-328.
[150] Li, H., Sze, K. H., Lu, G., & Ballester, P. J. *Wiley Interdiscip. Rev. Comput. Mol. Sci.*, **2021**, *11*(1), e1478.
[151] Eldridge, M. D., Murray, C. W., Auton, T. R., Paolini, G. V., & Mee, R. P. *J. Comput. Aided Mol.* **1997**, *11*, 425-445.
[152] Korb, O., Stutzle, T., & Exner, T. E. *J. Chem. Inf. Model*, **2009**, *49*(1), 84-96.
[153] Holloway, M. K., Wai, J. M., Halgren, T. A., Fitzgerald, P. M., Vacca, J. P., Dorsey, B. D., & Chen, L. J. *J. Med. Chem*, **1995**, *38*(2), 305-317.

By applying statistical methodologies, rules that delineate the favored geometric interactions are derived from these complex structures.[154]

These statistical functions serve a crucial purpose by enabling the establishment of a direct link between the thermodynamic state of the protein-ligand complex, which forms a dynamic system, and the likelihood of finding this complex in a specific microscopic state. To achieve this, the frequencies observed in the complexes are transformed into free enthalpy (energy) through the application of a Boltzmann distribution. Consequently, these potentials are referred to as potentials of mean force (PMF).[155,156]

c) Physics-based scoring functions:

Scoring functions rooted in physics principles or force fields, such as AMBER[157], GROMOS[158], and Tripos, employ a comprehensive approach to calculate the binding energy[159]. This computation involves aggregating the impacts of both bonded interactions (involving bond stretching, angle bending, and torsion angles) and non-bonded interactions (comprising van der Waals and electrostatic forces) within the protein-ligand complex. These interactions collectively represent the contribution of enthalpy to the overall energy.[160]

III-3-6-2 Machine-learning scoring functions

a) Consensus scoring functions

Consensus scoring functions involve the combination of multiple scoring methods to enhance the accuracy and reliability of predicting binding affinities between proteins and ligands[161]. By aggregating the results of different scoring functions, consensus scoring aims to reduce the impact of individual scoring function limitations and improve overall performance.[162] This approach leverages the strengths of various methods and increase hit rates, either by reducing the number of false positives or by statistically reducing the errors in the scores[163], thereby increasing the chances of identifying potential candidates with high

[154] Arrault, A. *Stratégies de docking-scoring assistées par analyse de données. Application au criblage virtuel des cibles thérapeutiques COX-2 et PPAR gamma* (Doctoral dissertation, Université d'Orléans), **2007**.
[155] Zheng, M., Xiong, B., Luo, C., Li, S., Liu, X., Shen, Q., Jiang, H. *J. Chem. Inf. Model*, **2011**, *51*(11), 2994-3004.
[156] Huang, S. Y., & Zou, X. *J. Comput. Chem.*, **2006**, *27*(15), 1866-1875.
[157] Lee, M. C., & Duan, Y. *Proteins: Structure, Function, and Bioinformatics*, **2004**, *55*(3), 620-634.
[158] Van Gunsteren, W. F., & Berendsen, H. J. *Angew. Chem., Int. Ed. Engl.*, **1990**, *29*(9), 992-1023.
[159] Su, M., Yang, Q., Du, Y., Feng, G., Liu, Z., Li, Y., & Wang, R. *J. Chem. Inf. Model*, **2018**, *59*(2), 895-913.
[160] Ruiz-Blanco, Y. B., Marrero-Ponce, Y., García, Y., Puris, A., Bello, R., Green, J., Sotomayor-Torres, C. M. *Chem. Phys. Lett*, **2014**, *610*, 135-140.
[161] Feher, M. *Drug Discov. Today*, **2006**, *11*(9-10), 421-428.
[162] Halperin, I., Ma, B., Wolfson, H., Nussinov, R. *Proteins: Structure, Function, and Bioinformatics*, **2002**, *47*(4), 409-443.
[163] Palacio-Rodríguez, K., Lans, I., Cavasotto, C. N., & Cossio, P. *Sci. Rep*, **2019**, *9*(1), 5142.

binding affinities.[164] The importance of molecular docking lies in its ability to provide valuable insights into the interactions between a potential drug and its target, which is critical for designing new drugs or optimizing existing ones.

Conclusion

In the present chapter we have highlighted the utility of the computational methodologies to explore the chemical data. From cheminformatics, bioinformationcs arriving to statistics constitute pivotal methodologies which revolutionized all the chemistry areas, especially for the drug design.

Design of experiments, DFT calculations and molecular docking are explored in the course of our thesis investigations and that with the main objective of designing reaction conditions and molecule structures as well as their bioactivity prediction.

[164] Ericksen, S. S., Wu, H., Zhang, H., Michael, L. A., Newton, M. A., Hoffmann, F. M., & Wildman, S. A. *J. Chem. Inf. Model*, **2017**, *57*(7), 1579-1590.

Part Two: Results and discussion

Chapter IV

Synthesis of α-aminophosphonates using diphenylphosphinic acid.

Introduction

Within the domain of synthetic chemistry, the quest for methodologies that are both efficient and sustainable stands as a fundamental pursuit. The escalating demand for streamlined synthetic processes underscores an imperative for systematic optimization strategies capable of augmenting reaction efficiency while concurrently minimizing resource consumption.

In response to this exigency, the application of Design of Experiments (DOE), a statistical methodology, has surfaced as a pivotal instrument in the realm of chemical synthesis. Functioning as a systematic framework for optimizing reaction parameters, DOE facilitates the simultaneous variation of multiple factors, empowering researchers to systematically untangle intricate interactions within a reaction system. This systematic approach culminates in the identification of optimal conditions that yield the desired outcomes, thereby advancing the efficiency and effectiveness of synthetic processes.

IV.1 Objective of the work

During the past decades, the *α*-aminophosphonates have been the subject of several in-depth researches in organic synthesis. In this work, we will contribute to the enrichment of organophosphorus compounds by a methodology development via the *Kabachnik-Fields* reaction using a novel organocatalyst under environmentally friendly conditions. The design of experiment method has been employed at the first time in the *Kabachnik-Fields* reaction to optimize the reaction parameters. This innovative methodology focuses on determining the ideal conditions by investigating the influence of three key factors: the catalyst quantity, temperature, and reaction time. Through this approach, we aspire to produce the α-aminophosphonates with excellent chemical yields, emphasizing both catalyst efficiency and eco-friendliness in the synthesis process.

IV.3 Results and discussion

IV.2 Choice of organocatalyst

In the continuation of our research, we have selected the phosphinic acid derivatives as an organocatalysts. Recently, our research group has been used the 1-oxo-1-hydroxy-2-c,5-t-diphenylphospholane as phosphinic acid derivative for the synthesis of bis *α*-aminophosphonates[1].

[1] Aissa, R., Guezane-Lakoud, S., Toffano, M., Gali, L., Aribi-Zouioueche, L. *Bioorganic & Medicinal Chemistry Letters*, **2021**, *41*, 128000.

The synthesis of diethyl *α*-aminophosphonate **IV.4** was accomplished by three components condensation in one pot via *Kabachnik-Fields* reaction. For that, we have chosen the condensation of aromatic aldehyde **IV.1** (115 mg, 1 mmol), aniline **IV.2** (99 mg, 1 mmol), and diethylphosphite **IV.3** (136 mg, 1.2 mmol) as model reaction in ethanol as green solvent at room temperature. (***Scheme 1).***

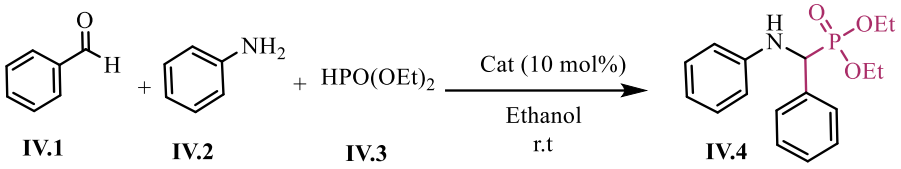

Scheme 1: The synthesis of diethyl *α*-aminophosphonate.

Initially, various organocatalysts were tested, including *Brønsted* acids such as (S, S)-1-oxo-1-hydroxy-2-c,5-*t*-diphenylphospholane (A), 1,1′-binaphtyl-2,2′-dihydrogene-phosphate (B), diphenylphosphinic acid (C), and diphenylphosphate acid (D). Additionally, proline derivatives like N-tert-butylpyrrolidine-2-carboxamide (E) and N-(2-trifluoroacetyl) pyrrolidine-2-carboxamide (F), as well as a Schiff base, namely (E)-1-(2-hydroxy-5-methoxybenzylidene-amino)-2,3-dihydro-1H-inden-2-ol (G), were investigated (***Figure 1***).

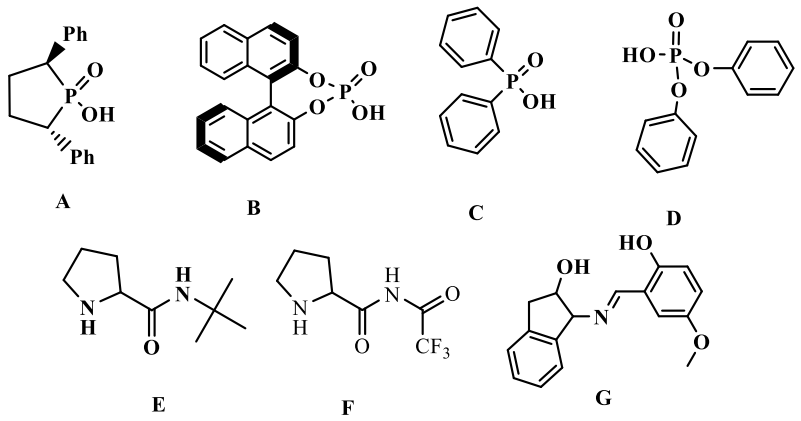

Figure 1: Different organocatalysts tested for the synthesis of *α*-aminophosphonates.

The catalyst screening involved the use of 10 mol% of each catalyst in ethanol at room temperature, and reactions were monitored for 6 hours. The progress of the reaction was tracked through thin layer chromatography (TLC) using an elution mixture of dichloromethane and methanol (80/20). (***Table1***).

Table 1: Test of organocatalysts for the synthesis of α-aminophosphonate.

Entry	**Organocatalyst (10 mol%)**	**Yield (%)[c]**
1[a]	--	--
2[b]	A	92
3	B	75
4	C	93
5	D	78
6	E	38
7	F	11
8	G	Trace

[a] Reaction conditions: aldehyde (1 mmol), aniline (1 mmol) and diethylphosphite (1.2 mmol) were stirred without catalyst in ethanol (2 mL), at 25°C, within 24 h. [b] Reaction conditions: aldehyde (1 mmol), aniline (1 mmol), and diethylphosphite (1.2 mmol) were stirred with the catalyst in ethanol (2 mL) at 25°C within 6 h. [c] Yield of the pure product purified by crystallization in hexane.

First, the multi-component reaction was conducted in ethanol without a catalyst, and even after 24 hours, no progress of reaction was noted, even by increasing the temperature up to 50 °C (***Table 1, entry 1***).

Subsequent experiments, as detailed in ***Table 1***, revealed that the employment of catalysts (**A)** and (**C)** led to the successful synthesis of the desired product with outstanding yields (92%, 93%) respectively (***Table 1, entries 2 and 3***). The enhanced activity of these catalysts is attributed to their relative lower acidity compared to the both catalysts (**B)** and (**D)**.

Regrettably, proline derivatives exhibited lower reactivities. The utilization of amido proline (**E**) and trifluoroacetoxy amido proline (**F**) resulted in α-aminophosphonate with yields of 38% and 11%, respectively (***Table 1, entries 6 and 7***). This diminished reactivity is likely attributed to the high acidity of (**E)** and (**F)**, stemming from their electron-withdrawing effects. Meanwhile, the limited solubility of Schiff base (**G**) remained a significant obstacle, hindering any progress in the reaction (***Table 1, entry 8***).

Considering the cost-effectiveness and ease of procurement of diphenylphosphinic acid (**C**) in contrast to the intricate preparation steps involved with (S, S)-1-oxo-1-hydroxy-2-c,5-*t*-

diphenylphospholane (**A**)[2,3], the (**C**) was chosen as the best one for the rest of our present investigation.

Diphenylphosphinic acid (DPPA or hdpp) (**C**) stands out as a versatile compound with specific properties. The presence of two aryl groups on the phosphorus atom contributes to the compound's stability by enhancing resonance. In addition, the phosphinic acid can be use as versatile ligand with specific electronic and steric properties that capable of forming a wide range of binding motif that have been utilized to improve the desired properties on the molecular level[4].

Bedolla-Medrano et *al*[5], have used the diphenylphosphinic acid as an organocatalyst (10 mol%, at 50°C) at the first time in the multicomponent condensation reaction involving the aromatic aldehyde, aniline, and diethylphosphite and the desired product was obtained with 76% chemical yield. Moreover, when combined with boronic acid (20 mol%), diphenylphosphinic acid (20 mol%) exhibits catalytic properties, displaying impressive efficacy in activating less reactive substrates such as *α,β*-unsaturated ketones **IV.6** and non-activated phenols[6] **IV.5** (***Scheme 2***). This catalytic action reaction leads to the formation of substituted 2H-chromenes **IV.7**, underscoring the versatile applications and transformative potential of diphenylphosphinic acid in various chemical processes.

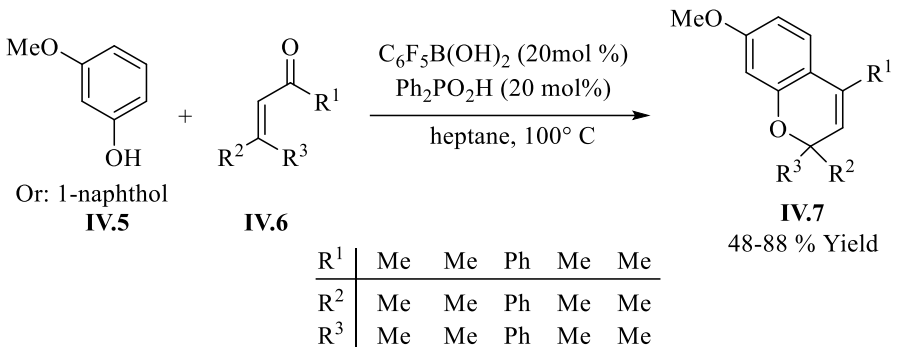

R^1	Me	Me	Ph	Me	Me
R^2	Me	Me	Ph	Me	Me
R^3	Me	Me	Ph	Me	Me

Scheme 2: Diphenylphosphinic acid catalyst the synthesis of 2H-chromenes.

In this study, we employed a full factorial design to systematically optimize the experimental framework, thereby minimizing the requisite number of trials and elucidating the optimal parameters governing the synthesis reaction of α-aminophosphonates. This investigation specifically utilized diphenylphosphinic acid as an innovative and efficacious catalyst within environmentally sustainable.

[2] Guillen, F., Rivard, M., Toffano, M., Legros, J. Y., Daran, J. C., & Fiaud, J. C. *Tetrahedron*, **2002**, *58*(29), 5895-5904.
[3] Guillen, F., & Fiaud, J. C. *Tetrahedron letters*, **1999**, *40*(15), 2939-2942.
[4] Kloda, M., Ondrušová, S., Lang, K., & Demel, J. *Coordination Chemistry Reviews*, **2021**, *433*, 213748.
[5] Bedolla-Medrano, M., Hernandez-Fernandez, E., & Ordonez, M. *Synlett*, **2014**, *25*(08), 1145-1149.
[6] Dimakos, V., Singh, T., & Taylor, M. S. *Organic & Biomolecular Chemistry*, **2016**, *14*(28), 6703-6711.

IV.3.1 Determination of factors and area of study

A comprehensive two-level full factorial model has been employed to systematically explore the impact of three critical factors namely, catalyst amount, medium temperature, and reaction time across a spectrum ranging from a lower level (-1) to a higher level (+1). To ensure a robust assessment of the model's clarity and curvature, the central point (0) was meticulously replicated thrice. These factors are the most studied parameters because of their influences on the reaction yield.

The total number of experiments (Enbr) undertaken is elucidated as follows:

$$E^{nbr} = 2^{\beta} + C_{(p)}$$

Here, β represents the number of operational factors, and $C_{(p)}$ denotes the count of center points utilized for assessing quadratic terms between the low and high factor levels. In this investigation, a total of eleven (11) experiments were conducted, encompassing various combinations of the studied factor levels. ***Table 2*** shows the selected operating factors and their corresponding levels in the experiment.

***Table 2*:** Coded levels for independent variables were used in the Full Factorial Design (2^3-FFD) Experiments.

Operating Factors	Symbols	Lower Level (-1)	Center point (0)	Higher Level (+1)
Catalyst amount (mol%)	Q_{Cat}	5	10	15
Reaction time (min)	T	15	30	60
Medium temperature (°C)	T°	25	40	50

IV.3.2 The response

The chemical yield (R%) was designated as the response (y) in order to attain the optimal conditions for the synthesis reaction of α-aminophosphonates.

IV.3.4 Performing tests

The optimization of α-aminophosphonate synthesis was systematically conducted through a comprehensive full factorial design, involving 11 experiments. Three distinct operating factors, each with varying levels, were considered in the experimental matrix, as outlined in ***Table 3***. The subsequent data from this table will be subjected to rigorous statistical analysis, aiming to derive accurate coefficients for the mathematical model that characterizes the response.

Table 3: Reaction conditions applied in Full Factorial Design (2^3-FFD) experiments for the synthesis of α-aminophosphonates under green conditions.

Run number	Operating factors						Chemical yields	
	Coded			Uncoded				
	X_1	X_2	X_3	t (min)	Q_{cat} (%)	T (°C)	R_{Exp} (%)	R_{Pred} (%)
1	-1	-1	-1	15	5	25	20.00	22.25
2	+1	-1	-1	60	5	25	40.00	37.75
3	1-	+1	-1	15	15	25	68.00	65.75
4	1+	1+	-1	60	15	25	70.00	72.25
5	1-	1-	+1	15	5	50	50.00	47.75
6	1+	1-	1+	60	5	50	60.00	62.25
7	1-	1+	1+	15	15	50	78.00	80.25
8	1+	1+	1+	60	15	50	88.00	85.75
9	0	0	0	30	10	40	90.00	90.00
10	0	0	0	30	10	40	90.00	90.00
11	0	0	0	30	10	40	90.00	90.00

The results obtained revealed a notable range in chemical yield (R%), spanning from 20% to 90%. This expansive experimental spectrum signifies an enhanced capability to encompass a diverse range of conditions, potentially incorporating the optimal conditions necessary for the desired outcome.

IV.3.5 Statistical results

IV.3.5.1 Determination of significant coefficients of the model

The determination of coefficients for the hypothesized model involved the application of MINITAB version 14 software, leveraging its advanced matrix calculation capabilities as outlined in ***Table 4***. This software, specialized in statistical processing, encompasses a diverse array of features. In the context of our study, it played a pivotal role in conducting regression and graphical analyses on experimental data pertinent to aminophosphonate synthesis. Furthermore, MINITAB proves versatile by accommodating both one-way and multi-way analysis of variance calculations, affirming its proficiency in handling diverse and intricate statistical analyses.

In this context, the interactions encompass: X_1X_2, X_1X_3, and X_2X_3. The corresponding effects matrix is detailed in ***Table 4***.

Table 4: Estimated regression coefficients for yield (R%).

	Terms	Coefficients
	Constant	*59.25*
t	**X_1**	*5.25*
Qcat	**X_2**	16.75
T°	**X_3**	*9.75*
t*Qcat	**$X_1.X_2$**	*-2.25*
t*T°	**$X_1.X_3$**	*- 0.25*
Qcat*T°	**$X_2.X_3$**	*-2.75*

A linear polynomial equation can be utilized to articulate the mathematical relationship between chemical yields and the tested operating parameters:

(✓) $R_{\%}=59.25 +5.25\ t +16.75\ Q_{cat} +9.75\ T° -2.25\ t*Q_{cat} – 0.25\ t*T° -2.75\ Q_{cat}*T° +30.75\ Ct\ Pt$

IV.3.5.2 Analysis of variance (ANOVA)

The ANOVA test was employed to assess the significant impact of operational factors and their interactions on chemical yield (R%). In ***Table 5***, the F-ratio, p-value, sum of squares, and mean square for each parameter are presented, derived from the preceding mathematical equations. P-values serve as a measure to ascertain the significance of each coefficient, elucidating the degree of interaction for each parameter. Statistical evaluation of this model was conducted using *Fisher's* statistical test or *Student's* t-test for analysis of variance.

Table 5: ANOVA test for quadratic models for the synthesis of α-aminophosphonates under green conditions.

Source	DF	Adj SS	Adj MS	F-Value	P-Value
Model	7	5390.05	770.01	57.04	0.003
Linear	3	3225.50	1075.17	79.64	0.002
T	1	220.50	220.50	16.33	0.027
Q cat	1	2244.50	2244.50	166.26	0.001
T°	1	760.50	760.50	56.33	0.005
2-Way Interactions	3	101.50	33.83	2.51	0.235
t*Q cat	1	40.50	40.50	3.00	0.182
t*T°	1	0.50	0.50	0.04	0.860

Q cat*T°	1	60.50	60.50	4.48	0.125
Curvature	1	2063.05	2063.05	152.82	0.001
Error	3	40.50	13.50		

S	**R-sq**	**R-sq(adj)**
3.67423	99.25%	97.51%

The quadratic regression analysis reveals a remarkably high F-value, equal to 57.04, signifying the pronounced significance of the model. Examination of the experimental data demonstrates that over 99% of the collected data can be effectively predicted by the adopted model. The R^2 value attains 99.25%, with an R^2 adj of 97.51%, indicating a well-adjusted model. This high level of correlation between the experimental and calculated values affirms the reliability of the model in accurately representing the chemical yield under varying operational conditions.

IV.3.5.3 Main individual effects

The graphical representation illustrating the impact of various factors is succinctly presented in ***Figure 2***, clearly delineating that the catalyst quantity (Qcat) exerts a significantly more positive influence than other factors.

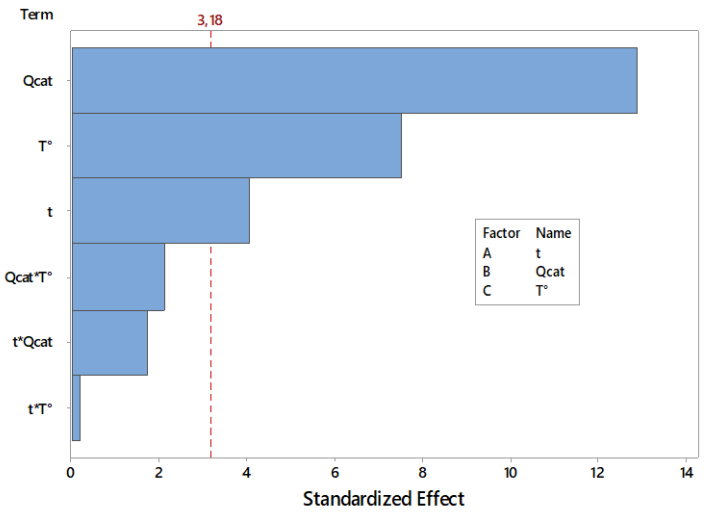

Figure 2: Pareto chart including the standardized effect of each factor on the chemical yields of the synthesis of α-aminophosphonates using diphenylphosphinic acid.

Additionally, the ***Figure 2*** and ***Table 5*** reveal that both reaction time (t) and temperature (T°) exhibit moderately positive effects.

Examining the hierarchy of factors influencing chemical yields, as depicted in ***Figure 3***, the catalyst quantity (Qcat) emerges as the foremost contributor with a substantial effect of 33.50, surpassing the moderate effects of medium temperature (19.50) and reaction time (10.50).

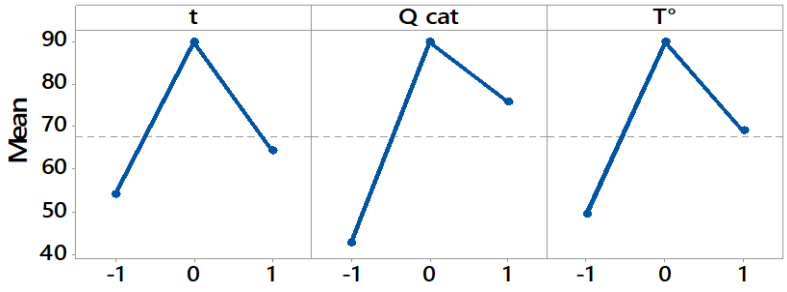

***Figure 3*:** Main effects of the operating factors for the synthesis of α-aminophosphonates using diphenylphosphinic acid.

IV.3.5.4 Interaction effects between operating factors

The interplay among the examined operational factors is elucidated in ***Figure 4***. The results gleaned from the analysis underscore the utmost significance of the interactions between Qcat/T° and t/Qcat, manifesting as substantial negative effects of -5.5 and -4.5, respectively.

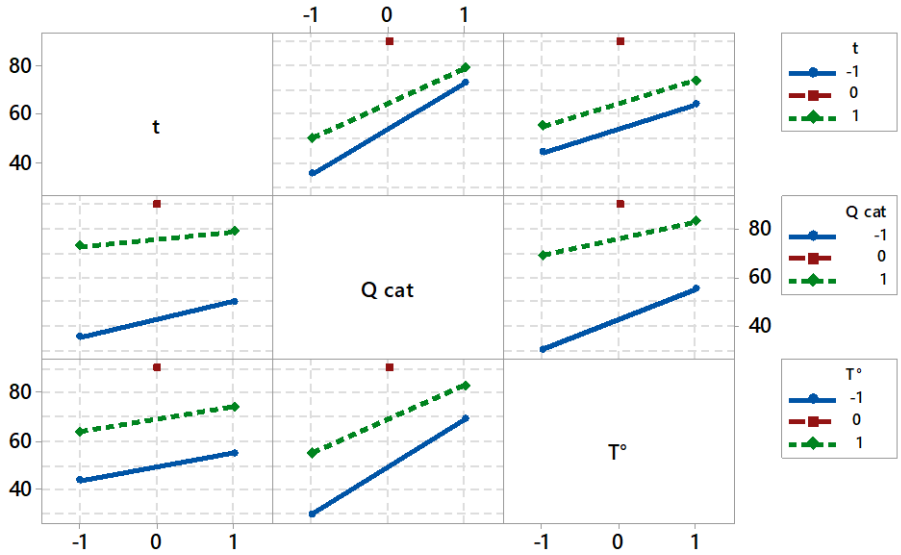

***Figure 4*:** Interactions effects between the operating factors for the synthesis of α-aminophosphonates using diphenylphosphinic acid.

This significance is further affirmed by the discernible non-parallel borders of these effects. Conversely, the interactions between reaction time (t) and the medium temperature effect exhibited an inconsequential impact, as evidenced by probabilities exceeding 0.05, notably 0.860. This observed phenomenon can be attributed to the absence of a synergistic effect between these operational factors.

IV.3.5.5 Determination of optimum conditions

The response surface plan serves as a valuable tool for visualizing the interdependencies among factors, aiding in the identification of optimal conditions for achieving a high chemical yield in the synthesis of *α*-aminophosphonates. This three-dimensional graphical grid represents the functional relationship between a response variable and two experimental factors. In our investigation, ***Figure 5*** showcases 3D surface plots illustrating the evolution of chemical yield in the synthesis of α-aminophosphonates using diphenylphosphinic acid as an efficient organocatalyst, specifically in relation to Qcat/T° and t/Qcat (***Figure 3***).

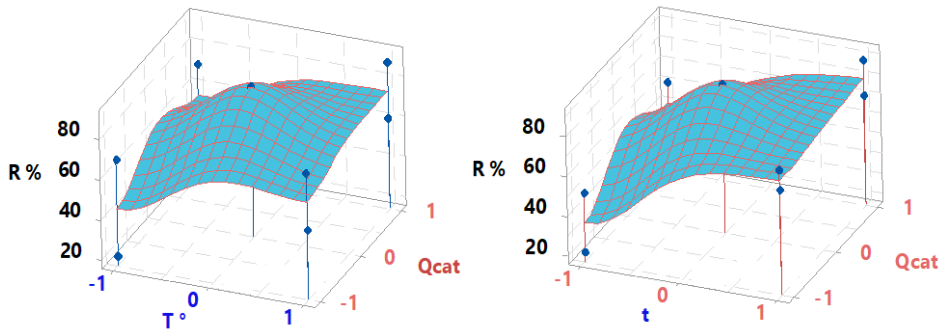

Figure 5: Three-dimensional surface plot of chemical yields as a function of Qcat/ T° and t/Qcat for the synthesis of *α*-aminophosphonates using diphenylphosphinic acid.

The results obtained from these plots reveal that the highest chemical yield (R% Exp) of 90.00% was attained when each factor was set at its optimal level, aligning well with the predicted chemical yield (R% pred) of 93.51%. Notably, the chemical yields (R%) exhibit a pronounced increase with the escalating amount of diphenylphosphinic acid, underscoring the intricate interplay among the studied factors. This observation reinforces the impact of the interaction effects. ***Table 6*** succinctly presents the optimal conditions under which the best chemical yields for the synthesis of *α*-aminophosphonates were achieved in our study.

Table 6: Optimum conditions for the synthesis of *α*-aminophosphonates using diphenylphosphinic acid as an efficient organocatalyst.

Operating Factors	Symbole	Optimum Values
Reaction time	t	30
Catalyst amount	Q_{cat}	10
Medium temperature	T°	40
Predicted chemical yield	R % $_{Pre}$	90.00%
Experimental chemical yield	R % $_{Exp}$	93.51%

IV.3.6 Characterization

The structure was confirmed by analytical and spectra data. The **^{1}H NMR** spectra showed the main characteristic peaks of *α*-aminophosphonate; two triplets between 114-1.31 ppm each exhibiting the same coupling constant (7.1 Hz) corresponding to 2(C**H$_3$**-CH$_2$-O) and three massifs between 3.63-4.18 ppm corresponding to 2(CH$_3$-C**H$_2$**-O), while the **H***C-P appeared in 4.84–4.755 ppm. The aromatic protons located between 6.61-7.52 ppm. (***Figure 6).***

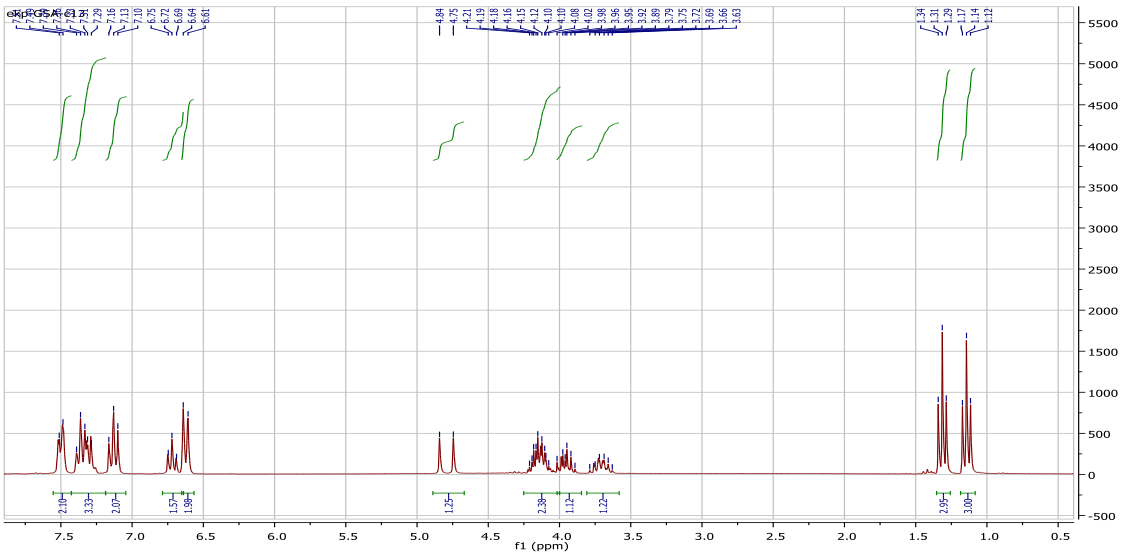

Figure 6: ^{1}H NMR spectrum of product IVl.

The **^{13}C NMR** analyses of *α*-aminophosphonate mentioned the presence of the phosphonate moiety; two doublets manifest at 16.37 and 16.46 ppm for the two methyl of ethoxy groups with a coupling constant ranging (*J*) 5.6 and 15.1 Hz for each one, and at 55 ppm for the **C**H$_2$- of ethoxy. For H***C**-P it is appeared at 63.27 ppm as doublet with

J^2_{CP}=6.9 Hz. In addition, the carbon atoms of aromatic ring have situated between 113-146 ppm. (***Figure 7).***

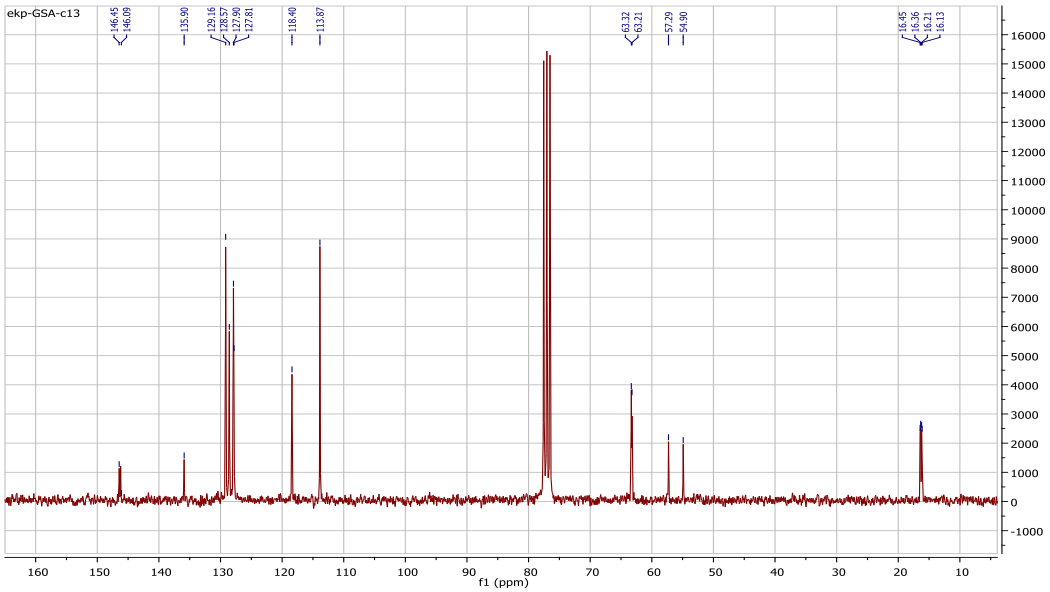

Figure 7: ^{13}C NMR spectrum of product IVl.

The **^{31}P NMR** confirms the structure of the *α*-aminophosphonates through the presence of a peak at approximately 22.46 ppm, corresponding to the phosphonate group. (***Figure 8).***

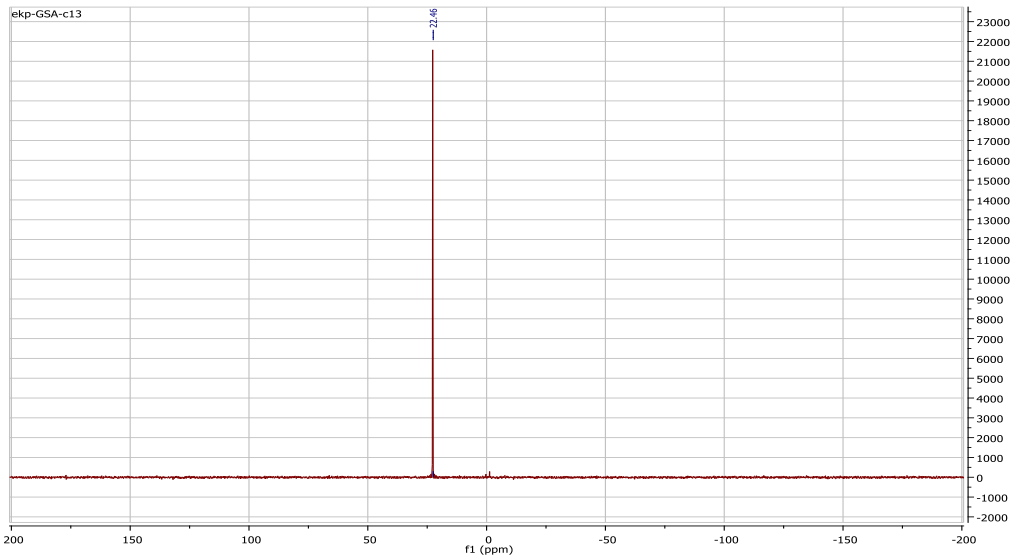

Figure 8: ^{31}P NMR spectrum of product IVl.

The **HRMS** data reveals a crude formula of $C_{17}H_{23}NO_3P$ and an atomic mass of [M + H+]: 320.140.

IV.3.7 Applied of the optimal conditions

After employing the optimized conditions from factorial experiments, we conducted an extensive exploration into the efficacy and constraints of multicomponent reactions (MCRs) applied to a diverse array of aromatic aldehydes and anilines featuring various electron-withdrawing and electron-donating groups in the presence of diethylphosphite. The reaction proceeds with 10 mol% of diphenylphosphinic acid as a *Brønsted* catalyst in ethanol at 40 °C within 30 minutes. The synthesis yielded noteworthy results.

The results in **Table 7** show the remarkable efficiency of diphenylphosphinic acid as an organocatalyst in the multicomponent *Kabachnik-Fields* reaction. When employing anilines in conjunction with benzaldehyde, 3-methoxybenzaldehyde, and 4-nitrobenzaldehyde, the *α*-aminophosphonates **IV.14a**, **IV.14b**, and **IV.14c** were obtained with outstanding chemical yields, reaching up to 90%, these results due to the electron effect of substitutes, which enhance the reactivity of the reaction. Similarly, toluidine paired with 1-naphthylbenzaldehyde, benzo[1,3]dioxole-5-carbaldehyde, and 4-fluorobenzaldehyde resulted in the formation of **IV.14d**, **IV.14e**, and **IV.14f** with excellent yields (90%, 91% and 80%) respectively. The methyl-trifluoroaniline partially decreases the nucleophilicity of aniline giving the desired products **IV.14g**, **IV.14h** and **IV.14i** with chemical yields (88, 78 and 87%) respectively.

This comprehensive study underscores the versatility of our approach across a range of substrates, delivering both high efficiency and notable yields in the synthesis of *α*-aminophosphonates.

Table 7: Diphenylphosphinic acid catalyzed *α*-aminophosphonates synthesis.

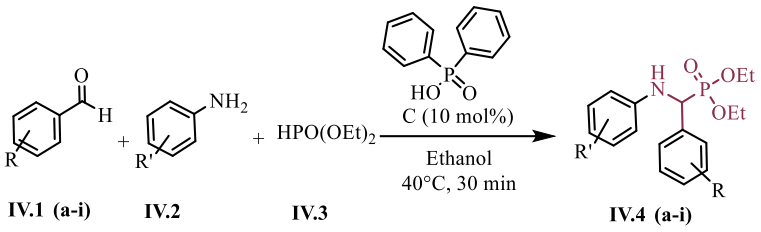

Product 4 **(yield)**[b]

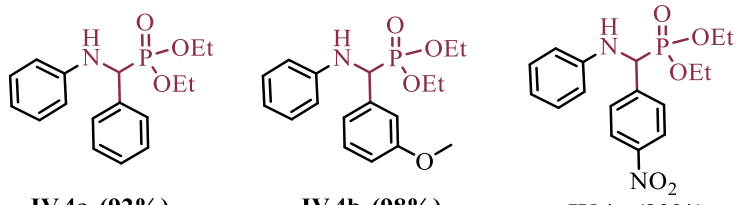

IV.4a (92%) **IV.4b (98%)** **IV.4c (90%)**

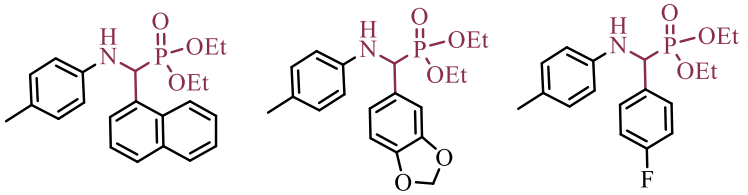

IV.4d (90%) **IV.4e (91%)** **IV.4f (80%)**

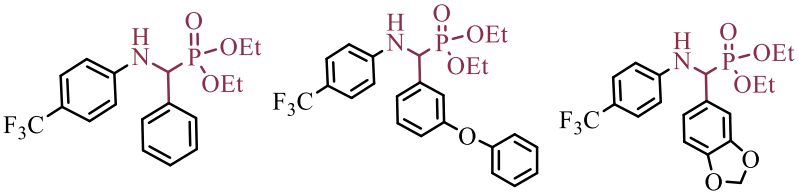

IV.4g (88%) **IV.4h (78%)** **IV.4i (87%)**

[a]The reaction was conducted using 1 mmol of benzaldehyde, 1 mmol of aniline, and 1.2 mmol of diethylphosphite in the presence of 10 mol% diphenylphosphoric acid. The reaction took place in 2 mL of ethanol at 40°C for 30 minutes. [b]Purification was performed through crystallization in hexane.

IV.3.8 Proposed mechanism

Based on the obtained results and drawing from our prior research, we propose a mechanistic pathway for the synthesis of *α*-aminophosphonates through a one-pot multicomponent condensation reaction involving aromatic aldehyde, amine, and diethylphosphite, catalyzed by diphenylphosphinic acid. Our hypothesis posits a pivotal role for the catalyst in the initial step, where it activates the carbonyl carbon of the aldehyde

through the formation of hydrogen bonds, facilitating the nucleophilic attack by the amine and resulting in the in situ formation of an imine intermediate.

Recognizing the reversible nature of imine formation, immediate trapping by the catalyst occurs, preventing the hydrolysis of the imine substrate to the amine and aldehyde in the presence of water. Subsequently, the coordinated catalyst enhances the electrophilicity of the imine, facilitating the nucleophilic attack of diethylphosphite. This concerted action leads to the formation of the desired *α*-aminophosphonates, with the simultaneous release of the catalyst (***Scheme 3***).

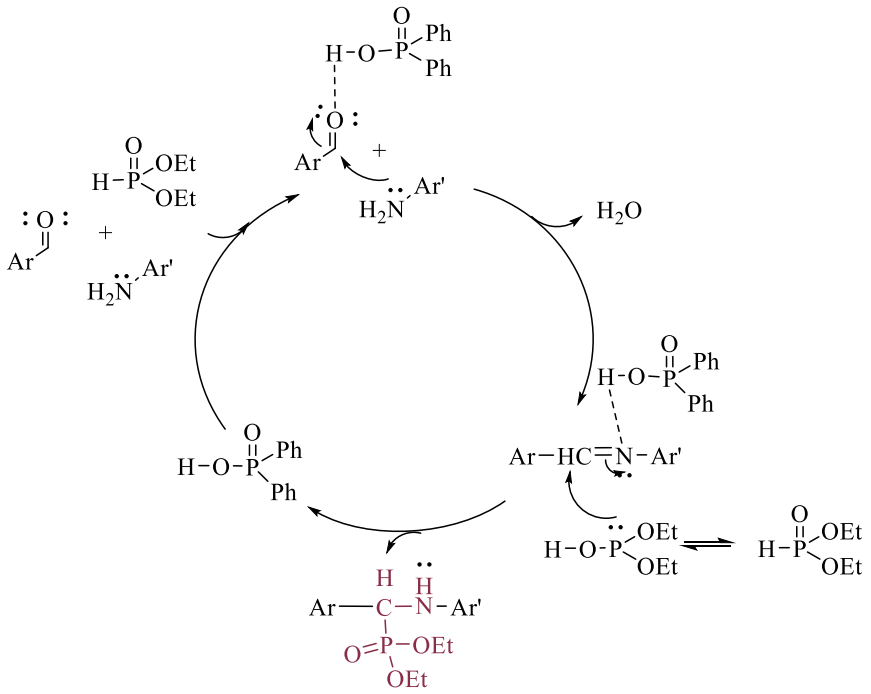

Scheme 3: Plausible reaction mechanism for the synthesis of *α*-aminophosphonates using diphenylphosphinic acid.

Conclusion

In this chapter, we have developed the synthesis of a series of *α*-aminophosphonates through multicomponent *Kabachnik-Fields,* employing the diphenylphosphinic acid as a *Bronsted* acid and an eco-compatible organocatalyst. Our study was dedicated to identifying the optimal conditions for enhancing the chemical yields of *α*-aminophosphonates. We adopted a comprehensive two-level experimental design method, focusing on three critical operating parameters: catalyst amount, reaction time, and medium temperature.

Our statistical analysis revealed that the quantity of diphenylphosphonic acid significantly influenced on the reaction yield. Furthermore, the regression analysis demonstrated a robust correlation between the experimentally obtained yields (R% Exp) and predicted yields (R% Pred), affirming the model's validity and practicality, with remarkable R^2 values reaching up to 99.25%.

The utilization of a full factorial experiment design in the synthesis of *α*-aminophosphonates played a pivotal role in uncovering optimal conditions for maximizing reaction yields. This approach allowed us not only to scrutinize individual factors but also to unravel the intricate interplay between variables. The success of this method is evident in the strong correlation observed between experimentally obtained yields and calculated values, as indicated by consistently high and significant R^2 values.

Chapter V

Synthesis of α-aminophosphonates using 2-Hydroxymethyl-18-Crown-6.

Introduction

The utilization of crown ethers as organocatalysts in multicomponent reactions constitutes a compelling and dynamic domain within organic synthesis. Recognized for their distinctive molecular architecture featuring a cyclic arrangement of oxygen atoms, crown ethers have evolved into versatile catalysts proficient in orchestrating intricate chemical transformations.

This chapter immerses itself in the fascinating realm of crown ether-mediated organocatalysis during multicomponent reactions, shedding light on the pivotal role these compounds play in facilitating the assembly of diverse substrates into sophisticated molecular architectures. As we navigate through the complexities of this catalytic strategy, a deeper understanding of the underlying principles, mechanisms, and synthetic applications emerges, underscoring the effectiveness of crown ethers in steering multicomponent reactions and making noteworthy contributions to the ever-expanding toolkit of modern organic synthesis.

V.1 Objective of the work

In order to extend our previous studies on the preparation of organophosphorus compounds derivatives, we investigate to develop a novel method for the synthesis of *α*-aminophosphonate derivatives via *Kabachnik-Fields* reaction through multicomponent in one pot of aromatic aldehyde, aniline and diethylphosphite using an organocatalyst under green conditions.

A pivotal focus of our research involves a meticulous examination of the impact of the crown ether as an organocatalyst with studying the influence of different parameters such as; solvent effect, quantity amount of catalyst and temperature on the outcomes of the reactions. This pioneering approach represents the first use of the crown ether as catalyst in the multicomponent *Kabachnik-Fields* reaction.

Because the potential activities of the *α*-aminophosphonates have widly described in the littérature, the docking molecular of our compounds has been carried out, after geometry optimization by DFT, in order to estimate their biological activity and to determine the banding interactions with the selected protein.

V.2 Bibliographic update of crown ether

Since its discovery by *Liittringhaus*[1] in **1937** and subsequent recognition by *Pedersen*[2] in **1967** for its ability to form stable complexes with alkali and alkaline earth metal salts, crown ethers have garnered significant interest across various scientific disciplines. Functioning as "host-guest" molecules, these compounds feature a hydrophobic ring enveloping a hydrophilic cavity, facilitating complex formation with metal ions[3]. Originally employed as solvent extraction reagents[4] and phase transfer catalysts[5], crown ethers have demonstrated ion-transport capabilities, particularly with sodium and potassium ions, enhancing their transport across cell membranes[6]. Additionally, they have proven beneficial as additives, enhancing the reactivity and selectivity of certain lipases[7]. Beyond this, crown ethers function as catalysts through noncovalent binding with both organic neutral and ionic species, promoting various reactions such as aldolization[8], allylic substitution, and asymmetric hydrogenation[9].

In this context, catalytic amounts of crown ethers combined with solid KOH or K_3PO_4 prove sufficient to activate 3-aryl phthalides **V.1** to facilitate the nucleophilic attack on *α,β*-unsaturated carbonyl **V.2**. This efficient activation leads to the successful execution of the diastereoselective arylogous *Michael* reaction resulting in a single diastereomer **V.3** with impressive yields and excellent diastereomeric excesses[10], as illustrated in ***Scheme 1***.

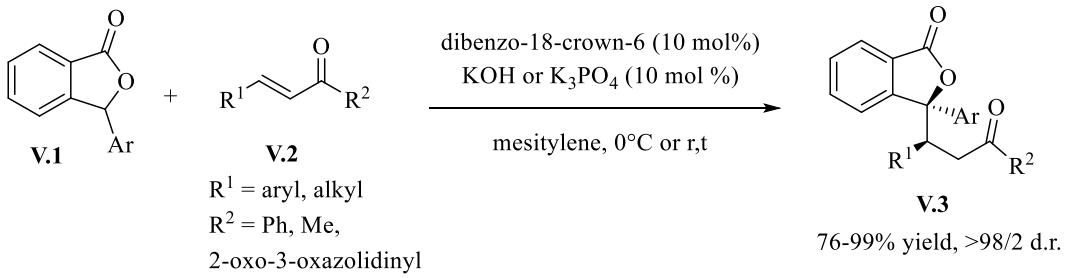

Scheme 1: Dibenzo-18-crown-6 catalyzed diastereoselective arylogous *Michael* reaction.

[1] Liittringhaus, A. *Justus Liebigs Ann. Chem*, **1937**, 528, 181,210.
[2] Pedersen, C. J. *J. Am. Chem. Soc*, **1967**, 89(10), 2495–2496.
[3] (a) Dix, J. P., Wittenbrink-Dix, A., & Vögtle, F. *Sci. Nat,* **1980**, *67*, 91-93. (b) Pedersen, C. J. *J. Am. Chem. Soc*, **1970**, *92*(2), 386-391.
[4] McDowell, A. *Sep Sci Technol*, **1988**, *23*(12-13), 1251-1268.
[5] Cinquini, M., & Tundo, P. *Synth* ***1976***, (08), 516-519.
[6] Lamb, J. D., Izatt, R. M., & Christensen, J. J. *Progr. Macro. Chem. J. Wiley & Sons, New York, NY*, **1981**, *2*, 41-90.
[7] Merabet, M., Melais, N., Boukachabia, M., Fiaud, J. C., & Zouioueche-Aribi, L. *J. Soc. Alg. Chim*, **2007**, *17*(2), 185.
[8] Nagayama, S., & Kobayashi, S. *J. Am. Chem. Soc*, **2000**, *122*(46), 11531-11532.
[9] Luo, Y., Ouyang, G., Tang, Y., He, Y. M., & Fan, Q. H. *J. Org. Chem*, **2020**, *85*(12), 8176-8184.
[10] Sicignano, M., Dentoni Litta, A., Schettini, R., De Riccardis, F., Pierri, G., Tedesco, C., & Della Sala, G. *Org. Lett*, **2017**, *19*(16), 4383-4386.

It is important the noted that the use of cown ethers as catalyst in multicomponent reaction is few described. Recently, the crown ether 18-crown-6 has been used as an efficient organocatalyst for reductive functionalization of CO_2 to N-containing benzoheterocyclics. Various benzimidazoles, benzoxazoles and benzothiazoles derivatives **V.5** could be respectively synthesized via the reductive cyclization of CO_2 with 1,2-phenylenediamine, 2-aminophenol and 2-aminothiophenol **V.4** by using 18-crown-6 catalyst with good to excellent yield (99% >yield >59%) (***Scheme 2***)[11].

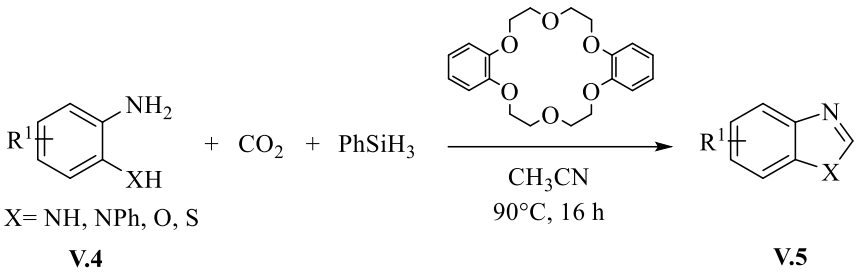

Scheme 2: 18-Crown-6 ether catalyzed synthesis of N-containing benzoheterocyclics through reductive cyclization.

In **2010**, *Masilamani-J* and *al*[12], have demonstrated a three component coupling of arynes **V.6** with N-heteroaromatics including quinolines derivatives **V.7** and terminal alkynes in the presence of KF and 18-crown-6 in THF at room temperature for 8h, obtaining N-arylated 1,2-dihydroaromatics-2-quinolinylalkynes **V.8** in good to moderate yields. The study shows that the crown ether increases the solubility of KF in the THF solution (***Scheme* 3**)

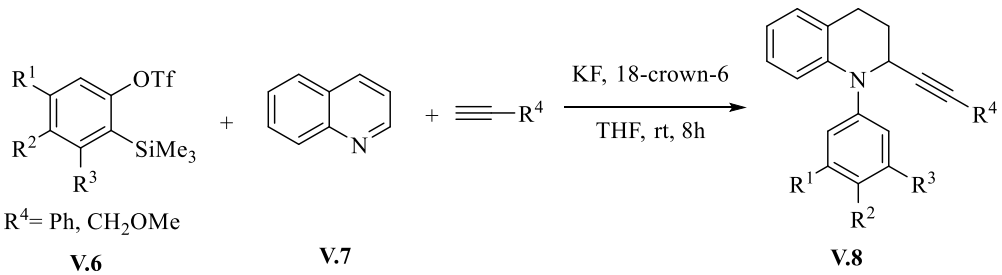

Scheme 3: KF/18-crown-6 used as catalyst for the N-arylated 1,2-dihydroaromatics-2-quinolinylalkynes synthesis.

In **2020**, and based on the work mentioned above, *Lim, T* and *al* [13]have used the crown ether as additive in the multicomponent phosphonylation for the *α*-aminophosphonates

[11] Ruxu Yao, Youjie Li, Jiahuan Wang, Jinzhu Chen , Yisheng Xu, *J. Catal*, **2023,** 418, 78–89
[12] Jeganmohan, M.; Bhuvaneswari, S.; Cheng, C.-H. *Chem. Asian J.* 2010, 5, 153–159.
[13] Lim, T., & Kim, B. M. *The Journal of Organic Chemistry*, **2020**, *85*(20), 13246-13255.

synthesis **V.11.** This reaction proceeds by the condensation of imine **V.9**, aryne **V.10**, and diethylphosphite, as depicted in ***scheme 4***.

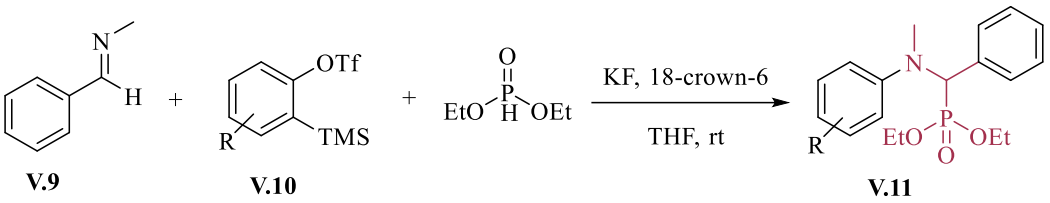

V.9 **V.10** **V.11**

R = 2-Me, 4-Me, 4-MeO, 4-F, 3-OMe

53-82% yield

Scheme 4: 18-crown-6 used as additive in the multicomponent phosphonylation of an aryne–imine adduct.

V.3 Results and discussion

V-3-1 Optimization of reaction conditions

The synthesis of *α*-aminophosphonates **V.14 (a-k)** was accomplished through one-pot condensation of three components using the *Kabachnik-Fields* reaction, employing crown ethers as organocatalysts. For that we conducted involving of benzaldehyde (1 mmol), aniline (1 mmol) and diethylphosphite (1.2 mmol) as a model reaction in THF. First, we examined the condensation without catalyst in THF, no progress of reaction was observed even after 24h at room temperature (***Table 1, entry 1***).

Several parameters were studied, such as; the catalytic amount of the organocatalysts, solvents effect, temperature and reaction time.

V-3-1-1 Effect of crown ether type

In this section, we have tested several crown ethers in a multicomponent reaction for the synthesis of *α*-aminophosphonate in order to identify which is the most effective one. The five crown ethers selected are: 18-crown-6 (A), 15-crown-5 (B), 12-crown-4 (C), 2-hydroxymethyl-18-crown-6 (D), and bibenzo-18-crown-6 (E). The catalysts screening was made with 5 mol % of each catalyst in THF (2 ml) at room temperature (***Figure 1***).

The progression of the reaction was monitored using thin-layer chromatography (TLC) with a dichloromethane elution.

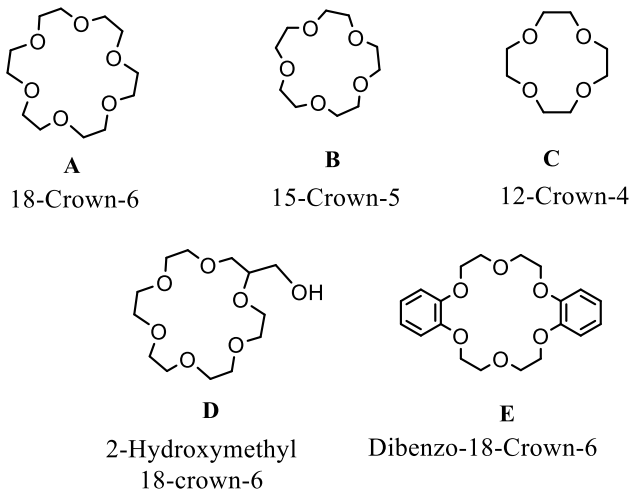

***Figure 1*:** Crown ethers tested.

Table 1 : Different organocatalysts tested[a]

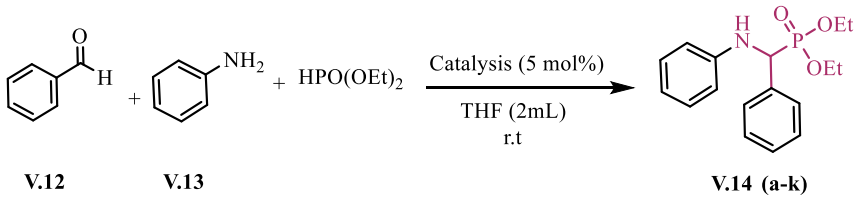

Entry	Catalyst (5 mol%)	Yield (%)[c]
1[b]	Free-catalyst	--
2	18-Crown -6 **(A)**	Traces
3	15-Crown -5 **(B)**	Traces
4	12-Crown -4 **(C)**	Traces
5	**2-Hydroxymethyl-18-Crown -6 (D)**	**91**
6	dibenzo-18-Crown -6 **(E)**	Traces

[a] Reaction conditions: benzaldehyde (1 mmol), aniline (1 mmol) and diethylphosphite (1.2 mmol) were stirred with catalyst (5 mol%) in THF (2 mL) at room temperature, within 24h,. [b] Yield of the pure product purified by crystallization in hexane.

Under these conditions, only 2-Hydroxymethyl-18-Crown-6 **(D)** can promote the multicomponent reaction, obtaining the desired product with excellent chemical yield (**91%)** (***Table 1, entry 5*).** However, the traces of product were obtained using the organocatalysts (**A, B, C** and **E**) (***Table 1***, ***entries 2, 3, 4*** and ***6*).** The efficiency of the 2-Hydroxymethyl-18-

Crown-6 **(D)** can be explained by the formation of hydrogen bonds with the carbonyl group of aldehyde, which, in turn, facilitated the nucleophilic attack of diethylphosphite. In a ground breaking development, the application of 2-Hydroxymethyl-18-Crown-6 ether as a polar moiety reagent has recently been documented for the first time.

III-3-1-2 Influence of the solvent nature

The influence of the hydrophobicity/hydrophilicity characteristics of the organic medium on the outcomes of our optimized reaction employing 2-Hydroxymethyl-18-crown-6 **(D)** over a 24 h at room temperature was also investigated. Various solvents with distinct hydrophobicities were tested, such as; THF (logP= 0.46), EtOH (logP= -0.18), CH_2Cl_2 (logP= 1.25), CH_3CN (logP= -0.37), AcOEt (logP= 0.73), and TBME (logP= 0.35).

Figure 2 illustrates the results, indicating that there is no significant correlation between the chemical yields of the desired product **V.14a** and the *logP* coefficient. Notably, THF emerged as the most favorable solvent, yielding the desired product with an excellent yield of 91%. Conversely, TBME, AcOEt, and CH_2Cl_2 resulted in low yields (<30%), while CH_3CN produced a 40% of chemical yield. EtOH, under the same conditions, afforded the desired product with a 56% yield.

These findings underscore the critical role of THF as solvent in optimizing reaction outcomes, showing the total disappearance of all reagents within 15min of stirring.

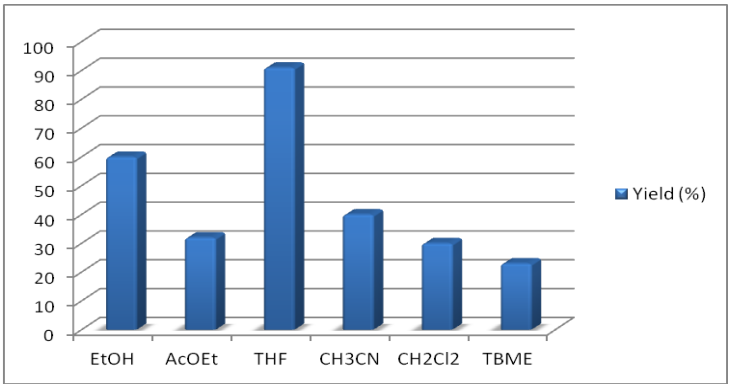

Figure.2: Impact of the organic solvent hydrophobicity's.

III-3-2 Exemplification

In order to validate the efficacy of optimal conditions using 2-Hydroxymethyl-18-crown-6 **(D)**, we implemented enhanced conditions for a multi-component reaction involving a range of substituted benzaldehydes and anilines, encompassing both electron-withdrawing and electron-donating groups and diethylphosphite. The results show that the efficiency of the

reactions 2-Hydroxymethyl-18-crown-6 used as novel organocatalyst in the multicomponent *Kabachnik-Field* reaction for the preparation of *α*-aminophosphonates. These derivatives were subsequently obtained through crystallization in hexane. The molecular structures of these synthesized *α*-aminophosphonates were confirmed through spectroscopic analyses, including ^{1}H, ^{13}C, and ^{31}P NMR, as well as high-resolution mass spectrometry (HRMS).

The outcomes of the multicomponent reactions dependent on the electronic effects of the substitutes. The use of benzaldehyde, 4-chlorobenzaldehyde, 4-nitrobenzaldehyde, 1-naphthaldehyde, 4-phenylbenzaldehyde, and 4-methoxybenzaldehyde with aniline resulted the corresponding products **V.14a**, **V.14b**, **V.14c**, **V.14d**, **V.14e**, and **V.14f**, with yields ranging from 80% to 93%. Similarly, employing toluidine in conjunction with the aforementioned series of aromatic aldehydes produced the corresponding products **V.14g**, **V.14h**, **V.14i**, **V.14j**, **V.14k**, and **V.14l**, with yields of up to 90%, attributed to the electron-donating nature of toluidine. (***Table 2***).

Table 2: 2-hydroxymethyl-18-crown-6 catalyzed the synthesis of diethyl *α*-aminophosphonates V.14a-r[a]

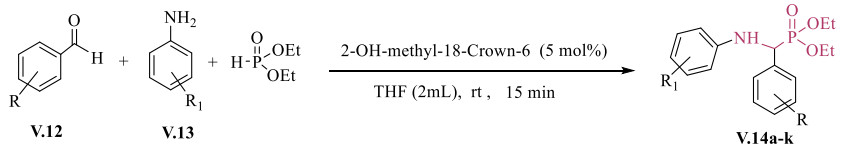

V.12 V.13 V.14a-k

Product V.14a-k (yield)[b]
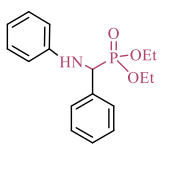 V.14a (91%)
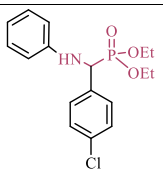 V.14b (80%)
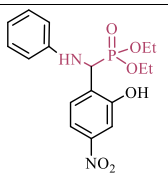 V.14c (93%)
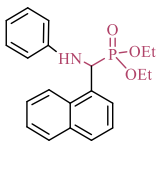 **V.14d(88%)**
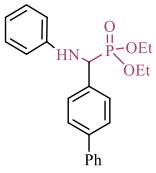 **V.14e (86%)**
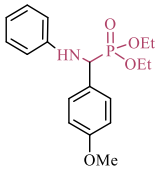 **V.14f (90%)**
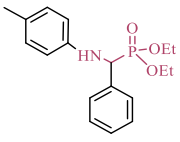 **V.14g (94%)**
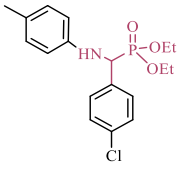 **V.14h (90%)**
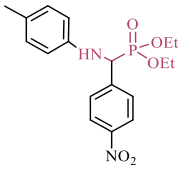 **V.14i (92%)**

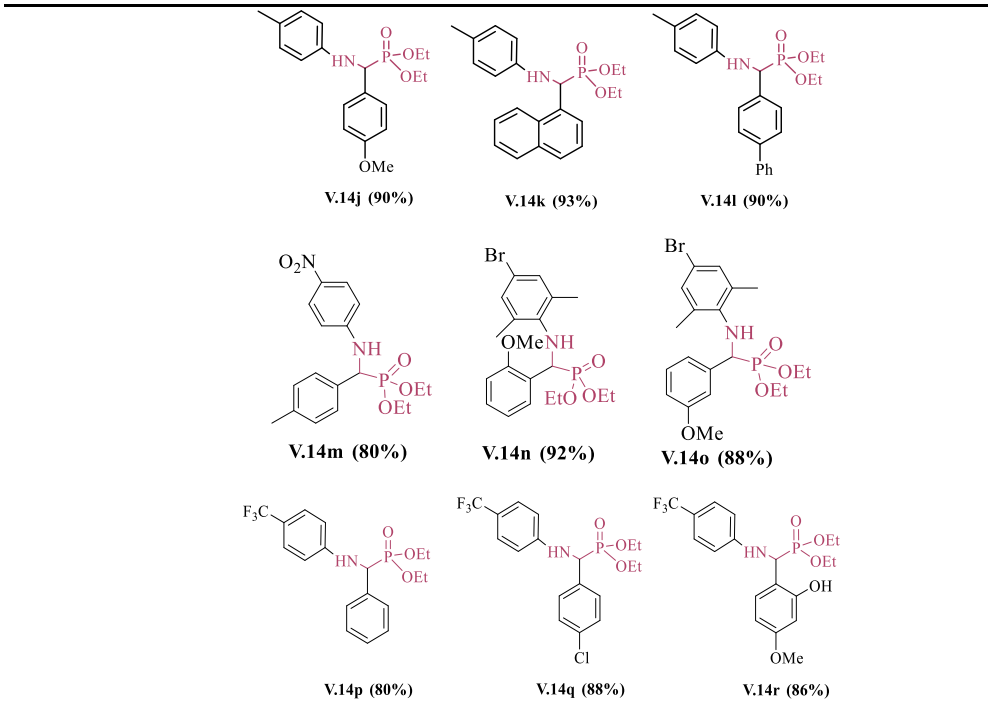

[a]Reaction Conditions: aromatic aldehyde (1 mmol), aniline (1 mmol), diethylphosphite (1,2 mmol), 2-Hydroxymethyl-18-crown-6 (5mol%), room temperature, in THF within 15 min. [b]Isolated yield after purification by crystallization from hexane.

When employing 4-nitroaniline with tolylbenzaldehyde, the desired product **4m** was obtained with an 80% yield. Furthermore, products **V.14n** and **V.14o** were synthesized with yields of 92% and 88%, respectively, through the use of 4-bromo-2,6-dimethylaniline with 2-methoxy and 3-methoxy benzaldehyde. Employing 4-trifluoromethan-aniline with benzaldehyde, 4-chlorobenzaldehyde, and 4-methoxybenzaldehyde lead to the *α*-aminophosphonates **V.14p**, **V.14q**, and **V.14r**, with chemical yields of 80%, 88% and 86%, respectively.

IV-3-3 Proposed mechanism

To understand the mechanism for the synthesis of *α*-aminophosphonates via a multicomponent reaction in the presence of 2-Hydroxymethyl-18-Crown-6 as a catalyst, we explored alternative alcohols under identical conditions, including ethanol, phenol, and 2-hydroxymethyl phenol. Our findings revealed that while ethanol and phenol produced only trace amounts of the desired product, 2-hydroxymethyl phenol demonstrated significant efficacy, yielding 60%.

Our investigation supports the assertion that the effectiveness of 2-Hydroxymethyl-18-Crown-6 stems from its ability to form hydrogen bonds of the hydroxyl group and the specific cavity structure of the crown ether. On the base of the viewpoints developed by our previous

work[14], we present a plausible pathway for the multicomponent reaction using 2-Hydroxymethyl-18 Crown-6 as a catalyst, summarized in ***Scheme 5***.

Our hypothesis posits that the catalytic function of this organocatalyst involves coordinating with the oxygen of benzaldehyde, enhancing their electrophilicity and facilitating the nucleophilic attack of aniline to form an imine. Subsequently, 2-hydroxymethyl-18-crown-6 coordinates with the imine through a hydrogen bond, facilitating the nucleophilic attack of diethylphosphite leading to obtain the desired product.

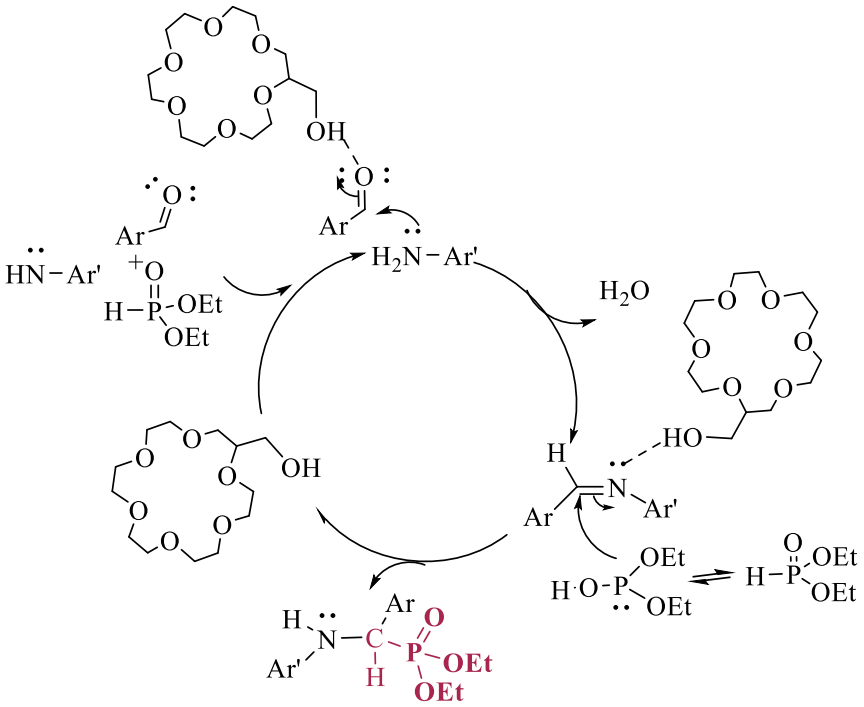

Scheme 5: Proposed mechanism of 2-Hydroxymethyl-18-Crown ether-6 catalyzed *α*-aminophosphonates synthesis.

Due to the wide medicinal applications of fluorinated *α*-aminophosphonates compounds, many studies have reported the interesting biological properties of trifluoromethyl *α*-aminophosphonates derivatives, which showed the cytotoxic activity toward cancer cells[15]. Herein, we have selected three synthesized 4-fluoro *α*-aminophosphonates (**V.14**p, **V.14**q and **V.14**r) then scrutinized them in quantum chemical calculations and

[14] (a) Aissa, R., Guezane-Lakoud, S., Gali, L., Toffano, M., Ignaczak, A., Adamiak, M., . Aribi-Zouioueche, L. *J. Mol. Struct*, **2022**, *1247*, 131336. (b) Guezane Lakoud, S., Merabet-Khelassi, M., & Aribi-Zouioueche, L. *Res. Chem. Intermed*, **2016**, *42*, 4403-4415.

[15] (a) Reddy, K. M. K., Sadik, S. M., Saichaithanya, N., Peddanna, K., Reddy, N. B., Sravya, G., Reddy, C. S. *Res. Chem. Intermed*,, **2017**, *43*, 7087-7103. (b) Dake, S., Raut, A., Kharat, D. S., Mhaske, K. R., Deshmukh, R. S., Pawar, S. M. *Bioorg. Med. Chem. Lett*, **2011**, *21*, 2527-2532.

modeling molecular study to determine the minimum energy molecular structure and to understand the correlation between the biological activity of *α*-aminophosphonates and their molecular structures[16].

V-4 Results of DFT study

V-4-1 Optimization of structures

In this study, we conducted geometry optimization for synthesized molecules (**V.14p**, **V.14q**, and **V.14r**) by employing the Density Functional Theory (DFT) method at the CAM-B3LYP level, using the 6-31 G (d, p) basis set as a starting point. This approach aimed to identify the most stable conformations of the investigated structures.

Figure 3 illustrates the calculated total energy values at the optimal stage for each molecule, namely -1619.4040 a.u, -2078.9989 a.u, and -1733.8816 a.u. These optimized structures serve as a foundation for subsequent calculations, enabling the determination of descriptor parameters and the estimation of various electronic properties for our diverse molecules.

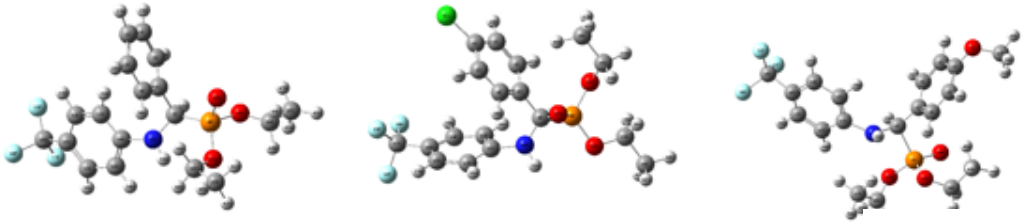

V.14p **V.14q** **V.14r**

Figure 3: Theoretical optimized structures of **V.14p, V.14q** and **V.14r** with CAM-B3LYP/6-31G (d,p) method.

V-4-2 Analysis of HOMO/LUMO frontier orbitals

Frontier Molecular Orbital analysis **HOMO, LUMO** energies, and energy gap calculations using Gaussian software, allows for predictions regarding the stability and reactivity of drug molecules.

A higher value of E_{HOMO} signifies a greater tendency for electron donation. From the ***Table 3,*** the results reveal that the compounds **V.14p** and **V.14q** exhibit E_{HOMO} values of -7.202 eV and -7.309 eV respectively, indicating their superior electron-accepting capabilities.

[16] (a) Turcheniuk, K. V., Kukhar, V. P., Röschenthaler, G. V., Aceña, J. L., Soloshonok, V. A., & Sorochinsky, A. E. *RSC adv*, **2013**, *3*(19), 6693-6716. (b) Cytlak, T., Kaźmierczak, M., Skibińska, M., & Koroniak, H. *Phosphorus, Sulfur, Silicon Relat. Elem*, **2017**, *192*(6), 602-620.

Conversely, the compound **V.14r** acts as a nucleophile, giving the highest HOMO energy (E_{HOMO} = -7.1021 eV), positioning it as an exceptional electron donor.

Furthermore, the calculated value of the HOMO-LUMO energy gap (ΔEgap) serves as an indicator of molecular reactivity. The energy gaps for the synthesized molecules range from 7.9146 eV to 8.0866 eV. Notably, smaller $E_{HOMO-LUMO}$ energy gaps suggest more stabilizing boundary interactions. Consequently, the results suggest that the compound **V.14q**, with the smallest energy gap, is the most stable and least reactive among the studied molecules.

Table 3: HOMO-LUMO energies of **V.14p**, **V.14q** and **V.14r** using DFT/ CAM-B3LYP/6-31G (d,p) method.

Compounds	E_{HOMO}(ev)	E_{LUMO} (ev)	ΔE (ev)
V.14p	–7.202	0.8846	8.0866
V.14q	–7.3097	0.6049	7.9146
V.14r	–7.1021	0.9088	8.0109

To elucidate the influence of the Highest Occupied Molecular Orbital (HOMO) and Lowest Unoccupied Molecular Orbital (LUMO) on molecular structures, visual representations of the surfaces were generated for **V.14p**, **V.14q**, and **V.14r** . As illustrated in ***Figure 4***, both the HOMO and LUMO are prominently localized around the aromatic ring and the amino group. Notably, the HOMO also extends its presence to include the CF3 group. This visualization provides valuable insights into the spatial distribution of electron density and reactivity patterns, contributing to a more thorough comprehension of the chemical behavior of these compounds.

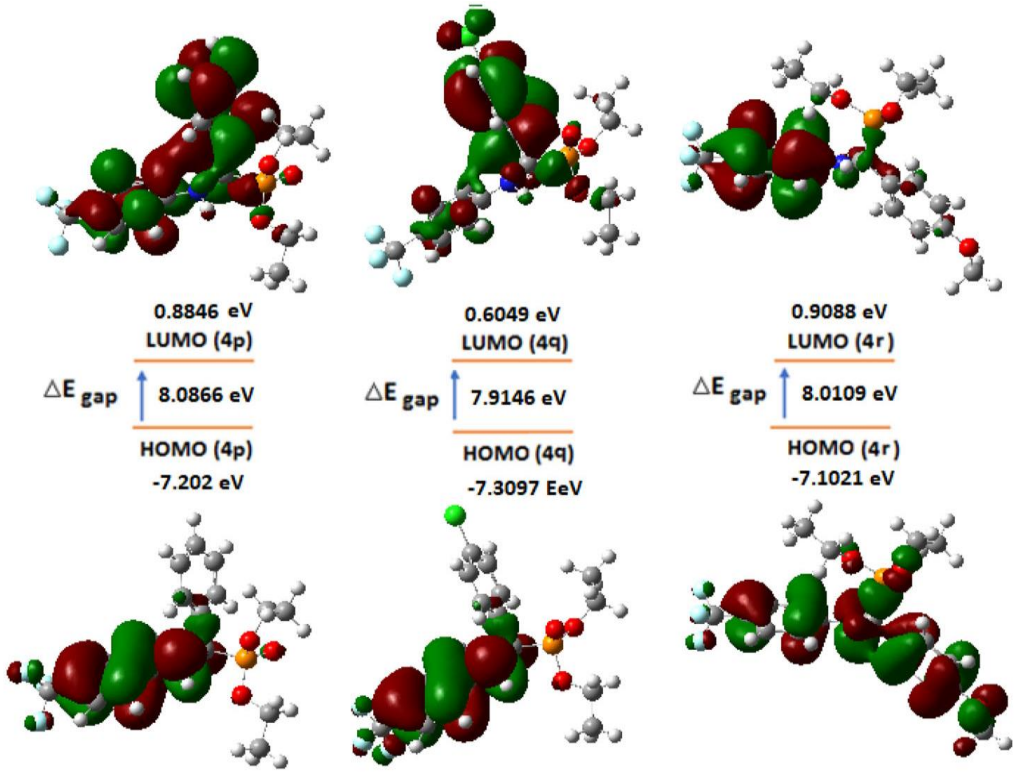

Figure 4: HOMO and LUMO orbitals of **V.14p, V.14q** and **V.14r** with CAM-B3LYP/6-31G (d,p) method.

V-4-3 Global reactivity descriptors

To assess the electrophilic/nucleophilic character and analyze the reactivity of the studied aminophosphonates, we employed the CAM-B3LYP/6-31G (d,p) method to calculate key static properties, such as: electronic chemical potential (μ), hardness (η), electronegativity (χ), overall electrophilicity index (ω), and dipole moment (μ). The results are summarized in the ***Table 4***.

Table 4**:** Calculated quantum chemical parameters of **V.14p, V.14q** and **V.14r** using DFT/CAM-B3LYP/6-31G (d,p) method.

Compounds	Dipole Moment DM(D)	Hardness η (ev)	Softness σ (ev)	Electronegativity χ (ev)	Electrophilicity ω (ev)
V.14p	5.0913	4.0433	0.2473	3.1587	1.2338
V.14q	6.0432	3.9573	0.2526	3.3524	1.4199
V.14r	3.2374	4.0054	0.2496	3.0966	1.1969

Specifically, the dipole moment (μ), reflecting the non-uniform charge distribution on different atoms, is a crucial electronic property. From the ***Table 4***, we observe that the value

of the dipole moment of **V.14q** is higher than **V.14p** and **V.14r** (6.0432 D *vs* 5.091 D and 3.2374 D) respectively. This discrepancy is attributed to the electronegativity difference introduced by Cl.

Furthermore, assessing the hardness (η) and local softness (r) of drug molecules provides insights into their resistance to electron cloud deformation or polarization[17]. These descriptors are pivotal for gauging reactivity and molecular stability, where chemical hardness corresponds to the energy gap between the LUMO and HOMO. As displayed the results, the high hardness values (4.033, 3.9573, and 4.0054 eV) for compounds **V.14p**, **V.14q**, and **V.14r** respectively indicate their stability and reduced reactivity.

Electronegativity (χ), representing an atom or molecule's affinity for electrons, giving 3.1587, eV 3.3524 eV and 3.0966 eV for **V.14p**, **V.14q**, and **V.14r** respectively. Furthermore, upon scrutiny of the results presented in the ***Table 4***, it is observed that the electrophilicity values for the examined compounds **V.14p**, **V.14q** and **V.14r** are 1.2338 eV, 1.4199 eV, and 1.1969 eV respectively. In line with the classification established by *Domingo* et *al*[18]. in **2002**, organic molecules are categorized into three groups based on their electrophilicity values: marginal electrophiles (values less than 0.8 eV), moderate electrophiles (values between 0.8 and 1.5 eV), and strong electrophiles (values greater than 1.5 eV). Applying this criterion, it can be deduced that the three ligands fall into the category of moderate electrophiles, indicating a moderate level of reactivity.

V-4-4 Molecular electrostatic potential

The Molecular Electrostatic Potential (MEP) serves as a crucial parameter in predicting and validating the reactivity of compounds as enzyme inhibitors. It provides insights into physicochemical property relationships by highlighting molecular structures' efficient centers governing electrophilic and nucleophilic reactions. Additionally, MEP is closely linked to electronic density.

In MEP, negative regions, depicted in red, signify electrophilic reactivity, while positive regions, shown in blue, indicate nucleophilic reactivity. The visualization in ***Figure 5*** reveals negative potentials concentrated at electronegative oxygen atoms (O21 and O26) attached to the phosphorous group, while positive potentials are evident at hydrogen atoms across all compounds.

[17] Issa, R. M., Awad, M. K., & Atlam, F. M. *Applied Surface Science*, **2008**, *255*(5), 2433-2441.
[18] Domingo, L. R., Aurell, M. J., Pérez, P. Contreras, R. *Tetrahedron*, **2002**, *58*(22), 4417-4423.

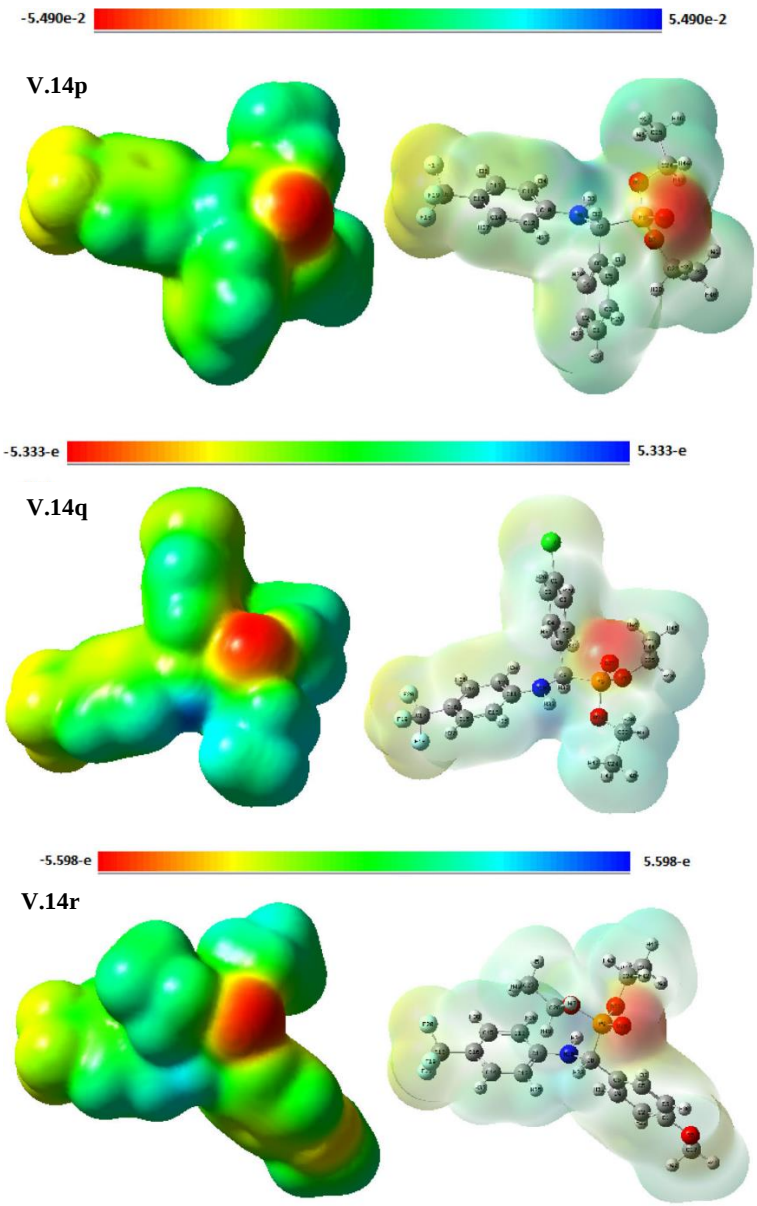

Figure 5: Molecular electrostatic potentials (MEP) for the investigated compounds.

As shown in the ***Figure 5***, the potential sites for electrophilic attacks are predominantly situated at heteroatoms. Conversely, the phenyl rings in the compounds exhibit negative regions. The MEP zones clearly delineate that negative positions align with electronegative atoms (N and O) and conjugated double bonds, while positive zones correspond to hydrogen atoms. This information contributes to a comprehensive understanding of the potential reactivity sites within the considered inhibitors.

V-5 Molecular docking studies

We performed *in silico* molecular docking analyses on three synthesized *α*-aminophosphonates (**V.14p**, **V.14q**, and **V.14r**) and compared their interactions with

Adriamycin. The objective was to discover the most probable mode of interaction with the topoisomerase-II enzyme receptor, employing AutoDock Vina as our computational tool. To simulate realistic conditions, the protein was maintained in a rigid conformation, while the ligands underwent flexible conformational adjustments during the docking simulations.

V-5-1 Methodology

V-5-1-1 Ligand Preparation

Ensuring reliable and reproducible results necessitates optimizing the ligand geometry before the docking process. We employed DFT calculations with the CAM-B3LYP/6-31(d,p) basis set using GAUSSIAN 09 to identify the most stable conformations. The resulting molecular structures were saved in pdb format. The final phase of ligand preparation involved the vina subroutine, which controlled ligand movements by specifying aromatic atoms, flexible bonds, and twist angles. The prepared ligand was then saved in pdbqt format for subsequent use by AutoDock.

V-5-1-2 Receptor Preparation

The 3D structure of the target protein, Human topoisomerase IIa (PDB ID: 1ZXM, Resolution: 1.87 Å), was retrieved from the RCSB Protein Data Bank. The preparation for docking unfolded through the following steps:

- Removal of water molecules surrounding the enzyme.
- Addition of hydrogen atoms to proteins, accompanied by the calculation of Kollman charges. The resulting structures were saved in PDBQT format.
- Identification of the active site of 1ZXM was accomplished by re-docking with ANP (phosphoaminophosphonic acid adenylate ester) onto specific binding pocket (Asn 163, Tyr 165, Glu 87, Thr 147, Ile 125, Asn 91, Asn 120, Ser 148, Ser 149, Phe 142, Thr 215, Asn 95, Gln 376, Arg 162, Lys 168)[19] (***Figure 6***)

[19] Wei, H., Ruthenburg, A. J., Bechis, S. K., Verdine, G. *L. J Biol Chem*, **2005**, *280*(44), 37041-37047.

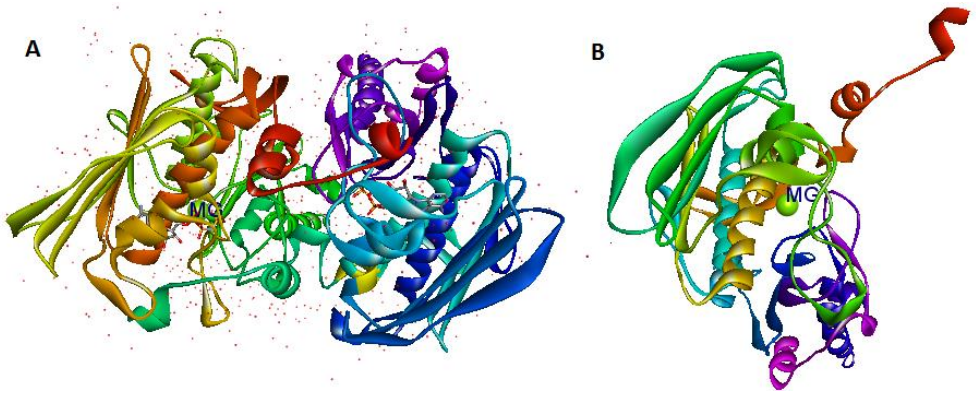

Figure 6: 3D structure of Human topoisomerase IIα (PDB ID: 1ZXM). A: before preparation, B: after preparation.

V-5-2 Results of molecular docking

To expedite energy evaluation, the receptor is embedded in a three-dimensional grid that extensively covers the active site of the studied protein, facilitating unimpeded ligand rotation within the site. The central coordinates of this grid are determined by X, Y, and Z, each dimension measured in Ångströms. The grid is then centered precisely on the ligand, and its dimensions are tailored to the sizes of all ligands under investigation. The specific binding site parameters derived from this approach include coordinates (X = 36.548, Y = 1.089, Z = 34.656) and a size of 40 Å along each axis (x = 40, y = 40, z = 40).

V-5-2-1 Re-docking:

Root Mean Square Deviation (RMSD) is a widely used metric for assessing and comparing molecular conformations. In our research, RMSD served to evaluate the accuracy of reproducing a known binding configuration by comparing the original ligand pose with the re-docked ligand into the active site. The RMSD index for binding topology between the original ligand and re-docked ligand into the active site was found to be 1.9438 Å.

V-5-2-2 Docking

To assess the affinity score and investigate drug interactions responsible for inhibiting the 1ZXM receptor, ligands were individually docked using Autodock Vina. As presented in ***Table 5***, the analysis revealed that among the various docking conformations of compounds, **V.14r** exhibited the highest docking score of 8.9 Kcal/mol, surpassing **V.14p** and **V.14q** with scores of -8.2 Kcal/mol, as well as the standard anticancer drug Adriamycin. This superior binding affinity can be attributed to the OCH_3 interaction, p-Alkyl interactions, and

conventional hydrogen bonding interactions within the active pocket of the topoisomerase-II enzyme.

Table 5: Binding scores and the Non-bonding interactions of **V.14p**, **V.14q**, **V.14r** and the ADM with amino acid residues of 1ZXM.

Compounds	Docking score (Kcal/ mol)	Amino acid with Hydrogen bonding Interaction	N Hydrogen bonding interaction (Distance (Å))	Hydrophobic interaction (Distances(Å)	Residues of binding site
V.14p	-8.2	Ser 149 Asn 95	1 (2.46) 1 (3.51)	Ala 167: Pi alkyl (4.69) Ile 217: Alkyl (4.52) Ale 118: Alkyl (5.34) Thr : Pi-Sigma Ile 141 : Pi alkyl (5.06) Ale 88 : Alkyl (5.36)	Ala 92, Ala 167, Ser 149, Asn 120, Asn 95, Ile 88, Ile 118, Ile 217, Ile 141, Thr 2015.
V.14q	-8.2	Ser 149	1 (2.54)	Ile 88 : Alkyl (5.45) Ala 167 : alkyl (4.18) Ala 167 : Pi-alkyl (4.77)	Asn 120, Ala 92, Ile 88, Ile 118, Ile 217, Ala 167, Ser 149.
V.14r	-8.9	Gly 164 Tyr 165 Asn 150 Ser 149 Ala 92	1 (2.32) 1 (1.97) 1 (2.71) 1 (1.73) 1 (3.24)		Gly 164, Tyr 165, Asn 91, Asn 120, Ala 92, Asn 150, Ser 149
Adriamycin (ADM)	-8.0	Asn 91 Ser 149 Ser 149 Ser 148 His 130	1 (3.55) 1 (2.29) 1 (2.31) 1 (3.07) 1 (2.77)	Ser 149: Pi-sigma (3.79) Ile 125 : Pi alkyl (5.05) Ile 125 : pi alkyl (5.43) Ile 141 : Pi- sigma (3.67) Ile 141 : Pi-sigma (3.41) His 130 : Pi-alkyl (5.01) His 137: Pi alkyl (5.48)	Asn 91, Ser 148, Ser 149, Ile 125, Ile 141, Leu 140, His 130, Val 137.

V-5-2-3 Ligand - protein interaction:

The 2D and 3D representations highlight that ADM binds to the 1ZXM receptor through a spectrum of interactions, encompassing Pi-sigma, Alkyl, and Pi-Alkyl interactions, along with conventional hydrogen bonding with Asn 91, Ser 148, and His 130. These critical residues were pinpointed within the active site, governing the enzymatic activity of 1ZXM. Notably, all three ligands share a common hydrogen bond interaction with Ser 149.

The stability of the docked ligand **V.14r** is exclusively attributed to hydrogen bond interactions between -OCH_3, precisely situated in the receptor's binding site. Additionally,

ligand **V.14r** uniquely engages in a direct interaction with the center of the Mg^{+2}: 309 metal, at a distance of 2.65 Å, constituting a crucial electrostatic interaction. In contrast, structures **V.14p** and **V.14q**, as well as ADM, rely on hydrophobic interactions for stability. ***(Figure 7)***

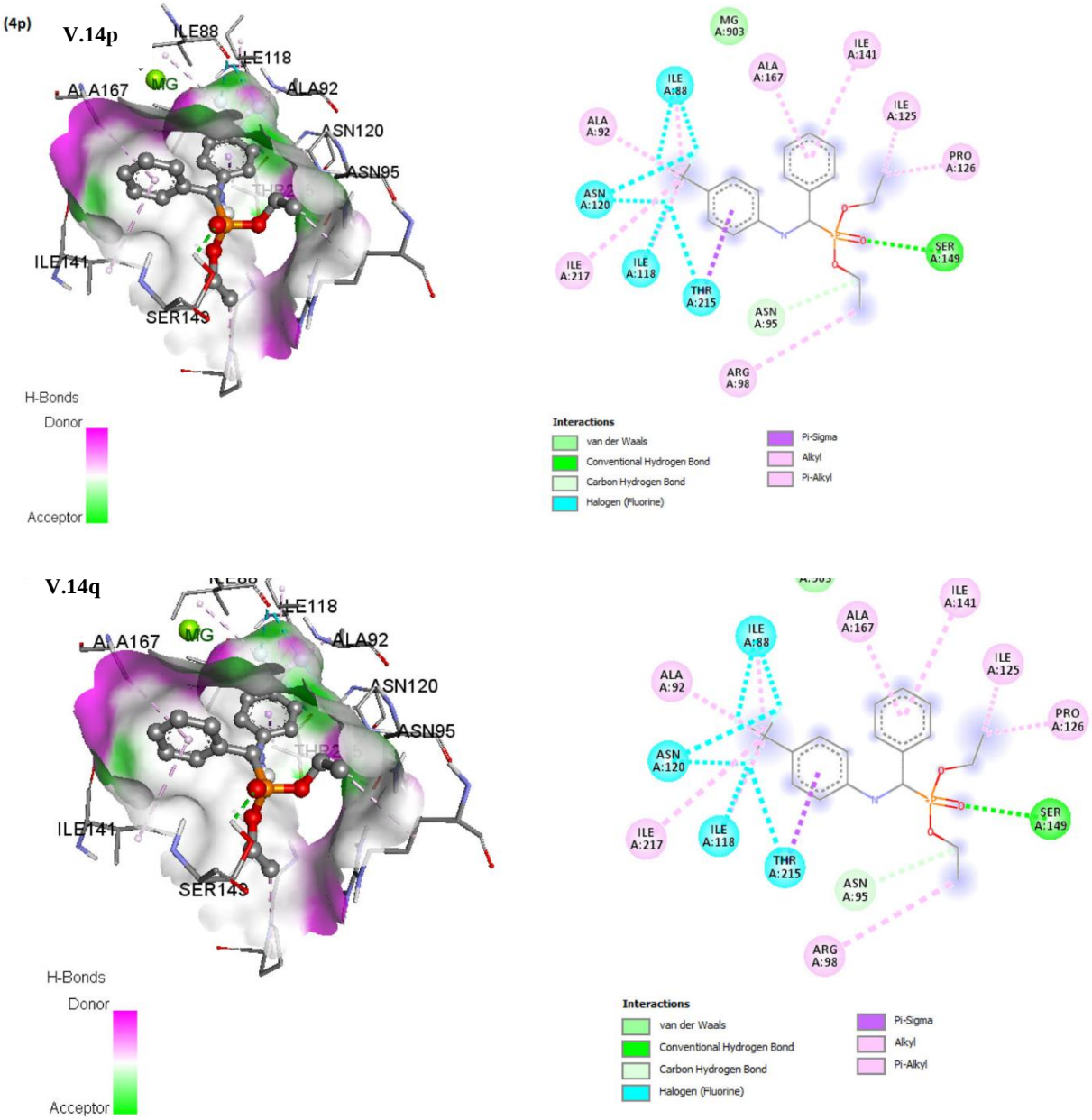

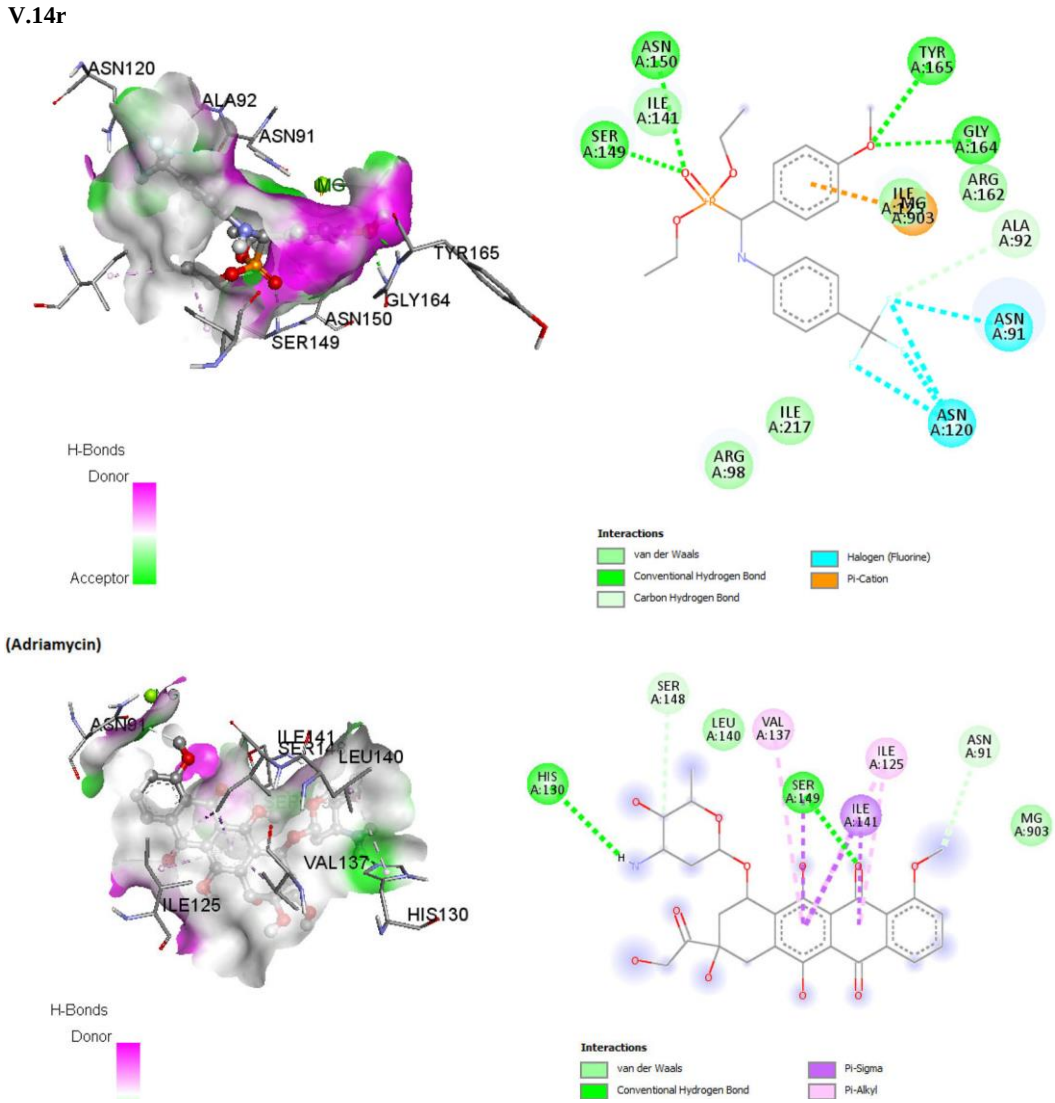

Figure 7: The docked 2D and 3D images of **V.14p**, **V.14q** and **V.14r** compounds and commercial drug (adriamycin) with 1ZXM receptor.

It's noteworthy that optimizing hydrophobic interactions at hydrogen bonding sites enhances binding affinity and drug efficacy[20].

Considering the number of hydrogen bonds with active site residues and the binding energy score, compound **V.14r** emerges as the most stable and exhibits a high affinity for the protein receptor. These findings position these ligands as potent anticancer agents, acting as inhibitors of topoisomerase II.

[20] Patil, R., Das, S., Stanley, A., Yadav, L., Sudhakar, A., Varma, A. K. *PloS one*, ***2010***, *5*(8), e12029.

V-6 ADMET prediction and drug likeness

V-6-1 Absorption and physicochemical properties

The drug-likeness properties, potential toxicity risks, and physicochemical characteristics were assessed using the Swiss-ADME server. This study focuses on the ADMET prediction of *α*-aminophosphonates **V.14p**, **V.14q**, and **V.14r**, and the findings are summarized in ***Table 6***. To evaluate their anti-proliferative and cytotoxic activities against breast cancer, prostate cancer, and stomach cancer cell lines, a comparative analysis was conducted with the established drug Adriamycin[21] (ADM).

Conforming to Lipinski's rule of five, the physicochemical properties of the synthesized *α*-aminophosphonates (**V.14p**, **V.14q**, and **V.14r**) were compared to those of ADM. Notably, **V.14p**, **V.14q**, and **V.14r** exhibited no violations of these rules, possessing molecular weights below 500 Da. This suggests their potential to traverse biological membranes efficiently. Furthermore, their log P values (<5) indicate a good membrane tolerance. The total polar surface area (TPSA), a key determinant of oral bioavailability, was within the recommended range (≤140 $Å^2$) for all synthesized molecules, signifying their high oral bioavailability. In contrast, ADM exceeded this threshold with a TPSA of 206.07 $Å^2$. (***Table 6***)

Table 6: The physicochemical properties of designed molecules for drug-likeness prediction based on *Lipinski's* rule of five.

Physicochemical properties	ADM	V.14p	V.14q	V.14r
Molecular weight g/mol	543.52	387.33	421.78	405.47
NHBA	12	6	6	4
NHBD	6	1	1	1
Consensus Log P $_{O/w}$	0.44	4.37	4.92	4.59
Log S	-3.46	-6.92	-7.50	-7.35
TPSA $(Å)^2$	206.07	57.37	57.37	66.60

Furthermore, assessing the oral bioavailability profile of compounds holds significant importance in evaluating the drug-likeness of a molecule and delineating its pharmacological potential. This evaluation is based on consideration of six key physicochemical properties: lipophilicity (lipo), size, polarity (polar), insolubility (insolu), flexibility (flex), and

[21] Liu, J. Z., Song, B. A., Fan, H. T., Bhadury, P. S., Wan, W. T., Yang, S., Zeng, S. *Eur. J. Med. Chem*, **2010**, *45*(11), 5108-5112.

unsaturation (insatu)[22]. Notably, the oral bioavailability radar reveals that all synthesized molecules consistently fall within the designated pink area, signifying an optimal range for the specified descriptors ***(Figure 8)***. This observation strongly suggests that the studied molecules exhibit drug-like characteristics.

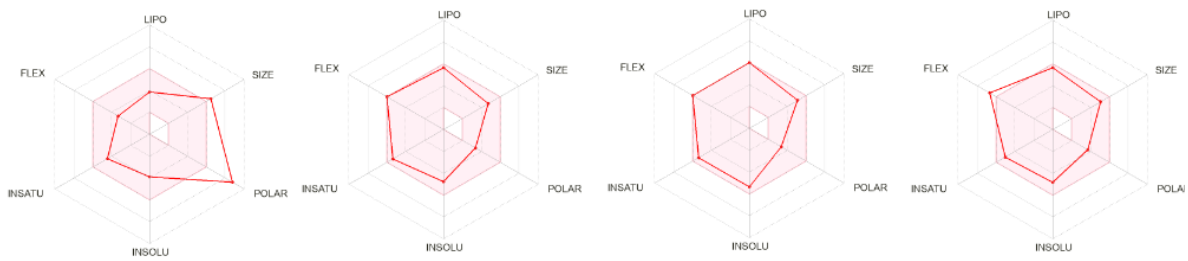

Adriamycin **V.14p** **V.14q** **V.14r**

Figure 8: Biovailability radars and physicochemical properties of Adriamycin, **V.14p**, **V.14q** and **V.14r**.

Moreover, the BOILEDEgg method stands out as a rapid and effective approach for assessing molecules in terms of their potential to penetrate the human blood-brain barrier (BBB) and undergo gastrointestinal absorption (GIA). This method, derived from a combination of lipophilicity and polarity[23], maps molecules onto the Egg diagram. Specifically, points within the Egg's yolk indicate molecules predicted to exhibit passive permeability through the BBB, while those in the white regions correspond to molecules anticipated to be passively absorbed through gastrointestinal absorption (GIA) processes (***Figure 9***).

[22] (a) Ramalingam, A., Mustafa, N., Chng, W. J., Medimagh, M., Sambandam, S., Issaoui, N. *Biomolecules*, **2022**, *12*(8), 1093.; (b) Ramalingam, A., Guerroudj, A. R., Sambandam, S., Kumar, A., Krishnamoorthy, R., Boukabcha, N, Elayaperumal, M. *J. Mol. Struct*, **2022**, *1269*, 133845.
[23] Daina, A., Michielin, O., & Zoete, V. *Scientific reports*, **2017**, *7*(1), 42717.

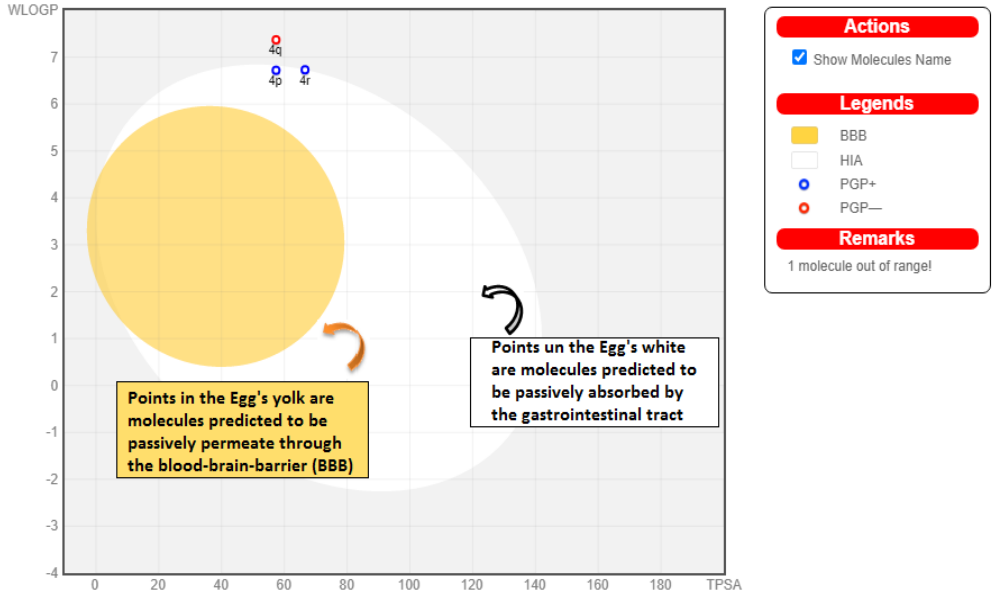

Figure 9: Overview of the BOILED-Egg construction for designed molecules **V.14p**, **V.14q**, **V.14r** and ADM from the SwissADME online sever.

Additionally, molecules exhibiting efflux (PGP+) and those not subject to efflux (PGP-) from the central nervous system by P-glycoprotein are visually represented as blue and red dots, respectively. Notably, the results indicate that none of the synthesized molecules demonstrated permeation across the blood-brain barrier. However, all of them were predicted to undergo passive absorption through the gastrointestinal tract, with PGP+ for **V.14p** and **V.14r**, and PGP- for **V.14q**, in comparison to ADM, which falls outside the specified range.

V-6-2 Distribution, metabolism and pharmacokinetic properties:

Pharmacokinetic properties serve as crucial indicators for assessing the potential therapeutic success of drug molecules, particularly those acting as potential inhibitors. Elevated gastrointestinal (GI) absorption is indicative of improved absorption from the intestinal tract upon oral administration. Notably, compounds **V.14p** and **V.14r** demonstrate high GI absorption compared to both ADM and **V.14q**, which exhibit lower GI absorption. However, it is important to highlight that, despite their high GI absorption, compounds **V.14p** and **V.14r** were found incapable of crossing the blood-brain barrier (BBB) partition, as depicted in ***Table 7***.

Table 7: Predicted pharmacokinetic and Drug-likeness properties of ADM, **V.14p**, **V.14q** and **V.14r**.

Pharmacokinetics properties	Adriamycin	V.14p	V.14q	V.14r
GI absorption	Low	High	Low	High
BBB permeant	No	No	No	No
P-gp substrate	Yes	Yes	No	Yes
CYP1A2 inhibitor	No	No	No	No
CYP2C19 inhibitor	No	Yes	Yes	Yes
CYP2C9 inhibitor	No	Yes	Yes	Yes
CYP2D6 inhibitor	No	Yes	Yes	Yes
CYP3A4 inhibitor	No	Yes	Yes	Yes
Log K_p (skin permeation)	-8.71 cm/s	-5.54 cm/s	-5.31 cm/s	-5.12 cm/s

GI absorption: gastrointestinal absorption; BBB: blood-brain barrier;
CYP: Cytochrome P450; P-gp substrate: Glycoprotein substrate P.

When predicting efflux mediated by P-glycoprotein, only **V.14q** emerges as a substrate. Notably, it has been reported that a molecule is more likely to engage in Drug-Drug Interactions (DDI) with other active compounds if it inhibits multiple CYP enzymes, particularly the isoforms (CYP1A2, CYP2C19, CYP2C9, CYP2D6, and CYP3A4) responsible for 90% of oxidative metabolic reactions[24]. Consequently, all the compounds were predicted to lack potency against CYP1A2 while serving as inhibitors for all CYP450 isoforms (CYP2C19, CYP2C9, CYP2D6, and CYP3A4), except for ADM.

Skin sensitization, a crucial safety assessment indicator, provides insights into a compound's potential to induce skin allergies upon administration[25]. Notably, the studied molecules (**ADM**, **V.14p**, **V.14q**, **V.14r**) exhibit low skin permeability at rates of 8.71 cm/s, 5.54 cm/s, 5.31 cm/s, and 5.12 cm/s, respectively. These results affirm that these compounds demonstrate a benign profile and may even serve as remedies for skin allergies[26].

V-6-3 Drug-likeness and bioavailability

Drug-likeness is determined by qualitative rules that assess the likelihood of a given molecule evolving into a viable oral drug, taking into account specific ranges of physicochemical properties[27]. In this context, *Veber's* rule is adhered to without any violation

[24] (a) Cheng, F., Yu, Y., Shen, J., Yang, L., Li, W., Liu, G, Tang, Y. *J. Chem. Inf. Model.*, **2011**, *51*(5), 996-1011. (b) Williams, J. A., Hyland, R., Jones, B. C., Smith, D. A., Hurst, S., Goosen, T. C., Ball, S. E. *Drug Metab. Dispos.*, **2004**, *32*(11), 1201-1208.
[25] Alves, V. M.,Muratov, E.,Fourches, D.,Strickland, J., Kleinstreuer, N., Andrade, C. H., & Tropsha, A. *Toxicol. Appl. Pharmacol*, **2015**, *284*(2), 273-280.
[26] (a) Abdelrheem, D. A., Rahman, A. A., Elsayed, K. N., Abd El-Mageed, H. R., Mohamed, H. S., & Ahmed, S. A. *J. Mol. Struct*, **2021**, *1225*, 129245. (b) Kavitha, N., & Alivelu, M. *Comput Theor Chem*, **2021**, *1201*, 113287.
[27] Daina, A., Michielin, O., & Zoete, V. *Sci. Rep*, **2017**, *7*(1), 42717.

for all synthesized products (**V.14p**, **V.14q**, and **V.14r**). Egan's rule is affirmed solely by **V.14r**, while *Mugge's* rule designates **V.14p** as a promising candidate for drug development.

In summary, these findings lead to the conclusion that the studied compounds exhibit the potential to be excellent drug candidates, as indicated in ***Table 8***.

Table 8: Drug-likeness profile and medicinal properties calculated for the studied molecule.

Drug-likeness	ADM	V.14p	V.14q	V.14r
Lipinski	No	Yes	Yes	Yes
Ghose	No	No	No	No
Veber	No	Yes	Yes	Yes
Egan	No	No	No	Yes
Muegge	No	Yes	No	No
Bioavailability Score	0.17	0.55	0.55	0.55
Synthetic accessibility (SA)	5.81	4.05	4.02	4.37

Conclusion

In this chapter, our research describe the development of a sustainable and environmentally friendly methodology for the synthesis of *α*-aminophosphonate derivatives utilizing 2-Hydroxymethyl-18-Crown-6 as a novel and efficient homogeneous organocatalyst. This innovative catalytic multicomponent reaction employing a mere 5 mol%, presents several notable advantages, including the efficient preparation of organophosphorus compounds under transition metal-free, environmentally friendly conditions, and a significantly shortened reaction time with excellent chemical yields. The structural elucidation of three CF_3 derivatives (**V.14p**, **V.14q**, and **V.14r**) was meticulously conducted through DFT/CAM-B3LYP/6-31G (d, p) calculations, providing insights into their geometrical parameters and electronic properties. Notably, the HOMO and LUMO distributions exhibited pronounced delocalization over the aromatic ring and the amino group, while the LUMO predominantly covered the CF_3 fragment. The calculated HOMO-LUMO energy gaps provided the justification for the observed charge transfer interactions within the molecules. Additionally, mapping the molecular electrostatic potential facilitated the prediction of sites susceptible to electrophilic and nucleophilic attacks. The identification of negative positions around electronegative atoms (N and O) and conjugated double bonds, alongside positive zones surrounding hydrogen atoms, enhances our understanding of potential reaction pathways. This comprehensive exploration contributes valuable insights into the catalytic and electronic properties of our synthesized compounds. In addition, the *in silico* docking study revealed that the docked conformations established robust hydrogen-bonding interactions within the active site of the enzyme. Notably, the three ligands, **V.14p**, **V.14q**, and **V.14r**, exhibited potent hydrogen bonding interactions with the active site of the topoisomerase-II enzyme, akin to Adriamycin. Among these ligands, **V.14r** uniquely demonstrated a direct electrostatic interaction with the center of the Mg^{2+}:309 metal, boasting the highest score energy (-8.9 kcal/mol). Impressively, **V.14r** seamlessly nestled into the active pocket of the enzyme, forming five hydrogen bond interactions, underscoring its exceptional stability and affinity for the receptor. Conversely, the stability of structures **V.14p** and **V.14q**, as well as Adriamycin, was underpinned by the presence of hydrophobic interactions.

Moreover, a comprehensive examination of the synthesized compounds for their potential as drugs, employing *Lipinski's* five rules and ADMET studies, was conducted in comparison to Adriamycin. The results unequivocally affirm the success of these compounds as promising candidates in drug discovery, with the potential to exert influence in anticancer

activity. The drug-likeness of the designed compounds was meticulously analyzed through oral bioavailability radar, revealing their high pharmacological potential. This integrated assessment positions the synthesized compounds as not only effective inhibitors but also as promising contenders for further exploration in the development of novel therapeutic agents.

Chapter VI

Enantioselective Biodeacylation of arylalkylacetates as key precursors of enantiopure organophosphorus compounds

Introduction

The preparation of enantiopure organophophorus compounds possessing a stereogenic carbon adjacent to the phophore atom still an important challenge either for the medicinal area or for the asymmetric synthesis. One of the synthetic approaches uses chiral alcohols as starting materials.[1]

For us at this stage of our investigations, we have envisaged the preparation of the enantiopure arylalkyl carbinols using one of the most efficient and simple strategy, which is well studied in our laboratory; It concerns the enzymatic kinetic resolution via deacylation of racemic aryl alkyl acetates.[2]

VI.1 Aim of the study

The study of the mode of action of enzyme during the enzymatic kinetic resolution of racemates constitutes one of the well studied investigations in our laboratory. In the fewer last year, this interest was focused on the study of the efficiency of the enzymatic kinetic resolution via deacylation in non-aqueous media.[3] Various parameters could modulate simultaneously the reactivity and the selectivity of this approach such as: the nature and amount of the lipase[4], the acyl donors[5], the solvent, the introduction of additives[6] as well as the water activity.

Concerning the deacylation of acetates in non-aqueous media, two efficient methodologies, in terms of reactivity and enantioselectivity, were established, the first one using stoichiometric amount of carbonate salts[3] as additives and the second one using the triethylamine[7] to improve the efficiency of the immobilized *Candida antarctica* lipase (*CAL-B*) as robust biocatalyst.

In the present study, we decided to combine the efficiency of the biodeacylation of racemic acetates in the presence of organic bases as additive to chemical synthetic path, such

[1] (a) Gbubele, J. D., & Olszewski, T. K. *Org & Biomol Chem*, **2021**, *19*(13), 2823-2846. (b) Kostoudi, S., & Pampalakis, G. *Int. J. Mol. Sci*, **2022**, *23*(6), 3395. (c) Kolodiazhnyi, O. I. *Russ. Chem. Rev.*, **2011**, *80*(9), 883.
[2] A. Zaïdi, M. Merabet-Khelassi, L. Aribi-Zouioueche, Catal. *Lett.* 145 (2015) 1054–1061.
[3] (a) M. Merabet-Khelassi, Z. Houiene, L. Aribi-Zouioueche, O. Riant, , *Tetrahedron: Asymmetry*. **2012,** 23, 828-833. (b) N. Braïa, M. Merabet-Khelassi, L. Aribi-Zouioueche, M. Toffano, *Biocatal. Biotransformation*. **2022**.
[4] M. Merabet-Khelassi, N. Bouzemi, J.C. Fiaud, O. Riant, L. Aribi-Zouioueche, C. R. *Chim.* **2011**, 14, 978-986
[5] (a) N.E. Benamara, M. Merabet-Khelassi, S. G. Lakoud, L. Aribi-Zouioueche, O. Riant, *ChemistrySelect.* 6 **2021**, 13941-13946. (b) Bouzemi, N., Debbeche, H., Aribi-Zouioueche, L., & Fiaud, J. C. *Tetrahedron lett*, **2012**, *45*(3), 627-630. (c) Melais, N., Aribi-Zouioueche, L., & Riant, O. . *Comptes Rendus Chimie*, **2016**, *19*(8), 971-977.
[6] (a) M. Merabet-Khelassi, L. Aribi-Zouioueche, O. Riant, T*etrahedron: Asymmetry*. **2008**, 19, 2378-2384. (b) F.Z. Belkacemi, M. Merabet-Khelassi, L. Aribi-Zouioueche, O. Riant, Res. *Chem. Intermed*. **2018**, 44, 6847-6860. (c) M. Merabet, N. Melais, M. Boukachabia, J.C. Fiaud, L. Zouioueche-Aribi, *J. Soc. Alg. Chim*. **2007**, 17 185.
[7] M. Merabet-Khelassi, A. Zaidi, L. Aribi-Zouioueche, *Enzyme Microb. Technol*. **2017**, 107, 1-6.

Arbuzov-Michaelis for the preparation of enantiopure organophosphorus compounds (***Scheme 1***).

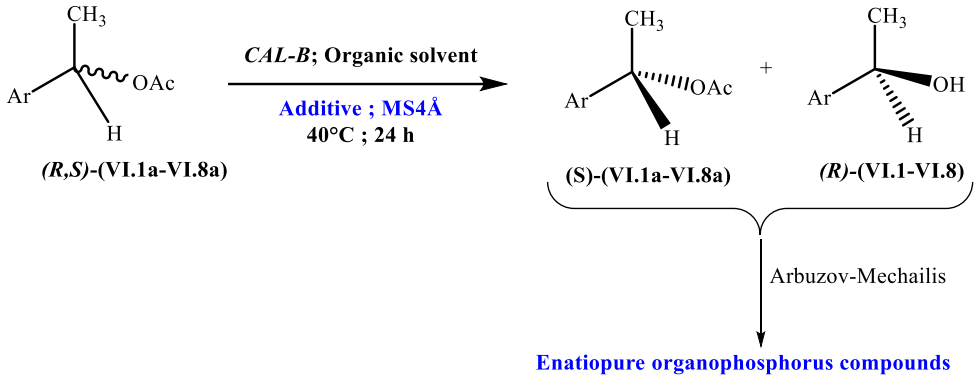

Scheme 1: Chemo-enzymatic investigated pathways to enantiopure organophosphorus compounds.

As biocatalyst, we have used the lipase from *Candida antarctica fraction* B (*CAL-B*), under an immobilized form. This enzyme belong to the class of hydrolytic enzymes (EC.3.1.1.3), it is widely used in industrial biotechnology for their several advantages such as the ease of use, biodegradable, and efficiency with less waste, non requirements for co-factors, stability in aqueous and organic solvents as well as their remarkable *chemo-*, *regio-* and *enantio*-selectivity[8]. To establish the adequate experimental conditions to reach our precursors under enantiopure forms, we have examined the promiscuous effect of some tertiary amines, simple and complex, as additives, in the deacylation of arylalkyl acetates catalyzed by lipases.

The study is carried out with two kinds of the *CAL-B*, from different suppliers, The *Novozym®435* lipase immobilized on hydrophobic carrier (acrylic resin) with Specific activity 10000 U/g and the *CHIRAZYME® L-2, c.-f. C2, lyo* with Specific activity 500 U/g. The reactions were performed in two organic solvents with different hydrophobicities.

VI.2 Results and discussion:

VI.2.1 Synthesis of racemic alcohols and their corresponding acetates:

The racemic alcohols **VI.2, VI.3, VI.6** were obtained quantitatively after reduction of the corresponding commercial ketones. Whilst the racemic acetates **VI.1a- VI.8a** were obtained by standard classical chemical acetylation of corresponding alcohols (***Scheme 2***).

[8] (a) U.T. Bornscheuer, R.J. Kazlauskas, Hydrolases in organic synthesis: regio- and stereoselective biotransformations, Weinheim: Wiley-VCH Verlag GmbH & Co. KGaA. **2005**. (b) D. Mendez-Sanchez, M. Lopez-Iglesias, V. Gotor-Fernandez, *Curr. Org. Chem.* **2016**, 20, 1186–1203.

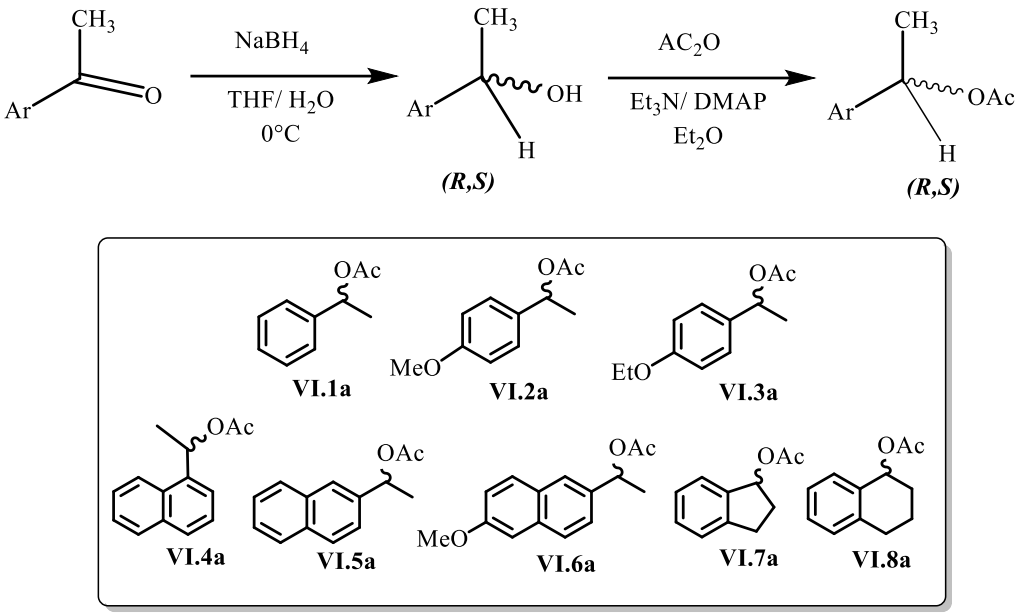

Scheme 2: Enzymatic deacylation of **VI.1a- VI.8a** in the presence of DABCO.

The structure of the synthesized alcohols and acetates were confirmed via e ^{1}H and ^{13}C NMR analyses.

VI.2.2 Study of Biodeacylation of *rac*-1-phenyl ethyl acetate VI.1a:

In order to determine the optimal conditions of the enzymatic deacylation of arylalkyl acetates, we have decided to explore the impact of the introduction of tertiary amines on the outcome of the this reaction using the phenylethyl acetate **VI.1a** as model of study, and an organic base, the triethylamine was chosen for finding the optimal conditions. The reactions are carried out in two organic solvents diisopropyl ether (DIPE, logP=1.9) and *tertio*-butylmethyl ether (TBME, logP=1.35) in the presence of molecular sieves 4Å (MS 4Å) as water regulator. The study was performed using the both selected lipases.

VI.2.3 Optimization of the threshold of the triethylamine

Firstly, for better apprehend the influence of the introduction of Et_3N on the outcome of the bio-deacylation, several amount loading of these non reactive base were examined (0, 0.2, 0.5, 1, 2, 3 equivalents). (***Scheme 3***)

The experiences were performed on 1 equivalent of acetate **VI.1a** diluted in 2 mL of organic solvent. 50 mg of *CAL-B* and 50 mg of MS 4Å were added. Blank reactions, without MS 4Å and Et_3N were performed and used as control reaction.

The mixture was stirred at 40°C for 24h. The evolution reactions were monitored by TLC. The reactions mixtures were filtered then evaporated in *vacuum*. The conversi

ons and the enantiomeric excesses of remained acetates ***(S)*- VI.1a** and the obtained alcohols ***(R)*- VI.1** were quantified by chiral GC. The obtained results are reported in ***table 1***.

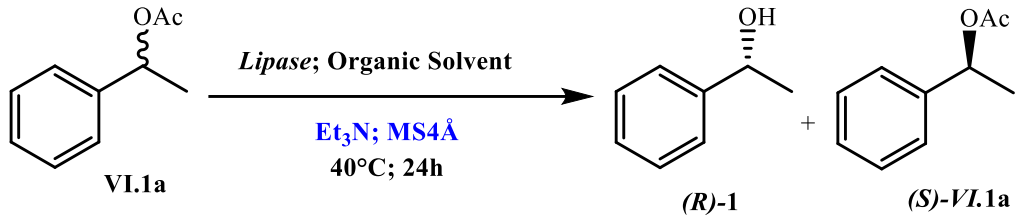

***Scheme 3*:** Enzymatic deacylation of VI.1 in the presence of Et_3N as basic additive.

As shown on ***table 1***, the *CAL-B* preparation has non negligible impact on the reactivity and the enantioselectivity during the deacylation of **VI.1a**, and that strongly related to the Et_3N loading. Also, the presence of the hydrolysis reaction in absence of both amine and molecular sieves in DIPE and TBME was detected with rates varying from Conv = 16.7% to Conv = 24.3% (***Entries: 1, 9, 17*** and ***25***). It is to be underline that the water implicated in the hydrolysis of acetates is probably brought from the lipase. Moreover, formation of the corresponding alcohol was not observed when Et_3N was used only.

Slight decrease of the conversion rates was recorded by adding an amount of molecular sieves as water regulator ($15.5\% \leq$ Conv $\leq 20.5\%$) (***Entries: 2, 10, 18*** and ***26***).

When the *CHIRAZYME® L-2, c.-f. C2, lyo* was exploited as biocatalyst in both organic solvents; a significant improvement of the conversion rates was observed when 2 equivalents of Et_3N were added and that without any perturbation of the lipase selectivity (E >>200). In DIPE from Conv = 20.5% to Conv = 31.8% and in TBME from Conv = 20.5% to Conv= 27.5% (***entries 2, 6*** versus ***10, 14***). A drastic enhancement of the reactivity was recorded in TBME when a large excesses of Et_3N (3 equivalent) was introduced and that in disfavor of the lipase selectivity; the selectivity factor pass from E>>200 to E= 38 and the conversion rates from Conv = 27.5% to Conv = 44.9% (***entry 14*** versus ***15***). Similar observations concerning the selectivity were noted in DIPE, but those on the reactivity were less important (***entries 6*** and ***7***).

Whilst, these perturbation were completely declined when the *Novozym®435* was used in the presence of excess of the Et_3N. The deacylation was performed with high selectivity regardless the amount of the base loading.

Table 1: Influence of Et_3N loading during the enzymatic deacylation of (VI.1)

Entry	Et_3N (equiv.)	Org. solvent (logP)	ee_S(%)[c]	ee_P(%)[c]	Conv(%)[d]	E[d]
		CHIRAZYME® L-2, c.-f. C2, lyo				
1[a]	0	DIPE (1.9)	31.2	> 99	23.9	> 200
2[b]	0		25.5	> 99	20.5	> 200
3[b]	0.2		33.4	> 99	25.2	> 200
4[b]	**0.5**		**34.2**	**> 99**	**25.7**	**> 200**
5[b]	**1**		**37.8**	**> 99**	**27.6**	**> 200**
6[b]	**2**		**46.1**	**> 99**	**31.8**	**> 200**
7[b]	3		46.1	89.4	34	28.2
8[b]	4		46.2	88.6	34.3	26.1
9[a]	0	TBME (1.35)	30.5	> 99	23.6	> 200
10[b]	0		25.5	> 99	20.5	> 200
11[b]	0.2		34.2	> 99	25.7	> 200
12[b]	**0.5**		**35.7**	**> 99**	**26.5**	**> 200**
13[b]	**1**		**39.2**	**> 99**	**28.4**	**> 200**
14[b]	**2**		**37.6**	**> 99**	**27.5**	**> 200**
15[b]	3		72.7	89.2	44.9	38
16[b]	4		29.8	83.3	26.3	14.7
		***Novozym*®435**				
17[a]	0	DIPE (1.9)	32	> 99	24.3	> 200
18[b]	0		18.3	> 99	15.5	> 200
19[b]	0.2		28.7	> 99	22.3	> 200
20[b]	0.5		35.8	> 99	26.4	> 200
21[b]	1		36.8	> 99	27	> 200
22[b]	2		46.9	> 99	32	> 200
23[b]	3		32.2	> 99	24.4	> 200
24[b]	4		27	> 99	21.3	> 200
25[a]	0	TBME (1.35)	20.1	> 99	16.7	> 200
26[b]	0		19.6	> 99	16.4	> 200
27[b]	0.2		14.4	> 99	12.6	> 200
28[b]	0.5		20.6	> 99	17.1	> 200
29[b]	1		25.5	> 99	20.3	> 200
30[b]	2		32.5	> 99	24.6	> 200
31[b]	3		40.9	> 99	29	> 200
32[b]	4		35	> 99	26	> 200

(a) 1mmol of (1a), 50 mg of *CAL-B*, 2 mL of organic solvent at 40°C during 24 hours.
(b) 1mmol of (1a), x equiv. of Et_3N , 50 mg of *CAL-B*, 50 mg of molecular sieves 4Å, 2 mL of organic solvent at 40°C during 24 hours.
(**c**) Enantiomeric excess of obtained alcohol and the remained acetate are measured by chiral GC.
(**d**) Conversion[9]: $Conv=ee_S/ee_P+ee_S$; Selectivity: $E = Ln [(1-C) (1-ee_S)]/ Ln [(1-C) (1+ee_S]$

As given results, the improvement of the reactivity was recorded from the addition of 0.5-1 equivalent of Et_3N, we maintain the minimum rate (0.5 equivalent of additive) as the activation rate of the deacylation in both solvents. We have undertaken these conditions with the other tertiary amines additives.

VI.2.4 Effect of the additive nature

The exploitation of organic bases as additives to optimize the reactivity and the selectivity of hydrolases has drawn attention in last two decades[10]. The most used is triethylamine and pyridine as non reactive bases, generally in the acylation reactions for the elimination the all trace of acidic residue from the enzyme microenvironment and preventing inhibition and denaturation of enzymes[11]. Whilst fewer examples were described, concerning their uses as additives during the hydrolysis reactions in aqueous media[12].

At this stage of the study, simple and complex bases (Lewis bases and Cinchona alkaloids) were selected to check the impact of their presence on the outcome of the bio-deacylation and that keeping the same above promiscuous conditions.

Besides the triethylamine (Et_3N: pk_a 10.75) the following additives were chosen: Pyridine (pk_a 5.25), 4-Dimethylaminopyridine (4-DMAP: pk_a 9.7), 1,4-Diazabicyclo[2.2.2]octane (DABCO : pk_a 8.8), Cinchonine (pk_a 9.15), Cinchonidine (pk_a 9.15), Quinine (pk_a 9.05) and Quinidine (pk_a 9.05) (***Figure 1***).

[9] (a) C.S. Chen, Y. Fujimoto, C.J. Sih, , *J. Am. Chem. Soc.***1982**, 104, 7294-7299.(b) H.B. Kagan, J.C. Fiaud, Kinetic Resolution Topics in Stereochemistry. E.L. Eliel, S.H. Wilen, Ed. J. Wiley & Sons, Inc. New York. **1988**, 18 249-330.
[10] Y.R. Liang, Q. Wu, X.F. Lin, *Chem. Rec*. **2017**, 17, 90-121.
[11] (a) B. Berger, C.G. Rabiller, K. Konigsberger, K. Faber, H. Griengl, *Tetrahedron: Asymmetry*. **1990**, 1, 541–546. (b) J.L.L. Rakels, A.J.J. Straathof, J.J. Heijnen, *Tetrahedron: Asymmetry*. **1994**, 5, 93–100. (c) P. Stead, H. Marley, M. Mahmoudian, G.Webb, D. Noble, Y.T. Ip, E. Piga, T. Rossi, S. Roberts, M.J. Dawson, *Tetrahedron: Asymmetry*. **1996**, 7, 2247–2250.
[12] M. Braner,, S.Z. ielonka, J. Grzeschik, S. Krah, S. Lieb, D. Petras, X. Wagner, I. Ahmed, S.H. Hüttenhain, *ChemCatChem* **2012**, 4, 2050–2054.

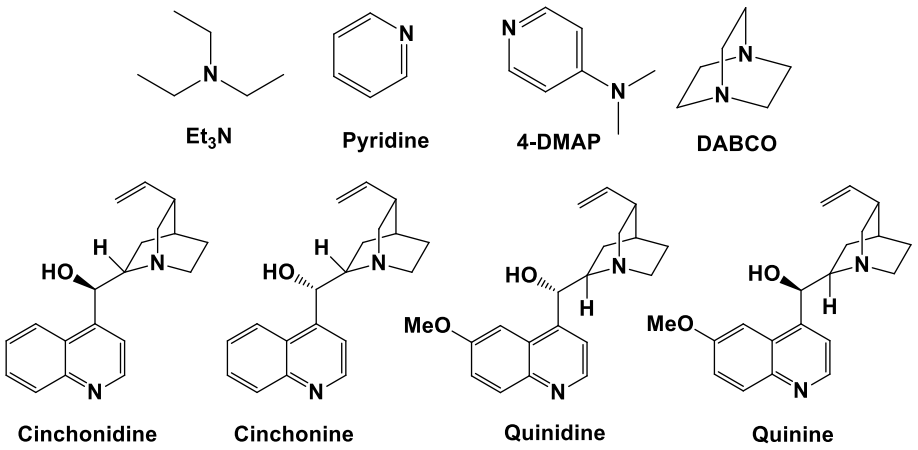

Figure 1: Structures of several chosen additives.

All experiences were performed on 1 equivalent of acetate **VI.1a** diluted in 2 mL of organic solvent in the presence of 50 mg of *CAL-B* and 50 mg of MS 4Å. After 24 h of stirring at 40°C the reactions mixtures were filtered then evaporated in *vacuum*. The conversions and the enantiomeric excesses of remained acetates ***(S)*- VI.1a** and the obtained alcohols ***(R)*- VI.1** were quantified by chiral GC after an acidic work-up (***Table 2***).

***Table 2*:** Influence of the additive nature on the enzymatic deacylation of **VI.1**.

Entry[a]	Org. Solvent	Additive	ee_S(%)[b]	ee_P(%)[b]	Conv(%)[c]	E[c]
		CHIRAZYME® L-2, c.-f. C2, lyo				
1	DIPE (1.9)	Et_3N	34.2	> 99	25.7	> 200
2		4-DMAP	35.6	> 99	26	> 200
3		**DABCO**	**81**	**> 99**	**44.8**	**> 200**
4		Pyridine	27.7	> 99	21.7	> 200
5		Cinchonine	23.3	> 99	18.9	> 200
6		Cinchonidine	25.1	> 99	20.1	> 200
7		Quinine	37.3	> 99	27.2	> 200
8		Quinidine	38	> 99	27.5	> 200
9	TBME (1.35)	Et_3N	35.7	> 99	26.5	> 200
10		4-DMAP	29.2	> 99	22.7	> 200
11		**DABCO**	**87.3**	**> 99**	**46.6**	**> 200**
12		Pyridine	25.3	> 99	20.4	> 200
13		Cinchonine	21.1	> 99	17.5	> 200
14		Cinchonidine	21.3	> 99	17.7	> 200

15		Quinine	29	> 99	22.7	> 200
16		Quinidine	28.7	> 99	22.5	> 200
		***Novozym*®435**				
17	TBME (1.35)	Et_3N	20.6	> 99	17.1	> 200
18		**4-DMAP**	**61.5**	**> 99**	**38.3**	**> 200**
19		**DABCO**	**79.9**	**> 99**	**44.7**	**> 200**
20		Pyridine	34.3	> 99	25.7	> 200
21		Cinchonine	34.4	> 99	25.8	> 200
22		Cinchonidine	30.2	> 99	23.4	> 200
23		Quinine	51.8	> 99	34.4	> 200
24		Quinidine	51.2	> 99	34.1	> 200

(a) 1mmol of (1a), 0.5 equiv. of additive , 50 mg of *CAL-B*, 50 mg of molecular sieves 4Å, 2 mL of organic solvent at 40°C during 24 hours.
(**b**) Enantiomeric excess of obtained alcohol and the remained acetate are measured by chiral GC.
(**c**) Conversion[13]: $Conv=ee_S/ee_P+ee_S$; Selectivity: $E = Ln [(1-C) (1-ee_S)]/ Ln [(1-C) (1+ee_S]$

As shown on ***table 2***, with both *CAL-B* preparations, the introduction of DABCO as additive improve significantly the conversion rate without any perturbation of the enantioselectivity in both used solvents (***entries 3, 11*** and ***19***).

At the best of our knowledge, the use of the DABCO as an enzyme activator in non-aqueous media for the EKR of racemates was not reported yet. The exploitation of this base as organocatalyst was only reported in promiscuous aldol reactions.[14]

It is to be underlined that no direct correlation between the pK_a values of several used additives and the conversion rates of acetate into alcohol was recorded.

In the case of *CHIRAZYME® L-2, c.-f. C2, lyo* used as biocatalyst, only the DABCO shows an activation role, the conversion rate was doubled and that compared to the other used additives. No significant influence of the addition of other bases and that independently to the solvent hydrophilicity.

Since the TBME is classed as replacement solvent of DIPE by *Pfizer* and for the above observations, we have opting to carry on our study in a more compatible solvent.

[13] (a) C.S. Chen, Y. Fujimoto, C.J. Sih, *J. Am. Chem. Soc*. **1989**, 104, 7294-7299.(b) H.B. Kagan, J.C. Fiaud, Kinetic Resolution Topics in Stereochemistry. E.L. Eliel, S.H. Wilen, Ed. J. Wiley & Sons, Inc. New York. **1988**, 18 249-330.
[14] J.W. Xue, J. Song, I.C.K. Manion, Y.H. He, Z. Guan, *J. Mol. Catal. B: Enzym*. **2016**, 124, 62–69.

Whilst, when the *Novozym®435* different degrees of activation were recorded using the chosen additives. The best conversion rates were achieved using the 4-DMAP and the DABCO, Conv = 38.3% and 44.7% respectively (***Entries 18*** and ***19***).

In order to validate this approach and checking the fact of the activation exhibited by the introduction of this Lewis base, we have decided to apply these optimized conditions of the kinetic bio-resolution *via* hydrolysis to series of secondary arylalkyl acetates **VI.2a-VI.8a.**

VI.2.5 Impact of the introduction of DABCO on the outcome of the bio-deacylation of some arylalkylacetates

The optimal conditions of the deacylation of acetates **VI.2a- VI.8a** catalyzed by both CAL-B preparation (***Scheme 4***), in the presence of DABCO was performed.

All experiments were performed on 1 mmole of racemic acetate, 0.5 equivalent of DABCO, in the presence of 50 mg of *CAL-B* preparations, 50 mg of molecular sieves in 2mL of TBME for 24 h, at 40 °C. The results are summarized in ***table 3***.

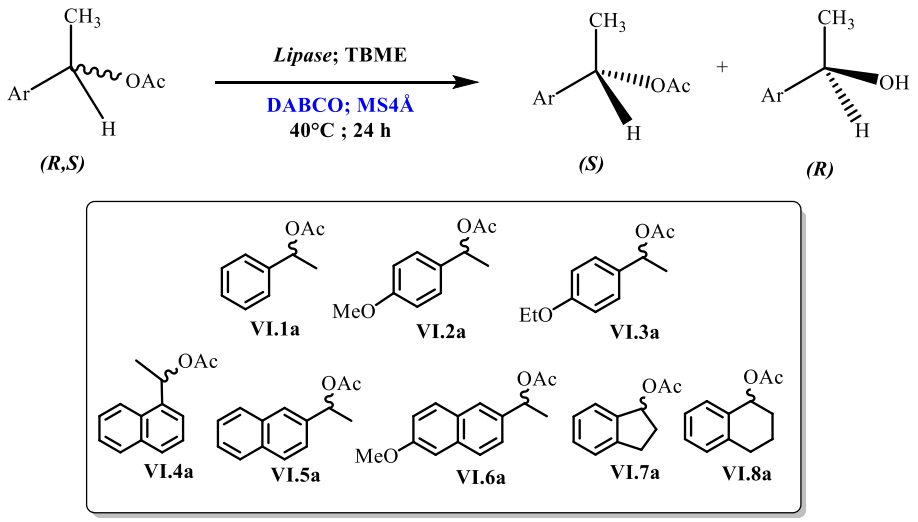

Scheme 4*: *CAL-B catalyzed the deacylation of **VI.2a- VI.8a** in the presence of DABCO.

Table 3: Impact of DABCO as additive on the outcome of the *CAL-B* deacylation.

Entry [a]	Acetate	ee_S(%)[b] (yield %)[d]	ee_P(%)[b](yield %)[d]	Conv(%)[c]	E [c]
CHIRAZYME® L-2, c.-f. C2, lyo					
1	**VI.1a**	87.3 (45)	> 99 (35)	46.6	> 200
2	**VI.2a**	75.6 (45)	>99 (34)	43.3	> 200
3	**VI.3a**	28.2 (70)	>99 (15)	22.2	> 200
4	**VI.4a**	> 99 (45)	> 99 (40)	50	>200
5	**VI.5a**	64.4 (50)	>99 (35)	39.4	> 200
6	**VI.6a**	9.6 (ND)	95.8 (ND)	9.1	120
7	**VI.7a**	3.9 (ND)	82.8 (ND)	4.6	11
8	**VI.8a**	66 (50)	>99 (35)	40	>200
***Novozym*®435**					
9	**VI.1a**	79.9 (50)	> 99 (38)	44.7	> 200
10	**VI.2a**	67.2 (48)	> 99 (35)	40.4	> 200
11	**VI.3a**	41.4 (60)	>99 (15)	29.5	> 200
12	**VI.4a**	> 99 (45)	> 99 (40)	50	>200
13	**VI.5a**	60 (60)	>99 (29)	37.7	> 200
14	**VI.6a**	72.6 (50)	>99 (35)	42	> 200
15	**VI.7a**	7.9 (ND)	94 (ND)	7.7	34
16	**VI.8a**	65.8 (60)	>99 (30)	39.9	> 200

(a) 1mmol of (1a), 0.5 equiv. of DABCO , 50 mg of *CAL-B*, 50 mg of molecular sieves 4Å, 2 mL of TBME at 40°C during 24 hours.
(**b**) Enantiomeric excess of obtained alcohol and the remained acetate are measured by chiral GC or HPLC.
(**c**) Conversion[15]: $Conv=ee_S/ee_P+ee_S$; Selectivity: $E =Ln [(1-C) (1-ee_S)]/ Ln [(1-C) (1+ee_S]$.
(d) Isolated Yields after separation on preparative TLC. **ND**: Not determined

The summarized results from ***table 3*** shows some similarities between both *CAL-B* preparations. From poor to excellent enantioselectivities, with slight to important differences in the conversion rates were recorded during the EKR of the selected arylalkylacetates (**VI.1a- VI.8a)** in the presence of DABCO under poor water conditions. *CHIRAZYME® L-2, c.-f. C2, lyo* and *Novozym®435* reveal the same behaviour toward all the resolved racemic acetates, except the structure **VI.7a**. Where the *Novozym®435* preparation exhibits the best

[15] a) C.S. Chen, Y. Fujimoto, C.J. Sih, *J. Am. Chem. Soc*. **1982**, 104, 7294-7299.(b) H.B. Kagan, J.C. Fiaud, Kinetic Resolution Topics in Stereochemistry. E.L. Eliel, S.H. Wilen, Ed. J. Wiley & Sons, Inc. New York. 18 **1988**, 249-330

reactivity and enantioselectivity under those promiscuous conditions compared to the *CHIRAZYME* preparation (***entry 6*** versus ***14***).

An ideal enzymatic kinetic resolution was recorded with the acetate **VI.4a** (Conv 50% and E>>200).

The following chromatograms illustrate the great impact of the introduction of DABCO during the deacylation of the structure **VI.6a**.

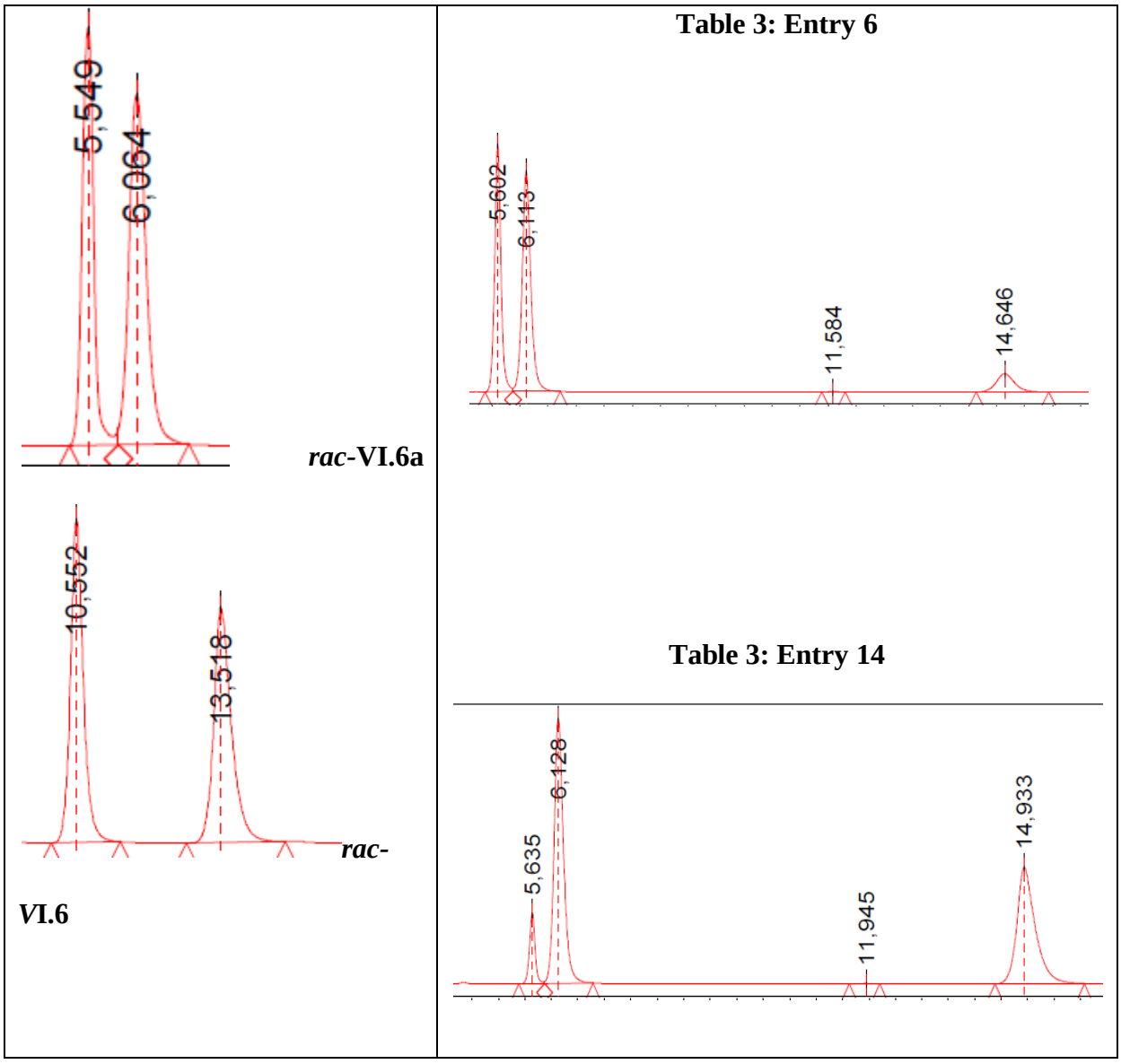

Chromatogram 1: Biodeacylation of VI.6a in the absence and in the presence of DABCO.

VI.2.6 Explanation and hypothesis

The obtained results using DABCO (pk_a 8.8) as additive for the deacylation of acetates **VI.1- VI.8** improve significantly the previous results when the Et_3N pk_a 10.75) was used, and that in terms of reactivity and enantioselectivity[16]. As others[17], we have attributed this fact to the basicity of the used additive, which acts in parallel on removing the acetic acids released during the deacylation of acetate from the enzyme microenvironment and preventing it inhibition and attenuation.

Another hypothesis was reported during the hydrolysis of 3-hydroxy fatty acid esters by Novozym 435 dissolved in Et_3N. The introduction of this base was enhanced reaction rates with moderate selectivities. The authors suggested that there was probably a special effect for sterically hindered amines especially amines with tertiary nitrogen atoms such as Et_3N and DABCO on the activation of the lipase and not only the basicity effects. They concluded that the acyl binding site of the enzyme may be activated by sterically hindered amines. Actually, our study support also this hypothesis, where we have observed that the presence of no reactive bases play role of enzyme activators without disturbing the lipase enantioselectivity, during the hydrolysis under promiscuous conditions without any introduction of external water. Exceptionally the use of strong bases such pyridine don't affect the enzyme enantioselectivity. Furthermore, we have shown that the use of chiral alkaloids (cinchonidine, cinchononine, quinine quinidine) as additives improve significantly the *Novozym®435* lipase reactivity despite their chirality. The same effects was reported by Guo and Sih, during the *Candida cylindracea lipase* (*CCL*) catalyzed hydrolysis of aryloxypropionic esters using either dextromethorphan (DM) or levomethorphan as enantiomerically pure additives[18].

Finally, we can conclude that use of two different preparation of *CAL-B* from different suppliers for the biodeacylation of some arylalkyl acetates under non-conventional conditions using the DABCO as enzyme activator shows some similarities. The presence of this amine improve significantly the reactivity without disturb the enantioselectivity one during the enzymatic kinetic resolution reactions.

VI.2.7 Preliminary result of the synthesis of enantiopure organophosphorus via *Arbuzov-Michaelis* reaction

For the synthesis of an enantiopure organophosphorus compounds, the *Arbuzov-Michaelis* reaction was applied, and as enantiopure alcohols, two structures were selected (*R*)-

[16] M. Merabet-Khelassi, A. Zaidi, L. Aribi-Zouioueche, *Enzyme Microb. Technol*. **2016**, 107, 1-6
[17] (a) Y.R. Liang, Q. Wu, X.F. Lin, *Chem. Rec.* **2017**, 17, 90-121. (b) F. Theil, *Tetrahedron.* **2000**, 19, 2905-2919
[18] Z. W. Guo, C. J. Sih, *J. Am. Chem. Soc.*, **1989**, 111, 6836-6841.

VI.9 and (*R*)- **VI.10** (1eq). (***Scheme 5***). a stochiometric amount of $ZnBr_2$ (1.2 eq) and a large excess of triethylphosphite (5 eq) were added.[19] The outcome of the reaction was followed via TLC.

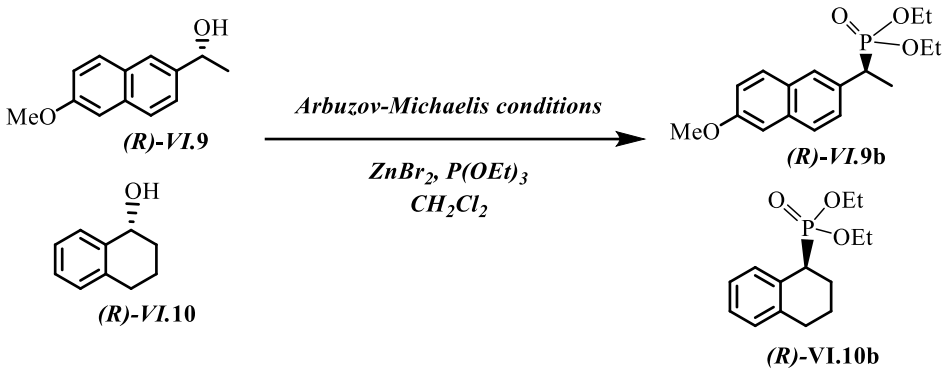

Scheme 5: Phosphorylation of enantiopure alcohols via *Arbuzov-Michaelis* reaction.

The TLC analyses show the apparition of new apolar spot. The confirmation of the structure of these novel products are in progress.

Conclusion

In the present chapter, we have described an important impact of the introduction of DABCO as an enzyme activator on the outcome of the kinetic resolution through deacylation of a set of arylalkyl acetates catalyzed by the *CAL-B* immobilized on hydrophobic carrier, and that under promiscuous conditions. A comparison of two *CAL-B* preparations from different suppliers was explored to this investigation.

After determination of the optimum conditions which allowing to the enantioenriched alcohol forms, using a tertiary amine, the Et_3N, as basic additive the impact of some simple and complex bases on the outcome of the reaction was also examined.

The results revealed no direct correlation between the pk_a values of several used additives and the *CAL-B* activation rates.

Among the used amines, simple or complex, the DABCO improved significantly the conversion rates of the enzymatic deacylation of phenylethyl acetate as the study model. The application of the optimum conditions on some arylalkyl acetates, confirm the efficiency of this basic organic additive as enzyme activator during the biodeacylation process.

[19] Rajeshwaran, G. G., Nandakumar, M., Sureshbabu, R., & Mohanakrishnan, A. K. *Organic letters*, **2011**, *13*(6), 1270-1273.

Conclusion

The objective of this thesis is to underscore the transformative potential of organophosphorus compounds as versatile building blocks across diverse applications, ranging from pharmaceuticals to agrochemicals. By delving into the realm of innovative organocatalysts and incorporating the tenets of green chemistry, this research endeavors to elevate the efficiency of organophosphorus compound synthesis. Beyond this immediate goal, the overarching objective is to make a substantive contribution to the broader vision of cultivating a more sustainable and responsible chemical industry.

The achieving results of this thesis are summarized as bellow:

Firstly, we synthesized a novel array of α-aminophosphonates through the three-component *Kabachnik-Fields* reaction, commencing with aniline and employing an aldehyde and diethylphosphite. This process adhered to the principles of green chemistry and leveraged the Design of Experiment (DoE) methodology. Initially, we assessed various catalysts to determine their effectiveness in influencing the reaction and facilitating the production of new α-aminophosphonates.

Our findings revealed that diphenylphosphinic acid emerged as the optimal catalyst, yielding α-aminophosphonates with exceptional efficiency. Subsequently, we conducted a comprehensive factorial experimental design to scrutinize the impact of three key factors: catalyst quantity, temperature, and reaction time. This systematic approach allowed us to pinpoint the optimal conditions that maximized the reaction yield. The results not only underscored the significance of diphenylphosphinic acid as a catalyst but also provided valuable insights into the interplay of crucial parameters in enhancing the synthesis of α-aminophosphonates.

The relationship between the yield and the three influencing factors was effectively captured through modeling. Statistical analyses confirmed the significance of the obtained model ($P < 0.05$), establishing a robust correlation between measured and adjusted values, as evidenced by an impressive R^2 of 99.25% and an adjusted R^2 of 97.51%.

The pursuit of optimal conditions, guided by an in-depth analysis of response surfaces and contour diagrams, led to the identification of peak efficiency at R=90%. This optimal performance was achieved under specific conditions: a temperature of 40°C, a reaction time of 10 minutes, and a catalyst quantity of 10 mol%.

The implementation of optimized conditions across a range of aromatic aldehydes and anilines, featuring diverse electron-withdrawing and electron-donating substituents, highlighted the efficacy of the diphenylphosphinic acid. This organocatalyst demonstrated its proficiency by yielding *α*-aminophosphonates with consistently high yields ranging from 78% to 98%.

In the second part, we successfully devised a methodology to synthesize *α*-aminophosphonates. After examination of various kind of crown ethers, we have find that the 2-Hydroxymethyl-18-crown-6 (5 mol%) is the most efficient as a homogeneous organocatalyst. The reactions conducted in the presence of tetrahydrofuran (THF) at room temperature. Employing this protocol, we achieved the anticipated products, completing the reactions within approximately 15 minutes and yielding satisfactory results ranging from 80% to 94%.

We also selected specific *α*-aminophosphonate derivatives synthesized substituted by trifluoromethyl in para position (**V.14p** , **V.14q** , and **V14.r**), then we delved into the prediction of chemical reactivity and explored the influence of substituents on specific *α*-aminophosphonate derivatives (**V.14p-V.14r**) synthesized. Leveraging various quantum descriptors (such as HOMO, LUMO, ΔEgap, and μ) and reactivity indices (η, μ, χ, ω) derived from density functional theory (DFT) using the CAM-B3LYP/6-31(d,p) basis set. Notably, our findings revealed that molecules **V.14p** and **V.14q** exhibit characteristics of electron acceptors, while compound **V.14r** demonstrates traits akin to an electron donor. The analysis of energy gaps elucidated that the **V.14q** derivative displays heightened reactivity, thus indicating lower stability compared to others.

Furthermore, we conducted an *in silico* study via molecular docking to elucidate the probable mode of interaction of these derivatives with the topoisomerase-II enzyme, juxtaposing them with Adriamycin (ADM). The outcomes highlighted that these three ligands **V.14p**, **V.14q**, and **V.14r** form hydrogen bonds within the enzyme's active site akin to Adriamycin. This resemblance positions them as potential inhibitors of topoisomerase II, thereby exhibiting promise as anticancer agents, which is also confirmed using *Lipinski's* five rules and ADMET studies.

Finally, we developed a new protocol for the preparation of enantiopure alcohols are a key precursors of enantiomerically pure phosphorus-containing arylcarbinols.

The selected method involves the deacylation of benzylic acetates with central chirality in a non-conventional medium. This process is catalyzed by *CAL-B* in the presence of seven tertiary amines, namely Triethylamine (Et_3N), Pyridine, 4-Dimethylaminopyridine (4-DMAP), 1,4-Diazabicyclo[2.2.2]octane (DABCO), Cinchonine, Cinchonidine, Quinine, and Quinidine, serving as activator enzymes.

Among the various examined amines, the introduction of DABCO as an additive improved the enantioselective deacylation of acetates with a high reactivity and selectivity. This noteworthy outcome prompted a comprehensive exploration of the deacylation of a series of benzylic acetates (**VI.a-VI.h**). Various parameters were explored, such as the *CAL-B* loading, The medium hydrophobicity, and the incorporation of DABCO as an activator.

The optimal results were attained with a catalytic amount of 25 mg of *CAL-B* in TBME (tert-butyl methyl ether). The obtained alcohols were recovered enantiopure (E>200) in favor of the (*R*)-enantiomer. This achievement highlights the efficiency of DABCO as an additive for enhancing the reactivity and the selectivity of the enzymatic kinetic resolution process.

- **Perspective**

Based on the findings presented, several avenues can be explored to further enhance and expand future research complementary to the work carried out during this thesis. The proposed perspectives include:

- ✓ Synthesis of enantiomerically pure organophosphonates and validation of their biological activity within this new family, specifically focusing on anticancer activity. Additionally, prediction of chemical reactivity is conducted through DFT, along with a molecular docking study to investigate interactions with the biological target.
- ✓ Evaluation of in vivo anticancer activity on biological models.
- ✓ Optimization and development of a new Kabachnick-Fields reaction approach enabling the formation of α-aminophosphonates in a single step under green chemistry conditions.
- ✓ Synthesis of new complex molecules within the same category for use as ligands with different metals.

Experimental protocols

1) Generality

- **Reagents and solvents**
- **Products**

All reagents were purchased from Sigma-Aldrich or Acros Company used without further purification.

- **Lipase**

The enzymes used in the kinetic resolution of racemic mixtures are commercial and are purchased from Sigma-Aldrich, Fluka and Amano. The Novozym®435 (CAL-B) lipase immobilized on hydrophobic carrier (acrylic resin) was purchased from STREM (Sold in collaboration with Novozymes A/S) with Specific activity 10000 U/g. The CHIRAZYME® L-2, c.-f. C2, lyo (CAL-B) was purchased from Boehringer Mannheim with Specific activity 500 kU. Both lipases were used without any pre-treatment.

- **Solvents**

The solvents used are of p.a. quality or distilled before use. The solvents used in HPLC are of HPLC quality, filtered and degassed before use.

2) Analytical equipment and techniques

The characteristics of the synthesized products were determined by the following different analytical methods:

- **Chromatographies:**

Reactions were monitored by thin-layer chromatography (TLC) carried out on 0.25-mm Merck silica gel plates (60F-254) using ultraviolet light (254 nm) as the visualizing agent and $KMnO_4$ solution as developing agents. The separation of the resulting alcohols and remaining acetates was performed by preparative TLC Glass plates with Silica gel $60F_{254}$ type *MERCK*.

- **Chiral GC analysis and/or chiral HPLC analysis conditions of all compounds:**

The chemical analysis was performed by gas chromatography (ThermoFinnigan Trace GC) equipped with an automatic autosampler and using a CHIRALSIL-DEX CB column (25 m; 0.25 mm; 0.25 µm) and by AGC Series 600 Gas Chromatograph using an Rt®-bDEXsm column (30 m; 0.32 mm; 0.25 µm). Furthermore, by a chiral stationary phase HPLC on Chiralpack IB column. Retention times of enantiomers *R* and *S* are reported in minutes.

- **NMR Spectroscopic**

NMR spectra were recorded with Bruker spectrometers operating at (300 MHz and 250 MHz for 1H, 75 MHz or 63 MHz for ^{13}C and 101 MHz or 121 MHz for ^{31}P). Chemical shift of Solvent reference peaks used were $CDCl_3$ (δ = 7.26 ppm) for 1H and (δ = 77ppm) for ^{13}C NMR spectra, while H_3PO_4 was used as external standard for chemical shift references for ^{31}P NMR. Couplings constants (J) are given in Hz, with the Following abbreviations multiplicity: s = singlet, d = doublet, t = triplet, q = quartet, m = multiplet, br = broad signal.

- **Mass spectrometry**

Mass spectrometry analyzes were taken on a Bruker MicrOTOF-Q spectrometer using electrospray ionization (ESI) analysis. The mass peaks are expressed in units of mass per elementary charge m/z.

- **Melting points**

Melting points were measured using Buchi Melting Point B-545.

3) Synthesis of *α*-aminophosphonates by diphenylphosphinic acid

- **General procedure**

The diphenylphosphinic acid (10 mol%) was added to the reaction mixture of aromatic aldehyde (122.12 mg, 1 mmol), aniline (93 mg, 1 mmol) and diethylphosphite (165 mg, 1.2 mmol) in ethanol (10 mL). The reaction was stirred at 40°C for 30 min. The progress of the reaction was monitored by TLC. The solvent was removed and the resulting residue was treated with HCl (1N) then washed with water (10 mL) and extracted with dichloromethane (10 mL×2). The organic phases were combined and evaporated in vacuum. The crude product was purified by crystallization in hexane. Complete experimental data have been provided (NMR spectra and HRMS).

- **Physico-chemical characteristics**

Diethyl[phenyl(phenylamino)methyl]phosphonate (IV.14a)

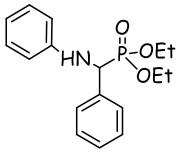

$C_{17}H_{23}NO_3P$
Molar mass: 320.14g/mol

Yield: 92%, as a white crystalline solid; **mp** 88°C. R_f: (0.43, 8/2. dichloromethane/methanol). **^{1}H NMR** (250 MHz, $CDCl_3$, 25°C) δ 7.52 -7.40 (m, 2H, ArH), 7.33-7.29 (m, 3H, ArH), 7.16 -7.10 (t, 2H, J =7.9 Hz, ArH), 6.75-6.69 (t, 1H, , J =7.3 Hz, ArH), 6.64 -6.61 (m, 2H, ArH), 4.84-4.75 (d, 1H, J_{HP}= 24.3 Hz, CHP), 4.18-4.10 (2H, m, -OCH_2- CH_3), 4.01-3.76 (1H, m, -OCH_2- CH_3), 3.74- 3.63

(1H, m, -OCH_2 CH_3), 1.31 (t, 3H, *J* = 7.1 Hz, -OCH_2-CH_3), 1.14 (t, 3H, *J* = 7.1 Hz, -OCH_2-CH_3). **^{13}C NMR** (63 MHz, $CDCl_3$, 25°C) δ 146.33 (d, J = 14.5 Hz); 136.00, 129.29, 128.74, 128.71, 128.00, 127.03, 118.40, 113.87, 63.27 (d, J^2_{CP} = 6.9 Hz), 57.29, 54.90, 16.46, (d, J^3_{CP} = 15.1), 16.37 (d, J^3_{CP} = 5.6 Hz). **^{31}P NMR** (101 MHz, $CDCl_3$, 25°C) δ 22.46 ppm. **HRMS (ESI)** m/z calcd for $C_{17}H_{23}NO_3P$ [M + H^+]: 320.1408; Found 320.1410.

Diethyl [(3-methoxyphenyl)(phenylamino)methyl] phosphonate (IV.14b)

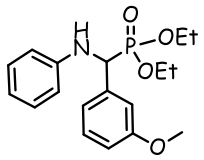

$C_{18}H_{26}NO_4P$
Molar mass: 351.14g/mol

Yield: 98%, as a white crystalline solid; mp103 °C. **R_f**: (0.41, 8/2. dichloromethane/methanol). **^{1}H NMR** (300 MHz, $CDCl_3$, 25 °C) δ 7.36–7.30 (m, 2H, HAr), 7.07–7.13 (m, 2H, HAr), 6.85 (d, *J*=7.3 Hz, 2H, H Ar), 6.66 (t, *J*=16.0 Hz, 1H, HAr), 6.58 (d, 2H, *J*=8.5Hz, HAr), 4.72 (d, *J*=24.4 Hz, 1H, CHP), 4.15 (m, 2H, OCH_2-CH_3), 3.91 (m, 1H, -OCH_2-CH_3), 3.77 (s, 3H, -OCH_3), 3.65–3.74 (m, 1H, -OCH_2-CH_3), 1.28 (t, 3H, *J*=7.0 Hz, -OCH_2-CH_3), 1.14 (t, 3H, *J*=7.0 Hz, -OCH_2-CH_3). **^{13}C NMR** (75 MHz, $CDCl_3$, 25°C): δ 159.40, 143.54 (d, *J*= 15.4 Hz), 129.24, 129.08, 129.01, 127.77, 127.73, 118.43, 114.16, 114.13, 63.39 (dd, J^2_{CP}=6.9, 3.9 Hz), 56.45, 55.33, 54.43, 16.60 (d, J^3_{CP}=14.9 Hz), 16.52 (d, J^3_{CP} = 5.9 Hz).**^{31}P NMR** (121 MHz, $CDCl_3$, 25 °C): δ 23.47 ppm.

Diethyl [4-nitrophenyl(phenylamino)methyl]phosphonate (IV.14c)

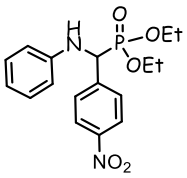

$C_{17}H_{23}N_2O_5P$
Molar mass: 362 g/mol

Yield: 90%, as a yellow crystalline solid; mp 89.2°C. **R_f:** (0.40, 8/2. dichloromethane/methanol). **^{1}H NMR** (400 MHz, $CDCl_3$, 25°C) δ 8.22-8.19 (d, 2H, ArH), 7.68-7.64 (dd, 2H, J_{HP} = 8.9, 2.3 Hz, ArH), 7.19-6.95 (m, 2H, ArH), 6.76-6.71 (t, 1H, *J* = 7.4 Hz, ArH), 6.56-6.52 (m, 2H, ArH), 4.88-4.81 (d, 1H, J_{HP} = 25.6 Hz, CHP), 4.25-4.11 (m, 2H, OCH_2-CH_3), 3.99-4.02 (m, 1H, -OCH_2-CH_3), 3. 97-3. 78 (m, 1H, -OCH_2-CH_3), 1.32 (t, 3H, J= 7.1 Hz, -OCH_2-CH_3), 1.21 (t, 3H, J= 7.1Hz, -OCH_2-CH_3). **^{13}C NMR** (101 MHz, $CDCl_3$, 25°C) δ 147.59, 145.71 (d, J = 16.6 Hz), 143.92 (d, *J* = 2.5 Hz), 129.35, 128.64 (d, *J* = 4.7 Hz), 123.75, 119.12, 113.81, 63.63 (dd, J^2 = 27.4, 6.8 Hz), 56.78, 55.31, 16.50 (d, J^3cp = 17.2 Hz), 16.24 (d, J^3cp = 5.5 Hz). **^{31}P NMR** (162 MHz, Chloroform-*d*) δ 20.80. **HRMS (ESI)** m/z calcd for $C_{17}H_{21}N_2O_5P$ [M + H^+]: 387.1094; Found 387.1080.

Diethyl[1-naphtyl(p-tolylamino)methyl]phosphonate (IV.14d)

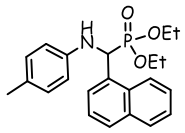

$C_{22}H_{28}NO_3P$
Molar mass: 385 g/mol

Yield: 90%, as a white crystalline solid; mp 145°C. **R_f**: (0.32, 8/2. dichloromethane/methanol). **^{1}H NMR** (300 MHz, $CDCl_3$, 25°C) δ 8.27 (d, 1H, J_{HP} = 8.5 Hz, HAr), 7.91 (d, 1H, *J* = 7.9 Hz HAr), 7.80-7.77 (m, 2H, HAr), 7. 63-7. 48 (m, 2H, HAr), 7.45 (t, 1H, *J* = 7.7 Hz, HAr), 6.67 (d, 2H, *J* = 8.48 Hz, HAr), 6.48 (d, 2H, *J* = 8.4 Hz, HAr), 4.64 (d, 1H, J_{HP} = 24.0 Hz, H_{CP}), 4.23-4.15 (m, 2H, -OCH_2-CH_3), 3.77-3.73 (m, 1H, -OCH_2-CH_3), 3. 28-3.17 (m, 1H, -OCH_2-CH_3), 2.16 (s, 3H, CH_3-Ph), 1.34 (t, 3H, *J* = 7.1 Hz, –OCH_2–CH_3), 0.75 (t, 3H, *J* = 7.1 Hz, –OCH_2–CH_3). **^{13}C NMR** (75 MHz, $CDCl_3$) δ 143.83 (d, *J* = 24.8 Hz), 133.81, 131.6 (d, *J*=19.7 Hz), 129.70, 129.00, 128.40, 127.50, 126.22, 125.64, 125.35 (d, *J* = 6.0 Hz), 123.00, 113.67, 63.63 (dd, J^2_{CP} = 27.4, 6.8 Hz), 20.33, 16.49 (d, J^3cp =5.9 Hz), 16.49 (d, J^3cp =5.9 Hz). **^{31}P NMR** (121 MHz, $CDCl_3$, 25°C): δ 23.07 ppm. **HRMS (ESI)** *m*/*z* calcd for $C_{22}H_{26}NO_3P$ [M + H^+]: 406.1532; Found 406.1542.

Diethyl [benzo [1,3]dioxol-5-yl((p-tolylamino) methyl]phosphonate (IV.14e)

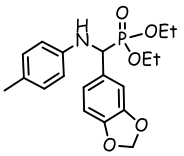

$C_{19}H_{26}NO_5P$
Molar mass: 375 g/mol

Yield: 91%, as a white crystalline solid; mp 115°C. **R_f**: (0.32, 8/2. dichloromethane/methanol). **^{1}H NMR** (300 MHz, $CDCl_3$, 25°C) δ 7.04 -6.89 (m, 4H, ArH), 6.77 (d, *J* = 8.0 Hz, 1H, ArH), 6.53 (d, *J*=8.5 Hz, 2H, ArH), 5.93-5.95 (dd, *J*=5.3, 1.4 Hz, 2H, O-CH_2-O), 4.66 (d, J_{HP} = 24.0 Hz, 1H, HCP), 4.27 – 4.07 (m, 3H, -OCH_2-CH_3+NH), 4.05 – 3.91 (m, 1H, -OCH_2-CH_3), 3.89 – 3.71 (m, 1H, -OCH_2-CH_3), 2.21 (s, 3H, CH_3Ph), 1.31 (t, *J* = 7.1 Hz, 3H, -OCH_2-CH_3), 1.19 (t, *J* = 7.1 Hz, 3H, -OCH_2-CH_3). **^{13}C NMR** (75 MHz, $CDCl_3$) δ 147.64 (d, *J* = 49.1 Hz), 143.78, 129.74 (d, *J* = 11.6 Hz), 121.35 (d, *J* = 6.5 Hz), 113.99, 108.21 (d, *J* = 13.9 Hz), 101.10, 63.84-62.26 (m), 57.01, 54.99, 20.36, 16.41 (d, J^3cp = 12.4 Hz), 16.19 (d, J^3cp = 5.7 Hz). **HRMS (ESI)** *m*/*z* calcd for $C_{19}H_{24}NNaO_5P$ [M + Na^+]: 400.128430; Found 400.1273. **^{31}P NMR** (121 MHz, $CDCl_3$) δ 22.65.

Diethyl [(4-fluorophenyl)(4-tolylamino)methyl] phosphonate (IV.14f)

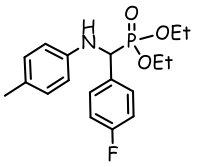

$C_{18}H_{25}NO_3PF$
Molar mass: 352 g/mol

Yield: 88%, as a white crystalline solid; mp 119°C. **R_f**: (0.36, 8/2. dichloromethane/methanol). **^{1}H NMR** (300 MHz, $CDCl_3$, 25°C) δ 7.43 (dd, J = 12.0, 4.0 Hz, 2H, HAr), 7.26 (m, 2H, HAr), 6.93 (d, 2H, *J* = 8.2 Hz, HAr), 6.48 (d, 2H, *J* = 8.5 Hz, HAr), 4.64–4.78 (m, 1H, HC*), 4.10–4.17 (m, 2H, -OCH_2-CH_3), 3.97–4.05 (m, 1H, -OCH_2-CH_3), 3.79–3.85 (m, 1H, -OCH_2-CH_3), 2.21 (s, 4H, CH_3-Ph+NH), 1.31 (t, 3H, *J*=7.1 Hz, -OCH_2-CH_3), 1.18 (t, 3H, *J* = 7.1 Hz, -OCH_2-CH_3). **^{13}C NMR:** (75 MHz, $CDCl_3$, 25 °C): δ 143.85 (d, *J* = 15.0 Hz), 134.84, 133.80, 133.76, 133.71, 129.83, 129.28,128.21,127.89,127.86, 128.03, 114.06, 63.59 (dd, J^2_{cp} = 12.1,7.0 Hz),56.89,54.89,20.47,16.59(d, J^3_{cp} = 13.7 Hz), 16.52 (d, J^3_{cp} = 5.8 Hz). ^{31}P NMR (121 MHz, $CDCl_3$) δ 22.69. **HRMS (ESI)** *m/z* calcd for $C_{18}H_{23}FNNaO_3P$ [M+ Na^+]: 374.1291; Found 374.1275. ^{31}P NMR (121 MHz, $CDCl_3$) δ 22.72.

Diethyl [(phenyl)(4-trifluoromethylamino)methyl] phosphonate (IV.14g)

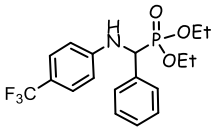

$C_{18}H_{22}NO_3PF_3$
Molar mass: 385 g/mol

Yield: 88%, as white crystalline solid. mp 140 °C. **R_f**: (0.40, 8/2. dichloromethane/methanol). **^{1}H NMR** (300 MHz, $CDCl_3$, 25 °C) δ = 7.49 (dd, *J*=7.7, 2.1 Hz, 2H, HAr), 7.26–7.40 (m, 5H, HAr), 6.62 (d, 2H, *J* = 8.5 Hz, HAr), 5.16–5.31 (t, *J* = 13.5 Hz, 1H, NH), 4.79 (dd, 1H, *J* = 24.2, 7.5 Hz, HC*), 4.10–4.20 (m, 2H, –OCH_2–CH_3), 3.90–4.08 (m, 1H, -OCH_2-CH_3), 3.61–3.70 (m, 1H, –OCH_2–CH_3), 1.31 (t, 3H, *J* = 7.1 Hz, –OCH_2–CH_3), 1.12 (t, 3H, *J*=7.0 Hz, –OCH_2–CH_3). **^{13}CNMR** (75MHz, $CDCl_3$, 25°C): δ 148.90 (d, *J* = 14.4 Hz), 135.13 (d, *J* =3.0 Hz), 128.91, 128.87, 128.38, 128.34, 127.90, 127.83, 126.68, 126.63, 113.16, 63.75 (dd, J^2_{cp} = 22.9, 7.0 Hz), 56.77, 54.77, 16.59 (d, J^3_{cp} = 19.0 Hz), 16.51 (d, J^3_{cp} = 5.8 Hz). **^{31}P NMR:** (121 MHz, $CDCl_3$, 25°C): δ 22.54 ppm.

Diethyl [3-phenoxyl(phenylamino)trifluoromethyl]phosphonate (IV.14h)

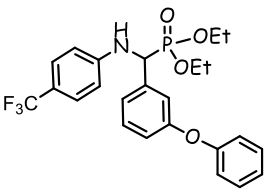

$C_{24}H_{26}NO_4PF_3$
Molar mass: 477 g/mol

Yield: 78%, as white crystalline solid. mp 155°C. **R_f**: (0.37, 8/2. dichloromethane/methanol). **^{1}H NMR** (360

MHz, $CDCl_3$, 25°C) δ 7.74-7.83 (m, 1H, HAr), 7.43-7.25 (m, 4H, HAr), 7.20 (d, *J* = 7.5 Hz, 1H, HAr), 7.13-7.05 (m, 2H, HAr), 6.93 (d, *J* = 7.6 Hz, 3H, HAr), 6.59 (d, *J* = 8.6 Hz, 2H, HAr), 5.53 (s, 1H, NH), 4.74 (d, *J* = 24.4 Hz, 1H, HC*), 4.20 – 4.06 (m, 2H), 4.05 – 3.93 (m, 1H, $–OCH_2–CH_3$), 3.84– 3.69 (m, 1H, $–OCH_2–CH_3$), 1.29 (t, *J* =7.1 Hz, 3H, $–OCH_2–CH_3$), 1.16 (t, *J* =7.1 Hz, 3H, $–OCH_2–CH_3$). **^{13}C NMR** (91 MHz, $CDCl_3$) δ 157.59, 156.82, 148.74 (d, *J*=14.3 Hz), 137.26, 129.92 (d, *J* = 30.6 Hz), 126.55, 123.45, 122.52 (d, *J* = 5.1 Hz), 120.35, 119.99, 118.83, 118.44, 118.14 (d, *J* = 5.3 Hz), 113.16, 63.49 (dd, *J* = 16.8, 6.9 Hz), 56.31, 54.64, 16.42 (d, J^3=5.8 Hz), 16.24 (d, J^3cp = 5.7 Hz). **^{31}P NMR** (162 MHz, $CDCl_3$) δ 21.54. **HRMS (ESI)** *m*/*z* calcd for $C_{24}H_{25}F_3NNaO_4P$ [M^+ Na^+]: 502.1365; Found 400.1343.

Diethyl [benzo [1,3]dioxol-5-yl((phenylamino)trifluoromethyl]phosphonate (IV.14i)

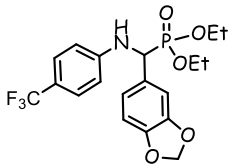

$C_{19}H_{23}NO_5PF_3$
Molar mass: 430 g/mol

Yield: 87%, as white crystalline solid. mp 148.2 °C. **R_f**: (0.34, 8/2. dichloromethane/methanol). **^{1}H NMR** (300 MHz, $CDCl_3$, 25°C) δ 7.36 (d, *J* = 8.5 Hz, 2H, HAr), 7.01 – 6.87 (m, 2H), 6.79 (d, *J* = 7.9 Hz, 1H), 6.64 (d, *J* = 8.5 Hz, 2H, HAr), 5.96 (dd, *J* = 3.8, 1.3 Hz, 2H, O-CH_2-O), 4.69 (d, *J* = 24.0 Hz, 1H, HC*), 4.23 – 4.06 (m, 2H, $–OCH_2–CH_3$), 4.05 – 3.92 (m, 1H, $–OCH_2–CH_3$), 3.76 (m, 1H, $–OCH_2–CH_3$), 1.32 (t, *J* = 7.1 Hz, 3H, $–OCH_2–CH_3$), 1.18 (t, *J* = 7.1 Hz, 3H, $–OCH_2–CH_3$). **^{13}C NMR** (101 MHz, $CDCl_3$) δ 148.88 (d, *J* = 34.5 Hz), 126.50, 121.32 (d, *J* =6.2 Hz), 120.14 (d, *J* = 34.6 Hz), 113.08, 108.42, 107.98 (d, *J* =4.2 Hz), 101.25, 63.56 (d, *J*=7.0 Hz), 63.28 (d, *J* = 7.0 Hz), 56.14, 54.62, 16.43 (d, J^3cp =5.6 Hz), 16.27 (d, J^3cp =5.5 Hz). **^{31}P NMR** (162 MHz, Chloroform-*d*) δ 21.87. **HRMS (ESI)** *m*/*z* calcd for $C_{19}H_{21}F_3NNaO_5P$ [M + Na^+]: 454.1001; Found 454.0991.

4) Synthesis of *α*-aminophosphonates by 2-Hydroxymethyl-18 crown ether-6

- **General procedure for the synthesis of diethyl phenyl *α*-aminophosphonates**

To the reaction mixture containing aromatic aldehyde(101.12 mg, 1 mmol), aniline (93 mg, 1 mmol), anddiethylphosphite (165 mg, 1.2 mmol) in ethanol, 2-Hydroxymethyl-18 crown ether-6 (5 mol%) wasadded, it was stirred within 15 min at room temperature. The reaction progress was monitored by TLC. The catalyst was removed by filtration. The filtrate waswashed by water (10 mL) and extracted with dichloromethane(10mL×2). The organic phases were combined andevaporated in vacuum. The crude product was purified bycrystallization in hexane to afford the aminophosphonatesderivatives V.14a-r. Complete experimental data have been provided (NMR spectra and HRMS) [13a, 14a].

- **Physico-chemical characteristics**

Diethyl [phenyl (phenylamino)methyl] phosphonate (V.14a)

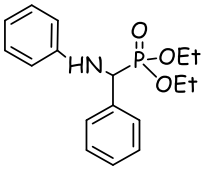

$C_{17}H_{23}NO_3P$
Molar mass: 320.14g/mol

Yield: 91%, as a white crystalline solid; mp 88°C. **R_f**: (0.43, 8/2. dichloromethane/methanol). **^{1}H NMR** (250 MHz, $CDCl_3$, 25°C): δ 7.52-7.29 (m, 6H, ArH), 7.16-7.10 (t, 1H, *J* = 7.9 Hz, ArH), 6.75-6.69 (t, 1H, *J* = 7.3 Hz, ArH), 6.64-6.61 (m, 2H, ArH), 4.84-4.75 (d, 1H, *J*HP = 24.3 Hz, CHP), 4.18-4.10 (2H, m, –OCH_2–CH_3), 4.01-3.76 (2H, m, –OCH_2–CH_3), 3.74-3.63 (1H, m, –OCH_2–CH_3), 1.31 (t, 3H, *J* = 7.1 Hz, –OCH2–CH3), 1.14 (t, 3H, *J* = 7.1 Hz, –OCH2– CH3). **^{13}C NMR** (63 MHz, CDCl3, 25°C): δ 146.33 (d,*J* = 14.5 Hz); 136.00, 129.29, 128.74, 128.71, 128.00, 127.03, 118.40, 113.87, 63.27 (d, J^2CP = 6.9 Hz), 57.29, 54.90, 16.46 (d, J^3 CP = 15.1), 16.37 (d, J^3 CP = 5.6 Hz). **^{31}P NMR** (101 MHz, $CDCl_3$, 25°C): δ 22.46 ppm. **HRMS (ESI)** *m*/*z* calcd for $C_{17}H_{23}NO_3P$ [*M* + H+]: 320.1408; Found 320.141.

Diethyl (4–chlorophenyl)(phenylamino) methylphosphonate (V.14b)

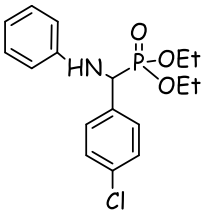

$C_{17}H_{22}NO_3PCl$
Molar mass: 354 g/mol

Yield: 80%, as a white crystalline solid. Mp 86.8 °C. **R_f**: (0.40, 8/2. dichloromethane/methanol). **^{1} HNMR** (300 MHz, $CDCl_3$, 25 °C): d = 1.18 (t, 3H, J = 7.0 Hz, –OCH_2–CH_3), 1.30 (t, 3H, J = 7.0 Hz, –OCH_2–CH_3), 3.75–3.80 (m, 1H, –OCH_2–CH_3), 3.92–4.06 (m, 1H, –OCH_2–CH_3), 4.05–4.21 (m, 2H, –OCH_2–CH_3),
4.75 (d, 1H, JHP = 24.5 Hz, CHP), 6.58 (dd, 2H, J = 8.6, 0.9 Hz, H Ar), 6.73(t, 1H, J = 7.4 Hz, H Ar), 7.13(dd, J = 8.5, 7.4 Hz, 2H, HAr), 7.21–7.38 (m, 2H, HAr), 7.44 (dd, J=8.6, 2.3 Hz, 2H, HAr). **^{13}CNMR**: (75 MHz, $CDCl_3$, 25 °C): d=146.01 (d, J=14.6 Hz), 134.60, 133.70, 129.26 128.19, 128.89, 128.86, 118.66, 113.83, 63.38 (d, J 2 = 6.8 Hz), 56.60, 54.61, 30.94, 16.36 (d, J 3 = 13.7 Hz), 16.36 (d, J^3 = 5.7 Hz). **^{31}P NMR:** (121 MHz, $CDCl_3$, 25 °C): d = 23.24 ppm.

Diethyl [4-nitrophenyl(phenylamino)methyl]phosphonate (V.14c)

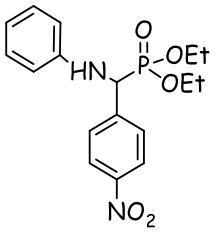

$C_{17}H_{22}N_2O_5P$
Molar mass: 365 g/mol

Yield: 93%, as a yellow crystalline solid; mp 89.2°C. **R_f**: (0.40, 8/2. dichloromethane/methanol). **^{1}HNMR** (250 MHz, CDCl3, 25°C): δ 8.22-8.19(m, 2H, ArH),7.69-7.64(dd, 2H, *J*HP = 8.80, 2.3 Hz, ArH), 7. 15-7.09 (m,2H, ArH), 6.77-6.71 (t, 2H, *J* = 7.4 Hz, ArH), 6.59-6.52 (m, 2H, ArH), 4.92-4.81(d, 1H, *J*HP = 25.2 Hz, CHP), 4.19-4.10 (m, 2H, –OCH_2–CH_3), 4.09-4.02(m, 1H, –OCH_2–CH_3), 3.99-3.95 (m, 1H, –OCH2–CH3), 1.30 (t, 3H, *J* = 7.00 Hz,–OCH2–CH3), 1.19 (t, 3H, *J* = 7.1 Hz, –OCH2–CH3).13C NMR (63 MHz, $CDCl_3$, 25°C): δ **^{13}C NMR** (63 MHz,$CDCl_3$): δ 147.59, 145.63 (d, *J* = 14.2 Hz), 144.04 (d,*J* = 2.5 Hz), 129.34, 128.63 (d, *J* = 4.9 Hz), 123.75, 119.10,113.79, 63.60 (dd, *J*2= 17.1, 6.9 Hz), 57.20, 54.84, 16.30 (dd,*J*3CP = 10.3, 5.5 Hz). **^{31}P NMR** (101 MHz, $CDCl_3$, 25°C):δ 21.31 ppm. **HRMS (ESI)** *m*/*z* calcd for $C_{17}H_{21}N_2O_5P$[*M* + Na^+]: 387.1094; Found 387.1080.

Diethyl [1-naphtyl(phenylamino) methyl]phosphonate (V.14d)

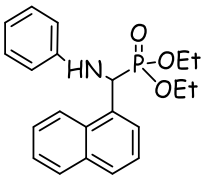

$C_{21}H_{25}NO_3P$
Molar mass: 370 g/mol

Yield: 88%, as a white crystalline solid; mp 123°C. **R_f**: (0.32, 8/2. dichloromethane/methanol). **^{1}H NMR** (250 MHz, $CDCl_3$, 25°C): δ 8.26 (d, 1H, *J*HP = 8.3 Hz, ArH), 7.89-7.44 (m, 6H, ArH), 7.05-7.02 (dd, 2H, *J* = 8.5, 7.4 Hz, ArH), 6.68-6.63 (dd, 1H, *J* = 10.6, 4.1 Hz, ArH), 6.57-6.53 (m, 2H, ArH), 5.60 (d, 1H, *J*HP = 24.1 Hz, CHP), 5.10 (s, 1H, NH), 4.25-4.13 (m, 2H, OCH2–CH3), 3.75-3.72(m, 1H,–O-CH_2–CH_3), 3.25-3.15(m, 1H, –OCH_2–CH_3), 1.33(t, 3H, *J* = 7.00 Hz, –OCH_2–CH_3), 0.70 (t, 3H, *J* = 7.1 Hz,–OCH_2–CH_3). **^{13}C NMR** (63 MHz, $CDCl_3$, 25°C): δ^{13}CNMR (63 MHz, $CDCl_3$): δ 146.11 (d, *J* = 13.9 Hz), 133.81,131.63 (d, *J* = 8.0 Hz), 129.09 (d, *J* = 10.6 Hz), 128.44,126.25, 126.05, 125.65, 125.37 (d, *J* = 5.8 Hz), 122.94,118.26, 113.57, 63.26 (dd, *J*2 CP = 12.4, 6.8 Hz), 52.67,50.25, 16.45 (d, J^3CP = 6.2 Hz), 15.75 (d, J^3CP = 5.7 Hz). **^{31}PNMR** (101 MHz, $CDCl_3$, 25°C): δ 22.98 ppm. **HRMS (ESI)** *m*/*z* calcd for $C_{21}H_{24}NO_3P$ [*M* + Na^+]: 392.1401; Found392.1386.

Diethyl [4-biphenyl(phenylamino)methyl]phosphonate (V.14e)

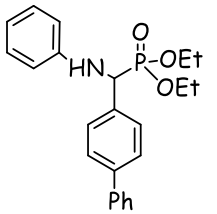

$C_{23}H_{27}NO_3P$
Molar mass: 396 g/mol

Yield: 86%, as a white crystalline solid; mp 158°C. **R_f**: (0.32, 8/2. dichloromethane/methanol). **^{1}HNMR** (300 MHz, $CDCl_3$): δ 7.64-7.53(m, 6H, ArH), 7.45 (t, *J* = 7.4 Hz, 2H, ArH), 7.36 (t, *J* = 6.7 Hz, 1H, ArH), 7.15 (t, *J* = 7.9 Hz, 2H, ArH), 6.74 (t, *J* = 7.3 Hz, 1H,ArH), 6.66 (d, *J* = 8.1 Hz, 2H, ArH), 4.89 (d, *J* = 7.5 Hz,^{1}H, HCP), 4.80 (d, *J* = 7.7 Hz, 1H, NH), 4.27-4.09 (m, 2H, –OCH_2–CH_3), 4.01-3.80 (m, 1H, –OCH2–CH3), 3.78-3.96 (m, 1H, –OCH_2–CH_3), 1.33 (t, *J* = 7.1 Hz, 3H, –OCH_2–CH_3), 1.18 (t, *J* = 7.1 Hz, 3H, –OCH_2–CH_3). **^{13}C NMR** (75 MHz, $CDCl_3$): δ 146.26 (d, *J* = 21.3 Hz), 140.70 (d, *J* = 6.8 Hz), 134.92, 129.22, 128.78, 128.72, 128.23 (d, *J* = 5.4 Hz), 127.35 (d, *J* = 2.9 Hz), 127.29, 127.02, 118.48, 113.88, 63.35 (d, J^2CP = 7.0 Hz), 56.81, 54.82, 16.47 (d, J^3CP = 5.8 Hz), 16.25 (d, J^3 CP = 6.1 Hz). **^{31}P NMR** (121 MHz, $CDCl_3$, 25°C): δ 22.58 ppm. **HRMS (ESI)** *m/z* calcd for $C_{23}H_{26}NO_3P$ [*M* + Na+]: 418.1550; Found 418.1542.

Diethyl [4-methoxy (phenylamino) methyl]phosphonate (V.14f)

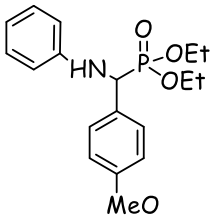

$C_{18}H_{25}NO_4P$
Molar mass: 350 g/mol

Yield: 90%, as Whitecrystalline solid. mp 103 °C. **R_f**: (0.39, 8/2. dichloromethane/methanol). **^{1}HNMR** (300 MHz, $CDCl_3$, 25 °C): d = 1.14 (t, 3H, J = 7.0 Hz, –OCH 2 –CH3), 1.28 (t, 3H, J = 7.0 Hz, –OCH_2–CH_3), 3.65–3.74 (m, 1H, –OCH_2–CH_3), 3.77 (s, 3H, –OCH 3), 3.91 (m, 1H, –OCH_2–CH_3), 4.15 (m, 2H, –OCH_2–CH_3), 4.72 (d, J = 24.4 Hz, 1H, CHP), 6.58 (d, 2H, J = Hz, HAr), 6.66 (t, J = 16.0 Hz, 1H, HAr), 6.85 (d, J = Hz, 2H, H Ar), 7.07–7.13 (m, 2H, HAr), 7.36–7.30 (m, 2H, H Ar). **^{13}C NMR**: (75 MHz, $CDCl_3$, 25 °C): d = 159.40, 143.54 (d, J = 15.4 Hz), 129.24, 129.08, 129.01, 127.77, 127.73, 118.43, 114.16, 114.13, 63.39 (dd, J 2 = 6.9, 3.9 Hz), 56.45, 55.33, 54.43, 16.60 (d, J^3 = 14.9 Hz), 16.52 (d, J 3 = 5.9 Hz). **^{31}P NMR**: (121 MHz, $CDCl_3$, 25 °C): d = 23.47 ppm.

Diethyl [phenyl(p-tolylamino)methyl]phosphonate (V.14g)

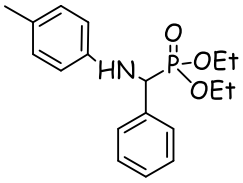

$C_{18}H_{25}NO_3P$
Molar mass: 334 g/mol

Yield: 94% as a white crystalline solid; mp 120°C. **R_f**: (0.41, 8/2. dichloromethane/methanol). **^{1}H NMR**(300 MHz, $CDCl_3$, 25°C): δ 7.49-7.47(m, 2H, ArH), 7.37-7.27(m, 3H, ArH), 6.93 (d, *J* = 8.3 Hz, 2H, ArH), 6.53(d, 2H, *J* = 8.4 Hz, ArH), 4.76 (d, *J* = 24.2 Hz, 2H, HCPand NH), 4.17-4.10(m, 2H, $–OCH_2–CH_3$), 4.00-3.92(m,1H, $–OCH_2–CH_3$), 3.74-3.66(m, 1H, $–OCH_2–CH_3$), 2.20(s, 3H, CH_3-Ph),1.30 (t, 3H, *J* = 7.1 Hz, $–OCH_2–CH_3$),1.13 (t, 3H, *J* = 7.1 Hz, $–OCH_2–CH_3$),**^{13}C NMR** (75 MHz,CDCl3, 25°C): δ^{13}C NMR (63 MHz, $CDCl_3$) δ 143.95 (d,*J* = 15.1 Hz), 135.98, 129.62, 128.50, 127.81 (d, *J* = 4.7 Hz),127.58, 113.96, 64.83-61.51(m), 57.54, 55.15, 20.31, 16.27(dd, J^3CP = 15.2, 5.7 Hz),**^{31}P NMR** (101 MHz, $CDCl_3$,25°C): δ 21.48 ppm. HRMS (ESI) *m*/*z* calcd for $C_{18}H_{24}NO_3P[M^+ Na^+]$: 356.1397; Found 356.1386.

Diethyl [4 chloro(p-tolylamino) methyl]phosphonate (V.14h)

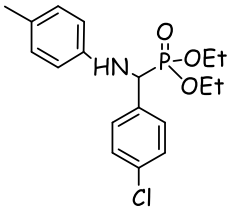

$C_{18}H_{24}NO_3PCl$
Molar mass: 368 g/mol

Yield: 76%, as White crystalline solid. Mp 119.5 °C. **R_f**: (0.39, 8/2. dichloromethane/methanol). **^{1}H NMR** (300 MHz, $CDCl_3$, 25 °C): d = 1.18 (t, 3H, J= 7.1 Hz, $–OCH_2–CH_3$), 1.31 (t, 3H, J = 7.1 Hz, $–OCH_2–CH_3$), 2.21 (s, 3H, CH_3–Ph), 3.79–3.85 (m, 1H, $–OCH_2–CH_3$), 3.97–4.05 (m, 1H, $–OCH_2–CH_3$), 4.10–4.17 (m, 2H, $–OCH_2–CH_3$), 4.64–4.78 (m, 2H, CH-NH), 6.48 (d, 2H, J = 8.5 Hz, HAr), 6.93 (d, 2H, J = 8.2 Hz, HAr), 7.26 (m, 2H, HAr), 7.43 (dd, J = 12.0, 4.0 Hz, 2H, HAr). **^{13}C NMR**: (75 MHz, $CDCl_3$, 25 °C): d = 143.85 (d, J = 15.0Hz), 134.84, 133.80, 133.76, 133.71, 129.83, 129.28, 128.21, 127.89, 127.86, 128.03, 114.06, 63.59 (dd, J 2 = 12.1, 7.0 Hz), 56.89, 54.89, 20.47, 16.59 (d, J 3 = 13.7 Hz), 16.52 (d, J 3 = 5.8 Hz). **^{31}P NMR**: (121 MHz, $CDCl_3$, 25 °C), δ= 22.69 ppm.

Diethyl [4-nitrophenyl (p-tolylamino) methyl]phosphonate (V.14i)

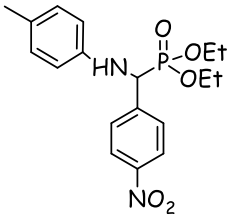

$C_{17}H_{24}N_2O_5P$
Molar mass: 367 g/mol

Yield: 92%, as a yellow crystalline solid; mp 158°C. **R_f**: (0.38, 8/2. dichloromethane/methanol). **^{1}H NMR** (300 MHz, $CDCl_3$, 25°C): δ 8.21 (d, *J* = 8.5 Hz,2H, ArH), 7.67 (dd, *J* = 8.8, 2.3 Hz, 2H, ArH), 6.94 (d,2H, *J* = 8.3 Hz, ArH), 6.46 (d, *J* = 8.4 Hz, 2H, ArH),4.85 (d, *J* = 25.1 Hz, 2H, HCP+NH), 4.20-4.02(m, 3H,–OCH_2–CH_3), 3.94-3.86(m, 1H, –OCH_2–CH_3), 2.35 (s,3H, CH_3-Ph),1.32 (t, 3H, *J* = 7.1 Hz, –OCH_2–CH_3), 1.21(t, 3H, *J* = 7.1 Hz, –OCH_2–CH_3). **^{13}C NMR** (75 MHz,$CDCl_3$, 25°C): δ 147.54, 144.20, 143.25 (d, *J* = 14.8 Hz), 129.86, 128.65 (d, *J* = 4.8 Hz), 128.62, 123.74, 113.93,63.58 (dd, J^2CP = 23.8, 6.9 Hz), 57.26, 55.29, 20.36, 16.45(d, J^3CP = 12.6 Hz), 16.30 (d, J^3 CP = 5.8 Hz). **^{31}P NMR**(121 MHz, $CDCl_3$, 25°C): δ=20.94 ppm. **HRMS (ESI)** *m*/*z* calcd for $C_{18}H_{24}N_2O_5P$ [M^+H^+]: 379.1412; Found379.1417.

Diethyl [4 methoxy(p-tolylamino) methyl]phosphonate (V.14j)

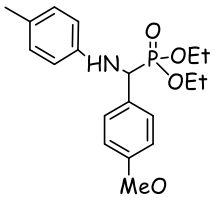

$C_{19}H_{27}NO_4P$
Molar mass: 364 g/mol

Yield: 90%, as White crystalline solid. mp 99 °C. **R_f**: (0.38, 8/2. dichloromethane/methanol). **^{1} H NMR** (300 MHz, $CDCl_3$, 25 °C): d = 1.14 (t, 3H, J= 7.1 Hz, –OCH_2–CH_3), 1.28 (t, 3H, J = 7.1 Hz, –OCH_2–CH_3), 2.18 (s, 3H, CH_3–Ph), 3.66–3.74 (m, 1H, –OCH_2–CH_3), 3.77 (s, 3H, –OCH_3), 3.91–3.96 (m,1H, –OCH_2–CH_3), 3.99–4.15 (m, 2H, –OCH_2–CH_3), 4.70 (d, J=24.5 Hz, 2H, CHP-NH), 6.49 (d, 2H, J = 8.4 Hz, HAr), 6.92 (dd, J = 16.0, 8.5 Hz, 4H, HAr), 7.26–7.39 (m, 2H, HAr). **^{13}C NMR**: (75 MHz, $CDCl_3$, 25°C): δ=159.20, 144.20 (d, J=15.4 Hz), 129.76, 129.08, 129.01, 127.92, 127.88, 127.68, 114.12, 63.38 (dd, J 2 = 6.9, 2.9 Hz), 56.74, 55.34, 54.72, 20.49, 16.63 (d, J^3=14.0 Hz), 16.55 (d, J 3 = 5.8 Hz).**^{31}P NMR**: (121 MHz, $CDCl_3$, 25 °C): δ= 23.59 ppm.

Diethyl [1-naphtyl (p-tolylamino) methyl]phosphonate (V.14k)

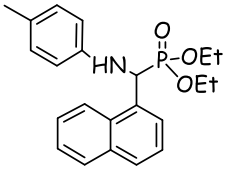

$C_{22}H_{27}NO_3P$

Molar mass: 384 g/mol

Yield: 93%, as a white crystalline solid; mp 145°C. **R_f**: (0.32, 8/2. dichloromethane/methanol). **^{1}H NMR** (300 MHz, $CDCl_3$, 25°C): δ 8.27 (d, 1H, *J*HP =

8.5 Hz, ArH),7.91 (d, 1H, *J* = 7.9 Hz ArH), 7.80-7.77(m, 2H, ArH), 7. 63-7.48 (m, 2H, ArH), 7.45 (t, 1H, *J* = 7.7 Hz, ArH), 6.67 (d, 2H,*J* = 8.48 Hz, ArH), 6.48 (d, 2H, *J* = 8.4 Hz, ArH), 4.64 (d,1H, *J*HP = 24.0 Hz, HCP), 4.23-4.15(m, 2H, –OCH_2–CH_3),3.77-3.73 (m, 1H, –OCH_2–CH_3), 3. 28-3.17 (m, 1H, –OCH_2– CH_3), 2.16 (s, 3H, CH3-Ph),1.34 (t, 3H, *J* = 7.1 Hz, –OCH_2–CH_3), 0.75 (t, 3H, *J* = 7.1 Hz, –OCH_2–CH_3). **^{13}C NMR**(75 MHz, $CDCl_3$) δ 143.83 (d, *J* = 24.8 Hz), 133.81, 131.6 (d, *J* = 19.7 Hz), 129.70, 129.00, 128.40, 127.50, 126.22,125.64, 125.35 (d, *J* = 6.0 Hz), 123.00, 113.67, 20.33, 16.49(d, *J* = 5.9 Hz), 15.79 (d, *J* = 5.9 Hz). **^{31}P NMR** (121 MHz,$CDCl_3$, 25°C): δ=23.07 ppm. **HRMS (ESI)** *m/z* calcd for$C_{22}H_{26}NO_3P$ [*M* $^+$ Na^+]: 406.1555; Found 406.1542.

Diethyl [4-biphenyl(p-tolylamino)methyl]phosphonate (V.14l)

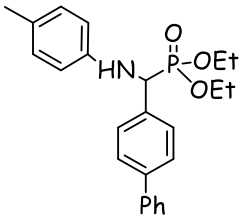

$C_{24}H_{29}NO_3P$
Molar mass: 410 g/mol

Yield: 90%, as a white crystalline solid; mp 140°C. **R_f:** (0.32, 8/2. dichloromethane/methanol). **^{1}H NMR** (300 MHz, $CDCl_3$, 25°C): δ7.42-7.59(m, 6H, ArH), 7.26-7.39(m, 3H, ArH), 6.93 (d, 2H, *J* = 8.2 Hz, ArH), 6.55 (d,2H, *J* = 8.4 Hz, ArH), 4.79 (d, 1H, *J* = 24.3 Hz, HCP), 4.10-4.18(m, 2H, OCH_2–CH_3), 3.84-4.01(m, 1H, –OCH_2–CH_3),3.71-3.81(m, 1H, –OCH_2–CH_3), 2.19 (s, 3H, CH_3-Ph),1.30 (t, 3H, *J* = 7.1 Hz, –OCH_2–CH_3), 1.15 (t, 3H, *J* = 7.0 Hz, –OCH_2–CH_3). **^{13}C NMR** (75 MHz, $CDCl_3$, 25°C): δ 143.82, 140.59, 129.67, 128.70, 128.20 (d, *J* = 5.5 Hz),127.66, 127.24 (d, *J* = 2.7 Hz), 126.96, 113.98, 63.31 (t, *J* = 7.0 Hz), 57.28, 54.87, 20.33, 16.38 (d, J^3 CP = 14.0 Hz), 16.16 (d, J^3CP = 5.5 Hz) **^{31}P NMR** (121 MHz, $CDCl_3$, 25°C):δ 22.71 ppm. **HRMS (ESI)** ***m/z*** calcd for $C_{24}H_{29}NO_3P$[*M* + H+]: 410.1876; Found 410.1879.

Diethyl [4-nitro phenyl (p-tolylamino) methyl] phosphonate (V.14m)

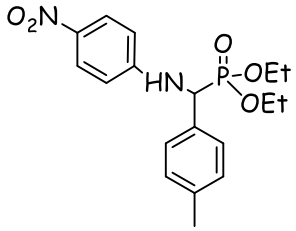

$C_{18}H_{24}N_2O_5P$
Molar mass: 379 g/mol

Yield: 80%, white crystalline solid, mp 137°C. **R_f**: (0.38, 8/2. dichloromethane/methanol). **^{1}H NMR** (360 MHz, Chloroform-*d*) δ 8.08- 8.00 (m, 2H, HAr), 7.36 (dd, *J* = 8.2, 2.2 Hz, 3H, HAr,), 7.19 (d, *J* = 8.2 Hz, 2H, HAr), 6.65-6.57 (m, 2H, HAr), 4.80 (dd, *J* = 23.7, 7.6 Hz, 1H, *CH), 4.25- 4.07 (m, 2H, -OCH_2-CH_3), 3.96 (m, 1H, -OCH_2-CH_3), 3.76-3.59 (m, 1H, -OCH_2-CH_3), 2.36 (d, *J* = 1.9 Hz, 3H, CH_3Ar), 1.34 (t, *J* = 7.0 Hz, 3H, -OCH_2-CH_3), 1.16 (t, *J* = 7.3 Hz, 3H, -OCH_2-CH_3). **^{13}C NMR** (91 MHz, Chloroform-*d*) δ 138.36 (d, *J* = 3.6 Hz), 131.40 (d, *J* = 3.3 Hz), 129.90- 129.35 (m), 127.61 (d, *J* = 5.4 Hz), 126.05, 112.45,

63.54 (dd, J = 48.3, 7.1 Hz), 56.18, 54.50, 16.43 (d, J^3_{CP} =5.8 Hz), 16.20 (d, J^3_{CP} = 5.7 Hz). **^{31}P NMR** (101 MHz, Acetone-d_6) δ 21.39. **HRMS (ESI)** m/z calcd for $C_{18}H_{23}N_2NaO_5P$ [M +Na^+]: 401.1239; Found. 401.1222.

Diethyl [2-methoxyphenyl (4-bromo, 2,6-dimethylamino) methyl] phosphonate (V.14n)

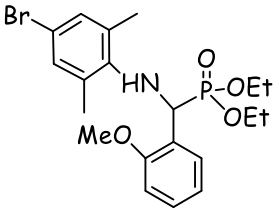

$C_{20}H_{28}NO_4PBr$
Molar mass: 457 g/mol

Yield: 92%. White crystalline solid, mp 106.8°C. **R$_f$**: (0.37, 8/2. dichloromethane/methanol). **^{1}H NMR** (360 MHz, Chloroform-d) δ 7.65 (d, J = 11.1 Hz, 2H, ArH), 7.27 (d, J = 9.9 Hz, 1H, ArH), 7.04 (d, J = 18.1 Hz, 3H, ArH), 6.85 (d, J = 8.3 Hz, 1H, ArH), 5.25 – 5.02 (m, 1H, -OCH_2-CH_3), 4.33 – 4.06 (m, 2H, -OCH_2-CH_3), 3.96 – 3.84 (m, 1H, -OCH_2-CH_3), 3.75 (s, 3H, -OCH_3), 3.71 – 3.58 (m, 1H, -OCH_2-CH_3), 2.24 (s, 6H, 2CH_3Ar), 1.29 (t, J = 7.1 Hz, 3H, -OCH_2-CH_3), 1.05 (t, J = 7.1 Hz, 3H, -OCH_2-CH_3). **^{13}C NMR** (91 MHz, Chloroform-d) δ 156.79 (d, J = 7.3Hz), 143.86 (d, J = 9.1 Hz), 131.08 (d, J = 5.3 Hz), 129.06, 125.86, 120.90 (d, J = 1.9 Hz), 113.70, 110.74, 63.23 – 62.23 (m), 55.62, 16.23 (dd, J^3_{CP} = 22.3, 5.7 Hz). **^{31}P NMR** (101 MHz, Acetone-d_6 25°C) δ 24.89 ppm. **HRMS (ESI)** m/z calcd for $C_{20}H_{28}BrNNaO_4P$ [M + Na^+]: 478.0753; Found 478.0742.

Diethyl [3-methoxyphenyl (4-bromo, 2,6-dimethylamino) methyl] phosphonate (V.14o)

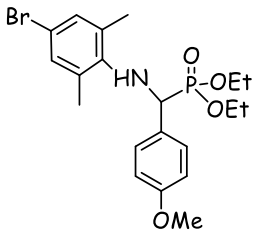

$C_{20}H_{28}NO_4PBr$
Molar mass: 457 g/mol

Yield: 88 %. White crystalline solid, mp 113°C. **R$_f$**: (0.37, 8/2. dichloromethane/methanol). **^{1}H NMR** (360 MHz, Chloroform-d) δ 7.33- 7.21 (m, 1H, ArH), 7.07 (s, 2H, ArH), 7.06-6.95 (m, 2H, ArH), 6.85 (d, J = 9.2 Hz, 1H, ArH), 4.53 – 4.34 (m, 1H, *CH), 4.23 – 4.09 (m, 2H, -OCH_2-CH_3), 3.95 (m, 1H, -OCH_2-CH_3), 3.81 (s, 3H, -OCH_3), 3.74-3.59 (m, 1H, -OCH_2-CH_3), 2.23 (s, 6H, 2CH_3Ar), 1.31 (t, J = 7.1 Hz, 3H, -OCH_2-CH_3), 1.09 (t, J = 7.1 Hz, 3H, -OCH_2-CH_3). **^{13}C NMR** (91 MHz, Chloroform-d) δ 131.35, 130.90, 129.42, 120.61 (d, J = 6.4 Hz), 113.80 (dd, J = 22.6, 15.9 Hz), 62.93 (dd, J = 34.7, 7.2 Hz), 18.73, 16.39 (d, J^3_{CP} = 6.2 Hz), 16.14 (d, J^3_{CP} = 5.9 Hz). **^{31}P NMR** (101 MHz, Acetone-d_6, 25°C) δ 23.93 ppm. **HRMS (ESI)** m/z calcd for $C_{20}H_{27}BrNNaO_4P$ [M+Na^+]: 478.0753; Found 478.0738.

Diethyl(phenyl)(4-trifluoromethyl)phenylamino) methylphosphonate (V.14p)

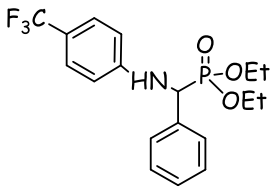

$C_{18}H_{22}NO_3PF_3$

Molar mass: 385 g/mol

Yield: 80%, as white crystalline solid. Mp 140°C. **R_f:** (0.40, 8/2. dichloromethane/methanol). **^{1}H NMR** (300 MHz, $CDCl_3$, 25 °C): d = 1.12 (t, 3H, J=7.0 Hz, $–OCH_2–CH_3$), 1.31 (t, 3H, J = 7.1 Hz, $–OCH_2–CH_3$), 3.61–3.70 (m, 1H, $–OCH_2–CH_3$), 3.90–4.08 (dp, J = 10.1, 7.1 Hz, 1H, $–OCH_2–CH_3$), 4.10–4.20 (m, 2H, $–OCH_2–CH_3$), 4.79 (dd, 1H, J = 24.2, 7.5 Hz, Ph–CH), 5.16–5.31 (m, 1H, NH), 6.62 (d, 2H, J = 8.5 Hz, H Ar), 7.26–7.40 (m, 5H, HAr), 7.49 (dd, J=7.7, 2.1 Hz, 2H, HAr). **^{13} C NMR**: (75 MHz, $CDCl_3$, 25 °C): d = 148.90 (d, J = 14.4 Hz), 135.13 (d, J = 3.0 Hz), 128.91, 128.87, 128.38, 128.34, 127.90, 127.83, 126.68, 126.63, 113.16, 63.75 (dd, J^2= 22.9, 7.0 Hz), 56.77, 54.77, 16.59 (d, J^3=19.0 Hz), 16.51 (d, J 3 = 5.8 Hz). **^{31}P NMR**: (121 MHz, $CDCl_3$, 25°C): δ= 22.54 ppm.

Diethyl (4-chlorophenyl)(4-trifluoromethylphenylamino) methylphosphonate (V.14q)

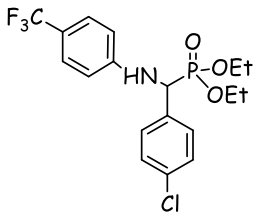

$C_{18}H_{21}NO_3PF_3Cl$

Molar mass: 419 g/mol

Yield: White crystalline solid. Mp 129 °C. **R_f**: (0.38, 8/2. dichloromethane/methanol). **^{1}H NMR** (300 MHz, $CDCl_3$, 25 °C): d = 1.18 (t, 3H, J = 6.9 Hz, $–OCH_2–CH_3$), 1.32 (t, 3H, J = 7.1 Hz, $–OCH_2–CH_3$), 3.72–3.81 (m,1H,$–OCH_2–CH_3$), 3.96–4.01(m,1H,$–OCH_2–CH_3$), 4.04–4.18 (m, 2H, $–OCH_2–CH_3$), 4.70 (dd,1H,J=24.4,7.3Hz,CHP), 5.16 (dd, 1H, J = 10.2, 7.5 Hz, –NH), 6.60 (d, 2H, J = 8.6 Hz, HAr),77.28–7.43(m,6H, H Ar). **^{13}C NMR**: (75 MHz, $CDCl_3$, 25 °C): d = 148.61 (d, J = 14.2 Hz),134.24 (d, J = 3.9 Hz), 134.19, 133.96, 133.92, 129.19, 129.12, 126.76, 126.71, 113.19, 63.71 (dd, J 2 = 11.2, 7.0 Hz), 56.27, 54.27, 16.60 (d, J 3 = 13.9 Hz), 16.53 (d, J 3 = 5.7 Hz). **^{31}P NMR**: (121 MHz, $CDCl_3$, 25 °C): δ = 21.87 pp.

Diethyl (4-methoxyphenyl)(4-trifluoromethylphenylamino) methylphosphonate (V.14r)

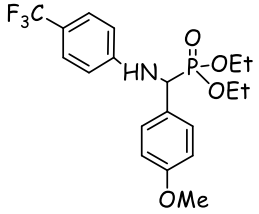

$C_{19}H_{24}NO_4PF_3$

Molar mass: 415 g/mol

Yield: 88%, as White crystalline solid. Mp111 °C. **R_f**: (0.38, 8/2. dichloromethane/methanol). **^{1}H NMR** (300

MHz, $CDCl_3$, 25 °C): d = 1.15 (t, 3H, J = 7.0 Hz, $–OCH_2$ $–CH_3$), 1.31 (t, 3H, J = 7.1 Hz, $–OCH_2–CH_3$), 3.63–3.72 (ddd, J = 10.1, 8.3, 7.1 Hz, 1H, $–OCH_2–CH_3$), 3.80 (s, 3H, $–OCH_3$), 3.95 (dt, J = 10.1, 7.1 Hz, 1H,$–OCH_2–CH_3$),4.13 (m,2H,$–OCH_2–CH_3$), 4.73 (dd, 1H, J = 23.8, 7.6 Hz, CHP), 5.15 (dd, J =9.7,7.8Hz,1H,–NH),6.63 (d, 2H, J = 8.5 Hz, HAr), 6.90 (d, 2H, J = 8.5 Hz, H Ar), 7.26–7.40 (m,4H,HAr).**^{13}C NMR**: (75 MHz, $CDCl_3$, 25 °C): d = 159.60, 148.16 (d, J = 14.3 Hz), 128.97, 126.96, 126.67, 114.35 (d, J= 2.3 Hz), 113.19, 63.70 (dd, J 2 = 24.1, 7.0 Hz), 56.10, 55.38, 54.08, 16.61 (d, J^3= 13.9 Hz), 16.54 (d, J^3= 5.8 Hz). **^{31}P NMR**: (121 MHz, $CDCl_3$, 25 °C): δ= 22.77 ppm.

5) Enzymatic deacylation of racemic acetates VI.1a- VI.8a

- ***General procedure for the reduction of ketones***

The racemic alcohols **VI.2**, **VI.3**, **VI.6** were obtained after reduction of the corresponding commercial ketones (1 equivalent) using 6 equivalents of $NaBH_4$ in a solution of (THF/water; 4/1 *v/v*). The reaction mixture was stirred under at 0 °C. The evolution of the reactions was monitored by TLC. After total consumption of ketones, the reaction mixture was neutralized by addition of a solution of (HCl, 1N). Then the organic layer was removed, and the aqueous layer was extracted with ethyl acetate (3 x 80 mL). The combined organic layers were dried over anhydrous $MgSO_4$ and concentrated to give the resulting alcohols in good yields.

- **NMR data and chromatographic characteristics of the racemic alcohols (VI.2, VI.3, VI.6)**

rac-1-(4-methoxyphenyl) ethanol (rac- VI.2)

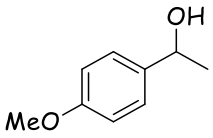

$C_9H_{12}O_2$

Molar mass: 152 g/mol

***rac*-1-(4-methoxyphenyl) ethanol (*rac*- VI.2):** Uncoloured oil. **Yield**: 92.1%. **R_f**: (0.24, 9/1. petroleum ether/ethyl acetate). **^{1}H NMR (300MHz, $CDCl_3$) δ** 7.32 (d, *J* = 8.7 Hz, 2H), 6.90 (d, *J* = 8.7 Hz, 2H), 4.87 (q, *J* = 6.4 Hz, 1H), 3.82 (s, 3H), 1.89 (s, 1H, -OH), 1.50 (d, *J* = 6.4 Hz, 3H). **^{13}C NMR (75 MHz, $CDCl_3$) δ** 158.97, 138.01, 126.66, 113.84, 69.97, 55.29, 25.03. **Chiral GC**: Isothermal 103°C. **Retention time**: t_R = 18.64 min t_S = 19.58 min.

rac-1-(4-ethoxyphenyl) ethanol (rac- *VI.*3)

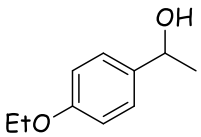

$C_{10}H_{14}O_2$

Molar mass: 166 g/mol

***rac*-1-(4-ethoxyphenyl) ethanol (*rac*- VI.3):** White Crystals. Yield: 99 %. **R_f**: (0.29, 9/1. petroleum ether/ethyl acetate). **mp:** 41°C. **^{1}H NMR (300MHz, $CDCl_3$) δ** 7.30 (d, *J* = 8.7 Hz, 2H), 6.89 (d, *J* = 8.7 Hz, 2H), 4.86 (q, *J* = 6.4 Hz, 1H), 4.05 (q, *J* = 7.0 Hz, 2H), 1.87 (s, 1H, -OH), 1.64 – 1.21 (m, 6H). **^{13}C NMR (75MHz, $CDCl_3$) δ** 158.34, 137.84, 126.65,

114.41, 70.00, 63.46, 24.99, 14.85. **Chiral GC**: Isothermal 103°C. **Retention time**: t_R = 26.08 min, t_S = 27.83 min.

rac-1-(6-methoxynaphthalen-2-yl) ethanol (rac- VI.6)

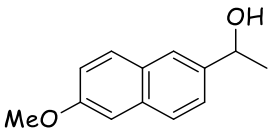

$C_{13}H_{15}O_2$

Molar mass: 203 g/mol

***rac*-1-(6-methoxynaphthalen-2-yl) ethanol (*rac*- VI.6):** White solid. Yield: 96.6 %. **R_f**: (0.11, 9/1. petroleum ether/ethyl acetate). **mp:** 113-115°C. **^{1}H NMR (300MHz, $CDCl_3$) δ** 7.72 (dd, *J* = 8.3, 3.4 Hz, 3H), 7.47 (dd, *J* = 8.6, 1.7 Hz, 1H), 7.21 – 7.03 (m, 2H), 5.03 (q, *J* = 6.4 Hz, 1H), 3.91 (s, 3H), 1.92 (s, 1H), 1.57 (d, *J* = 6.4 Hz, 3H). **^{13}C NMR (75 MHz, $CDCl_3$) δ** 157.67, 140.93, 134.06, 129.41, 128.75, 127.18, 124.38, 123.78, 118.96, 105.71, 70.53, 55.31, 25.07. **Chiral GC**: Isothermal 103°C. **Retention time**: t_R = 10.55 min, t_S = 13.51 min. Flow rate: 1 ml/min.

- **General procedure for the chemical acylation of racemic alcohols VI.1- VI.8:**

The racemic acetates **VI.1- VI.8** were obtained by standard classical chemical acetylation of corresponding alcohols, according to the following procedure: to 1 equivalent of racemic alcohol **1-8**, 1.2 equivalent of triethylamine and 0.1 equivalent of 4-dimethylaminopyridine (DMAP) dissolved in 4 mL of ether, 1.5 equivalent of acetic anhydride were added slowly. The evolution of the reactions was monitored by TLC. The acetates are obtained pure after standard work up, in good yields. The ^{1}H and ^{13}C NMR spectra of these products were in good agreement with the literature.

- **General procedure for the enzymatic deacylation of racemic acetates VI.1a- VI.8a:**

To 1mmol of the racemic acetates **VI.1a- VI.8a** dissolved in 2 mL of organic solvent, 50 mg of the *CAL-B* (*Novozym®435* or *CHIRAZYME® L-2, c.-f. C2, lyo*) and 50 mg of molecular sieves 4Å were added. The suspension was stirred at 40 °C for 24 hours. The reaction mixture was filtered and concentrated in *vacuum* and an acidic extraction was performed to remove the amine excess. The remaining acetate and the produced alcohol were separated by preparative TLC (petroleum ether/ethyl acetate: 90/10) and analyzed by chiral GC or Chiral HPLC.

- **NMR data chromatographic characteristics of the racemic acetates (VI.1a- VI.8a):**

rac-Phenylethyl acetate (rac- VI.1a)

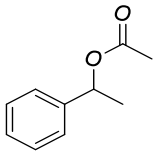

$C_{10}H_{12}O_2$

Molar mass: 164 g/mol

***rac*-Phenylethyl acetate (*rac*- VI.1a)** : Uncoloured oil. Yield: 86 %. **R_f**: (0.87, 9/1. petroleum ether/ethyl acetate). **^{1}H NMR (300MHz, $CDCl_3$) δ** 7.51 – 7.20 (m, 5H), 5.92 (q, *J* = 6.6 Hz, 1H), 2.10 (s, 3H), 1.57 (d, *J* =

6.6 Hz, 3H). **^{13}C NMR (75MHz, $CDCl_3$) δ** 170.32, 141.68, 128.50, 127.87, 126.10, 72.31, 22.22, 21.37. **Chiral GC**: Isothermal 120°C. **Retention time**: t_S = 4.08 min, t_R = 5.25 min.

rac-1-(4-methoxyphenyl)ethyl acetate (rac- VI.2a)

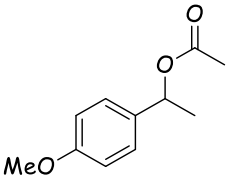

$C_{11}H_{14}O_3$
Molar mass: 194 g/mol

***rac*-1-(4-methoxyphenyl)ethyl acetate (*rac*- VI.2a) :** Uncoloured oil. **Yield**: 77%. **R_f**: (0.74, 9/1. petroleum ether/ethyl acetate). **^{1}H NMR (300MHz, $CDCl_3$) δ** 7.32 (d, *J* = 8.6 Hz, 2H), 6.90 (d, *J* = 8.8 Hz, 2H), 5.88 (q, *J* = 6.6 Hz, 1H), 3.82 (s, 3H), 2.07 (s, 3H), 1.55 (d, *J* = 6.6 Hz, 3H). **^{13}C NMR (75MHz, $CDCl_3$) δ** 170.37, 159.27, 133.74, 127.60, 113.83, 72.01, 55.26, 21.95, 21.40. **Chiral GC**: Isothermal 103°C. **Retention time**: t_R = 22.33 min t_S = 24.12 min.

rac-1-(4-ethoxyphenyl)ethyl acetate (rac- VI.3a)

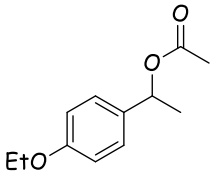

$C_{12}H_{16}O_3$
Molar mass: 208 g/mol

***rac*-1-(4-ethoxyphenyl)ethyl acetate (*rac*-VI.3a) :** Uncoloured oil. **Yield**: 88%. **R_f**: (0.75, 9/1. petroleum ether/ethyl acetate). **^{1}H NMR (300MHz, $CDCl_3$) δ** 7.30 (d, *J* = 8.6 Hz, 2H), 6.98 – 6.70 (m, 2H), 5.87 (q, *J* = 6.6 Hz, 1H), 4.04 (q, *J* = 7.0 Hz, 2H), 2.06 (d, *J* = 3.2 Hz, 3H), 1.54 (d, *J* = 6.6 Hz, 3H), 1.43 (t, *J* = 7.0 Hz, 3H). **^{13}C NMR (75MHz, $CDCl_3$) δ** 170.37, 158.65, 133.55, 127.58, 114.36, 72.03, 63.43, 21.93, 21.41, 14.83. **Chiral GC**: Isothermal 103°C. **Retention time**: t_S = 34.6 min, t_R = 36.6 min.

rac-1-(naphthalen-1-yl)ethyl acetate (rac- VI.4a)

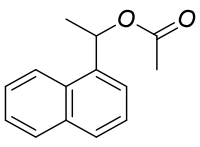

$C_{14}H_{14}O_2$
Molar mass: 214 g/mol

***rac*-1-(naphthalen-1-yl)ethyl acetate (*rac*- VI.4a) :** Uncoloured oil. Yield: 94%. **R_f**: (0.61, 9/1. petroleum ether/ethyl acetate). **(250MHz, $CDCl_3$) δ** 1.72 (d, *J*=6.5 Hz, 3H), 2.14 (s, 3H), 6.65 (q, *J*=6.75 Hz, 1H), 7.46-7.56 (m, 5H), 7.56 (d, *J*=1.75 Hz, 1H), 7.59 (d, *J*=2.12 Hz, 1H), 7.62 (d, *J*=3.25 Hz, 1H). **^{13}C NMR (75MHz, $CDCl_3$) δ** 170.37, 137.48, 133.89, 130.32, 128.98, 128.51, 126.37, 125.73, 125.42, 123.24, 123.21, 69.49, 30.39, 21.75, 21.40.

***rac*-1-(naphthalen-2-yl)ethyl acetate (*rac*- VI.5a)**

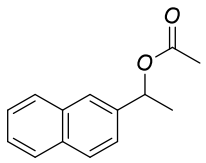

$C_{14}H_{14}O_2$
Molar mass: 214 g/mol

***rac*-1-(naphthalen-2-yl)ethyl acetate (*rac*- VI.5a) :** Uncoloured oil. **Yield**: 92%. **R_f**: (0.72, 9/1. petroleum ether/ethyl acetate). **^{1}H NMR (300MHz, $CDCl_3$) δ** 7.80 (m, 4H), 7.45 (m, 3H), 6.05 (q, *J* = 6.6 Hz, 1H), 2.07 (s, 3H), 1.60 (d, *J* = 6.6 Hz, 3H). **^{13}C NMR (75MHz, $CDCl_3$) δ** 170.50, 139.24, 133.42, 133.25, 128.59, 128.25, 127.89, 126.45, 126.27, 125.24, 124.31, 72.64, 22.40, 21.57. **Chiral GC**: Isothermal 100°C. **Retention time**: t_S = 4.98 min, t_R = 5.37 min.

***rac*-1-(6-methoxynaphthalen-2-yl)ethyl acetate (*rac*- VI.6a)**

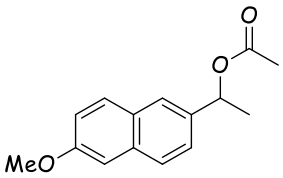

$C_{15}H_{16}O_3$
Molar mass: 244 g/mol

***rac*-1-(6-methoxynaphthalen-2-yl)ethyl acetate (*rac*- VI.6a):** White solid. **Yield**: 89%. **R_f**: (0.49, 9/1. petroleum ether/ethyl acetate). **mp: 58-61** °C. **^{1}H NMR (300MHz, $CDCl_3$): δ** 7.76 – 7.67 (m, 3H), 7.49 – 7.39 (m, 1H), 7.22 – 7.07 (m, 2H), 6.02 (q, *J* = 6.6 Hz, 1H), 3.90 (s, 3H), 2.08 (s, 3H), 1.60 (d, *J* = 6.6 Hz, 3H). **^{13}C NMR (75MHz, $CDCl_3$) δ** 170.35, 139.10, 133.28, 133.11, 128.45, 128.11, 127.75, 126.31, 126.13, 125.10, 124.17, 72.50, 22.26, 21.43. **Chiral GC**: Isothermal 100°C. **Retention time**: t_S = 5.54 min, t_R= 6.06 min. Flow rate: 1 ml/min.

***rac*-2,3-dihydro-1H-inden-yl acetate (*rac*- VI.7a)**

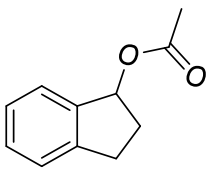

$C_{11}H_{12}O_2$
Molar mass: 176 g/mol

***rac*-2,3-dihydro-1H-inden-yl acetate (*rac*- VI.7a):** Uncoloured oil. **Yield**: 85 %. **R_f**: (0.83 , 9/1. petroleum ether/ethyl acetate). **^{1}H NMR (300MHz, $CDCl_3$) δ** 7.40 (d, *J* = 7.4 Hz, 1H), 7.30 – 7.06 (m, 3H), 6.18 (dd, *J* = 7.0, 3.7 Hz, 1H), 3.08 (m, 1H), 2.84 (m, 1H), 2.46 (m, 1H), 2.18 – 1.81 (m, 4H). **^{13}C NMR (75MHz, $CDCl_3$) δ** 171.14, 144.43, 141.10, 128.99, 126.74, 125.60, 124.84, 78.41, 32.32, 30.22, 21.30. **Chiral GC**: Isothermal 100°C. **Retention time** t_S = 36.7 min, t_R =

37.01 min. T_{column} = 60 °C for 5 min, after 140°C for 0 min.

rac-1,2,3,4-tetrahydronaphthalen-1-yl acetate (rac- VI.8a)

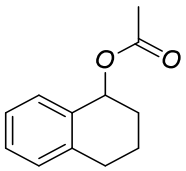

$C_{12}H_{14}O_2$
Molar mass: 190 g/mol

***rac*-1,2,3,4-tetrahydronaphthalen-1-yl acetate (*rac*- VI.8a):** Uncoloured oil. **Yield**: 75 %. **R_f**: (0.72, 9/1. petroleum ether/ethyl acetate). **^{1}H NMR (300MHz, $CDCl_3$) δ** 7.42 – 6.93 (m, 4H), 5.98 (t, *J* = 4.2 Hz, 1H), 2.76 (m, 2H), 2.08 – 2.01 (m, 3H), 2.01 – 1.69 (m, 4H). **^{13}C NMR (75MHz, $CDCl_3$) δ** 170.72, 137.92, 134.64, 129.49, 129.12, 128.13, 126.13, 70.01, 29.16, 29.03, 21.46, 18.89. **Chiral GC**: Isothermal 100°C. **Retention time:** t_S = 60.25 min, t_R = 61.57 min. T_{column} = 90 °C for 35 min, after 120 °C for 20 min.

Annex

❖ **Spectral data**

▪ ***α*-aminophosphonates synthesized by diphenylphosphinic acid**

^{1}H, ^{13}C, ^{31}P NMR and HRMS of diethoxy (phenyl)(phenylamino)methylphosphoryle IV.14a:

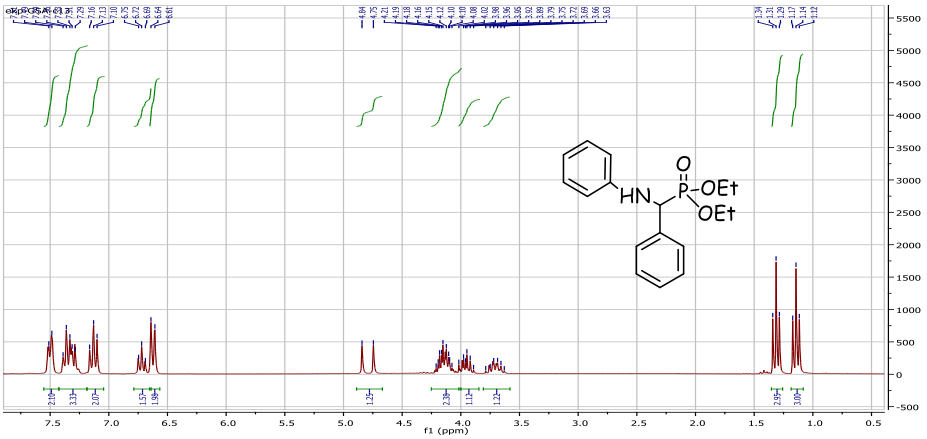

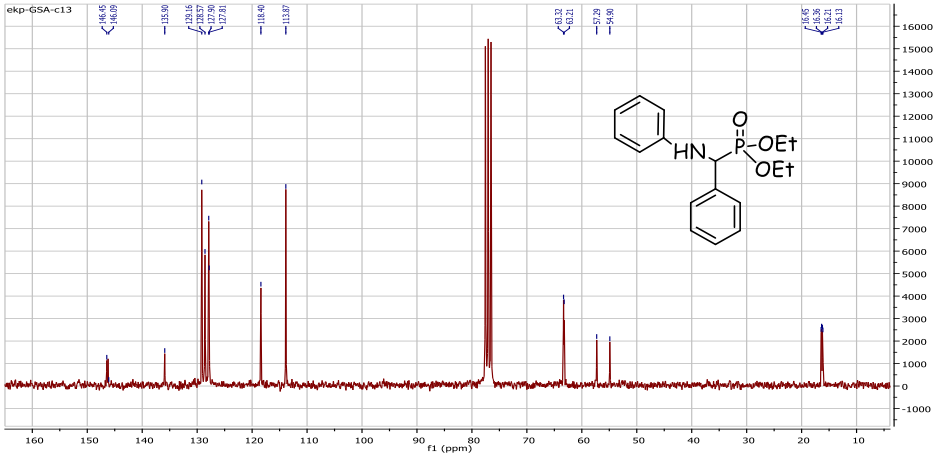

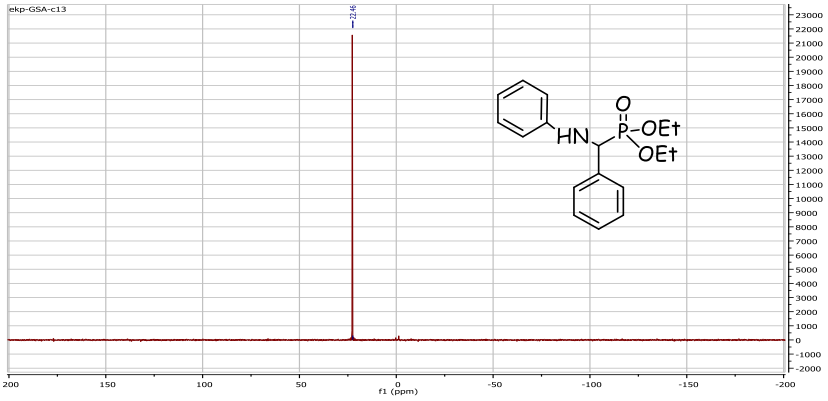

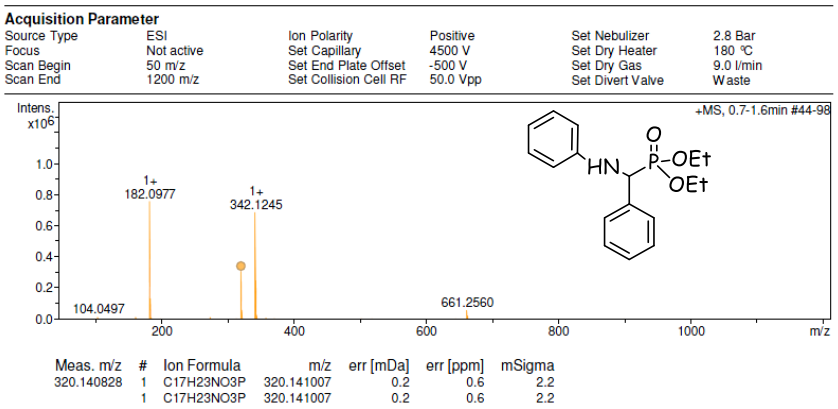

^{1}H, ^{13}C and ^{31}P NMR of Diethyl (3-methoxyphenyl) (phenylaminomethyl) phosphonate (IV.14b)

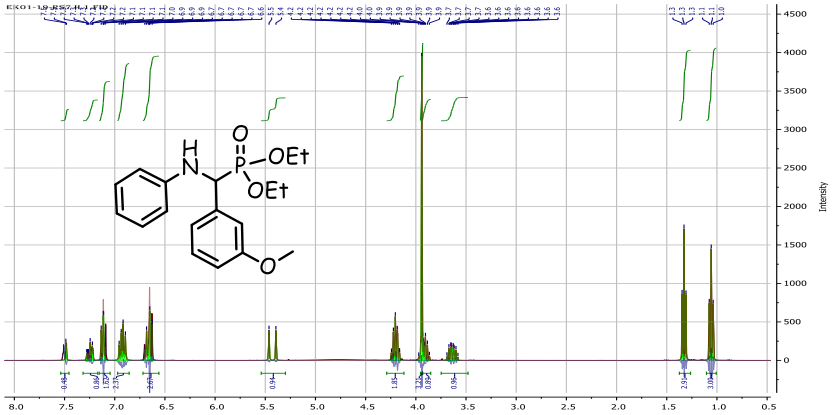

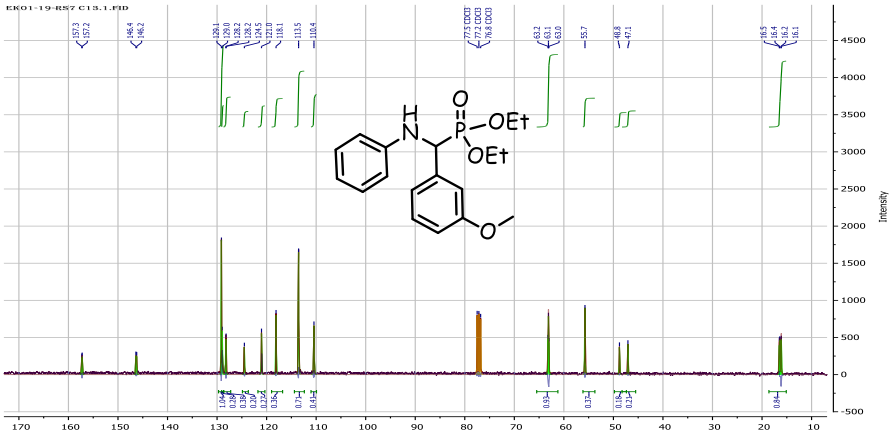

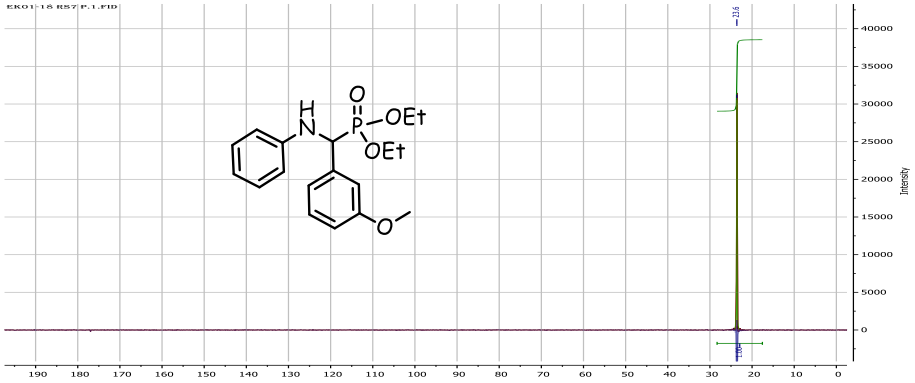

^{1}H, ^{13}C, ^{31}P NMR and HRMS of diethyl [4-nitrophenyl(phenylamino)methyl]phosphonate (IV.14c)

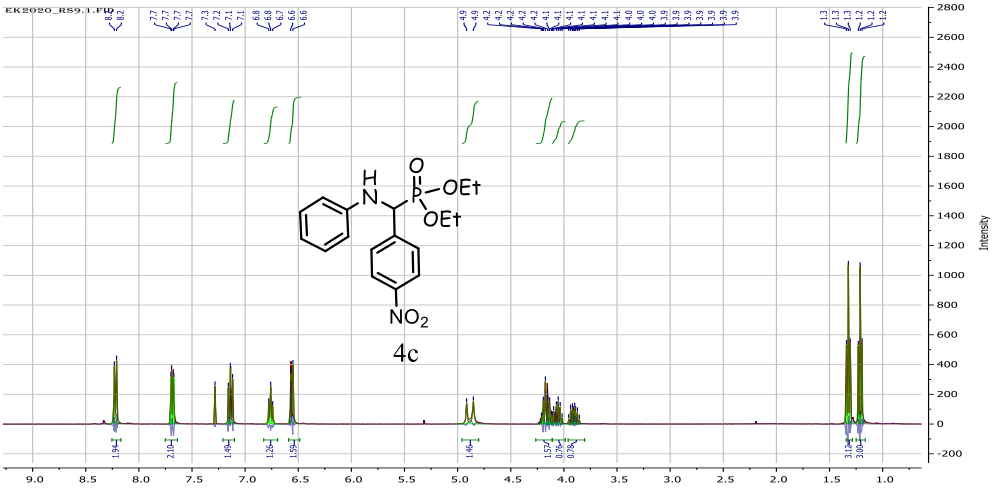

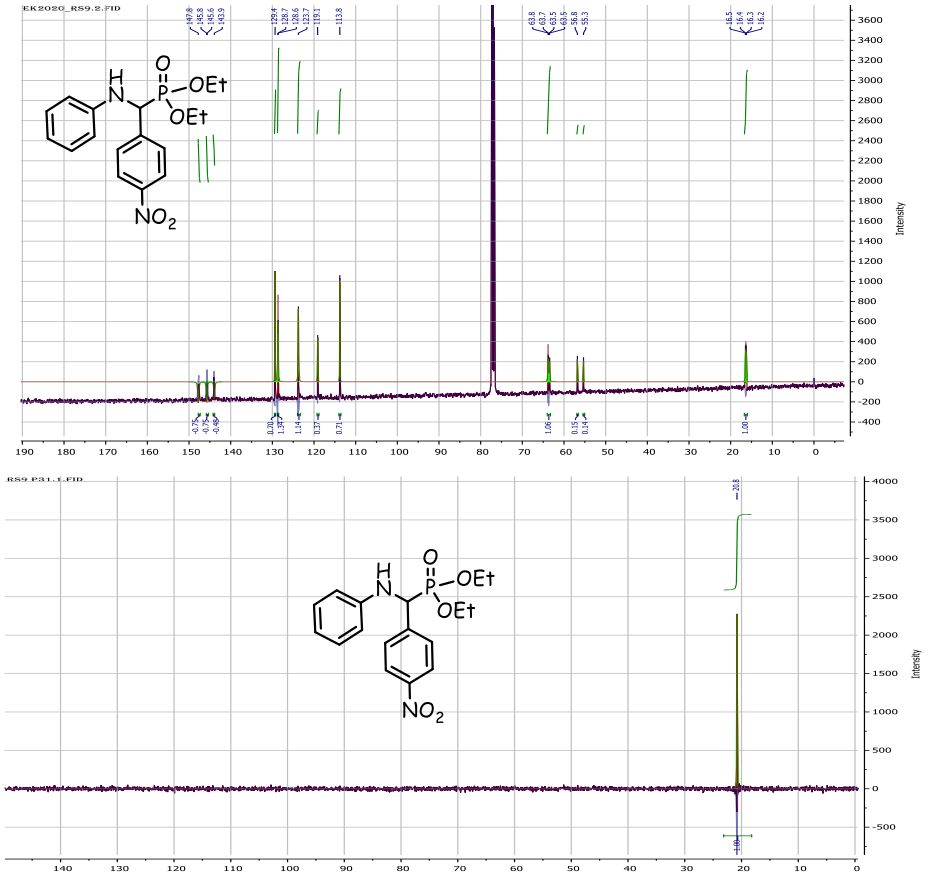

Acquisition Parameter

Source Type	ESI	Ion Polarity	Positive	Set Nebulizer	2.8 Bar
Focus	Not active	Set Capillary	4500 V	Set Dry Heater	180 °C
Scan Begin	50 m/z	Set End Plate Offset	-500 V	Set Dry Gas	9.0 l/min
Scan End	1200 m/z	Set Collision Cell RF	50.0 Vpp	Set Divert Valve	Waste

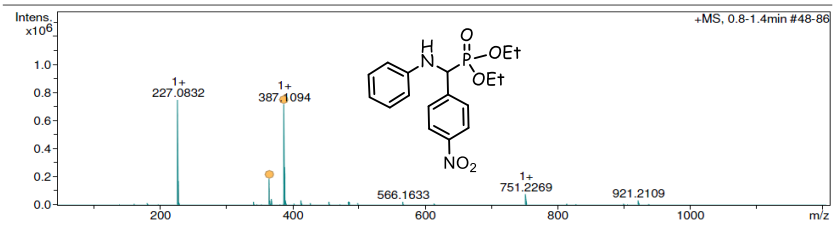

Meas. m/z	#	Ion Formula	m/z	err [mDa]	err [ppm]	mSigma
365.125321	1	C17H22N2O5P	365.126085	0.8	2.1	0.9
	1	C17H22N2O5P	365.126085	0.8	2.1	0.9
387.109424	1	C17H21N2NaO5P	387.108029	1.4	3.6	106.3
	1	C17H21N2NaO5P	387.108029	1.4	3.6	106.3
	1	C17H21N2NaO5P	387.108029	1.4	3.6	106.3

^{1}H, ^{13}C, ^{31}P NMR and HRMS of diethyl[1-naphtyl(p-tolylamino)methyl]phosphonate (IV.14d)

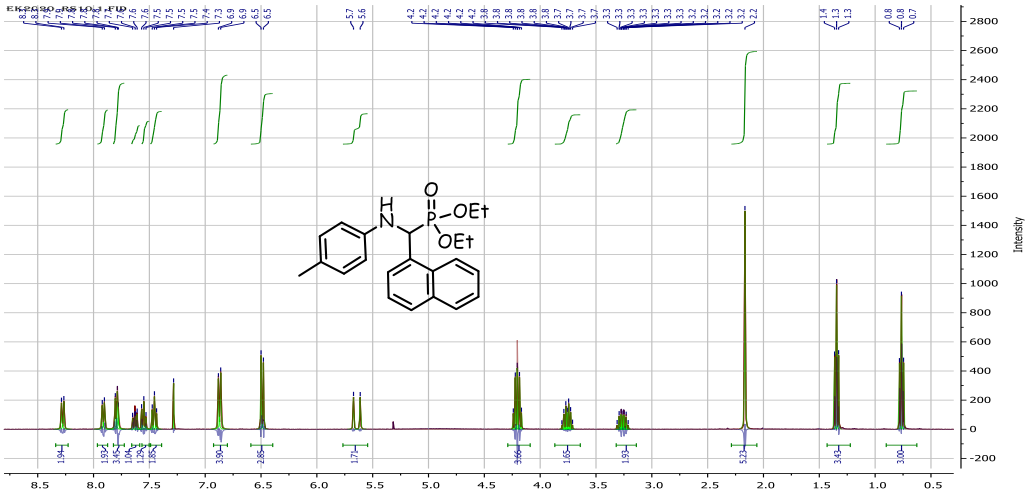

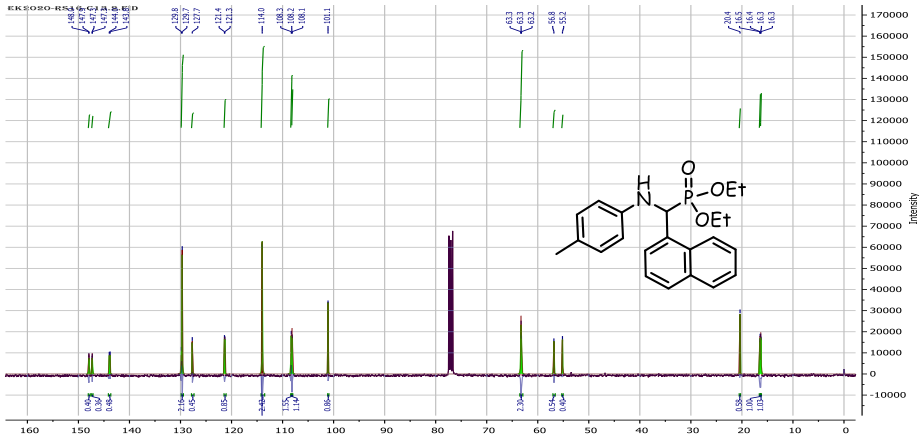

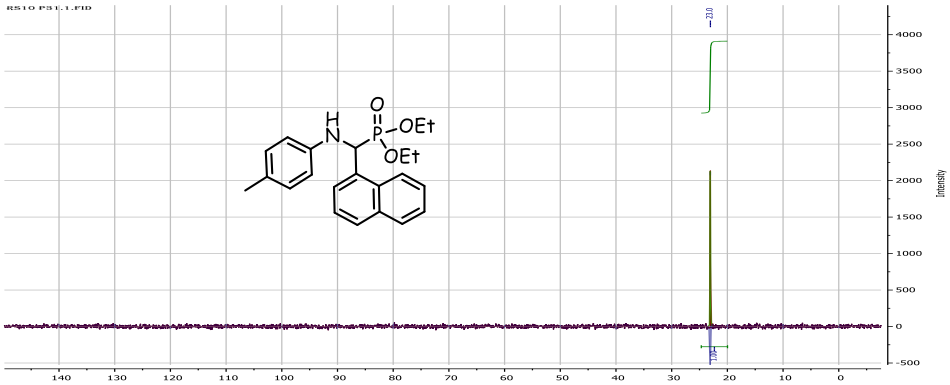

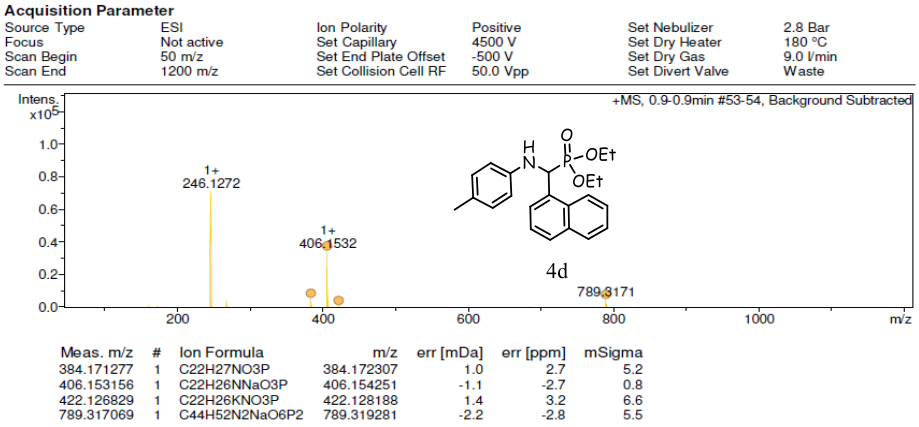

^{1}H, ^{13}C, ^{31}P NMR and HRMS of diethyl [benzo [1,3]dioxol-5-yl((p-tolylamino) methyl]phosphonate (IV.14e)

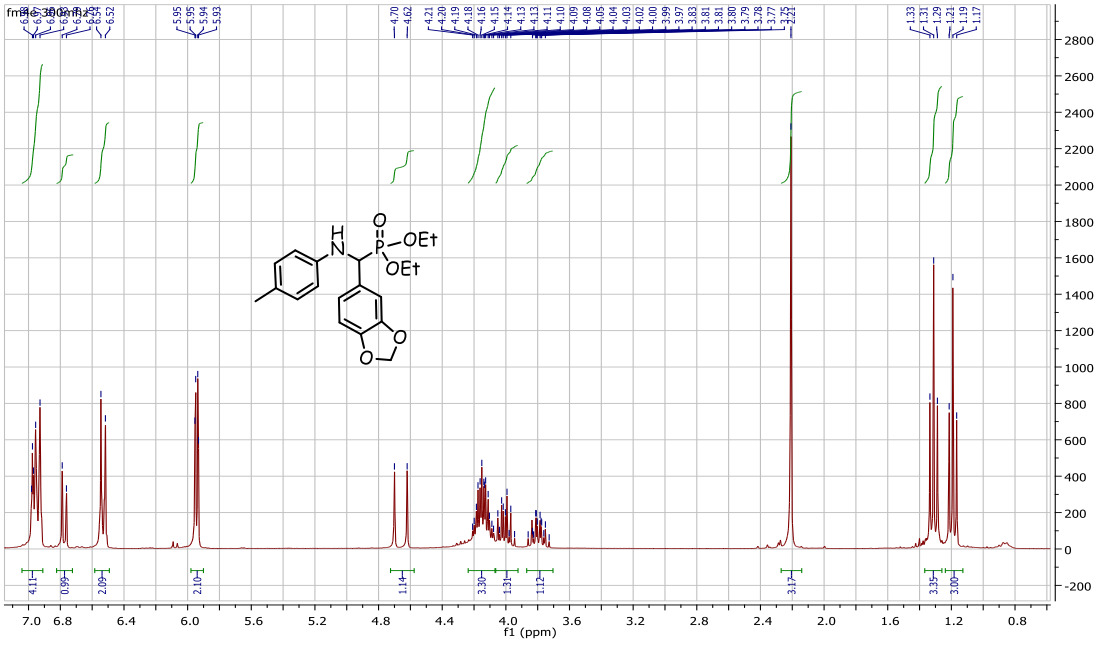

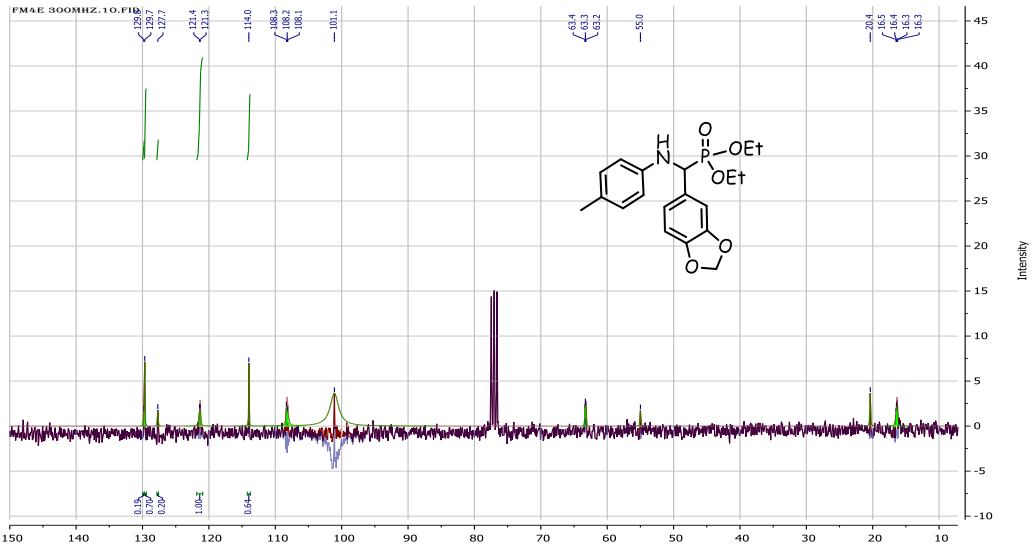

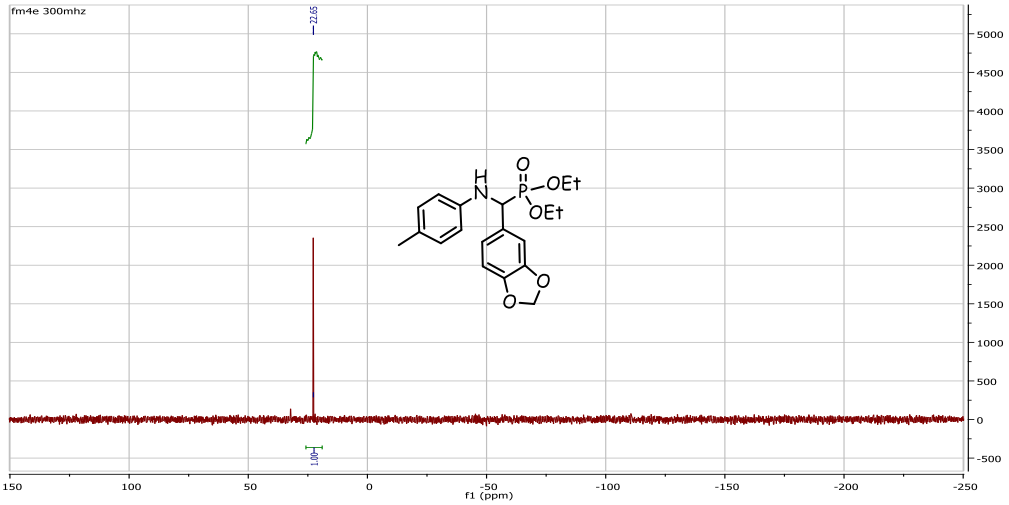

Acquisition Parameter

Source Type	ESI	Ion Polarity	Positive	Set Nebulizer	2.8 Bar
Focus	Not active	Set Capillary	4500 V	Set Dry Heater	180 °C
Scan Begin	50 m/z	Set End Plate Offset	-500 V	Set Dry Gas	9.0 l/min
Scan End	1200 m/z	Set Collision Cell RF	50.0 Vpp	Set Divert Valve	Waste

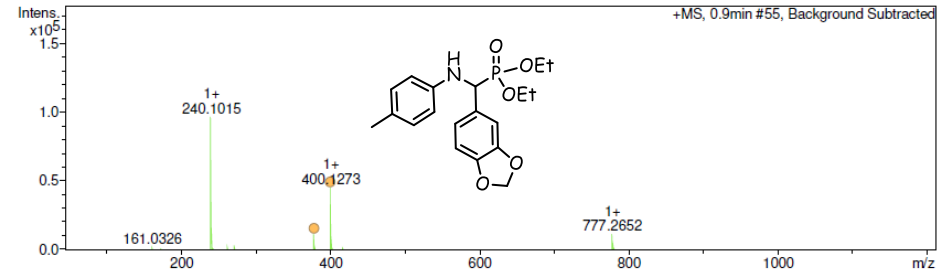

Meas. m/z	#	Ion Formula	m/z	err [mDa]	err [ppm]	mSigma
378.145334	1	C19H25NO5P	378.146486	-1.2	-3.0	2.7
400.127295	1	C19H24NNaO5P	400.128430	-1.1	-2.8	0.8

^{1}H, ^{13}C, ^{31}P NMR and HRMS of diethyl [(4-fluorophenyl)(4-tolylamino)methyl] phosphonate (IV.14f)

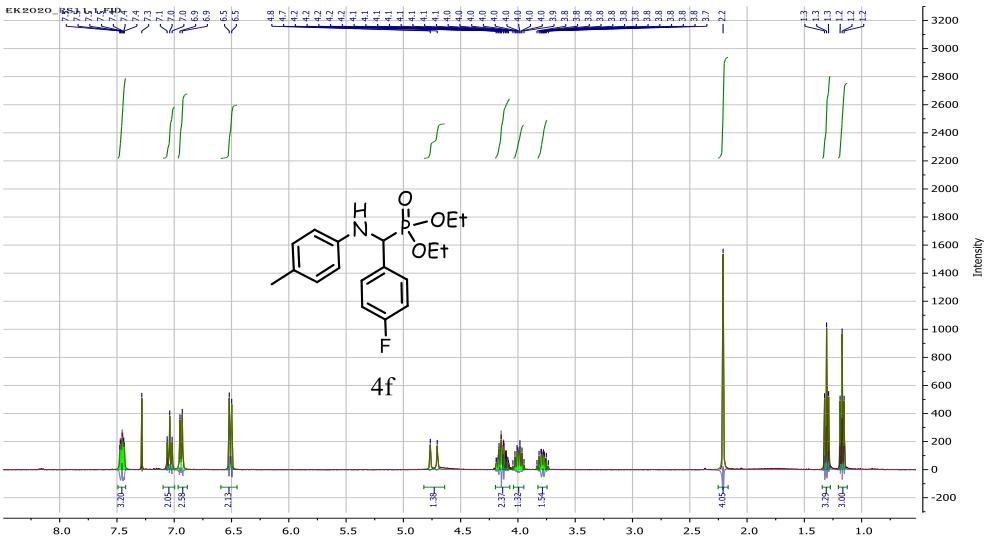

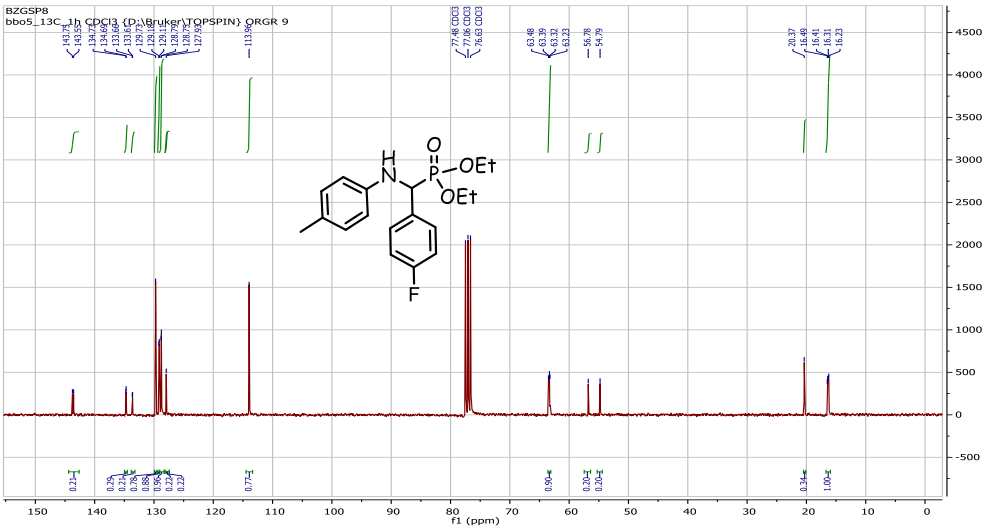

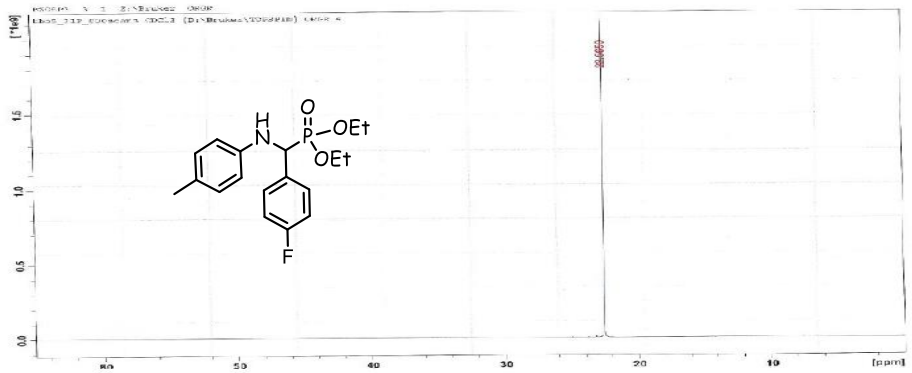

Acquisition Parameter

Source Type	ESI	Ion Polarity	Positive	Set Nebulizer	2.8 Bar
Focus	Not active	Set Capillary	4500 V	Set Dry Heater	180 °C
Scan Begin	50 m/z	Set End Plate Offset	-500 V	Set Dry Gas	9.0 l/min
Scan End	1200 m/z	Set Collision Cell RF	50.0 Vpp	Set Divert Valve	Waste

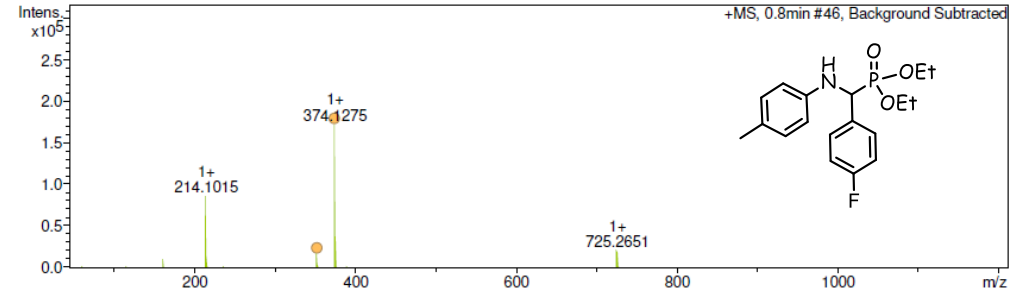

Meas. m/z	#	Ion Formula	m/z	err [mDa]	err [ppm]	mSigma
352.145492	1	C18H24FNO3P	352.147235	1.7	4.9	1.1
374.127465	1	C18H23FNNaO3P	374.129179	1.7	4.6	8.5

^{1}H, ^{13}C and ^{31}P NMR of diethyl [(phenyl)(4-trifluoromethylamino)methyl] phosphonate (IV.14g)

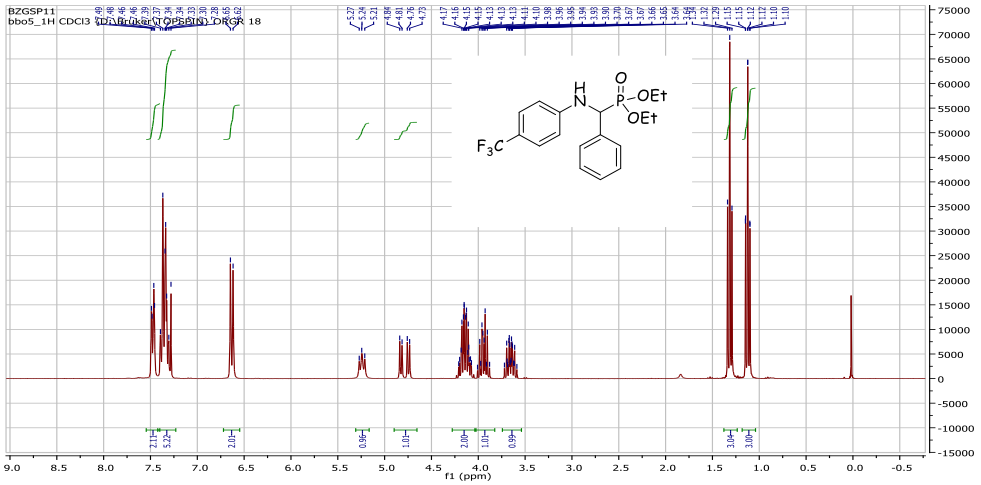

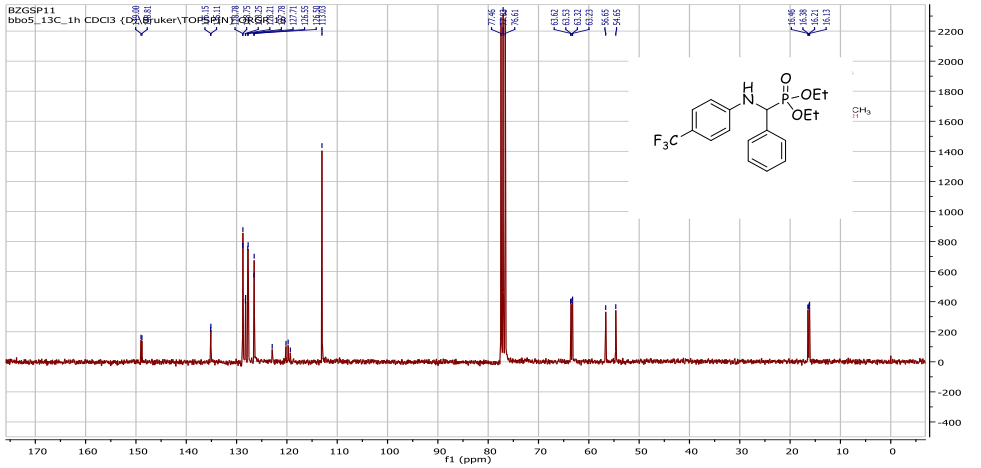

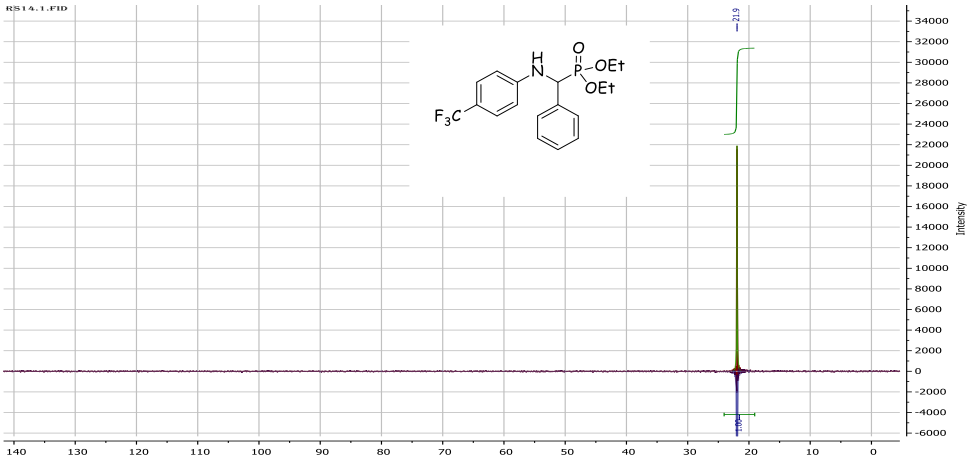

^{1}H, ^{13}C, ^{31}P NMR and HRMS of diethyl [3-phenoxyl(phenylamino)trifluoromethyl]phosphonate (IV.14h)

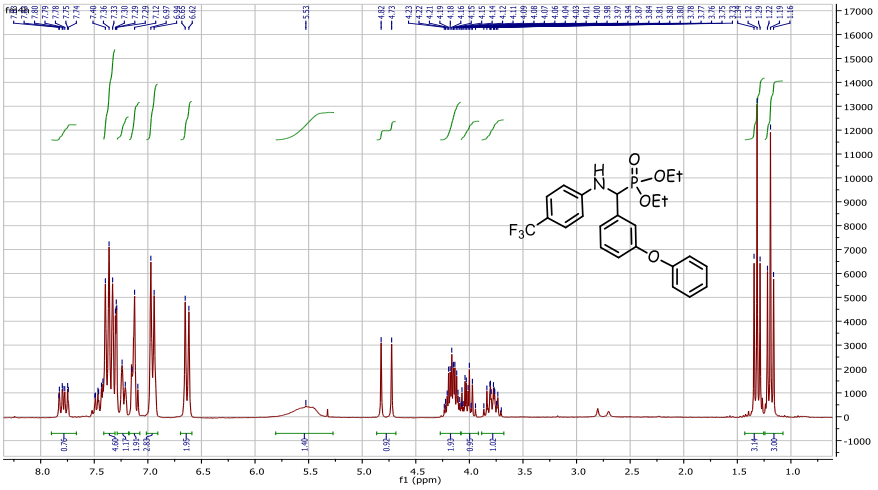

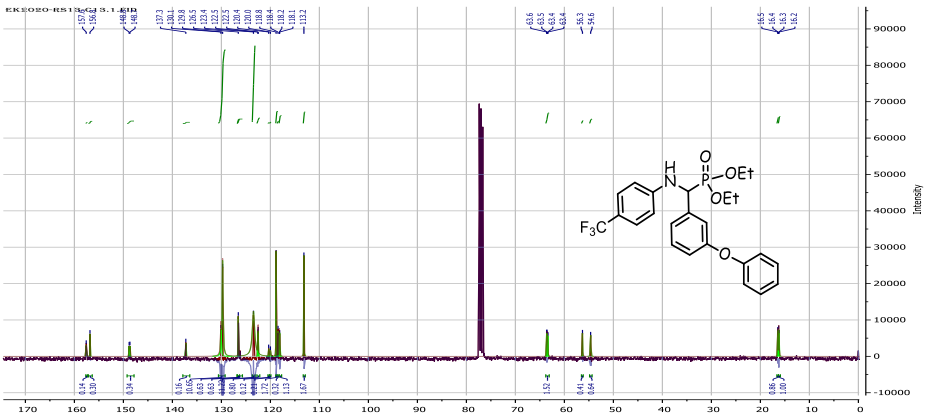

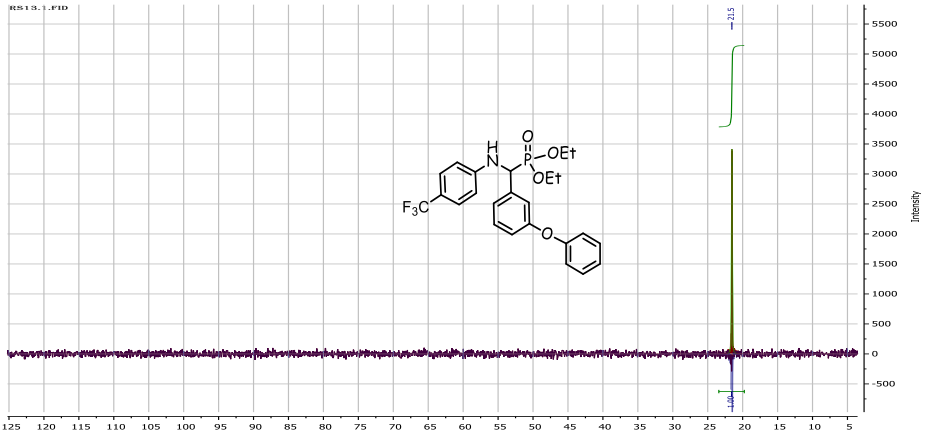

Acquisition Parameter

Source Type	ESI	Ion Polarity	Positive	Set Nebulizer	2.8 Bar
Focus	Not active	Set Capillary	4500 V	Set Dry Heater	180 °C
Scan Begin	50 m/z	Set End Plate Offset	-500 V	Set Dry Gas	9.0 l/min
Scan End	1200 m/z	Set Collision Cell RF	50.0 Vpp	Set Divert Valve	Waste

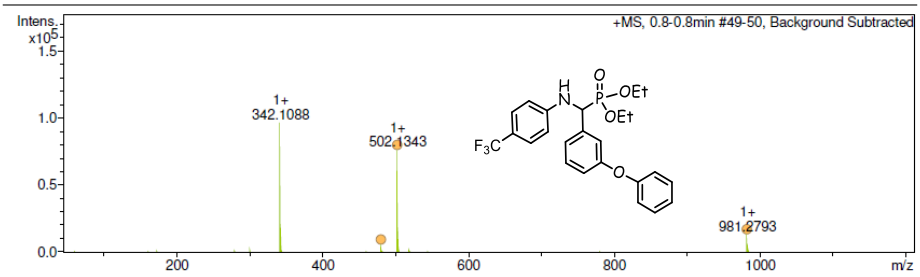

Meas. m/z	#	Ion Formula	m/z	err [mDa]	err [ppm]	mSigma
480.152826	1	C24H26F3NO4P	480.154606	1.8	3.7	57.5
502.134273	1	C24H25F3NNaO4P	502.136550	2.3	4.5	12.1
981.279296	1	C48H50F6N2NaO8P2	981.283880	-4.6	-4.7	18.0

^{1}H, ^{13}C, ^{31}P NMR and HRMS of diethyl [benzo [1,3]dioxol-5-yl((phenylamino)trifluoromethyl]phosphonate (IV.14i)

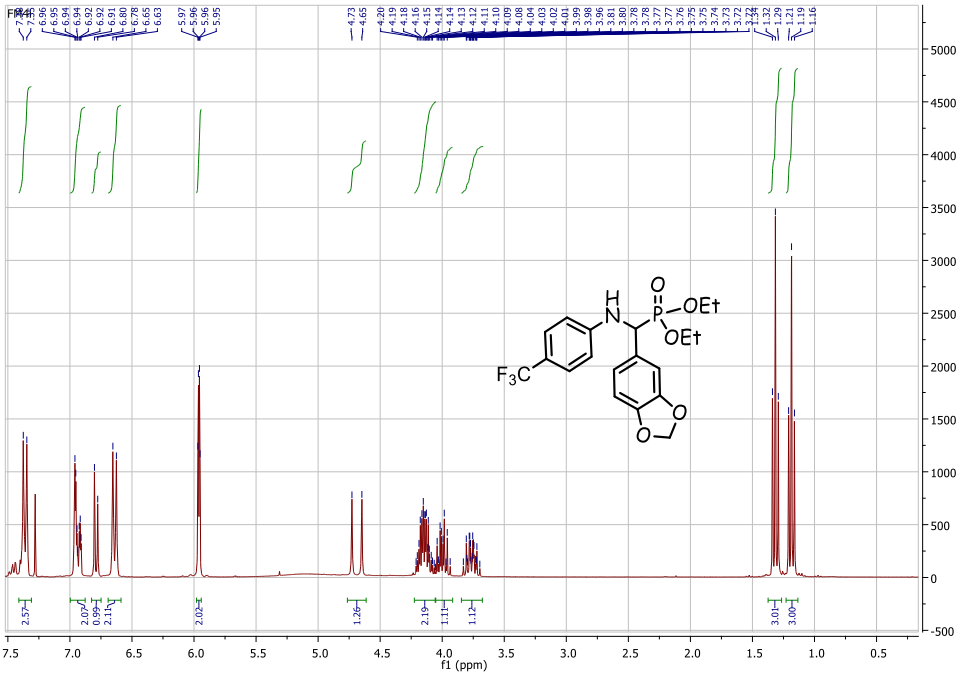

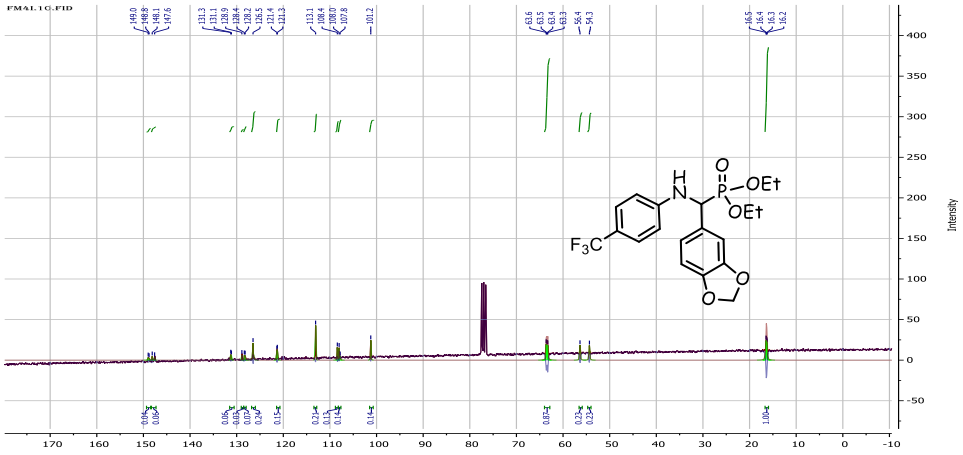

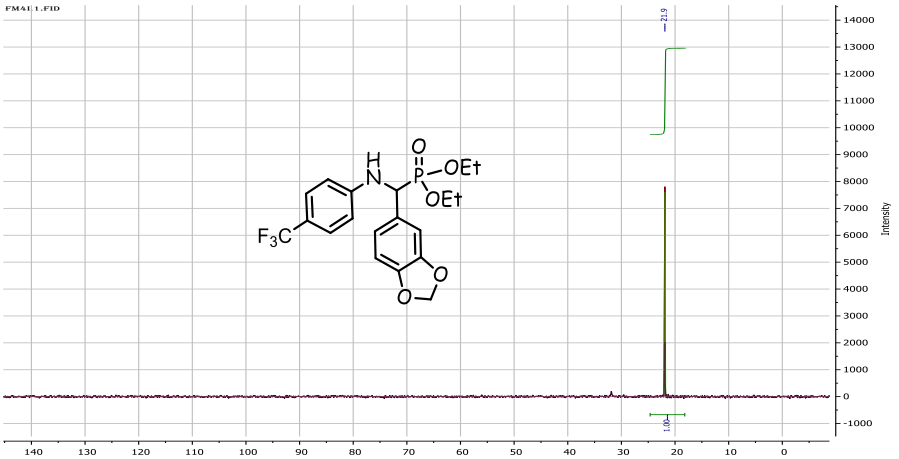

Acquisition Parameter

Source Type	ESI	Ion Polarity	Positive	Set Nebulizer	2.8 Bar
Focus	Not active	Set Capillary	4500 V	Set Dry Heater	180 °C
Scan Begin	50 m/z	Set End Plate Offset	-500 V	Set Dry Gas	9.0 l/min
Scan End	1200 m/z	Set Collision Cell RF	50.0 Vpp	Set Divert Valve	Waste

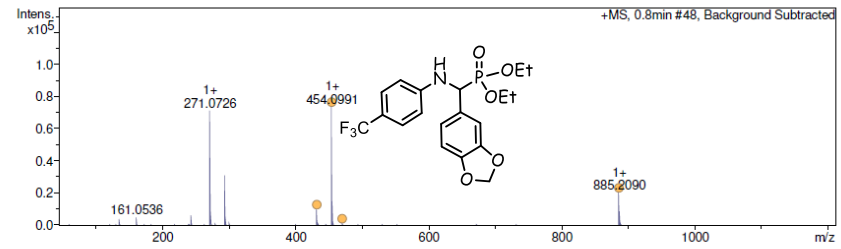

Meas. m/z	#	Ion Formula	m/z	err [mDa]	err [ppm]	mSigma
432.117254	1	C19H22F3NO5P	432.118221	-1.0	-2.2	37.3
454.099136	1	C19H21F3NNaO5P	454.100165	-1.0	-2.3	5.3
470.072824	1	C19H21F3KNO5P	470.074102	1.3	2.7	27.3
885.208986	1	C38H42F6N2NaO10P2	885.211109	-2.1	-2.4	4.1

- ***α*-aminophosphonates synthesized by 2-Hydroxymethyl-18-Crown -6**

^{1}H, ^{13}C, ^{31}P NMR and HRMS of diethoxy (phenyl)(phenylamino)methylphosphoryle V.14a:

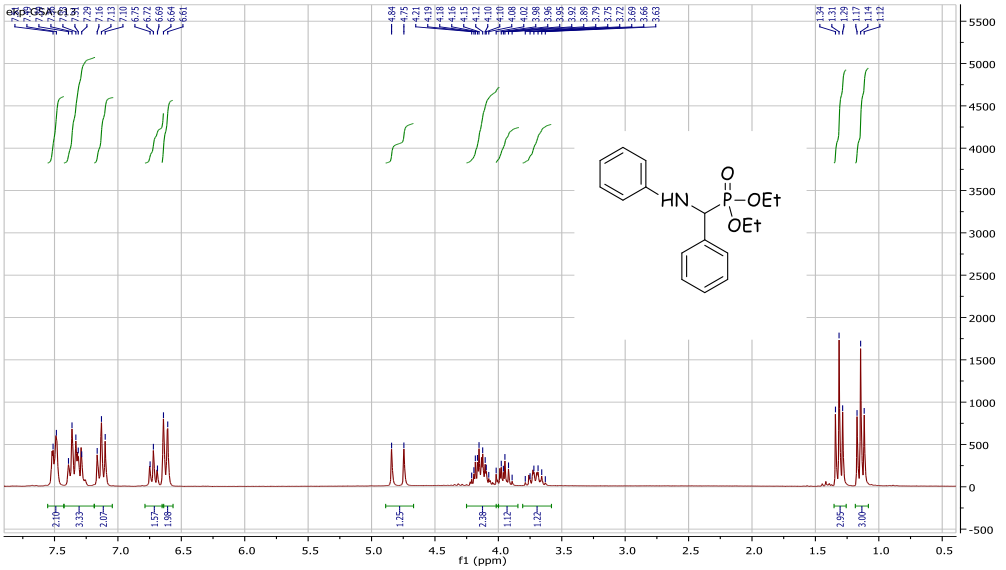

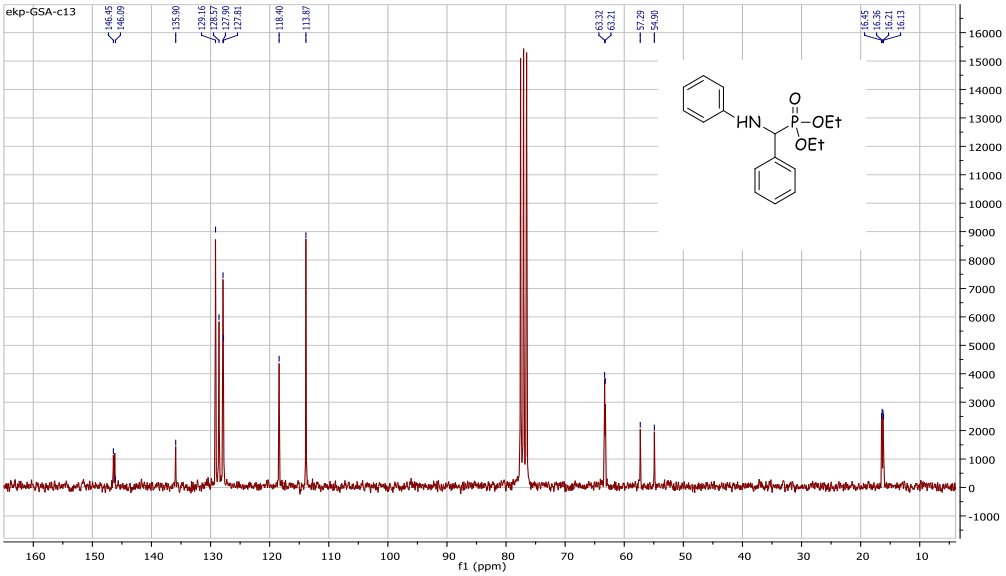

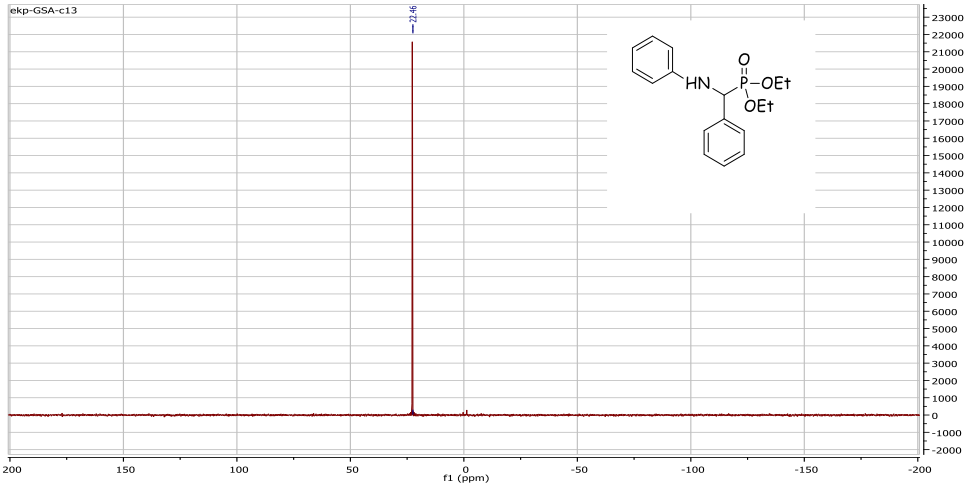

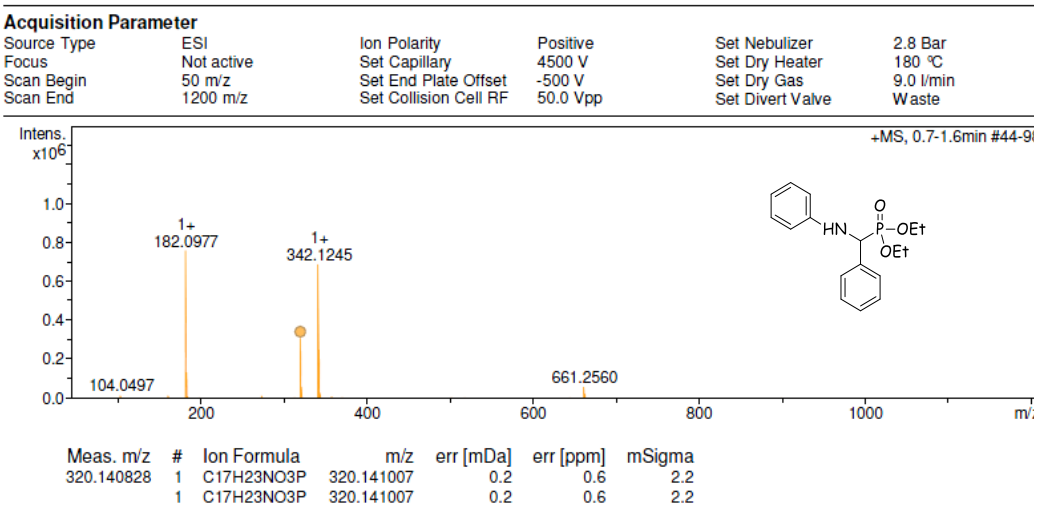

***^{1}H, ^{13}C and ^{31}P NMR of*diethyl (4–chlorophenyl)(phenylamino) methylphosphonate (*V.*14b):**

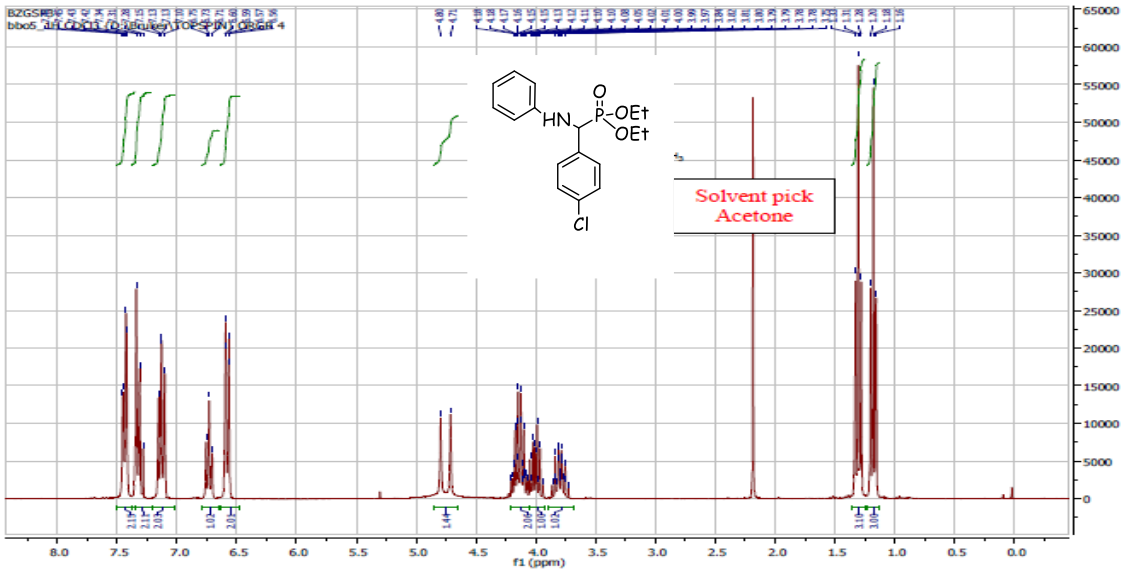

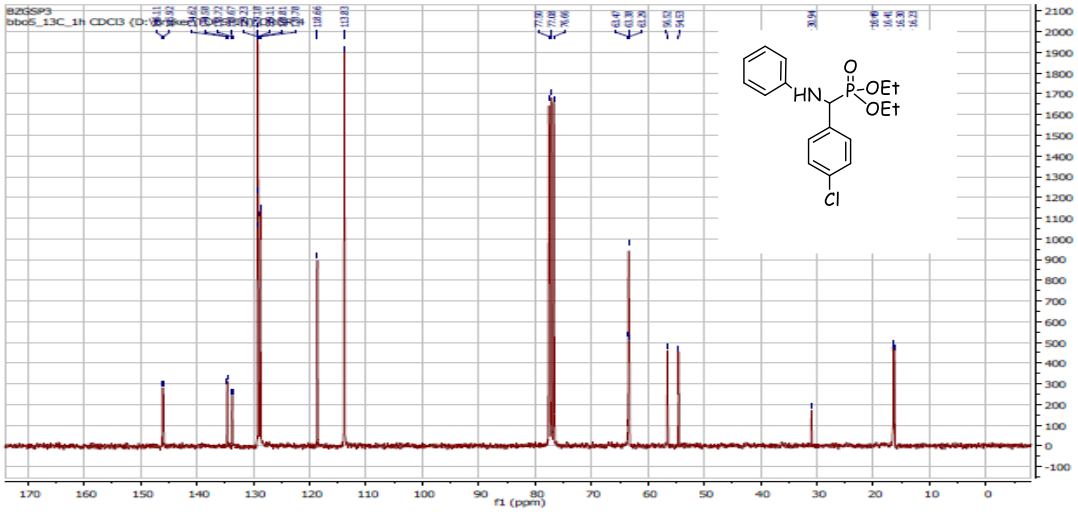

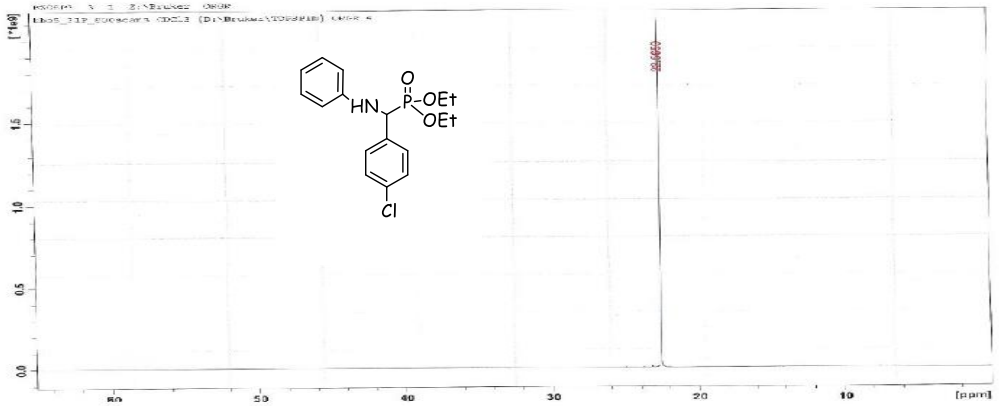

***^{1}H, ^{13}C, ^{31}P NMR and HRMS of* Diethyl [4-nitrophenyl(phenylamino)methyl]phosphonate (4c):**

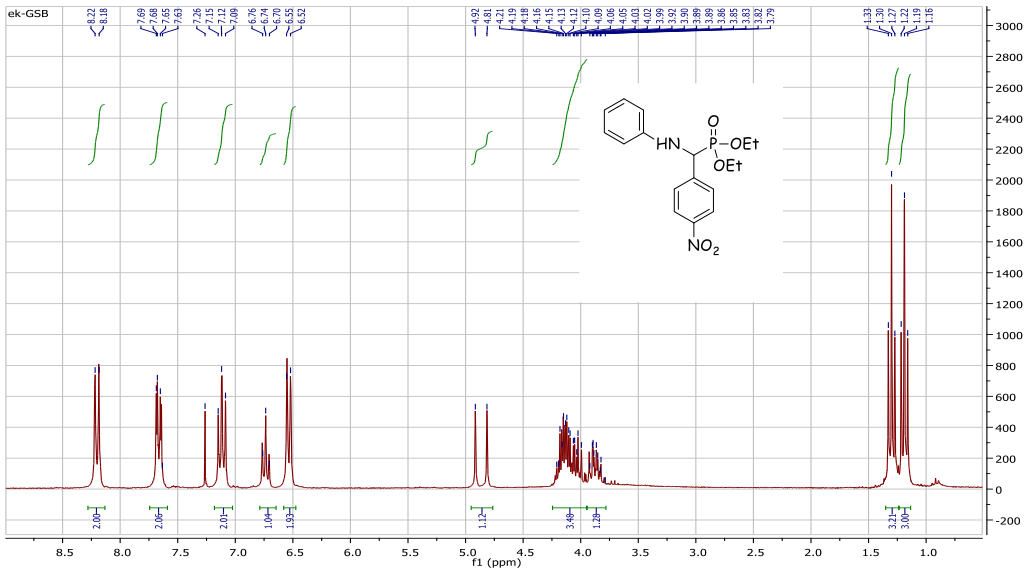

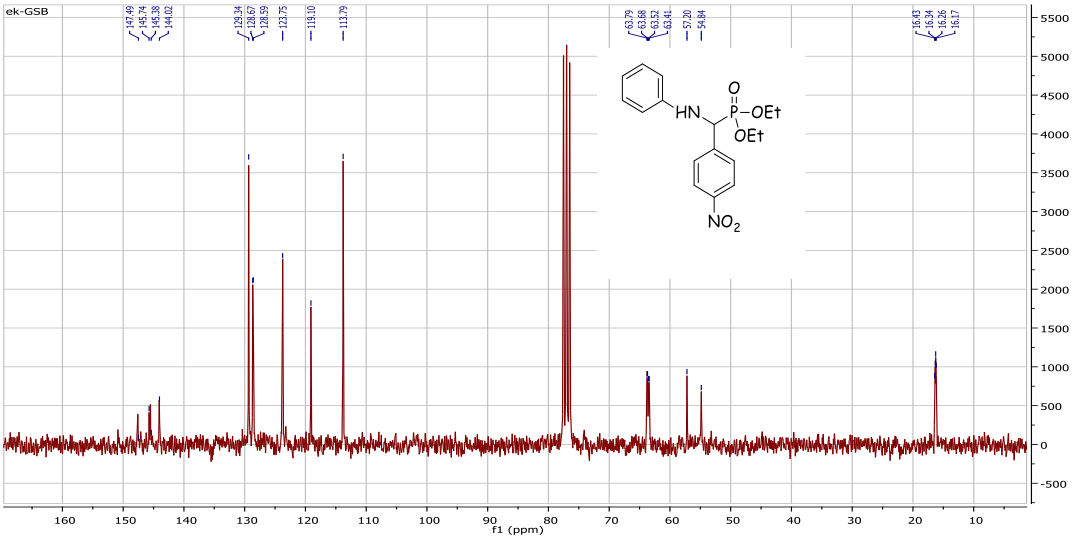

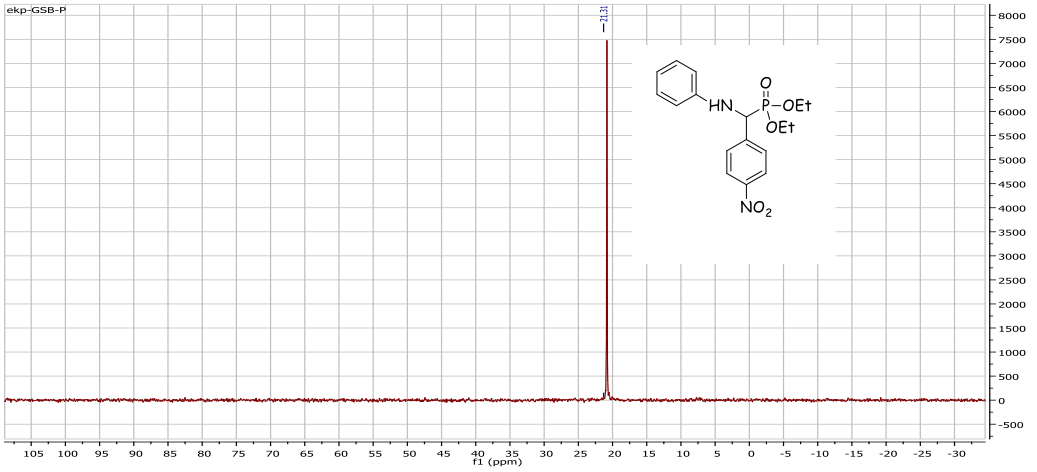

Acquisition Parameter

Source Type	ESI	Ion Polarity	Positive	Set Nebulizer	2.8 Bar
Focus	Not active	Set Capillary	4500 V	Set Dry Heater	180 °C
Scan Begin	50 m/z	Set End Plate Offset	-500 V	Set Dry Gas	9.0 l/min
Scan End	1200 m/z	Set Collision Cell RF	50.0 Vpp	Set Divert Valve	Waste

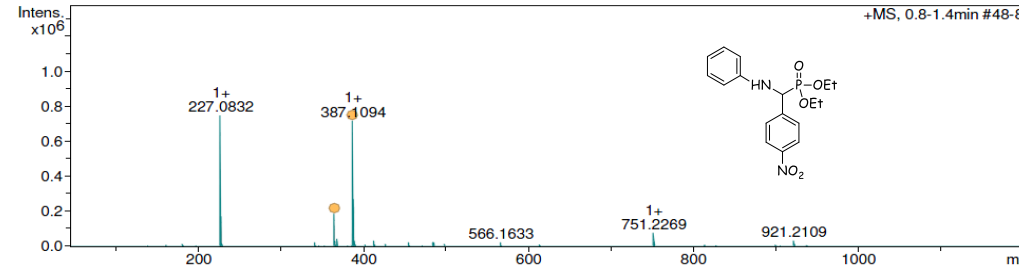

Meas. m/z	#	Ion Formula	m/z	err [mDa]	err [ppm]	mSigma
365.125321	1	C17H22N2O5P	365.126085	0.8	2.1	0.9
	1	C17H22N2O5P	365.126085	0.8	2.1	0.9
387.109424	1	C17H21N2NaO5P	387.108029	1.4	3.6	106.3
	1	C17H21N2NaO5P	387.108029	1.4	3.6	106.3

^{1}H, ^{13}C, ^{31}P NMR and HRMS of diethyl [1-naphtyl (phenylamino) methyl]phosphonate (V.14d)

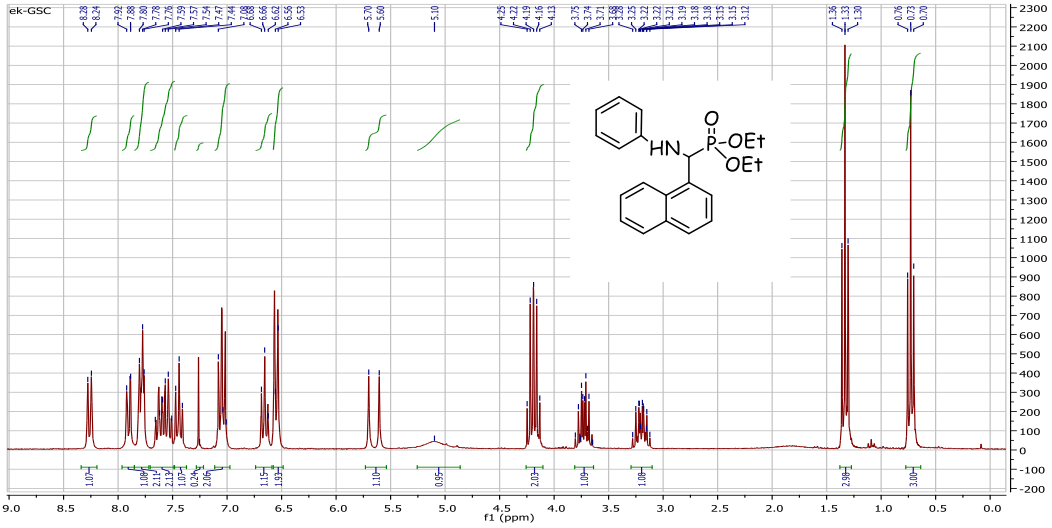

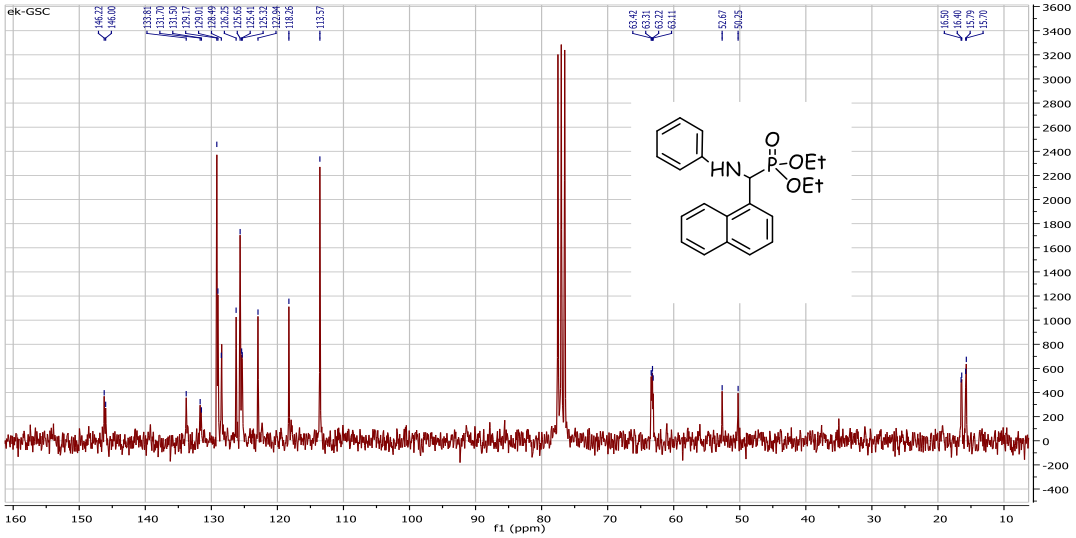

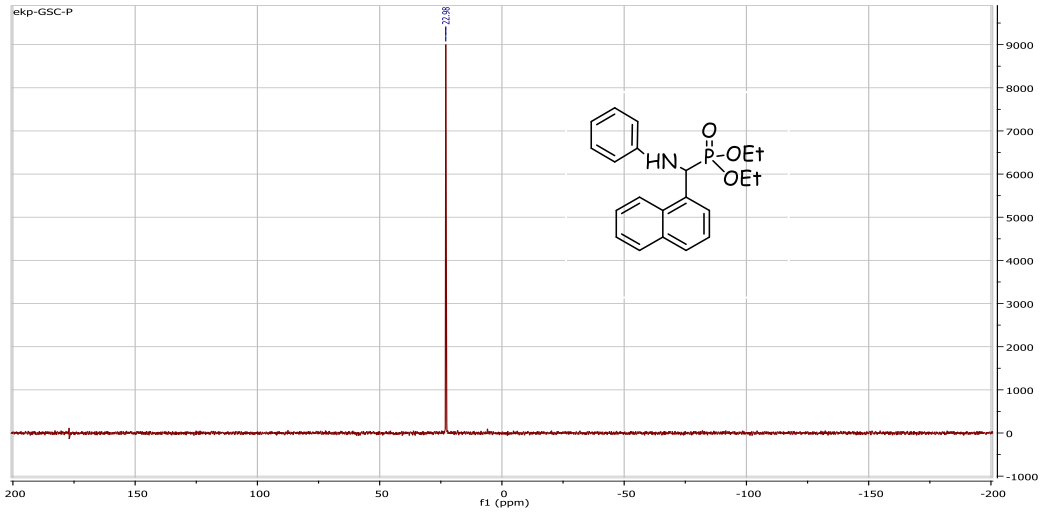

Acquisition Parameter

Source Type	ESI	Ion Polarity	Positive	Set Nebulizer	2.8 Bar
Focus	Not active	Set Capillary	4500 V	Set Dry Heater	180 °C
Scan Begin	50 m/z	Set End Plate Offset	-500 V	Set Dry Gas	9.0 l/min
Scan End	1200 m/z	Set Collision Cell RF	50.0 Vpp	Set Divert Valve	Waste

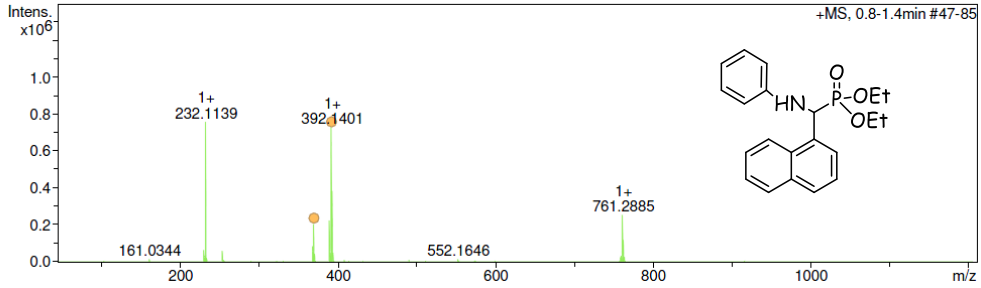

Meas. m/z	#	Ion Formula	m/z	err [mDa]	err [ppm]	mSigma
370.155854	1	C21H25NO3P	370.156657	-0.8	-2.2	3.6
	1	C21H25NO3P	370.156657	-0.8	-2.2	3.6
392.140113	1	C21H24NNaO3P	392.138601	1.5	3.9	172.3
	1	C21H24NNaO3P	392.138601	1.5	3.9	172.3
	1	C21H24NNaO3P	392.138601	1.5	3.9	172.3

^{1}H, ^{13}C, ^{31}P NMR and HRMS ofdiethyl [4-biphenyl(phenylamino)methyl]phosphonate (V.14e)

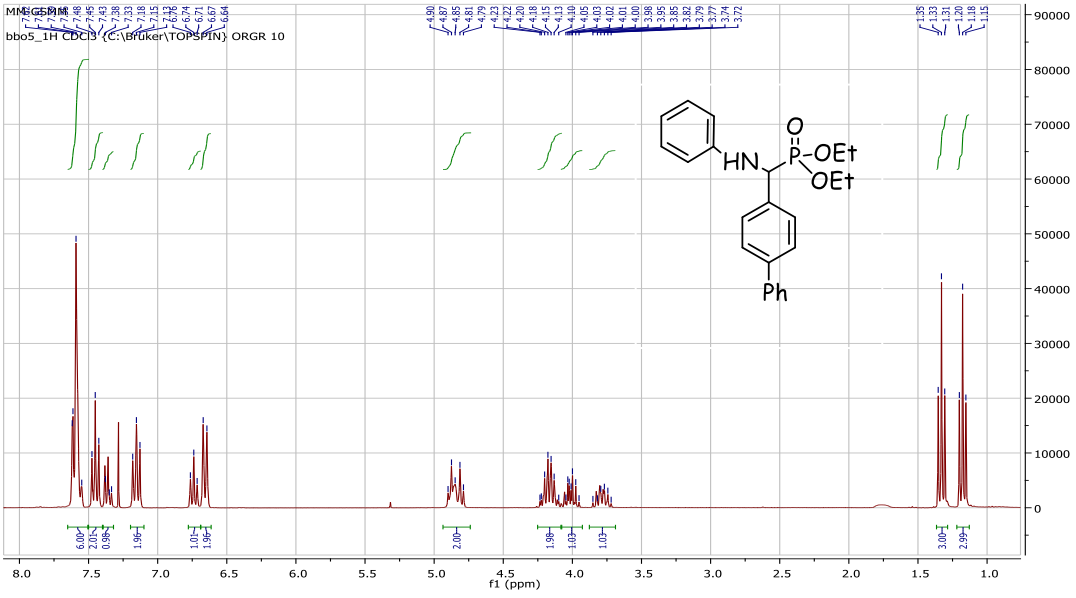

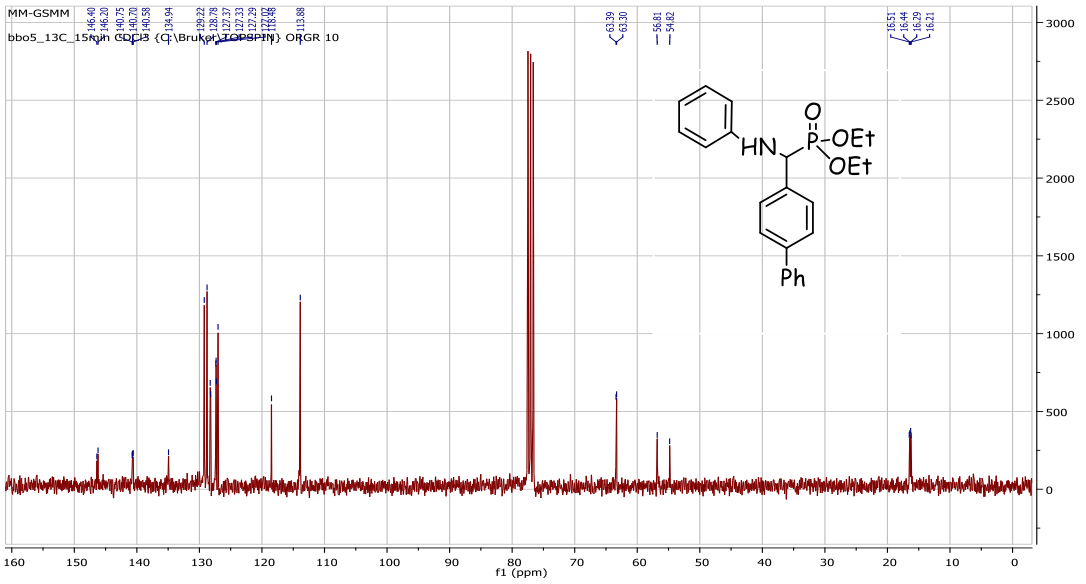

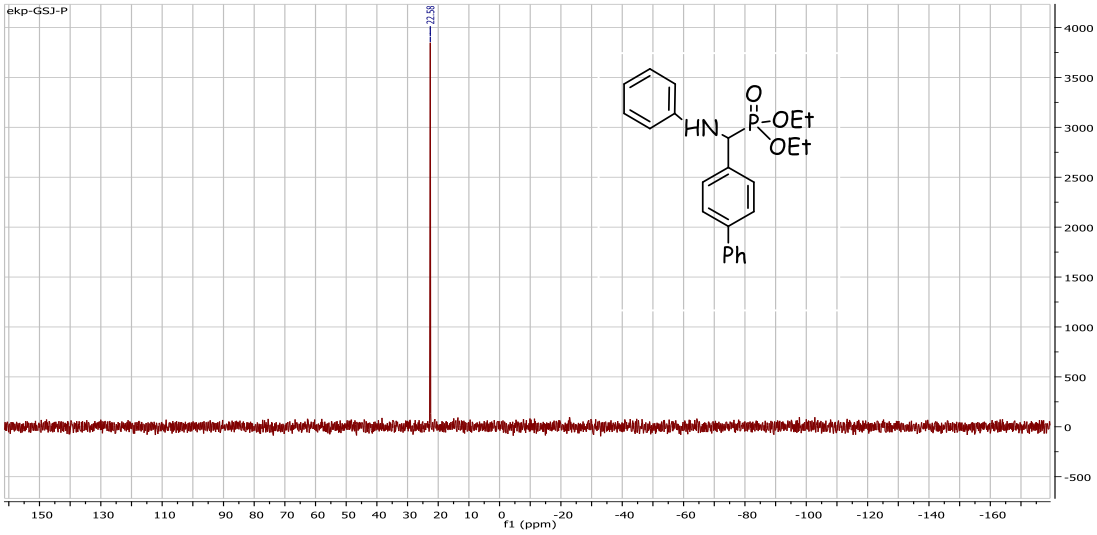

Acquisition Parameter

Source Type	ESI	Ion Polarity	Positive	Set Nebulizer	2.8 Bar
Focus	Not active	Set Capillary	4500 V	Set Dry Heater	180 °C
Scan Begin	50 m/z	Set End Plate Offset	-500 V	Set Dry Gas	9.0 l/min
Scan End	1200 m/z	Set Collision Cell RF	50.0 Vpp	Set Divert Valve	Waste

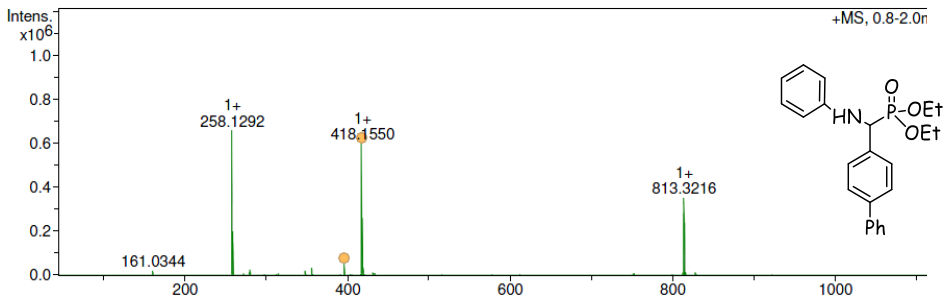

Meas. m/z	#	Ion Formula	m/z	err [mDa]	err [ppm]	mSigma
396.171124	1	C23H27NO3P	396.172307	1.2	3.0	2.9
	1	C23H27NO3P	396.172307	1.2	3.0	2.9
418.155006	1	C23H26NNaO3P	418.154251	-0.8	-1.8	90.8
	1	C23H26NNaO3P	418.154251	-0.8	-1.8	90.8

^{1}H, ^{13}C, ^{31}P NMR and HRMS of diethyl [phenyl(p-tolylamino)methyl]phosphonate (V.14g)

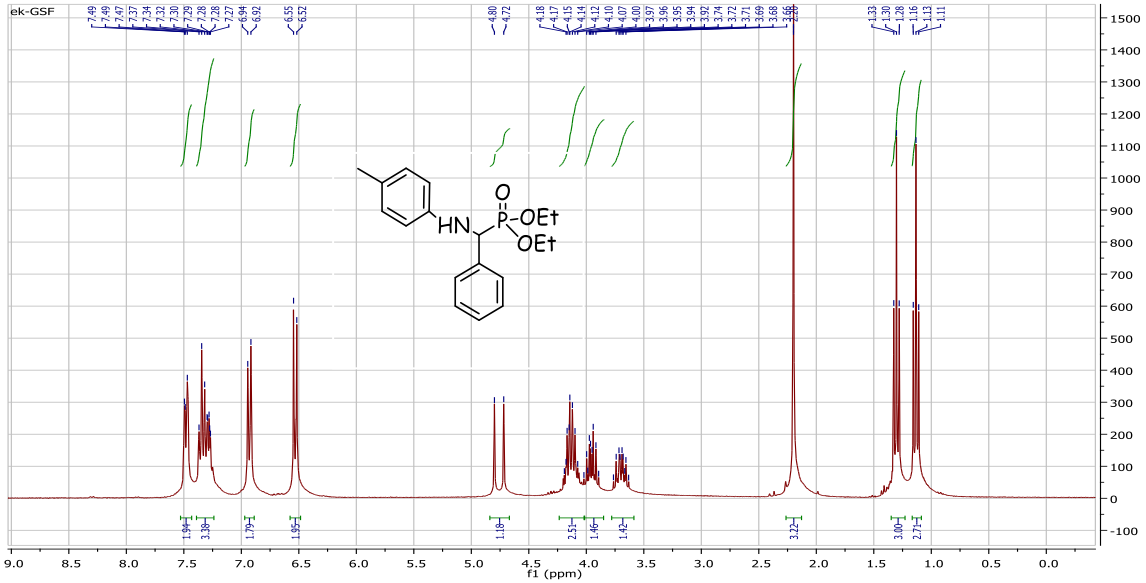

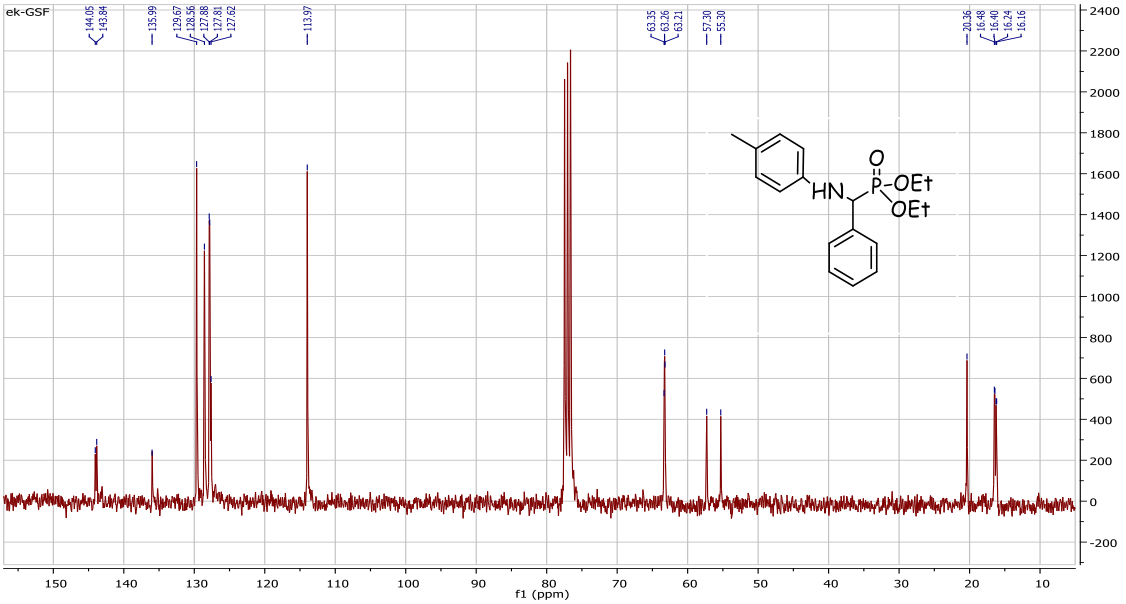

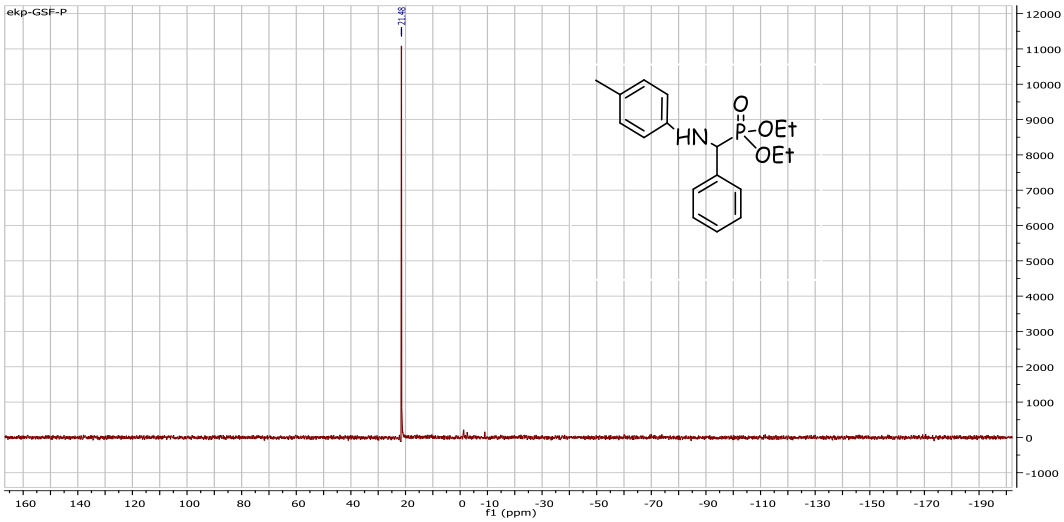

Acquisition Parameter

Source Type	ESI	Ion Polarity	Positive	Set Nebulizer	2.8 Bar
Focus	Not active	Set Capillary	4500 V	Set Dry Heater	180 °C
Scan Begin	50 m/z	Set End Plate Offset	-500 V	Set Dry Gas	9.0 l/min
Scan End	1200 m/z	Set Collision Cell RF	50.0 Vpp	Set Divert Valve	Waste

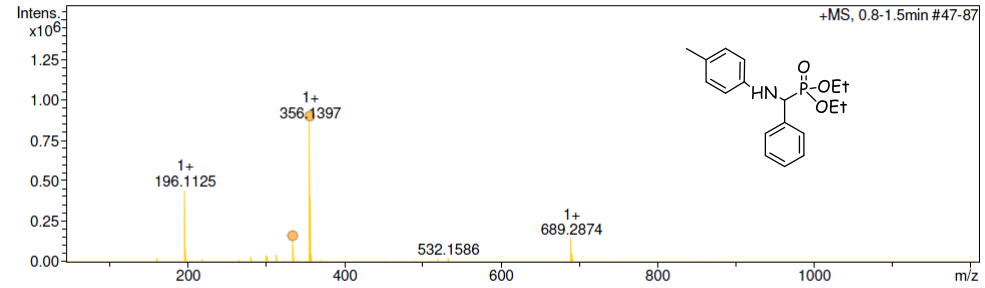

Meas. m/z	#	Ion Formula	m/z	err [mDa]	err [ppm]	mSigma
334.155823	1	C18H25NO3P	334.156657	-0.8	-2.5	5.3
	1	C18H25NO3P	334.156657	-0.8	-2.5	5.3
356.139691	1	C18H24NNaO3P	356.138601	-1.1	-3.1	151.3
	1	C18H24NNaO3P	356.138601	-1.1	-3.1	151.3
	1	C18H24NNaO3P	356.138601	-1.1	-3.1	151.3

***^{1}H, ^{13}C and ^{31}P NMR of* diethyl [4 chloro (p-tolylamino) methyl]phosphonate (*V.14*h)**

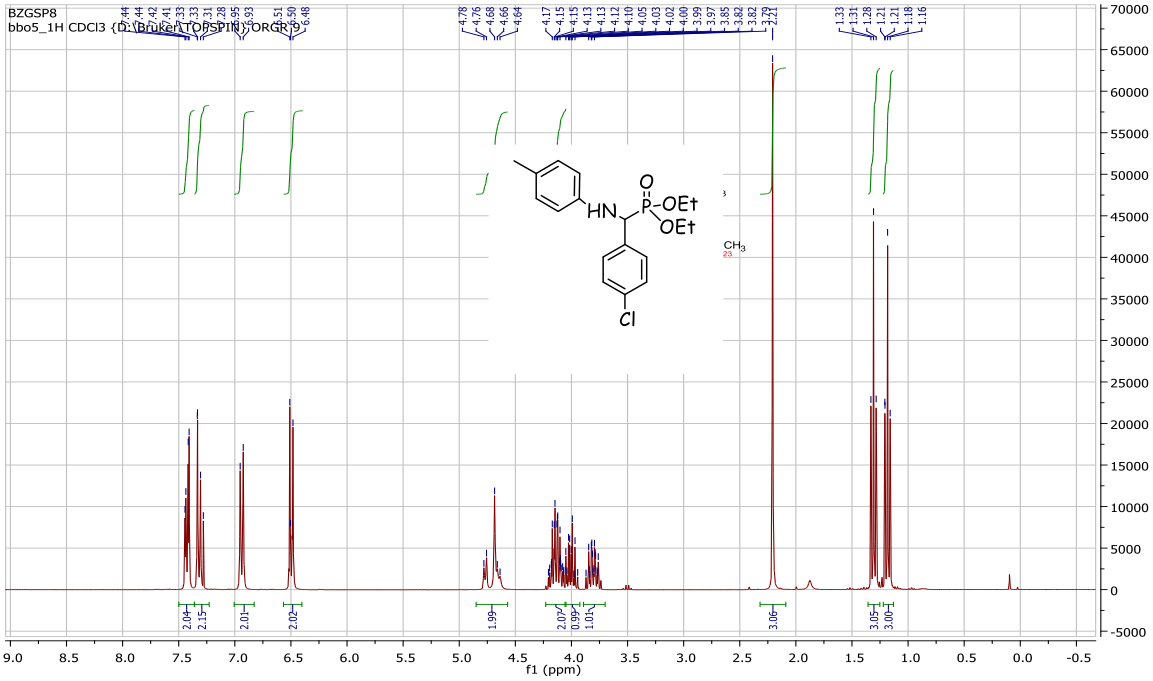
BZGSP8
bbo5_1H CDCl3 {D:\Bruker\TOPSPIN}
HN
O
P-OEt
OEt
Cl
f1 (ppm)

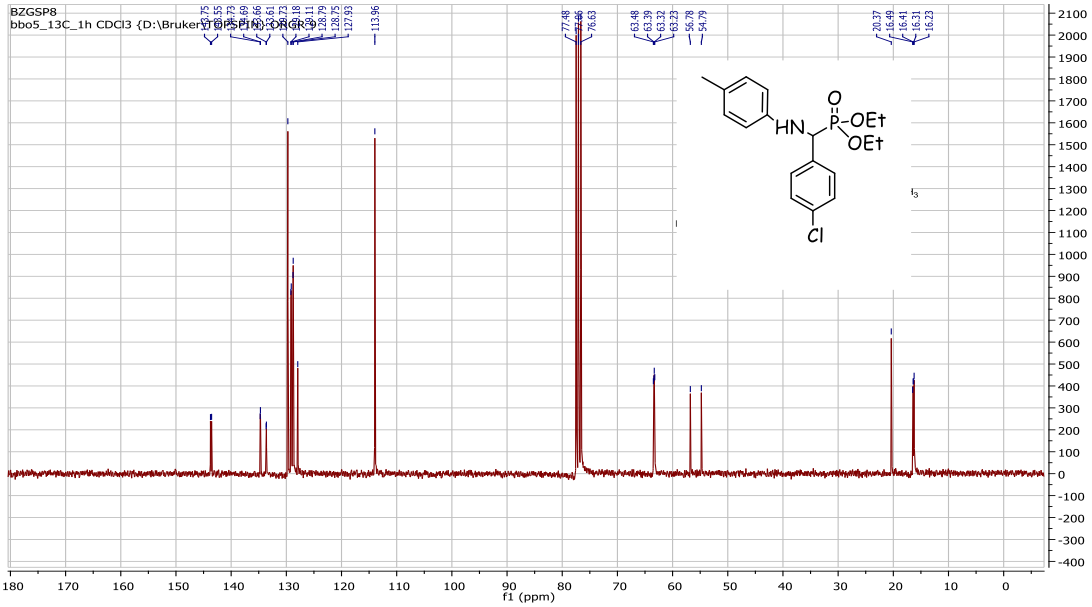
BZGSP8
bbo5_13C_1h CDCl3 {D:\Bruker\TOPSPIN}
HN
O
P-OEt
OEt
Cl
f1 (ppm)

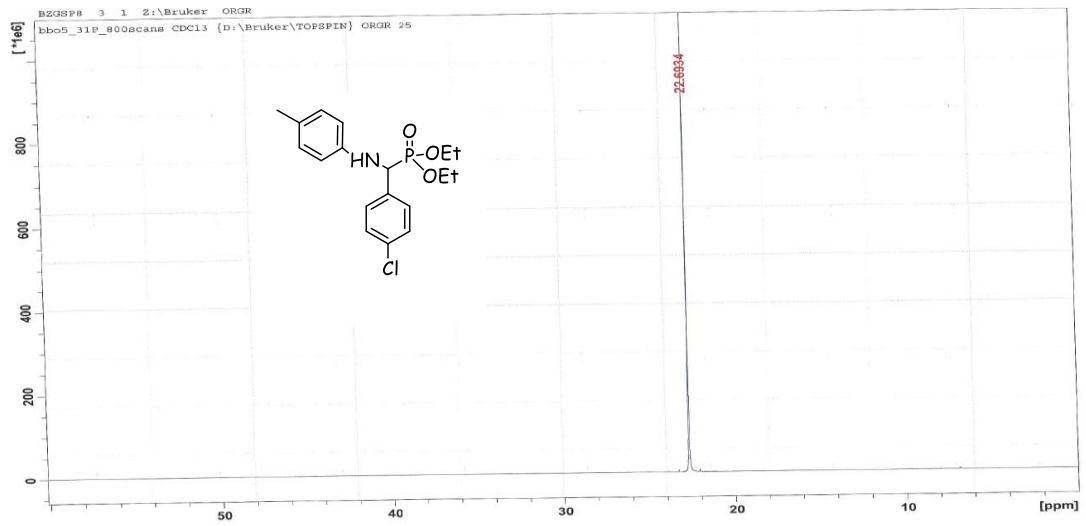

^{1}H, ^{13}C, ^{31}P NMR and HRMS of diethyl [4-nitrophenyl (p-tolylamino) methyl]phosphonate (V.14i)

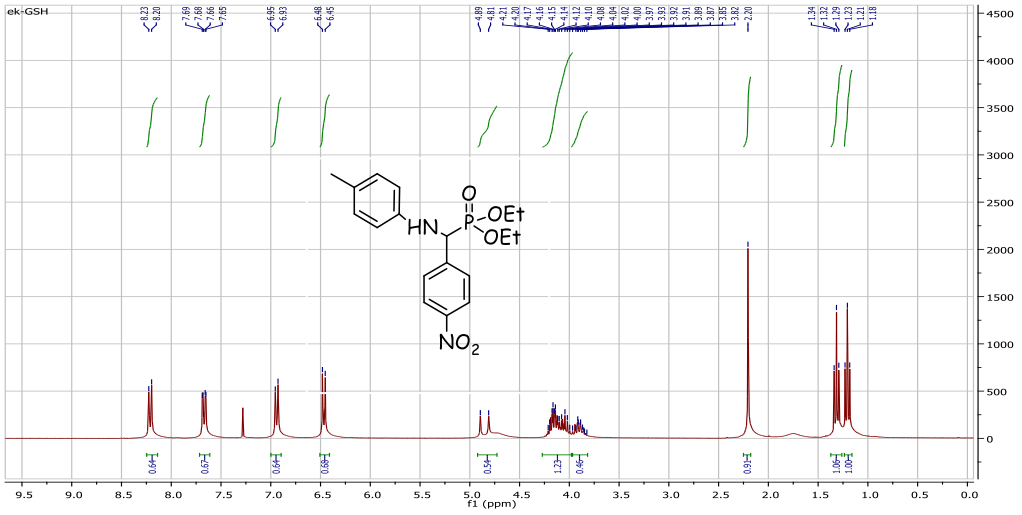

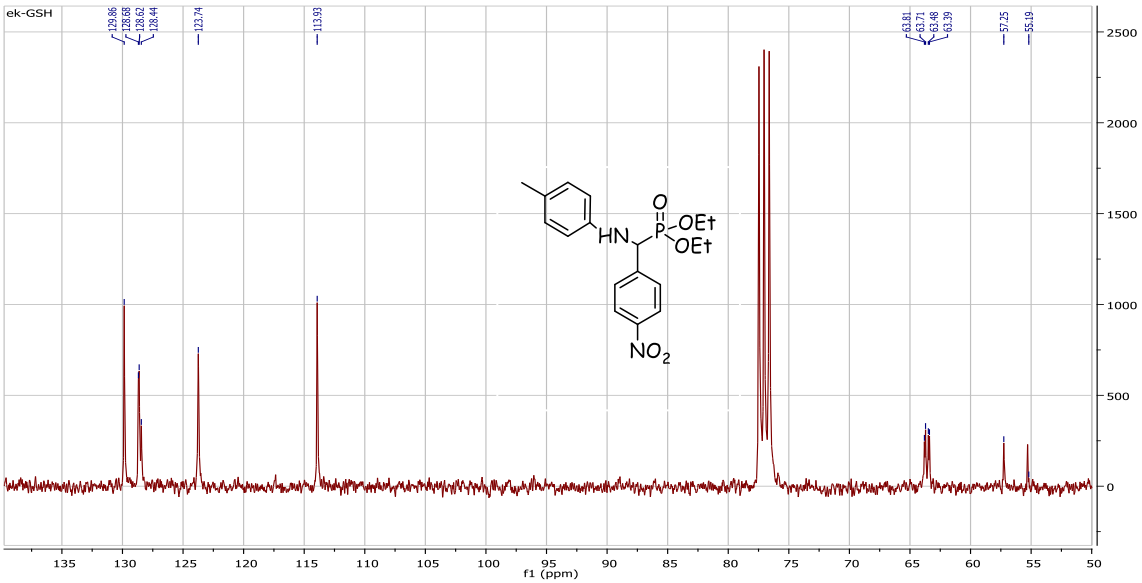

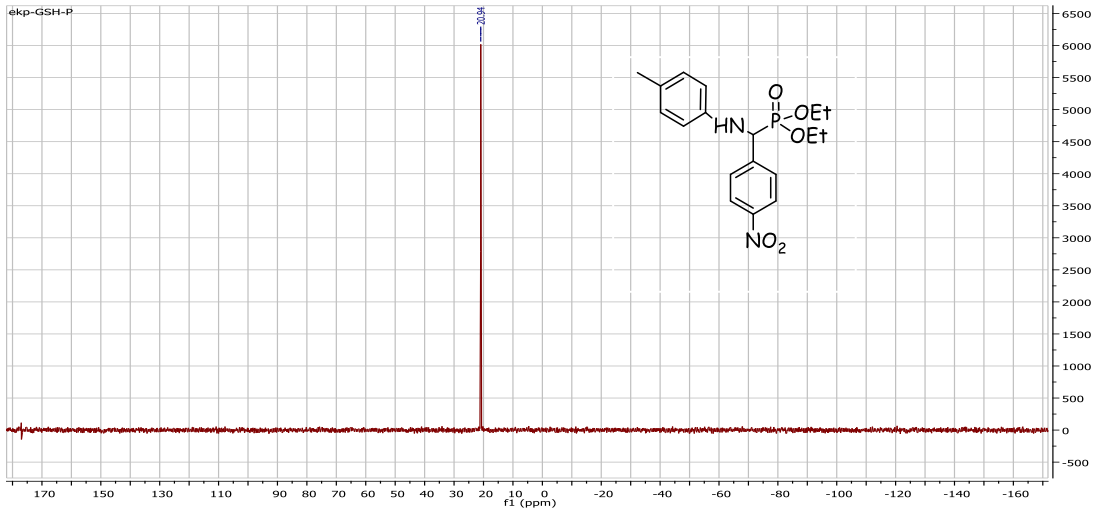

Acquisition Parameter

Source Type	ESI	Ion Polarity	Positive	Set Nebulizer	2.8 Bar
Focus	Not active	Set Capillary	4500 V	Set Dry Heater	180 °C
Scan Begin	50 m/z	Set End Plate Offset	-500 V	Set Dry Gas	9.0 l/min
Scan End	1200 m/z	Set Collision Cell RF	50.0 Vpp	Set Divert Valve	Waste

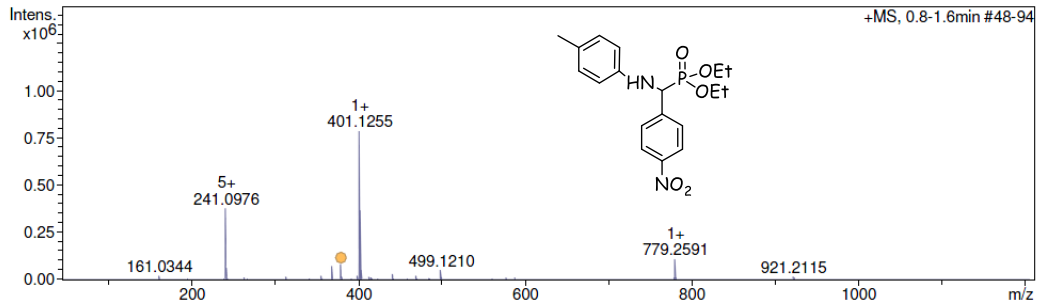

Meas. m/z	#	Ion Formula	m/z	err [mDa]	err [ppm]	mSigma
379.141225	1	C18H24N2O5P	379.141735	-0.5	-1.3	1.2
	1	C18H24N2O5P	379.141735	-0.5	-1.3	1.2

^{1}H, ^{13}C, ^{31}P NMR and HRMS of diethyl [4 methoxy(p-tolylamino) methyl]phosphonate (V.14j)

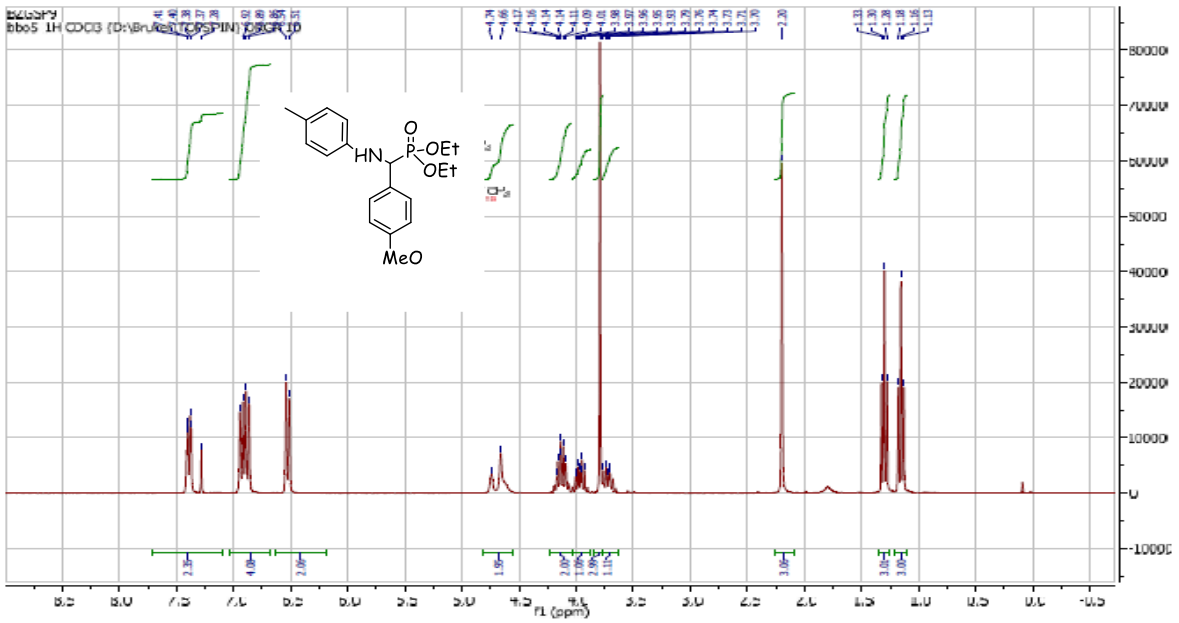
HN
O
P-OEt
OEt
MeO
f1 (ppm)

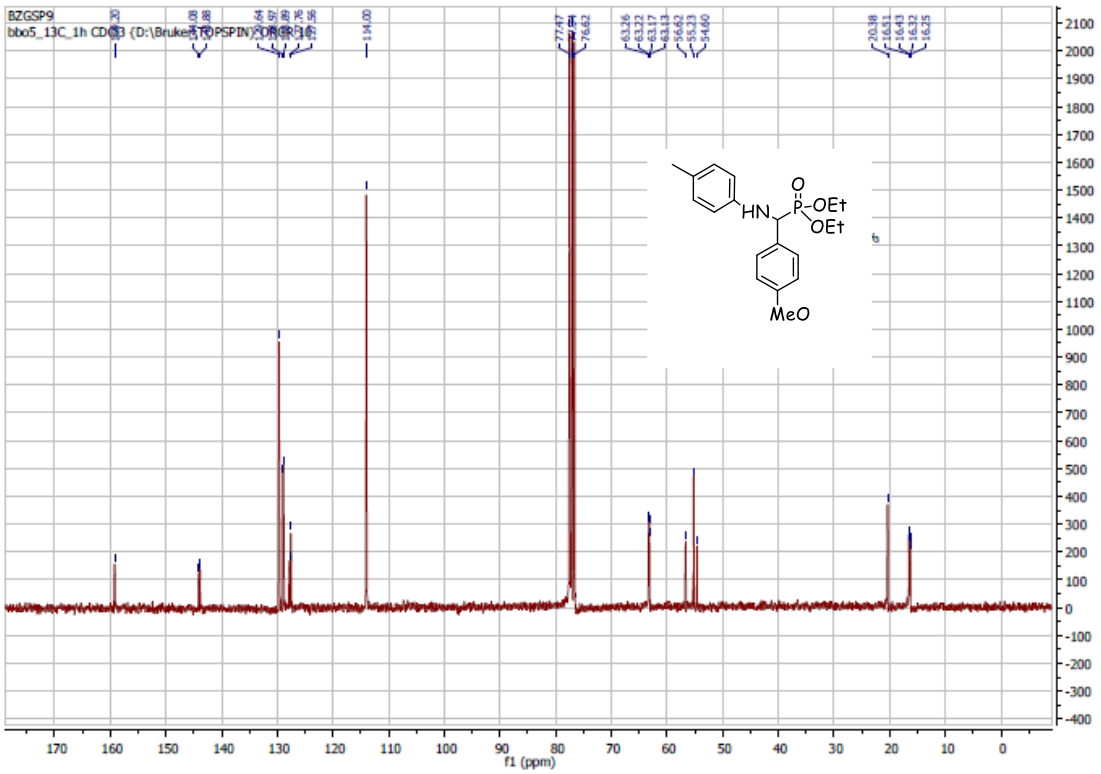
HN
O
P-OEt
OEt
MeO
f1 (ppm)

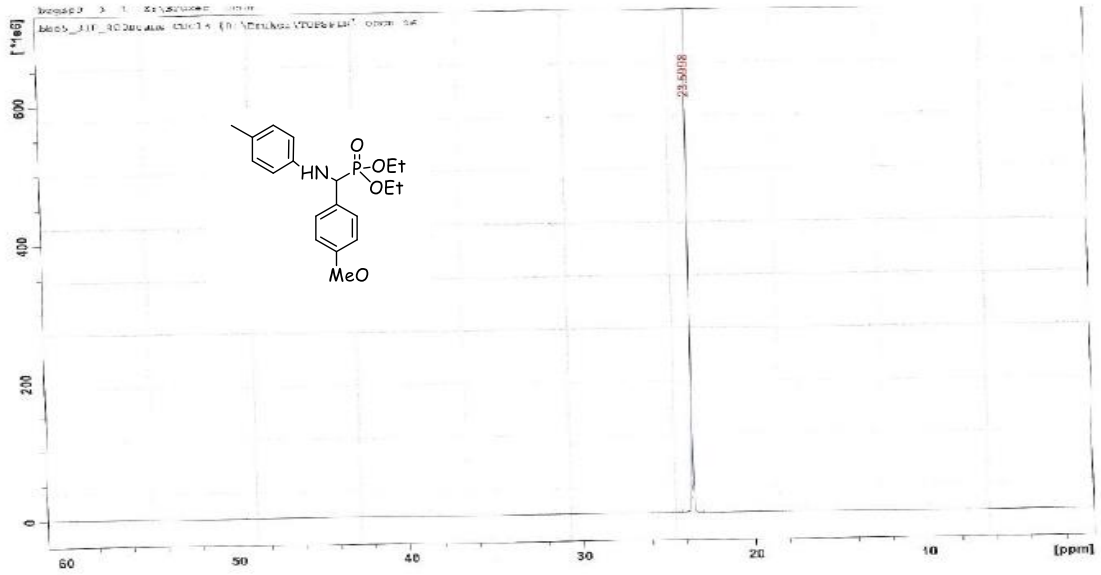

^{1}H, ^{13}C, ^{31}P NMR and HRMS of diethyl[1-naphtyl (p-tolylamino) methyl]phosphonate (V.14k)

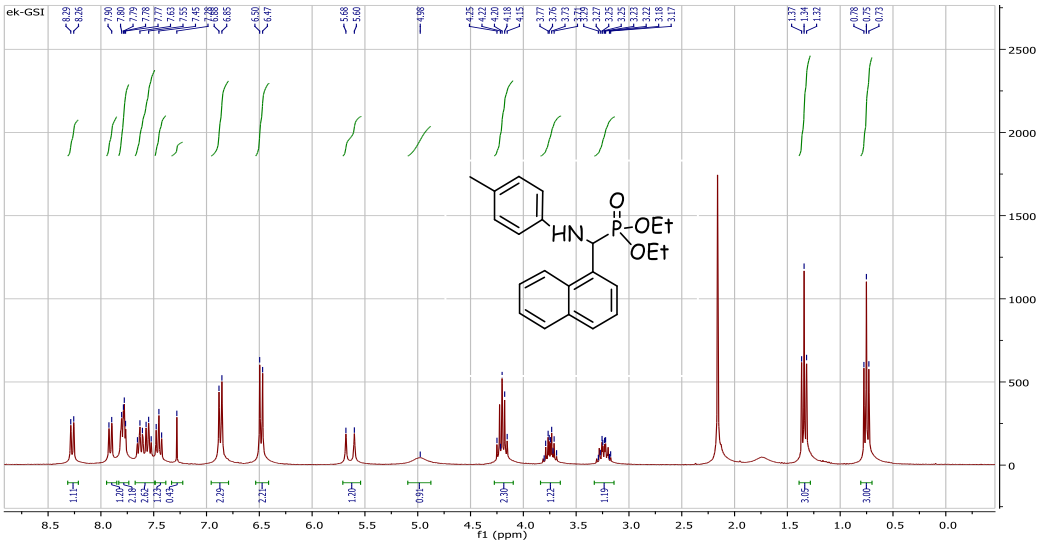

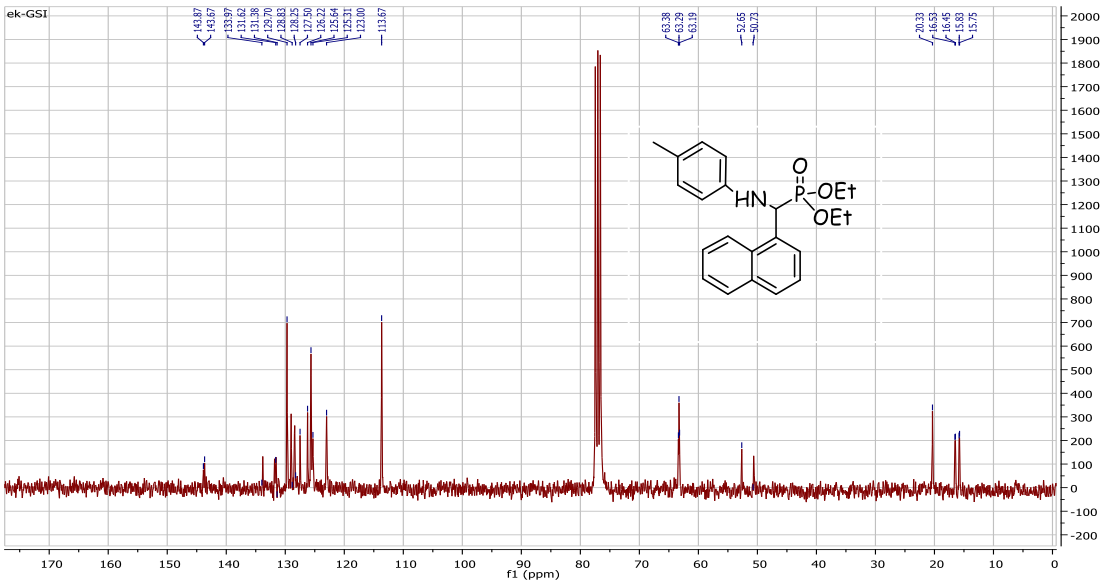

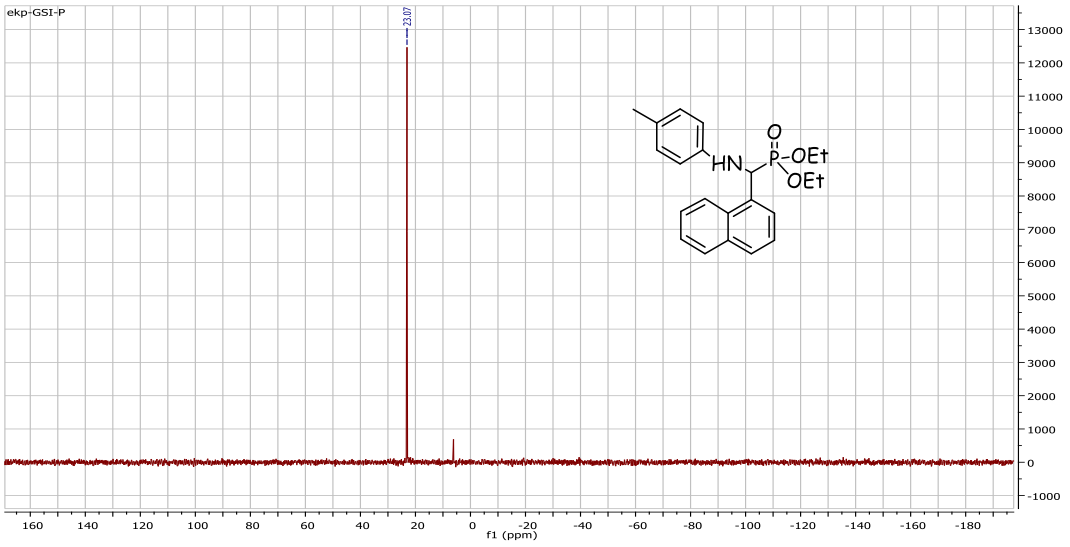

Acquisition Parameter

Source Type	ESI	Ion Polarity	Positive	Set Nebulizer	2.8 Bar
Focus	Not active	Set Capillary	4500 V	Set Dry Heater	180 °C
Scan Begin	50 m/z	Set End Plate Offset	-500 V	Set Dry Gas	9.0 l/min
Scan End	1200 m/z	Set Collision Cell RF	50.0 Vpp	Set Divert Valve	Waste

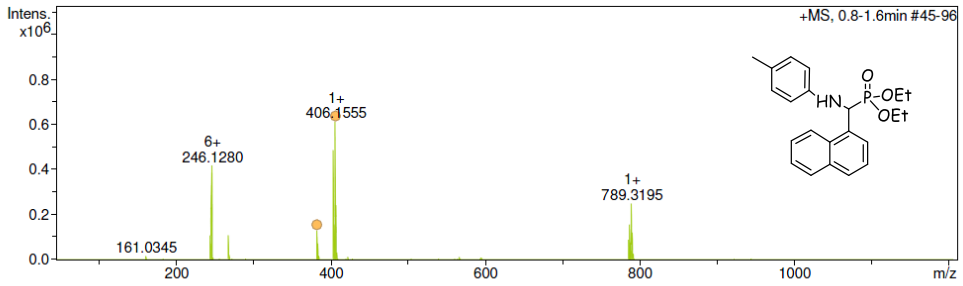

Meas. m/z	#	Ion Formula	m/z	err [mDa]	err [ppm]	mSigma
382.155759	1	C22H25NO3P	382.156657	-0.9	-2.3	272.3
	1	C22H25NO3P	382.156657	-0.9	-2.3	272.3
406.155519	1	C22H26NNaO3P	406.154251	1.3	3.1	76.1
	1	C22H26NNaO3P	406.154251	1.3	3.1	76.1
	1	C22H26NNaO3P	406.154251	1.3	3.1	76.1

^{1}H, ^{13}C, ^{31}P NMR and HRMS of diethyl [4-biphenyl(p-tolylamino)methyl]phosphonate (V.14l)

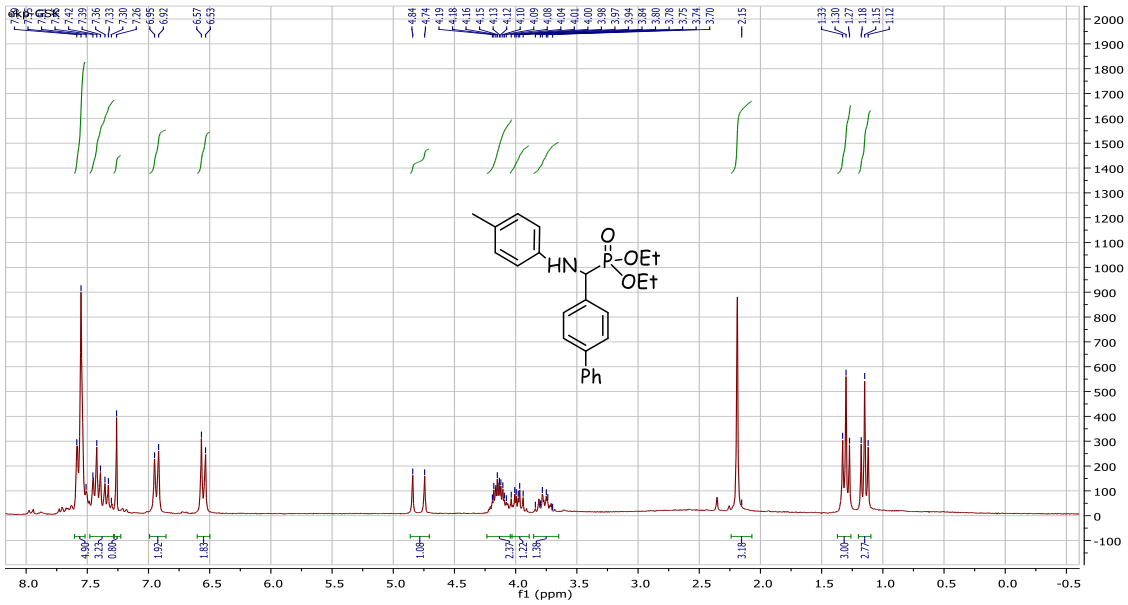

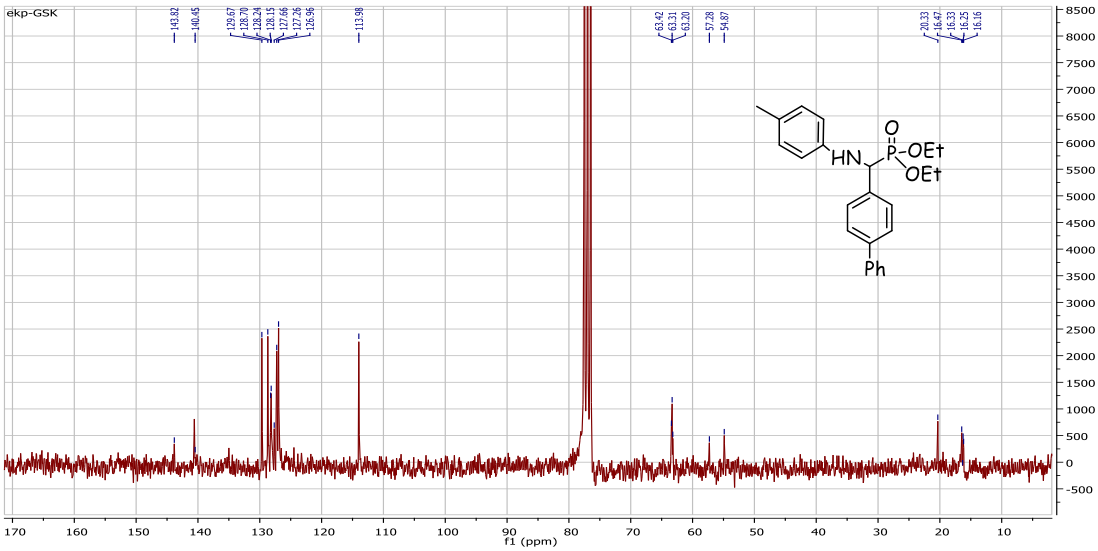

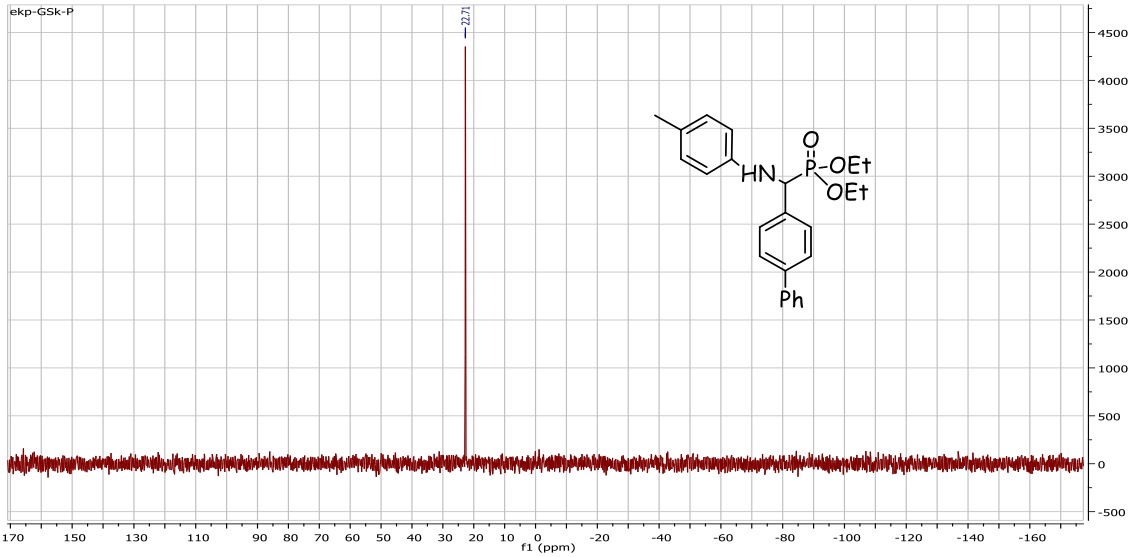

Acquisition Parameter

Source Type	ESI	Ion Polarity	Positive	Set Nebulizer	2.8 Bar
Focus	Not active	Set Capillary	4500 V	Set Dry Heater	180 °C
Scan Begin	50 m/z	Set End Plate Offset	-500 V	Set Dry Gas	9.0 l/min
Scan End	1200 m/z	Set Collision Cell RF	50.0 Vpp	Set Divert Valve	Waste

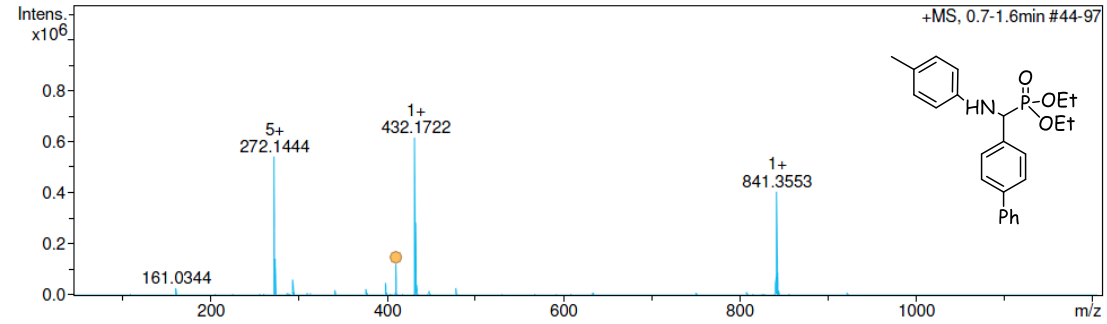

Meas. m/z	#	Ion Formula	m/z	err [mDa]	err [ppm]	mSigma
410.187633	1	C24H29NO3P	410.187957	-0.3	-0.8	3.6
	1	C24H29NO3P	410.187957	-0.3	-0.8	3.6

^{1}H, ^{13}C, ^{31}P NMR and HRMS of diethyl [4-nitro phenyl (p-tolylamino) methyl] phosphonate (V.14m)

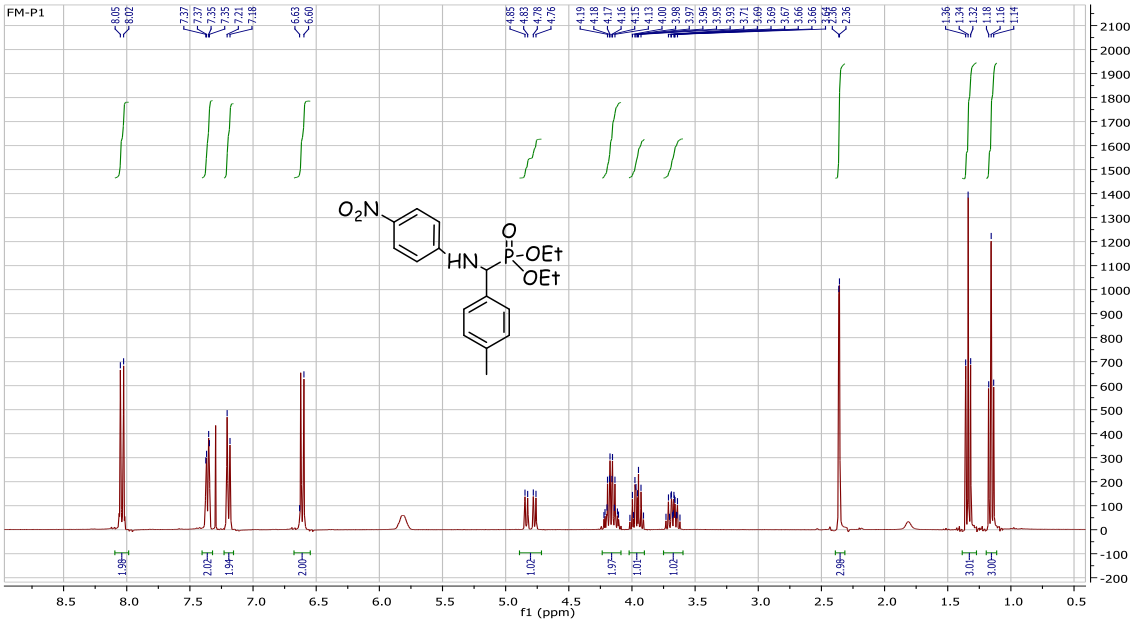

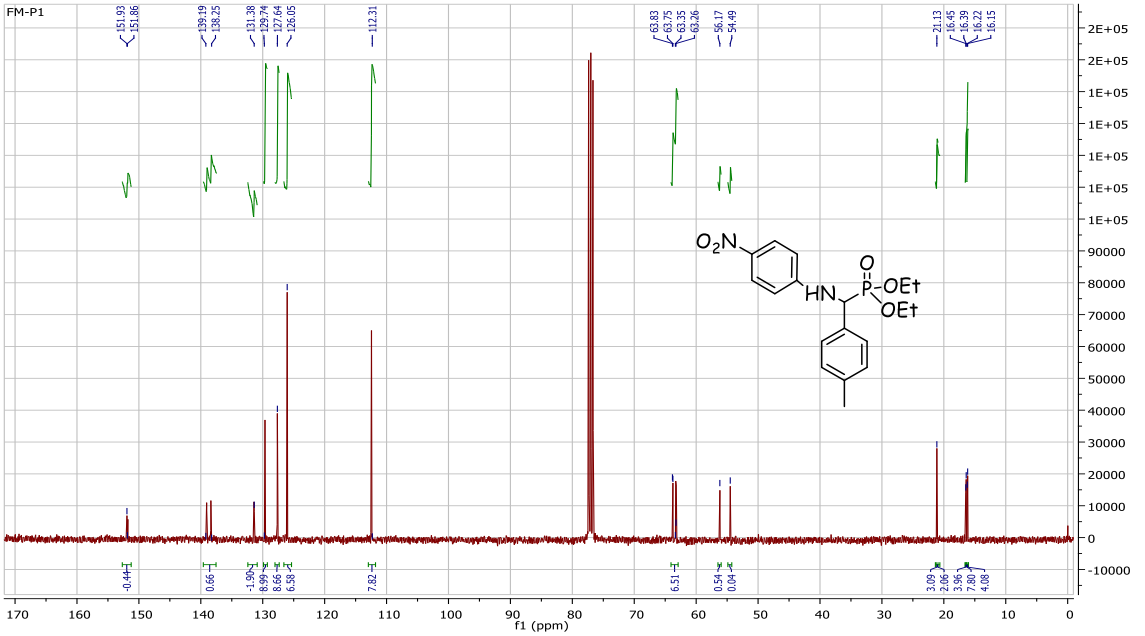
FM-P1
151.93
151.86
139.19
138.25
131.38
129.74
127.64
126.05
112.31
63.83
63.75
63.35
63.26
56.17
54.49
21.13
16.45
16.39
16.22
16.15
O_2N
HN
O
P-OEt
OEt
f1 (ppm)

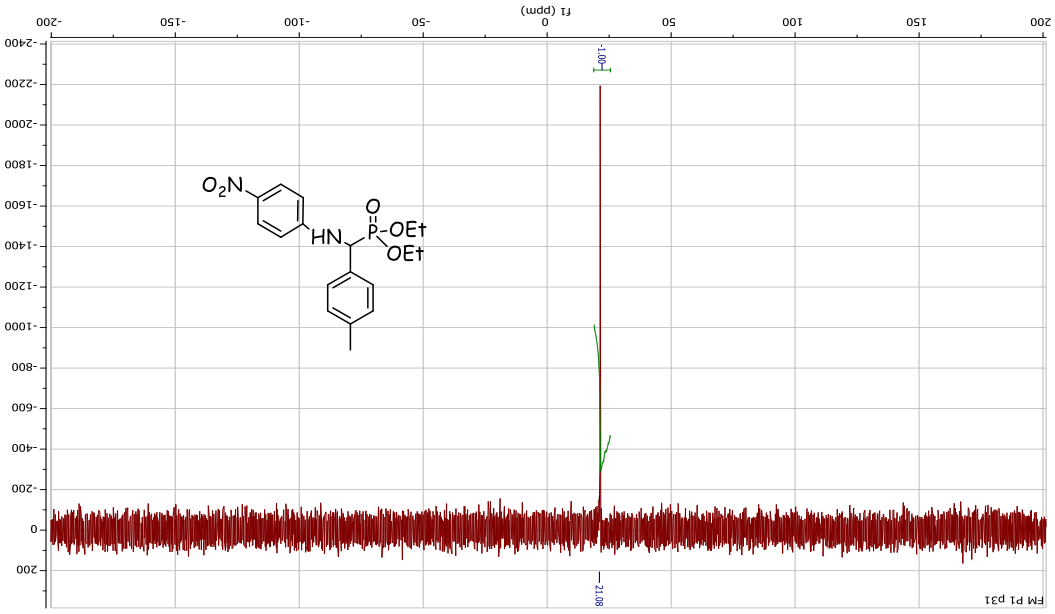
f1 (ppm)
1.00
21.08
O_2N
HN
O
P-OEt
OEt
FM P1 p31

Acquisition Parameter

Source Type	ESI	Ion Polarity	Positive	Set Nebulizer	2.8 Bar
Focus	Not active	Set Capillary	4500 V	Set Dry Heater	180 °C
Scan Begin	50 m/z	Set End Plate Offset	-500 V	Set Dry Gas	9.0 l/min
Scan End	1200 m/z	Set Collision Cell RF	50.0 Vpp	Set Divert Valve	Waste

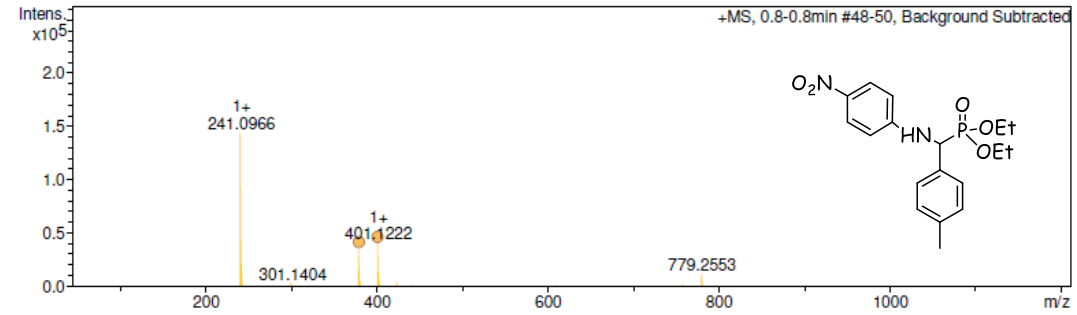

Meas. m/z	#	Ion Formula	m/z	err [mDa]	err [ppm]	mSigma
379.140392	1	C18H24N2O5P	379.141735	-1.3	-3.5	0.7
401.122199	1	C18H23N2NaO5P	401.123679	-1.5	-3.7	2.0

^{1}H, ^{13}C, ^{31}P NMR and HRMS of diethyl [2-methoxyphenyl (4-bromo, 2,6-dimethylamino) methyl] phosphonate (V.14n)

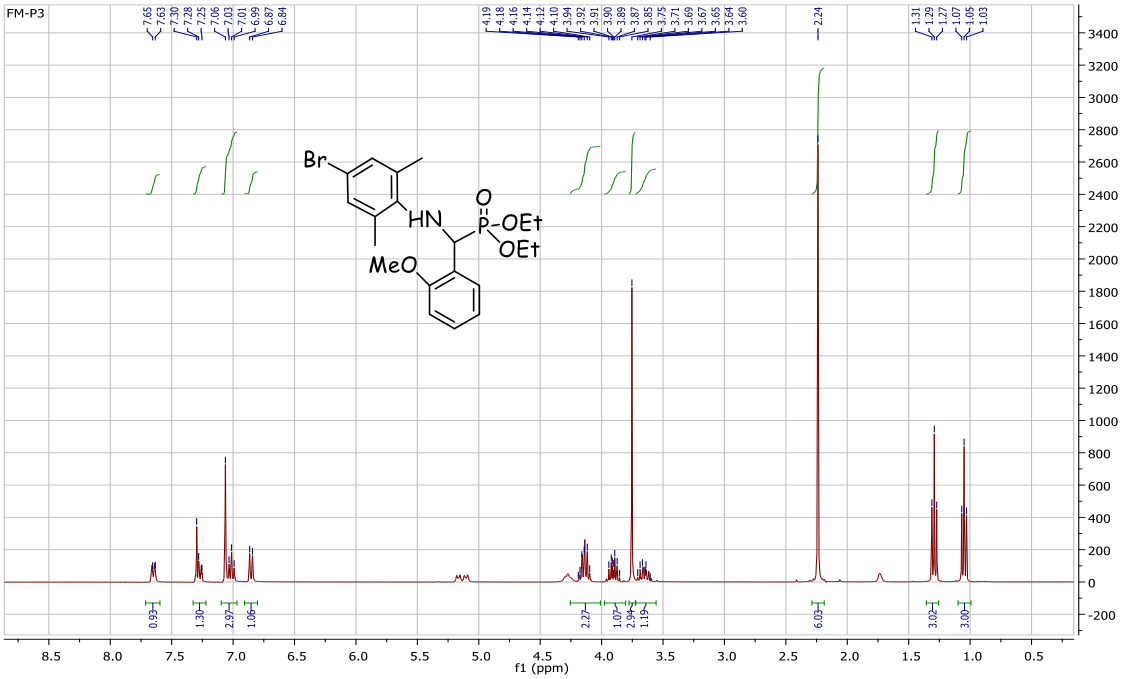

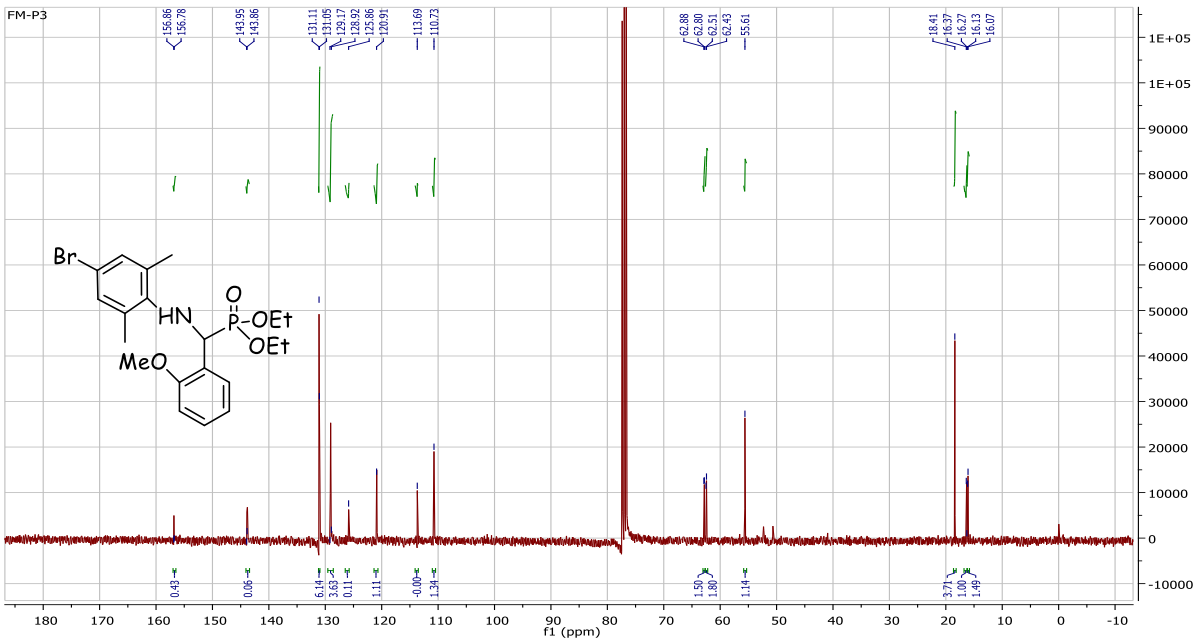
FM-P3
Br
HN
O
P-OEt
OEt
MeO
f1 (ppm)

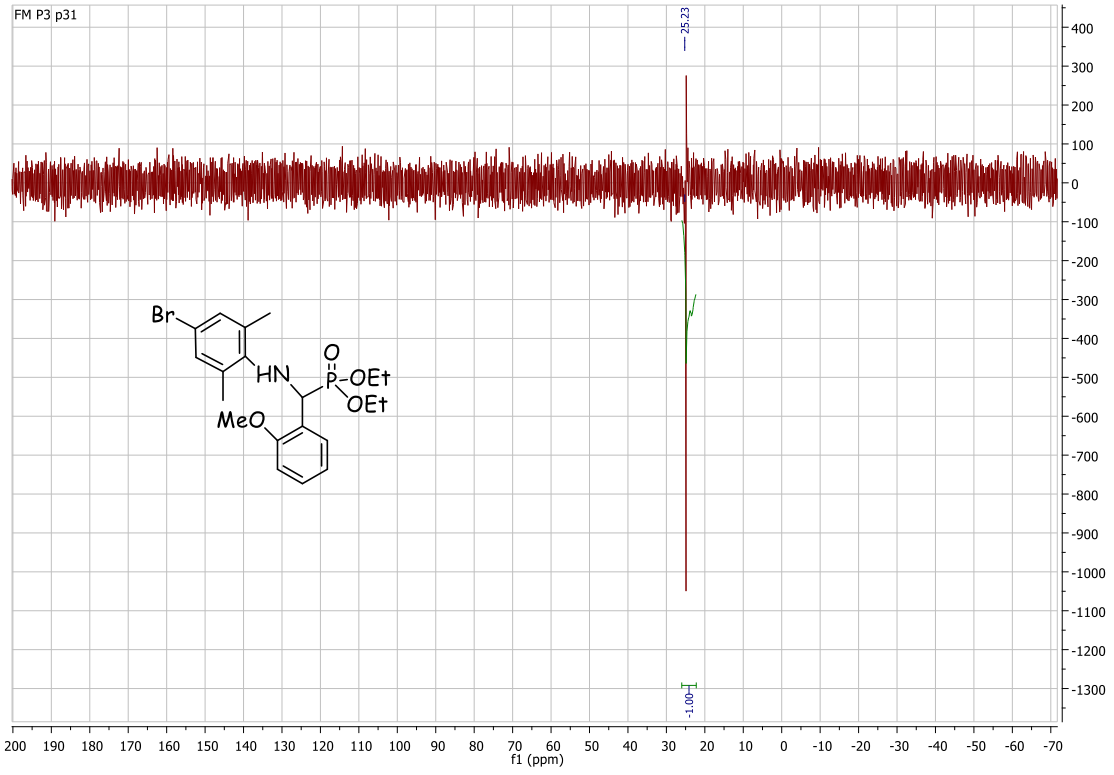
FM P3 p31
Br
HN
O
P-OEt
OEt
MeO
f1 (ppm)

Acquisition Parameter

Source Type	ESI	Ion Polarity	Positive	Set Nebulizer	2.8 Bar
Focus	Not active	Set Capillary	4500 V	Set Dry Heater	180 °C
Scan Begin	50 m/z	Set End Plate Offset	-500 V	Set Dry Gas	9.0 l/min
Scan End	1200 m/z	Set Collision Cell RF	50.0 Vpp	Set Divert Valve	Waste

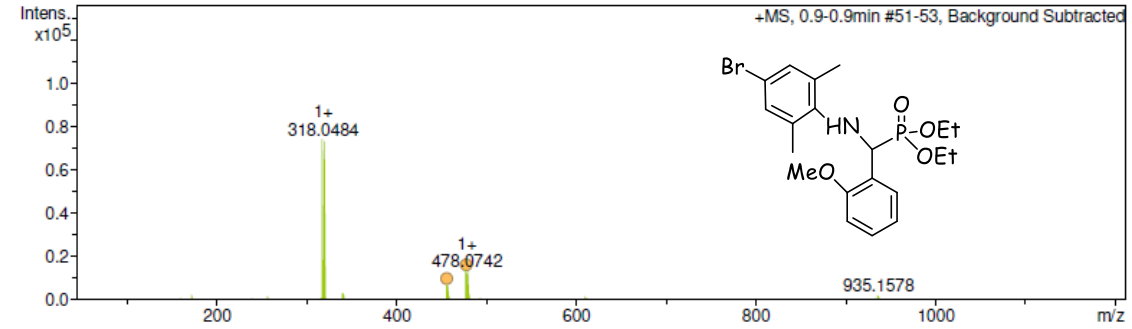

Meas. m/z	#	Ion Formula	m/z	err [mDa]	err [ppm]	mSigma
456.092391	1	C20H28BrNO4P	456.093384	1.0	2.2	16.1
478.074159	1	C20H27BrNNaO4P	478.075328	1.2	2.4	8.0

^{1}H, ^{13}C, ^{31}P NMR and HRMS of diethyl [3-methoxyphenyl (4-bromo, 2,6-dimethylamino) methyl] phosphonate (V.14o)

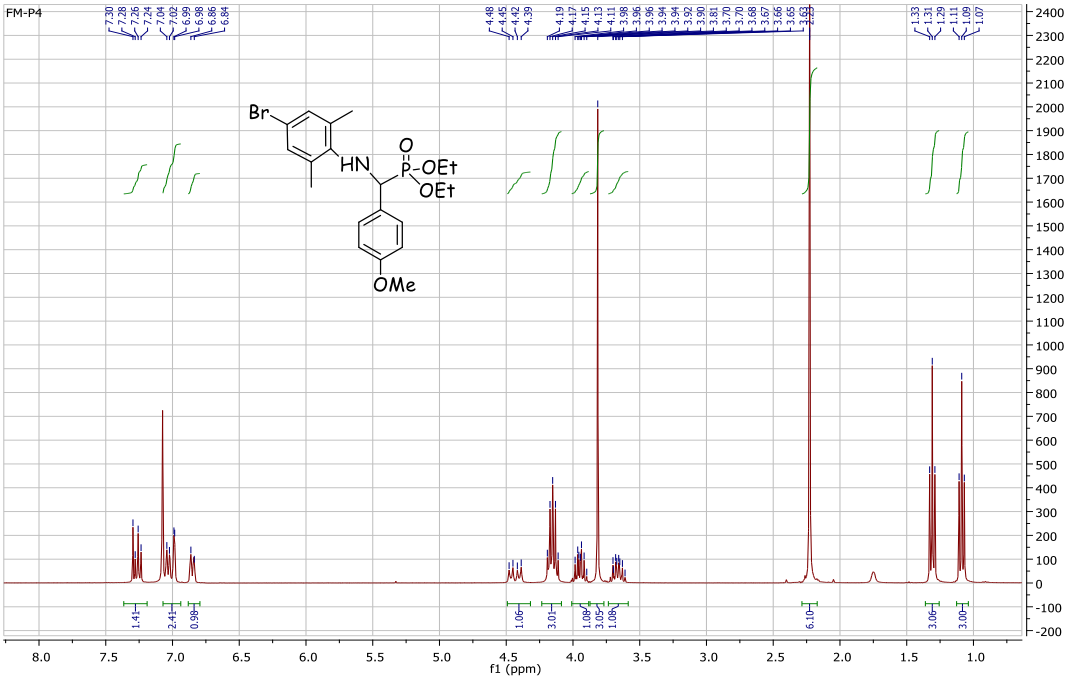

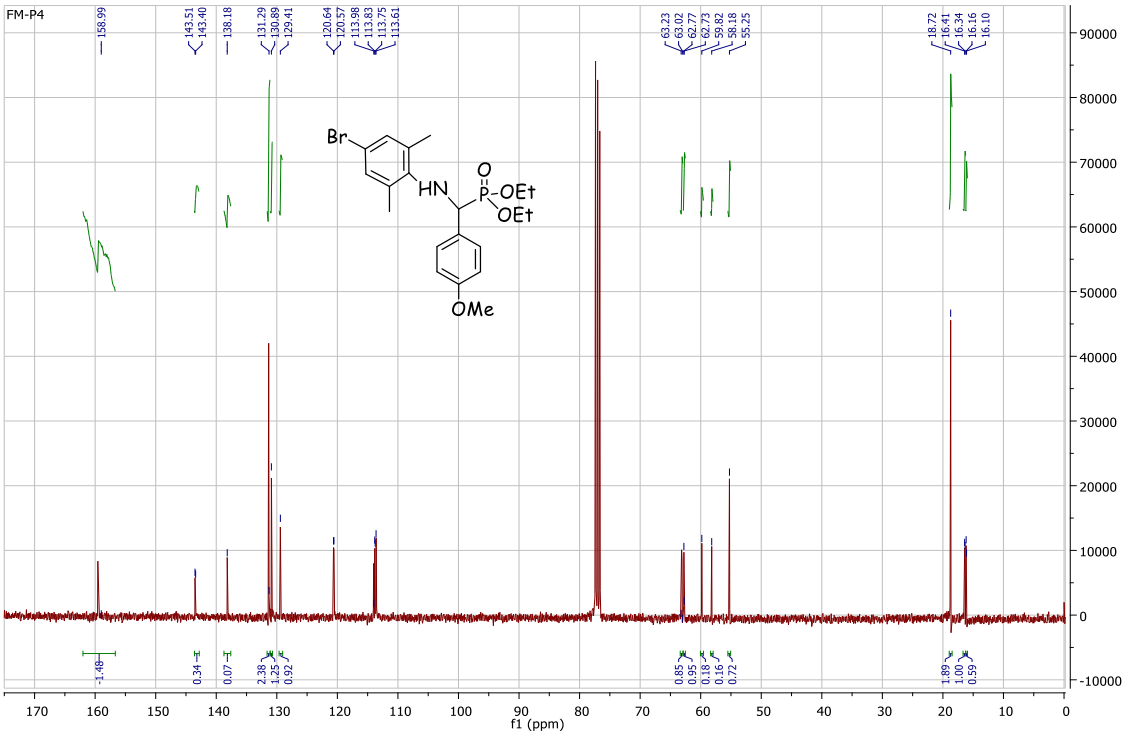
FM-P4
158.99
143.51
143.40
138.18
131.29
130.89
129.41
120.64
120.57
113.98
113.83
113.75
113.61
63.23
63.02
62.77
62.73
59.82
58.18
55.25
18.72
16.41
16.34
16.16
16.10
Br
HN
O
P-OEt
OEt
OMe
1.48
0.34
0.07
2.38
1.25
0.92
0.85
0.95
0.18
0.16
0.72
1.89
1.00
0.59
f1 (ppm)

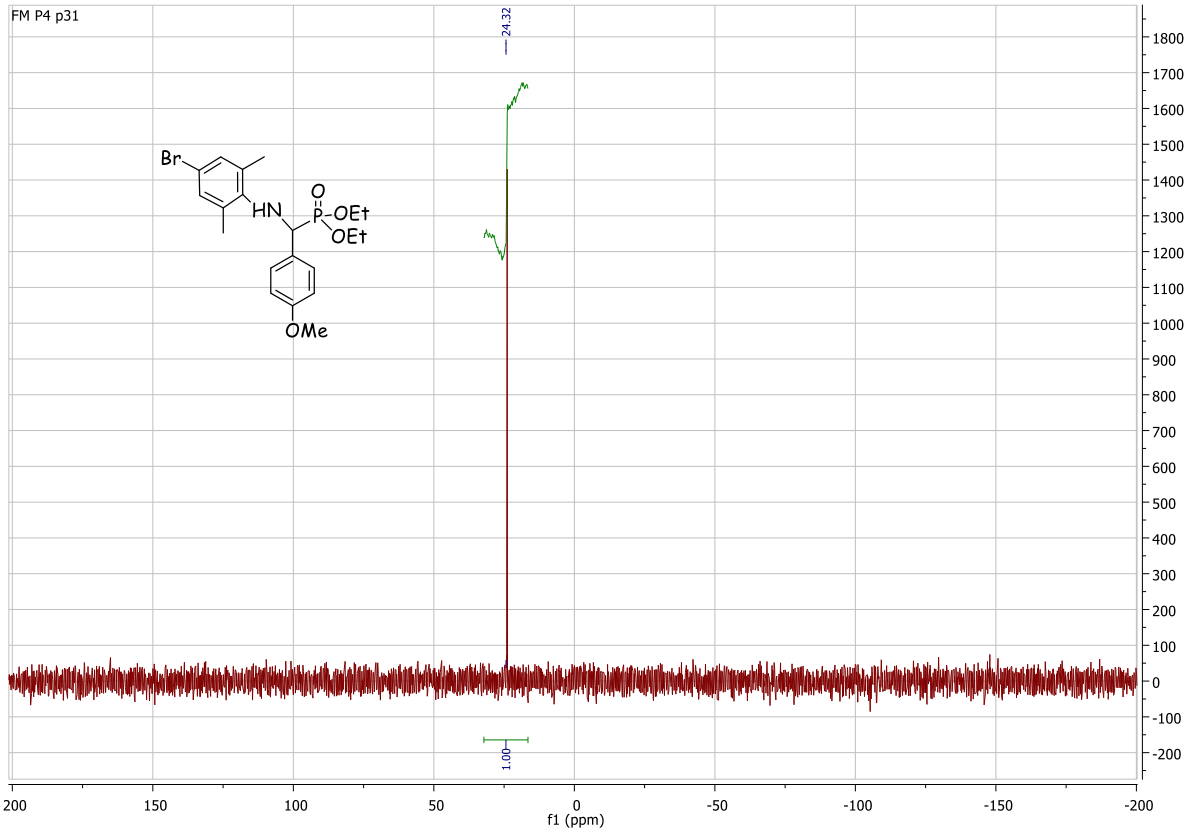
FM P4 p31
24.32
Br
HN
O
P-OEt
OEt
OMe
1.00
f1 (ppm)

Acquisition Parameter

Source Type	ESI	Ion Polarity	Positive	Set Nebulizer	2.8 Bar
Focus	Not active	Set Capillary	4500 V	Set Dry Heater	180 °C
Scan Begin	50 m/z	Set End Plate Offset	-500 V	Set Dry Gas	9.0 l/min
Scan End	1200 m/z	Set Collision Cell RF	50.0 Vpp	Set Divert Valve	Waste

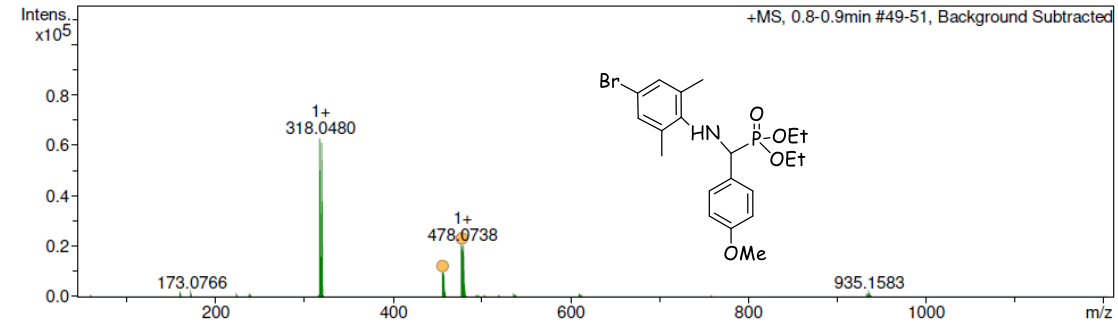

Meas. m/z	#	Ion Formula	m/z	err [mDa]	err [ppm]	mSigma
456.091985	1	C20H28BrNO4P	456.093384	1.4	3.1	7.9
478.073790	1	C20H27BrNNaO4P	478.075328	-1.5	-3.2	9.5

^{1}H, ^{13}C and ^{31}P NMR of diethyl (phenyl) (4-trifluoromethyl)phenylamino) methylphosphonate (V.14p)

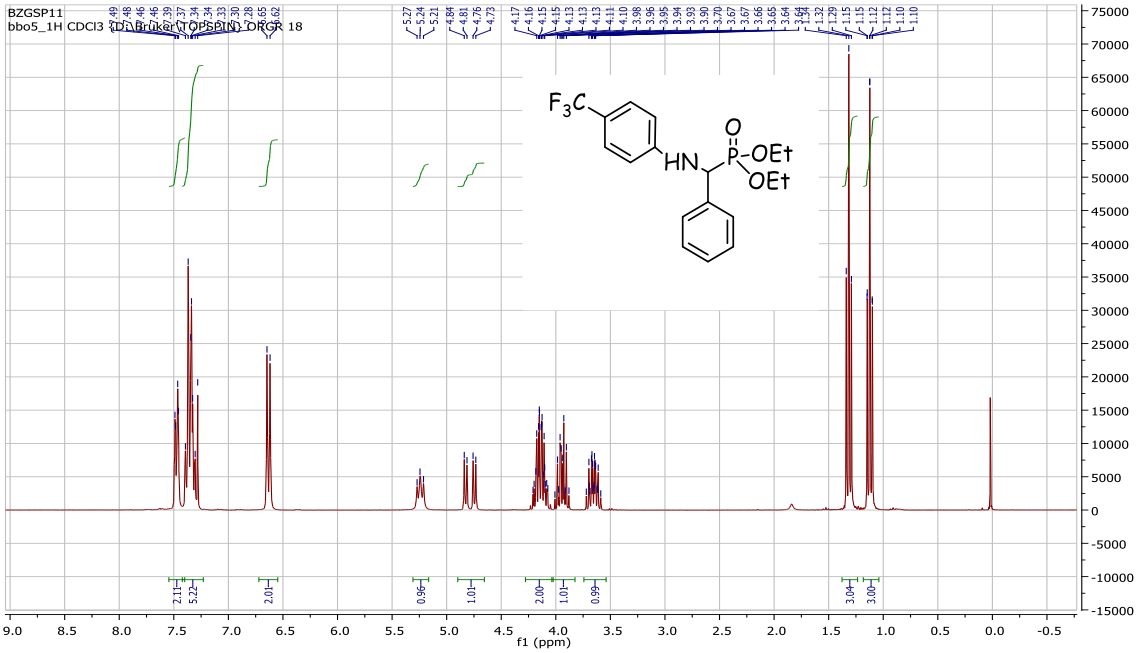

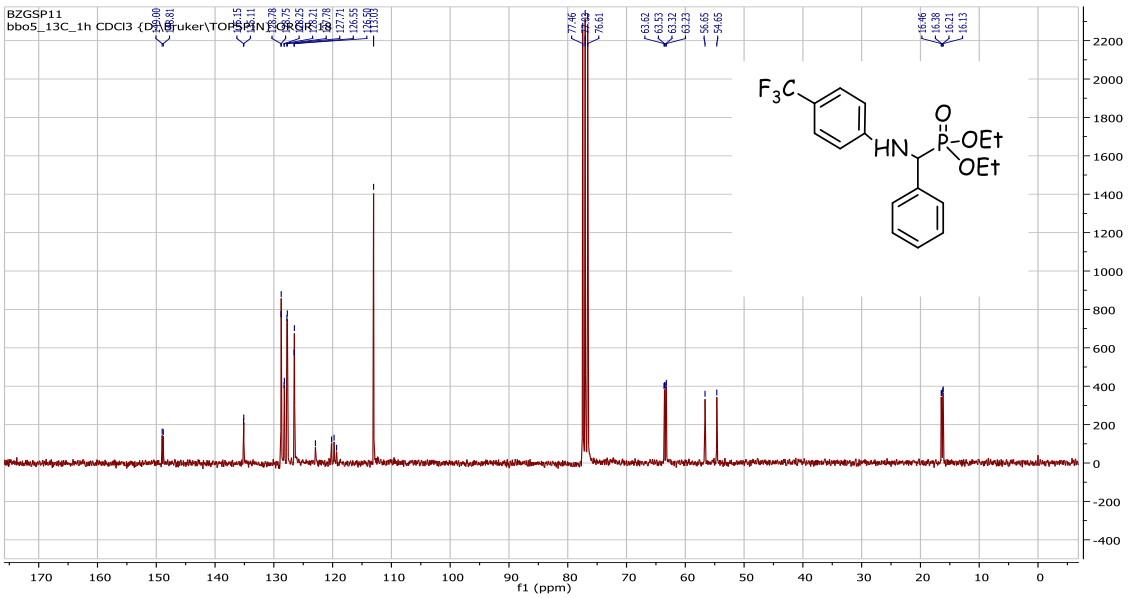
BZGSP11
bbo5_13C_1h CDCl3 {D:\Bruker\TOPSPIN} ORGR 18
F3C
HN
O
P-OEt
OEt
f1 (ppm)

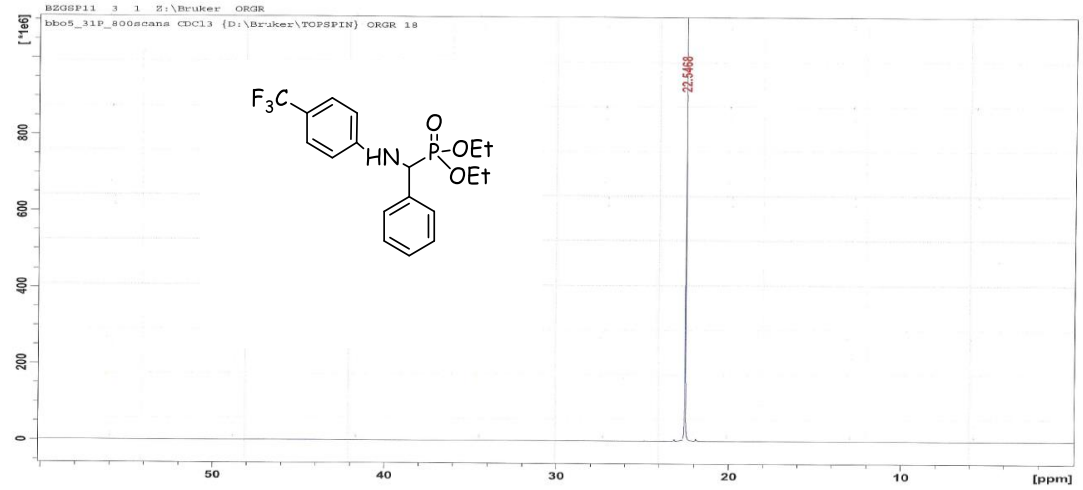
BZGSP11 3 1 Z:\Bruker ORGR
bbo5_31P_800scans CDCl3 {D:\Bruker\TOPSPIN} ORGR 18
22.5468
F3C
HN
O
P-OEt
OEt
[*1e6]
[ppm]

^{1}H, $^{13}C$and^{31}P NMR of diethyl (4-chlorophenyl)(4-trifluoromethylphenylamino) methylphosphonate (V.14q)

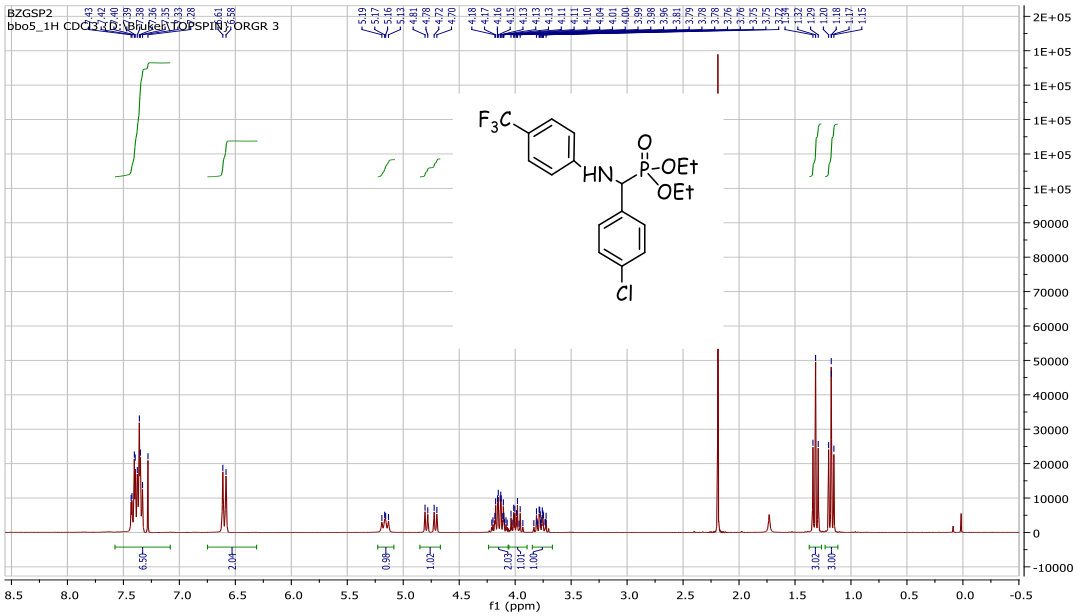

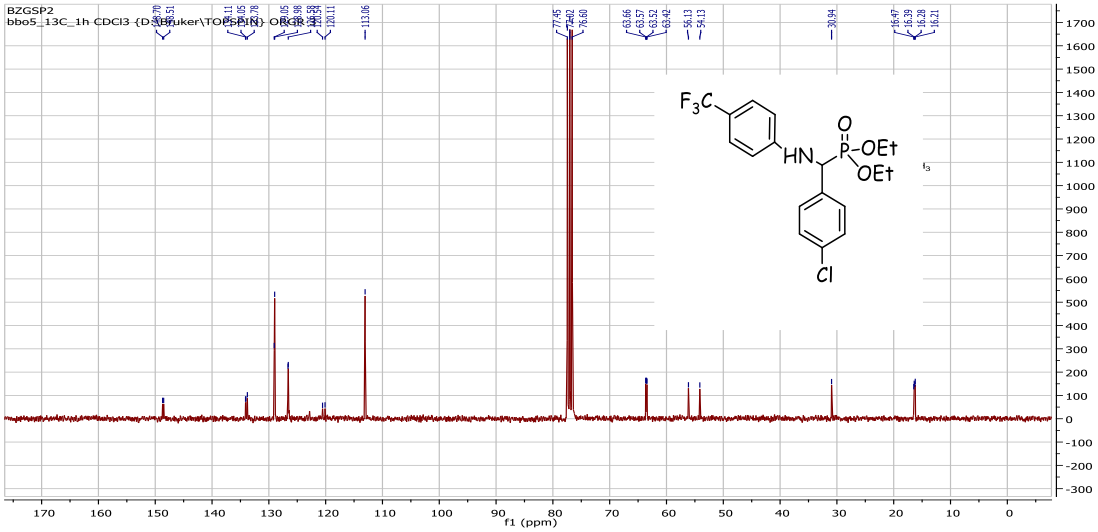

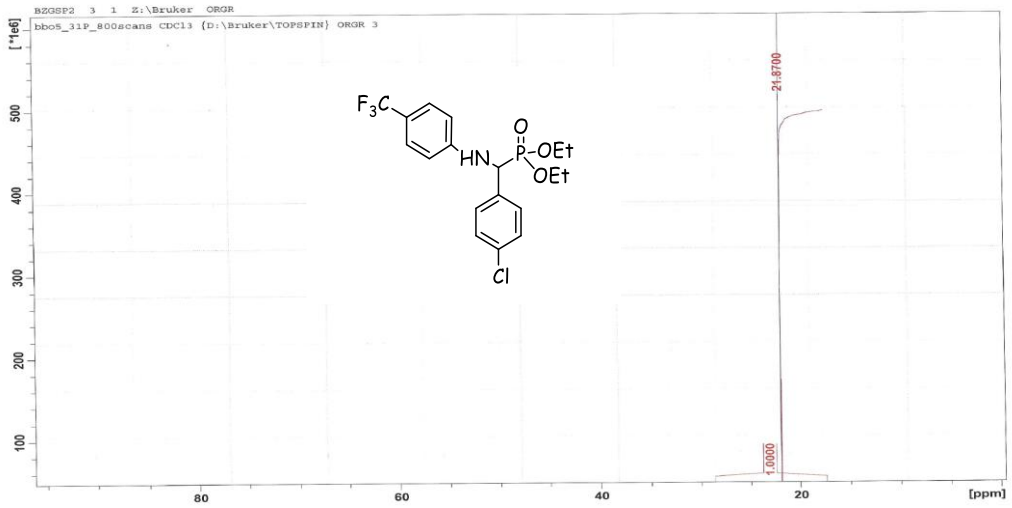

^{1}H, ^{13}C and^{31}P NMR of diethyl (4-methoxyphenyl)(4-trifluoromethylphenylamino) methylphosphonate (V.14r)

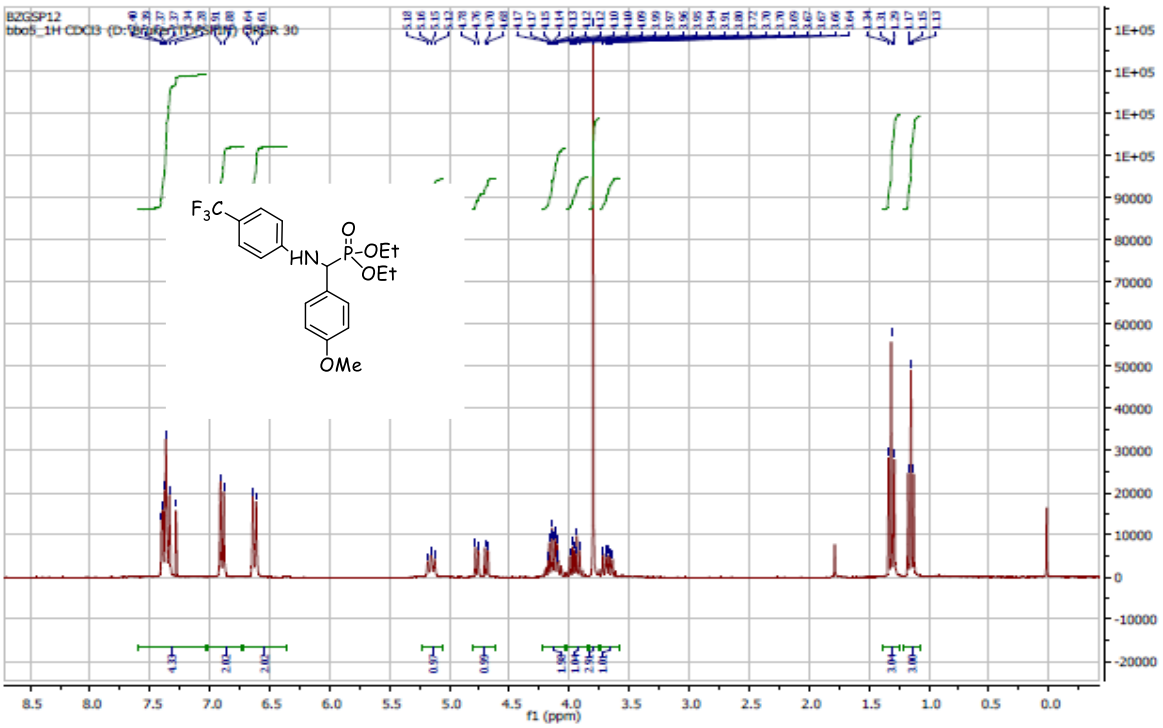

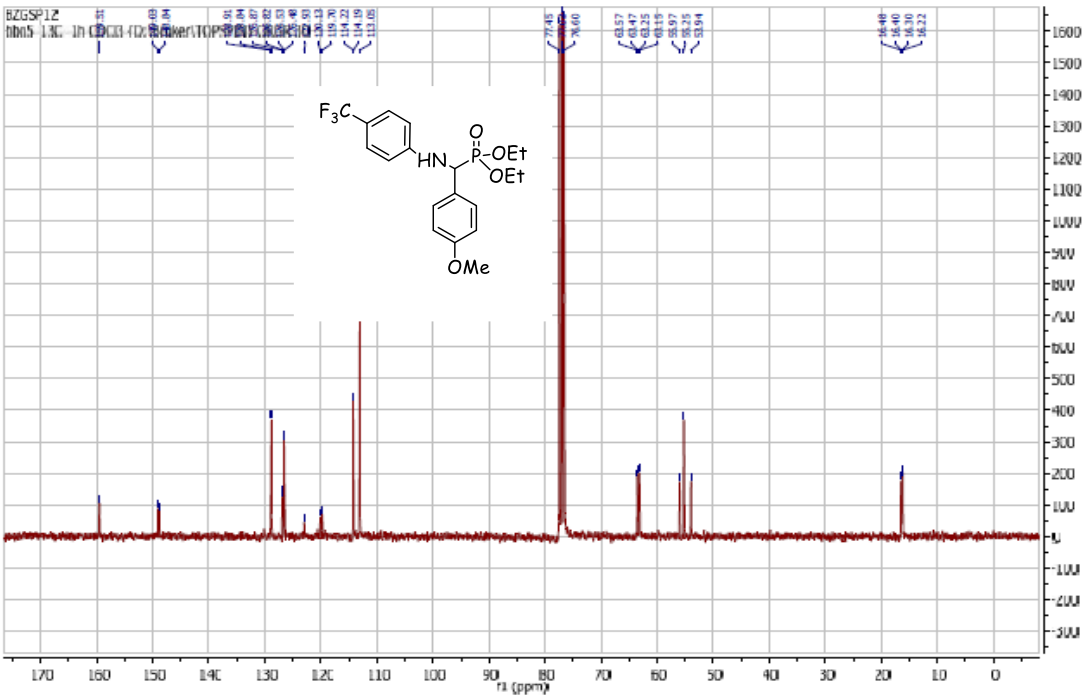

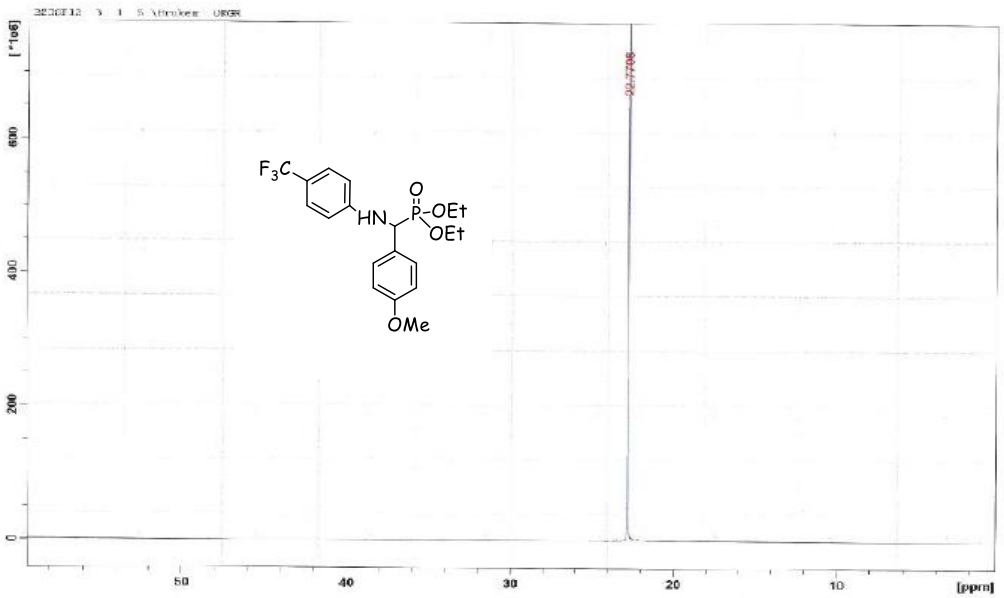

- **NMR spectra of kenitic resolution of acetates**

^{1}H and ^{13}C NMR of rac-1-(4-methoxyphenyl) ethanol (rac- VI.2)

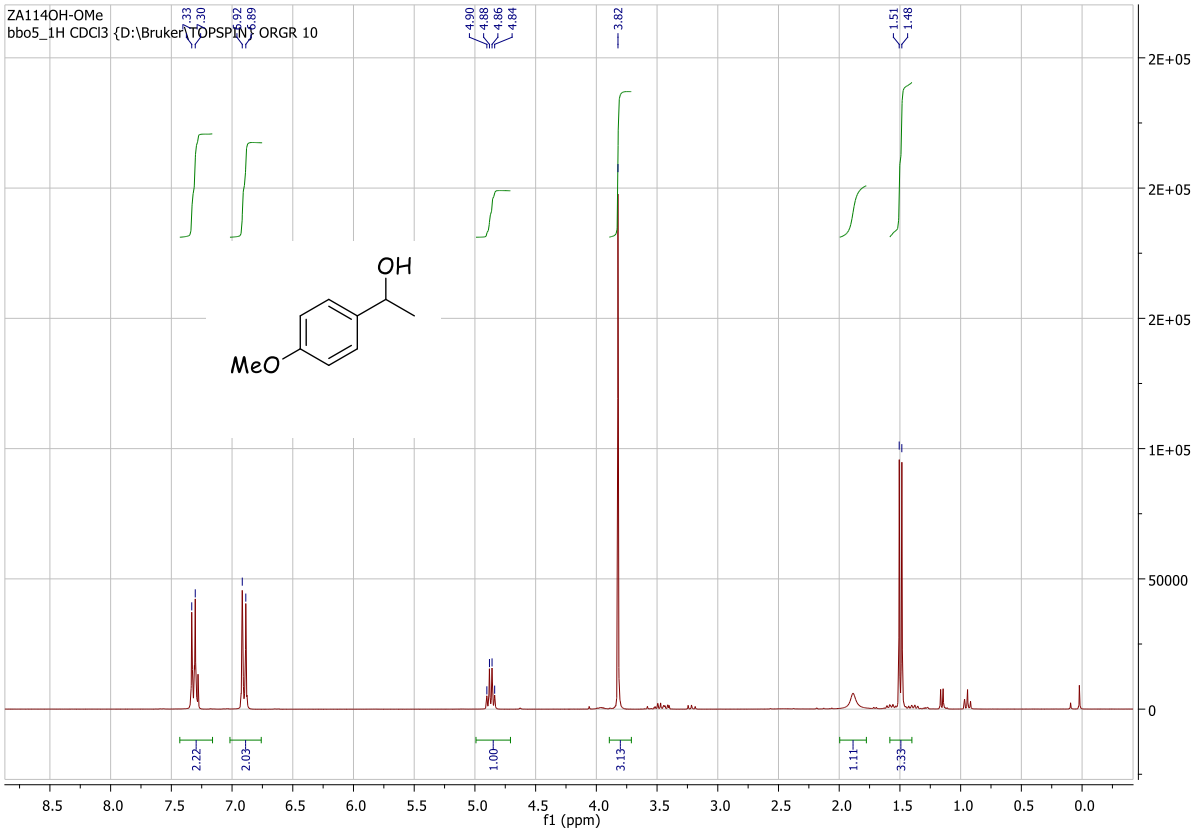

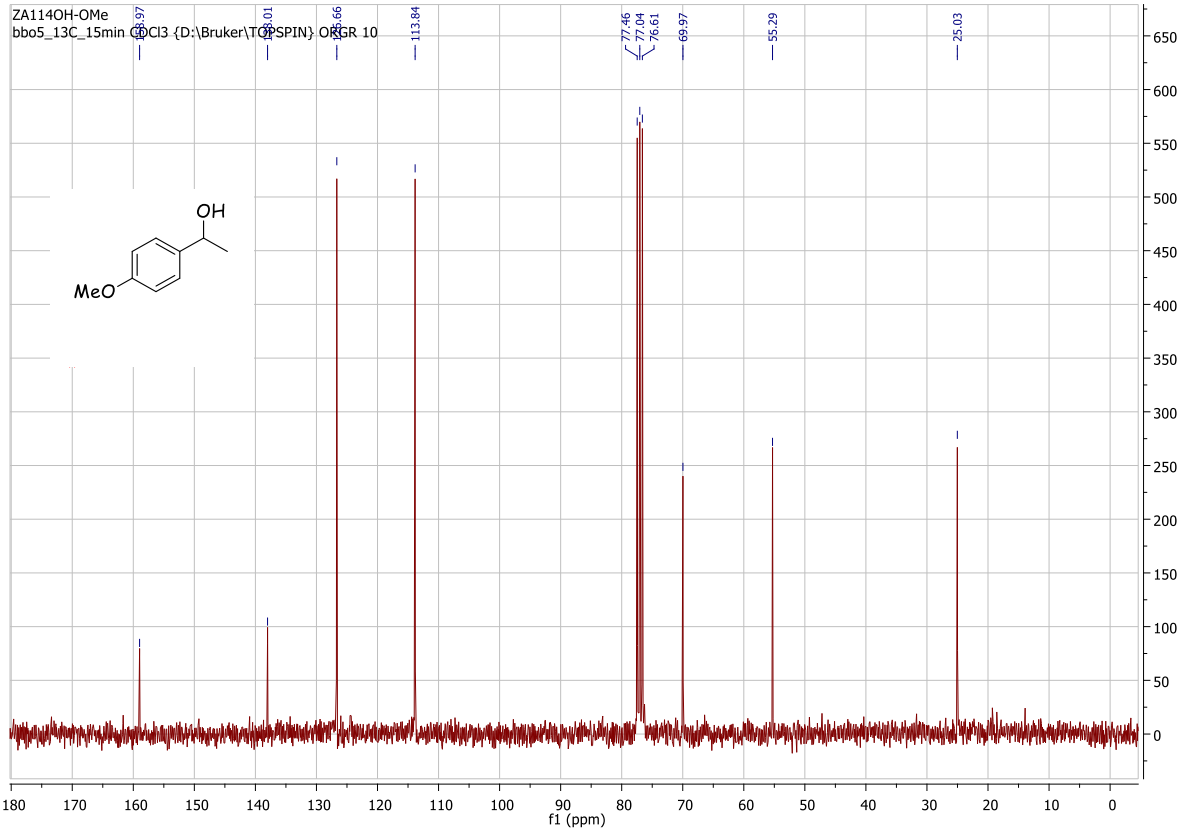

^{1}H and ^{13}C NMR of rac-1-(4-ethoxyphenyl) ethanol (rac- VI.3)

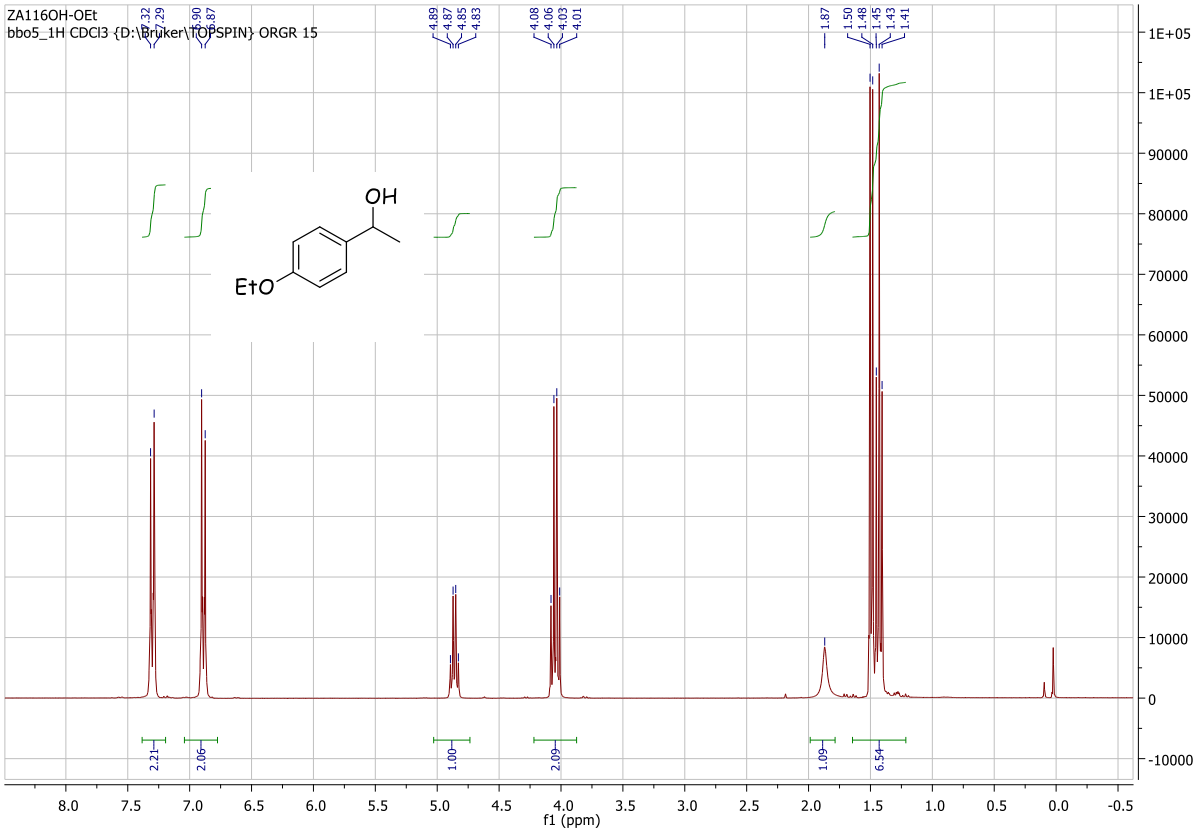

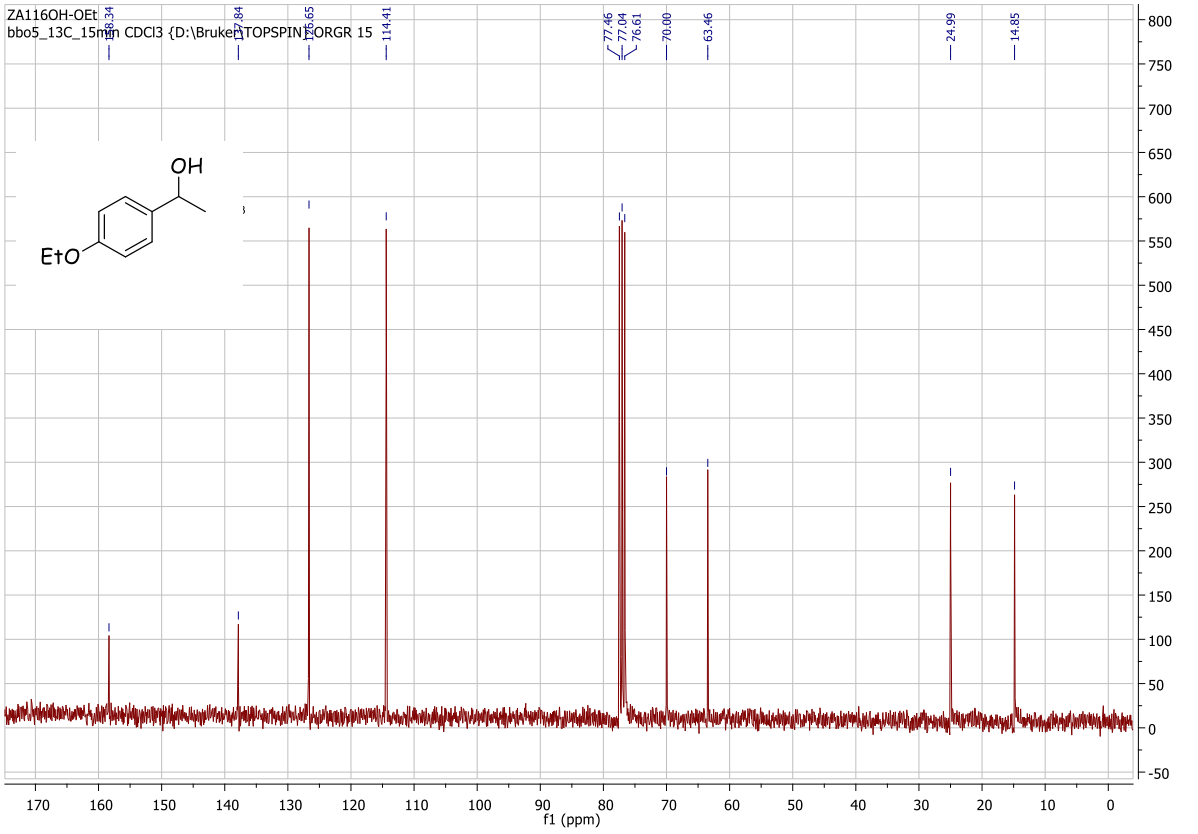

[1]H and [13]C NMR of rac-1-(6-methoxynaphthalen-2-yl) ethanol (rac- VI.6)

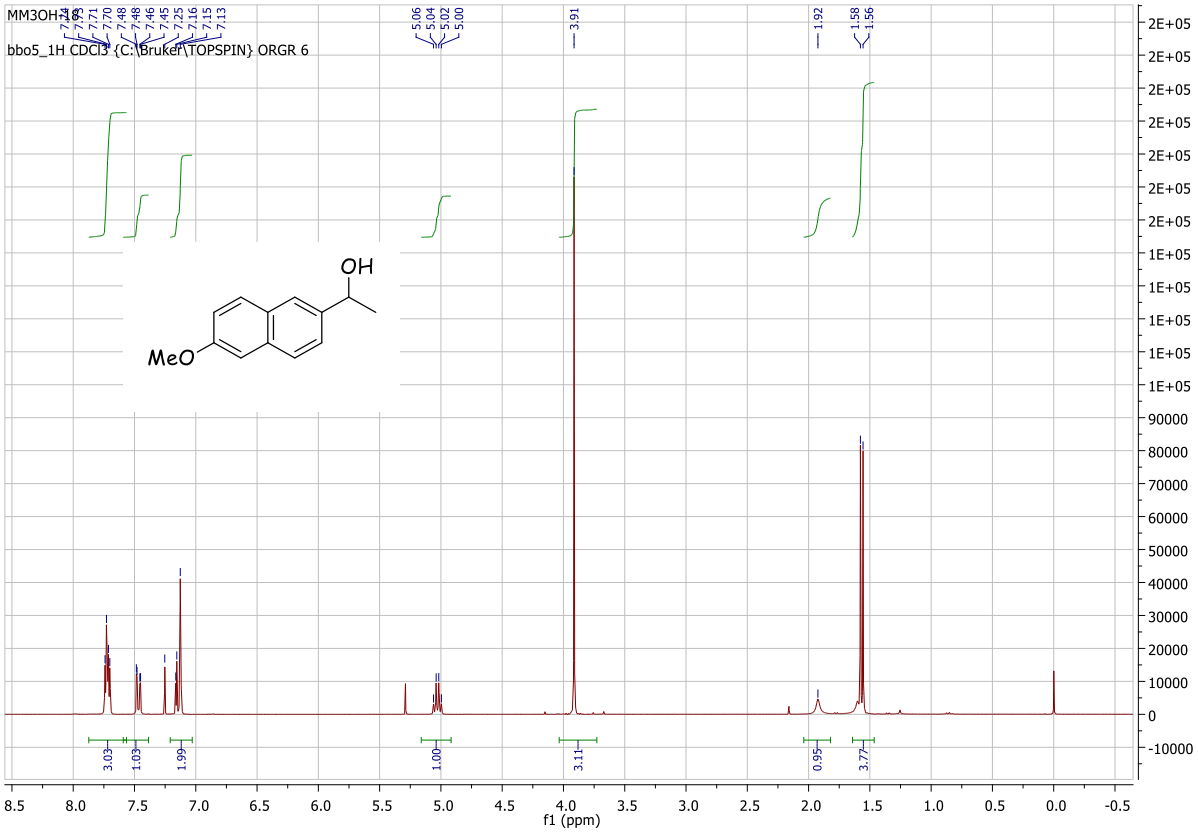

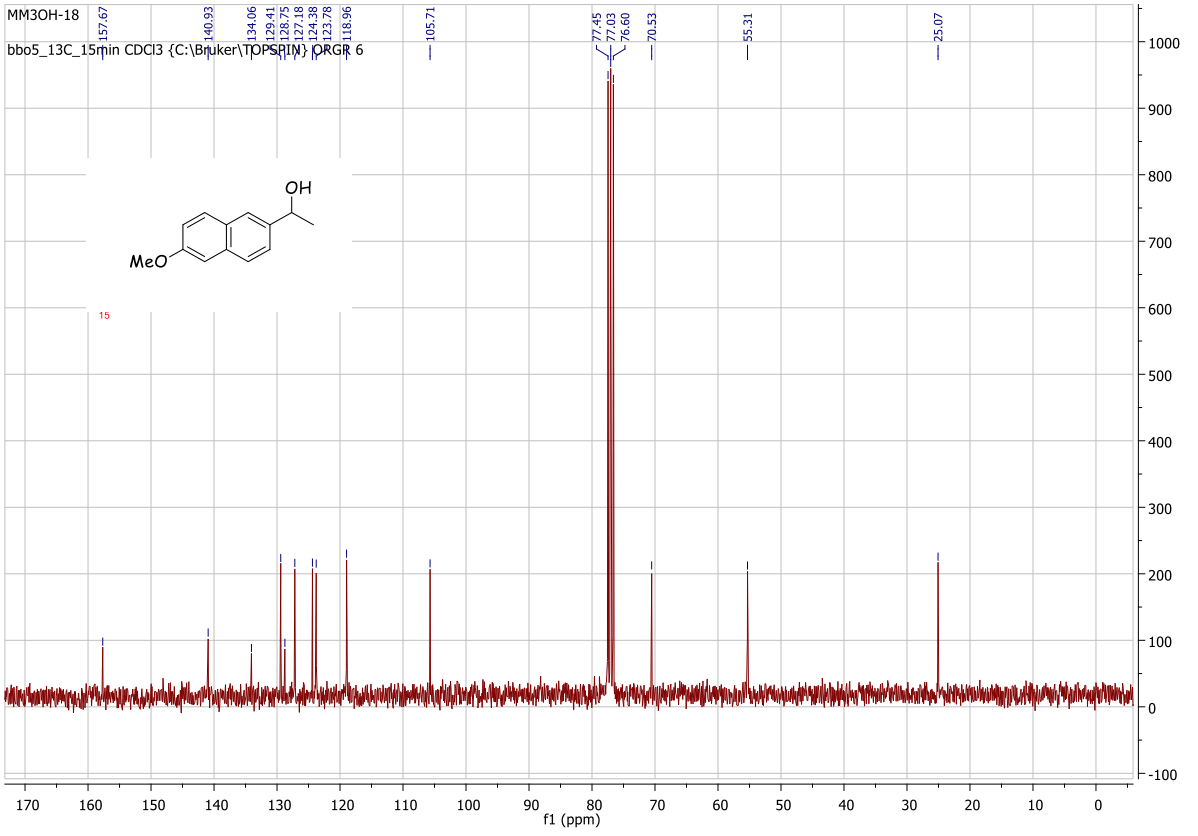

^{1}H and ^{13}C NMR of rac-Phenylethyl acetate (rac- VI.1a)

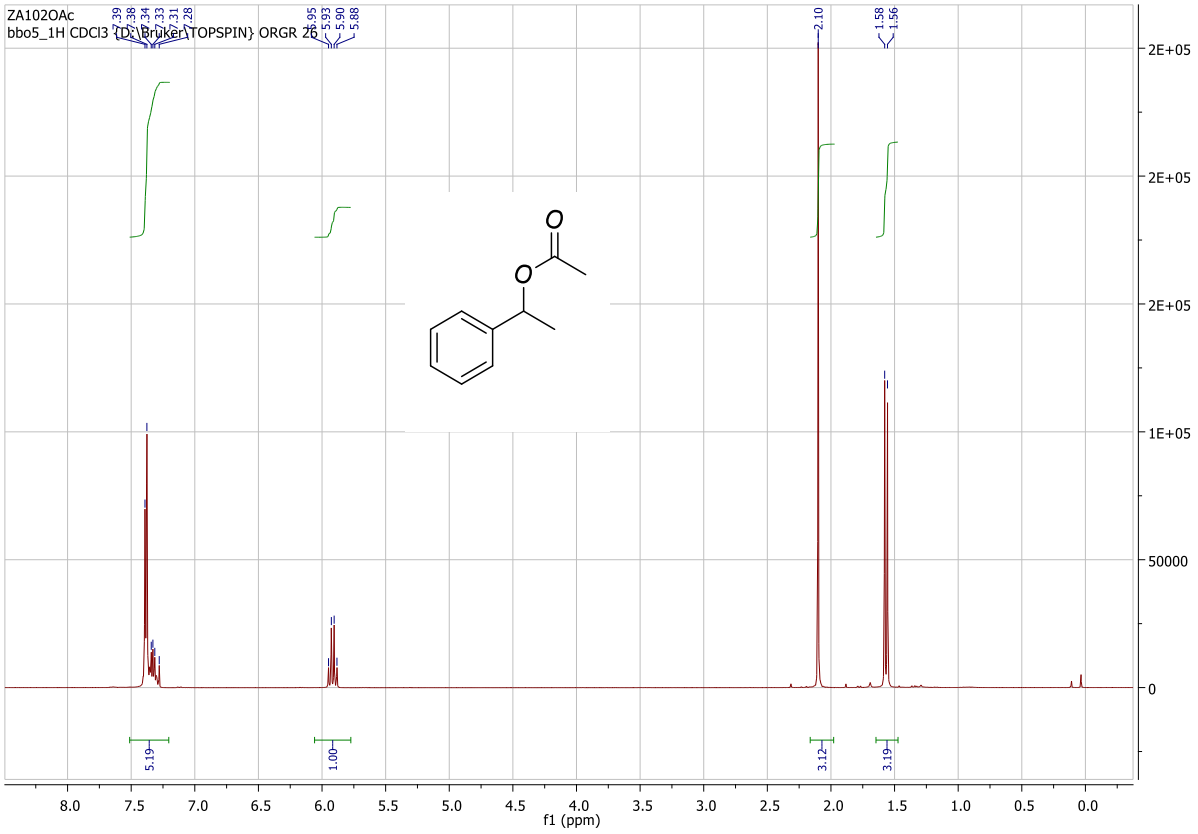

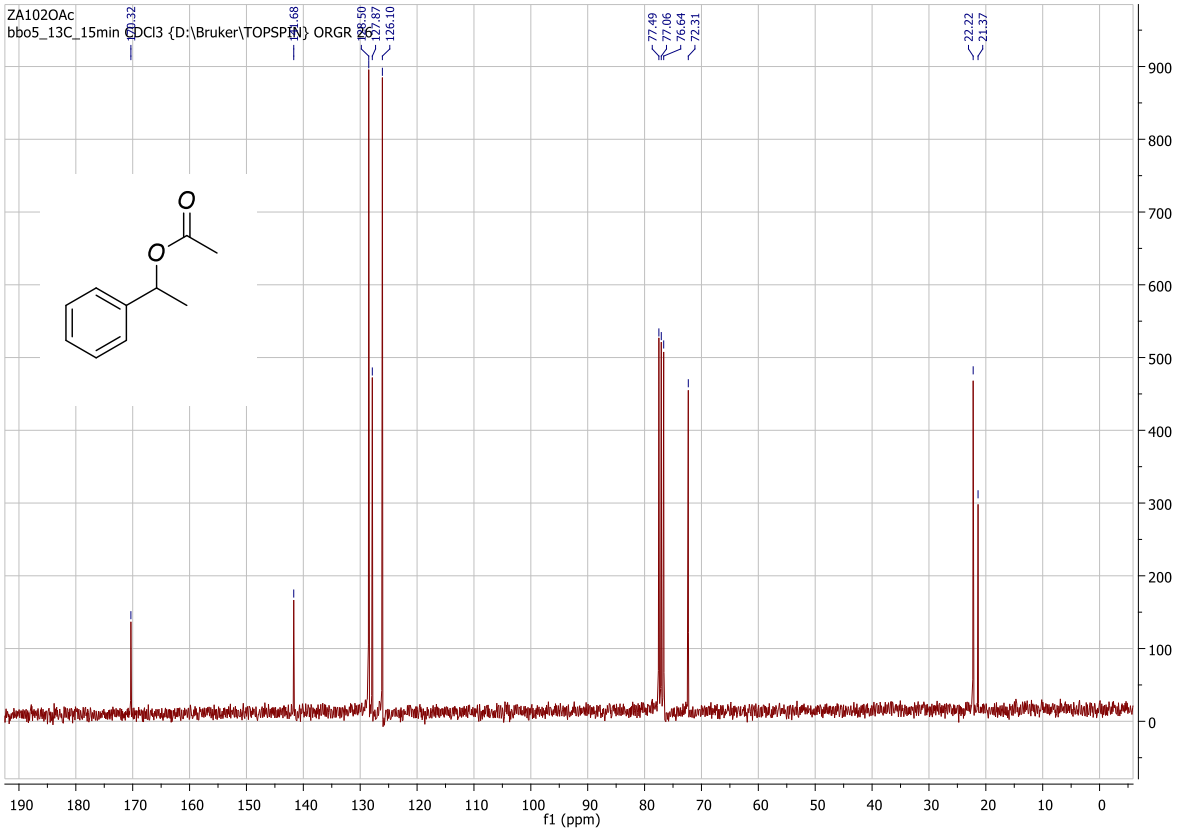

[1]H and [13]C NMR of rac-1-(4-methoxyphenyl)ethyl acetate (rac- VI.2a)

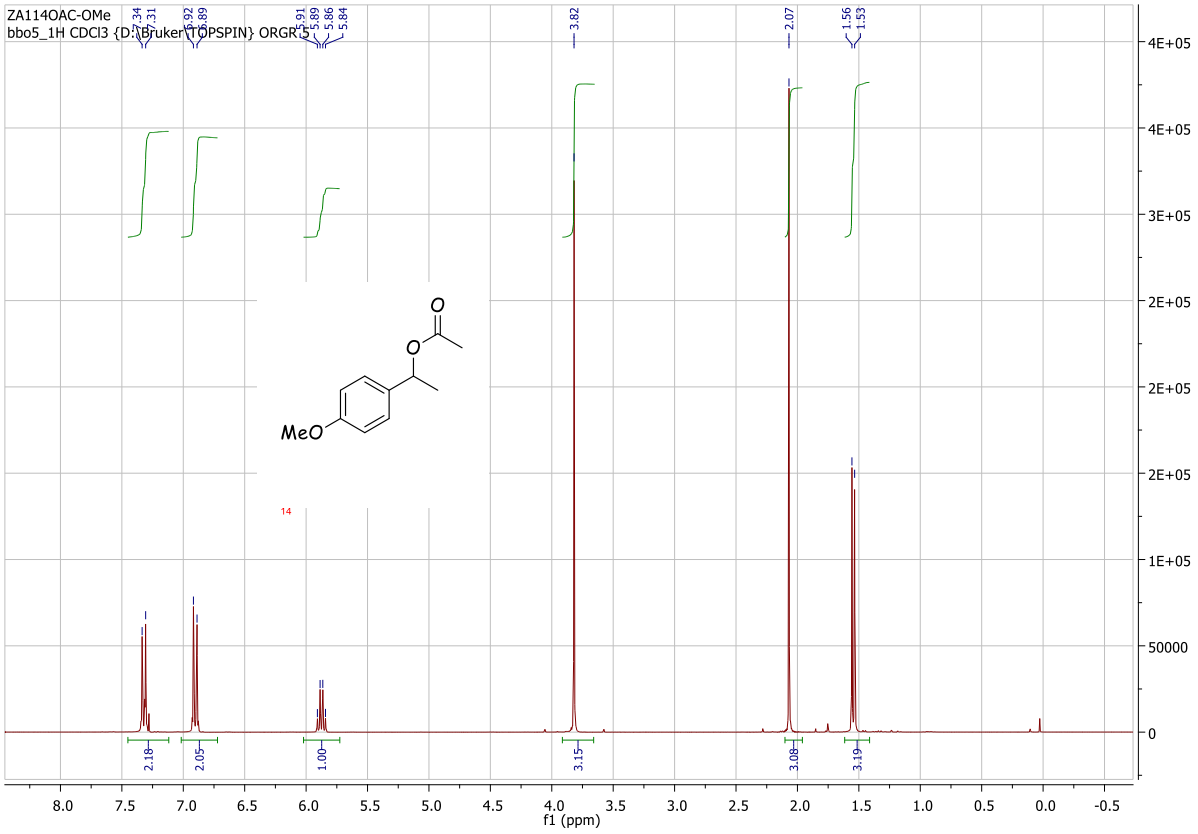
ZA114OAC-OMe
bbo5_1H CDCl3 {D:\Bruker\TOPSPIN} ORGR 5
7.34
7.31
6.92
6.89
5.91
5.89
5.86
5.84
3.82
2.07
1.56
1.53
O
O
MeO
14
2.18
2.05
1.00
3.15
3.08
3.19
4E+05
4E+05
3E+05
2E+05
2E+05
2E+05
1E+05
50000
0
8.0
7.5
7.0
6.5
6.0
5.5
5.0
4.5
4.0
3.5
3.0
2.5
2.0
1.5
1.0
0.5
0.0
-0.5
f1 (ppm)

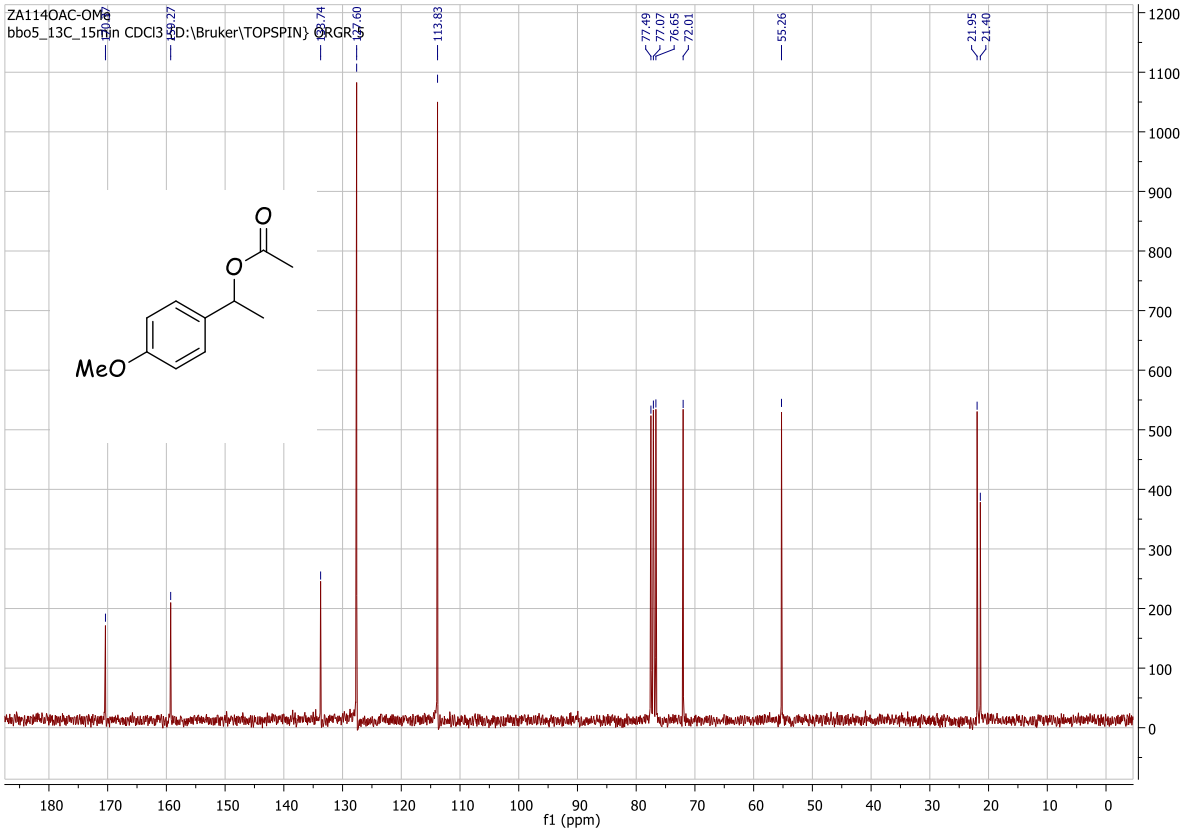
ZA114OAC-OMe
bbo5_13C_15min CDCl3 {D:\Bruker\TOPSPIN} ORGR 5
170.27
159.27
127.74
127.60
113.83
77.49
77.07
76.65
72.01
55.26
21.95
21.40
O
O
MeO
1200
1100
1000
900
800
700
600
500
400
300
200
100
0
180
170
160
150
140
130
120
110
100
90
80
70
60
50
40
30
20
10
0
f1 (ppm)

^{1}H and ^{13}C NMR of rac-1-(4-ethoxyphenyl)ethyl acetate (rac- VI.3a)

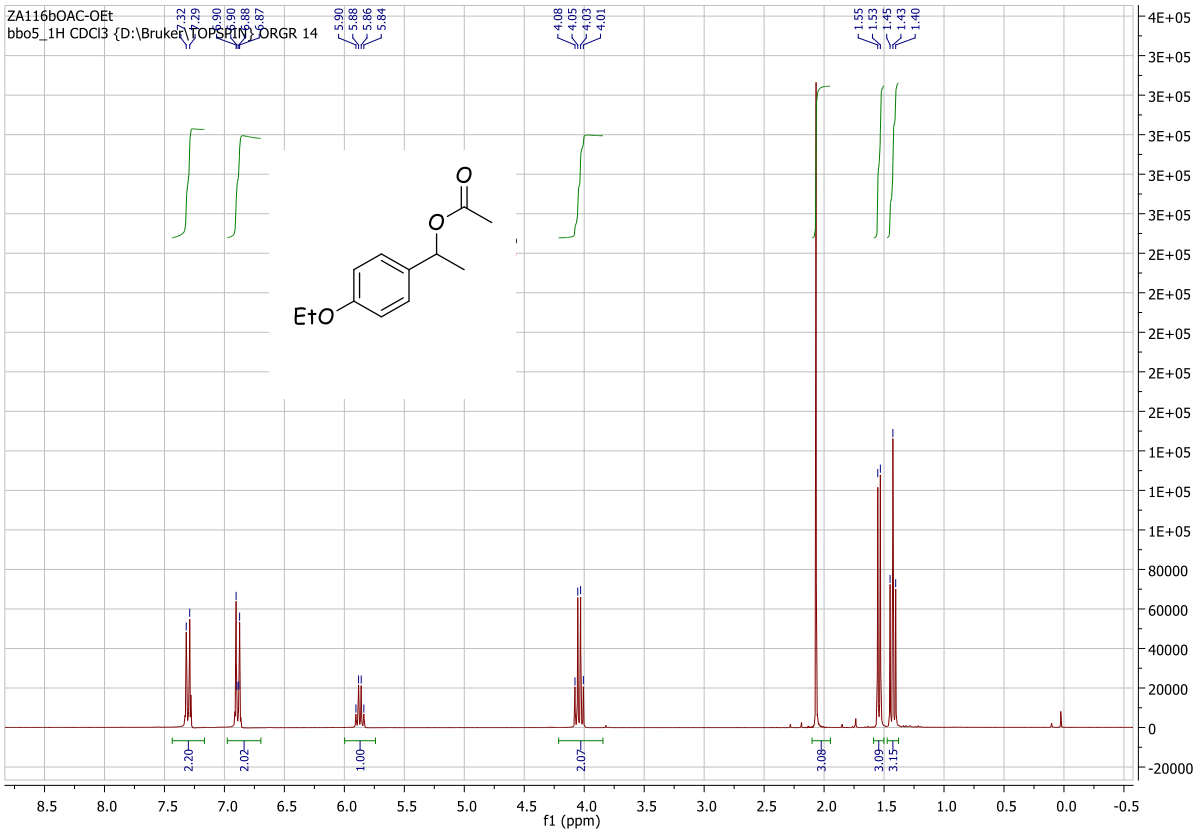

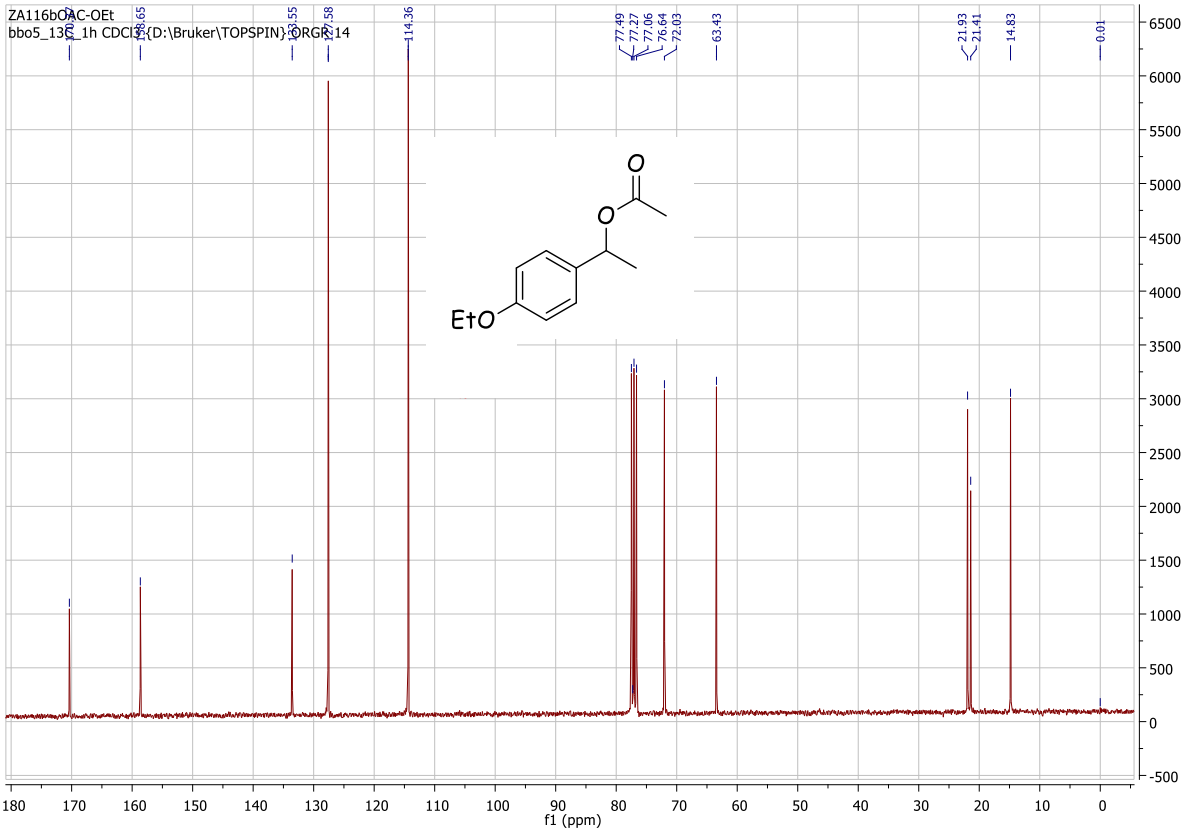

[1]H and [13]C NMR ofrac-1-(naphthalen-1-yl)ethyl acetate (rac- VI.4a)

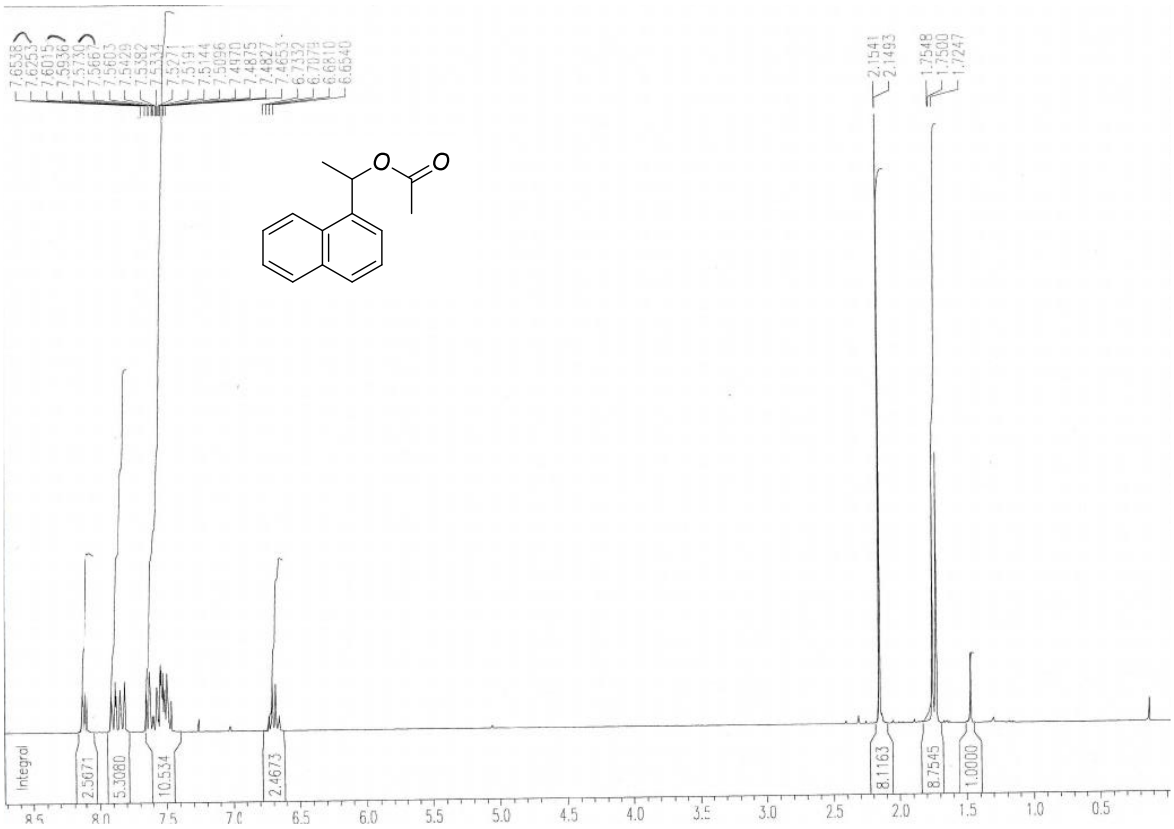

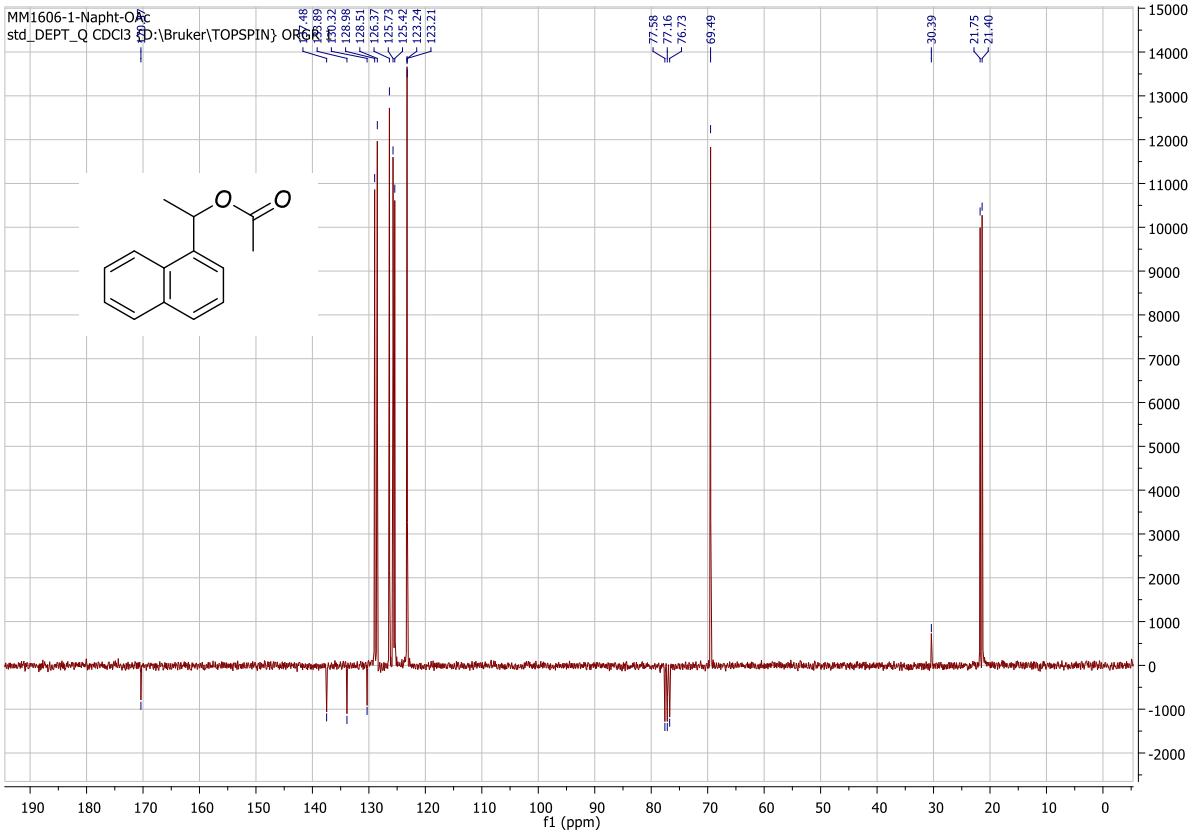

[1]H and [13]C NMR of rac-1-(naphthalen-2-yl)ethyl acetate (rac-VI.5a)

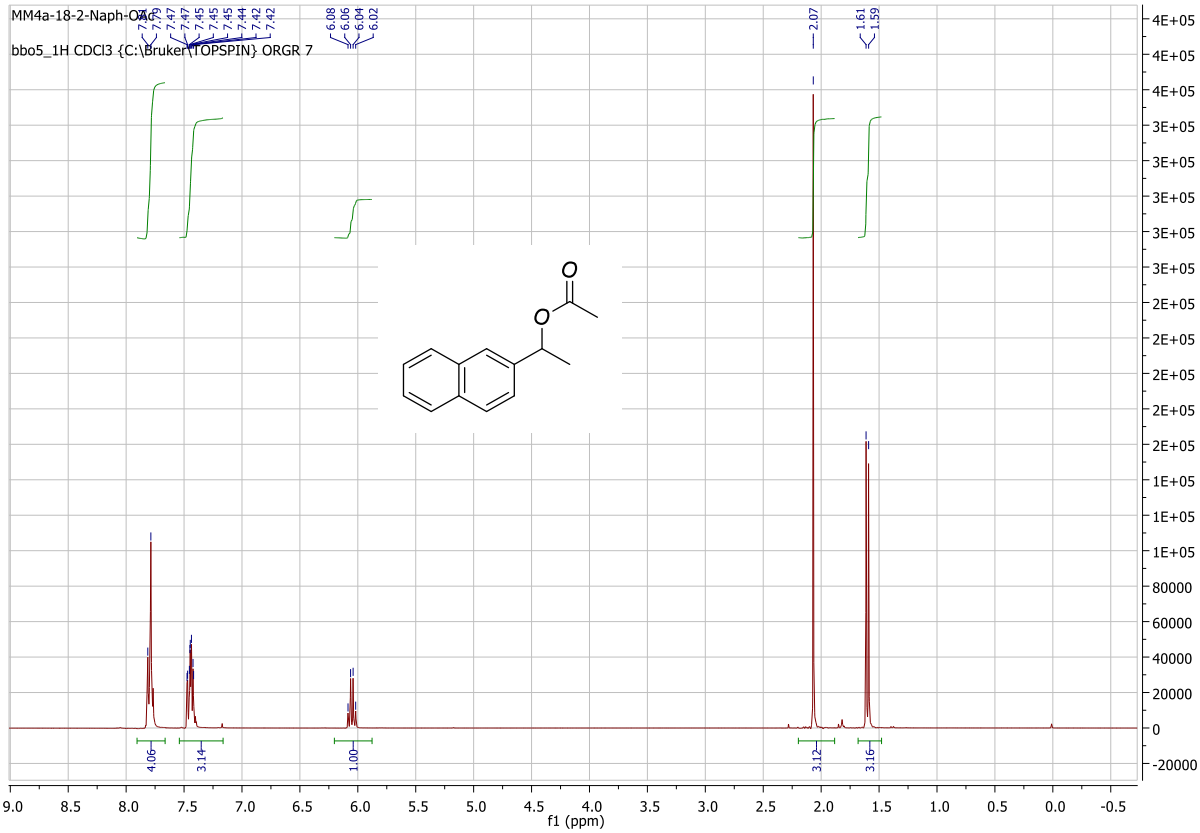

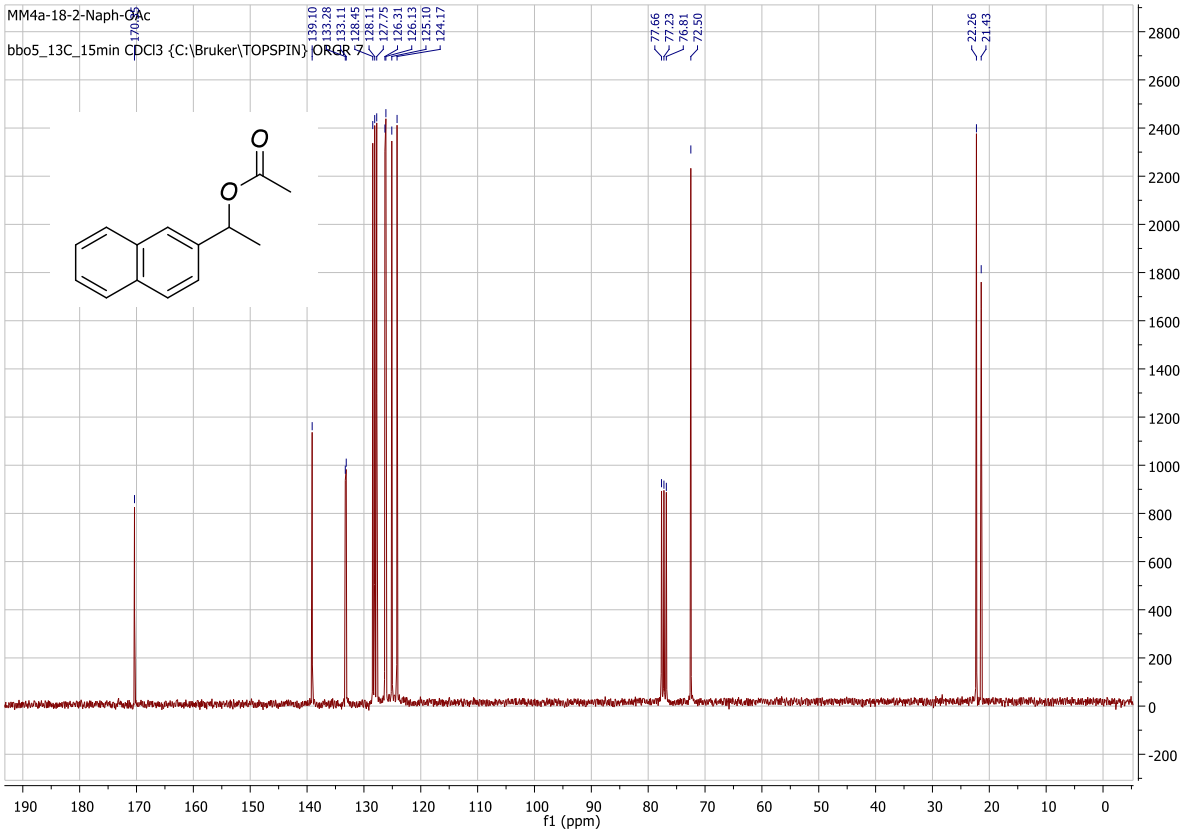

[1]H and [13]C NMR of rac-2,3-dihydro-1H-inden-yl acetate (rac-VI.7a)

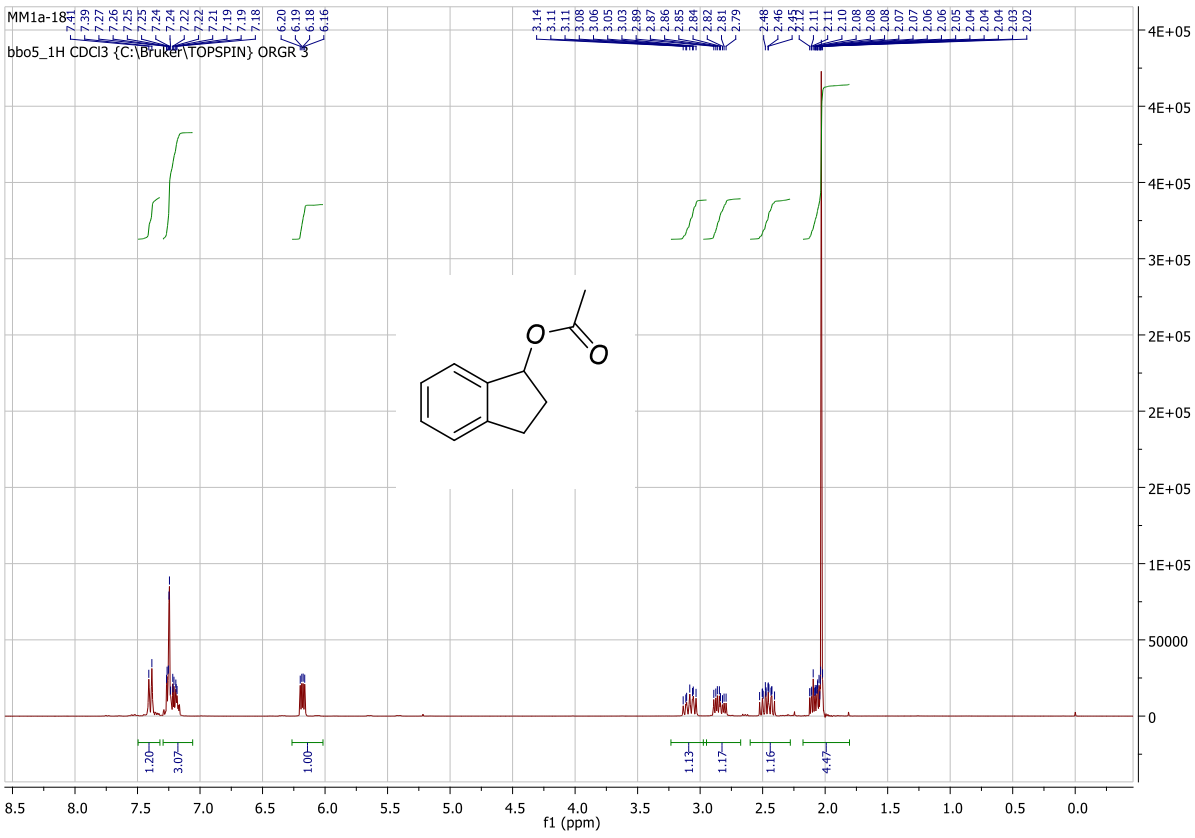

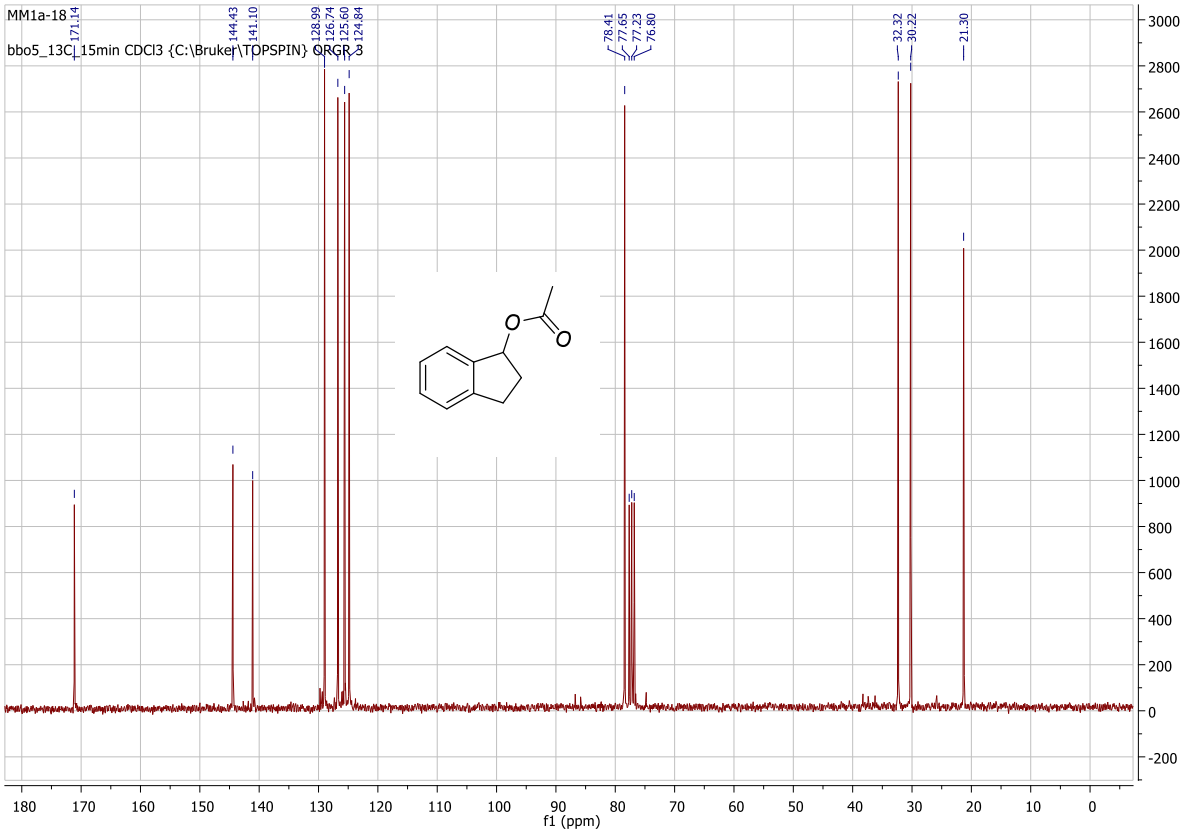

^{1}H and ^{13}C NMR of rac-1,2,3,4-tetrahydronaphthalen-1-yl acetate (rac-VI.8a)

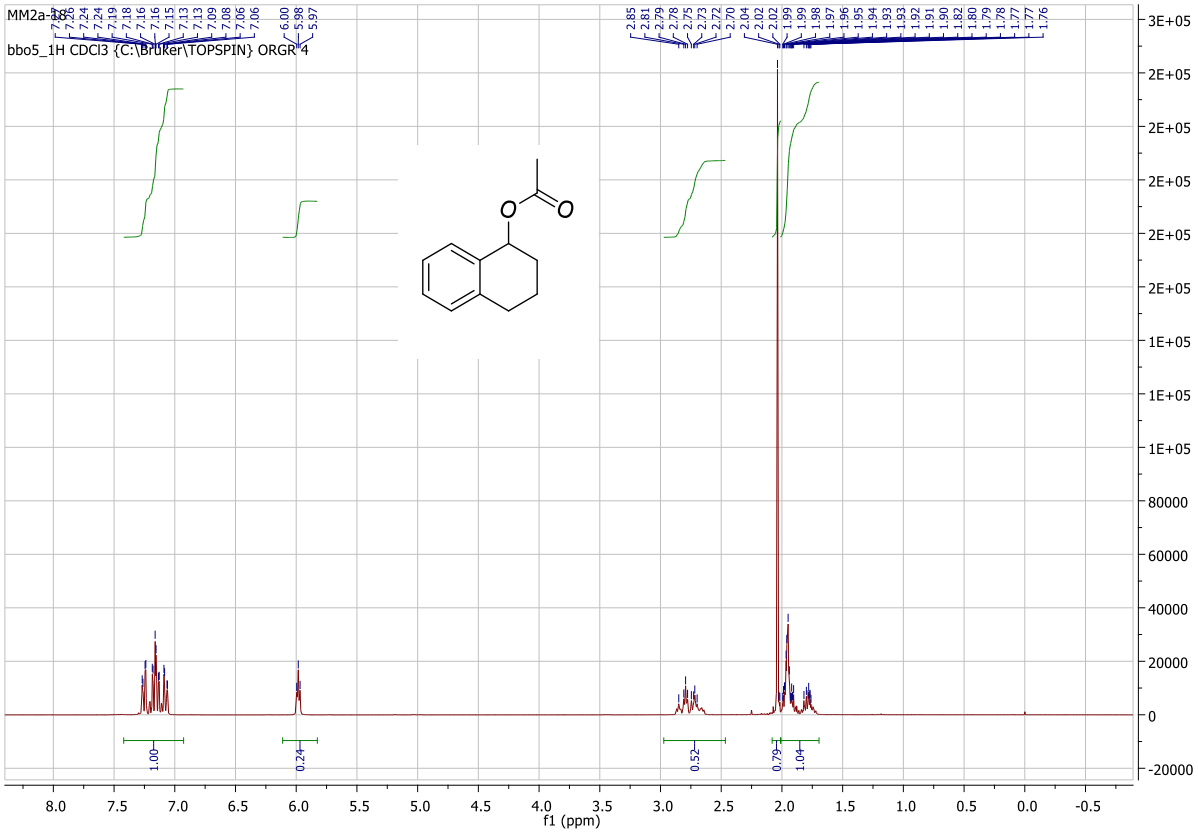

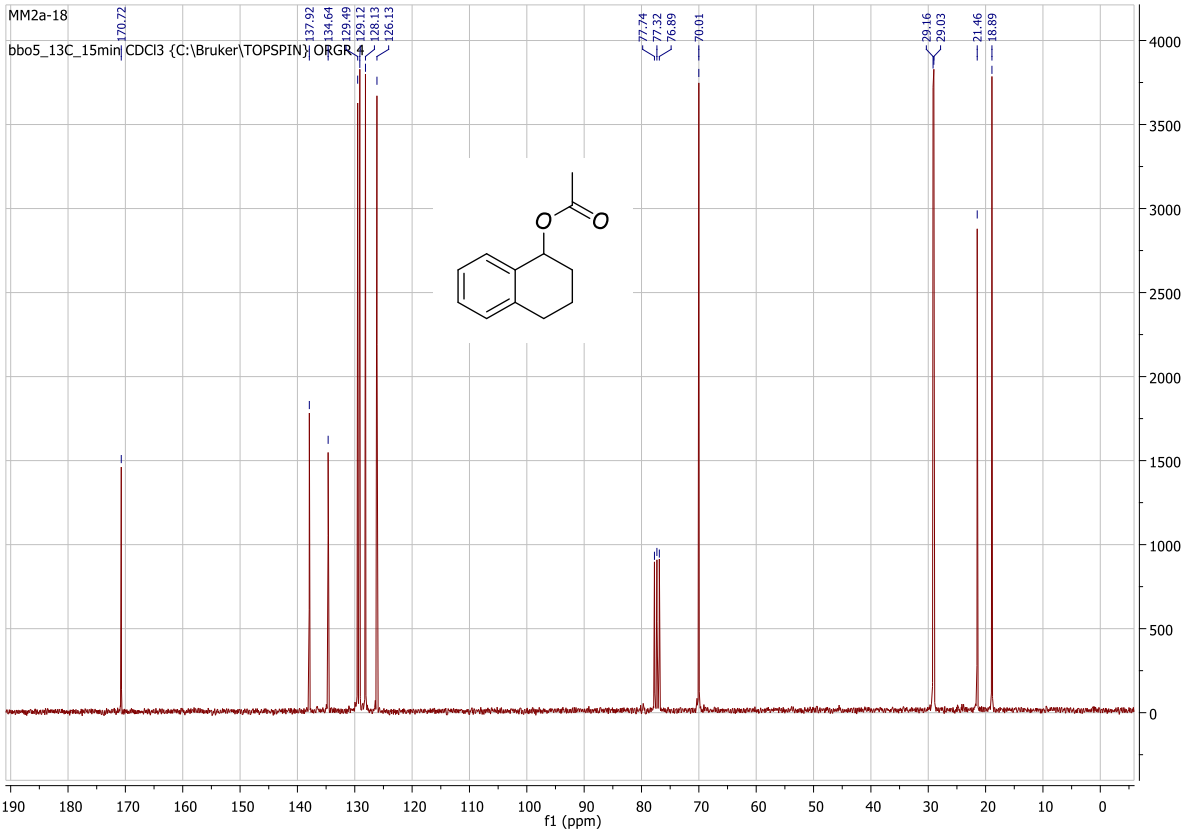

Chromatograms of some markedly results.

***rac-VI.*1a + *rac-VI.*1**	**Table 2: Entry 1** 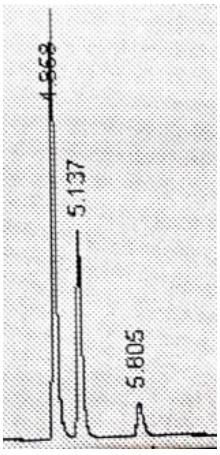 **Table 2: Entry 3**

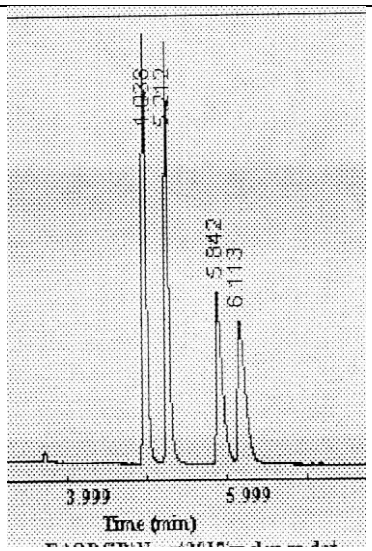

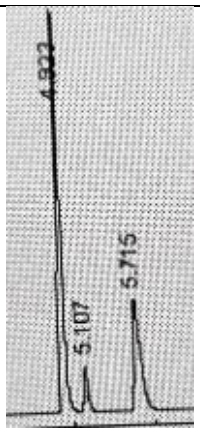

Table 2: Entry 11

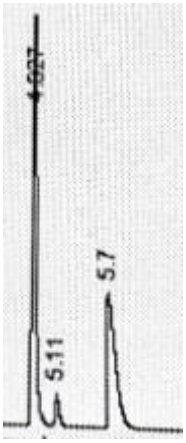

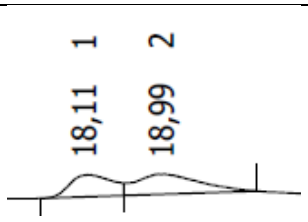

rac-VI.2

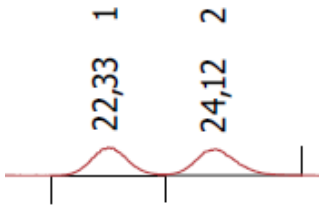

rac-VI.2a

Table 3: Entry 2

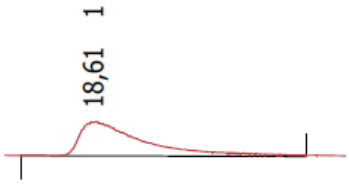

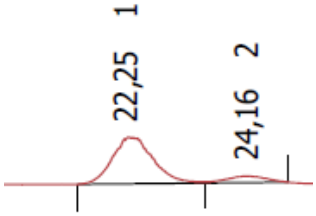

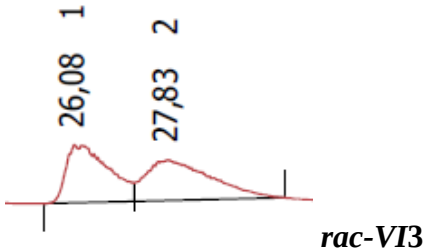

*rac-VI*3

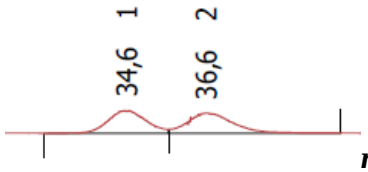

rac-

***VI*.3a**

Table 3: Entry 3

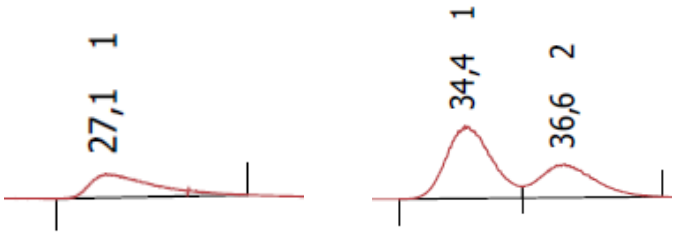

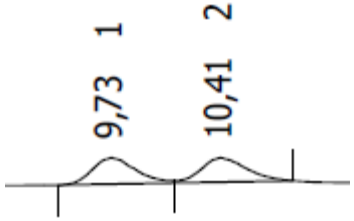

rac-

***VI*.4**

Table 3: Entry 12

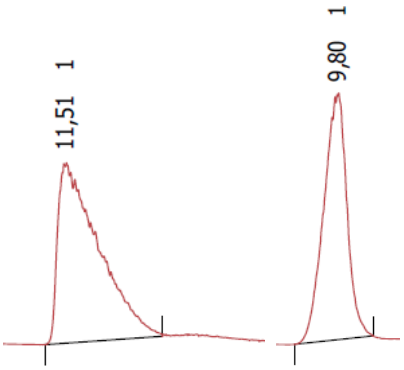

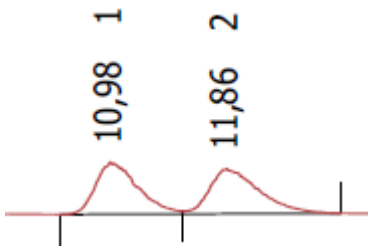

rac-

***VI*.5**

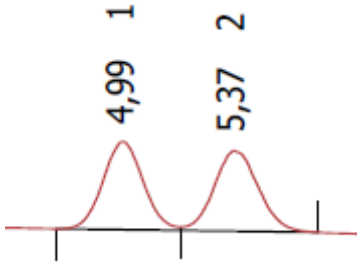

rac-

Table 3: Entry 13

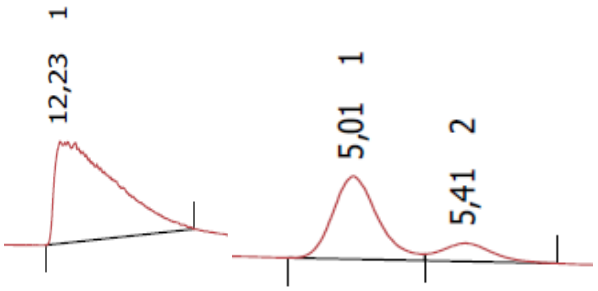

***VI*.5a**	
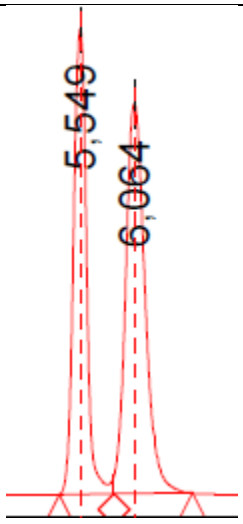 ***rac-VI*.6a** 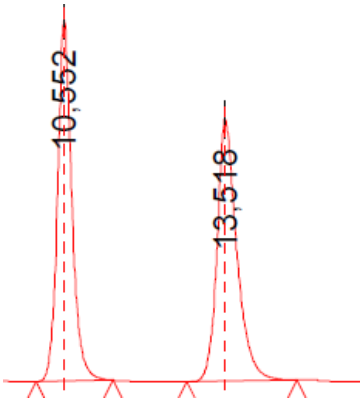 ***rac-VI*.6**	**Table 3: Entry 6** 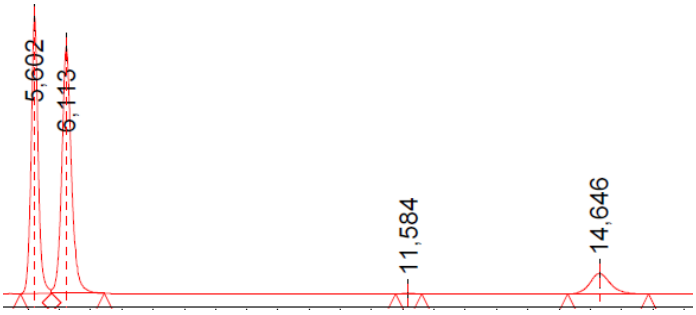 **Table 3: Entry 14** 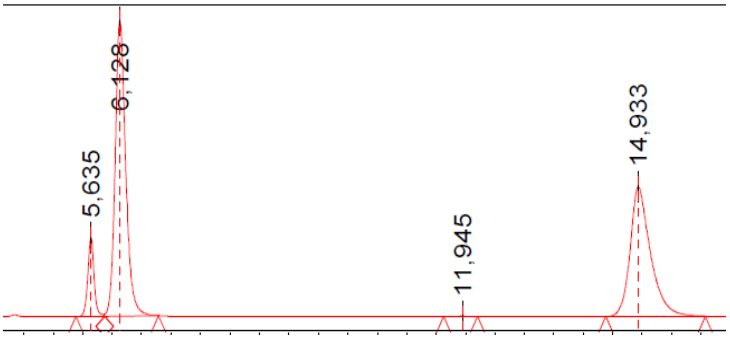

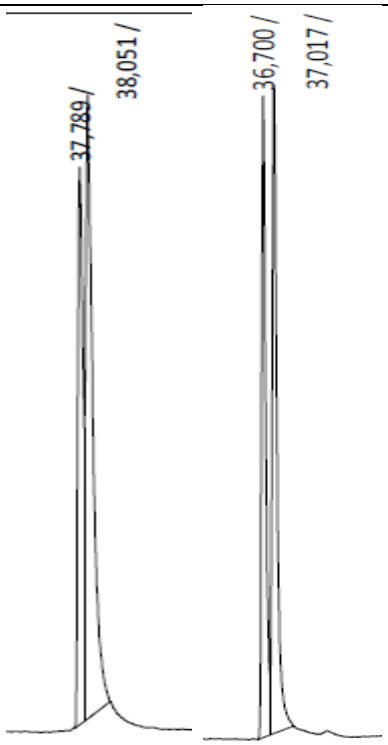

***rac-VI*.7a** ***rac-VI*.7**

Table 3: Entry 7

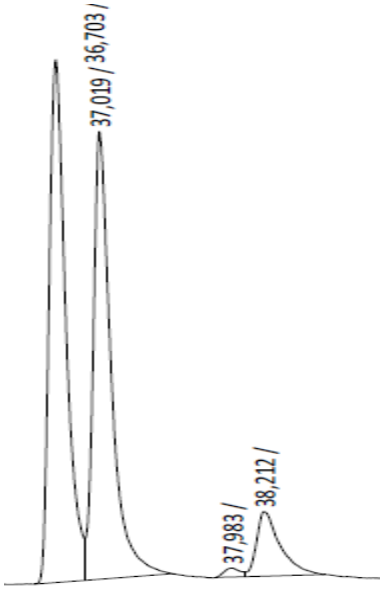

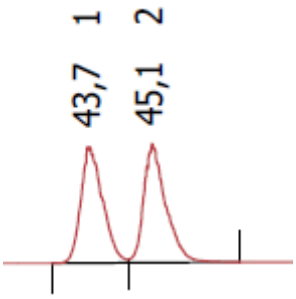

***rac-VI*.8a**

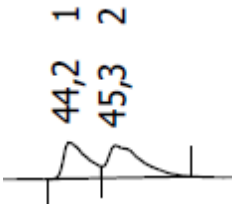

***rac-VI*.8**

Table 3: Entry 8

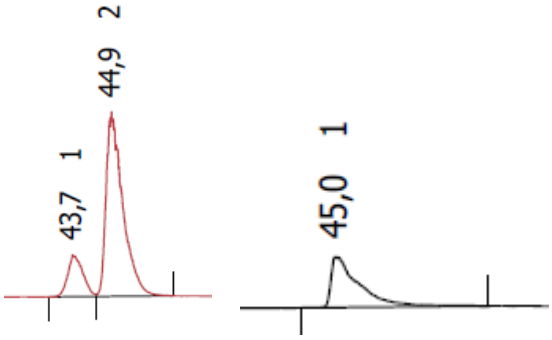

Reaction Kinetics, Mechanisms and Catalysis (2023) 136:165–182
https://doi.org/10.1007/s11144-022-02329-0

Full factorial optimization of *α*-aminophosphonates synthesis using diphenylphosphinic acid as efficient organocatalyst

Meriem Ferrah[1] · Samia Guezane-Lakoud[1] · Hacene Bendjeffal[2] · Rym Aissa[1] · Mounia Merabet-Khelassi[1] · Martial Toffano[3] · Louisa Aribi-Zouioueche[1]

Received: 2 October 2022 / Accepted: 11 November 2022 / Published online: 21 November 2022

Abstract

Diphenylphosphinic acid was used as an efficient and simple catalyst for the synthesis of the α-aminophosphonates by multicomponent *Kabachnik-Fields* reaction in one pot of aromatic aldehyde, aniline and diethylphosphite. Three physicochemical factors including catalyst amount, reaction time and medium temperature were optimized using a full factorial experiment design (FFD). Additionally, a quadratic polynomial regression model was applied for the analysis of the experimental data at a confidence level of 95% with p-values < 0.05. The high signification effect of the reaction time and the medium temperature on the α-aminophosphonates synthesis were confirmed by the statistical analysis. Besides, the diphenylphosphinic acid amount showed an effect on the reaction yield. ANOVA exhibited that the coefficient determination of this model up to 99.25%. This eco-friendly procedure was extended for the preparation of series of the α-aminophosphonates in ethanol as green solvent, giving the desired products with high chemical yields up to 90%.

Keywords α-aminophosphonates · Full factorial experiment · Diphenylphosphonic acid · *Kabachnik-Fields* reaction · Organocatalyst

✉ Samia Guezane-Lakoud
samia.guezanelakoud@univ-annaba.dz

[1] Ecocompatible Asymmetric Catalysis Laboratory (LCAE), Badji Mokhtar Annaba-University, B.P 12, 23000 Annaba, Algeria

[2] Laboratory of Physical Chemistry and Biology of Materials, Higher Normal School of Technological Education (ENSET), 21000 Skikda, Algeria

[3] Equipe de Catalyse Moléculaire-ICMMO Bât 420, Université Paris-Saclay, Saclay, France

Introduction

As an important class in organic synthesis, medicinal chemistry and biological activities, organophosphorus compounds have attracted an intensively growing interest and fascinating applications in agricultural and industrial [1–3]. The α-aminophosphonates has represented, from its discovery by *Kabachnik-Fields* [4, 5] to nowadays an important class of organophosphorus compounds due to their analogs amino acid, and mimic transition states of active peptides [6–8]. The α-aminophosphonates have shown an outstandingly broad spectrum of pharmacological and physiological effectiveness [9–11], and they were used as inhibitors of the angiotensin-converting enzyme [12], antiviral [13], antibiotic [14], antibacterial [15], antitumoral [16], anti-HIV [17], antihypertensive [18], anti-tuberculosis agents [19], anti-oxidant [20, 21], anticorrosion [22], herbicides, fungicides and insecticides [23, 24]. In reactivity terms, the α-aminophosphonates were used as a key intermediate in HWE reaction [25], as organocatalyst in the Petasis Boronic Acid, *Mannich* reaction [26], in asymmetric *Michael* addition [27], and for the preparation of complexes as tridentate ligands [28].

Meanwhile, the multicomponent reaction via *Kabachnik-Fields* is still a crucial and highly valuable method for their synthesis using a wide range of catalysts, such as *Lewis* and *Brønsted* acids [29–31], organocatalysts [32–34], nano-materials [35], heteropolyacids [36] and β-cyclodextrin [37].

Due to the overwhelming development of the α-aminophosphonates in synthetic and biological fields, the efficient catalysts are widely requested for their preparation and increase their productivity. Unfortunately, few investigations were dedicated to developing this multicomponent reaction under green conditions; many reactions used costly catalysts, a stoichiometric amount of catalysts, long reaction time, and production of by-products. The last one can cause a considerable ecological problem related to their chemical properties. Therefore, the development of a new effective catalytic process using a low-cost and eco-friendly catalyst is considered a valuable approach to preparing these compounds.

In the continuation of our ongoing research interest for novel synthetic derivatives of organophosphorus compounds [38–42], herein, we report the successful employ of diphenylphosphinic acid as an efficient catalyst in multicomponent condensation reaction aromatic aldehyde, aniline, and diethylphosphite. However, the diphenylphosphinic acid was previously tested in multicomponent reaction and the desired product was obtained with 76% chemical yield [43]. Nevertheless, this catalytic process is sensitive to various operational parameters, including the catalyst amount, reaction time and medium temperature. Furthermore, studying the effect of each factor alone is considered a rather tedious and costly synthetic process (time, cost and energy depenses). For these reasons, we have opting to use the full factorial design for diminution of the experimental difficulties by the optimization of all the affecting parameters together at the same time to optimize the effectiveness of our proposed target under green conditions reaction.

Experimental section

General

All reagents were purchased from Sigma-Aldrich or Acros Company used without further purification. Reactions were monitored by thin-layer chromatography (TLC) carried out on 0.25-mm Merck silica gel plates (60F-254) using ultraviolet light (254 nm) as the visualizing agent and $KMnO_4$ solution as developing agents. NMR spectra were recorded with Bruker spectrometers operating at (400, 360, 300, and 250 MHz for 1H, 90, 75 or 63 MHz for ^{13}C, and 162, 101 or 121 MHz for ^{31}P). The chemical shift of Solvent reference peaks used were $CDCl_3$ ($\delta = 7.26$ ppm) for 1H and ($\delta = 77$ ppm) for ^{13}C NMR spectra, while H_3PO_4 was used as external standard for chemical shift references for ^{31}P NMR. Couplings constants (*J*) are given in Hz, with the following abbreviations multiplicity: s = singlet, d = doublet, t = triplet, q = quartet, m = multiplet, br = broad signal. Mass spectra were taken by a MicrOTOF-Q Bruker spectrometer using electrospray ionization (ESI) analysis. Melting points were measured using Buchi Melting Point B-545.

General procedure for the synthesis of α-aminophosphonates 4a-4i

The diphenylphosphinic acid (10 mol%) was added to the reaction mixture of aromatic aldehyde (122.12 mg, 1 mmol), aniline (93 mg, 1 mmol) and diethylphosphite (165 mg, 1.2 mmol) in ethanol (10 mL). The reaction was stirred at 40 °C for 30 min. The progress of the reaction was monitored by TLC. The solvent was removed and the resulting residue was treated with HCl (1 N) then washed with water (10 ml) and extracted with dichloromethane (10 ml × 2). The organic phases were combined and evaporated in vacuum. The crude product was purified by crystallization in hexane. Complete experimental data have been provided (NMR spectra and HRMS).

Diethyl [Phenyl(phenylamino)methyl] phosphonate (4a)

Yield: 92%, as a white crystalline solid; mp 88 °C. ^1H NMR (250 MHz, $CDCl_3$, 25 °C) δ 7.52–7.40 (m, 2H, HAr), 7.33–7.29 (m, 3H, HAr), 7.16–7.10 (t, 2H, J = 7.9 Hz, HAr), 6.75–6.69 (t, 1H,, J = 7.3 Hz, HAr), 6.64–6.61 (m, 2H, HAr), 4.84–4.75 (d, 1H, $J_{HP} = 24.3$ Hz, HC*), 4.18–4.10 (2H, m, –O–CH_2–CH_3), 4.01–3.76 (1H, m, –O–CH_2–CH_3), 3.74–3.63 (1H, m, –O–CH_2 CH_3), 1.31 (t, 3H, J = 7.1 Hz, –O–CH_2–-CH_3), 1.14 (t, 3H, J = 7.1 Hz, –O–CH_2–CH_3). ^{13}C NMR (63 MHz, $CDCl_3$, 25 °C) δ 146.33 (d, J = 14.5 Hz); 136.00, 129.29, 128.74, 128.71, 128.00, 127.03, 118.40, 113.87, 63.27 (d, $J^2_{CP} = 6.9$ Hz), 57.29, 54.90, 16.46, (d, $J^3_{CP} = 15.1$), 16.37 (d, $J^3_{CP} = 5.6$ Hz). ^{31}P NMR (101 MHz, $CDCl_3$, 25 °C) δ 22.46 ppm. HRMS (ESI) m/z calcd for $C_{17}H_{23}NO_3P$ [M + H^+]: 320.1408; Found 320.1410.

Diethyl (3-methoxyphenyl) (phenylaminomethyl) phosphonate (4b)

Yield: 98%, as a white crystalline solid; mp103 °C.^{1}H NMR (300 MHz, $CDCl_3$, 25 °C) δ 7.36–7.30 (m, 2H, HAr), 7.07–7.13 (m, 2H, HAr), 6.85 (d, $J=7.3$ Hz, 2H, H Ar), 6.66 (t,$J=16.0$ Hz, 1H, HAr), 6.58 (d, 2H, $J=8.5$ Hz, HAr), 4.72 (d, $J=24.4$ Hz, 1H, CHP), 4.15 (m, 2H, OCH_2–CH_3), 3.91(m, 1H, –OCH_2–CH_3), 3.77 (s, 3H, –OCH_3), 3.65–3.74 (m,1H, –OCH_2–CH_3), 1.28 (t, 3H, $J=7.0$ Hz, –OCH_2–CH_3), 1.14 (t, 3H, $J=7.0$ Hz, –OCH_2–-CH_3). ^{13}C NMR (75 MHz,$CDCl_3$, 25 °C) δ 159.40, 143.54 (d, $J=15.4$ Hz), 129.24, 129.08, 129.01, 127.77, 127.73, 118.43, 114.16, 114.13,63.39 (dd, $J^2_{CP}=6.9$, 3.9 Hz), 56.45, 55.33, 54.43, 16.60 (d, $J^3_{C\,P}=14.9$ Hz), 16.52 (d,$J^3_{CP}=5.9$ Hz).^{31}P NMR (121 MHz, $CDCl_3$, 25 °C) δ 23.47 ppm.

Diethyl [4-nitrophenyl(phenylamino)methyl]phosphonate (4c)

Yield: 90%, as a yellow crystalline solid; mp 89.2 °C. ^{1}H NMR (400 MHz, $CDCl_3$, 25 °C) δ 8.22–8.19 (d, 2H, ArH), 7.68–7.64 (dd, 2H, $J_{HP}=8.9$, 2.3 Hz, ArH), 7.19–6.95 (m, 2H, ArH), 6.76–6.71 (t, 1H, $J=7.4$ Hz, ArH), 6.56–6.52 (m, 2H, ArH), 4.88–4.81 (d, 1H, $J_{HP}=25.6$ Hz, CHP), 4.25–4.11 (m, 2H, OCH_2–CH_3), 3.99–4.02 (m, 1H, –OCH_2–CH_3), 3. 97–3. 78 (m, 1H, –OCH_2–CH_3), 1.32 (t, 3H, J = 7.1 Hz, –OCH_2–CH_3), 1.21 (t, 3H, J = 7.1 Hz, –OCH_2–CH_3). ^{13}C NMR (101 MHz, $CDCl_3$, 25 °C) δ 147.59, 145.71 (d, J = 16.6 Hz), 143.92 (d, $J=2.5$ Hz), 129.35, 128.64 (d, $J=4.7$ Hz), 123.75, 119.12, 113.81, 63.63 (dd, $J^2=27.4$, 6.8 Hz), 56.78, 55.31, 16.50 (d, $J^3cp=17.2$ Hz), 16.24 (d, $J^3cp=5.5$ Hz). ^{31}P NMR (162 MHz, Chloroform-*d*) δ 20.80. HRMS (ESI) m/z calcd for $C_{17}H_{21}N_2O_5P$ [M + H$^+$]: 387.1094; Found 387.1080.

Diethyl[1-naphtyl(p-tolylamino)methyl]phosphonate (4d)

Yield: 90%, as a white crystalline solid; mp 145 °C. ^{1}H NMR (300 MHz, $CDCl_3$, 25 °C) δ 8.27 (d, 1H, $J_{HP}=8.5$ Hz, HAr), 7.91 (d, 1H, $J=7.9$ Hz HAr), 7.80–7.77 (m, 2H, HAr), 7. 63–7. 48 (m, 2H, HAr), 7.45 (t, 1H, $J=7.7$ Hz, HAr), 6.67 (d, 2H, $J=8.48$ Hz, HAr), 6.48 (d, 2H, $J=8.4$ Hz, HAr), 4.64 (d, 1H, $J_{HP}=24.0$ Hz, H_{CP}), 4.23–4.15 (m, 2H, –OCH_2–CH_3), 3.77–3.73 (m, 1H, –OCH_2–CH_3), 3. 28–3.17 (m, 1H, –OCH_2–CH_3), 2.16 (s, 3H, CH_3–Ph), 1.34 (t, 3H, $J=7.1$ Hz, –OCH_2–CH_3), 0.75 (t, 3H, $J=7.1$ Hz, –OCH_2–CH_3). ^{13}C NMR (75 MHz, $CDCl_3$) δ 143.83 (d, $J=24.8$ Hz), 133.81, 131.6 (d, $J=19.7$ Hz), 129.70, 129.00, 128.40, 127.50, 126.22, 125.64, 125.35 (d, $J=6.0$ Hz), 123.00, 113.67, 63.63 (dd, $J^2_{CP}=27.4$, 6.8 Hz), 20.33, 16.49 (d, $J^3cp=5.9$ Hz), 16.49 (d, $J^3cp=5.9$ Hz). ^{31}P NMR (121 MHz, $CDCl_3$, 25 °C): δ 23.07 ppm. HRMS (ESI) *m/z* calcd for $C_{22}H_{26}NO_3P$ [M + H$^+$]: 406.1532; Found 406.1542.

Diethyl [benzo [1, 3]dioxol-5-yl((p-tolylamino) methyl]phosphonate (4e)

Yield: 91%, as a white crystalline solid; mp 115 °C. ^{1}H NMR (300 MHz, $CDCl_3$, 25 °C) δ 7.04–6.89 (m, 4H, ArH), 6.77 (d, $J=8.0$ Hz, 1H, ArH), 6.53 (d, $J=8.5$ Hz,

2H, ArH), 5.93–5.95 (dd, $J=5.3$, 1.4 Hz, 2H, O–CH_2–O), 4.66 (d, $J_{HP}=24.0$ Hz, 1H, HCP), 4.27–4.07 (m, 3H, –OCH_2–CH_3 + NH), 4.05–3.91 (m, 1H, –OCH_2–CH_3), 3.89–3.71 (m, 1H, –OCH_2–CH_3), 2.21 (s, 3H, CH_3Ph), 1.31 (t, $J=7.1$ Hz, 3H, –OCH_2–CH_3), 1.19 (t, $J=7.1$ Hz, 3H, –OCH_2–CH_3). ^{13}C NMR (75 MHz, $CDCl_3$) δ 147.64 (d, $J=49.1$ Hz), 143.78, 129.74 (d, $J=11.6$ Hz), 121.35 (d, $J=6.5$ Hz), 113.99, 108.21 (d, $J=13.9$ Hz), 101.10, 63.84–62.26 (m), 57.01, 54.99, 20.36, 16.41 (d, $J^3cp=12.4$ Hz), 16.19 (d, $J^3cp=5.7$ Hz).. HRMS (ESI) *m/z* calcd for $C_{19}H_{24}NNaO_5P$ [M + Na^+]: 400.128430; Found 400.1273. ^{31}P NMR (121 MHz, $CDCl_3$) δ 22.65.

Diethyl [(4-fluorophenyl)(4-tolylamino)methyl] phosphonate (4f)

Yield: 88%, as a white crystalline solid; mp 119 °C. ^{1}H NMR (300 MHz, $CDCl_3$, 25 °C) δ 7.43 (dd, $J=12.0$, 4.0 Hz, 2H, HAr), 7.26 (m, 2H, HAr), 6.93 (d, 2H, $J=8.2$ Hz, HAr), 6.48 (d, 2H, $J=8.5$ Hz, HAr), 4.64–4.78 (m, 1H, HC*), 4.10–4.17 (m, 2H, –OCH_2–CH_3), 3.97–4.05 (m, 1H, –OCH_2–CH_3), 3.79–3.85 (m, 1H, –OCH_2–CH_3), 2.21 (s, 4H, CH_3–Ph + NH), 1.31 (t, 3H, $J=7.1$ Hz, –OCH_2–CH_3), 1.18 (t, 3H, $J=7.1$ Hz, –OCH_2–CH_3). ^{13}C NMR: (75 MHz, $CDCl_3$, 25 °C): δ 143.85 (d, $J=15.0$ Hz), 134.84, 133.80, 133.76, 133.71, 129.83, 129.28,128.21,127.89,127.86, 128.03, 114.06, 63.59 (dd, $J^2_{cp}=12.1$,7.0 Hz),56.89, 54.89,20.47,16.59(d, $J^3_{cp}=13.7$ Hz), 16.52 (d, $J^3_{cp}=5.8$ Hz). ^{31}P NMR (121 MHz, $CDCl_3$) δ 22.69. HRMS (ESI) *m/z* calcd for $C_{18}H_{23}FNNaO_3P$ [M + Na^+]: 374.1291; Found 374.1275. ^{31}P NMR (121 MHz, $CDCl_3$) δ 22.72.

Diethyl [(phenyl)(4-trifluoromethylamino)methyl] phosphonate (4 g)

Yield: 88%, as white crystalline solid. mp 140 °C. ^{1}H NMR (300 MHz, $CDCl_3$, 25 °C) δ = 7.49 (dd, $J=7.7$, 2.1 Hz, 2H, HAr), 7.26–7.40 (m, 5H, HAr), 6.62 (d, 2H, $J=8.5$ Hz, HAr), 5.16–5.31 (t, $J=13.5$ Hz, 1H, NH), 4.79 (dd, 1H, $J=24.2$, 7.5 Hz, HC*), 4.10–4.20 (m, 2H, –OCH_2–CH_3), 3.90–4.08 (m, 1H, -OCH_2-CH_3), 3.61–3.70 (m, 1H, –OCH_2–CH_3), 1.31 (t, 3H, $J=7.1$ Hz, –OCH_2–CH_3), 1.12 (t, 3H, $J=7.0$ Hz, –OCH_2–CH_3). ^{13}CNMR (75 MHz, $CDCl_3$, 25 °C): δ 148.90 (d, $J=14.4$ Hz), 135.13 (d, $J=3.0$ Hz), 128.91, 128.87, 128.38, 128.34, 127.90, 127.83, 126.68, 126.63, 113.16, 63.75 (dd, $J^2_{cp}=22.9$, 7.0 Hz), 56.77, 54.77, 16.59 (d, $J^3_{cp}=19.0$ Hz), 16.51 (d, $J^3_{cp}=5.8$ Hz). ^{31}P NMR: (121 MHz, $CDCl_3$, 25 °C): δ 22.54 ppm.

Diethyl [3-phenoxyl(phenylamino)trifluoromethyl] phosphonate (4 h)

Yield: 78%, as white crystalline solid. mp 155 °C. ^{1}H NMR (360 MHz, $CDCl_3$, 25 °C) δ 7.74–7.83 (m, 1H, HAr), 7.43–7.25 (m, 4H, HAr), 7.20 (d, $J=7.5$ Hz, 1H, HAr), 7.13–7.05 (m, 2H, HAr), 6.93 (d, $J=7.6$ Hz, 3H, HAr), 6.59 (d, $J=8.6$ Hz, 2H, HAr), 5.53 (s, 1H, NH), 4.74 (d, $J=24.4$ Hz, 1H, HC*), 4.20–4.06 (m, 2H), 4.05–3.93 (m, 1H, –OCH_2–CH_3), 3.84–3.69 (m, 1H, –OCH_2–CH_3), 1.29 (t, $J=7.1$ Hz, 3H, –OCH_2–CH_3), 1.16 (t, $J=7.1$ Hz, 3H, –OCH_2–CH_3). ^{13}C NMR (91 MHz, $CDCl_3$) δ 157.59, 156.82, 148.74 (d, $J=14.3$ Hz), 137.26, 129.92 (d, $J=30.6$ Hz), 126.55, 123.45, 122.52 (d, $J=5.1$ Hz), 120.35, 119.99, 118.83, 118.44,

118.14 (d, $J=5.3$ Hz), 113.16, 63.49 (dd, $J=16.8$, 6.9 Hz), 56.31, 54.64, 16.42 (d, $J^3=5.8$ Hz), 16.24 (d, $J^3cp=5.7$ Hz). ^{31}P NMR (162 MHz, $CDCl_3$) δ 21.54. HRMS (ESI) *m/z* calcd for $C_{24}H_{25}F_3NNaO_4P$ [$M^+ Na^+$]: 502.1365; Found 400.1343.

Diethyl [benzo [1,3]dioxol-5-yl((phenylamino)trifluoro-methyl] phosphonate (4i)

Yield: 87%, as white crystalline solid. mp 148.2 °C. ^{1}H NMR (300 MHz, $CDCl_3$, 25 °C) δ 7.36 (d, $J=8.5$ Hz, 2H, HAr), 7.01–6.87 (m, 2H), 6.79 (d, $J=7.9$ Hz, 1H), 6.64 (d, $J=8.5$ Hz, 2H, HAr), 5.96 (dd, $J=3.8$, 1.3 Hz, 2H, O-CH_2-O), 4.69 (d, $J=24.0$ Hz, 1H, HC*), 4.23–4.06 (m, 2H, –OCH_2–CH_3), 4.05–3.92 (m, 1H, –OCH_2–CH_3), 3.76 (m, 1H, –OCH_2–CH_3), 1.32 (t, $J=7.1$ Hz, 3H, –OCH_2–CH_3), 1.18 (t, $J=7.1$ Hz, 3H, –OCH_2–CH_3). ^{13}C NMR (101 MHz, $CDCl_3$) δ 148.88 (d, $J=34.5$ Hz), 126.50, 121.32 (d, $J=6.2$ Hz), 120.14 (d, $J=34.6$ Hz), 113.08, 108.42, 107.98 (d, $J=4.2$ Hz), 101.25, 63.56 (d, $J=7.0$ Hz), 63.28 (d, $J=7.0$ Hz), 56.14, 54.62, 16.43 (d, $J^3cp=5.6$ Hz), 16.27 (d, $J^3cp=5.5$ Hz). ^{31}P NMR (162 MHz, Chloroform-*d*) δ 21.87. HRMS (ESI) *m/z* calcd for $C_{19}H_{21}F_3NNaO_5P$ [M + Na^+]: 454.1001; Found 454.0991.

Experimental design

A statistical approach was chosen to optimizing the synthesis reaction of α-aminophosphonates using diphenylphosphinic acid as a new and efficient catalyst under green conditions. A full factorial model of two levels with three operating factors was selected in a first approach (2^3), and each factor takes two values including a low and high level. Table 1 shows the selected operating factors and their levels in the experiment. All synthesis experiments were realized with three repetitions at the central point ($C_{(P)}$).

The chemical yield (R%) was chosen as the answer (*y*) to achieve the optimal conditions of the synthesis reaction of α-aminophosphonates. Data analyzes were performed using statistical software (Minitab18), which allows us to determine the main effects and the interactions between the factors tested. In this study, the total number of experiments (E^{nbr}) performed was reported as follows:

$$E^{nbr} = 2^{\beta} + C_{(p)} \tag{1}$$

Here β is the number of operating factors, and $C_{(p)}$ symbolizes the number of center points used to test for quadratic terms between low and high levels; these central points

Table 1 Coded levels for independent variables were used in the Full Factorial Design (2^3-FFD) Experiments

Operating factors	Units	Symbols	Lower level (−1)	Center point (0)	Higher level (+1)
Catalyst amount	mol.%	Q_{Cat}	5	10	15
Reaction time	min	t	15	30	60
Medium temperature	°C	T°	25	40	50

were used to estimate the clarity and curving of the applied model. So, eleven (11) experiments were conducted in this investigation, including a combination of the factor levels studied. The results of the factorial design, given in terms of the theoretical response (y) and a regression model, can be expressed by Eq. (2):

$$y = \delta_0 + \sum_{i=1}^{4} \delta_i x_i + \sum_{i=1}^{3} \sum_{j=i+1}^{4} \delta_{ij} x_i x_j + \sum_{i=1}^{2} \sum_{j=i+1}^{3} \sum_{k=j+1}^{4} \delta_{ijk} x_i x_j x_k \quad (2)$$

Here δ_0 is the result average value; δ_1, δ_2, and δ_3 correspond to the linear coefficients; and δ_{12}, α_{13}, δ_{23}, and δ_{123} interaction coefficients between the operating factors and η means the residual term. The symbols Q_{Cat}, t and $T°$ symbolize the tested variables in the model.

Results and discussion

The synthesis of diethyl α-aminophosphonate compounds was realized by multi-components *Kabachnik–Fields* reaction. For that, we have chosen the condensation in one pot of aromatic aldehyde (115 mg, 1 mmol), aniline (99 mg, 1 mmol), and diethylphosphite (136 mg, 1.2 mmol) as reaction models.

Table 2 Test of organocatalysts for the synthesis of α-aminophosphonate **4a**

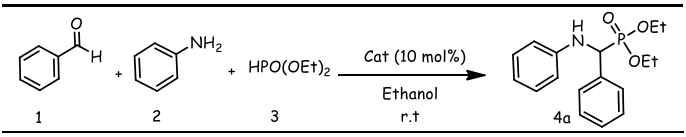

Entry	Organocatalyst (10 mol%)	Yield (%)[c]
1[a]	–	–
2[b]	A	92
3	B	75
4	C	93
5	D	78
6	E	38
7	F	11
8	G	Trace

[a]Reaction conditions: aldehyde (1 mmol), aniline (1 mmol) and diethylphosphite (1.2 mmol) were stirred without catalyst in ethanol (2 mL), at 25 °C, within 24 h

[b]Reaction conditions: aldehyde (1 mmol), aniline (1 mmol), and diethylphosphite (1.2 mmol) were stirred with the catalyst in ethanol (2 mL) at 25 °C within 6 h.

[c] Yield of the pure product purified by crystallization in hexane

Organocatalyts screening

First, the multi-component reaction was performed without catalyst in ethanol, no progress of reaction was observed after 24 h even by increasing the temperature up to 50 °C (Table 2, entry 1). We have tested different kinds of organocatalysts; Brønsted acids such as (*S, S*)-1-oxo-1-hydroxy-2-c,5-*t*-diphenylphospholane (A), 1,1′-binaphtyl-2,2′-dihydrogene-phosphate (B), diphenyl-phosphinic acid (C) and diphenylphosphate acid (D), prolines derivatives such as *N*-*tert*-butylpyrrolidine-2-carboxamide (E) and *N*-(2-trifluoroacetyl) pyrrolidine-2-carboxamide (F), and Schiff base such as (*E*)-1-(2-hydroxy-5-methoxybenzylidene-amino)-2,3-dihydro-1H-inden-2-ol (G) (Fig. 1). The catalysts screening was made with 10 mol.% in ethanol at room temperature within 6 h.

The high activity of (A) and (C) can be attributed to their relative lower acidity compared to (B) and (D). Owing to the commercial availability at low cost of the organocatalyst (C) compared to the tedious preparation steps of the (A) [44, 45], the first one was chosen as the best one for the rest of our present investigation.

Unfortunately, the proline derivatives have shown lower reactivities, the use of the amido proline (E) and trifluoroacetoxy amido proline (F) furnish the α- aminophosphonate 4a with 38% and 11% yields, respectively (Table 2, entries 6 and 7). These results were probably due to the high acidity (E) and (F), exhibited by their electron-withdrawing effects. While a problem of the low solubility of the Schiff base (G) still the main cause for no progress of the reaction (Table 2, entry 8).

Modeling and optimization of α-aminophosphonates synthesis

Full factorial optimization of the synthesis of α-aminophosphonates was performed as a matrix of 11 experiments under the influence of three operating factors with different levels, as shown in Table 3. The obtained results showed that the chemical yield ($R_{\%}$) varied from 20 to 90%; this vast experimental zone can be seen as an improvement for this behavior as it could include the required optimal conditions. The normal probability plot, Pareto plot, surface plots, individual/interaction

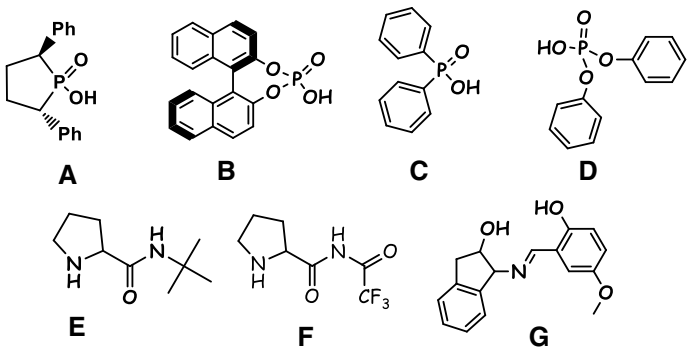

Fig. 1 Different organocatalysts tested for the synthesis of α-aminophosphonates

Table 3 Reaction conditions applied in Full Factorial Design (2^3-FFD) experiments for the synthesis of α-aminophosphonates under green conditions

Run number	Operating factors			Chemical yields	
	t (min)	Q_{cat} (%)	T (°C)	R_{Exp} (%)	R_{Pred} (%)
1	15	5	25	20.00	22.25
2	60	5	25	40.00	37.75
3	15	15	25	68.00	65.75
4	60	15	25	70.00	72.25
5	15	5	50	50.00	47.75
6	60	5	50	60.00	62.25
7	15	15	50	78.00	80.25
8	60	15	50	88.00	85.75
9	30	10	40	90.00	90.00
10	30	10	40	90.00	90.00
11	30	10	40	90.00	90.00

Table 4 ANOVA test for quadratic models for the synthesis of α-aminophosphonates under green conditions

Source	DF	Adj SS	Adj MS	*F*-value	*p*-value
Model	7	5390.05	770.01	57.04	0.003
Linear	3	3225.50	1075.17	79.64	0.002
t	1	220.50	220.50	16.33	0.027
Q cat	1	2244.50	2244.50	166.26	0.001
T°	1	760.50	760.50	56.33	0.005
2-Way Interactions	3	101.50	33.83	2.51	0.235
t*Q cat	1	40.50	40.50	3.00	0.182
t*T°	1	0.50	0.50	0.04	0.860
Q cat*T°	1	60.50	60.50	4.48	0.125
Curvature	1	2063.05	2063.05	152.82	0.001
Error	3	40.50	13.50		
S	R-sq	R-sq(adj)			
3.67423	99.25%	97.51%			

effects, and optimization plots of the fitted values were examined. Analysis of variance and *p*-value significance levels were estimated to verify the significance of the effect of operating factors on chemical yield. After discarding insignificant terms (i.e., Q_{cat}*$T°$*t), the resulting model was reduced to determine all workable terms ($Q_{cat,}$ $T°$ *and t).*

The ANOVA test was used to determine the significant effect of operating factors and their interactions on chemical yield (R%). Table 4 shows the *F*-ratio, *p*-value, sum of squares and mean square of each parameter. Data rank can be judged by its *p*-value, with values earlier than zero denoting greater significance. The *p*-value should be less than or equal to 0.05 to examine statistical significance with up to a

95% confidence level. In the case of the adopted model, the statistical treatment generated *p*-values and *F*-values (probability > *F*, indicating the insignificant probabilities), and therefore one could establish the significance of each variable. The variable under study could be more significant when the absolute *F*-value became greater and the *p*-value became lesser. Statistical testing of this model was performed using Fisher's statistical test or Student's *t*-test for analysis of variance. Accordingly, the quadratic regression shows that the assumed model had a very large *F*-value, on the order of 57.04, indicating a height signification of the model. The analysis of the experimental data indicates that more than 99% of the obtained data can be well predicted by the adopted model with an R^2 reaching 99.25% and R^2_{adj} of 97.51%, indicating that the terms included in recommended model have been measured remarkably enough to make satisfactory predictions.

This section aimed to define the optimal condition for maximum chemical yields of the synthesis of α-aminophosphonates. The correctness of the model was confirmed by comparing the experimental data as function of the predicted responses generated by the adopted model. The results obtained showed good agreement between the experimental chemical yields and the predicted values. The predicted response of the model was consistent with the experimental data. In this study, the influence of five independent factors on the response function was examined by a full factorial design to determine the optimal conditions.

In this study, the influence of five independent factors on the response function was examined by a full factorial design to determine the optimal conditions. The mathematical relationship between five important variables and the response can be estimated by a quadratic polynomial equation (Eq. 3):

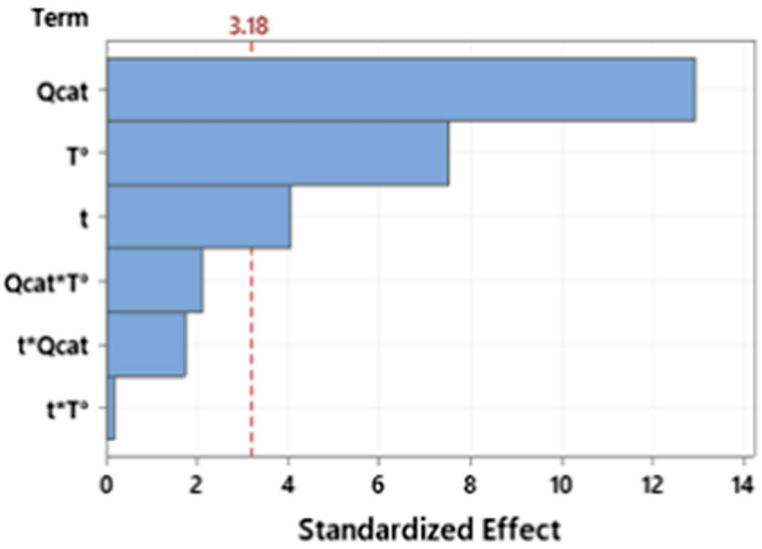

Fig. 2 Pareto chart including the effect of each factor on the chemical yields of the synthesis of α-aminophosphonates using diphenylphosphinic acid

$$(y)R\% = 59,25 + 5,25t + 16,75Q_{cat} + 9,75T^{\circ} - 2,25t * Q_{cat} - 0,25t * T^{\circ} - 2,75Q_{cat} * T^{\circ} + 30,75CtPt \quad (3)$$

The statistical data of the selected significant model terms are summarized in Table 3 to describe the chemical yields as a function of the operating parameters tested.

Main individual effects

The individual effects of each operational factor on the chemical yields of the synthesis of α-aminophosphonates under green conditions are summarized in Fig. 2. According to the results obtained, we found that the amount of catalyst (Q_{cat}) has a highly positive effect, which is essentially due to the good catalytic performance and high reactivity of diphenylphosphinic acid **C**, reinforced by its *pKa* values (2.30) as a *Brønsted* acid catalyst compared with the Pka of **A** and phosphoric acid **B** and **D** (3.3, 3.37 and 3.7). Also, the reaction time (t) and temperature (T°) have a medium positive effect, while the other terms were not significant, with a *p*-value higher than 0.05 as shown in the Pareto chart (Fig. 3) and Table 4. These results showed good agreement between the predicted and experimental values for the chemical yields as summarized in Table 3, the main reaction factors were the catalyst amount (Q_{cat}) with an effect of 33.50 > medium temperature effect (19.50) > the effect of reaction time (10.50).

Interaction effects between operating factors

The interaction effects between the investigated operating factors are shown in Fig. 4. The interactions between Q_{cat}/T° and t/ Q_{cat} were the most significant with a

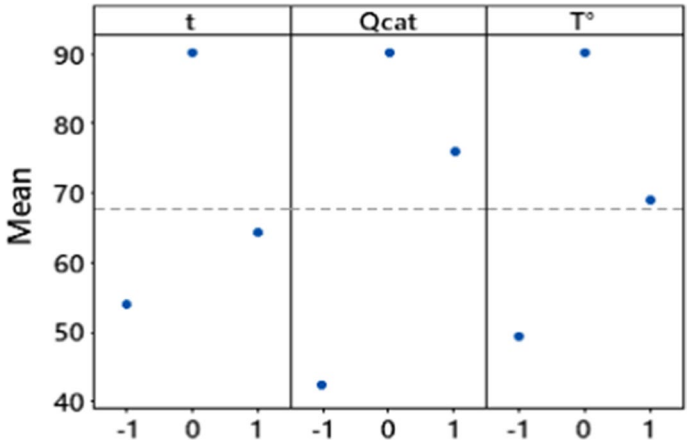

Fig. 3 Main effects of the operating factors: reaction time (t), amount of catalyst (Q_{cat}) and temperature (T°) for the α-aminophosphonates synthetized using diphenylphosphonic acid

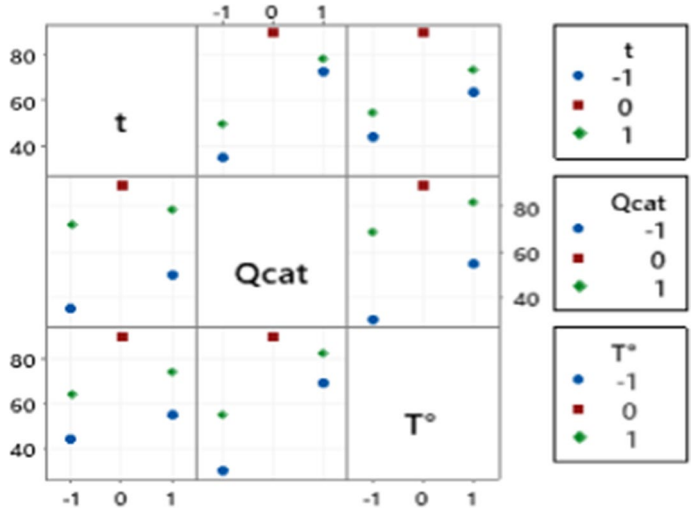

Fig. 4 Interactions effects between the operating factors (t, Q_{cat} and T°) for the synthesis of α-aminophosphonates using diphenylphosphinic acid

negative effect of -5.5 and −4.5 respectively, which was confirmed by the non-parallel borders of the effects. Therefore, the interactions between reaction time (t) and medium temperature effect represented an insignificant effect, which was confirmed by limits, which were easily found at p values less than 0.05, this phenomenon can be explained by the absence of a synergetic effect between these operating factors.

Determination of optimum conditions

In our study, the main optimization goal was to determine the ideal conditions for the synthesis of α-aminophosphonates using diphenylphosphinic acid as an efficient organocatalyst. The request-target was the synthesis of α-aminophosphonates in their maximum values in a minimum time in order to obtain the high chemical yield.

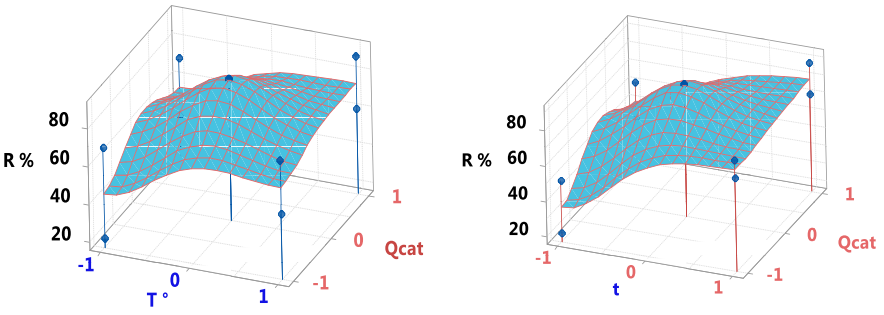

Fig. 5 Three-dimensional surface plot of chemical yields as a function of Q_{cat}/T° and t/Q_{cat} for the synthesis of α-aminophosphonates using diphenylphosphinic acid

Table 5 Optimum conditions for the synthesis of α-aminophosphonates using diphenylphosphinic acid as an efficient organocatalyst

Operating factors	Symbole	Optimums values
Reaction time	t	30 min
Catalyst amount	Q_{cat}	10 mol.%
Medium temperature	T°	40 °C
Predicted chemical yield	R $\%_{Pre}$	90.00%
Experimental chemical yield	R $\%_{Exp}$	93.51%

The obtained results indicated that the highest chemical yield $R_{\%Exp}$ (90.00%) was achieved when each factor value was placed at the optimal level, which was in good agreement with the predicted chemical yield $R_{\%pred}$ (93.51%). Fig. 5 exhibits the 3D surface plots of chemical yield evolution as a function of *Qcat/T°* and *t /Qcat* for the synthesis of *α*-aminophosphonates. As can be observed, the chemical yields (R%) highly increase with the increasing amount of diphenylphosphinic acid, at the same time, this phenomenon can be explained by the interaction between the effects of the studied factors.

The best chemical yields of the *α*-aminophosphonate synthesis were obtained under optimum conditions are shown in Table 5. It is anticipated that this behavior may open the way to applying this model for the synthesis of a matrix of MCRs on a series of variously substituted aromatic aldehydes and anilines with electron-withdrawing and electron-donating groups.

Applied of the optimal conditions

Based on the optimal conditions of the factorial experiments study, we have investigated the effectiveness and limitations of the MCRs on a series of variously substituted aromatic aldehydes and anilines with electron-withdrawing and electron-donating groups. The reaction proceeds in the presence of diphenylphosphinic acid (10 mol.%) in ethanol at 40 °C within 30 min. The results summarized in Table 6 showed the high efficiency of diphenylphosphinic acid as *Brønsted* catalyst in *Kabachnik-Fields* reaction. The use of aniline with benzaldehyde, 3-methoxybenzaldehyde, and 4-nitrobenzaldehyde leads to the *α*-aminophosphonates **4a**, **4b** and **4c** with excellent chemical yields (up to 90%). Similarly in the presence of toluidine with 1-naphtylbenzaldehyde, dioxobenzaldehyde and 4-fluorobenzldehyde, the **4d**, **4e** and **4f** are obtained in excellent yields (90%, 91% and 80%). The methyl-trifluoro aniline partially decreases the nucleophilicity of aniline giving the desired products **4g, 4h** and **4i** with **88, 78** and **87%**.

According to the obtained results and based on our previous work, we propose a mechanism for the synthesis of *α*-aminophosphonates via multicomponent condensation reaction in one pot of aromatic aldehyde, amine and diethylphosphite catalyzed by a diphenylphosphinic acid. It was reasonably supposed that in the first step the catalyst plays a crucial role to activate electrophilically the carbonyl carbon of the aldehyde

Table 6 Diphenylphosphinic acid catalyzed α-aminophosphonates synthesis[a]

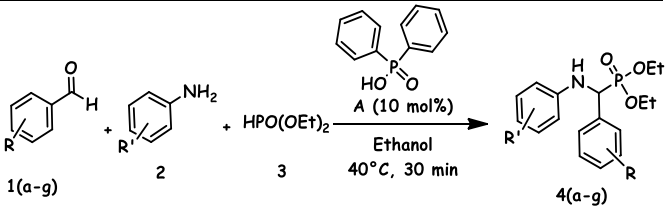

Product **4** (yield)[b]		
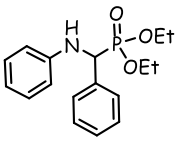	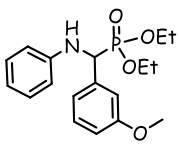	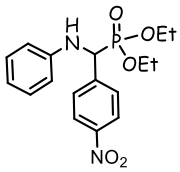
4a (92%)	4b (98%)	4c (90%)
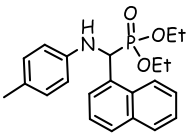	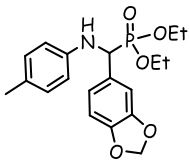	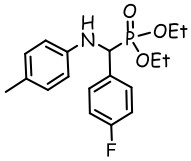
4d (90%)	4e (91%)	4f (80%)
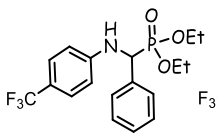	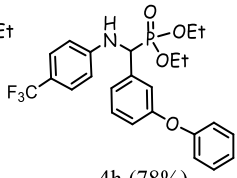	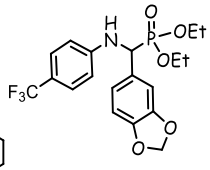
4g (88%)	4h (78%)	4i (87%)

[a]Reaction conditions: benzaldehyde (1 mmol), aniline (1 mmol) and diethylphosphite (1.2 mmol), Ethanol (2 ml), diphenylphosphinic acid (10 mol.%), 40 °C, 30 min

[b]Yield of the pure product, purified by crystallization from hexane

which promotes the nucleophilic attack by the amine to form the imine intermediate. Because of its formation is a reversible process, it is trapped immediately by the catalyst which prevents hydrolysis of the imine substrate to the amine and aldehyde by water formed. The coordination of catalyst active the imine and renders it more electrophile for facilitate the nucleophilic attack of the diethylphosphite which leads to the formation of the desired α-aminophosphonates with simultaneous release of the catalyst (Scheme 1).

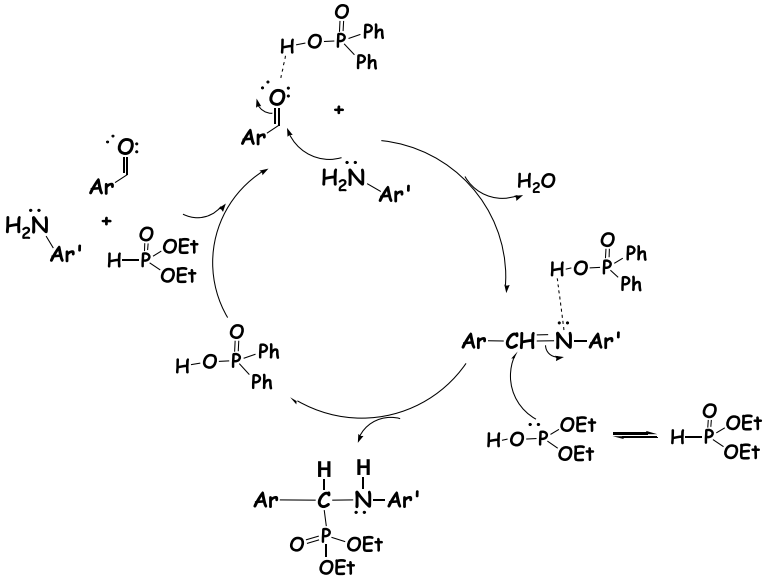

Scheme 1 Plausible reaction mechanism for the synthesis of aminophosphonates using diphenylphosphinic acid

Conclusions

In conclusion, we have described a novel and highly efficient protocol for the synthesis of α-aminophosphonates via multicomponent condensation reaction under green conditions, using diphenylphosphinic acid as Bronsted acid and eco-compatible organocatalyst. The full factorial experiment design was successfully used to establish the optimal conditions for optimizing the reaction yield. The regression analysis showed a good correlation between the obtained reaction yields ($R\%_{Exp}$) and predicted yields ($R\%_{Pred}$), which confirmed the validity and practicability of the model, with high and significant R^2 values up to 99.25%. The statistic treatment indicated that the diphenylphosphonic acid amount, reaction time, and medium temperature have high signification positive effects on the α-aminophosphonates synthesis. The application of the optimization conditions on a series of variously substituted aromatic aldehydes and aromatic amines with electron-withdrawing and electron-donating groups showed the effectiveness of this catalyst gave the α-aminophosphonates in chemical yields.

Supplementary Information The online version contains supplementary material available at https://doi.org/10.1007/s11144-022-02329-0.

Acknowledgements The General Directorate of Scientific Research and Technological Development (DGRSDT) is gratefully acknowledged for financial support of this work. The technical support provided by Emilie KOLODZIEJ is highly appreciated.

Author contributions All authors contributed to this manuscript. MF: Synthesis of molecules. SGL: wrote, conceived and designed the study and Methodology, HB: Wrote and designed the full factorial

experiment. RA: Investigation. MMK: wrote and investigated. MT: performed the data analysis and wrote this manuscript. LAZ: Wrote and revised.

Funding This research did not receive any specific grant from funding agencies in the public, commercial, or not-for-profit sectors.

Data availability In good to excellent chemical yields (from 78% to 98%).

Declarations

Conflict of interest The authors declare that they have no known competing financial interests or personal relationships that could have appeared to influence the work reported in this paper.

References

1. Horsman GP, Zechel DL (2017) Phosphonate biochemistry. Chem Rev 117:5704–5783
2. Arizpe AF, Sayago J, Jimenez AI, Ordonez M, Cativiela C (2011) Stereodivergent synthesis of two novel α-aminophosphonic acids characterised by a cis-fused octahydroindole system. Eur J Org Chem 2011:3074–3081
3. Wendels S, Chavez T, Bonnet M, Salmeia KA, Gaan S (2017) Recent developments in organophosphorus flame retardants containing P-C bond and their applications. Materials 10:784
4. Fields EK (1952) The synthesis of esters of substituted amino phosphonic acids[1a]. J Am Chem Soc 74:1528–1531
5. Kabachnik MI, Medved TY (1952) New synthesis of aminophosphonic acids. In Dokl Akad Nauk SSSR 83:689–692
6. Schoepp DD, Johnson BG (1989) Inhibition of excitatory amino acid-stimulated phosphoinositide hydrolysis. J Neurochem 53:1865–1870
7. George A, Veis A (2008) Phosphorylated proteins and control over apatite nucleation, crystal growth, and inhibition. Chem Rev 108:4670–4693
8. Kafarski P, Lejczak B (1991) Biological activity of aminophosphonic acids. Phosphorus Sulfur Silicon Relat Elem 63:193–215
9. Orsini F, Sello G, Sisti M (2010) Aminophosphonic acids and derivatives: synthesis and biological applications. Curr Med Chem 17:264–289
10. Mucha A, Kafarski P, Berlicki Ł (2011) Remarkable potential of the α-aminophosphonate/phosphinate structural motif in medicinal chemistry. J Med Chem 54:5955–5980
11. Han W, Mayer P, Ofial AR (2010) Ofial, iron-catalyzed oxidative mono-and bis- phosphonation of *N, N*-dialkylaniline. Adv Synth Catal 352:1667–1676
12. Kim H, Chin J, Choi H, Baek K, Lee TG, Park SE, Wang W, Hahn D, Yang I, Lee J, Mun B, Ekins M, Nam SJ, Kang H (2013) Unique phosphorus-containing iodinated polyacetylenes from a Korean sponge placospongia sp. Org Lett 15:100–103
13. Clercq ED, Holý A (2005) Acyclic nucleoside phosphonates: a key class of antiviral. Drugs Nat Rev Drug Discov. 4:928–940
14. Ali N, Zakir S, Patel M, Farooqui M (2012) Synthesis of new aminophosphonate system bearing Indazole moiety and their biological activity. Eur J Med Chem 50:39–43
15. Sampath C, Harika P, Revaprasadu N (2016) Design, green synthesis, anti-microbial, and antioxidant activities of novel α-aminophosphonates via Kabachnik-Fields reaction. Phosphorus Sulfur Silicon Relat Elem 191:1081–1085
16. Kotsikorou E, Oldfield E (2003) A quantitative structure-activity relationship and pharmacophore modeling investigation of aryl-X and heterocyclic bisphosphonates as bone resorption agents. J Med Chem 46:2932–2944
17. Lacbay CM, Mancuso J, Lin YS, Bennett N, Götte M, Tsantrizos YS (2014) Modular assembly of purine-like bisphosphonates as inhibitors of HIV-1 reverse transcriptase. J Med Chem 57:7435–7449

18. Rozenfeld R, Iturrioz X, Okada M, Maigret B, Llorens-Cortes C (2003) Contribution of molecular modeling and site-directed mutagenesis to the identification of a new residue, glutamate 215, involved in the exopeptidase specificity of aminopeptidase A. Biochemistry 42:14785–14793
19. Mulla SAR, Pathan MY, Chavan SS, Gample SP, Sarkar D (2014) Highly efficient one-pot multicomponent synthesis of α-aminophosphonates and bis- α-aminophosphonates catalyzed dodecatungstophosphoric acid (DTP/SiO2) at ambient temperature and their antitubercular evaluation. RSC Adv 4:7666–7672
20. Aissa R, Guezane-Lakoud S, Toffano M, Gali L, Aribi-Zouioueche L (2021) Fiaud's acid, a novel organocatalyst for diastereoselective bis α-aminophosphonates synthesis with in-vitro biological evaluation of antifungal, antioxidant and enzymes inhibition potential. Bioorg Med Chem Lett 41:128000
21. Onita N, Şişu I, Penescu M, Purcarea VL, Kurunczi L (2010) Characterization and biological activity of some α-aminophosphonates. Farmacia 58:531
22. Moumeni O, Chafaa S, Kerkour R, Benbouguerra K, Chafai N (2020) New thiophene-derived α-aminophosphonic acids: Synthesis under microwave irradiations, antioxidant and antifungal activities, DFT investigations and SARS-CoV-2 main protease inhibition. J Mol Struct 93:1206–1276
23. Devineni SR, Doddaga S, Donka R, Chamarthi NR (2013) $CeCl_3 \cdot 7H_2O$-SiO_2: Catalyst promoted microwave assisted neat synthesis, antifungal and antioxidant activities of α-diaminophosphonates. Chin Chem Lett 24:759–763
24. Rao AJ, Rao PV, Rao VK, Mohan C, Raju CN, Reddy CS (2010) Microwave assisted one-pot synthesis of novel α-aminophosphonates and their biological activity. Bull Korean Chem Soc 31:1863–1868
25. Kobayashi K, Tanaka KIII, Kogen H (2018) Recent topics of the natural product synthesis by Horner–Wadsworth–Emmons reaction. Tetrahedron Lett 59:568–582
26. Shevchuk MV, Sorochinsky AE, Khilya VP, Romanenko VD, Kukhar VP (2010) Utilization of aminophosphonates in the Petasis boronic acid Mannich reaction. Synlett 1:73–76
27. Chen L, You Y, Zhang ML, Zhao JQ, Zuo J, Zhang XM, Yuan WC, Xu XY (2015) Organocatalytic asymmetric Michael addition of 3-substituted oxindoles to α, β-unsaturated acyl phosphonates for the synthesis of 3, 3′-disubstituted oxindoles with chiral squaramides. Org Biomol Chem 13:4413–4417
28. Lipowska M, Klenc J, Taylor AT, Marzilli LG (2019) fac-99mTc/Re-tricarbonyl complexes with tridentate aminocarboxy-phosphonate ligands: suitability of the phosphonate group in chelate ligand design of new imaging agents. Inorg Chim Act 486:529–537
29. Lakoud SG, Merabet-Khelassi M, Aribi-Zouioueche L (2016) $NiSO_4.6H_2O$ as a new, efficient, and reusable catalyst for the α-aminophosphonates synthesis under mild and eco-friendly conditions. Res Chem Intermediat 42:4403–4415
30. Dindulkar SD, Reddy MV, Jeong YT (2012) Cd $(ClO_4)_2 \cdot xH_2O$ as a novel catalyst for the synthesis of α-aminophosphonates under solvent-free conditions. Catal Commun 17:114–117
31. Bhagat S, Chakraborti AK (2007) An extremely efficient three-component reaction of aldehydes/ketones, amines, and phosphites (Kabachnik– fields reaction) for the synthesis of α-aminophosphonates catalyzed by magnesium perchlorate. J Org Chem 7:21263–21270
32. Pham TS, Balazs L, Petnehazy I, Jaszay Z (2010) Enantioselective Michael addition of diethyl cyanomethyl-phosphonate to chalcones using bifunctional Cinchona-derived organocatalysts: synthesis of chiral precursors of α-substituted β-aminophosphonates. Tetrahedron Asymmetry 21:346–351
33. Pham TS, Czirok JB, Balazs L, Pal K, Kubinyi M, Bitter I, Jaszay Z (2011) BINOL-based azacrown ether catalyzed enantioselective Michael addition: asymmetric synthesis of α-aminophosphonates. Tetrahedron Asymmetry 22:480–486
34. Laschat S, Kunz H (1992) Carbohydrates as chiral templates: stereoselective synthesis of (R)-and (S)-α-aminophosphonic acid derivatives. Synthesis 1992:90–95
35. Reddy BS, Krishna AS, Ganesh AV, Kumar GN (2011) Nano Fe_3O_4 as magnetically recyclable catalyst for the synthesis of α-aminophosphonates in solvent-free conditions. Tetrahedron Lett 52:1359–1362
36. Heydari A, Hamadi H, Pourayoubi MA (2007) A new one-pot synthesis of α-aminophosphonates catalyzed by $H_3PW_{12}O_{40}$. Catal Commun 8:1224–1226

37. Rostamnia S, Doustkhah E (2015) Synthesis of water-dispersed magnetic nanoparticles (H_2O-DMNPs) of β-cyclodextrin modified Fe_3O_4 and its catalytic application in Kabachnik-fields multicomponent reaction. J Magn Magn Mater 386:111–116
38. Aissa R, Guezane-Lakoud S, Gali L, Toffano M, Ignaczak A, Adamiak M, Merabet-Khelassi M, Guillot R, Aribi-Zouioueche L (2022) New promising generation of phosphates α-aminophosphonates: design, synthesis, in-vitro biological evaluation and computational study. J Mol Struct 1247:131336
39. Guezane-Lakoud S, Aissa R, Guillot R, Toffano M, Aribi-Zouioueche L (2020) Novel one-pot access to diastereoisomeric tertiary phospholanes oxides by using enantiomerically pure phospholane oxides under catalyst-free conditions. ChemistrySelect 5:379–383
40. Aissa R, Guezane-Lakoud S, Kolodziej E, Toffano M, Aribi-Zouioueche L (2019) Diastereoselective synthesis of bis(α-amino-phosphonates) by lipase catalytic promiscuity. N J Chem 43:8153–8159
41. Guezane-Lakoud S, Toffano M, Aribi- Zouioueche L (2017) Promiscuous lipase catalyzed a new P-C bond formation: green and efficient protocol for one-pot synthesis of α-amino-phosphonates. Heteroat Chem 28:e21408
42. Guezane Lakoud S, Lecouvey M, Berrebah H, Aouf NE (2015) Synthesis of chiral phosphonoacetamides and their toxic effects on *Paramecium sp*. Org Commun 8:1–8
43. Bedolla-Medrano M, Hernández-Fernández E, Ordóñez M (2014) Phenylphosphonic acid as efficient and recyclable catalyst in the synthesis of α-aminophosphonates under solvent-free conditions. Synlett 25:1145–1149
44. Guillen F, Rivard M, Toffano M, Legros JY, Daran JC, Fiaud JC (2002) Synthesis and first applications of a new family of chiral monophosphine ligand: 2, 5-diphenylphosphospholanes. Tetrahedron 58:5895–5904
45. Guillen F, Fiaud JC (1999) Enantiomerically pure 1, 2, 5-triphenylphospholane through the synthesis and resolution of the chiral trans-(2,5)-diphenylphospholanic acid. Tetrahedron Lett 40:2939–2942

Journal of Biomolecular Structure and Dynamics

ISSN: (Print) (Online) Journal homepage: https://www.tandfonline.com/loi/tbsd20

2-Hydroxymethyl-18-crown-6 as an efficient organocatalyst for α-aminophosphonates synthesized under eco-friendly conditions, DFT, molecular docking and ADME/T studies

Samia Guezane-Lakoud, Meriem Ferrah, Mounia Merabet-Khelassi, Nourhane Touil, Martial Toffano & Louisa Aribi-Zouioueche

To cite this article: Samia Guezane-Lakoud, Meriem Ferrah, Mounia Merabet-Khelassi, Nourhane Touil, Martial Toffano & Louisa Aribi-Zouioueche (2023): 2-Hydroxymethyl-18-crown-6 as an efficient organocatalyst for α-aminophosphonates synthesized under eco-friendly conditions, DFT, molecular docking and ADME/T studies, Journal of Biomolecular Structure and Dynamics, DOI: 10.1080/07391102.2023.2213336

To link to this article: https://doi.org/10.1080/07391102.2023.2213336

JOURNAL OF BIOMOLECULAR STRUCTURE AND DYNAMICS
https://doi.org/10.1080/07391102.2023.2213336

2-Hydroxymethyl-18-crown-6 as an efficient organocatalyst for α-aminophosphonates synthesized under eco-friendly conditions, DFT, molecular docking and ADME/T studies

Samia Guezane-Lakoud[a], Meriem Ferrah[a], Mounia Merabet-Khelassi[a], Nourhane Touil[a], Martial Toffano[b] and Louisa Aribi-Zouioueche[a]

[a]Ecocompatible Asymmetric Catalysis Laboratory (LCAE) Badji Mokhtar Annaba-University, Annaba, Algeria; [b]Equipe de Catalyse Moléculaire-ICMMO Bât 420. Université Paris-Saclay, Paris, France

Communicated by Ramaswamy H. Sarma

ABSTRACT

Eco-friendly and simple procedure has been developed for the synthesis of α-aminophosphonates that act as topoisomerase II α-inhibiting anticancer agent, using 2-hydroxymethyl-18-crown-6 as an unexpected homogeneous organocatalyst in multicomponents reaction of aromatic aldehyde, aniline and diethylphosphite in one pot *via Kabachnik–Fields* reaction. This efficient method proceeds with catalytic amount, transition metal-free, at room temperature within short reaction time, giving the α-aminophosphonates derivatives **(4a–r)** in high chemical yields (up to 80%). Theoretical DFT calculations of three compounds **(4p, 4q** and **4r)** were carried out in a gas phase at CAM-B3LYP 6-31G (d,p) basis set to predict the molecular geometries and chemical reactivity descriptors. The frontier orbital energies (HOMO/LUMO) were described the charge transfer and used to predict structure-activity relationship study. Molecular electrostatic potential (MEP) has also been analyzed. Molecular docking studies are implemented to analyze the binding energy and compared with Adriamycin against 1ZXM receptor which to be considered as antitumor candidates. *In silico* pharmacological ADMET properties as Drug likeness and oral activity have been carried out based on Lipinski's rule of five.

ARTICLE HISTORY
Received 17 February 2023
Accepted 4 May 2023

KEYWORDS
α-Aminophosphonates; crown ether; *Kabachnik–Fields* reaction; DFT; molecular docking; ADMET prediction

1. Introduction

Among the types of phosphonates derivatives, systems containing nitrogen, oxygen and phosphore atoms have the most biological and biochemical aspects (Mucha et al., 2011; Schug & Lindner, 2005). Considerable attention is continuously devoted to α-aminophosphonates because of analogy with amino acid. These compounds exhibit significant biological and pharmacological activities, they are employed as enzyme inhibitor (Grzywa & Sieńczyk, 2013; Maier, 1990), cholinesterase inhibitors (Uparkar et al., 2022), inhibitors of UDP-galactopyranose mutase, also as antitumor agents (Pan et al., 2007), and growth inhibition on *Paramecium* sp. (Guezane-Lakoud et al., 2015). In agrochemistry, a number of α-aminophosphonates derivatives are used as fungicidal and herbicidal agents (Bonarska et al., 2002; Maier & Diel, 1991). Due to their outstanding properties, the construction of α-aminophosphonates compounds remains an important and demanding topic in chemical synthesis. Various approaches were described to synthesize their derivatives *via Kabachnik–Fields* reaction using *Lewis* and *Brønsted* acids (Aissa et al., 2022; Lakoud et al., 2016; Laschat & Kunz, 1992; Sivala et al., 2016; Yadav et al., 2001), lipase (Aissa et al., 2019; Guezane-Lakoud et al., 2017), oxalic acid (Vahda et al., 2008) ionic liquid (Rostamnia & Amini, 2014), organocatalyst (Aissa et al., 2021; Ferrah et al., 2022), heteropolyacids (Heydari et al., 2007) and β-cyclodextrin (Rostamnia & Doustkhah, 2015). However, the catalytic process suffers many drawbacks, such as the use of the high temperature, long reaction times, metal-catalyst, drastic reaction conditions, stoichiometric amount of catalyst and tedious workup of the purification. There is still a strong demand for new efficient and easy methods to reduce the difficulties for the synthesis of α-aminophosphonates. Herein, we envisioned the use of the crown ether as a new type of organocatalyst for the multicomponent *Kabachnik–Fields* reaction. Crown ethers represent, from its discovery by *Liittringhaus'* in 1937 (Liittringhaus, 1937), then by *Pedersen* in 1967 for the formation of stable complexes with salts of alkali and alkaline earth metals (Pedersen, 1967), a great interest as structure-specific in many areas of science. Crown ethers include as 'host-guest' due to the presence of a hydrophobic ring surrounding a hydrophilic cavity leading to the complex formation with metal ions (Dix et al., 1980; Pedersen, 1970). Some of the first uses of crown ethers were as solvent extraction reagents (Mcdowell, 1988), phase transfer catalysis (Cinquini & Tundo, 1976), and they have a property of ion-transport and form complexes with specific ions, particularly of sodium and potassium ions and facilitate their transport across cell

CONTACT Guezane-Lakoud Samia samia.guezanelakoud@univ-annaba.dz

Supplemental data for this article can be accessed online at https://doi.org/10.1080/07391102.2023.2213336.

membranes (Lamb et al., 1981), also they have been used as additive to improve the reactivity and selectivity of some lipases (Merabet et al., 2007).Chiral crown ethers have been also used in asymmetric chemistry as chiral selectors and reported the separation of amino acids and drug enantiomers (Hyun, 2012). On the other hand, crown ethers are numerously used as catalysts by noncovalent binding with the organic neutral and ionic species to promote various reactions such as aldolization (Nagayama & Kobayashi, 2000), *Michael* reaction (Pham et al., 2011), allylic substitution and asymmetric hydrogenation (Luo et al., 2020). In addition, the introduction of amine-substituted by crown ether as a reagent has been reported to produce α-aminophosphonates based on the combination of radiation-induced graft polymerization (Omichi et al., 2019). Herein, we have evaluated for the first time the use of crown ether as an efficient homogeneous organocatalyst for the synthesis of various α-aminophosphonates from aromatic aldehydes, anilines and diethylphosphite *via* multicomponents reaction under mild conditions. On the other hand, the DFT study, in *silico* molecular docking and ADMET prediction of various derivatives of α-aminophosphonates have been widely described (Aita et al., 2021; Kerkour et al., 2023; Mirzaei et al., 2018). In this context, we have carried out the prediction of molecular geometry parameters, HOMO-LUMO orbitals, intramolecular charge transfer and molecular electrostatic potential in CAM-B3LYP/6-31G (d,p) level of theory to investigate the physicochemical properties of the characterized structure of **4p**, **4q** and **4r** as target molecules. As mentioned above, α-aminophosphonates have antitumoral activities. The 1ZXM protein was chosen for molecular docking studies in order to predict the potential 1ZXM binding affinity and binding interactions of the examined compounds. Pharmacological ADMET properties as Drug likeness of the compounds were assessed based on Lipinski's rule of five.

2. Materials and methods

2.1. Chemistry

All reagents were purchased from Sigma-Aldrich or Acros Company used without further purification. Reactions were monitored by thin layer chromatography (TLC) carried out on 0.25-mm Merck silica gel plates (60F-254) using ultraviolet light (254 nm) as the visualizing agent and $KMnO_4$ solution as developing agents. NMR spectra were recorded with Bruker spectrometers operating at (360, 300 and 250 MHz for 1H, 90, 75 or 63 MHz for ^{13}C and 101 MHz or 121 MHz for ^{31}P). Chemical shift of Solvent reference peaks used were $CDCl_3$ ($\delta = 7.26$ ppm) for 1H and ($\delta = 77$ ppm) for ^{13}C NMR spectra, while H_3PO_4 was used as external standard for chemical shift references for ^{31}P NMR. Couplings constants (*J*) are given in Hz, with the Following abbreviations multiplicity: s = singlet, d = doublet, t = triplet, q = quartet, m = multiplet, br = broad signal. Mass spectra were taken by a MicrOTOF-Q Bruker spectrometer using electrospray ionization (ESI) analysis. Melting points were measured using Buchi Melting Point B-545.

2.2. General experimental procedure for the synthesis of diethyl phenyl α-aminophosphonates 4a–r

To the reaction mixture containing aromatic aldehyde (101.12 mg, 1 mmol), aniline (93 mg, 1 mmol) and diethylphosphite (165 mg, 1.2 mmol) in THF (2 mL), 2-hydroxymethyl-18-crown ether-6 (5 mol%) was added, it was stirred within 15 min at room temperature. The reaction progress was monitored by TLC. The mixture was extracted with dichloromethane (10 mL × 2). The organic phases were combined and evaporated in vacuum. The crude product was purified by crystallization in hexane to afford the α-aminophosphonates derivatives 4a-r with good to excellent chemical yields.

2.2.1. Diethyl [phenyl (phenylamino) methyl] phosphonate (4a)

White crystalline solid, 91% yield, mp 88 °C. ^1H NMR (250 MHz, $CDCl_3$, 25 °C) δ 7.52–7.29 (m, 6H, HAr), 7.16–7.10 (t, 1H, $J = 7.9$ Hz, HAr), 6.75–6.69 (t, 1H, $J = 7.3$ Hz, HAr), 6.64–6.61 (m, 2H, HAr), 4.84–4.75 (d, 1H, $J_{HP} = 24.3$ Hz, CHP), 4.18–4.10 (2H, m, $-OCH_2-CH_3$), 4.01–3.76 (2H, m, $-OCH_2-CH_3$), 3.74–3.63 (1H, m, $-OCH_2-CH_3$), 1.31 (t, 3H, $J = 7.1$ Hz, $-OCH_2-CH_3$), 1.14 (t, 3H, $J = 7.1$ Hz, $-OCH_2-CH_3$). ^{13}C NMR (63 MHz, $CDCl_3$, 25 °C): δ 146.33 (d, $J = 14.5$ Hz); 136.00, 129.29, 128.74, 128.71, 128.00, 127.03, 118.40, 113.87, 63.27 (d, J^2 CP = 6.9 Hz), 57.29, 54.90, 16.46 (d, $J^3_{CP} = 15.1$), 16.37 (d, $J^3_{CP} = 5.6$ Hz). ^{31}P NMR (101 MHz, $CDCl_3$, 25 °C) δ 22.46 ppm. HRMS (ESI) *m/z* calcd for $C_{17}H_{23}NO_3P$ $[M+H^+]$: 320.1408; Found 320.141.

2.2.2. Diethyl [4-chlorophenyl (phenylamino) methyl] phosphonate (4b)

White crystalline solid, 80% yield, mp: 86.8 °C. ^{1} HNMR (300 MHz, $CDCl_3$, 25 °C) δ 7.44 (dd, $J = 8.6$, 2.3 Hz, 2H, HAr), 7.21–7.38 (m, 2H, HAr), 7.13 (dd, $J = 8.5$, 7.4 Hz, 2H, HAr), 6.73 (t, 1H, $J = 7.4$ Hz, HAr), 6.58 (dd, 2H, $J = 8.6$, 0.9 Hz, HAr), 4.75 (d, 1H, $J_{HP} = 24.5$ Hz, CHP), 4.05–4.21 (m, 2H, $-OCH_2-CH_3$), 3.92–4.06 (m, 1H, $-OCH_2-CH_3$), 3.75–3.80 (m, 1H, $-OCH_2-CH_3$), 1.30 (t, 3H, $J = 7.0$ Hz, $-OCH_2-CH_3$), 1.18 (t, 3H, $J = 7.0$ Hz, $-OCH_2-CH_3$), ^{13}CNMR (75 MHz, $CDCl_3$, 25 °C) δ 146.01 (d, $J = 14.6$ Hz), 134.60, 133.70, 129.26 128.19, 128.89, 128.86, 118.66, 113.83, 63.38 (d, J^2=6.8 Hz), 56.60, 54.61, 30.94, 16.36 (d, J^3_{CP}=13.7 Hz), 16.36 (d, J^3_{CP}=5.7 Hz). ^{31}P NMR (121 MHz, $CDCl_3$, 25 °C) δ 23.24 ppm.

2.2.3. Diethyl [4-nitrophenyl (phenylamino) methyl] phosphonate (4c)

Yellow crystalline solid, 93% yield, mp 89.2 °C. ^1H NMR (250 MHz, $CDCl_3$, 25 °C) δ 8.22–8.19 (m, 2H, HAr), 7.69–7.64 (dd, 2H, $J_{HP} = 8.80$, 2.3 Hz, HAr), 7. 15–7. 09 (m, 2H, HAr), 6.77–6.71 (t, 2H, $J = 7.4$ Hz, HAr), 6.59–6.52 (m, 2H, HAr), 4.92–4.81 (d, 1H, $J_{HP} = 25.2$ Hz, CHP), 4.19–4.10 (m, 2H, $-OCH_2-CH_3$), 4.09–4.02 (m, 1H, $-OCH_2-CH_3$), 3. 99–3. 95 (m, 1H, $-OCH_2-CH_3$), 1.30 (t, 3H, $J = 7.00$ Hz, $-OCH_2-CH_3$), 1.19 (t, 3H, $J = 7.1$ Hz, $-OCH_2-CH_3$). ^{13}C NMR (63 MHz, $CDCl_3$, 25 °C) δ 147.59, 145.63 (d, $J = 14.2$ Hz), 144.04 (d, $J = 2.5$ Hz), 129.34,

128.63 (d, $J = 4.9$ Hz), 123.75, 119.10, 113.79, 63.60 (dd, $J^2 =$ 17.1, 6.9 Hz), 57.20, 54.84, 16.30 (dd, $J^3_{CP} = 10.3, 5.5$ Hz). ^{31}P NMR (101 MHz, $CDCl_3$, 25 °C): δ 21.31 ppm. HRMS (ESI) *m/z* calcd for $C_{17}H_{21}N_2O_5P$ [M + H$^+$]: 387.1094; Found 387.1080.

2.2.4. Diethyl [1-naphtyl (phenylamino) methyl] phosphonate (4d)

White crystalline solid, 88% yield; mp 123 °C. ^{1}H NMR (250 MHz, $CDCl_3$, 25 °C) δ 8.26 (d, 1H, $J_{HP} = 8.3$ Hz, HAr), 7.89–7.44 (m, 6H, HAr), 7.05–7.02 (dd, 2H, $J = 8.5, 7.4$ Hz, HAr), 6.68–6.63 (dd, 1H, $J = 10.6, 4.1$ Hz, HAr), 6.57–6.53 (m, 2H, HAr), 5.60 (d, 1H, $J_{HP} = 24.1$ Hz, CHP), 5.10 (s, 1H, NH), 4.25–4.13 (m, 2H, –OCH_2–CH_3), 3.75–3.72 (m, 1H, –OCH_2–CH_3), 3.25–3.15 (m, 1H, –OCH_2–CH_3), 1.33 (t, 3H, $J = 7.00$ Hz, –OCH_2–CH_3), 0.70 (t, 3H, $J = 7.1$ Hz, –OCH_2–CH_3). ^{13}C NMR (63 MHz, $CDCl_3$, 25 °C) δ 146.11 (d, $J = 13.9$ Hz), 133.81, 131.63 (d, $J = 8.0$ Hz), 129.09 (d, $J = 10.6$ Hz), 128.44, 126.25, 126.05, 125.65, 125.37 (d, $J = 5.8$ Hz), 122.94, 118.26, 113.57, 63.26 (dd, $J^2_{CP} = 12.4, 6.8$ Hz), 52.67, 50.25, 16.45 (d, $J^3_{CP} = 6.2$ Hz), 15.75 (d, $J^3_{CP} = 5.7$ Hz). ^{31}P NMR (101 MHz, $CDCl_3$, 25 °C): δ 22.98 ppm. HRMS (ESI) *m/z* calcd for $C_{21}H_{24}NO_3P$ [$M + H^+$]: 392.1401; Found 392.1386.

2.2.5. Diethyl [4-biphenyl (phenylamino) methyl] phosphonate (4e)

White crystalline solid, yield: 86%; mp 158 °C. ^{1}H NMR (300 MHz, $CDCl_3$) δ 7.64–7.53 (m, 6H, HAr), 7.45 (t, $J = 7.4$ Hz, 2H, HAr), 7.36 (t, $J = 6.7$ Hz, 1H, HAr), 7.15 (t, $J = 7.9$ Hz, 2H, HAr), 6.74 (t, $J = 7.3$ Hz, 1H, HAr), 6.66 (d, $J = 8.1$ Hz, 2H, HAr), 4.89 (d, $J = 7.5$ Hz, ^{1}H, HCP), 4.80 (d, $J = 7.7$ Hz, 1H, NH), 4.27–4.09 (m, 2H, –OCH_2–CH_3), 4.01–3.80 (m, 1H, –OCH_2–CH_3), 3.78–3.96 (m, 1H, –OCH_2–CH_3), 1.33 (t, $J = 7.1$ Hz, 3H, –OCH_2–CH_3), 1.18 (t, $J = 7.1$ Hz, 3H, –OCH_2–CH_3). ^{13}C NMR (75 MHz, $CDCl_3$, 25 °C) δ 146.26 (d, $J = 21.3$ Hz), 140.70 (d, $J = 6.8$ Hz), 134.92, 129.22, 128.78, 128.72, 128.23 (d, $J = 5.4$ Hz), 127.35 (d, $J = 2.9$ Hz), 127.29, 127.02, 118.48, 113.88, 63.35 (d, $J^2_{CP} =$ 7.0 Hz), 56.81, 54.82, 16.47 (d, $J^3_{CP} = 5.8$ Hz), 16.25 (d, $J^3_{CP} =$ 6.1 Hz). ^{31}P NMR (121 MHz, $CDCl_3$, 25 °C): δ 22.58 ppm. HRMS (ESI) *m/z* calcd for $C_{23}H_{26}NO_3P$ [$M + H^+$]: 418.1550; Found 418.1542.

2.2.6. Diethyl [4-methoxyphenyl (phenylamino) methyl] phosphonate (4f)

White crystalline solid, yield: 90%; mp 103 °C. ^{1}H NMR (300 MHz, $CDCl_3$, 25 °C) δ 7.36–7.30 (m, 2H, ArH), 7.07–7.13 (m, 2H, HAr), 6.85 (d, *J*=Hz, 2H, HAr), 6.66 (t, $J = 16.0$ Hz, 1H, HAr), 6.58 (d, 2H, J = Hz, HAr), 4.72 (d, $J = 24.4$ Hz, 1H, CHP), 4.15 (m, 2H, –OCH_2–CH_3), 3.91 (m, 1H, –OCH_2–CH_3), 3.77 (s, 3H, –OCH_3), 3.65–3.74 (m, 1H, –OCH_2–CH_3), 1.28 (t, 3H, $J = 7.0$ Hz, –OCH_2–CH_3), 1.14 (t, 3H, $J = 7.0$ Hz, –OCH_2–CH_3), 4.89 (d, $J = 7.5$ Hz, ^{1}H, HCP), 4.80 (d, $J = 7.7$ Hz, 1H, NH), 4.27–4.09 (m, 2H, –OCH_2–CH_3), 4.01–3.80 (m, 1H, –OCH_2–CH_3), 3.78–3.96 (m, 1H, –OCH_2–CH_3), 1.33 (t, $J = 7.1$ Hz, 3H, –OCH_2–CH_3), 1.18 (t, $J = 7.1$ Hz, 3H, –OCH_2–CH_3). ^{13}C NMR (75 MHz, $CDCl_3$, 25 °C) δ 146.26 (d, $J = 21.3$ Hz), 140.70 (d, $J = 6.8$ Hz), 134.92, 129.22, 128.78, 128.72, 128.23 (d, $J = 5.4$ Hz), 127.35 (d, $J = 2.9$ Hz), 127.29, 127.02, 118.48, 113.88, 63.35 (d, $J^2_{CP} =$ 7.0 Hz), 56.81, 54.82, 16.47 (d, $J^3_{CP} = 5.8$ Hz), 16.25 (d, $J^3_{CP} =$ 6.1 Hz). ^{31}P NMR (121 MHz, $CDCl_3$, 25 °C): δ 22.58 ppm. HRMS (ESI) *m/z* calcd for $C_{23}H_{26}NO_3P$ [$M + H^+$]: 418.1550; Found 418.1542.

2.2.7. Diethyl [phenyl (p-tolylamino) methyl] phosphonate (4g)

Yield: 94% as a white crystalline solid; mp 120 °C. ^{1}H NMR (300 MHz, $CDCl_3$, 25 °C) δ 7.49–7.47 (m, 2H, HAr), 7.37–7.27 (m, 3H, HAr), 6.93 (d, $J = 8.3$ Hz, 2H, HAr), 6.53 (d, 2H, $J = 8.4$ Hz, HAr), 4.76 (d, $J = 24.2$ Hz, 2H, HCP and NH), 4.17–4.10 (m, 2H, –OCH_2–CH_3), 4.00–3.92 (m, 1H, –OCH_2–CH_3), 3.74–3.66 (m, 1H, –OCH_2–CH_3), 2.20 (s, 3H, CH_3–Ph), 1.30 (t, 3H, $J = 7.1$ Hz, –OCH_2–CH_3), 1.13 (t, 3H, $J = 7.1$ Hz, –OCH_2–CH_3). ^{13}C NMR (75 MHz, $CDCl_3$, 25 °C) δ 143.95 (d, $J = 15.1$ Hz), 135.98, 129.62, 128.50, 127.81 (d, $J = 4.7$ Hz), 127.58, 113.96, 64.83–61.51 (m), 57.54, 55.15, 20.31, 16.27 (dd, $J^3_{CP} = 15.2, 5.7$ Hz), ^{31}P NMR (101 MHz, $CDCl_3$, 25 °C) δ 21.48 ppm. HRMS (ESI) *m/z* calcd for $C_{18}H_{24}NO_3P$ [$M + H^+$]: 356.1397; Found 356.1386.

2.2.8. Diethyl [4 chlorophenyl (p-tolylamino) methyl] phosphonate (4h)

White crystalline solid, 90% yield, mp 119.5 °C. ^{1} HNMR (300 MHz, $CDCl_3$, 25 °C) δ 7.43 (dd, $J = 12.0, 4.0$ Hz, 2H, HAr), 7.26 (m, 2H, HAr), 6.93(d, 2H, $J = 8.2$ Hz, HAr), 6.48(d, 2H, $J = 8.5$ Hz, HAr), 4.64–4.78(m, 2H, CH–NH), 4.10–4.17(m, 2H, –OCH_2–CH_3), 3.97–4.05(m, 1H, –OCH_2–CH_3), 3.79–3.85(m, 1H, –OCH_2–CH_3), 2.21 (s, 3H, CH_3–Ph), 1.31 (t, 3H, $J = 7.1$ Hz, –OCH_2–CH_3), 1.18 (t, 3H, $J = 7.1$ Hz, –OCH_2–CH_3). ^{13}C NMR (75 MHz, $CDCl_3$, 25 °C) δ 143.85 (d, $J = 15.0$ Hz), 134.84, 133.80, 133.76, 133.71, 129.83, 129.28, 128.21, 127.89, 127.86, 128.03, 114.06, 63.59 (dd, $J^2 =$ 12.1, 7.0 Hz), 56.89, 54.89, 20.47, 16.59 (d, $J^3_{CP} = 13.7$ Hz), 16.52 (d, $J^3_{CP} = 5.8$ Hz). ^{31}P NMR (121 MHz, $CDCl_3$, 25 °C) δ 22.69 ppm.

2.2.9. Diethyl [4-nitrophenyl (p-tolylamino) methyl] phosphonate (4i)

Yellow crystalline solid, 92% yield; mp 158 °C. ^{1}H NMR (300 MHz, $CDCl_3$, 25 °C) δ 8.21 (d, $J = 8.5$ Hz, 2H, HAr), 7.67 (dd, $J = 8.8, 2.3$ Hz, 2H, HAr), 6.94 (d, 2H, $J = 8.3$ Hz, HAr), 6.46 (d, $J = 8.4$ Hz, 2H, HAr), 4.85 (d, $J = 25.1$ Hz, 2H, HCP + NH), 4.20–4.02 (m, 3H, –OCH_2–CH_3), 3.94–3.86 (m, 1H, –OCH_2–CH_3), 2.35 (s, 3H, CH_3–Ph), 1.32 (t, 3H, $J = 7.1$ Hz, –OCH_2–CH_3), 1.21 (t, 3H, $J = 7.1$ Hz, –OCH_2–CH_3). ^{13}C NMR (75 MHz, $CDCl_3$, 25 °C) δ 147.54, 144.20, 143.25 (d, $J = 14.8$ Hz), 129.86, 128.65 (d, $J = 4.8$ Hz), 128.62, 123.74, 113.93, 63.58 (dd, J^2 CP = 23.8, 6.9 Hz), 57.26, 55.29, 20.36, 16.45 (d, $J^3_{CP} = 12.6$ Hz), 16.30 (d, $J^3_{CP} = 5.8$ Hz). ^{31}P NMR (121 MHz, $CDCl_3$, 25 °C) δ 20.94 ppm. HRMS (ESI) *m/z* calcd for $C_{18}H_{24}N_2O_5P$ [$M + H^+$]: 379.1412; Found 379.1417.

2.2.10. Diethyl [4-methoxy phenyl (p-tolylamino) methyl] phosphonate (4j)

White crystalline solid, 90% yield; mp 99 °C. ^{1} HNMR (300 MHz, $CDCl_3$, 25 °C) δ 7.26–7.39 (m, 2H, HAr),6.92(dd, J = 16.0, 8.5 Hz, 4H, HAr), 6.49 (d, 2H, J = 8.4 Hz, HAr), 4.70 (d, J = 24.5 Hz, 2H, CHP–NH),3.99–4.15 (m, 2H, –OCH_2–CH_3),3.91–3.96 (m, 1H, –OCH_2–CH_3), 3.77(s, 3H, –OCH_3), 3.66–3.74 (m, 1H, –OCH_2–CH_3), 2.18 (s, 3H, CH_3Ar), 1.28 (t, 3H, J = 7.1 Hz, –OCH_2–CH_3), 1.14 (t, 3H, J = 7.1 Hz, –OCH_2–CH_3). ^{13}CNMR (75 MHz, $CDCl_3$, 25 °C) δ159.20, 144.20 (d, J = 15.4 Hz), 129.76, 129.08, 129.01, 127.92, 127.88, 127.68, 114.12, 63.38 (dd, J^2 = 6.9, 2.9 Hz), 56.74, 55.34, 54.72, 20.49, 16.63 (d, J^3_{CP} = 14.0 Hz), 16.55 (d, J^3_{CP} = 5.8 Hz). ^{31}P NMR (121 MHz, $CDCl_3$, 25 °C) δ 23.59 ppm.

2.2.11. Diethyl [1-naphtyl (p-tolylamino) methyl] phosphonate (4k)

White crystalline solid, 93% yield; mp 145 °C. ^{1}H NMR (300 MHz, $CDCl_3$, 25 °C) δ 8.27 (d, 1H, J_{HP} = 8.5 Hz, HAr), 7.91 (d, 1H, J = 7.9 Hz, HAr), 7.80–7.77 (m, 2H, HAr), 7.63–7.48 (m, 2H, HAr), 7.45 (t, 1H, J = 7.7 Hz, HAr), 6.67 (d, 2H, J = 8.48 Hz, HAr), 6.48 (d, 2H, J = 8.4 Hz, HAr), 4.64 (d, 1H, J_{HP} = 24.0 Hz, HCP), 4.23–4.15 (m, 2H, –OCH_2–CH_3), 3.77–3.73 (m, 1H, –OCH_2–CH_3), 3.28–3.17 (m, 1H, –OCH_2–CH_3), 2.16 (s, 3H, CH_3–Ph), 1.34 (t, 3H, J = 7.1 Hz, –OCH_2–CH_3), 0.75 (t, 3H, J = 7.1 Hz, –OCH_2–CH_3). ^{13}C NMR (75 MHz, $CDCl_3$) δ 143.83 (d, J = 24.8 Hz), 133.81, 131.6 (d, J = 19.7 Hz), 129.70, 129.00, 128.40, 127.50, 126.22, 125.64, 125.35 (d, J = 6.0 Hz), 123.00, 113.67, 20.33, 16.49 (dd, J^3_{CP} = 5.9, 5.9 Hz). ^{31}P NMR (121 MHz, $CDCl_3$, 25 °C) δ 23.07 ppm. HRMS (ESI) *m/z* calcd for $C_{22}H_{26}NO_3P$ [$M + H^+$]: 406.1555; Found 406.1542.

2.2.12. Diethyl [4-biphenyl (p-tolylamino) methyl] phosphonate (4l)

White crystalline solid, yield 90%; mp 140 °C. ^{1}H NMR (300 MHz, $CDCl_3$, 25 °C) δ 7.42–7.59 (m, 6H, ArH), 7.26–7.39 (m, 3H, HAr), 6.93 (d, 2H, J = 8.2 Hz, HAr), 6.55 (d, 2H, J = 8.4 Hz, HAr), 4.79 (d, 1H, J = 24.3 Hz, HCP), 4.10–4.18 (m, 2H, –OCH_2–CH_3), 3.84–4.01 (m, 1H, –OCH_2–CH_3), 3.71–3.81 (m, 1H, –OCH_2–CH_3), 2.19 (s, 3H, CH_3Ar), 1.30 (t, 3H, J = 7.1 Hz, –OCH_2–CH_3), 1.15 (t, 3H, J = 7.0 Hz, –OCH_2–CH_3). ^{13}C NMR (75 MHz, $CDCl_3$, 25 °C) δ 143.82, 140.59, 129.67, 128.70, 128.20 (d, J = 5.5 Hz), 127.66, 127.24 (d, J = 2.7 Hz), 126.96, 113.98, 63.31 (t, J = 7.0 Hz), 57.28, 54.87, 20.33, 16.38 (d, J^3_{CP} = 14.0 Hz), 16.16 (d, J^3_{CP} = 5.5 Hz) ^{31}P NMR (121 MHz, $CDCl_3$, 25 °C): δ 22.71 ppm. HRMS (ESI) *m/z* calcd for $C_{24}H_{29}NO_3P$ [$M + H^+$]: 410.1876; Found 410.1879.

2.2.13. Diethyl [4-nitro phenyl (p-tolylamino) methyl] phosphonate (4m)

White crystalline solid, yield 80%; mp 137 °C. ^{1}H NMR (360 MHz, Chloroform-*d*) δ 8.08–8.00 (m, 2H, HAr), 7.36 (dd, J = 8.2, 2.2 Hz, 3H, HAr,), 7.19 (d, J = 8.2 Hz, 2H, HAr), 6.65–6.57 (m, 2H, HAr), 4.80 (dd, J = 23.7, 7.6 Hz, 1H, *CH), 4.25–4.07 (m, 2H, –OCH_2–CH_3), 3.96 (m, 1H, –OCH_2–CH_3), 3.76–3.59 (m, 1H, –OCH_2–CH_3), 2.36 (d, J = 1.9 Hz, 3H, CH_3Ar), 1.34 (t, J = 7.0 Hz, 3H, –OCH_2–CH_3), 1.16 (t, J = 7.3 Hz, 3H, –OCH_2–CH_3). ^{13}C NMR (91 MHz, Chloroform-*d*) δ 138.36 (d, J = 3.6 Hz), 131.40 (d, J = 3.3 Hz), 129.90–129.35 (m), 127.61 (d, J = 5.4 Hz), 126.05, 112.45, 63.54 (dd, J = 48.3, 7.1 Hz), 56.18, 54.50, 16.43 (d, J^3_{CP} =5.8 Hz), 16.20 (d, J^3_{CP} = 5.7 Hz). ^{31}P NMR (101 MHz, Acetone-d_6) δ 21.39. HRMS (ESI) *m/z* calcd for $C_{18}H_{23}N_2NaO_5P$ [M + Na^+]: 401.1239; Found. 401.1222.

2.2.14. Diethyl [2-methoxyphenyl (4-bromo,2,6-dimethylamino) methyl] phosphonate (4n)

White crystalline solid, yield 92%; mp 106.8 °C. ^{1}H NMR (360 MHz, Chloroform-*d*) δ 7.65 (d, J = 11.1 Hz, 2H, ArH), 7.27 (d, J = 9.9 Hz, 1H, ArH), 7.04 (d, J = 18.1 Hz, 3H, ArH), 6.85 (d, J = 8.3 Hz, 1H, ArH), 5.25 − 5.02 (m, 1H, –OCH_2–CH_3), 4.33 − 4.06 (m, 2H, –OCH_2–CH_3), 3.96 − 3.84 (m, 1H, –OCH_2–CH_3), 3.75 (s, 3H, –OCH_3), 3.71 − 3.58 (m, 1H, –OCH_2–CH_3), 2.24 (s, 6H, 2CH_3Ar), 1.29 (t, J = 7.1 Hz, 3H, –OCH_2–CH_3), 1.05 (t, J = 7.1 Hz, 3H, –OCH_2–CH_3). ^{13}C NMR (91 MHz, Chloroform-*d*) δ 156.79 (d, J = 7.3 Hz), 143.86 (d, J = 9.1 Hz), 131.08 (d, J = 5.3 Hz), 129.06, 125.86, 120.90 (d, J = 1.9 Hz), 113.70, 110.74, 63.23 − 62.23 (m), 55.62, 16.23 (dd, J^3_{CP} = 22.3, 5.7 Hz). ^{31}P NMR (101 MHz, Acetone-d_6 25 °C) δ 24.89 ppm. HRMS (ESI) *m/z* calcd for $C_{20}H_{28}BrNNaO_4P$ [M + Na^+]: 478.0753; Found 478.0742.

2.2.15. Diethyl [3-methoxyphenyl (4-bromo,2,6-dimethylamino) methyl] phosphonate (4o)

White crystalline solid, yield 88%; mp 113 °C. ^{1}H NMR (360 MHz, Chloroform-*d*) δ 7.33–7.21 (m, 1H, ArH), 7.07 (s, 2H, ArH), 7.06–6.95 (m, 2H, ArH), 6.85 (d, J = 9.2 Hz, 1H, ArH), 4.53 − 4.34 (m, 1H, *CH), 4.23 − 4.09 (m, 2H, –OCH_2–CH_3), 3.95 (m, 1H, –OCH_2–CH_3), 3.81 (s, 3H, –OCH_3), 3.74–3.59 (m, 1H, –OCH_2–CH_3), 2.23 (s, 6H, 2CH_3Ar), 1.31 (t, J = 7.1 Hz, 3H, –OCH_2–CH_3), 1.09 (t, J = 7.1 Hz, 3H, –OCH_2–CH_3). ^{13}C NMR (91 MHz, Chloroform-*d*) δ 131.35, 130.90, 129.42, 120.61 (d, J = 6.4 Hz), 113.80 (dd, J = 22.6, 15.9 Hz), 62.93 (dd, J = 34.7, 7.2 Hz), 18.73, 16.39 (d, J^3_{CP} = 6.2 Hz), 16.14 (d, J^3_{CP} = 5.9 Hz). ^{31}P NMR (101 MHz, Acetone-d_6, 25 °C) δ 23.93 ppm. HRMS (ESI) *m/z* calcd for $C_{20}H_{27}BrNNaO_4P$ [M +Na^+]: 478.0753; Found 478.0738.

2.2.16. Diethyl [4-trifluoromethyl phenyl (phenylamino) methyl] phosphonate (4p)

White crystalline solid, yield 80%; mp 140 °C. ^{1}HNMR (300 MHz, $CDCl_3$, 25 °C) δ 1.12 (t, 3H, J = 7.0 Hz, –OCH_2–CH_3), 1.31 (t, 3H, J = 7.1 Hz, –OCH_2–CH_3), 3.61–3.70 (m, 1H, –OCH_2–CH_3), 3.90–4.08 (dp, J = 10.1, 7.1 Hz, 1H, –OCH_2–CH_3), 4.10–4.20 (m, 2H, –OCH_2–CH_3), 4.79 (dd, 1H, J = 24.2, 7.5 Hz, Ph–CH), 5.16–5.31 (m, 1H, NH), 6.62 (d, 2H, J = 8.5 Hz, HAr), 7.26–7.40 (m, 5H, HAr),7.49 (dd, J = 7.7,2.1 Hz, 2H, HAr).^{13}CNMR (75 MHz, $CDCl_3$, 25 °C) δ 148.90 (d, J = 14.4 Hz), 135.13(d, J = 3.0 Hz), 128.91, 128.87, 128.38, 128.34, 127.90, 127.83, 126.68, 126.63, 113.16, 63.75 (dd, J^2_{CP} = 22.9,7.0 Hz), 56.77, 54.77, 16.59 (d, J^3_{CP} = 19.0 Hz), 16.51 (d, J^3_{Cp} = 5.8 Hz).^{31}P NMR (121 MHz, $CDCl_3$, 25 °C) δ = 22.54 ppm.

2.2.17. Diethyl [4-chlorophenyl (4-trifluoromethylphenylamino) methyl] phosphonate (4q)

White crystalline solid, yield 80%; mp 129 °C. ^{1}HNMR (300 MHz, $CDCl_3$, 25 °C): δ = 1.18 (t, 3H, *J* = 6.9 Hz, –OCH_2–CH_3), 1.32 (t, 3H, *J* = 7.1 Hz, –OCH_2–CH_3), 3.72–3.81 (m, 1H, –OCH_2–CH_3), 3.96–4.01(m,1H, –OCH_2–CH_3),4.04–4.18 (m, 2H, –OCH_2–CH_3), 4.70 (dd, 1H, *J* = 24.4,7.3 Hz,CHP),5.16 (dd, 1H, *J* = 10.2, 7.5 Hz, –NH), 6.60 (d, 2H, *J* = 8.6 Hz, HAr), 77.28–7.43 (m, 6H, HAr).^{13}CNMR (75 MHz, $CDCl_3$, 25 °C) δ 148.61 (d, *J* = 14.2 Hz),134.24 (d, *J* = 3.9 Hz), 134.19, 133.96, 133.92, 129.19, 129.12, 126.76, 126.71, 113.19, 63.71 (dd, J^2 = 11.2, 7.0 Hz), 56.27, 54.27, 16.60 (d, J^3_{CP} = 13.9 Hz),16.53 (d, J^3_{CP} = 5.7 Hz). ^{31}P NMR (121 MHz, $CDCl_3$, 25 °C) δ 21.87 ppm.

2.2.18. Diethyl [4-methoxyphenyl (4-trifluoromethylphenylamino) methyl] phosphonate (4r)

White crystalline solid, yield 88%; mp 111 °C. ^{1}HNMR (300 MHz, $CDCl_3$, 25 °C) δ 7.26–7.40 (m, 4H, HAr), 6.90 (d, 2H, *J* = 8.5 Hz, HAr), 6.63 (d, 2H, *J* = 8.5 Hz, HAr), 5.15 (dd, *J* = 9.7,7.8 Hz, 1H, –NH), 4.73 (dd, 1H, *J* = 23.8, 7.6 Hz, CHP), 4.13 (m, 2H, –OCH_2–CH_3), 3.95 (m, 1H, –OCH_2–CH_3), 3.80 (s, 3H, –OCH_3), 3.63–3.72 (m, 1H, –OCH_2–CH_3), 1.31 (t, 3H, *J* = 7.1 Hz, –OCH_2–CH_3), δ 1.15 (t, 3H, *J* = 7.0 Hz, –OCH_2 –CH_3). ^{13}C NMR (75 MHz, $CDCl_3$, 25 °C) δ 159.60, 148.16 (d, *J* = 14.3 Hz), 128.97, 126.96, 126.67, 114.35 (d, *J* = 2.3 Hz), 113.19, 63.70 (dd, J^2=24.1,7.0 Hz), 56.10, 55.38, 54.08, 16.61 (d, J^3_{CP} = 13.9 Hz), 16.54 (d, J^3_{CP} = 5.8 Hz). ^{31}P NMR (121 MHz, $CDCl_3$, 25 °C) δ 22.77 ppm.

2.3. Computational details

2.3.1. Quantum chemical calculations

All quantum chemical calculations were performed using DFT method in the Gaussian 09 program package (Frisch et al., 2009). Gauss View 5.0.8 computer program was used to visualize the results (Dennington et al., 2009). The geometries were optimized at the long-range corrected (CAM-B3LYP) functional (Yanai et al., 2004) with standard 6-31G (d, p) basis set (Becke, 1993). The calculated energies of the highest occupied molecular orbital (E_{HOMO}) and lowest unoccupied molecular orbital (E_{LUMO}) have been used to determine various quantum chemical parameters such as the energy gap (ΔE_{gap}), the dipole moment (μ), chemical hardness (η), chemical softness (σ), electronegativity (χ) and global electrophilicity index (ω), using the following equations (Feng et al., 2018; Kohn & Sham, 1965).

$$\Delta E_{gap} = E_{LUMO} - E_{HOMO} \quad (1)$$

$$\eta = \frac{E_{LUMO} - E_{HOMO}}{2} \quad (2)$$

$$\sigma = \frac{1}{\eta} \quad (3)$$

$$\chi = -\frac{(E_{HOMO} + E_{LUMO})}{2} \quad (4)$$

$$\omega = \left(\frac{\chi^2}{2\eta}\right) \quad (5)$$

2.3.2. In silico drug-likeness and ADMET prediction

In order to screen the physicochemical characteristics, pharmacokinetic behavior and the drug likeness; in *silico* ADME (Absorption, Distribution, Metabolism and Excretion) parameters and toxicity prediction of the designed compounds were calculated using the SwissADME (http://www.swissadme.ch) (Daina et al., 2017). Lipinski's rule of five, Ghose, Veber, Egan, Muegge and synthetic accessibility were prerequisite to ensure drug-like properties when using rational drug design. (mol. wt. ≤ 500 Da; log P o/*w* ≤ 5; HBD ≤ 5; HBA ≤ 10). Solubility (LogS): Should be > −4. Van der Walls topological polar surface area (TPSA) value is (≤140 Å^2) (Lipinski, 2016; Olasupo et al., 2020).

2.3.3. Molecular docking studies

A molecular docking study of the three α-aminophosphonates synthesized (**4p, 4q** and **4r**) and Adriamycin (ADM) taken as reference was performed using Auto-DockTools (ADT) (Morris et al., 2009), software and AutoDock Vina program, (Oleg & Olson, 2010), and the 3D structure of target protein Human topoisomerase IIα (PDB ID: 1ZXM, Resolution: 1.87 Å) (Wei et al., 2005) was obtained from RCSB protein data bank. All ligands were geometrically optimized by DFT calculation. The docked poses and ligand-protein interactions were visualized using the Discover Studio Visualizer software (Chung-Kiak & Han-Ping, 2016). The analysis of the docked models was performed to investigate the binding affinity and the nature of the intermolecular bonding interactions between each species and the target proteins. The modes of interactions of the ligand with proteins were determined by investigating their favorable orientations of binding.

3. Results and discussion

3.1. Synthesis

Herein, in our quest for developing the optimization reaction conditions we performed using the condensation of aromatic aldehyde (1 mmol), aniline (1 mmol) and diethylphosphite (1.2 mmol) as study model. First, we have used blank reaction without catalyst then we have investigated the effect of several crown ethers as organocatalysts in the multicomponents reaction for the synthesis of α-aminophsphonate. To determine the best catalyst, we have selected: 18-crown-6 **(A)**, 15-crown-5 **(B)**, 12-crown-4 **(C)**, 2-hydroxymethyl-18-crown-6 **(D)** and bibenzo-18-crown-6 **(E)** (Figure. 1). All these catalysts were loading at 5 mol%, and the reactions carried in THF at room temperature within 24 h.

The obtained results show that no reaction was observed without catalyst (Table 1, entry 1), and traces of products appear using the organocatalysts chosen whatever the crown's size, such as; 18-crown-6 **(A),** 15-crown-5 **(B)**, 12-crown-4 **(C)** and dibenzo-18-crown-6 **(E)** (Table 1, entries 2, 3, 4 and 6**)**. Therefore, the hydroxymethyl linked to 18-crown-6 **(D)** led to obtain the desired product with excellent yield (91%) (Table 1, entry 5). These results explained by the efficiency of the catalyst to activate the carbonyl of aromatic

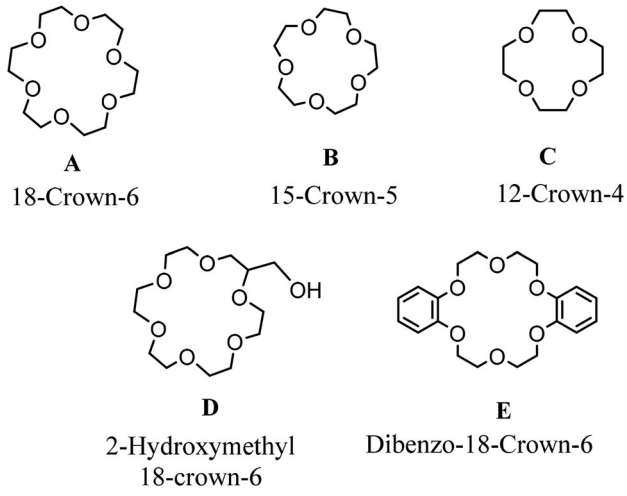

Figure 1. Crown ethers tested.

Table 1. Different catalysts tested.[a]

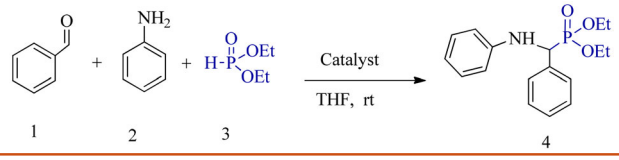

Entry	Catalyst (5 mol%)	Yield (%)[c]
1[b]	Free-catalyst	–
2	18-Crown-6 **(A)**	Traces
3	15-Crown-5 **(B)**	Traces
4	12-Crown-4 **(C)**	Traces
5	**2-Hydroxymethyl-18-crown-6 (D)**	**91**
6	Dibenzo-18-crown-6 **(E)**	Traces

[a]Reaction conditions: benzaldehyde (1 mmol), aniline (1 mmol) and diethylphosphite (1.2 mmol) were stirred with catalyst (5 mol%) in THF (2 mL) at room temperature, within 24 h.
[b]Reaction without catalyst.
[c]Yield of the pure product purified by crystallization in hexane.

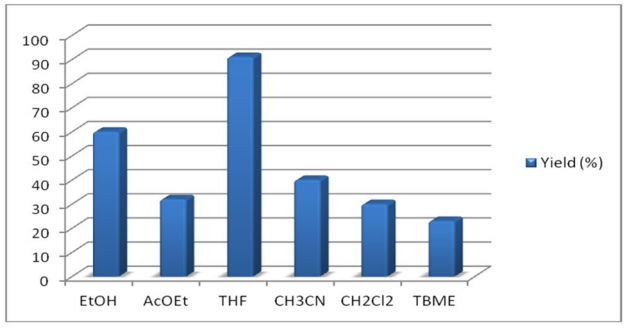

Figure 2. Impact of the organic solvent hydrophobicity's (reaction conditions: 2-hydroxymethyl-18-crown-6 (5 mol%), 2 mL of solvent, rt, 24 h).

aldehyde which facilitate the nucleophilic attack of diethylphosphite. The best recorded results were shown using of 2-hydroxymethyl-18-crown-6 **(D)** (5 mol %) in THF (2 mL) at room temperature giving the α-aminophosphonate **4a** in 91% yield.

Owing the encouraged results obtained with the 2-hydroxymethyl-18-crown-6 **(D)** described above, we have envisaged to checking the impact of the hydrophobicity-hydrophilicity of the organic medium on the outcome of our optimized reaction. For that, several organic solvents have been tested, such as: THF (logP = 0.46), EtOH (logP = −0.18), CH_2Cl_2 (logP = 1.25), CH_3CN (logP = −0.37), AcOEt (logP = 0.73) and TBME (logP = 0.35). The recorded results reveal that no significant correlation between the chemical yields of the product **4a** and the logP coefficient. The best result was recorded in THF as solvent giving the desired product with excellent yield (91%). Low yields of the reactions were observed in TBME, AcOEt and CH_2Cl_2 (<30%), while 40% chemical yield was obtained in CH_3CN. In EtOH, the desired product was recovered in 66% yield under the same conditions, which illustrated in Figure. 2. The α-aminophosphonate was easily obtained by crystallization from hexane. In addition, it is important to underline the total disappearance of all reagents in THF within 15 min of stirring.

In order to validate the optimum conditions using 2-Hydroxymethyl-18-crown-6 **(D)**, we applied them on a set of substituted benzaldehyde and aniline with electron-withdrawing and electron-donating. The results summarized in Table 2 showed the efficiency of 2-hydroxymethyl-18 crown-6 **(D)**, used as novel organocatalyst in the MCRs by *Kabachnik–Fields* reaction for P-C bond formation by α-aminophosphonates preparation.

All the chemical yields showed in the Table 2 were obtained by crystallization in hexane. The chemical yields of multicomponent reactions depend on the nature of electronic effects of the substrates. The use of benzaldehyde, 4-chlorobenzaldehyde, 4-nitrobenzaldehyde, 1-naphtaldehyde, 4-phenylbenzaldehyde and 4-methoxybenzaldehyde with aniline leads, respectively to **4a**, **4b, 4c 4d, 4e** and **4f** with yields between 80 and 93%. Similarly, using toluidine with the above series of aromatic aldehydes gives the **4g**, **4h, 4i, 4j, 4k** and **4l** with best results up to 90% yields, this due to the electron donating of toluidine.

The use of 4-nitroaniline with tolylbenzaldehyde gives the desired product **4m** with 80%, and the two products **4n** and **4o** are obtained with 92 and 88% yields by using 4-bromo, 2,6-dimethylaniline with 2-methoxy and 3 methoxy benzaldehyde respectively. The employ of 4-trifluoromethananiline with benzaldehyde, 4-chlorobenzaldehyde and 4-methoxybenz-aldehyde gives the α-aminophosphonaes **4p, 4q** and **4r** with 80%, 88% and 86% chemical yields respectively.

In order to understand the mechanism for the synthesis of α-aminophosphonates by multicomponents reaction using 2-hydroxymethyl-18-crown-6 as catalyst, we tested some other alcohols as catalysts in the same conditions, such as: ethanol, phenol and 2-hydroxymethyl phenol. The results show that traces of desired product were obtained using ethanol and phenol, however, a good yield (60%) was obtained using 2-hydroxymethyl phenol. In our case, we confirmed that the efficiency of 2-hydroxymethyl-18 crown-6 is due to the hydrogen bond with OH and the specificity of the crown ether cavity. Combining the viewpoints developed by our previous work (Aissa et al., 2022; Lakoud et al., 2016), and based on our above described observations, we proposed herein a mechanism for the multicomponents reaction using 2-Hydroxymethyl-18 Crown-6 as catalyst, as summarized in Scheme 1. However, we suppose that this

Table 2. 2-Hydroxymethyl-18-crown-6 catalyzed the synthesis of diethyl α-aminophosphonates **4a–r**.[a]

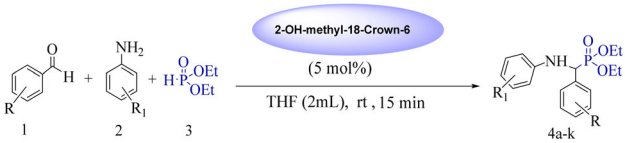

*Product **4a–r** (yield)*[b]

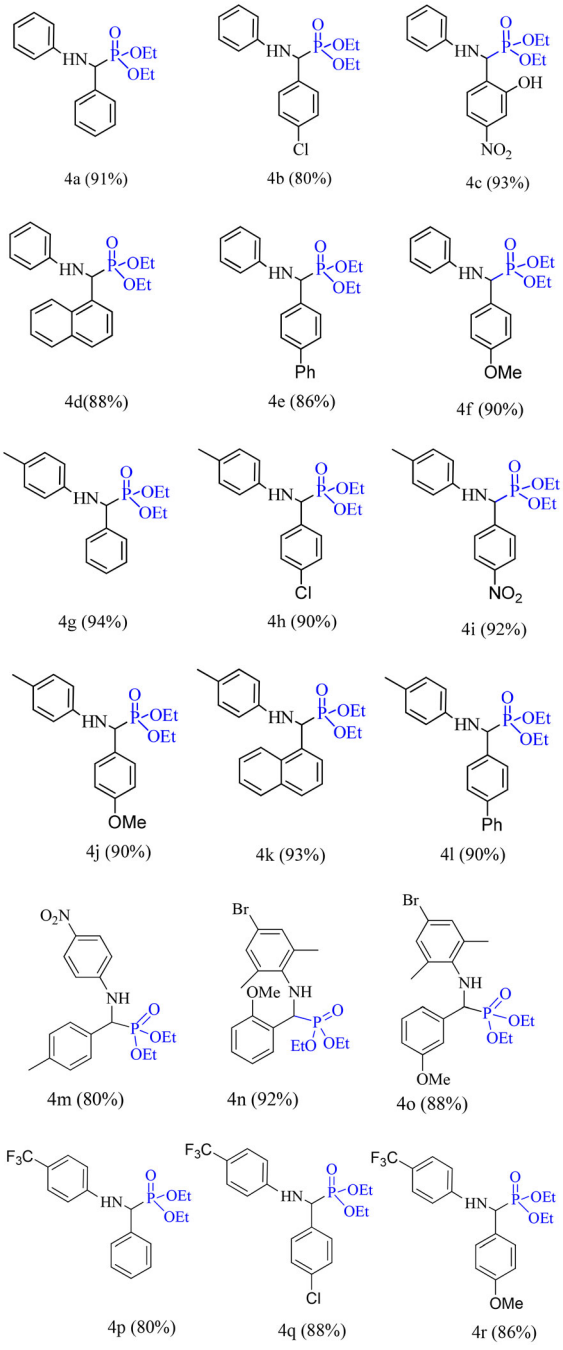

[a]Reaction conditions: aromatic aldehyde (1 mmol), aniline (1 mmol), diethylphosphite (1,2 mmol), 2-hydroxymethyl-18-crown-6 (5 mol%), room temperature, in THF within 15 min.
[b]Isolated yield after purification by crystallization from hexane.

organocatalyst plays a crucial role for the P–C bond formation. First, the 2-hydroxymethyl-18 Crown ether-6 probably coordinates the oxygen of benzaldehyde to accelerate the

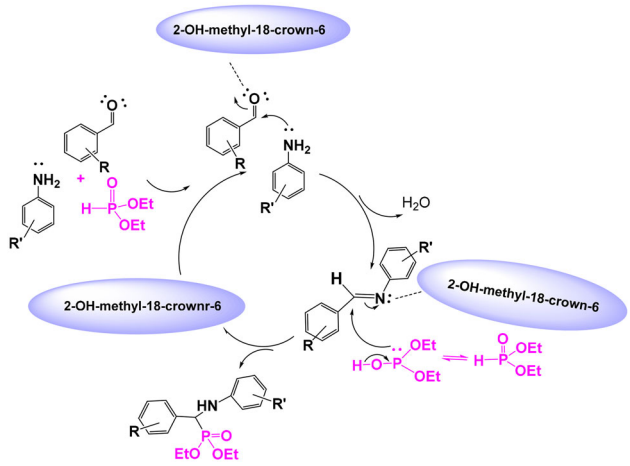

Scheme 1. Proposed mechanism of 2-hydroxymethyl-18-crown ether-6 catalyzed α-aminophosphonates synthesis.

nucleophilic attack of aniline to form an imine, then the 2-hydroxymethyl-18 crown ether-6 coordinates the imine by hydrogen bond to facilitate the nucleophilic attack of diethylphosphite to obtain the desired product.

Due to wide medicinal applications of fluorinated α-aminophosphonates compounds, many studies have reported the interesting biological properties of trifluoromethyl α-aminophosphonates derivatives, which showed the cytotoxic activity toward cancer cells (Kandula et al., 2017; Satish et al., 2018). Herein, we have scrutinized the three synthesized α-aminophosphonates (**4p, 4q** and **4r**) in quantum chemical calculations and modeling molecular study to determine the minimum energy molecular structure and to understand the correlation between the biological activity of α-aminophosphonates and their molecular structures (Cytlak et al., 2017; Turcheniuk et al., 2013).

3.2. DFT study

3.2.1. Optimization of structures

The geometry optimization of molecules synthesized (**4p**, **4q** and **4r**) was performed by minimizing the energy using DFT method at the CAM-B3LYP level with the base 6-31 G (d, p), and showed in Figure 3. The calculated values of total energy for each molecule at the optimal stage were: −1619.4040 a.u, −2078.9989 a.u and −1733.8816 a.u respectively, which signify the energy of the more stable conformation of the studied structures.

3.2.2. Frontier molecular orbital analysis

Frontier Molecular Orbitals HOMO (Highest Occupied Molecular Orbital) and LUMO (Lowest Unoccupied Molecular Orbital), or HOMO is directly related to ionization potential and can examined the aptitude of a molecule to contribute electrons to an electrophilic species, and LUMO is directly related to electron affinity and can determine the ability of a molecule to accept electrons from nucleophilic species (Elfily, 2020; Xavier & Periandy, 2015). These orbitals can describe significantly the stability and reactivity of drug molecules (Abraham et al., 2017; Asiri et al., 2011). So, the capacity of a

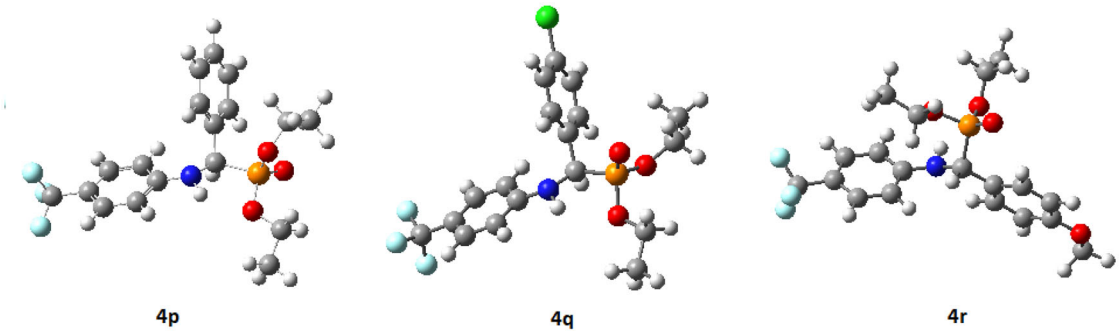

Figure 3. Theoretical optimized structures of **4p, 4q** and **4r** with CAM-B3LYP/6-31G (d,p) method.

Table 3. Calculated quantum chemical parameters of **4p, 4q** and **4r** using DFT/CAM-B3LYP/6-31G (d,p) method.

Compounds	E_{HOMO} (ev)	E_{LUMO} (ev)	ΔE (ev)	Dipole moment DM(D)	Hardness η (ev)	Softness σ (ev)	Electronegativity χ (ev)	Electrophilicity ω (ev)
4p	−7.202	0.8846	8.0866	5.0913	4.0433	0.2473	3.1587	1.2338
4q	−7.3097	0.6049	7.9146	6.0432	3.9573	0.2526	3.3524	1.4199
4r	−7.1021	0.9088	8.0109	3.2374	4.0054	0.2496	3.0966	1.1969

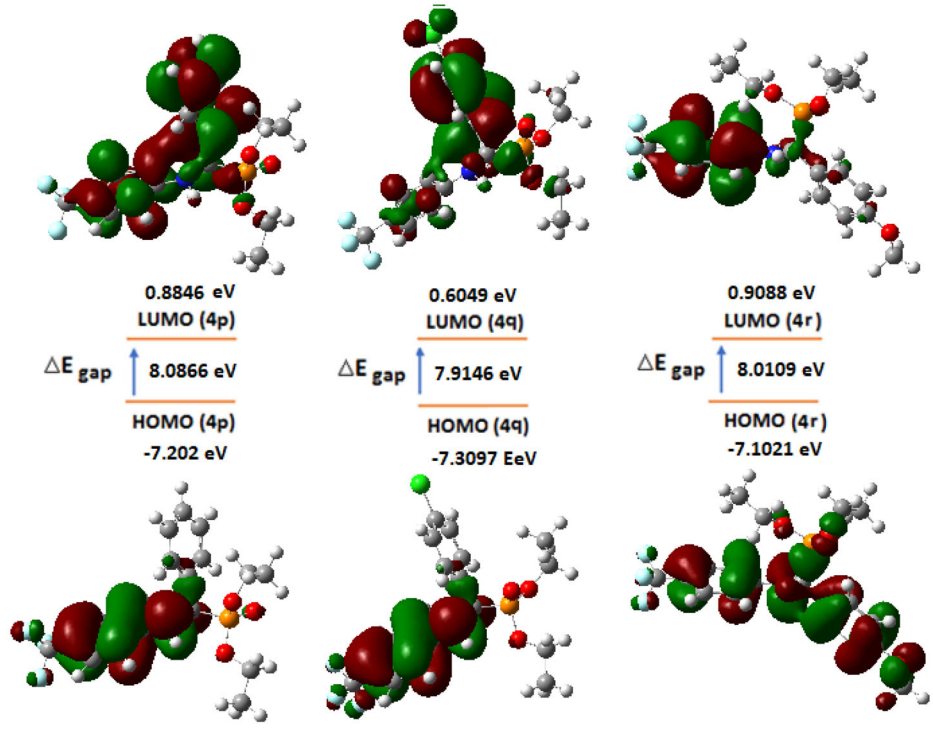

Figure 4. HOMO and LUMO orbitals of **4p, 4q** and **4r** with CAM-B3LYP/6-31G (d,p) method.

molecule to give electrons to an acceptor species is favored by the high values of E_{HOMO}, whereas the ability of a molecule to take electrons is preferred by the low values of E_{LUMO} (Mekky et al., 2015). Furthermore, the estimated value of HOMO-LUMO energy (ΔEgap) of drug molecules shows the energy required to excite a molecule's electrons. If the Δ*Egap* is small, molecules can be highly chemically reactive and unstable and readily excited, whereas if the Δ*Egap* is big, molecules can be very stable and less chemically reactive (Kosar & Albayrak, 2011).

Higher value of E_{HOMO} indicates a better tendency toward the donating electrons, the Table 3 show that the molecule **4p** and **4q** (E_{HOMO} = −7.202 eV and −7.309 eV) respectively are the most molecules have the ability to accept electrons, while **4r** has the highest HOMO energy (E_{HOMO} = −7.1021 eV) that allows it to be the best electron donor molecule.

The calculations show that the energy gap of **4p**, **4q** and **4r** are 8.0866 eV, 7.9146 eV and 8.0109 eV respectively as shown in Table 3, the compounds **4p** and **4r** have relatively higher energy gap than **4q,** which signifies the liberation of electrons to an acceptor molecule. Moreover, the calculated value of Δ Egap indicates the highly reactive molecules.

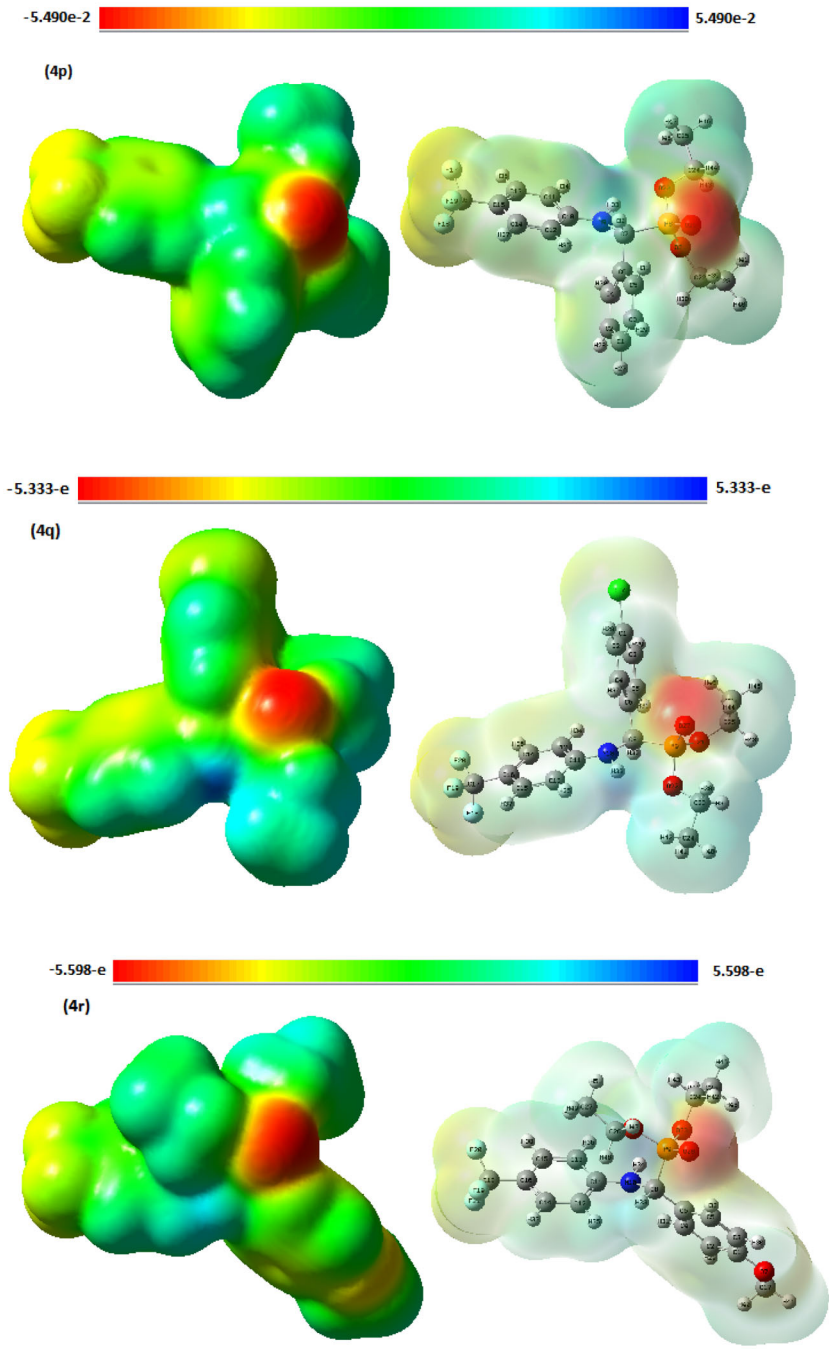

Figure 5. Molecular electrostatic potentials (MEP) for the investigated compounds.

Figure 4 illustrates the calculated HOMO and LUMO orbitals for the **4p, 4q** and **4r** ligands of α-aminophosphonates derivatives, which revealed that the HOMO and LUMO are frequently located on the aromatic ring and the amino group and on CF_3 group just for HOMO. On the outer hand, Table 3 shows that the studied molecules have an elevated value of E_{LUMO} and lower of E_{HOMO}.

3.2.3. Global reactivity descriptors

The polarity of pharmacological molecules is denoted by the dipole moment (μ), which is an important electronic property that results from the non-uniform distribution of charges on the different atoms. Table 3 shows that the calculated values of dipole moments in the case of **4q** (6.0432 D) is more superior than **4p** and **4r** (5.091 D and 3.2374 D) respectively, it can be explained by the difference in electronegativity caused by Cl. Furthermore, the hardness (η) and local softness (σ) of drug molecules can be used to assess their resistance to deformation of their electron clouds or polarization (Raafat et al., 2008). These two descriptors are essential properties to measure reactivity and the molecular stability of molecules. Chemical hardness corresponds to the energy gap between the LUMO and HOMO. The larger energy gap indicates that the molecule is harder and more stable therefore less reactive. As shown in Table 3, it can be seen that the

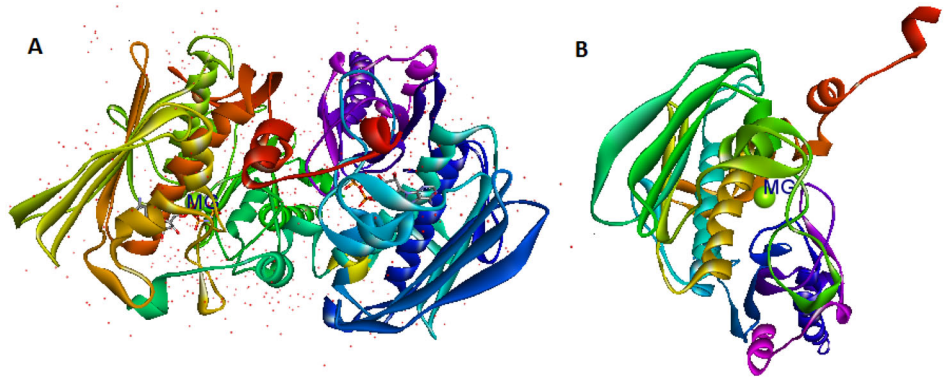

Figure 6. Crystalline structure of Human topoisomerase IIα (PDB ID: 1ZXM). A: No prepared, B: prepared.

Table 4. Binding scores and the non-bonding interactions of **4p**, **4q**, **4r** and the **ADM** with amino acid residues of 1ZXM.

Compounds	Docking score (Kcal/ mol)	Amino acid with hydrogen bonding interaction	N hydrogen bonding interaction [distance (Å)]	Hydrophobic interaction [distances (Å)]	Residues of binding site
4p	−8.2	Ser 149 Asn 95	1 (2.46) 1 (3.51)	Ala 167: Pi alkyl (4.69) Ile 217: Alkyl (4.52) Ale 118 : Alkyl (5.34) Thr 215 : Pi-Sigma Ile 141: Pi alkyl (5.06) Ale 88 : Alkyl (5.36)	Ala 92, Ala 167, Ser 149, Asn 120, Asn 95, Ile 88, Ile 118, Ile 217, Ile 141, Thr 215
4q	−8.2	Ser 149	1 (2.45)	Ile 88 : Alkyl (5.45) Ala 167 : alkyl (4.18) Ala 167 : Pi-alkyl (4.77)	Asn 120, Ala 92, Ile 88, Ile 118, Ile 217, Ala 167, Ser 149
4r	−8.9	Gly 164 Tyr 165 Asn 150 Ser 149 Ala 92	1 (2.32) 1 (1.97) 1 (2.71) 1 (1.73) 1 (3.24)		Gly 164, Tyr 165, Asn 91, Asn 120, Ala 92, Asn 150, Ser 149
Adriamycin (ADM)	−8.0	Asn 91 Ser 149 Ser 149 Ser 148 His 130	1 (3.55) 1 (2.29) 1 (2.31) 1 (3.07) 1 (2.77)	Ser 149 : Pi-sigma (3.79) Ile 125: Pi alkyl (5.05) Ile 125: Pi alkyl (5.43) Ile 141: Pi-sigma (3.67) Ile 141: Pi-sigma (3.41) His 130: Pi alkyl (5.01) His 137: Pi alkyl (5.48)	Asn 91, Ser 148, Ser 149, Ile, 125, Ile 141, Leu 140, His 130, Val 137

three compounds **4p, 4q** and **4r** are stable because they present high values of hardness (4.033, 3.9573 and 4.0054 eV).

Electronegativity (χ) is the tendency to attract electrons of an atom, molecule or solid substance to itself. The calculated electronegativity of **4p, 4q** and **4r** is found to be 3.1587, 3.3524 and 3.0966 eV respectively. The electrophilicity index (ω) measures the capacity of species to accept electrons (the electrophilic tendency). We can divide organic molecules into three categories based on their electrophilicity values: marginal electrophiles with a value of less than 0.8 eV, moderate electrophiles between 0.8 and 1.5 eV, and strong electrophiles with a value greater than 1.5 eV (Domingo et al., 2002). In this case, all values of 1.2338 eV, 1.4199 eV and 1.1969 eV for the investigated ligands **4p, 4q** and **4r** respectively are moderate electrophiles.

3.2.4. Molecular electrostatic potential

The molecular electrostatic potential (MEP) is an important parameter to be predicted to verify the evidence regarding the investigated reactivity of the compounds as enzyme inhibitors, it can be an indicator for expecting physiochemical property relationships with the molecular structure to determine the efficient centers accountable for electrophilic and nucleophilic reactions. Moreover, MEP is associated to the electronic density. The negative regions of MEP are related to electrophilic reactivity demonstrated in the red color, and the positive ones to nucleophilic reactivity demonstrated in blue color.

The visualization of the Figure 5 show that negative potentials are presented at electronegative oxygen atoms attached to the phosphorous group O21 and O26, whereas positive potentials are presented at hydrogen atoms for all compounds. Obviously through Figure 5 that for the considered inhibitors, the possible sites for electrophilic attack are generally located at heteroatom. Otherwise, the phenyl rings of the considered compounds have a negative region. It is clear from the obtained zones of MEP that the negative possible positions are about electronegative atoms (N and O) and the conjugated double bonds, contrariwise the positive possible zones are about the hydrogen atoms.

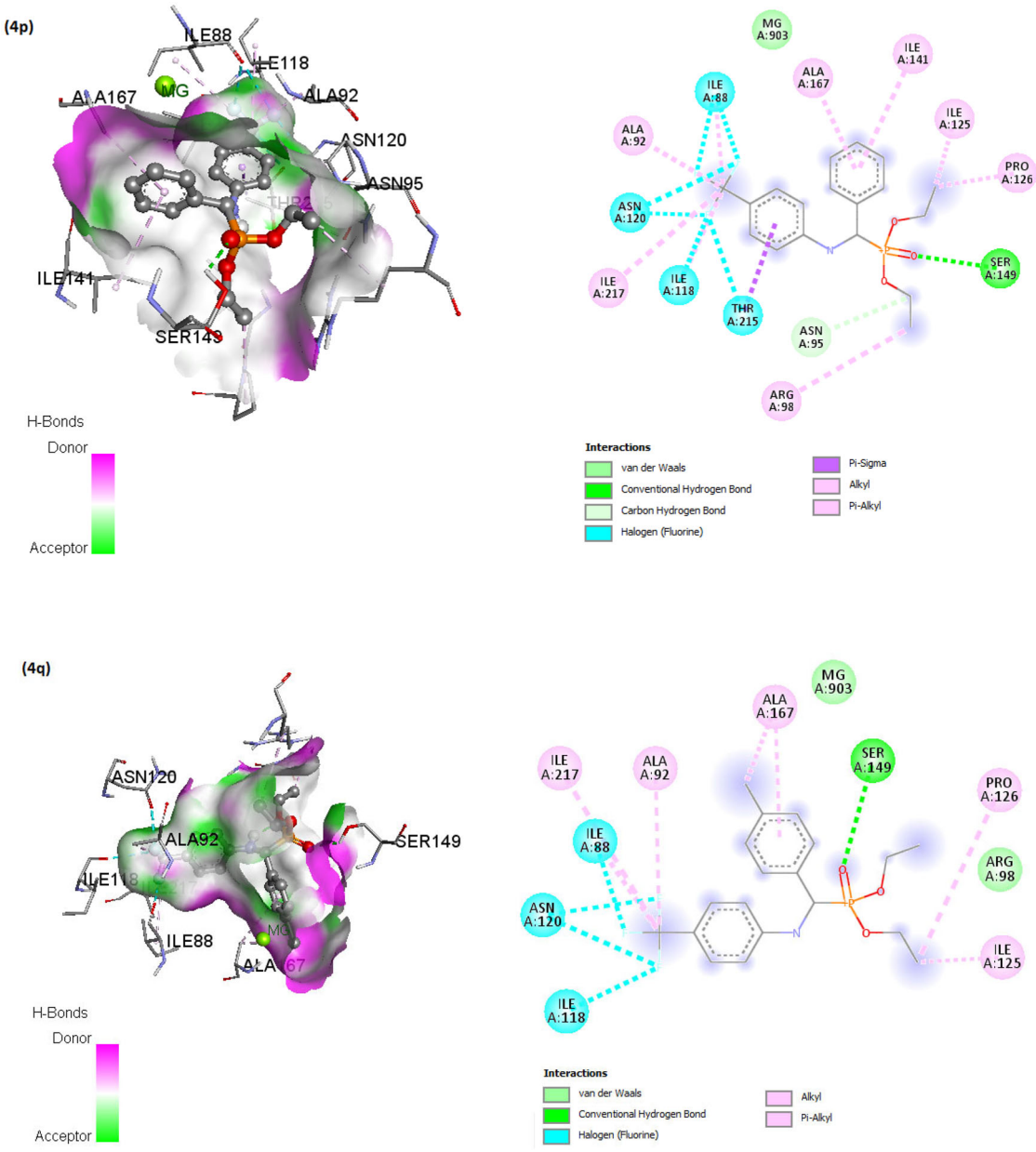

Figure 7. The docked 2D and 3D images of **4p**, **4q** and **4r** compounds and commercial drug Adriamycin with 1ZXM receptor.

3.3. Molecular docking studies

In *silico* molecular docking was applied to probe interactions of ligand with protein. Prior to the docking calculations, water molecules around the enzyme were removed, hydrogen atoms were added and the *Kollman* charge was calculated. The active site of 1ZXM was done by re-docking with ANP (phosphoaminophosphonic acid adenylate ester) onto the binding site (Asn 163, Tyr 165, Glu 87, Thr 147, Ile 125, Asn 91, Asn 120, Ser 148, Ser 149, Phe 142, Thr 215, Asn 95, Gln 376, Arg 162, Lys 168) (Figure 6) (Wei et al., 2005). The binding site parameters obtained are ($X = 36.548$, $Y = -1.089$; $Z = 34.656$ and size $x = 40$, $y = 40$, $z = 40$). The RMSD index of binding topology between the original ligand and re-docked ligand onto the active site is 1.9438 Å.

The molecular docking between synthesized ligands and the 1ZXM receptor was executed to define the appropriate conformation of each ligand in the receptor and the secondary forces resulting between the active amino acids of the receptor and ligand. The protein was kept in a rigid conformation whilst the ligand was in flexible conformation. The best conformations of the ligands were analyzed for their binding interactions and were evaluated by binding free energies (S-score, Kcal/mol), and bonds interactions between ligand atoms and active site residues.

It was established that among the different docking conformations of compounds, **4r** is shown as the highest docking scores −8.9 Kcal/mol compared to **4p** and **4q** (-8.2 Kcal/mol) as well as the standard anticancer drug Adriamycin (Table 4), this due to the OCH_3 interaction, and π-Alkyl interactions, also to conventional hydrogen bonding interactions with active pocket of topoisomerase-II enzyme.

As shown in Figure 7 and detailed in Table 4, only the ligand **4r** has a direct interaction with the center of the

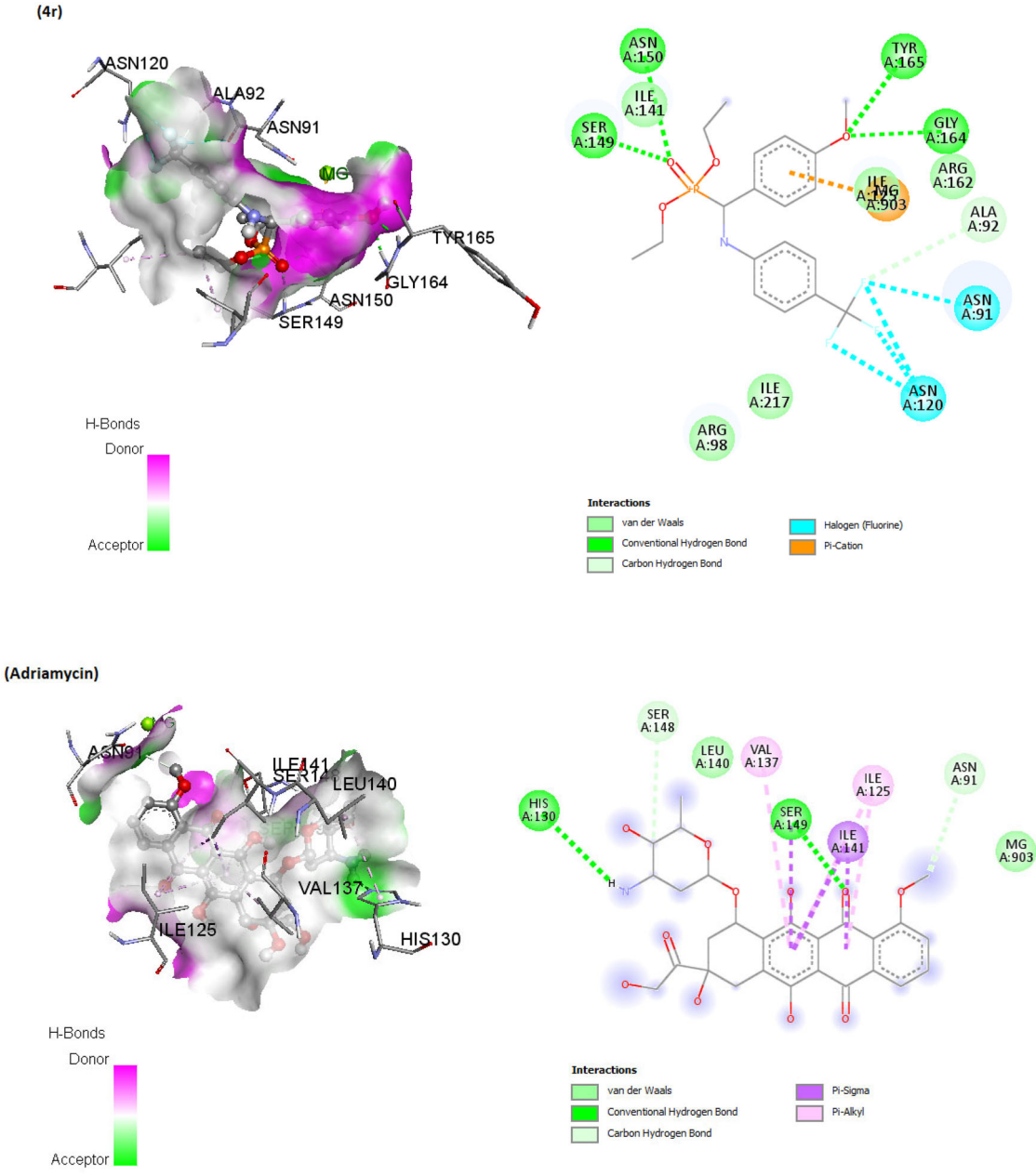

Figure 7. Continued.

Table 5. The physicochemical properties of designed molecules for drug-likeness Pre-diction based on Lipinski's rule of five.

Physicochemical properties	ADM	4p	4q	4r
Molecular weight g/mol	543.52 g/mol	387.33 g/mol	421.78 g/mol	405.47 g/mol
NHBA	12	6	6	4
NHBD	6	1	1	1
Consensus Log P $_{O/w}$	0.44	4.37	4.92	4.59
Log S	–3.46	–6.92	–7.50	–7.35
TPSA (Å)^2	206.07	57.37	57.37	66.60

Mg^{+2}:309 metal, the distance of this electrostatic interaction was 2.65 Å.

Furthermore, the ADM binds to 1ZXM receptor through various interactions, including Pi-sigma, Alkyl and Pi-Alkyl interactions as well as conventional hydrogen bond with Asn 91, Ser 148 and His 130. Those residues were identified in the active site that drives the enzymatic activity of the 1ZXM. The three ligands have a common hydrogen bond interaction with the Ser 149. The stability of the docked ligand **4r** is due exclusively to the hydrogen bond interactions between the -OCH_3 and the P = O moieties to the binding site of the receptor. However, for the structures **4p** and **4q** as well as the ADM, their stability was supported by the presence of hydrophobic interactions. It has been reported

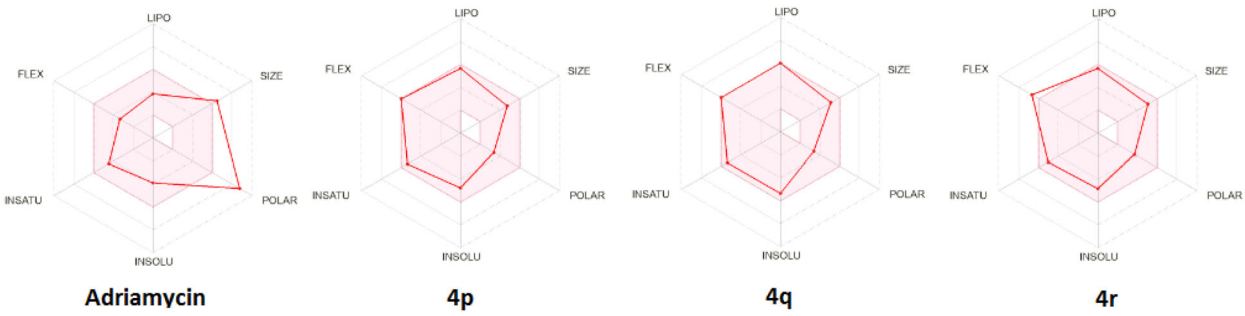

Figure 8. Biovailability radars and physicochemical properties of Adriamycin, **4p**, **4q** and **4r**.

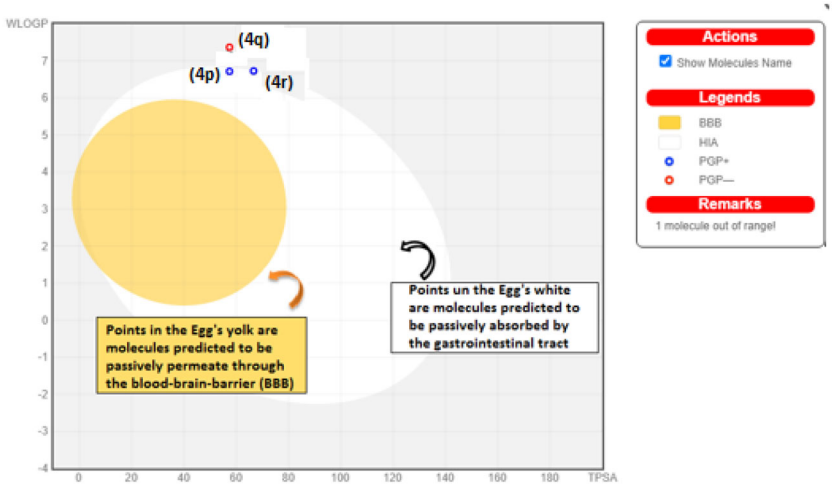

Figure 9. Overview of the BOILED-Egg construction for designed molecules **4p**, **4q**, **4r** and **ADM** from the SwissADME online sever.

that the binding affinity and drug efficacy associated with hydrophobic interactions can be optimized by incorporating them at the site of the hydrogen bonding (Patil et al., 2010). Finally, taken in account a number of hydrogen binding to the site active residues and the binding energy score, the compound **4r** shows as the most stable and presents a high affinity to the protein receptor.

3.4. ADMET prediction and drug likeness

3.4.1. Absorption and physicochemical properties

The drug-likness properties and potential toxicity risk as well as the physicochemical properties were predicted using Swiss-ADME server. In the present study, the ADMET prediction of the α-aminophosphonates **4p**, **4q** and **4r** are treated and summarized in two Tables 4 and 5. A comparison with commercial drug Adriamycin (ADM) was chosen for their anti-proliferation activities cytotoxicity activity against three types of human cancer cell lines, breast cancer, prostate cancer and stomach cancer cells (Jing-Zi et al., 2010).

Based on the physicochemical properties with their ranges as described the Lipinski's rule of five, a violation of those rules was examined for the **ADM** compared to the synthesized α-aminophosphonates (**4p**, **4q** and **4r)**. The results show no violation of the rules for **4p**, **4q** and **4r,** they have a molecular weight are less than 500 Da, which suggests that they can move easily across biological membranes. In addition, these molecules were well tolerated by cell membranes and this is confirmed by their log *p* value (<5). The total polar surface area (TPSA) it is a stronger indicator of whether molecule is orally active or not. All molecules synthesized are respect the rule of the TPSA (≤140 Å^2) which indicates that they have a high oral biovailability, compared to Adriamycin having (TPSA = 206.07 Å^2). Table 5.

Moreover, the oral bioavailability radar of compounds is very important for analyzing the drug-likeness of a molecule and defining its pharmacological potential, by taking into consideration the six physicochemical properties such as; lipophilicity (lipo), size, polarity (polar), insolubility (insolu), flexibility (flex) and unsaturation (insatu) (Arulraj et al., 2022a; 2022b). Consequently, the oral bioavailability radar show that all synthesized molecules fall entirely inside the pink area representing the optimal range of the mentioned descriptors, thus indicating that the studied molecules could be considered druglike (Figure 8**)**.

Further, one of the fast and efficient approaches to examine molecules for the human blood-brain barrier (BBB) penetration and gastrointestinal absorption (GIA) is the BOILED-Egg method, which is derived from lipohilicity and polarity (Daina & Zoete, 2016). As such, points in the Egg's yolk correspond to molecules predicted to passively permeate through the BBB and white correspond to molecules predicted to be passively absorbed by the gastrointestinal absorption (GIA) (Figure 9). Furthermore, molecules found to

Table 6. Predicted pharmacokinetic and drug-likeness properties of **ADM**, **4p**, **4q** and **4r**.

Pharmacokinetics properties	ADM	4p	4q	4r
GI absorption	Low	High	Low	High
BBB permeant	No	No	No	No
P-gp substrate	Yes	Yes	No	Yes
CYP1A2 inhibitor	No	No	No	No
CYP2C19 inhibitor	No	Yes	Yes	Yes
CYP2C9 inhibitor	No	Yes	Yes	Yes
CYP2D6 inhibitor	No	Yes	Yes	Yes
CYP3A4 inhibitor	No	Yes	Yes	Yes
Log K_p (skin permeation)	−8.71 cm/s	−5.54 cm/s	−5.31 cm/s	−5.12 cm/s

GI absorption: gastrointestinal absorption; BBB: blood–brain barrier; CYP: Cytochrome P450; P-gp substrate: glycoprotein substrate P.

be effluated (PGP+) and not to be effluated (PGP-) from the central nervous system by the P-glycoprotein are shown as blue and red dots, respectively. According to the results, none of the synthesized molecules displayed permeation through the blood-brain barrier, whereas all were predicted to be passively absorbed by the gastrointestinal property with the PGP + for **4p** and **4r**, and with the PGP- for **4q** compared to Adriamycin, which is out of range.

3.4.2. Distribution, metabolism and pharmacokinetic properties

Pharmacokinetic properties are another important indicator of the likelihood of therapeutic success for drug molecules like these potential inhibitors. High GI absorption denotes that the compound could be better absorbed from the intestinal tract upon oral administration. It is noted that **4p** and **4r** exhibit high GI absorption compared to ADM and **4q** compounds which exibit low GI absorption, however it was found to be unable to cross the blood-brain barrier (BBB) partition, is depicted in Table 6.

In predicting, the efflux by p-glycoprotein, only **4q** comes out as the substrate. In fact, it was reported that a given molecule could more likely take part in Drug-Drug Interactions (DDI) with other active molecules if it inhibits more CYP enzymes (Cheng et al., 2011), especially the isoforms (CYP1A2, CYP2C19, CYP2C9, CYP2D6 and CYP3A4) which are responsible of 90% for oxidative metabolic reactions (Williams et al., 2004). Therefore, all compounds were predicted to show no potency against CYP1A2, and are inhibitors of at least of all the CYP450 isoforms (CYP2C19, CYP2C9, CYP2D6 and CYP3A4) except ADM. Skin sensitization is a safety assessment indicator that provides information on a compound's ability to induce skin allergy when administered (Alves et al., 2015), the studied molecules (**ADM, 4p**, **4q**, **4r)** show low skin permeability at −8.71 cm/s, −5.54 cm/s, −5.31 cm/s and −5.12 cm/s respectively. Here, the results proved that these compounds are harmless and cure for skin allergies (Abdelrheem et al., 2021; Kavitha & Alivelu, 2021).

3.4.3. Drug-likeness and bioavailability

Drug-likeness is defined by rules that evaluate qualitatively the chance for a given molecule to become a possible oral drug with respect to its bioavailability by considering ranges of specific physicochemical properties (Daina et al., 2017). Veber's rule shows non-violation for all synthesized products (**4p**, **4q** and **4r**). Egan's rule is verified only by **4r**. Mugge's rule indicates that **4p** can be considered as good drugs. Based on these results, it can be concluded that the studied compounds have to potential to become excellent drug candidates (Table 7).

Table 7. Drug-likeness profile and medicinal properties calculated for the studied molecule.

Drug-likeness	ADM	4p	4q	4r
Lipinski	No	Yes	Yes	Yes
Ghose	No	No	No	No
Veber	No	Yes	Yes	Yes
Egan	No	No	No	Yes
Muegge	No	Yes	No	No
Bioavailability score	0.17	0.55	0.55	0.55
Synthetic accessibility (SA)	5.81	4.05	4.02	4.37

4. Conclusion

In conclusion, we have developed a sustainable and an eco-friendly methodology for the preparation of α-aminophosphonates derivatives **(4a-r)** using 2-hydroxymethyl-18-crown-6 as an efficient homogeneous organocatalyst. This new catalytic multicomponent reaction using 5 mol% has number of advantages; including a substantial preparation of organophosphorus compounds under environmental friendliness transition metal-free conditions and short reaction time. Three structures of CF_3 derivatives (**4p, 4q** and **4r**) were selected and optimized by the DFT/CAM-B3LYP/6-31G (d,p) calculations to reveal its geometrical parameters and electronic properties. The HOMO and LUMO are mainly delocalized over the aromatic ring and the amino group, while the LUMO is mainly spread over the CF_3 fragment. HOMO and LUMO energy gaps justify the eventual charge transfer interactions taking place within the molecules. The molecular electrostatic potential has been mapped for predicting sites of electrophilic and nucleophilic attack, we have mentioned that the negative possible positions are about electronegative atoms (N and O) and the conjugated double bonds, and the positive possible zones are about the hydrogen atoms. In *silico* docking study showed that the docked conformations also formed an H-bonding interaction within the active site of enzyme. The three ligands **4p, 4q** and **4r** have shown potent hydrogen bonding interactions with active site of topoisomerase-II enzyme as Adriamycin. Depending on the results, only the ligand **4r** has a direct electrostatic interaction with the center of the Mg^{+2}:309 metal, it has the highest score energy (-8.9 Kcal/mol) and is deeply fitted the active pocket of the enzyme forming five hydrogen bond interactions, which reflects high stability and affinity of this molecule to the receptor. However, for the structures **4p** and **4q** as well as the Adriamycin, their stability was supported by the presence of hydrophobic interactions. In addition, the synthesized compounds (**4p, 4q** and **4r**) were examined for their potential as drugs using Lipinski's five rules and ADMET studies compared to Adriamycin, the results confirm the success of these potential inhibitors as candidates in drug

discovery, which may have an influence in anticancer activity. Drug-likeness of designed compounds is analyzed by oral bioavailability radar and show their high pharmacological potential.

Acknowledgments

The Algerian Ministry of Education and Scientific Research (DGRSDT, FNR) is gratefully acknowledged for financial support of this work. The technical support provided by Emilie KOLODZIEJ is highly appreciated.

Disclosure statement

The authors declare that they have no known competing financial interests or personal relationships that could have appeared to influence the work reported in this paper.

Funding

The author(s) reported there is no funding associated with the work featured in this article.

References

Aissa, R., Guezane-Lakoud, S., Gali, L., Toffano, M., Ignaczak, A., Adamiak, M., Merabet-Khelassi, M., Guillot, R., & Aribi-Zouioueche, L. (2022). New promising generation of phosphates α-aminophosphonates: Design, Synthesis, In-vitro biological evaluation and Computational study. *Journal of Molecular Structure*, *1247*(17), 131336. https://doi.org/10.1016/j.molstruc.2021.131336

Aissa, R., Guezane-Lakoud, S., Kolodziej, E., Toffano, M., & Aribi-Zouioueche, L. (2019). Diastereoselective synthesis of bis(a-aminophosphonates) by lipase catalytic promiscuity. *New Journal of Chemistry*, *43*(21), 8153–8159. https://doi.org/10.1039/C8NJ06235H

Aissa, R., Guezane-Lakoud, S., Toffano, M., Gali, L., & Aribi-Zouioueche, L. (2021). Fiaud's acid, a novel organocatalyst for diastereoselective bis α-aminophosphonates synthesis with *in-vitro* biological evaluation of antifungal, antioxidant and enzymes inhibition potential. *Bioorganic & Medicinal Chemistry Letters*, *41*(1), 128000. https://doi.org/10.1016/j.bmcl.2021.128000

Asiri, A. M., Karabacak, M., Kurt, M., & Alamry, K. A. (2011). Synthesis, molcecular conformation, vibrational and electronic transition, isometric chemical shift, polarizability and hyperpolarizability analysis of 3-(4-Methoxy-phenyl)-2-(4-nitro phenyl)-acrylonitrile: A combined experiment and theoretical analysis. *Spectrochimica Acta. Part A, Molecular and Biomolecular Spectroscopy*, *82*(1), 444–455. https://doi.org/10.1016/j.saa.2011.07.076

Arulraj, R., Nurulhuda, M., Wee Joo, C., Mouna, M., Sivakumar, S., & Noureddine, I. (2022a). 3-Chloro-3-methyl-2,6-diarylpiperidin-4-ones as anti-cancer agents: Synthesis, biological evaluation, molecular docking, and in silico ADMET prediction. *Biomolecules*, *12*(8), 1093. https://doi.org/10.3390/biom12081093

Arulraj, R., Ahlam Roufieda, G., Sivakumar, S., Anitha, K., Rajkumar, K., Nourdine, B., Abdelkader, C., & Manikandan, E. (2022b). Synthesis, vibrational spectra, Hirshfeld surface analysis, DFT calculations, and in silico ADMET study of 3-(2-chloroethyl)-2,6-bis(4-fluorophenyl)piperidin-4-one: A potent anti-Alzheimer agent. *Journal of Molecular Structure*, *1269*, 133845. https://doi.org/10.1016/j.molstruc.2022.133845

Alves, V. M., Muratov, E., Fourches, D., Strickland, J., Kleinstreuer, N., Andrade, C. H., & Tropsha, A. (2015). Predicting chemically-induced skin reactions. Part II: QSAR models of skin permeability and the relationships between skin permeability and skin sensitization. *Toxicology and Applied Pharmacology*, *284*(2), 262–272. https://doi.org/10.1016/j.taap.2014.12.013

Abdelrheem, D. A., Rahman, A. A., Elsayed, N. M., Abd El-Mageed, H. R., Mohamed, H. S., & Ahmed, S. A. (2021). Isolation, characterization, in vitro anticancer activity, DFT calculations, molecular docking, bioactivity score, drug-likeness and admet studies of eight phytoconstituents from brown alga sargassum platycarpum. *Journal of Molecular Structure*, *1225*, 129245. https://doi.org/10.1016/j.molstruc.2020.129245

Abraham, C. S., Prasana, J. C., & Muthu, S. (2017). Quantum mechanical, spectroscopic and docking studies of 2-amino-3-bromo-5-nitropyridine by density functional method. *Spectrochimica Acta. Part A, Molecular and Biomolecular Spectroscopy*, *181*, 153–163. https://doi.org/10.1016/j.saa.2017.03.045

Aita, S., Badavath, V. N., Gundluru, M., Sudileti, M., Nemallapudi, B. R., Gundala, S., Zyryanov, G. V., Chamarti, N. R., & Cirandur, S. R. (2021). Novel α-aminophosphonates of imatinib Intermediate: Synthesis, anticancer Activity, human Abl tyrosine kinase Inhibition, ADME and toxicity prediction. *Bioorganic Chemistry*, *109*, 104718. https://doi.org/10.1016/j.bioorg.2021.104718

Bonarska, D., Kleszczynska, H., & Sarapuk, J. (2002). Antioxidative activity of some phenoxy and organophosphorous compounds. *Cellular & Molecular Biology Letters*, *7*(3), 929–935.

Becke, A. D. (1993). Density-functional thermochemistry III. The role of exact exchange. *The Journal of Chemical Physics*, *98*(7), 5648–5652. https://doi.org/10.1063/1.464913

Cinquini, M., & Tundo, P. (1976). Synthesis of alkyl-substituted crown ethers: efficient phase-transfer catalysts. *Synthesis*, *1976*(08), 516–519. https://doi.org/10.1055/s-1976-24101

Chung-Kiak, P., & Han-Ping, D. S. (2016). Density functional based tight binding (DFTB) study on the thermal evolution of amorphous carbon. *Graphene*, *5*, 51–54. https://doi.org/10.4236/graphene.2016.52006

Cytlak, T., Kaźmierczak, M., Skibińska, M., & Koroniak, H. (2017). Latest achievements in the preparation of fluorinated aminophosphonates and aminophosphonic acids. *Phosphorus, Sulfur, and Silicon and the Related Elements*, *192*(6), 602–620. https://doi.org/10.1080/10426507.2017.1287706

Cheng, F., Yu, Y., Shen, J., Yang, L., Li, W., Liu, G., Lee, P. W., & Tang, Y. (2011). Classification of cytochrome P450 inhibitors and noninhibitors using combined classifiers. *Journal of Chemical Information and Modeling*, *51*(5), 996–1011. https://doi.org/10.1021/ci200028n

Dennington, R., Keith, T., Millam, J., & Inc, S. (2009). V.5. GaussView.

Dix, J. P., Wittenbrink-Dix, A., & Vögtle, F. (1980). Ion-selective steering of the reaction rate and of the catalyst activity by crown-ether complexation. *Naturwissenschaften*, *67*(2), 91–93. https://doi.org/10.1007/BF01054694

Daina, A., Michielin, O., & Zoete, V. (2017). SwissADME: A free web tool to evaluate pharmacokinetics, drug-likeness and medicinal chemistry friendliness of small molecules. *Scientific Reports*, *7*, 42717. https://doi.org/10.1038/srep42717

Domingo, L. R., Aurell, M. J., Pérez, P., & Contreras, R. (2002). Quantitative characterization of the global electrophilicity power of common diene/dienophile pairs in Diels-Alder reactions. *Tetrahedron*, *58*(22), 4417–4423. https://doi.org/10.1016/S0040-4020(02)00410-6

Daina, A., & Zoete, V. (2016). A BOILED-egg to predict gastrointestinal absorption and brain penetration of small molecules. *ChemMedChem*. *11*(11), 1117–1121. https://doi.org/10.1002/cmdc.201600182

Elfily, A. A. (2020). Ribavirin, sofosbuvir remdesivir, galidesivir, and tenofovir against SARS-Cov-2 RNA dependent RNA polymerase (RdRp): A molecular docking study. *Life Sciences*, *253*, 117592. https://doi.org/10.1016/j.lfs.2020.117592

Ferrah, M., Samia, G.-L., Bendjeffal, H., Aissa, R., Merabet-Khelassi, M., Toffano, M., & Aribi-Zouioueche, L. (2022). Full factorial optimization of α-aminophosphonates synthesis using diphenylphosphinic acid as efficientorganocatalyst. *Reaction Kinetics, Mechanisms and Catalysis*. https://doi.org/10.1007/s11144-022-02329-0

Frisch, M. J., Trucks, G. W., Schlegel, H. B., Scuseria, G. E., Robb, M. A., Cheeseman, J. R., Scalmani, G., Barone, V., Mennucci, B., Petersson, G. A., Nakatsuji, H., Caricato, M., Li, X., Hratchian, H. P., Izmaylov, A. F., Bloino, J., Zheng, G., Sonnenberg, J. L., Hada, M., … Gaussian, D. J. (2009). *09, Revision A.02*. Gaussian, Inc.

Feng, L., Yang, H., Cui, X., Chen, D., & Li, G. (2018). Experimental and theoretical investigation on corrosion inhibitive properties of steel rebar by a newly designed environmentally friendly inhibitor formula. *RSC Advances*, *8*(12), 6507–6518. https://doi.org/10.1039/C7RA13045G

Grzywa, R., & Sieńczyk, M. (2013). Phosphonic esters and their application of protease control. *Current Pharmaceutical Design*, *19*(6), 1154–1178. https://doi.org/10.2174/1381612811319060014

Guezane-Lakoud, S., Lecouvey, M., Berrebah, H., & Aouf, N. E. (2015). Synthesis of chiral phosphonoacetamides and their toxic effects on Paramecium sp. *Organic Communications*, *8*, 1–8.

Guezane-Lakoud, S., Toffano, M., & Aribi-Zouioueche, L. (2017). Promiscuous lipase catalyzed a new P–C bond formation: Green and efficient protocol for one-pot synthesis of α-aminophosphonates. *Heteroatom Chemistry*, *28*(6), e21408. https://doi.org/10.1002/hc.21408

Heydari, A., Hamadi, H., & Pourayoubi, M. (2007). A new one-pot synthesis of α-amino phosphonates catalyzed by $H_3PW_{12}O_{40}$. *Catalysis Communications*, *8*(8), 1224–1226. https://doi.org/10.1016/j.catcom.2006.11.008

Hyun, M. H. (2012). Chromatographic separations and analysis: Chiral crown ether-based chiral stationary phases. In E. M. Carreira & H. Yamamoto (Eds.), *Comprehensive chirality* (Vol. 8, pp. 263–285). ISBN 9780080951683 Elsevier. https://doi.org/10.1016/B978-0-08-095167-6.00827-2

Jing-Zi, L., Bao-An, S., Hui-Tao, F., Pinaki, S. B., Wen-Ting, W., Song, Y., Weiming, X., Jian, W., Lin-Hong, J., Xue, W., De-Yu, H., & Song, Z. (2010). Synthesis and *in vitro* study of pseudo-peptide thioureas containing α-aminophosphonate moiety as potential antitumor agents. *European Journal of Medicinal Chemistry*, *45*(11), 5108–5112. https://doi.org/10.1016/j.ejmech.2010.08.021

Kohn, W., & Sham, L. J. (1965). Quantum density oscillations in an inhomogeneous electron gas. *Physical Review*, *137*(6A), A1697–A1705. https://doi.org/10.1103/PhysRev.137.A1697

Kandula, M. K. R., Shaik, M. S., Nagaripati, S., Kotha, P., Bakthavatchala, R., Sravya, G., Grigory, Z., & Cirandur, S. R. (2017). One-pot green synthesis and cytotoxicity of new α-aminophosphonates. *Research on Chemical Intermediates*, *43*(12), 7087–7103. https://doi.org/10.1007/s11164-017-3060-y

Kosar, B., & Albayrak, C. (2011). Spectroscopic investigations and quantium chemical computational study of (E)-4-methoxy-2-[(p-tolylimino) methyl phenyl]. *Spectrochimica Acta. Part A, Molecular and Biomolecular Spectroscopy*, *78*(1), 160–167. https://doi.org/10.1016/j.saa.2010.09.016

Kavitha, N., & Alivelu, M. (2021). Investigation of structures, QTAIM, RDG, ADMET, and docking properties of SASC compound using experimental and theoretical approach. *Computational and Theoretical Chemistry*, *1201*, 113287. https://doi.org/10.1016/j.comptc.2021.113287

Kerkour, R., Chafai, N., Moumeni, O., & Chafaa, S. (2023). Novel α-aminophosphonates derivates synthesis, theoretical calculation, Molecular docking, and in silico prediction of potential inhibition of SARS-CoV-2. *Journal of Molecular Structure*, *1272*, 134196. https://doi.org/10.1016/j.molstruc.2022.134196

Lakoud, S. G., Merabet-Khelassi, M., & Aribi-Zouioueche, L. (2016). $NiSO_4$-$6H_2O$ as a new, efficient, and reusable catalyst for the α-aminophosphonates synthesis under mild and eco-friendly conditions. *Research on Chemical Intermediates*, *42*(5), 4403–4415. https://doi.org/10.1007/s11164-015-2283-z

Laschat, S., & Kunz, H. (1992). Carbohydrates as chiral templates: Stereoselective synthesis of (*R*)- and (*S*)-α-aminophosphonic acid derivatives. *Synthesis*, *1992*(1/2), 90–95. https://doi.org/10.1055/s-1992-34155

Lamb, J. D., Izatt, R. M., & Christensen, J. J. (1981). In R. M. Izatt and J. J. Christensen (Eds.), *Progress in macrocyclic chemistry* (Vol. 2, pp. 41–90). Jhon Wiley & Sons.

Liittringhaus, A. (1937). Hydroquinone or 1.5 and 1.6 dihydroxynaphtalemen cyclic polyethers. *Justus Liebigs Annalen Der Chemie*, *528*, 181–210. https://doi.org/10.1002/jlac.19375280112

Luo, Y., Ouyang, G., Tang, Y., Y-M, H., & Q-H, F. (2020). Diaza-crown ether-bridged chiral diphosphoramidite ligands: Synthesis and applications in asymmetric catalysis. *The Journal of Organic Chemistry*, *85*(12), 8176–8184. https://doi.org/10.1021/acs.joc.0c00223

Lipinski, C. A. (2016). Rule of five in 2015 and beyond: Target and ligand structural limitations, ligand chemistry structure and drug discovery project decisions. *Advanced Drug Delivery Reviews*, *101*, 34–41. https://doi.org/10.1016/j.addr.2016.04.029

Maier, L. (1990). Organic phosphorus compounds 91.[1]synthesis and properties of 1-amino-2-arylethylphosphonic and-phosphinic acids as well as -phosphine oxides. *Phosphorus, Sulfur, and Silicon and the Related Elements*, *53*(1-4), 43–67. https://doi.org/10.1080/10426509008038012

Maier, L., & Diel, P. J. (1991). Organic phosphorus compounds 94 preparation, physical and biological properties of amino-arylmethylphosphonic- and-phosphonous acids. *Phosphorus, Sulfur, and Silicon and the Related Elements*, *57*(1-2), 57–64. https://doi.org/10.1080/10426509108038831

Mcdowell, W. J. (1988). Crown ethers as solvent extraction reagents: Where do we stand? *Separation Science and Technology*, *23*(12-13), 1251–1268. https://doi.org/10.1080/01496398808075628

Mekky, A. H., Hlhaes, H. G., El-Okr, M. M., Al-Aboudi, A. S., & Ibrahim, M. A. (2015). Effect of solvents on the electronic properties of fullerene base systems: Molecular modelling. *Journal of Computational and Applied Mathematics*, *4*(1), 1–4. https://doi.org/10.4172/2168-9679.1000203

Merabet, M., Melais, N., Boukachabia, M., Fiaud, J. C., & Zouioueche-Aribi, L. (2007). Effet d'un ether couronne sur le systeme catalytique dans la reaction d'acylation du 1-acenaphtenol avec la lipase de candida cylindracea. *Journal De la Société Algerienne De Chimie*, *17*(2), 185–194.

Morris, G. M., Huey, R., Lindstrom, W., Sanner, M. F., Belew, R. K., Goodsell, D. S., & Olson, A. J. (2009). AutoDock4 and AutoDockTools4: Automated Docking with Selective Receptor Flexiblity. *Journal of Computational Chemistry*, *30*(16), 2785–2791. https://doi.org/10.1002/jcc.21256

Mirzaei, M., Hossein, E., Bagherjeri, F. A., Mirzaei, M., & Farhadipour, A. (2018). Investigation of non-covalent and hydrogen bonding interactions on the formation of crystalline networks and supramolecular synthons of series of α-aminophosphonates: Cristallography and DFT studies. *Journal of Molecular Structure*, *1163*, 316–326. https://doi.org/10.1016/j.molstruc.2018.03.014

Mucha, A., Kafarski, P., & Berlicki, Ł. (2011). Remarkable potential of the α-aminophosphonate/phosphinate structural motif in medicinal chemistry. *Journal of Medicinal Chemistry*, *54*(17), 5955–5980. https://doi.org/10.1021/jm200587f

Nagayama, S., & Kobayashi, S. (2000). A novel chiral lead (II) catalyst for enantioselective aldol reactions in aqueous media. *Journal of the American Chemical Society*, *122*(46), 11531–11532. https://doi.org/10.1021/ja001234l

Omichi, M., Yamashita, S., Okura, Y., Ikutomo, R., Ueki, Y., Seko, N., & Kakuchi, R. (2019). Surface engineering of fluoropolymer films via the attachment of crown ether derivatives based on the combination of radiation-induced graft polymerization and the *Kabachnik–Fields* reaction. *Polymers*, *11*(8), 1337. https://doi.org/10.3390/polym11081337

Olasupo, S. B., Uzairu, A., Shallangwa, G. A., & Uba, S. (2020). Profiling the antidepressant properties of phenyl piperidine derivatives as inhibitors of serotonin transporter (SERT) via cheminformatics modeling, molecular docking and ADMET predictions. *Scientific African*, *9*, e00517. https://doi.org/10.1016/j.sciaf.2020.e00517

Oleg, T., & Olson, A. J. (2010). AutoDock Vina: Improving the speed and accuracy of docking with a new scoring function, efficient optimization, and multithreading. *Journal of Computational Chemistry*, *31*, 254–261. https://doi.org/10.1002/jcc.21334

Pan, W., Ansiaux, C., & Vincent, S. P. (2007). Synthesis of acyclic galactitol-and lyxitol-aminophosphonates as inhibitors of UDP-galactopyranose mutase. *Tetrahedron Letters*, *48*(25), 4353–4356. https://doi.org/10.1016/j.tetlet.2007.04.113

Patil, R., Das, S., Stanley, A., Yadav, L., Sudhakar, A., & Varma, A. K. (2010). Optimized hydrophobic interactions and hydrogen bonding at the target-ligand interface leads the pathways of drug-designing. *PloS One*, *5*(8), e12029. https://doi.org/10.1371/journal.pone.0012029

Pedersen, C. J. (1967). Cyclic polyethers and their complexes with metal salts. *Journal of the American Chemical Society*, *89*(10), 2495–2496. https://doi.org/10.1021/ja00986a052

Pedersen, C. J. (1970). Crystalline Salt Complexes of Macrocyclic Polyethers. *Journal of the American Chemical Society*, *92*, 386–391. https://doi.org/10.1021/ja00705a605

Pham, T. S., Czirok, J. B., Balazs, L., Pal, K., Kubinyi, M., Bitter, I., & Jaszay, Z. (2011). BINOL-based azacrown ether catalyzed enantioselective Michael addition: Asymmetric synthesis of α-aminophosphonates. *Tetrahedron: Asymmetry*. *22*(4), 480–486. https://doi.org/10.1016/j.tetasy.2011.02.002

Rostamnia, S., & Doustkhah, E. (2015). Synthesis of water-dispersed magnetic nanoparticles (H_2O-DMNPs) of β-cyclodextrin modified Fe_3O_4 and its catalytic application in Kabachnik–Fields multicomponent reaction. *Journal of Magnetism and Magnetic Materials*, *386*, 111–116. https://doi.org/10.1016/j.jmmm.2015.03.064

Rostamnia, S., & Amini, M. (2014). Ultrasonic and Lewis acid ionic liquid catalytic system for Kabachnik–Fields reaction. *Chemical Papers*, *68*(6), 834–837. https://doi.org/10.2478/s11696-013-0516-4

Raafat, M., Mohamed, I. A., & Faten, M. K. A. (2008). Quantum chemical studies on the inhibition of corrosion of copper surface by substituted uracils. *Applied Surface Science*, *255*, 2433–2441. https://doi.org/10.1016/j.apsusc.2008.07.155

Schug, K. A., & Lindner, W. (2005). Noncovalent binding between guanidinium and anionic groups: Focus on biological- and synthetic-based arginine/guanidinium interactions with phosph[on]ate and sulf[on]ate residues. *Chemical Reviews*, *105*(1), 67–114. https://doi.org/10.1021/cr040603j

Satish, U. D., Kiran, R., Kharat, A. R., Yadav, S. U. S., Manoj, G. D., Jaiprakash, N. S., & Rajendra, P. P. (2018). Synthesis of novel α-aminophosphonate derivatives, biological evaluation as potent antiproliferative agents and molecular docking. *ChemistrySelect*, *3*(20), 5552–5558. https://doi.org/10.1002/slct.201800798

Sivala, M. R., Devineni, S. R., Golla, M., Medarametla, V., Pothuru, G. K., & Chamarthi, N. R. (2016). A heterogeneous catalyst, SiO_2-$ZnBr_2$: An efficient neat access for α-aminophosphonates and antimicrobial activity evaluation. *Journal of Chemical Sciences*, *128*(8), 1303–1313. https://doi.org/10.1007/s12039-016-1113-1

Turcheniuk, K. V., Kukhar, V. P., Roschenthaler, G. V., Acena, J. L., Soloshonok, V. A., & Sorochinsky, A. E. (2013). Recent advances in the synthesis of fluorinated aminophosphonates and aminophosphonic acids. *RSC Advances*, *3*(19), 6693–6716. https://doi.org/10.1039/c3ra22891f

Uparkar, J. J., Dhavan, P. P., Jadhav, B. L., & Pawar, S. D. (2022). Design, synthesis and biological evaluation of furan based α-aminophosphonate derivatives as anti-Alzheimer agent. *Journal of the Iranian Chemical Society*, *19*(7), 3103–3116. https://doi.org/10.1007/s13738-022-02515-w

Vahda, S. M., Baharfar, R., Tajbakhsh, M., Heydari, A., Baghbanian, S. M., & Khaksar, S. (2008). Organocatalytic synthesis of α-hydroxy and α-aminophosphonates. *Tetrahedron Letters*, *49*(46), 6501–6504. https://doi.org/10.1016/j.tetlet.2008.08.094

Wei, H., Ruthenburg, A. J., Bechis, S. K., & Verdine, G. L. (2005). Nucleotide-dependent domain movement in the ATPase domain of a human type IIA DNA topoisomerase. *The Journal of Biological Chemistry*, *280*(44), 37041–37047. https://doi.org/10.1074/jbc.M506520200

Williams, J. A., Hyland, R., Jones, B. C., Smith, D. A., Hurst, S., Goosen, T. C., Peterkin, V., Koup, J. R., & Ball, S. E. (2004). Drug-drug interactions for UDP-glucuronosyltransferase substrates: A pharmacokinetic explanation for typically observed low exposure (AUCi/AUC) ratios. *Drug Metabolism and Disposition: The Biological Fate of Chemicals*, *32*(11), 1201–1208. https://doi.org/10.1124/dmd.104.000794

Xavier, S., & Periandy, S. (2015). Spectroscopic (FT-IR, FT-Raman, UV and NMR) investigation on 1-phenyl-2-nitropropene by quantum computational calculations. *Spectrochimica Acta. Part A, Molecular and Biomolecular Spectroscopy*, *149*, 216–230. https://doi.org/10.1016/j.saa.2015.04.055

Yadav, J. S., Reddy, B. V. S., Raj, K. S., Reddy, K. B., & Prasad, A. R. (2001). Zr^{4+}catalyzed efficient synthesis of α-aminophosphonates. *Synthesis*, *2001*(15), 2277–2280. https://doi.org/10.1055/s-2001-18444

Yanai, T., Tew, D., & Handy, N. (2004). New hybrid exchange-correlation functional using the Coulomb attenuating method (CAM-B3LYP). *Chemical Physics Letters*, *393*(1-3), 51–57. https://doi.org/10.1002/chir.22384

Enzyme and Microbial Technology 162 (2023) 110145

Contents lists available at ScienceDirect

Enzyme and Microbial Technology

journal homepage: www.elsevier.com/locate/enzmictec

Enantioselective bio-deacylation of arylalkyl acetates using tertiary amines as additive under promiscuous conditions

Meriem Ferrah, NourElhouda Benamara, Mounia Merabet-Khelassi [*,1], Samia Guezane Lakoud [2], Louisa Aribi-Zouioueche [3]

Ecocompatible Asymmetric Catalysis Laboratory (L.C.A.E), Badji Mokhtar Annaba University, B.P 12, Annaba 23000, Algeria

ARTICLE INFO

Keywords:
Bio-deacylation
Enzymatic Kinetic Resolution
Tertiary amine
DABCO
CAL-B
Promiscuous conditions

ABSTRACT

Herein, we describe the impact of the introduction of tertiary amines as additive during the enzymatic kinetic resolution via deacylation of some arylalkyl acetates **1a-8a** under promiscuous conditions. Two *CAL-B* preparations were examined: *Novozym®435* and *CHIRAZYME® L-2, c.-f. C2, lyo*. The influence of the introduction of seven amines is checked: Triethylamine (Et_3N), Pyridine, 4-Dimethylaminopyridine (4-DMAP), 1,4-Diazabicyclo [2.2.2]octane (DABCO), Cinchonine, Cinchonidine, Quinine and Quinidine; and that in two organic solvent: diisopropylether (DIPE) and tertiobutylmethyl ether (TBME).

Among the examined amines, the use of DABCO as additive recorded the best results in terms of reactivity and selectivity. It was to be highlighted that this additive was reported as an enzyme activator for the first time in the enzymatic kinetic resolution via hydrolysis of racemic acetates under non-aqueous conditions. Both *CAL-B* preparations showed the same behavior in the presence of the chosen additives during the biodeacylation of the resolved acetates. No direct correlation between the pK_a values of several used additives and the *CAL-B* activation rates has been revealed.

An ideal enzymatic kinetic resolution was recorded with the acetate **4a** (Conv 50% and E > >200).

1. Introduction

The hydrolytic enzymes (EC.3.1.1.3) are widely used in industrial biotechnology for their several advantages such as the ease of use, biodegradable, and efficiency with less waste, non requirements for co-factors, stability in aqueous and organic solvents as well as their remarkable *chemo-*, *regio-* and *enantio*-selectivity [1,2]. Furthermore they are known from their substrate and condition promiscuity what makes them efficient tools in organic synthesis and allows to development of greener processes [3–6].

Among them, the lipase from *Candida antarctica fraction* B (*CAL-B*), under an immobilized form, is one of the most popular lipases, qualified as very robust biocatalyst in various non-conventional media, with high catalytic efficiency especially for kinetic resolution of racemates [7,8]. The exclusive properties of immobilized *CAL-B* such as: Facile recoveries, thermo-stability, being environmentally benign are making it attractive for wide applications in pharmaceuticals, food technology, organic synthesis, paper industry and laundry [9,10]. This is due to their stability in poor water organic solvents, facilitating else the solubility of large panel of substrates [11,12].

In our previous works, the *Candida Antarctica lipase* immobilized on acrylic resin (*CAL-B*) was successfully used for the acylation and deacylation of arylalkylcarbinols [13,14] and primary 1,2-disubstituted ferrocene derivatives [15,16]. We have demonstrated an important influence of some parameters on control reactivity and enantioselectivity in the enzymatic kinetic resolution of racemates, such as, the nature and amount of the lipase [17], the acyl donors [18], the solvent, the introduction of additives [19–21] as well as the water activity. The later factor impacts crucially the enzymatic activity in hydrophobic organic solvents and may induce a competitive hydrolysis reaction [22].

Owing this parallel reaction, especially, when using *CAL-B* as catalysts, two efficient and practical ways for the enzymatic kinetic

* Corresponding author.
E-mail addresses: mounia.merabet@univ-annaba.dz, mounia.merabet@gmail.com (M. Merabet-Khelassi).
[1] http://orcid.org/0000-0002-7149-5878
[2] https://orcid.org/0000-0001-6969-0730
[3] http://orcid.org/0000-0002-2619-7206

https://doi.org/10.1016/j.enzmictec.2022.110145
Received 9 August 2022; Received in revised form 16 October 2022; Accepted 17 October 2022
Available online 19 October 2022

deacylation were successfully described, and that, in the presence of stoichiometric amount of carbonate salts (1 equivalent) [23–27] and triethylamine (2 equivalents) [28] as additives in non aqueous media catalyzed by the *CAL-B* (Supplier: Sigma-Aldrich; UA>10,000 U/g). Those methods present numerous advantages by expanding the panel of substrates insoluble or unstable in the aqueous media and allow us to reduce the work up steps when dealing with scale up application.

The exploitation of organic bases as additives to optimize the reactivity and the selectivity of hydrolases has drawn attention in last two decades [29]. The most used is triethylamine and pyridine as non reactive bases, generally in the acylation reactions for the elimination the all trace of acidic residue from the enzyme microenvironment and preventing inhibition and denaturation of enzymes [30–32]. Whilst fewer examples were described, concerning their uses as additives during the hydrolysis reactions in aqueous media [33].

Herein, in the continuity of our investigations in this field, especially to improve the enzymatic hydrolysis in water-poor environment or in the anhydrous organic solvent, we have examined the promiscuous effect of some tertiary amines, simple and complex, as additives, in the deacylation of arylalkyl acetates catalyzed by lipases.

The study is carried out with two kinds of the *CAL-B*, from different suppliers, and that, in two organic solvents with different hydrophobicities.

2. Materials and methods

2.1. Chemicals and materials

All reagents and solvents were of analytical grade and were used as purchased from Sigma-Aldrich, TCI and STREM. The *Novozym®435 (CAL-B)* lipase immobilized on hydrophobic carrier (acrylic resin) was purchased from STREM (Sold in collaboration with Novozymes A/S) with Specific activity 10,000 U/g. The *CHIRAZYME® L-2, c.-f. C2, lyo (CAL-B)* was purchased from Boehringer Mannheim with Specific activity 500 kU. Both lipases were used without any pre-treatment. Reactions were monitored using TLC aluminum plates with Silica gel 60 F_{254} type *MERCK* 5179, 250 *mesh* using UV light as a visualizing agent. The separation of the resulting alcohols and remaining acetates was performed by preparative TLC Glass plates with Silica gel 60 F_{254} type *MERCK*.

2.2. Instrumentations

The spectroscopic characterisation was performed with Brüker spectrometers (300 MHz for ^{1}H, 75 MHz for ^{13}C). Chemical shifts were reported in δ ppm from tetramethylsilane with the solvent resonance as an internal standard for ^{1}H NMR and chloroform-d (δ 77.0 ppm) for ^{13}C NMR. The enantiomeric excesses were measured by gas chromatography on Thermo-Finnigan Trace GC, equipped with an automatic autosampler, using a CHIRALSIL-DEX CB column (25 m; 0.25 mm; 0.25 μm) and by AGC Series 600 Gas Chromatograph using an Rt®-bDEXsm column (30 m; 0.32 mm; 0.25 μm). Furthermore, by a chiral stationary phase HPLC on Chiralpack IB column. Retention times were reported in minutes.

2.3. General procedure for the reduction of ketones

The racemic alcohols **2, 3, 6** were obtained after reduction of the corresponding commercial ketones (1 equivalent) using 6 equivalents of $NaBH_4$ in a solution of (THF/water; 4/1 *v/v*). The reaction mixture was stirred under at 0 °C. The evolution of the reactions was monitored by TLC. After total consumption of ketones, the reaction mixture was neutralized by addition of a solution of (HCl, 1 N). Then the organic layer was removed, and the aqueous layer was extracted with ethyl acetate (3 ×80 mL). The combined organic layers were dried over anhydrous $MgSO_4$ and concentrated to quantify the isolated yields. The ^{1}H and ^{13}C NMR spectra of these products were in good agreement with the literature [28].

2.4. General procedure for the chemical acylation of racemic alcohols 1–8

The racemic acetates **1a-8a** were obtained by standard classical chemical acetylation of corresponding alcohols, according to the following procedure: to 1 equivalent of racemic alcohol **1–8**, 1.2 equivalent of triethylamine and 0.1 equivalent of 4-dimethylaminopyridine (DMAP) dissolved in 4 mL of ether, 1.5 equivalent of acetic anhydride were added slowly. The evolution of the reactions was monitored by TLC. The acetates are obtained pure after standard work up, in good yields. The ^{1}H and ^{13}C NMR spectra of these products were in good agreement with the literature.

2.5. General procedure for the enzymatic deacylation of racemic acetates 1a-8a

To 1 mmol of the racemic acetates **1a-8a** dissolved in 2 mL of organic solvent and the indicated amount of amine, 50 mg of the *CAL-B* (*Novozym®435* or *CHIRAZYME® L-2, c.-f. C2, lyo*). 50 mg of molecular sieves 4 Å, drying over night at 100 °C, were added. The suspension was stirred at 40 °C for 24 h. The reaction mixture was filtered and concentrated in *vacuum* and an acidic extraction was performed to remove the amine excess. The remaining acetate and the produced alcohol were separated by preparative TLC (petroleum ether/ethyl acetate: 90/10) and analyzed by chiral GC or Chiral HPLC.

3. Results and discussion

For the present investigation we have decided to study the impact of the introduction of tertiary amines on the outcome of the enzymatic deacylation of arylalkyl acetates catalyzed by lipase *CAL-B*. Two *CAL-B* lipase preparations were selected: the *Novozym®435* (10,000 U/g) and the *CHIRAZYME®* L-2, c.-f. C2, lyo (500 kU). The phenylethyl acetate **1a** was selected as model of study, and an organic base, the triethylamine was chosen for finding the optimal conditions. The reactions are carried out in two organic solvents diisopropyl ether (DIPE, logP=1.9) and *tertio*-butylmethyl ether (TBME, logP=1.35) in the presence of molecular sieves 4 Å (MS 4 Å) as water regulator.

3.1. Optimization of the triethylamine loading

Initially, for better apprehend the influence of the introduction of Et_3N on the outcome of the bio-deacylation, several amount loading of these non reactive base were examined (0, 0.2, 0.5, 1, 2, 3 equivalents). (Scheme 1).

The experiences were performed on 1 equivalent of acetate **1a** diluted in 2 mL of organic solvent. 50 mg of *CAL-B* and 50 mg of MS 4 Å were added. Blank reactions, without MS 4 Å and Et_3N were performed and used as control reaction.

The mixture was stirred at 40 °C for 24 h. The evolution reactions were monitored by TLC. The reactions mixtures were filtered then evaporated in *vacuum*. The conversions and the enantiomeric excesses of remained acetates ***(S)*-1a** and the obtained alcohols ***(R)*-1** were quantified by chiral GC. The obtained results are reported in Table 1.

As described on Table 1, the *CAL-B* preparation has non negligible impact on the reactivity and the enantioselectivity during the deacylation of **1a**, and that strongly related to the Et_3N loading. Also, the presence of the hydrolysis reaction in absence of both amine and molecular sieves in DIPE and TBME was detected with rates varying from Conv = 16.7% to Conv = 24.3% (Entries: 1, 9, 17 & 25). It is to be underline that the water implicated in the hydrolysis of acetates is probably brought from the lipase. Moreover, formation of the corresponding alcohol was not observed when Et_3N was used only.

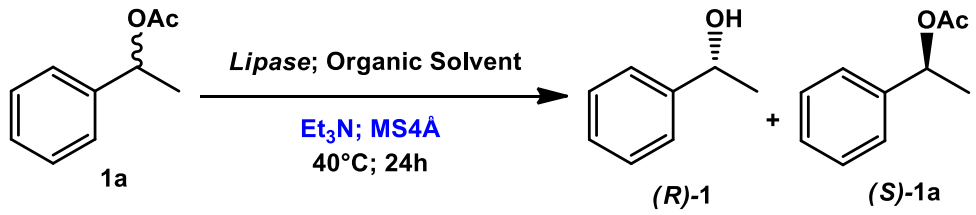

Scheme 1. : Enzymatic deacylation of **1a** in the presence of Et_3N as basic additive.

Table 1
Influence of Et_3N loading during the enzymatic deacylation of (1a).

Entry	Et_3N (equiv.)	Org. solvent (logP)	ee_S (%)[a]	ee_P (%)[a]	Conv (%)[b]	E[b]
CHIRAZYME® L-2, c.-f. C2, lyo						
1[c]	0	DIPE (1.9)	31.2	> 99	23.9	> 200
2[d]	0		25.5	> 99	20.5	> 200
3[d]	0.2		33.4	> 99	25.2	> 200
4[d]	0.5		34.2	> 99	25.7	> 200
5[d]	1		37.8	> 99	27.6	> 200
6[d]	2		46.1	> 99	31.8	> 200
7[d]	3		46.1	89.4	34	28.2
8[d]	4		46.2	88.6	34.3	26.1
9[c]	0	TBME (1.35)	30.5	> 99	23.6	> 200
10[d]	0		25.5	> 99	20.5	> 200
11[d]	0.2		34.2	> 99	25.7	> 200
12[d]	0.5		35.7	> 99	26.5	> 200
13[d]	1		39.2	> 99	28.4	> 200
14[d]	2		37.6	> 99	27.5	> 200
15[d]	3		72.7	89.2	44.9	38
16[d]	4		29.8	83.3	26.3	14.7
Novozym®435						
17[c]	0	DIPE (1.9)	32	> 99	24.3	> 200
18[d]	0		18.3	> 99	15.5	> 200
19[d]	0.2		28.7	> 99	22.3	> 200
20[d]	0.5		35.8	> 99	26.4	> 200
21[d]	1		36.8	> 99	27	> 200
22[d]	2		46.9	> 99	32	> 200
23[d]	3		32.2	> 99	24.4	> 200
24[d]	4		27	> 99	21.3	> 200
25[c]	0	TBME (1.35)	20.1	> 99	16.7	> 200
26[d]	0		19.6	> 99	16.4	> 200
27[d]	0.2		14.4	> 99	12.6	> 200
28[d]	0.5		20.6	> 99	17.1	> 200
29[d]	1		25.5	> 99	20.3	> 200
30[d]	2		32.5	> 99	24.6	> 200
31[d]	3		40.9	> 99	29	> 200
32[d]	4		35	> 99	26	> 200

[a] Enantiomeric excess of obtained alcohol and the remained acetate are measured by chiral GC.

[b] Conversion [34,35]: Conv=$ee_S/ee_P + ee_S$; Selectivity: E = Ln [(1-C) (1-ee_S)]/ Ln [(1-C) (1 +ee_S]

[c] 1 mmol of (1a), 50 mg of *CAL-B*, 2 mL of organic solvent at 40 °C during 24 h.

[d] 1 mmol of (1a), x equiv. of Et_3N, 50 mg of *CAL-B*, 50 mg of molecular sieves 4 Å, 2 mL of organic solvent at 40 °C during 24 h.

Slight decrease of the conversion rates was recorded by adding an amount of molecular sieves as water regulator (15.5% ≤ Conv ≤ 20.5%) (Entries: 2, 10, 18 & 26).

When the *CHIRAZYME® L-2, c.-f. C2, lyo* was exploited as biocatalyst in both organic solvents; a significant improvement of the conversion rates was observed when 2 equivalents of Et_3N were added and that without any perturbation of the lipase selectivity (E > >200). In DIPE from Conv = 20.5% to Conv = 31.8% and in TBME from Conv = 20.5% to Conv= 27.5% (entries 2, 6 versus 10, 14). A drastic enhancement of the reactivity was recorded in TBME when a large excesses of Et_3N (3 equivalent) was introduced and that in disfavor of the lipase selectivity; the selectivity factor pass from E > >200 to E = 38 and the conversion rates from Conv = 27.5% to Conv = 44.9% (entry 14 versus 15). Similar observations concerning the selectivity were noted in DIPE, but those on the reactivity were less important (entries 6 & 7).

Whilst, these perturbation were completely declined when the *Novozym®435* was used in the presence of excess of the Et_3N. The deacylation was performed with high selectivity regardless the amount of the base loading.

Since, the improvement of the reactivity was recorded from the addition of 0.5–1 equivalent of Et_3N, we were decided to maintain the minimum rate (0.5 equivalent of additive) as the activation rate of the deacylation in both solvents, and we have applied these conditions using several tertiary amines as additive.

3.2. *Effect of the additive nature*

At this stage of study, simple and complex bases (Lewis bases and Cinchona alkaloids) were selected to check the impact of their presence on the outcome of the bio-deacylation and that keeping the same above promiscuous conditions.

Besides the triethylamine (Et_3N: pk_a 10.75) the following additives were chosen: Pyridine (pk_a 5.25), 4-Dimethylaminopyridine (4-DMAP: pk_a 9.7), 1,4-Diazabicyclo[2.2.2]octane (DABCO: pk_a 8.8), Cinchonine (pk_a 9.15), Cinchonidine (pk_a 9.15), Quinine (pk_a 9.05) and Quinidine (pk_a 9.05) (Fig. 1).

All experiences were performed on 1 equivalent of acetate **1a** diluted in 2 mL of organic solvent in the presence of 50 mg of *CAL-B* and 50 mg of MS 4 Å. After 24 h of stirring at 40 °C the reactions mixtures were filtered then evaporated in *vacuum*. The conversions and the enantiomeric excesses of remained acetates ***(S)*-1a** and the obtained alcohols ***(R)*-1** were quantified by chiral GC after an acidic work-up (Table 2).

As shown on Table 2, with both *CAL-B* preparations, the use of DABCO as additive improve significantly the conversion rate without any perturbation of the enantioselectivity behavior and that in both used solvents (entries 3, 11 & 19). At the best of our knowledge, the use of the DABCO as enzyme activator in non-aqueous media for the kinetic bio-resolution of racemates was not described yet. Their use was only reported in promiscuous aldol reactions [36].

Also, there is not a direct correlation between the pK_a values of several used additives and the *CAL-B* activation rates. It is important to note that no deactivation influence of the *CAL-B* was noted when using a base with low pK_a value, the pyridine (entries 4, 12 & 20).

When the *CHIRAZYME® L-2, c.-f. C2, lyo* is used, only the DABCO play the role of enzyme activator, where the conversion rate was doubled and that compared to the other used additives. No significant influence of the addition of other bases and that independently to the solvent hydrophilicity. Since the TBME is classed as replacement solvent of DIPE by *Pfizer* and for the above observations, we have opting to carry on our study in a more compatible solvent.

Whilst, when the *Novozym®435* different degrees of activation were recorded using the chosen additives. The best conversion rates were achieved using the 4-DMAP and the DABCO, Conv = 38.3% and 44.7% respectively (Entries 18 & 19).

In order to validate this approach and checking the fact of the activation exhibited by the introduction of this Lewis base, we have decided to apply these optimized conditions of the kinetic bio-resolution via hydrolysis to series of secondary arylalkyl acetates **2a-8a.**

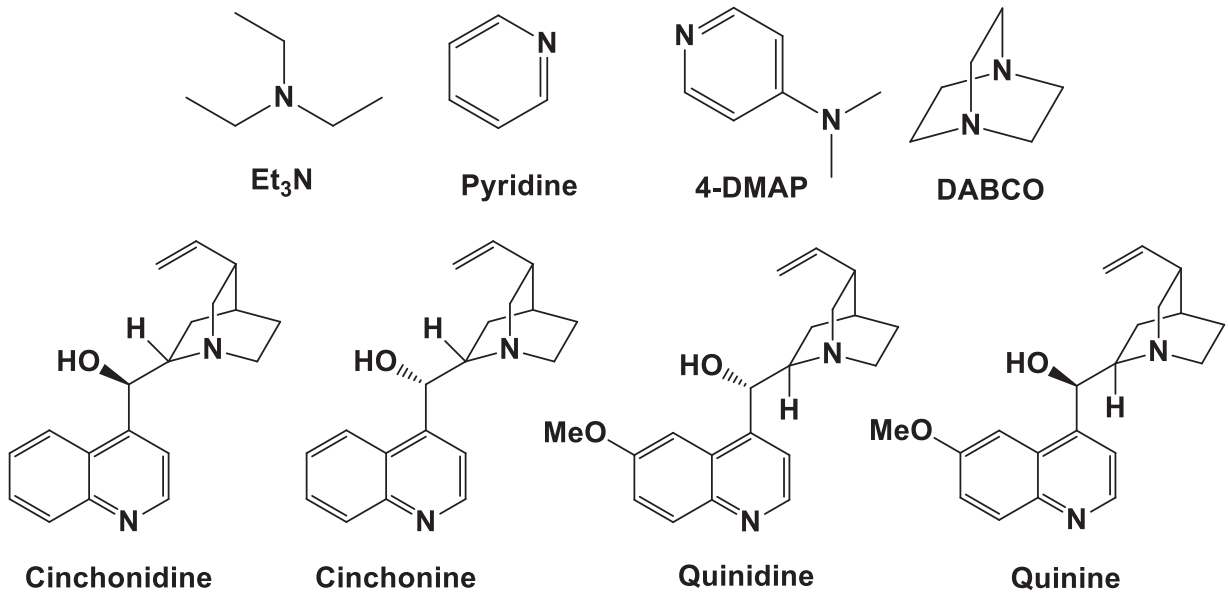

Fig. 1. : Structures of several chosen additives.

Table 2
Influence of the additive nature on the enzymatic deacylation of **1a**.

Entry[a]	Org. Solvent	Additive	ee_S (%)[b]	ee_P (%)[b]	Conv (%)[c]	E[c]
CHIRAZYME® L-2, c.-f. C2, lyo						
1	DIPE (1.9)	Et_3N	34.2	> 99	25.7	> 200
2		4-DMAP	35.6	> 99	26	> 200
3		DABCO	81	> 99	44.8	> 200
4		Pyridine	27.7	> 99	21.7	> 200
5		Cinchonine	23.3	> 99	18.9	> 200
6		Cinchonidine	25.1	> 99	20.1	> 200
7		Quinine	37.3	> 99	27.2	> 200
8		Quinidine	38	> 99	27.5	> 200
9	TBME	Et_3N	35.7	> 99	26.5	> 200
10	(1.35)	4-DMAP	29.2	> 99	22.7	> 200
11		DABCO	87.3	> 99	46.6	> 200
12		Pyridine	25.3	> 99	20.4	> 200
13		Cinchonine	21.1	> 99	17.5	> 200
14		Cinchonidine	21.3	> 99	17.7	> 200
15		Quinine	29	> 99	22.7	> 200
16		Quinidine	28.7	> 99	22.5	> 200
Novozym®435						
17	TBME	Et_3N	20.6	> 99	17.1	> 200
18	(1.35)	4-DMAP	61.5	> 99	38.3	> 200
19		DABCO	79.9	> 99	44.7	> 200
20		Pyridine	34.3	> 99	25.7	> 200
21		Cinchonine	34.4	> 99	25.8	> 200
22		Cinchonidine	30.2	> 99	23.4	> 200
23		Quinine	51.8	> 99	34.4	> 200
24		Quinidine	51.2	> 99	34.1	> 200

[a] 1 mmol of (1a), 0.5 equiv. of additive, 50 mg of *CAL-B*, 50 mg of molecular sieves 4 Å, 2 mL of organic solvent at 40 °C during 24 h.

[b] Enantiomeric excess of obtained alcohol and the remained acetate are measured by chiral GC.

[c] Conversion [34,35]: Conv=$ee_S/ee_P + ee_S$; Selectivity: E = Ln [(1-C) (1-ee_S)]/ Ln [(1-C) (1 +ee_S]

3.3. Scope on the impact of the introduction of DABCO during the bio-deacylation of some arylalkylacetates

The *CAL-B* catalyzed deacylation of acetates **2a-8a** (Scheme 2), under the new reaction's conditions, in the presence of DABCO was performed. All experiments were carried out on 1 mmole of racemic acetate, 0.5 equivalent of DABCO, in the presence of 50 mg of *CAL-B* preparations, 50 mg of molecular sieves in 2 mL of TBME for 24 h, at 40 °C. The results are summarized in Table 3.

The described results reported on Table 3 shows that both *CAL-B* preparations gave poor to excellent enantioselectivities albeit with slight to important differences in the conversion rates, during the bio-deacylation of arylalkylacetates (**1a-8a)** in the presence of DABCO under poor water conditions. *CHIRAZYME® L-2, c.-f. C2, lyo* and *Novozym®435* reveal the same behaviour toward all the resolved racemic acetates, except the structure **7a**. Where the *Novozym®435* preparation exhibits the best reactivity and enantioselectivity under those promiscuous conditions compared to the *CHIRAZYME* preparation (entry 6 versus 14).

An ideal enzymatic kinetic resolution was recorded with the acetate **4a** (Conv 50% and E > >200).

The obtained results using DABCO (pk_a 8.8) as additive for the deacylation of acetates **1a-8a** improve significantly the previous results when the Et_3N pk_a 10.75) was used, and that in terms of reactivity and enantioselectivity [28]. As others [29,37], we have attributed this fact to the basicity of the used additive, which acts in parallel on removing the acetic acids released during the deacylation of acetate from the enzyme microenvironment and preventing it inhibition and attenuation. Another hypothesis was reported during the hydrolysis of 3-hydroxy fatty acid esters by Novozym 435 dissolved in Et_3N. The introduction of this base was enhanced reaction rates with moderate selectivities [29]. The authors suggested that there was probably a special effect for sterically hindered amines especially amines with tertiary nitrogen atoms such as Et_3N and DABCO on the activation of the lipase and not only the basicity effects. They concluded that the acyl binding site of the enzyme may be activated by sterically hindered amines. Actually, our study support also this hypothesis, where we have observed that the presence of no reactive bases play role of enzyme activators without disturbing the lipase enantioselectivity, during the hydrolysis under promiscuous conditions without any introduction of external water. Exceptionally the use of strong bases such pyridine don't affect the enzyme enantioselectivity. Furthermore, we have shown that the use of chiral alkaloids (cinchonidine, cinchononine, quinine quinidine) as additives improve significantly the *Novozym®435* lipase reactivity despite their chirality. The same effects was reported by Guo and Sih, during the *Candida cylindracea lipase* (*CCL*) catalyzed hydrolysis of aryloxypropionic esters using either dextromethorphan (DM) or levomethorphan as enantiomerically pure additives [38].

Finally, we can conclude that use of two different preparation of *CAL-B* from different suppliers for the biodeacylation of some arylalkyl

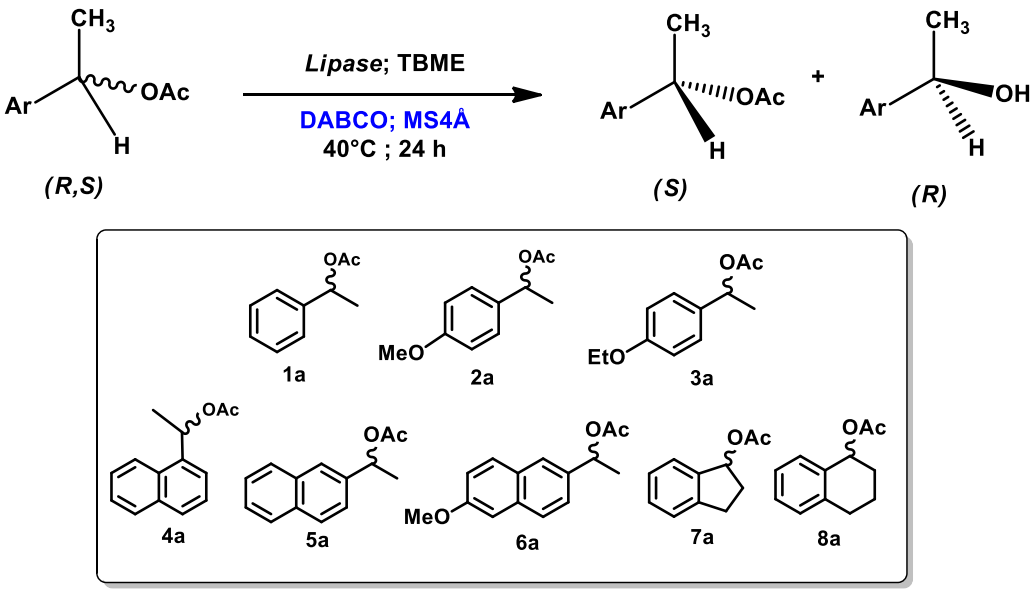

Scheme 2. Enzymatic deacylation of **2a-8a** in the presence of DABCO.

Table 3
Effect of DABCO as additive on the outcome of the *CAL-B* deacylation of some arylalkyl acetates.

Entry[a]	Acetate	ee_S (%)[b] (yield %)[c]	ee_P (%)[b] (yield %)[c]	Conv (%)[d]	E[d]
CHIRAZYME® L-2, c.-f. C2, lyo					
1	1a	87.3 (45)	> 99 (35)	46.6	> 200
2	2a	75.6 (45)	> 99 (34)	43.3	> 200
3	3a	28.2 (70)	> 99 (15)	22.2	> 200
4	4a	> 99 (45)	> 99 (40)	50	> 200
5	5a	64.4 (50)	> 99 (35)	39.4	> 200
6	6a	9.6 (ND)	95.8 (ND)	9.1	120
7	7a	3.9 (ND)	82.8 (ND)	4.6	11
8	8a	66 (50)	> 99 (35)	40	> 200
Novozym®435					
9	1a	79.9 (50)	> 99 (38)	44.7	> 200
10	2a	67.2 (48)	> 99 (35)	40.4	> 200
11	3a	41.4 (60)	> 99 (15)	29.5	> 200
12	4a	> 99 (45)	> 99 (40)	50	> 200
13	5a	60 (60)	> 99 (29)	37.7	> 200
14	6a	72.6 (50)	> 99 (35)	42	> 200
15	7a	7.9 (ND)	94 (ND)	7.7	34
16	8a	65.8 (60)	> 99 (30)	39.9	> 200

[a] 1 mmol of (1a), 0.5 equiv. of DABCO, 50 mg of *CAL-B*, 50 mg of molecular sieves 4 Å, 2 mL of TBME at 40 °C during 24 h.
[b] Enantiomeric excess of obtained alcohol and the remained acetate are measured by chiral GC or HPLC.
[c] Isolated Yields after separation on preparative TLC. **ND**: Not determined
[d] Conversion [34,35]: Conv=$ee_S/ee_P + ee_S$; Selectivity: E = Ln [(1-C) (1-ee_S)]/ Ln [(1-C) (1 +ee_S].

acetates under non-conventional conditions using the DABCO as enzyme activator shows some similarities. The presence of this amine improve significantly the reactivity without disturb the enantioselectivity one during the enzymatic kinetic resolution reactions.

4. Conclusion

The present study describes for the first time a significant impact of the introduction of DABCO as an activator enzyme during the kinetic resolution via biodeacylation of some arylalkyl acetates catalyzed by lipase *CAL-B* under promiscuous conditions. Two *CAL-B* preparations from different suppliers were subjected to this investigation.

The optimum conditions were appointed initially using a tertiary amine, the Et_3N. The impact of some simple and complex bases on the outcome of the reaction was also examined. No direct correlation between the pk_a values of several used additives and the *CAL-B* activation rates. From the examined amines, the DABCO gave an improvement of the conversion rates of the enzymatic deacylation was noticed with the phenylethyl acetate as the study model. An application of the optimum conditions on some arylalkyl acetates, improves significantly the efficiency of this basic organic additive as enzyme activator during the biodeacylation process.

CRediT authorship contribution statement

Meriem Ferrah, NourElHouda Benamara, Mounia Merabet-Khelassi carried out all the experimental works and performed all spectral and chromatographic analyses. Mounia Merabet-Khelassi and Samia Guezane-Lakoud interpreted the results and carried out the first draft of the manuscript. Mounia merabet-Khelassi and Louisa Aribi-Zouioueche conceived, designed and supervised the study. Mounia Merabet-Khelassi and Louisa Aribi-Zouioueche corrected and wrote the final manuscript. All authors read and approved the final version of this manuscript.

Declaration of Competing Interest

The authors declare no conflict of interest.

Data Availability

No data was used for the research described in the article.

Acknowledgements

Algerian Ministry of Higher Education and Scientific Research (MESRS, FNR 2000) is gratefully acknowledged for the financial support of this work. Prof. Olivier RIANT (IMCN/UCL- Louvain-La-Neuve, Belgium) is acknowledged for his assistance and the welcome of NourElHouda Benamara and Mounia Merabet-Khelassi to perform specific analyses.

Appendix A. Supporting information

Supplementary data associated with this article can be found in the online version at doi:10.1016/j.enzmictec.2022.110145.

References

[1] U.T. Bornscheuer, R.J. Kazlauskas, Hydrolases in organic synthesis: regio- and stereoselective biotransformations. GmbH & Co. KGaA, Wiley-VCH Verlag, Weinheim, 2005.

[2] D. Mendez-Sanchez, M. Lopez-Iglesias, V. Gotor-Fernandez, Hydrolases in organic chemistry. Recent achievements in the synthesis of pharmaceuticals, Curr. Org. Chem. 20 (2016) 1186–1203, https://doi.org/10.2174/1385272819666150819190956.

[3] M. Kapoor, M.N. Gupta, Lipase promiscuity and its biochemical applications, Process Biochem. 47 (2012) 555–569, https://doi.org/10.1016/j.procbio.2012.01.011.

[4] K. Hult, P. Berglund, Enzyme promiscuity: mechanism and applications, Trends Biotechnol. 25 (2007) 231–238, https://doi.org/10.1016/j.tibtech.2007.03.002.

[5] O.V. Kharissova, B.I. Kharisov, C.M. Oliva González, Y.P. Méndez, I. López, Greener synthesis of chemical compounds and materials, R. Soc. Open Sci. 6 (2019), 191378, https://doi.org/10.1098/rsos.191378.

[6] E. Busto, V. Gotor-Fernandez, V. Gotor, Hydrolases: catalytically promiscuous enzymes for non-conventional reactions in organic synthesis, Chem. Soc. Rev. 39 (2010) 4504–4523, https://doi.org/10.1039/C003811C.

[7] K. Faber. Biotransformations in Organic Chemistry, sixth ed., Springer-Verlag, Berlin, 2011.

[8] R.A. Sheldon, Green Biocatalysis, in: R.N. Patel (Ed.), Biocatalysis and green chemistry, Wiley online library, 2011. Chap1, 1-15.

[9] C. Ortiz, M.L. Ferreira, O. Barbosa, J.C. dos Santos, R.C. Rodrigues, Á. Berenguer-Murcia, L.E. Briand, R. Fernandez-Lafuente, Novozym 435: the "perfect" lipase immobilized biocatalyst? Catal. Sci. Technol. 9 (2019) 2380–2420, https://doi.org/10.1039/C9CY00415G.

[10] A. Idris, A. Bukhari, Immobilized Candida antarctica lipase B: hydration, stripping off and application in ring opening polyester synthesis, Biotechnol. Adv. 30 (2012) 550–563, https://doi.org/10.1016/j.biotechadv.2011.10.002.

[11] D. Rotticci, J. Ottosson, T. Norin, K. Hult, Candida antarctica lipase B a tool for the preparation of optically active alcohols. Enzymes in nonaqueous solvents, Humana Press Inc., 2001, pp. 261–276.

[12] R.N. Lima, C.S. dos Anjos, E.V.M. Orozco, A.L.M. Porto, Versatility of Candida antarctica lipase in the amide bond formation applied in organic synthesis and biotechnological processes, Mol. Catal. 466 (2019) 75–105, https://doi.org/10.1016/j.mcat.2019.01.007.

[13] A. Zaïdi, M. Merabet-Khelassi, L. Aribi-Zouioueche, CAL-B-catalyzed enantioselective deacetylation of some benzylic acetate derivatives via alcoholysis in non-aqueous media, Catal. Lett. 145 (2015) 1054–1061, https://doi.org/10.1007/s10562-014-1470-7.

[14] S. Razi, S. Zeror, M. Merabet-Khelassi, E. Kolodziej, M. Toffano, L. Aribi-Zouioueche, Two approaches for CAL-B-catalyzed enantioselective deacylation of a set of α-Phenyl ethyl esters: organic solvent with sodium carbonate and micro-aqueous medium, Catal. Lett. 151 (2021) 2603–2611, https://doi.org/10.1007/s10562-020-03525-0.

[15] M. Merabet-Khellasi, L. Aribi-Zouioueche, O. Riant, Chemoenzymatic synthesis of optically active 1, 2-disubstituted ferrocenes with planar chirality, Tetrahedron.: Asymmetry 20 (2009) 1371–1377, https://doi.org/10.1016/j.tetasy.2009.04.014.

[16] M. Merabet-Khelassi, L. Aribi-Zouioueche, O. Riant, Synthesis of 1,2-disubstituted aminoarylferrocene as direct route to enantioenriched 2-hydroxymethyl-1-phenylferrocene via enzymatic kinetic resolution, Res. Chem. Intermed. 43 (2017) 5293–5303, https://doi.org/10.1007/s11164-017-2926-3.

[17] M. Merabet-Khelassi, N. Bouzemi, J.C. Fiaud, O. Riant, L. Aribi-Zouioueche, Effect of the amount of lipase on enantioselectivity in the kinetic resolution by enzymatic acylation of arylalkylcarbinols, C. R. Chim. 14 (2011) 978–986, https://doi.org/10.1016/j.crci.2011.07.005.

[18] N.E. Benamara, M. Merabet-Khelassi, S.G. Lakoud, L. Aribi-Zouioueche, O. Riant, Enantioselective enzymatic synthesis of (R)-Phenyl alkyl esters and their analogue amides using fatty acids as green acyl donors, ChemistrySelect 6 (2021) 13941–13946, https://doi.org/10.1002/slct.202103831.

[19] M. Merabet-Khelassi, L. Aribi-Zouioueche, O. Riant, Effect of alkaloids on the activity and selectivity of Candida rugosa lipase in the kinetic resolution of 2-hydroxymethyl-1-phenylthioferrocene with planar chirality, Tetrahedron.: Asymmetry 19 (2008) 2378–2384, https://doi.org/10.1016/j.tetasy.2008.10.009.

[20] F.Z. Belkacemi, M. Merabet-Khelassi, L. Aribi-Zouioueche, O. Riant, Production of l-menthyl acetate through kinetic resolution by Candida cylindracea lipase: effects of alkaloids as additives, Res. Chem. Intermed. 44 (2018) 6847–6860, https://doi.org/10.1007/s11164-018-3525-7.

[21] M. Merabet, N. Melais, M. Boukachabia, J.C. Fiaud, L. Zouioueche-Aribi, Effet d'un éther couronne sur le système catalytique dans la réaction d'acylation du 1-acenaphtenol avec la lipase de candida cylindracea, J. Soc. Alg. Chim. 17 (2007) 185.

[22] A.L. Serdakowski, J.S. Dordick, Enzyme activation for organic solvents made easy, Trends Biotechnol. 26 (2008) 48–54, https://doi.org/10.1016/j.tibtech.2007.10.007.

[23] M. Merabet-Khelassi, Z. Houiene, L. Aribi-Zouioueche, O. Riant, Green methodology for enzymatic hydrolysis of acetates in non-aqueous media via carbonate salts, Tetrahedron.: Asymmetry 23 (2012) 828–833, https://doi.org/10.1016/j.tetasy.2012.06.001.

[24] A. Alalla, M. Merabet-Khelassi, O. Riant, L. Aribi-Zouioueche, Easy kinetic resolution of some β-amino alcohols by Candida antarctica lipase B catalyzed hydrolysis in organic media, Tetrahedron.: Asymmetry 27 (2016) 1253–1259, https://doi.org/10.1016/j.tetasy.2016.10.003.

[25] N. Braia, M. Merabet-Khelassi, L. Aribi-Zouioueche, Efficient access to both enantiomers of 3–(1–hydroxyethyl) phenol by regioselective and enantioselective CAL-B–catalyzed hydrolysis of diacetate in organic media by sodium carbonate, Chirality 30 (2018) 1312–1320, https://doi.org/10.1002/chir.23025.

[26] F.Z. Belkacemi, M. Merabet-Khelassi, L. Aribi-Zouioueche, O. Riant, Diastereoselective and enantioselective alkaline-hydrolysis of 2-aryl-1-cyclohexyl acetate: a CAL-B catalyzed deacylation/acylation tandem process, Tetrahedron.: Asymmetry 28 (2017) 1644–1650, https://doi.org/10.1016/j.tetasy.2017.09.010.

[27] N. Braïa, M. Merabet-Khelassi, L. Aribi-Zouioueche, M. Toffano, Practical access to (S)-heterocyclic aromatic acetates via CAL-B/Na_2CO_3 deacylation and Mitsunobu reaction protocol, Biocatal. Biotrans. (2022), https://doi.org/10.1080/10242422.2022.2030726.

[28] M. Merabet-Khelassi, A. Zaidi, L. Aribi-Zouioueche, CAL-B-Catalyzed deacylation of benzylic acetates: Effect of amines addition. Comparison of several approaches, Enzym. Microb. Technol. 107 (2017) 1–6, https://doi.org/10.1016/j.enzmictec.2017.07.005.

[29] Y.R. Liang, Q. Wu, X.F. Lin, Effect of additives on the selectivity and reactivity of enzymes, Chem. Rec. 17 (2017) 90–121, https://doi.org/10.1002/tcr.201600016.

[30] B. Berger, C.G. Rabiller, K. Konigsberger, K. Faber, H. Griengl, Enzymatic acylation using acid anhydrides: crucial removal of acid, Tetrahedron.: Asymmetry 1 (1990) 541–546, https://doi.org/10.1016/S0957-4166(00)80545-5.

[31] J.L.L. Rakels, A.J.J. Straathof, J.J. Heijnen, Improvement of enantioselective enzymatic ester hydrolysis in organic solvents, Tetrahedron.: Asymmetry 5 (1994) 93–100, https://doi.org/10.1016/S0957-4166(00)80488-7.

[32] P. Stead, H. Marley, M. Mahmoudian, G. Webb, D. Noble, Y.T. Ip, E. Piga, T. Rossi, S. Roberts, M.J. Dawson, Efficient procedures for the large-scale preparation of (1S, 2S)-trans-2-methoxycyclohexanol, a key chiral intermediate in the synthesis of tricyclic β-lactam antibiotics, Tetrahedron.: Asymmetry 7 (1996) 2247–2250, https://doi.org/10.1016/0957-4166(96)00279-0.

[33] M. Braner, S.Z. ielonka, J. Grzeschik, S. Krah, S. Lieb, D. Petras, X. Wagner, I. Ahmed, S.H. Hüttenhain, Hydrolysis of fatty acid esters by Candida Antarctica lipase B (Novozym 435) dissolved in anhydrous triethylamine, ChemCatChem 4 (2012) 2050–2054, https://doi.org/10.1002/cctc.201200355.

[34] C.S. Chen, Y. Fujimoto, C.J. Sih, Quantitative analyses of biochemical kinetic resolutions of enantiomers, J. Am. Chem. Soc. 104 (1982) 7294–7299, https://doi.org/10.1021/ja00389a064.

[35] H.B. Kagan, J.C. Fiaud, Kinetic Resolution Topics, in: E.L. Stereochemistry, S. H. Eliel (Eds.), Wilen, 18, J. Wiley & Sons, Inc, New York, 1988, pp. 249–330.

[36] J.W. Xue, J. Song, I.C.K. Manion, Y.H. He, Z. Guan, Asymmetric morita–baylis–hillman reaction catalyzed by pepsin, J. Mol. Catal. B: Enzym. 124 (2016) 62–69, https://doi.org/10.1016/j.molcatb.2015.12.002.

[37] F. Theil, Enhancement of selectivity and reactivity of lipases by additives, Tetrahedron 19 (2000) 2905–2919, https://doi.org/10.1016/S0040-4020(00)00041-7.

[38] Z.W. Guo, C.J. Sih, Enantioselective inhibition: strategy for improving the enantioselectivity of biocatalytic systems, J. Am. Chem. Soc. 111 (1989) 6836–6841, https://doi.org/10.1021/ja00199a053.